VYSOKÉ UČENÍ TECHNICKÉ V BRNĚ
FAKULTA CHEMICKÁ

Recent Advances in Polysaccharides-based Biological Macromolecules for Tissue Engineering: From Preparation to Medical Applications

HABILITAČNÍ PRÁCE V OBORU MAKROMOLEKULÁRNÍ CHEMIE

Dr. Abdelmohsen Abdellatif, Ph.D.

Brno, 2023

Habilitační práce

Recent Advances in Polysaccharides-based Biological Macromolecules for Tissue Engineering: From Preparation to Medical Applications

Dr. Abdelmohsen Abdellatif, Ph.D.

2023

Abdel-mohsen@ceitec.vutbr.ccz

https://www.vut.cz/lide/abdelmohsen-moustafa-abdellatif-161078#navigace-vizitka

https://scholar.google.cz/citations?hl=en&user=1aJxGZkAAAAJ&view_op=list_works&sortby=pubdate

S C O P U S I D : 35751774400

ORCID ID: 0000-0002-1232-2301

Table of contents:

Abstract

The habilitation thesis titled " **Recent Advances in Polysaccharides-based Biological Macromolecules for Tissue Engineering: From Preparation to Medical Applications**" presents original and relevant research results obtained during the author's research career in chemical modification polysaccharides and their applications, particularly in the medical area. The thesis summarizes the significant results sustained by the publication of 12 ISI papers and 1 US patent, with the author contributing as the first author and/or corresponding author.

Various procedures for chemical modification, preparation of nanocomposites, and fabrication of different material shapes via different techniques were employed to produce various polysaccharide surface modifications and their applications. The preparation of different polysaccharide derivatives and their composites was deeply characterized regarding material properties, with special attention paid to their medical applications. The thesis also documents original results showing improvements in the biological properties of different polysaccharides and their composites, such as antibacterial and biocompatibility. The selected activity is considered relevant in terms of originality and importance for the author's future Research and academic career development. My academic activity will be focused on the correlation between research and education, the promotion of innovation in applied research and educational methodologies, collaboration with industry, and student needs and expectations.

Keywords:

Polysaccharides, chemical modifications, nanocomposite, antibacterial, wound dressing, nanotechnology

<u>Arrangement of the habilitation thesis</u>.

The thesis is structured into three parts:

<u>Chapter 1:</u> Introduction and Motivation

<u>Chapter 2:</u> Describes the preparation and investigation of wound dressing materials based on polysaccharides, involving various techniques and assays to create materials with unique properties and investigate their potential for use in tissue engineering areas.

<u>Chapter 3:</u> Conclusion and briefly summarize the author's future scientific and teaching activities.

<u>Chapter: 4</u> List of publications output related to the habilitation thesis, including nine articles published in high-impact journals and one USA Patent to which the author contributed as the first author and/or corresponding author.

Acknowledgments

Chapter 1: Introduction and Motivation

Uses of natural and synthetic polymers have gained considerable attention in tissue engineering applications due to their favorable properties, such as tunable mechanical properties, biocompatibility, biodegradability, and ease of processing. However, one of the main disadvantages of using synthetic polymers in tissue engineering applications is their potential for inducing an immune response or inflammation in the body due to their non-biodegradable nature or the release of toxic degradation products. Additionally, synthetic polymers cannot mimic the complex architecture and biochemical cues found in natural tissues, limiting their ability to support proper cell behavior and tissue regeneration.

The motivation of the work in this thesis is to create functional wound dressing materials from different polysaccharides and their composites and derivatives. The broadly defined goals investigate the effects of material performance, composition and functionality on their biological properties. The work in this thesis has three foci: 1) Development and preparation of new materials based on different polysaccharides; 2) Investigation of the relationships between the material properties and their performances; 3) Applications of the prepared materials in tissue regeneration, especially for skin tissue regeneration.

The mystery of life is in biological macromolecules. Biological macromolecules are large molecules essential to living organisms' structure and function. There are four important classes of biological macromolecules: carbohydrates, lipids, proteins, and nucleic acids[1-3]. Carbohydrates, proteins, and nucleic acids naturally exist as long-chain polymers, while lipids are smaller, and in a true sense, these are all considered biopolymers[1]. Carbohydrates are the storage form of energy and meet the demand as and when required. Carbohydrates are the most widely found organic compounds. These are well-known as essential sources of life or sustaining life itself[4]. These are optically active polyhydroxy aldehydes or ketones. There are broadly three major classes of carbohydrates: monosaccharides, oligosaccharides, and polysaccharides[5]. Carbohydrates are nature's most abundant organic compounds essential for many biological processes. They are found in a wide range of organisms, including plants, microorganisms, animal tissues, and bodily fluids such as blood and tissue fluids[1, 6].

Polysaccharides: Structure, properties, and chemical functionalization

Polysaccharides are important biomolecules widely used in the medical and pharmaceutical fields due to their biodegradability, biocompatibility, and bioactivity[7]. They are composed of long chains of monosaccharides, which are simple sugars linked in various ways to create different polysaccharides. Polysaccharides can be classified based on surface charge, chain structure, source, and monomer composition. The specific type and function of polysaccharides vary depending on the source, and many polysaccharides have unique properties that make them useful for various applications[1, 5, 8]. Polysaccharides have been found to have a number of properties that make them effective wound-healing agents. For example, they can help promote cell growth and proliferation, stimulate angiogenesis (forming new blood vessels), and provide a protective barrier against bacterial infection. Many types of polysaccharides **(Fig. 1)** have been studied for their wound-healing properties, including chitosan, hyaluronic acid, alginate, cellulose, schizophyllan, and carrageenan[8-11].

The chemical functionalization of polysaccharides involves the covalent attachment of various chemical groups to the polysaccharide backbone. This process can modify polysaccharides' physical, chemical, and biological properties, making them more versatile for specific applications. The functionalization can be achieved through various methods, including oxidation, esterification, etherification, amidation, and click chemistry[12-15].

Chemical functionalization of polysaccharides can lead to the development of new materials with improved properties such as increased mechanical strength, thermal stability, and water solubility. It can also enhance the biocompatibility and biodegradability of polysaccharides, making them suitable for various biomedical applications such as drug delivery, tissue engineering, and wound healing.
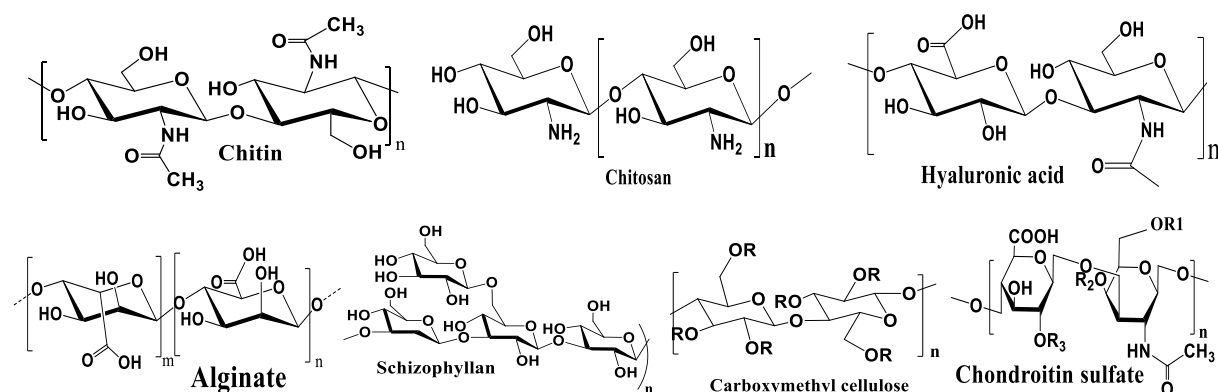

Fig. 1. Chemical structure of polysaccharides: chitin, chitosan, hyaluronic acid, alginate, schizophyllan, carboxymethyl cellulose and chondroitin sulfate.

Polysaccharide-based nanocomposites

Nanotechnology can be described as the controlled processing of materials consisting of at least one component with one dimension smaller than 100 nm. This technology aims to combine all core areas of science; chemistry, physics, biology, and material science to establish and achieve new materials with peculiar properties that can be exploited to develop and produce advanced biomedical and electronic devices, advanced high-performance materials, and other consumer products[16-18]. Polysaccharides have taken an interesting high position among biomaterials for advanced applications in pharmaceuticals and medicine due to their biocompatibility, biodegradability, and versatility. However, their poor mechanical properties can limit their applications, highlighting the need for modification and improvement. Polysaccharide-based nanocomposites have emerged as a promising solution to enhance polysaccharide-based biomaterials' mechanical properties and functionality. Incorporating nanoscale materials with high specific surface area and favorable inherent properties can significantly improve the performance of polysaccharides-based matrices[18]. Nanocomposites have a range of potential applications in tissue engineering, drug delivery, gene therapy, and wound dressings[16, 19]. For example, polysaccharide-based nanocomposites containing metal nanoparticles like silver, gold, and zinc oxide nanoparticles can be used as a wound dressing material for skin regeneration but also reveal improved physical, chemical and mechanical properties[8, 20-23]. Combining each component in nanocomposite with tunable properties is desirable for a specific application.

Overall, nanotechnology in polysaccharide-based biomaterials holds great promise for expanding their applications and benefits in various fields of medicine and pharmaceuticals[10, 11, 24-26].

Advanced applications of polysaccharides in tissue engineering

Tissue engineering is an interdisciplinary field that combines principles from biology, chemistry, engineering, and medicine to develop innovative solutions to medical problems. The goal of tissue engineering is to create functional and viable tissues or organs that can be transplanted into patients to restore or replace damaged or diseased tissue. One of the most significant advantages of tissue engineering is that it offers a potentially permanent solution for organ failure rather than just treating the condition's symptoms. Tissue engineering also has the potential to reduce the need for organ transplantation, which is currently limited by a shortage of donor organs. Selecting the right cell type is crucial for the success of tissue engineering. The cell can be obtained by different means, such as being harvested from the target organ, developed from stem cells, taken from grown cell lines in the lab, or directly taken from the

patient, reducing the chances of rejection. Both human tissue and synthetic polymer can be used for the supporting structure. Organs such as bladders, small arteries, trachea, and skin grafts are examples of tissue-engineered implants in humans.

Skin plays an essential role in preserving the body from the attack of the stimuli that come from outside. There are two main approaches to rescuing damaged skin: Autografts and allografts are practical approaches for saving highly injured skin (for instance, a high percentage of burnt skin), but they may cause immune responses such as morbidity. Hence, polysaccharides-based tissue engineering seems to be a perfect approach to healing tissue damage as an alternative for natural skin. In addition to having good mechanical properties, appropriate polysaccharides-based biomaterials for skin scaffold fabrication have to support cell attachment, growth, proliferation, differentiation, and migration, besides enablingc ell–cell signaling (fibroblasts, keratinocytes, as well as melanocytes as the foremost three types of skin cells) and the minimum possible immunogenic response[27-31]. Various polysaccharide-based biomaterials and nano additives with good mechanical and biological properties have been reported[26, 32]. Polysaccharides are great potent options among different biomaterials that can be utilized for skin tissue engineering. Although hydrophilicity is crucial in all biomaterials used in tissue engineering, it is underscored for skin scaffolds. The polysaccharide-based nanocomposite is a great biodegradable 3D structure to entrap a large amount of water[33]. Also, several reports on polysaccharides-based nanocomposites simulate human skin's biological and mechanical properties for tissue regeneration [28, 34].

Polysaccharide-based wound dressing

Wound healing is a complex and dynamic process that involves various cellular and molecular events. The four phases of wound healing are coagulation, inflammation, proliferation, and remodeling, a complex and slow process. Many internal (diabetes, vascular diseases, malignant tumors) and external factors (scalding burns, mechanical) are prone to skin trauma. Nondiabtetic or minor wounds can heal themselves, but large wounds and some pathological wounds heal too slowly and can become infected by bacteria and airborne dust particles during the healing process. Therefore, effectively promoting wound healing and repairing damaged skin is still a great clinical challenge.

Polysaccharide-based wound dressings are materials used to protect wounds from environmental microorganisms and promote skin tissue regeneration. Various wound dressings have been designed to protect, debride and absorb excess exudate while treating burns, trauma and chronic wounds. The ideal wound dressing should achieve fast wound healing to reduce potential patient suffering.

Traditional wound dressings, such as gauze and cotton, protect wounds from contamination and do not actively participate in wound healing.

More advanced dressings were designed to be biologically active alone or release biologically active ingredients in the dressing, such as adding antibacterial agents, which can facilitate moisture management, and controlling infection, assist tissue regeneration and accelerate wound healing. The functional and innovative wound dressing should have a unique performance like moisture management, permeability, non-toxicity, biocompatibility, adhesive properties, absorption capacity, sterility, bacterial Barrier, ease of use and cost-effectiveness.
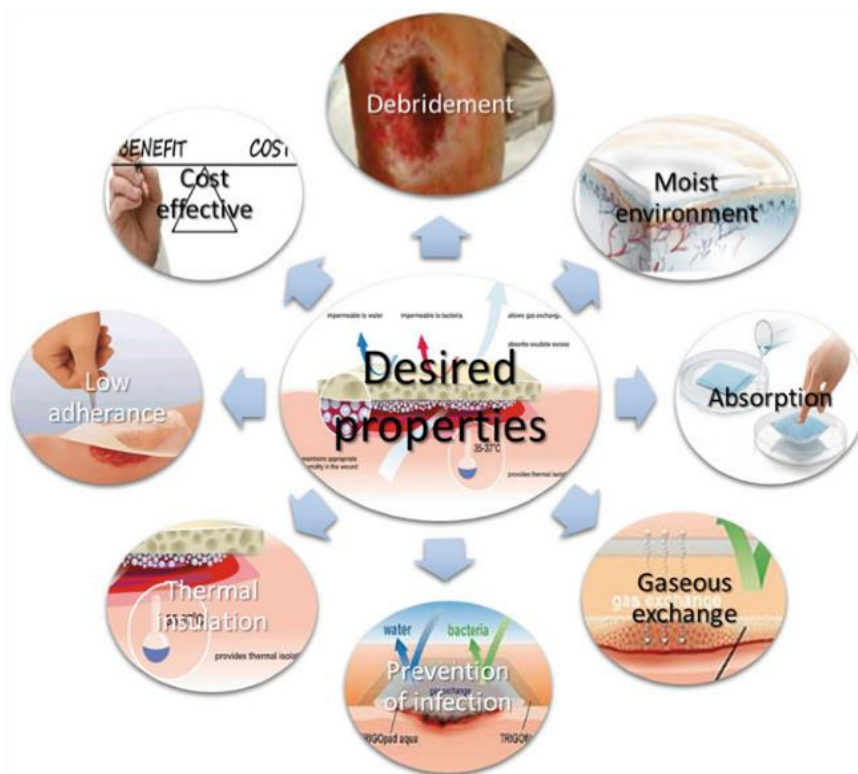
Fig. 2. Desired properties of wound dressing based on polysaccharides

Polysaccharides such as chitosan, alginate, hyaluronan, schizoplyllan, bacterial cellulose, dextrin, and carboxymethyl cellulose have been widely used in developing wound dressings due to their biocompatibility and biodegradability. These dressings can be made into different forms to suit wounds and applications, including gels, scaffolds, membranes, films, foams, and micro/nanofibers mats. Some benefits of polysaccharide-based wound dressings include reducing pain, accelerating wound healing, and minimizing scarring. They can also be used to treat a variety of wounds, including burns, pressure ulcers, diabetic ulcers, and surgical wounds.

Overall, polysaccharide-based wound dressings have shown great promise in wound care, and ongoing research is focused on improving their efficacy and developing new formulations for different applications. In order to enhance the antibacterial properties of wound dressings, various antibacterial agents have been incorporated into the dressings, including antibiotics (tetracycline, octenidine dihydrochloride, ciprofloxacin, gentamicin and sulfa-diazine), nanoparticles (metal/metal oxide nanoparticles) and natural products (honey, essential oils and chitosan[35]. The fact that no single dressing can be suitable for managing all wounds is the main contributor to the wide range of dressings. Modern dressings have been developed based on all discoveries regarding desired properties. The latter are classified mainly according to the materials from which they are produced.

In this habilitation thesis, I will highlight and discuss only two examples of polysaccharides (chitosan and hyaluronan) and their derivatives

The motivation behind the habilitation thesis:

Due to the limitations of traditional wound dressings in terms of their ability to maintain their integrity and durability over time, especially when exposed to fluids and exudates from the wound. Research in wound dressing materials engineering using polysaccharides and their derivatives is ongoing, and there is still much work to be done to understand these materials' structural and morphological impact. Further research could develop new wound dressings with improved properties and interactions between polysaccharide derivatives and other types of substances, such as nanoparticles or polymers.

Given these challenges, I introduce this thesis about my efforts during the last years to fabricate a new series of wound dressing materials that could overcome many disadvantages of traditional wound dressing. This research has significant potential for medical applications, technological optimization, and developing new composite materials with functional properties, making it an important area of basic and applied materials engineering research.

The aim of the habilitation thesis:

1. Development and preparation of new materials based on polysaccharides and polysaccharides wastes,
2. Investigation of the relationships between the material properties and performances,
3. Applications of the prepared materials in tissue regeneration, especially for skin tissue regeneration.

Chapter 2

Uses of different polysaccharides and their composites in tissue regeneration applications

This part focuses on fabricating and engineering wound dressing materials from cationic and anionic polysaccharides like chitin/chitosan and hyaluronan and their chemical modifications, such as detailing polysaccharide-based use within the broader context of the engineering of skin and other tissues **[P1-13]**.

This chapter is divided into two parts: The first part focuses on using chitosan polysaccharide and their derivatives and composites for tissue regeneration. The second part will concentrate on hyaluronan's different forms in medical applications. The main effort was focused on the preparation, characterization and evaluation of the prepared materials using different techniques with study on how to improve the biocompatibility and biological properties of the prepared materials.

Now, I will briefly discuss this research's examples, which document changes in material characteristics after modification.

Part A will address the applications and uses of cationic polysaccharides (chitin/chitosan) for tissue regeneration application, especially for skin regeneration **[P1-6].**

During my work, I used new sources of biowastes to prepare new wound dressing materials. The morphology of the synthesized bio-waste polysaccharide (chitin/chitosan-glucan complex) depends on the preparation and treatment process.

Chitosan and glucan are the most important components of the cell walls of fungi. They occur in different states depending on the specific fungal species. Some fungi have chitosan and glucan as covalently bonded complexes, while others have them as separate components in the cell wall. I successfully prepared chitin, chitosan and the chitosan-β-glucan complex in different forms (powder, microfiber, hollow fibers), and I could use them with another additive to fabricate a series of new wound dressing materials. First, I will describe the fabrication of new wound dressing materials based on chitosan covalently bonded to β-glucan **[P1-4].**

In manuscript **[P1],** a New wound dressing material based on chitin/chitosan-glucan microfiber (CGF) and collagen (CO) was prepared using EDC/NHS system as a crosslinker agent**.** The physicochemical and mechanical properties of native collagen were improved after grafting with CGF. A hybrid bioscaffold exhibits a higher reduction rate against different bacteria types than a control sample. From the results, a new type of wound dressing enhanced the mechanical, chemical and biological properties of native collagen.

[P1] R. M. Abdel-Rahman, V. Vishakha, I. Kelnar, J. Jancar, **A.M. Abdel-Mohsen***. Synergist performance of collagen-g-chitosan-glucan fiber biohybrid scaffold with tunable properties. International Journal of biological macromolecules **2022,** 202, 671-680. **(IF = 8.02)**
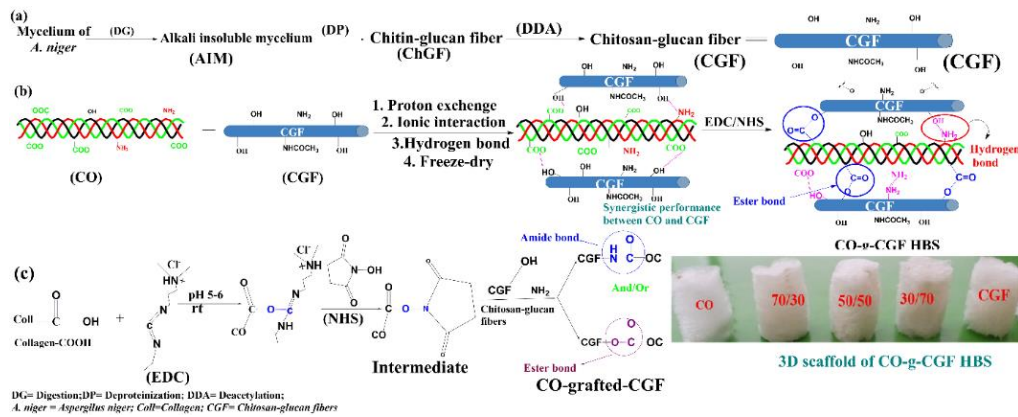
Fig.3. Representative extraction sequences of CGF and chemical modification with collagen (CO)

It was the first time to prepare hollow natural microfibers for skin regeneration and new cell carrier **[P2]**. A new dressing scaffold made of chitosan-glucan complex (CSGC) hollow fibers with collagen (CO) encapsulated aloe vera (AV). The main interesting point in this study is synthesized hollow microfibers from bio-wastes exhibited an inner diameter of 600 ± 250 nm and an outer fiber diameter of 2.5 ± 0.5 µm that could be used as a carrier for different drugs and small bioactive molecules like growth factors and nanoparticles, which was never seen before. Various properties of the fabricated system were investigated, including morphology, mechanical properties, pore size, porosity, swelling ability, and degradation behavior. We found that the presence of different ratios of hollow fibers (CSGC) in the scaffold significantly improved its physicochemical properties in a concentration-dependent manner. The mechanical properties of the scaffold were enhanced by encapsulating the AV inside the matrix. The hydrolytic stability of collagen was improved significantly with any external crosslinker after adding the CSGC. The obtained results suggest that the new CO/CSGC dressing scaffold has the potential for clinical skin regeneration.
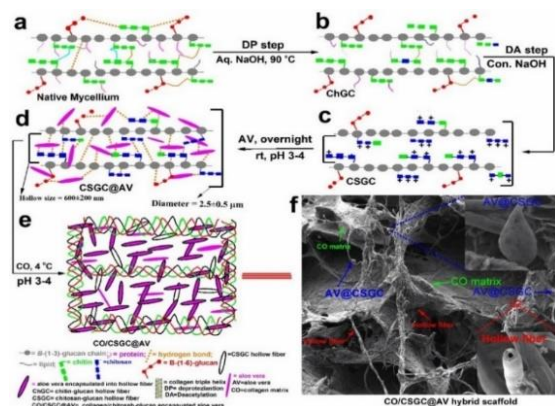
Scheme 1. Schematic illustration extracting sequence process of hollow fibers, hollow fibers encapsulated aloe vera and engineered dressing scaffolds.

Notes: (a) native mycelium beads after fermentation; **(b)** mycelium beads after deproteinization step (DP) (chitin-glucan hollow fiber complex (ChGC)); **(c)** chitosan-glucan hollow fiber after deacetylation step (CSGC); **(d)** hollow fiber encapsulated aloe vera (CSGC@AV); **(e)** collagen/chitosan-glucan hollow fiber encapsulated aloe vera (CO/CSGC@AV; **(f)** CO/CSGC@AV dressing scaffold.

[P2] <u>A.M. Abdel-Mohsen</u>*, Rasha M Abdel-Rahman, I Kubena, L Kobera, Z. Spotez, M Zboncak, R Prikryl, J Brus, J Jancar. Chitosan-glucan Complex Hollow Fibers Reinforced Collagen Wound Dressing Embedded with Aloe vera. Part I: Preparation and Characterization. Carbohydrate Polymers. **2020,** 115708. **(IF = 10.7)**

[P3] <u>A.M. Abdel-Mohsen</u>*, Rasha M. Abdelrahman, J. Frankova, M. Steinhart, J. Jancar. Chitosan-glucan Complex Hollow Fibers Reinforced Collagen Wound Dressing Embedded with Aloe vera. Part II: multifunctional properties to promote wound healing. International Journal of Pharmaceutics. **2020,** 582, 119349. **(IF = 6.5)**
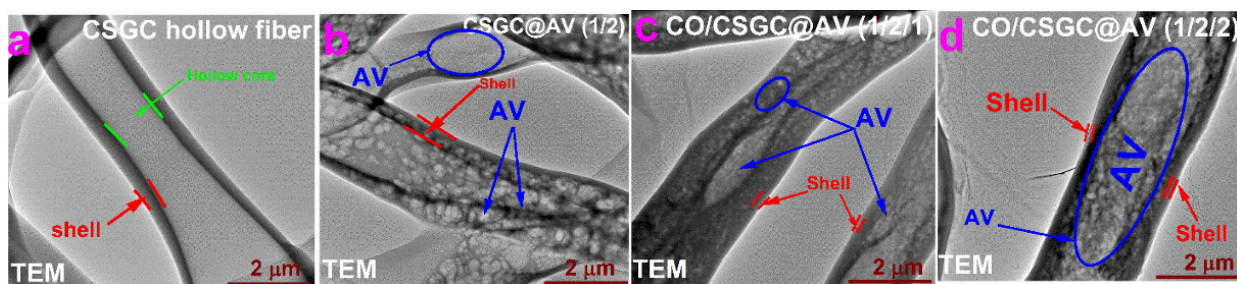
Fig. 4. TEM of CO/CSGC@AV wound dressing scaffold
(a) TEM of native CSGC; **(b)** CSGC@AV (1/2); **(c)** CO/CSGC@AV (1/2/1); **(d)** CO/CSGC@AV (1/2/2).

Another type of wound dressing based on powder chitin/chitosan-glucan complex was prepared using a green solvent (urea/sodium hydroxide) to fabricate. I have developed a chitin/chitosan-glucan complex (ChCsGC) wound dressing material, a promising step towards sustainable and eco-friendly wound healing solutions **[P4]**. The extracted complex was in <u>powder</u> form (due to the extraction and treatment process). The dissolution of ChCsGC in a pre-cooled urea/NaOH solution is a novel approach to achieve a homogeneous and uniform solution, which is necessary for fabricating nonwoven microfibers mats through a wet-dry-spinning technique for the first time. The mechanical properties of the ChCsGC nonwoven mats were improved by changing the coagulation bath components (from acid/alcohol ratio), indicating the importance of optimizing the fabrication process to achieve the desired properties, especially mechanical properties.

The excellent antibacterial activity of the ChCsGC nonwoven mats against different types of bacteria is a significant advantage for wound dressing applications, as infections are a common complication in wound healing. ChCsGC nonwoven mats show high biocompatibility compared with the control sample. The healing properties of the ChCsGC nonwoven mats revealed that the new wound dressing material from biowastes and their promising properties make it a potential candidate for commercialization and clinical use.
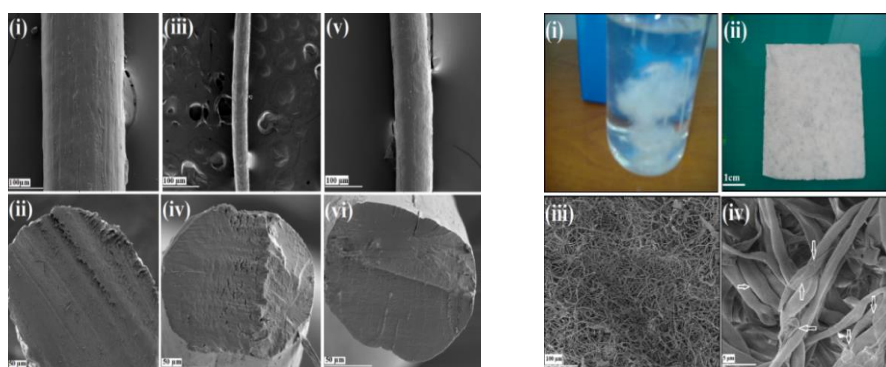
Fig. 5. Scanning electron microscopy of ChCsGC fibers in different coagulation bath compositions 5 % acetic acid/ isopropyl alcohol (i, ii); 10 % acetic acid/isopropyl alcohol (iii, iv); 15 % acetic acid/isopropyl alcohol (v, vi) **(A);** Photograph of short nonwoven fibers in wet-state (i); complex nonwoven sheet (ii), scale bar is 1 cm; SEM of complex nonwoven sheet with task bar 100 µm (b); SEM of a nonwoven sheet with task bar 5 µm **(B).**

[P4] <u>A.M. Abdel-Mohsen*,</u> J. Jancar, D. Massoud, Z. Fohlerova, H. Elhadidy, Z. Spotz, A. Hebeish. Novel chitin/chitosan-glucan wound dressing: Isolation, characterization, antibacterial activity and wound healing properties. International Journal of Pharmaceutics. **2016**, 510, 86–99. **(IF = 6.5).**
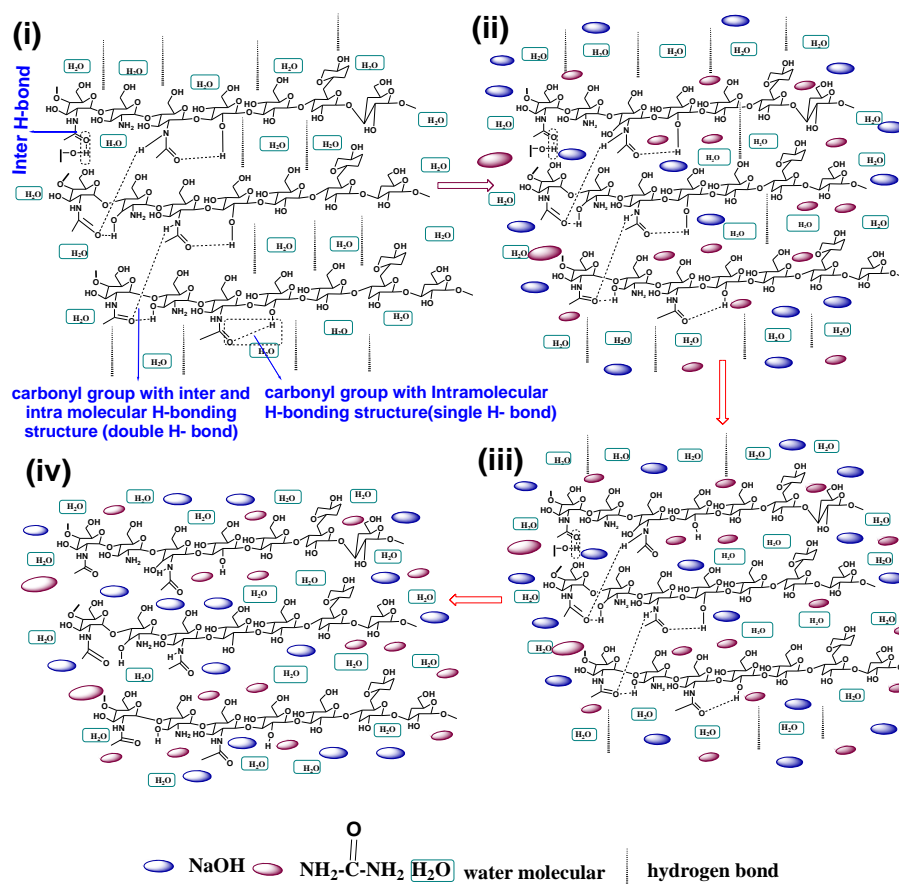
Scheme. 2. Illustration of the dissolution process of ChCsGC; ChCsGC immersed in 6 wt. % NaOH/8 wt. % urea aqueous solution at room temperature; **(i)** water molecules enter into the chitin molecular chain facilitated by the NaOH; **(ii)** water molecules freeze and expand at the freezing temperature and break the inter-and intra-hydrogen bond; **(iii)** promoting solubility of the ChCsGC **(iv).**
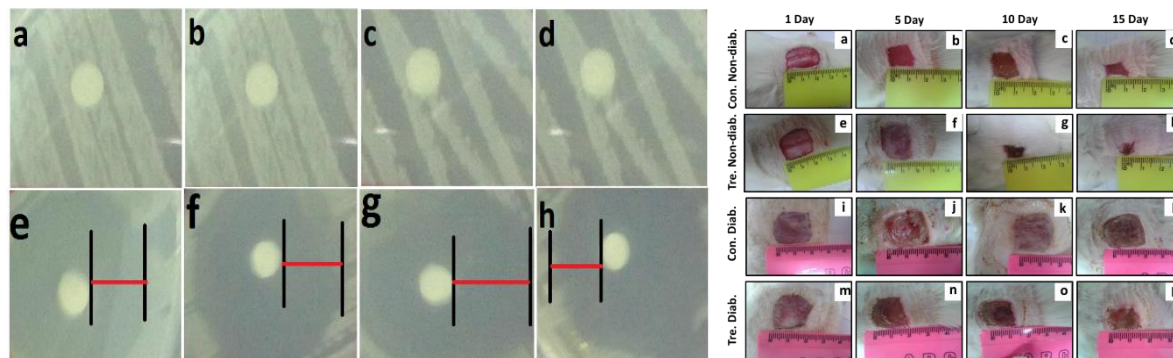

Fig. 6. Inhibition Zone assays of *bacillus subtilis* (a), *escherichia coli* (b); *staphylococcus aureus* (c); *klebsiella pneumoniae* (d) as control sample. ChCsGC nonwoven mats against *bacillus subtilis* (e), *escherichia coli* (f); *staphylococcus aureus* (g), *klebsiella pneumoniae* (h) **(A).** Macroscopic observation of the surface healing dressed with a nonwoven sheet (gauze) from cellulosic material (control-non-diabetic) at 1st, 5th, 10th and 15th days after surgery (a-d), respectively; healing of wound dressed with the ChCsGC sheet (non-diabetic) at 1st, 5rd, 10th and 15th days after operation (e-h), respectively; wound surface dressed with a nonwoven sheet (gauze) from cellulosic material (control diabetic) at 1st, 5rd, 10th and 15th days after operation (i-l), respectively; healing of wound dressed with nonwoven ChCsGC sheet (diabetic) at 1st, 5rd, 10th and 15th days after the operation (m-p), respectively **(B).**

[P4] **A.M. Abdel-Mohsen,** J. Jancar, D. Massoud, Z. Fohlerova, H. Elhadidy, Z. Spotz, A. Hebeish. Novel chitin/chitosan-glucan wound dressing: Isolation, characterization, antibacterial activity and wound healing properties. International Journal of Pharmaceutics 510 (**2016**) 86–99. (**IF = 6.51**)

Here, I used free chitosan, which I could successfully extract from animal sources. This study **[P5]** investigated and optimized the conditions to extract Chitin and chitosan from shrimp shells (Brazilian Atlantic Ocean). The biological properties of these materials were affected by the extraction process, which impacted their potential effectiveness as wound dressings. Furthermore, chitosan with a high degree of deacetylation (DDA), zero % of protein and a high yield percentage were obtained by sequence process (DMPA> DPMA> DAPM> DAMP). The new sources of Chitin and chitosan show high antibacterial activity against gram-negative bacteria (*E. coli*) compared with commercial chitosan (*Sigma-Aldrich*). This new source of chitin and chitosan opened a new research field for one company in Brazil to commercialize and produce Chitin and chitosan from local sources. The results conclude that chitin and chitosan from shrimp shells have high DDA, thermal stability and excellent antibacterial activity compared with other commercial sources that could be used in different medical and pharmaceutical applications.
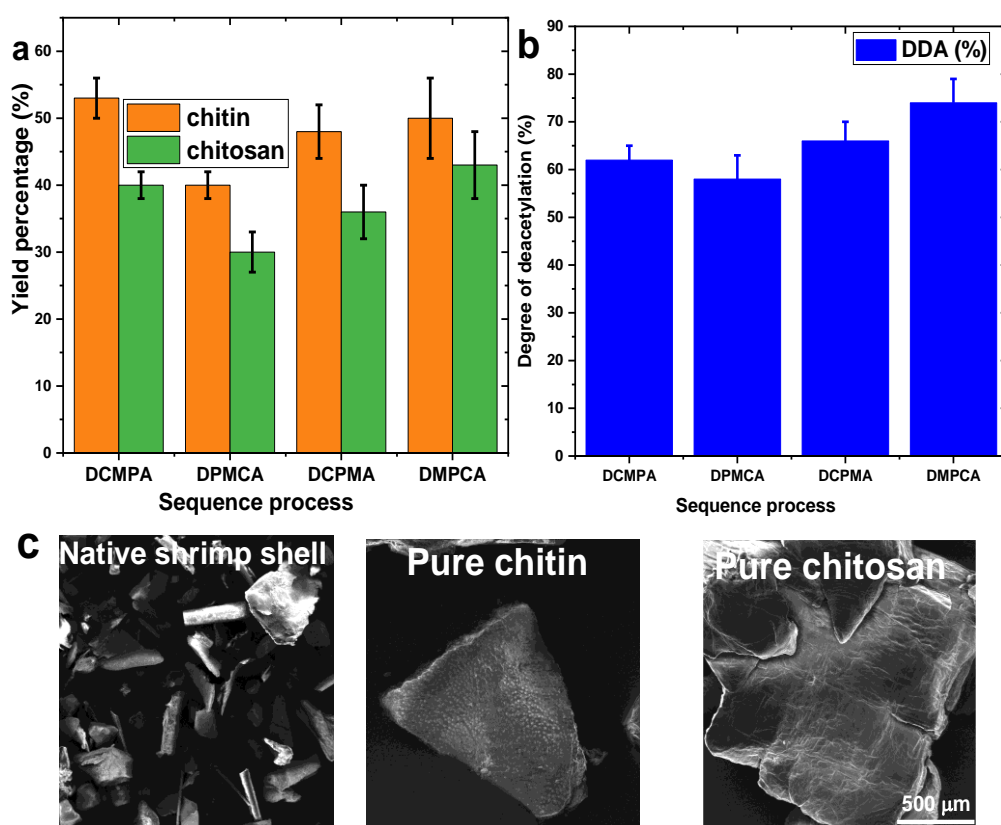
Fig. 7. Extraction sequence process of Chitin and chitosan on yield percent **(a)**; Sequence process on (DDA %) **(b)**, SEM of native shrimp shell, Chitin and chitosan **(c)**.
DMPA: demineralization, deproteinization, deacetylation; **DPMA**: deproteinization, demineralization, deacetylation; **DAPM**: deacetylation, deproteinization, demineralization; **DAMP**: deacetylation, demineralization, deproteinization.

[P5] Rasha M. Abdel-Rahman**, A.M. Abdel-Mohsen***, R. Hrdina, T. Pinto. Chitin and chitosan from Brazilian Atlantic Coast: Isolation, characterization, and antibacterial activity. International Journal of Biological Macromolecules. **2015,** 107, 107-120 **(IF = 8.02)**

Then, I succeeded in studying an eco-friendly process to prepare new wound dressing mats based on chitosan as cationic and hyaluronan as anionic polysaccharides (chitosan, hyaluronan) described in **[P6]**. Pure chitosan was prepared according to **[P5]** and was used for treatment by pad-dry-cure technique in the presence of a crosslinker agent (citric acid). Then, another layer of hyaluronan was immobilized into chitosan/ nonwoven fabrics by the same above. Chitosan/hyaluronan shows a well-distributed morphology on the fibers, as confirmed by scanning electron microscopy. The wound dressing material exhibited high antibacterial activity against two types of bacteria. The new dressing materials were also non-toxic to mouse fibroblast and keratinocyte cell lines. In addition, the composite of chitosan/hyaluronan viscose nonwoven fabrics enhanced the healing properties of diabetic and non-diabetic rats compared to the control sample, indicating the potential for use as a wound healing agent**.**

This study suggests that these novel wound dressing materials based on chitosan/hyaluronan/nonwoven fabrics may have the potential as a drug carrier for the better treatment of wound defects and promote wound healing**.**
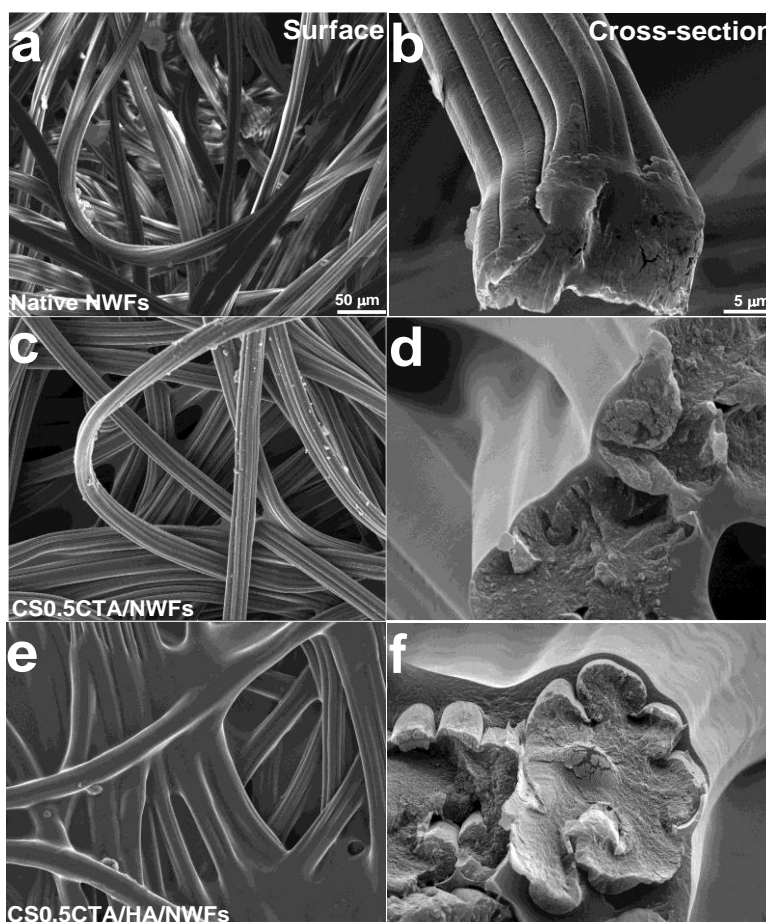
Fig. 8. Scanning electron microscopy of Chitosan/hyaluronan wound dressing layered. Native NWFs (a, b); CS$_{0.5}$CTA//NWFs (c, d); CS0.5CTA/HA/NWFs (e, f).

[P6] Rasha M. Abdel-Rahman**, A.M. Abdel-Mohsen***, R. Hrdina, L. Burgert, Z. Fohlerova, D. Pavlinak. Sayed, J. Jancar. Wound dressing based on chitosan/hyaluronan/nonwoven fabrics: Preparation, characterization, and medical applications. International Journal of Biological Macromolecules. **2016**, 89, 725–736. **(IF = 8.02).**

Also, we synthesized a novel fluorescent chitosan derivative with potential applications as a marker for tumors and as a carrier for targeted drug delivery **[P7].** The fluorescent label was synthesized by reacting cyanuric chloride with 9-amino anthracene, and the intermediate was then reacted with extracted chitosan in different molar ratios to yield different degrees of substitution of the fluorescent polymer.

The structure of the synthesized chitosan-g-4,6-dichloro-1,3,5-triazin-9-yl)-9-amino anthracene was confirmed using a range of analytical techniques, including NMR, FTIR, TGA and X-ray diffraction. The absorption and fluorescence spectra of the fluorescent label were measured in both solution and solid phases. The synthesized fluorescent chitosan derivative showed fluorescence in both the solid and solution phases.

In conclusion, these findings suggest that the prepared fluorescent chitosan derivative could be used as a marker for different tumors and a carrier for targeted drug delivery applications. Further Research is needed to evaluate the effectiveness of this compound in vitro and in vivo on the biocompatibility properties of the prepared materials.
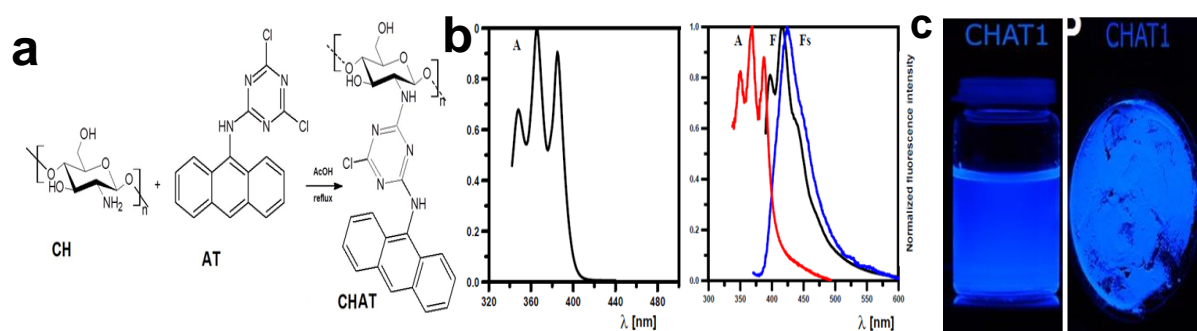
Fig. 9. Synthesis of chitosan-g-(4, 6-dichloro-1,3,5-triazin-9-yl)-9-aminoanthracene (CHAT) (a); absorption (A) spectrum of AT (left), absorption (A) spectrum and fluorescence spectra in solution (F) and in the solid phase (Fs) of CHAT1 **(b);** CHAT1-3 in aqueous solution (left); and in the solid phase under irradiation of UV light (right) **(c).**

[P7] Hana Prichystalova, Numan Almonasy, **A. M. Abdel-Mohsen***, Rasha. M. Abdel-Rahman, Libor Kobera, Moustafa M. G. Fouda, Zdenek Spotz, L.Vojtova, Ladislav Burgert, J. Jancar. Synthesis, characterization, and antibacterial activity of new fluorescent chitosan derivatives. International Journal of Biological Macromolecules. **2014**, 65, 234–240.**(IF = 8.02)**

Part B: Anionic polysaccharides-based wound dressing

This part **[P8-13]** will focus on preparing different wound dressing materials from anionic polysaccharides and their modifications to be used in medical applications. The effects of structure properties, chemical compositions, and morphology on biological properties were investigated and evaluated. The use of sodium hyaluronate (HA) in medical applications is attractive due to its biodegradable, biocompatible, and non-toxic properties. However, its poor stability and lack of antibacterial activity have limited its use in wound dressings.

In this part, I used hyaluronan as anionic polysaccharides incorporated with various additives such as Zinc oxide nanoparticles (ZnO-NPs), chitin nanowhiskers, PVA, and AgNPs to prepare different wound dressing materials with high-performance properties.

Zinc oxide nanoparticles (ZnO-NPs) were incorporated into the HA via in situ synthesis, with HA as a reducing and stabilizing agent **[P8]**. Uniform with the spherical shape of zinc oxide nanoparticles (50 ± 10 nm) was evenly distributed throughout the hyaluronan/polyvinyl alcohol (HA/PVA) matrix, providing stability and preventing NPs from dropping off the network, thus reducing their toxicity. The nanocomposite membrane (HA/PVA/ZnO-NPs) demonstrated significant antibacterial activity against both Gram-positive and Gram-negative bacteria while also promoting the attachment and growth of normal human dermal fibroblasts (NHDF) and human primary osteogenic sarcoma (Saos-2) without toxicity. The in vivo studies showed that the nanocomposite PVA/HA/ZnO-NPs membrane promoted wound healing in infected wounds compared to the control sample. These results demonstrate that HA-based nanocomposite can be an effective antibacterial wound dressing material.
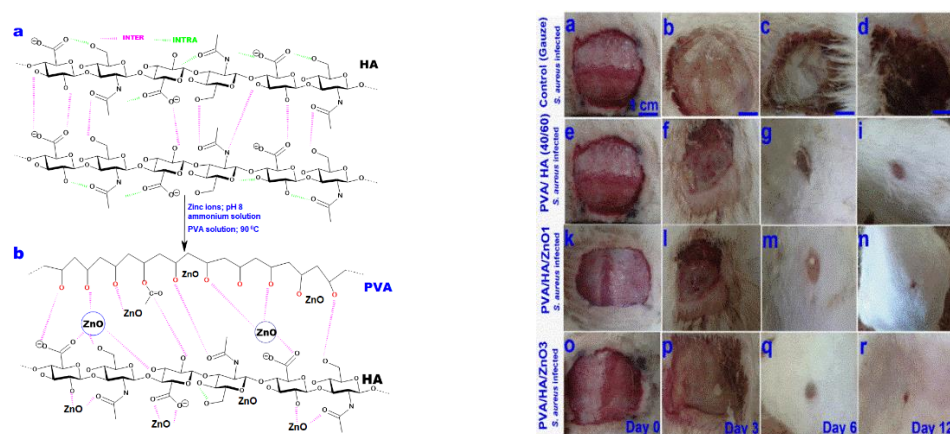
Fig 10. Representative synthesis of ZnO-NPs using HA and PVA
Chemical structure of hyaluronan with intra and inter-hydrogen bonds **(left side)**; *In-situ* synthesis of zinc oxide nanoparticles using hyaluronan/ polyvinyl alcohol **(b)** Photographs of the healing process of an infected wound with *E. coli* bacteria after 3, 6 and 12 days of treatments **(c) (right side).**

[P8] R. M. Abdel-Rahman, J. Frankova, R. Sklenarova, L. Kapralkova, I. Kelnar, **A. M. Abdel-Mohsen***. Hyaluronan/zinc oxide nanocomposite-based Membrane: Preparation, Characterization, In vitro and In vivo Evaluation. ACS Applied Polymer Materials. ACS Appl. Polym. Mater. **2022**, 4, 7723−7738. **(IF = 4.85)**

We successfully enhanced the performance properties of hyaluronan film by using chitin nanowhiskers as nanofiller material to improve the chemical, mechanical, and biological properties of plain hyaluronan film **[P9].** There were no significant effects of acid concentration treatments on the DDA of deacetylated chitin nanowhiskers (ChNWs) but reduced dimensions of the NWs. By adding the NWs as nanofiller, the mechanical properties of native HA were enhanced due to the formation of solid interfacial bonding between ChNWs and HA. The nanocomposite films also exhibited good antibacterial properties against different types of bacteria, which improved with the increased volume fraction of the NWs loaded into the HA compared with native HA film. These nanocomposite films show non-toxic properties that enhance the cell viability of NHDF and Saos-2, making the nanocomposite film suitable for drug-carrier applications and tissue regeneration. This study is significant as it provides an alternative way to prepare sustainable, environmentally friendly, edible biofilms using seafood waste.

In conclusion, this work shows important implications for developing new materials for biomedical and drug carrier applications that are environmentally friendly and cost-effective**.**
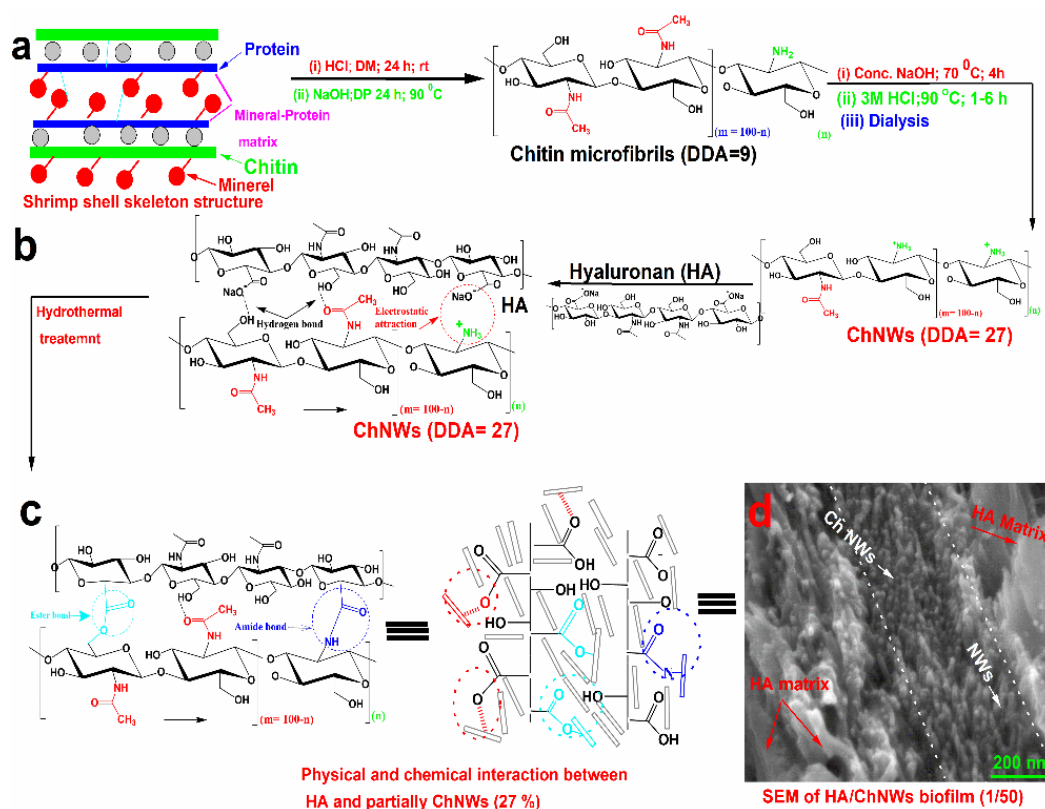
Scheme 3. Representative mechanism of extraction and partially deacetylated chitin nanowhiskers ChNWs) proposed interactions with hyaluronan (HA) and hydrothermal treatment.

[P9] A.M. Abdel-Mohsen*, Rasha M. Abdelrahman**,** M. Zboncak, J. Frankova, P. Lepcio, L. Kobera, M. Steinhart, D. Pavlinak Z. Spotaz, R. Sklenářévá, J. Brus, J. Jancar. Hyaluronan biofilms reinforced with partially deacetylated chitin nanowhiskers: Extraction, fabrication, *in-vitro* and antibacterial properties of advanced nanocomposites. Carbohydrate Polymers**, 2020,** 235,115951. **(IF = 10.72)**

Electrospun nanofibers in biomedical applications have gained much attention due to their high surface area-to-volume ratio, large porosity, and high mechanical strength. New nanofiber mats were fabricated from nanocomposite hyaluronan/silver nanoparticles **[P10].** Polyvinyl alcohol/hyaluronan (PVA/HA) solutions were electrospun to produce nanofiber mats, and silver nanoparticles (AgNPs) were incorporated into the mats by *in-situ* chemical reduction of silver ions (Ag^+). The size and shape of the NPs were controlled and optimized by investigating the reaction conditions (time, temperature, conc., and the ratio of HA/Ag^+). The presence of AgNPs improved the mechanical properties of the HA nonwoven mats. The stability of the nonwoven mats was enhanced in the presence of NPs. In conclusion, this study provides valuable insights into the fabrication and characterization of PVA/HA-AgNPs nanofiber mats and highlights their potential in biomedical applications.
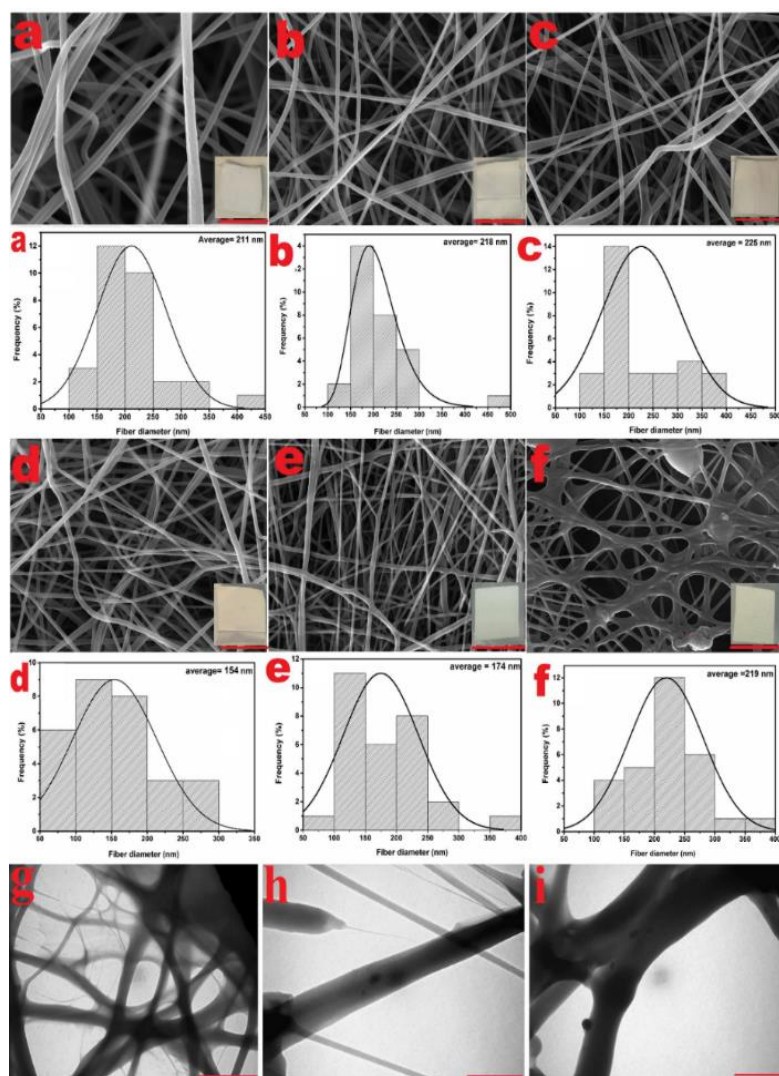
Fig. 11. Representative SEM and histograms of electrospun mats of HA/PVA/AgNPs.

Experimental conditions: **(a)** SEM and histograms of PVA/HA-AgNPs (100/0); **(b)** SEM and histograms of PVA PVA/HA-AgNPs (95/5); **(c)** SEM and histograms of PVA/HA-AgNPs (90/10); **(d)** SEM and histograms of PVA/HA-AgNPs (80/20); **(e)** SEM and histograms of PVA/HA-AgNPs (60/40); **(f)** SEM and histograms of PVA/HA-AgNPs (50/50). SEM-2 µm scale bar, TEM scale bars (500 nm), and histograms were done using 200 points.

[P10] <u>**AM Abdel-Mohsen**</u>, D Pavliňák, M Cileková, P Lepcio, RM Abdel-Rahman, J Jančář.
Electrospinning of hyaluronan/polyvinyl alcohol in the presence of in-situ silver nanoparticles: Preparation and characterization. International journal of biological macromolecules, **2019,** 139, 730-739. **(IF = 8.02)**

Furthermore, different novel short-staple nonwoven dressing materials from other polysaccharides (hyaluronan, chitosan, carboxymethyl cellulose, Chitin, alginate, oxidized cellulose, and carrageenan) were developed by wet-dry-spinning technique in presence and absence of different metal ions, and metal nanoparticles **[P12, 13].** In patent **[P12]** and manuscript **[P13],** we innovated a simple and easy process to prepare wound dressing paper sheets for different wound dressing.

Native hyaluronan with different molecular weights, hyaluronan/ chitosan, hyaluronan/ carboxymethyl cellulose, hyaluronan/ alginate, hyaluronan/ oxidized cellulose was used for fabricating 2D wound dressing sheets with a density 15 g/ m3 by wet-rotating spinning technique [P11]. The mechanical properties and stability were improved by adding metal ions (zinc and copper) to the coagulation bath [P11]. In-situ formed hyaluronan/silver (HA/Ag) nanoparticles (NPs) and their evaluation for antibacterial and wound healing properties [P12]. The micro and nonwoven mats' fiber/fabrics were prepared using wet-spinning and wet-rotating spinning techniques. The nanocomposite HA/AgNPs with uniform size of NPs (25 ± 2 nm) improved the mechanical and thermal stability after the generation of NPs compared with native HA. The antibacterial activity of the composite nonwoven fabrics was evaluated against E. coli, showing significant bactericidal activity. In-vivo animal tests using non-diabetic and diabetic rat models demonstrated that the wound dressing had strong healing efficacy and significantly accelerated the healing process compared to plain HA fabrics. The study suggests that the new HA/Ag-NPs nonwoven mats wound dressing can be used in treating wounds and chronic ulcers as well as cell carriers and tissue engineering applications.
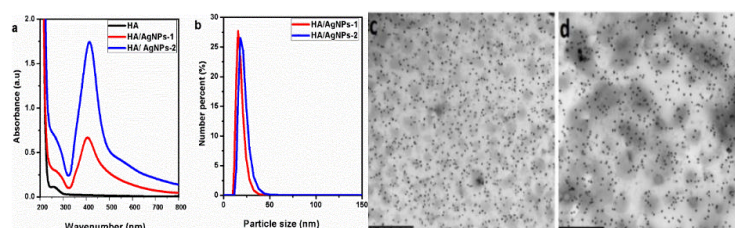

Fig. 12: UV/Vis spectra of plain HA and HA/Ag-NPs-1mg and HA/Ag-NPs-2 mg (**a**); DLS of HA/ Ag-NPs-1mg and HA/Ag-NPs-2mg (**b**), TEM of HA/Ag-NPs-1mg (**c**); TEM of HA/ Ag-NPs-2 mg (**d**); scale bars =1µm.
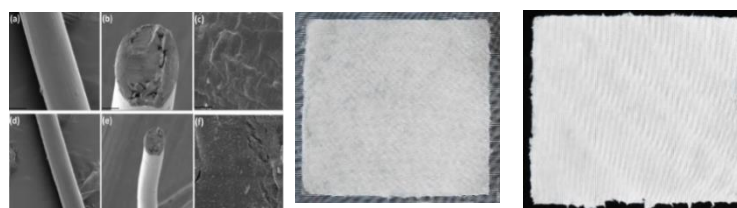
Fig.13. Scanning electron micrographs of plain HA fibers (**a**); cross-section of HA fibers (**b**); HA fibers at high magnification (**c**); HA/ Ag-NPs-1 mg fiber; (**d**); cross-section of HA/ Ag-NPs-1 mg fiber (**e**); HA/ Ag-NPs-1 mg fiber at high magnification (**f**); HA/ Ag-NPs-2 mg fiber; (**d**); cross-section of HA/ Ag-NPs-2 mg fiber (**e**). Scale bars for a, d (100 µm); b, e (50 µm), and c, f (2 µm). Staple wound dressing from native HA (**middle**); Hyaluronan/ chitosan staple wound dressing sheet (**right side**).

[P11] Ladislav Burgert, Radim Hrdina, Vladimir Velebny, **Abdelmohsen Abdellatif**, , Lubos Sobotka,Dzianis Smirnou. Method of preparation of polysaccharide microfibres, wound covers a method for producing the wound covers. **2015**, US 2015/0119783 A1,

[P12] **A.M. Abdel-Mohsen***, J. Jancar, R.M. Abdel-Rahman, L. Vojtek, P. Hyršl, M. Duskova, H. Nejezchlebová. A novel in situ silver/hyaluronan bio-nanocomposite fabrics for wound and chronic ulcer dressing: In vitro and in vivo evaluations. International Journal of Pharmaceutics. **2017**, 520, 241-253**. (IF = 6.5)**

In manuscript **[P13],** we investigated the impact of different molecular weights of hyaluronan (Low-**HA2**, Medium-**HA3** and High-**HA4**), with and without silver nanoparticles (AgNPs), on wound healing in older rats and diabetic rats. The results showed that a granulation and dermal construction deficiency accompanied impaired wound healing in older rats. However, treatment with HA2 or HA4 improved these processes and reduced the number of pathogenic bacteria on wounds in the first 24 hours. The wound size was significantly smaller in the HA4-treated group (high molecular weight HA) than in other groups (HA2, HA3). In the diabetic model, inflammatory cytokine levels were impaired, but treatment with HA4 normalized their levels.

Moreover, HA4 recovered oxidative and toxicity markers in diabetic models. This suggests HA4 improves granulation and inflammatory mediators in impaired older and diabetic rat wound healing. In conclusion, the study highlights the potential therapeutic benefits of HA4 in enhancing wound healing in older and diabetic rats. Further Research is needed to understand the underlying mechanisms of HA4 therapeutic effects and to assess its safety and efficacy in human clinical trials.
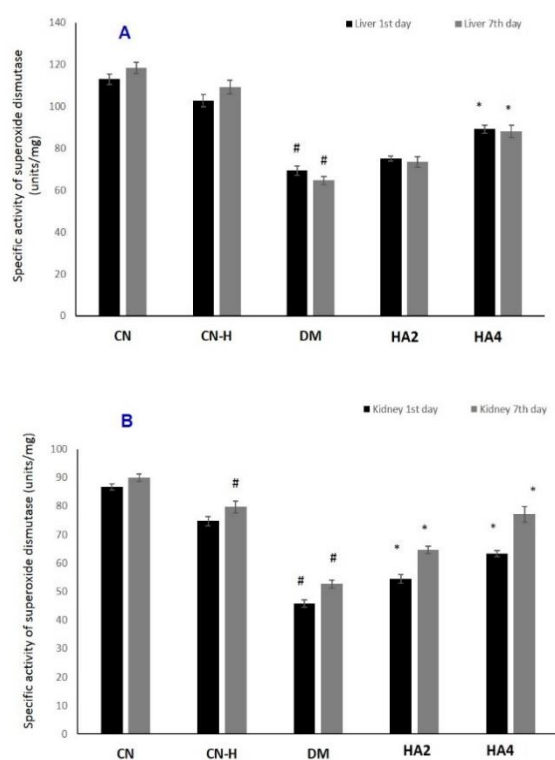
Liver: After 1st day of the treatment, group DM showed a decline in the specific activity of SOD by 38.55 %, while the CN-H demonstrated merely an 8.96 % decrease compared to the control. Among the combination groups, HA2 and HA4 exhibited an increase in their activity by 8.35% and 28.44 % with respect to the group DM. After the 7th day of the treatment, the animals showed similar but stronger patterns. DM group demonstrated a decrease in activity by 45.35 %, while HA2 and HA4 showed an increase by 13.67 % and 35.94 %, respectively, compared to group DM (Fig. 12A).

Kidney: After 1st day of the treatment, the DM group showed a dip in activity by 47.19%, whereas HA2 and HA4 demonstrated a rise in activity by 18.75% and 38.28% in the same sequence. After the 7th day of the treatment, the decline in the DM group was found to be 41.39 %, while the group – HA2 and HA4 showed an increase of 22.78 % and 46.35 % with respect to the DM group (Fig. 12 B).

Fig. 14. Effect of HA2 and HA4 on antioxidant enzymes and proteins of diabetic rats Superoxide dismutase (SOD).

[P13] <u>A.M. Abdel-Mohsen*,</u> Moustafa M.G. Fouda, Hossam Ebaide, Iftekhar Hassane, Jameel Al-Tamimie, Rasha M. Abdel-Rahman, Ali Metwalli, Ibrahim Alhazzae, Ahmed Radye, Ayman El-Fahama, J. Jancar. Wound healing of different molecular weights of hyaluronan; in-vivo study. International Journal of Biological Macromolecules. **2016,** 89, 582–591. **(IF = 8.02).**

Referencess

[1] A.K. Dhara, A.K. Nayak, Chapter 1 - Biological macromolecules: sources, properties, and functions, in: A.K. Nayak, A.K. Dhara, D. Pal (Eds.), Biological Macromolecules, Academic Press2022, pp. 3-22.

[2] T.B. Hughes, N.L. Dang, G.P. Miller, S.J. Swamidass, Modeling Reactivity to Biological Macromolecules with a Deep Multitask Network, ACS Central Science 2(8) (2016) 529-537.

[3] R. Fernandez-Leiro, S.H.W. Scheres, Unravelling biological macromolecules with cryo-electron microscopy, Nature 537(7620) (2016) 339-346.

[4] Y. Xu, H. Zhang, X.-W. Liu, Antimicrobial Carbohydrate-Based Macromolecules: Their Structures and Activities, The Journal of Organic Chemistry 85(24) (2020) 15827-15836.

[5] K.M. Hoang, N.R. Lees, S.B. Herzon, General Method for the Synthesis of α- or β-Deoxyaminoglycosides Bearing Basic Nitrogen, Journal of the American Chemical Society 143(7) (2021) 2777-2783.

[6] M. Delbianco, P. Bharate, S. Varela-Aramburu, P.H. Seeberger, Carbohydrates in Supramolecular Chemistry, Chemical Reviews 116(4) (2016) 1693-1752.

[7] R.M. Abdel-Rahman, R. Hrdina, A.M. Abdel-Mohsen, M.M.G. Fouda, A.Y. Soliman, F.K. Mohamed, K. Mohsin, T.D. Pinto, Chitin and chitosan from Brazilian Atlantic Coast: Isolation, characterization and antibacterial activity, International Journal of Biological Macromolecules 80 (2015) 107-120.

[8] A.M. Abdel-Mohsen, R.M. Abdel-Rahman, M.M.G. Fouda, L. Vojtova, L. Uhrova, A.F. Hassan, S.S. Al-Deyab, I.E. El-Shamy, J. Jancar, Preparation, characterization and cytotoxicity of schizophyllan/silver nanoparticle composite, Carbohydrate Polymers 102 (2014) 238-245.

[9] A.M. Abdel-Mohsen, J. Frankova, R.M. Abdel-Rahman, A.A. Salem, N.M. Sahffie, I. Kubena, J. Jancar, Chitosan-glucan complex hollow fibers reinforced collagen wound dressing embedded with aloe vera. II. Multifunctional properties to promote cutaneous wound healing, International Journal of Pharmaceutics 582 (2020) 119349.

[10] A.M. Abdel-Mohsen, R.M. Abdel-Rahman, R. Hrdina, A. Imramovský, L. Burgert, A.S. Aly, Antibacterial cotton fabrics treated with core–shell nanoparticles, International Journal of Biological Macromolecules 50(5) (2012) 1245-1253.

[11] A.M. Abdel-Mohsen, R. Hrdina, L. Burgert, G. Krylová, R.M. Abdel-Rahman, A. Krejčová, M. Steinhart, L. Beneš, Green synthesis of hyaluronan fibers with silver nanoparticles, Carbohydrate Polymers 89(2) (2012) 411-422.

[12] X. Meng, K.J. Edgar, "Click" reactions in polysaccharide modification, Progress in Polymer Science 53 (2016) 52-85.

[13] R. Xiao, M.W. Grinstaff, Chemical synthesis of polysaccharides and polysaccharide mimetics, Progress in Polymer Science 74 (2017) 78-116.

[14] O. Garcia-Valdez, P. Champagne, M.F. Cunningham, Graft modification of natural polysaccharides via reversible deactivation radical polymerization, Progress in Polymer Science 76 (2018) 151-173.

[15] K. Kurita, Controlled functionalization of the polysaccharide chitin, Progress in Polymer Science 26(9) (2001) 1921-1971.

[16] S. Merino, C. Martín, K. Kostarelos, M. Prato, E. Vázquez, Nanocomposite Hydrogels: 3D Polymer–Nanoparticle Synergies for On-Demand Drug Delivery, ACS Nano 9(5) (2015) 4686-4697.

[17] Z. Cai, H. Zhang, Y. Wei, F. Cong, Hyaluronan-Inorganic Nanohybrid Materials for Biomedical Applications, Biomacromolecules 18(6) (2017) 1677-1696.

[18] T. Nezakati, A. Seifalian, A. Tan, A.M. Seifalian, Conductive Polymers: Opportunities and Challenges in Biomedical Applications, Chemical Reviews 118(14) (2018) 6766-6843.

[19] A. Pardo, M. Gómez-Florit, S. Barbosa, P. Taboada, R.M.A. Domingues, M.E. Gomes, Magnetic Nanocomposite Hydrogels for Tissue Engineering: Design Concepts and Remote Actuation Strategies to Control Cell Fate, ACS Nano 15(1) (2021) 175-209.

[20] M.S.A.S. Shah, M. Nag, T. Kalagara, S. Singh, S.V. Manorama, Silver on PEG-PU-TiO2 Polymer Nanocomposite Films: An Excellent System for Antibacterial Applications, Chemistry of Materials 20(7) (2008) 2455-2460.

[21] J. Yu, W. Ha, J.-n. Sun, Y.-p. Shi, Supramolecular Hybrid Hydrogel Based on Host–Guest Interaction and Its Application in Drug Delivery, ACS Applied Materials & Interfaces 6(22) (2014) 19544-19551.

[22] S. Dutta Choudhury, R. Badugu, K. Ray, J.R. Lakowicz, Silver–Gold Nanocomposite Substrates for Metal-Enhanced Fluorescence: Ensemble and Single-Molecule Spectroscopic Studies, The Journal of Physical Chemistry C 116(8) (2012) 5042-5048.

[23] A. Regiel-Futyra, M. Kus-Liśkiewicz, V. Sebastian, S. Irusta, M. Arruebo, G. Stochel, A. Kyzioł, Development of Noncytotoxic Chitosan–Gold Nanocomposites as Efficient Antibacterial Materials, ACS Applied Materials & Interfaces 7(2) (2015) 1087-1099.

[24] H.B. Ahmed, A.M. Abdel-Mohsen, H.E. Emam, Green-assisted tool for nanogold synthesis based on alginate as a biological macromolecule, RSC Advances 6(78) (2016) 73974-73985.

[25] A.M. Abdel-Mohsen, A.S. Aly, R. Hrdina, A.T. El-Aref, A novel method for the preparation of silver/chitosan-O-methoxy polyethylene glycol core shell nanoparticles, Journal of Polymers and the Environment 20(2) (2012) 459-468.

[26] A.M. Abdel-Mohsen, D. Pavliňák, M. Čileková, P. Lepcio, R.M. Abdel-Rahman, J. Jančář, Electrospinning of hyaluronan/polyvinyl alcohol in presence of in-situ silver nanoparticles: Preparation and characterization, International Journal of Biological Macromolecules 139 (2019) 730-739.

[27] Y.D. Nokoorani, A. Shamloo, M. Bahadoran, H. Moravvej, Fabrication and characterization of scaffolds containing different amounts of allantoin for skin tissue engineering, Scientific Reports 11(1) (2021) 16164.

[28] M. Sheikholeslam, M.E.E. Wright, M.G. Jeschke, S. Amini-Nik, Biomaterials for Skin Substitutes, Advanced Healthcare Materials 7(5) (2018) 1700897.

[29] L. Suamte, A. Tirkey, J. Barman, P. Jayasekhar Babu, Various manufacturing methods and ideal properties of scaffolds for tissue engineering applications, Smart Materials in Manufacturing 1 (2023) 100011.

[30] D.R. Griffin, M.M. Archang, C.-H. Kuan, W.M. Weaver, J.S. Weinstein, A.C. Feng, A. Ruccia, E. Sideris, V. Ragkousis, J. Koh, M.V. Plikus, D. Di Carlo, T. Segura, P.O. Scumpia, Activating an adaptive immune response from a hydrogel scaffold imparts regenerative wound healing, Nature Materials 20(4) (2021) 560-569.

[31] A.K. Gaharwar, I. Singh, A. Khademhosseini, Engineered biomaterials for in situ tissue regeneration, Nature Reviews Materials 5(9) (2020) 686-705.

[32] R.M. Abdel-Rahman, J. Frankova, R. Sklenarova, L. Kapralkova, I. Kelnar, A.M. Abdel-Mohsen, Hyaluronan/Zinc Oxide Nanocomposite-Based Membrane: Preparation, Characterization, and In Vitro and In Vivo Evaluation, ACS Applied Polymer Materials 4(10) (2022) 7723-7738.

[33] D.R. Griffin, W.M. Weaver, P.O. Scumpia, D. Di Carlo, T. Segura, Accelerated wound healing by injectable microporous gel scaffolds assembled from annealed building blocks, Nature Materials 14(7) (2015) 737-744.

[34] R. Jayakumar, M. Prabaharan, S.V. Nair, S. Tokura, H. Tamura, N. Selvamurugan, Novel carboxymethyl derivatives of chitin and chitosan materials and their biomedical applications, Progress in Materials Science 55(7) (2010) 675-709.

[35] D. Simões, S.P. Miguel, M.P. Ribeiro, P. Coutinho, A.G. Mendonça, I.J. Correia, Recent advances on antimicrobial wound dressing: A review, European Journal of Pharmaceutics and Biopharmaceutics 127 (2018) 130-141.

Chapter 3

<u>Conclusion</u>

The scientific work described in this thesis covers a set of directions for using polysaccharides in medical applications with a focus on tissue regeneration. The performance properties of the prepared materials, combined with their biological properties, offer unique possibilities to produce different novel wound dressing materials for specific disease treatments. One main objective of the thesis is to understand the relationships between the different chemical compositions and performance on the biological properties of the prepared materials.

In our work, we have focused entirely on different types of polysaccharides, chemical modification, preparation of bionanocomposites, characterization of the prepared materials and evaluation of the prepared materials against various bacteria and stem cells. In this thesis, the outlined work shows how these functional biomaterials can be interfaced with living cells and accelerate healing performance. Substantial effort was made to understand the fundamental mechanisms involved, covering the antibacterial and cell viability.

One of the main achievements of our efforts is the new hollow fibrils with functional properties like antibacterial, wound healing, and biocompatibility scaffold, which is a promising system for wound healing applications. Ongoing work is targeted at optimizing the conditions to enhance the properties of the prepared materials for skin regeneration applications while also focusing on uses for control drug delivery purposes.

Overall, the work presented in the thesis appears to have the potential to advance the field of polysaccharides-based biological macromolecules and tissue regeneration and offer new treatment options for patients with various medical conditions.

The papers reporting on this research have been published in leading high-impact journals and so far, have received 2200 citations (google Scholar) which accounts for the recognition of the work by other researchers.

<u>Summarize the author's future scientific and teaching activities</u>

In terms of teaching and after discussion with the guarantor, the applicant plans to continue innovating lectures and exercises related to using biomaterials in medical and environmental applications, incorporating modern trends and technological approaches to make the classes more interesting and attractive to the students. The applicant is also the guarantor of the English version of the Biomaterial course and plans to participate in the education of students through bachelor and diploma theses.

I will generate more subjects for Ph.D. students at the Institute of macromolecular chemistry, Czech Academy of Sciences, Prague, Czech Republic.

In 2019, one Ph.D. student (Ing. Bystřícky zdeněk) completed his Ph. D. study (I was co-supervisor), and also, in 2016, completed my Ph.D. student (MSc. Ahmed Saad). This year 2023, one Ph.D. student (MSc. Rasha Radwan) will defend her study (I am co-supervisor). Last September (2022), a new Ph.D. student started his study at CEITEC under my direct supervision.

Scientific perspective, I would outline several visions for the future related to my scientific work:

- As part of my MŠMT project: Ministry of Education, Culture, Sport and Science (MŠMT) for the next five years (INTER-ACTION-LUAUS23). I focus on fundamental research in generating organic nanotubes based on polysaccharides, their derivatives and proteins like collagen and silk fibroin, and their self-assembly process and uses as new drug carrier materials.

- Within the framework of the newly adopted TAČR at CEITEC BUT (TN02000033) using the 3D printing and bioprinting techniques in medical and industrial applications, I will participate in the solution of this project as a team member focusing on chemical modification of different polysaccharides and oligosaccharides and shaping the synthesized materials for medical and industrial applications.

- One of the interesting areas is superabsorbent hydrogels for medical and agricultural applications. I have developed new materials mainly based on polysaccharides and their derivatives with acrylate free to be used as new fertilizer carriers and control the release of different nutrients.

One of my main tasks will be acquiring new projects, not only national projects but also international projects.

Chapter 4

List of Publications related to the thesis:

NO.	Title	Q	IF	Citation
P1	R. M. Abdel-Rahman, V. Vishakha, I. Kelnar, J. Jancar, **A.M. Abdel-Mohsen***. Synergist performance of collagen-g-chitosan-glucan fiber biohybrid scaffold with tunable properties. International Journal of biological macromolecules **2022**, 202, 671-680.	Q1	8.02	3
P2	**A.M. Abdel-Mohsen***, R. M Abdel-Rahman, I Kubena, L Kobera, Z. Spotez, M Zboncak, R Prikryl, J Brus, J Jancar. Chitosan-glucan Complex Hollow Fibers Reinforced Collagen Wound Dressing Embedded with Aloe vera. Part I: Preparation and Characterization. Carbohydrate Polymers. **2020**, 115708.	Q1	10.7	37
P3	**A.M. Abdel-Mohsen***, R. M. Abdelrahman, J. Frankova, M. Steinhart, J. Jancar. Chitosan-glucan Complex Hollow Fibers Reinforced Collagen Wound Dressing Embedded with Aloe vera. Part II: multifunctional properties to promote wound healing. International Journal of Pharmaceutics. **2020**, 582, 119349.	Q1	6.5	28
P4	**A.M. Abdel-Mohsen***, J. Jancar, D. Massoud, Z. Fohlerova, H. Elhadidy, Z. Spotz, A. Hebeish. Novel chitin/chitosan-glucan wound dressing: Isolation, characterization, antibacterial activity and healing properties. International Journal of Pharmaceutics. **2016**, 510, 86–99.	Q1	6.5	74
P5	R. M. Abdel-Rahman, **A.M. Abdel-Mohsen***, R. Hrdina, T. Pinto. Chitin and chitosan from Brazilian Atlantic Coast: Isolation, characterization, and antibacterial activity. International Journal of Biological Macromolecules. **2015**, 107, 107-120	Q1	8.02	80
P6	R. M. Abdel-Rahman, **A.M. Abdel-Mohsen***, R. Hrdina, L. Burgert, Z. Fohlerova, D. Pavlinak. Sayed, J. Jancar. Wound dressing based on chitosan/hyaluronan/nonwoven fabrics: Preparation, characterization, and medical applications. International Journal of Biological Macromolecules. **2016**, 89, 725–736.	Q1	8.02	57
P7	Hana Prichystalova, Numan Almonasy, **A. M. Abdel-Mohsen***, R. M. Abdel-Rahman, Libor Kobera, Moustafa M. G. Fouda, Zdenek Spotz, L.Vojtova, Ladislav Burgert, J. Jancar. Synthesis, characterization, and antibacterial activity of new fluorescent chitosan derivatives. International Journal of Biological Macromolecules. **2014**, 65, 234–240	Q1	8.02	41
P8	R. M. Abdel-Rahman, J. Frankova, R. Sklenarova, L. Kapralkova, I. Kelnar, **A. M. Abdel-Mohsen***. Hyaluronan/zinc oxide nanocomposite-based Membrane: Preparation, Characterization, In vitro and In vivo Evaluation. ACS Applied Polymer Materials. ACS Appl. Polym. Mater. **2022**, 4, 7723−7738.	Q1	4.8	1
P9	**A.M. Abdel-Mohsen***, R. M. Abdelrahman, M. Zboncak, J. Frankova, P. Lepcio, L. Kobera, M. Steinhart, D. Pavlinak Z. Spotaz, R. Sklenářévá, J. Brus, J. Jancar. Hyaluronan biofilms reinforced with partially deacetylated chitin nanowhiskers: Extraction, fabrication, *in-vitro* and antibacterial properties of advanced nanocomposites. Carbohydrate Polymers, **2020**, 235,115951.	Q1	10.7	17
P10	**AM Abdel-Mohsen***, D Pavliňák, M Čileková, P Lepcio, R.M .AbdelRahman, J Jančář. Electrospinning of hyaluronan/polyvinyl alcohol in presence of in-situ silver nanoparticles: Preparation and characterization. International journal of biological macromolecules, **2019**, 139, 730-739.	Q1	8.02	30
P11	Ladislav Burgert, Radim Hrdina, Vladimir Velebny, **Abdelmohsen Abdellatif,** Romana Sulakova, Lubos Sobotka, Jiri Betakm, Dzianis Smirnou. Method of preparation of polysaccharide microfibres, wound covers comprising the obtained microfibres, method for producing the wound covers. **2015**, US 2015/0119783 A1.	P		1
P12	**A.M. Abdel-Mohsen***, J. Jancar, R.M. Abdel-Rahman, L. Vojtek, P. Hyršl, M. Duskova, H. Nejezchlebová. A novel in situ silver/hyaluronan bio-nanocomposite fabrics for wound and chronic ulcer dressing: In-vitro and in-vivo evaluations. International Journal of Pharmaceutics. **2017**, 520, 241-253.	Q1	6.5	55
P13	**A.M. Abdel-Mohsen***, Moustafa M.G. Fouda, Hossam Ebaide, Iftekhar Hassane, Jameel Al-Tamimie, R. M. Abdel-Rahman, Ahmed Radye, Ayman El-Fahama, J. Jancar. Wound healing of different molecular weights of hyaluronan; in-vivo study. International Journal of Biological Macromolecules. **2016**, 89, 582–591.	Q1	8.02	48

*Corresponding author

Publication 1
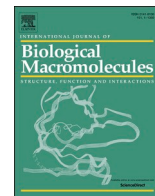
Synergistic performance of collagen-g-chitosan-glucan fiber biohybrid scaffold with tunable properties

R.M. Abdel-Rahman [a], V. Vishakha [b], I. Kelnar [a], J. Jancar [b], A.M. Abdel-Mohsen [a,b,c,*]

[a] Institute of Macromolecular Chemistry, Czech Academy of Sciences, Heyrovského nám. 2, Praha 162 06, Czech Republic
[b] CEITEC-Central European Institute of Technology, Brno University of Technology, Purkyňova 656/123, Brno 61200, Czech Republic
[c] Department of Pretreatment and Finishing of Cellulosic Fibers, Textile Research Division, National Research Centre, 33 EL Buhouth St., Dokki, Giza 12622, Egypt

ARTICLE INFO

ABSTRACT

Hybrid biocomposite scaffolds (HBS) that serve as a carrier for cell proliferation and differentiation are increasingly used for tissue regeneration. 3D hybrid scaffold based on collagen-grafted-chitosan-glucan fiber (CO-g-CGF-HBS) was prepared by freeze-drying technique. The swelling percentage, hydrolytic stability, and modulus of elasticity of HBS were enhanced after the chemical modification of CO with CGF. Pore size and porosity of HBS were decreased with an increased CGF ratio. HBS exhibits a higher reduction rate against different types of bacteria compared with a control sample. Thus, chemical modification of CO with different ratios of CGF significantly improved the physicochemical, antibacterial properties of HBS.

1. Introduction

Protein is the main component of the extracellular matrix (ECM) in many mammalian tissues. Collagen type I (CO) has been extensively investigated for different biomedical applications [1,2], and nano-fibrillar collagen structure existing in many organs (bone, cornea, skin, tendon) was considered its characteristic feature, based on which the excellent mechanical and other functional performances of tissues are guaranteed [3,4]. Collagen was consider as one of the most inter-esting proteins that has been used for various purposes in tissue engi-neering thanks to its brilliant and unique properties, like biocompatibility [5], biodegradability [6] and low cytotoxicity [7]. However, the biodegradation rate and poor mechanical properties of native collagen are critical issues limiting the further application of CO. Chemical crosslinking step of collagen-based scaffolds was an effective method to control the degradability rate and optimize the physico-chemical and mechanical properties of collagen [8–10]. For the above reasons, the crosslinking step of collagen has become one of the most significant steps in preparing collagen-based scaffolds. Currently, two different types of crosslinking processes were used to improve the chemical, physical and mechanical properties of the collagen-based

scaffolds: chemical [11] and physical methods [12].

Chitin and chitosan biopolymers offer excellent biological charac-teristics, which have paved the way for their purposes in medicine and drug-delivery applications [2] or as a scaffold for tissue regeneration [13]. Indeed, chitosan has good mucoadhesive characteristics due to its polycationic nature [14], which increases the adhesion to mucosa and thus the contact time for drug penetration. Chitosan consider one of the main components of different fungi cell walls, such as *Gongronella* spp., *Penicillium*, *Aspergillus niger* (*A. niger*), and *Schizophyllum commune* (*S. commune*) [15,16].

Chitin-glucan complex from mycelia Tremella fuciformis with controlled ratio of chemical composition of the complex between glu-caose amine and *N*-acetyl glucose amine glucosamine and glucose (GlcN:Glc = 26:74 mol%) has been extracted in powder form [17]. White button and pleurotus ostreatus mushrooms were used as a new source to extract chitin-glucan complex with controlled the degree of deacetylation. Unfortunately, the isolated complex exhibited small particle form [18–20]. Chitin-glucan and chitosan-glucan complex were isolated from *Aspergillus niger* in powder form and used for wastewater treatment applications [21–24]. The fungal cell wall was used to extract chitin-glucan complex in powder morphology and fabrication

---

nanopapers was obtained from dispersed solution and have been used for heavy metal adsorption [25–27]. Hollow fibers from chitin and chitosan-glucan complex with controlled the degree of deacetylation have been extracted from mycelium of shizophyllum commune fungi and used as new wound dressing material [28–30]. New soft hydrogel with low porosity was fabricated using chitin-glucan complex dissolved under harsh alkaline conditions using concentrated sodium hydroxide. The extracted complex was in powder form with a low degree of deacetylation [28,30–33]. From all sources which we mentioned above, all chitin-glucan and chitosan-glucan complex was extracted only in powder form, neither short nor longer micro/nanofibers obtained. So far, there wasn't no literature information about extraction of fiber-based chitin-glucan or chitosan-glucan complex from mycelium of aspergillus niger.

Extraction of chitin-glucan (ChGF) or chitosan-glucan CGF (CGF) in fiber forms from non-animal sources (mushrooms, bacteria, fungi) has several benefits over animal sources like shrimps, crabs, crawfish shells, lobsters [34,35]. These include: In our study, (I) ChGF or CGF are extracted for the first time in the form of microfiber from *Aspergillus niger* (*A. niger*) with controlled fiber dimensions between 2.5 and 3 ± 0.5 μm; (II) A raw biopolymer that was constant in composition and available throughout the year [36]; (III) Free-heavy metal attached to starting material [37]; (IV) Removal of minerals was not necessary for the extraction of chitosan from fungal mycelia [38]. The individual chains of CGF were agglomerated into microfibrils with hydrogen bonds and, together with the chemically crosslinked network of glucan, they result in a mechanically robust and rigid structure [28,39–41]. The goal of the present work was to synthesize new hybrid biocomposite scaffold (HBS) by chemical modification of collagen (CO) with fiber based-chitosan-glucan CGF fibers (CO-g-CGF) and to investigate the effects of different composition on physicochemical, mechanical and antibacterial properties of the synthesized HBS.

2. Experimental

2.1. Materials

Water-insoluble dermal collagen type I with partial hydrochloride of purified bovine was supplied as a 10 wt% suspension from VUP (Brno, Czechia). The suspension of CO I was lyophilized using (ALPHA 1–4 LSC, CHRIST, Germany) at -90 °C for 48 h to obtain dry CO sheets. *Mycelium* was produced from *Aspergillus niger* (*A. niger*) strain as a source of ChGF and CGF (Brno, Czechia). *N*-(3-dimethylamino propyl)-*N*-ethyl-carbodiimide hydrochloride (EDC), NHS (N-hydroxy succinimide) are purchased from Sigma-Aldrich (Brno, Czechia), sodium hydroxide, acetic acid, ethanol, hydrochloric acid, and isopropyl alcohol was purchased from Lach-Ner, s.r.o., (Czechia). All chemicals are used without further purification.

2.2. Preparation of CGF and CO-g-CGF

Chitin-glucan (ChGF) and chitosan-glucan complex fibers (CGF) were extracted from the industrial strain of the Aspergillus niger (*A. niger*) cell wall by a chemical treatment process. Briefly, 10 g of native *mycelium* (fermented from *A. niger)* was treated with 1% NaOH at room temperature (RT) for 5 h, filtered off and washed with Milli-Q water to neutral pH. The obtained *mycelium* in a wet state was treated with 5% of sodium hydroxide at 90 °C for 10 h, filtered off, and the insoluble part was collected. The insoluble alkaline *mycelium* (IAM) was washed three times with Milli-Q water until pH neutral, then treated with 75% isopropyl alcohol and absolute isopropyl alcohol (IPA). The product was dried at 70 °C; chitin-glucan CGF fiber (ChGF) yield was 85%. 5 g of dry ChGF was dispersed in 25% NaOH at 50 °C using a water bath for 5 h combined with mechanical stirrer with a large pitch blade impeller at high speed (2000 rpm). The product was filtered off, washed until pH neutral, and dried at 50 °C. In the final step, wet alkali-insoluble

material of chitosan-glucan CGF fibers was treated with 1 M acetic acid at 50 °C for 2 h to remove the acid-soluble chitosan (C) and branched glucan (G), then filtered, washed with distilled water until pH neutral and dried at 50 °C for 24 h. From SEM, the chitosan-glucan complex fibers showed a diameter about 2.5 ± 0.5 μm with microfiber length about 300–500 μm (Fig. S1).

Hybrid biocomposite scaffolds (HBS) collagen-grafted-chitosan-glucan CGF fibers (CO-g-CGF) were synthesized via chemical modification of CO with CGF in the presence of EDC/NHS as a crosslinking agent. Different weight ratios of CGF were added to the CO solution as described in Table 1. CO (0.5 wt%) and CGF (0.5 wt%) were mixed in Milli-Q water, swelled for 48 h at 4 ± 2 °C with pH about 4.5, then homogenized for 20 min using an IKA disintegrator. The dispersed solutions are subsequently centrifuged at 4000 rpm (4 °C) for 10 min to remove air bubbles, frozen in 48-well culture plates at -25 °C overnight and subsequently lyophilized at -90 °C for 48 h.

CO-g-CGF-HBS was crosslinked with 50 mM EDC/25 mM NHS using 90% ethanol solution at pH 6.5. Carbodiimide crosslinking was achieved by immersing the native CO, CSGC, and CO-g-CGF-HBS in EDC into ethanol at RT. After the dispersion of CO, CGF and CO/CGF at RT (22 ± 2 °C) for 5 h, HBS was washed in 0.1 M $Na_2HPO_4.12H_2O$, twice for 1 h, followed by washing with Milli-Q water for 2 h (changing the medium every 30 min). All samples (Table 1) were frozen and lyophilized again, as described above. Native CO, CGF and HBS were coded as (100/0; 70/30; 50/50; 30/70; 0/100) corresponding to CO/CGF ratios, respectively. The crosslinked density between collagen and chitosan-glucan complex fiber in the presence of EDC/NHS was measured using 2,4,6-trinitrobenzene sulfonic acid (TNBS) to determine the free amino groups collagen by UV-VIS spectroscopy and lysine as a standard amino acid for the calibration curve [42–45].

2.3. Characterization

Hydrolytic degradation of CO-g-CSGCF-HBS was measured using phosphate buffer solution (pH 7.4) in an incubator at 37 °C. Cylindrical samples were weighed W_1, submerged in PBS (pH 7.4), and kept in an incubator at 37 °C. A piece of each dried HBS was weighed and immersed in 10 ml of phosphate buffer saline solution (PBS, pH 7.4) at 37 °C for a certain time, and the swollen samples were gently pressed between filter papers to remove the excess water remaining from the surface of HBS and weighed (W_w). Each value was averaged from five parallel measurements. The swelling ratio of the scaffold was defined as the ratio of weight of the swollen samples (W_s) to initial weight (W_i) at different swelling times (0 to two months) according to the following Eq. (1).

After different time inverters (7, 14, 28, 56 days), samples were washed with water to remove the rest of the buffer saline salts and gently pressed between two filter papers to remove the excess water. The final mass was recorded (W_2) and used to calculate the weight loss percentage from the following Eq. (2). The porosity of the native and HBS was

Table 1
Different compositions of grafted hybrid biocomposite scaffold (HBS) using different ratios between CO and CGF.

Sample codes	Weight ratio between CO to CGF	Wt. of CO (g)	Wt. of CGF (g)
Native CO scaffold	0	0.5	0
CO-g-CGF (70/30)	70/30	0.375	0.125
CO-g-CGF (50/50)	50/50	0.25	0.25
CO-g-CGF (30/70)	30/70	0.125	0.375
Native CGF scaffold	0	0	0.5

measured using the Archimedes principle [46,47], and ethanol was used as a liquid medium for 2 h at room temperature. The porosity percentage was calculated from the following Eq. (3).

$$\text{Swelling percentage} = \frac{Ws - Wi}{Wi} \times 100 \qquad (1)$$

$$\text{Weight loss} = \left(100 - \frac{W1 - W2}{W1}\right) \qquad (2)$$

$$\text{Porosity (\%)} = \frac{M2 - M1}{M2 - M3} \times 100 \qquad (3)$$

where M_1 was the dry weight of the scaffolds, M_2 was the weight of scaffolds saturated with ethanol, and M_3 was the weight of scaffolds suspended in ethanol. Five samples were used to calculate the standard division ($\pm$SD).

Young's modulus of elasticity of the collagen, chitosan-glucan complex fiber, and hybrid bioscaffold was measured at room temperature using a Zwick/Roel traction machine. The loading velocity was 1 mm/min. The specimens had a cylindrical shape (about 12 mm in height and 6 mm in diameter) and a native and HBS with different ratios (100/0; 70/30; 50/50; 30/70 and 0/100) were tested and evaluated. Each group had five specimens. The mechanical loading was applied until the scaffold was compressed up to 50% of its original height. The compressive moduli were determined to apply linear regression to a part of the stress-strain curves at 2–10% strain (initial modulus E_{init}). The stress was defined as the force divided by the initial area, and the strain was defined as the deformation of the specimen (height) divided by the initial height of the specimen. Because of not exactly the cylindrical shape of specimens, the initial area of each specimen was determined using software Ellipse 3D (ViDiTo, Košice, Slovak Republic). Each specimen was captured using a camera, and the perimeter of the initial area was manually marked using Freehand plugin of Ellipse.

The antibacterial test was done using the Shake-Flask method [48–52]. A certain concentration of living organisms (*Escherichia coli* (*G*-) and *Staphylococcus aureus* (*G*+)) was suspended in an Erlenmeyer flask (1–2 10^5 / ml of microorganism). The test solution was shaken for 24 h (320 rpm) at 25 °C (Control sample). After adding native (CO, CSGCF) and CO-g-CSGCF (70/30, 50/50, 30/70) of HBS, the reduction rate of living microorganisms was estimated by comparing the number of microorganisms before adding the scaffolds according to the following Eq. (4).

$$\text{Reduction rate (\%)} = \frac{[A1 - A2]}{A1} \times 100 \qquad (4)$$

where $A1 =$ the number of microorganisms without a scaffold, $A2 =$ number of microorganisms with a scaffold after incubation. Data were shown as mean ($\pm$ SD; $n = 4$).

X-ray diffraction patterns were collected on a device: D-8 Advance diffractometer (Bruker AXS, Germany) with Bragg-Brentano (θ-θ) goniometer (radius 217.5 mm) equipped with a secondary beam curved graphite monochromator and Na (Tl) I scintillation detector. The generator was operated at 40 kV and 30 mA. The scan was completed at room temperature from 5 to 30° (2θ) in 0.02° step with a counting time of 8 s per step. Thermal decomposition of HBS was evaluated using a thermo-gravimetric instrument (TG, Entsch 209F3), Al_2O_3 crucible under the heating rate of 10 °C/ min (with data collecting rate of 40 points per Kelvin). Attenuated total reflectance Fourier transforms infrared spectroscopy (ATR-FTIR) was performed using a Nicolet Impact 400 D ATR-FTIR spectrophotometer (Nicolet, Prague, CZ) equipped with a ZnSe crystal for the ATR-FTIR spectroscopy. Absorbance is measured as a function of wavenumber (cm^{-1}) between 4000 cm^{-1} and 600 cm^{-1} with a resolution of 8 cm^{-1}.

The structure and surface morphology of the HBS was visualized using scanning electron microscopy (MIRA 3, Brno, Czechia). HBS was cut with a razor scalpel after being frozen, coated with a layer of gold/

palladium (20 nm), then observed under secondary electron emission mode with high voltage of 10 kV. The histograms were plotted from the average pore size by measure (250–300) of pores chosen randomly throughout the surface and central cross-section of native CO, CGF and HBS samples. The image analysis program (Image J) was used to determine the average diameter of pores, and at least 100–150 pores were assessed from 10 SEM photos. Statistical analysis: Data analysis was carried out using A nova: Single Factor Test and T-Test: Two-Sample Assuming Equal Variances. Error bars represent mean $\pm$ standard deviation (SD) of measurements p values < 0.05 were considered statistically significant (*p < 0.01, **p < 0.0001, and ***p < 0.00001). All experiments were performed in triplicate, and data were given as mean $\pm$ standard deviation and graphs were drawn in OriginPro 2019b.

3. Results and discussion

3.1. Extraction and chemical modification of CGF

ChGF and CGF were extracted from the *mycelium* of *A. niger* using different sequence steps, as shown in Fig. 1. Fig. 1a explores the sequencing process of acid-base treatments to remove the non-bonded impurities linked to the cell wall matrix like proteins, lipids, dyes; this step was called the digestion process [28,30,41]. The insoluble alkaline *mycelium* (IAM) was treated with NaOH to hydrolyze the chemical bonds between lipids-proteins-dyes matrix to obtain pure ChGF (Deproteinization step, (DP). In the final step (deacetylation process), ChGF was treated with highly concentrated NaOH to remove the acetyl groups from the ChGF chain (deacetylation step (DDA). A large pitch blade impeller was used to prevent destroying the CGF fibers. The insoluble CGF was filtered, washed several times with a mixture of alcohol-water (80/20 *v*/v), then dried at 70 °C for 24 h. The degree of deacetylation (DDA) of CGF was 71% (measured by ss-NMR spectroscopy, Fig. S2). The fiber diameter was about 2.5 $\pm$ 0.5 μm with a length of about 300–500 μm (Fig. S1).

Hybrid biocomposite scaffolds (HBS) were synthesized by chemical modification of CO with CGF. Collagen and CGF fiber (DDA = 71%) were mixed for 10 min to obtain homogenized, well dispersed and one-phase material from both solutions. The blending was done using an IKA homogenizer at 8000/min in a slightly acid medium (pH 4.5) and a lower temperature of 0 °C for 30 min. The physical synergistic interactions (proton exchange, ionic interaction, hydrogen bonds) between the CO and CGF functional groups (Fig. 1b) were generated.

Mixture of CO and CGF were centrifuged at 4000 rpm for 5 min to remove air bubbles and to obtain homogenous pores from the CO-CGF composite. The blended mixture was transferred into 48 well plates and agitated at −30 °C about 24 h. After agitation, the samples were dried in a freeze drier at −90 °C for 48 h. During the freeze-drying step, the interactions between CO/CGF were improved and enhanced as described below (Fig. 1b).

EDC/NHS was employed as a crosslinking agent of collagen scaffold materials [53] due to the low toxicity and higher stability of the CO scaffold after the crosslinking step. There were many physical and non-ionic interactions between the functional groups of CO and CGF (Fig. 1b) created after the modification of CO with CGF. The synergistic performance during the chemical interactions between CO and CGF was significantly improved after using EDC and NHS as crosslinking and catalyzing agents. The crosslinked density between collagen and chitosan-glucan complex fiber was 0.2, 0.4, 0.5 for HBS with 70/30, 50/50, and 30/70, respectively.

Fig. 1c shows the proposed chemical interaction mechanism between -COO$^-$ in CO helical structure and –OH groups in CGF. Due to the lower ratio of chitosan (C) to glucan (G) in the CGF composition (Fig. S1; 9: 1) [41], the possibility of interaction of -COO$^-$ (in CO) with OH (in chitosan and glucan chains) was higher than that of -NH$_2$ groups in chitosan. New chemical bonds were generated, and they improve mechanical stability, swelling, degradation of the hybrid scaffold, which
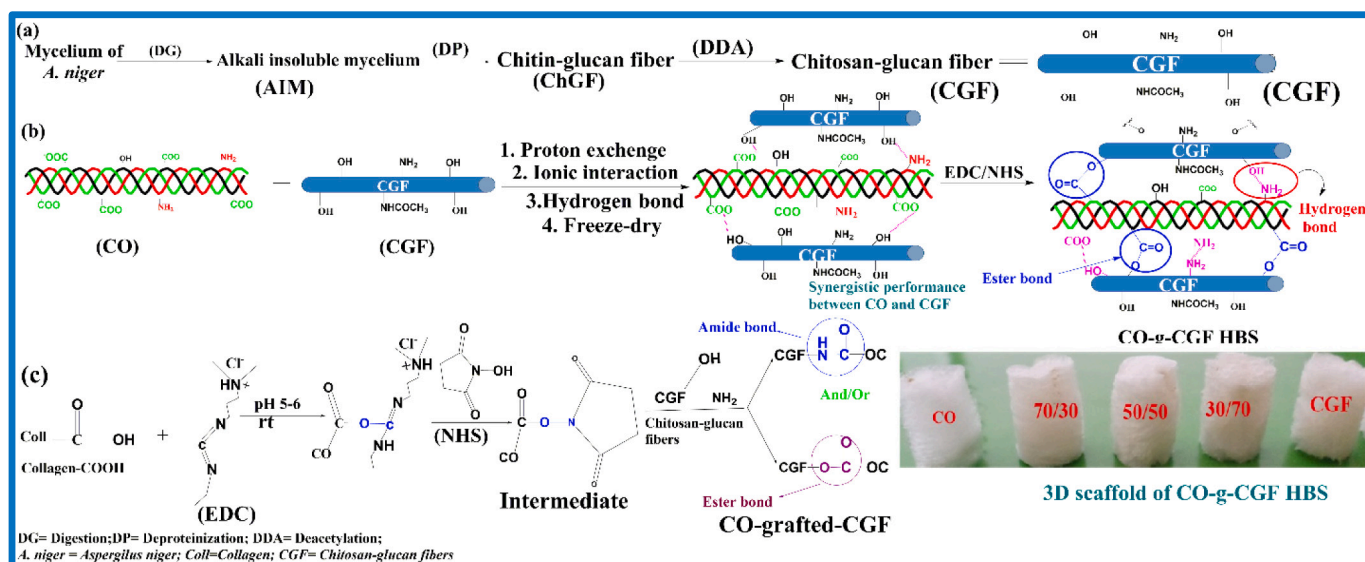
Fig. 1. Representative extraction sequences of CGF and chemical modification of collagen (CO).

was an essential point of applications of 3D scaffold tissue engineering as described in the following sections.

3.2. Physicochemical properties of HBS

One of the significant purposes of the addition of CGF to CO was to improve the interaction between complex functional groups (amino and hydroxyl) with collagen (carboxylic and amino) groups that function as binding sites to increase the EDC/NHS crosslinking efficiency. Fig. 2 shows the FTIR spectra of the natives CO, CGF and HBS with different ratio between CO and CGF. The absorption peaks of crosslinked native CO scaffold appear at 3500 cm^{-1} for -OH groups, 3278 cm^{-1} for amide A, 3072 cm^{-1} for amide B, 2930 cm^{-1} for asymmetrical stretch CH$_2$, 1646 cm^{-1} for amide I, 1548 cm^{-1} for amide II, 1250 cm^{-1} for amide III, and at 750500 cm^{-1} for amide (IV-VII) [28,41,54,55]. From the FTIR spectrum of native CO, we confirmed that there wasn't denaturation of native CO scaffold during preparation steps and crosslinking via EDC/NHS mixture.

CGF shows specific peaks at 3320 cm^{-1} corresponding to -OH of (Ch, C, G) compositions and 2930 cm^{-1} related to an asymmetrical stretch of methylene groups of the CGF (Fig. 2). The characteristic vibration peak
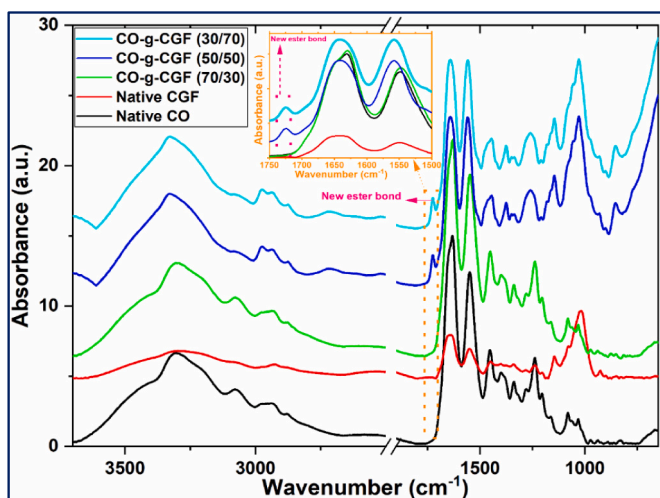
for carbonyl groups in chitin at 1650 cm^{-1} and 1550 cm^{-1} was related to the free amino groups of the chitosan (part of CGF). The peaks at 1070 and 1040 cm^{-1} were characteristic of ether linkage (-C-O-C-) between chitin, chitosan, and glucan polymers. The β-anomeric configuration was signalized by absorption at 890 and 1371 cm^{-1}.

A hybrid biocomposite scaffold (HBS) shows another new peak at 1732 cm^{-1} suggesting the formation of chemical ester bonds (-O-C=O$^-$) between CO and CGF [10,41,56,57] that improve the synergistic performance between CO and CGF. The intensity of the new peak was slightly increased with increasing the CGF grafting ratios (Fig. 2). The absorptions bands were shifted due to interaction between CO and CGF, which indicates the occurrence of molecular interactions in the hybrid synthesis process. Such a band involves the -OH group of CGF (in C and G parts) and carboxylic groups of CO. The sharp and strong peak at 1130 cm^{-1} in the hybrid scaffold spectrum relates to -C-O-C- ether linkage in CO and CGF. After the chemical modification of CO by CGF, the peak corresponding to amide I shifted from 1629 to 1641 cm^{-1} due to the interactions with functional groups of CGF.

The thermal stability of native CO, CGF and HBS were measured and evaluated as shown in Fig. 3. Native CO scaffold shows two different peaks characteristic of the two-stage sample devastation due to higher temperature. In the first stage (between 25 and 75 °C), the peak with a maximum of 70 °C (mass loss approx. 15%) was due to the evaporation of absorbed water (non-bonded) to the native CO scaffold. In the second stage (between 225 and 375 °C), the peak maximum was 330 °C (mass loss approx. 55%). The DTG curve, the significant degradation occurs in three steps at 240, 330, 340 °C, was caused by concurrent collagen degradation processes such as depolymerization, dehydration, and decomposition of mono CO chain unit followed by the formation of the charred residue. The DTG peak above 340 °C was attributed to the oxidation and breakdown of charred residue to low molecular weight gaseous products.

The native CGF scaffold shows three different peaks, as shown in Fig. 3(a, b); these peaks were representatives of the three-stage sample destruction. The first stage (between 25 and 75 °C) with a maximum peak at 56 °C (mass loss approx. 5%) relates to the evaporation of water absorbed to Ch, C and G compositions in the CGF chains. In the second and third stages (between 210 and 340 °C), the maximum of the second peak was at 260 °C (mass loss approx. 28%), maximum of the third peak was at 270 °C (mass loss approx. 38%) that were attributed to release of water bonded to different functional groups in CGF (-OH,-NHCOCH$_3$ and -NH$_2$) and small molecular products liberated on thermal

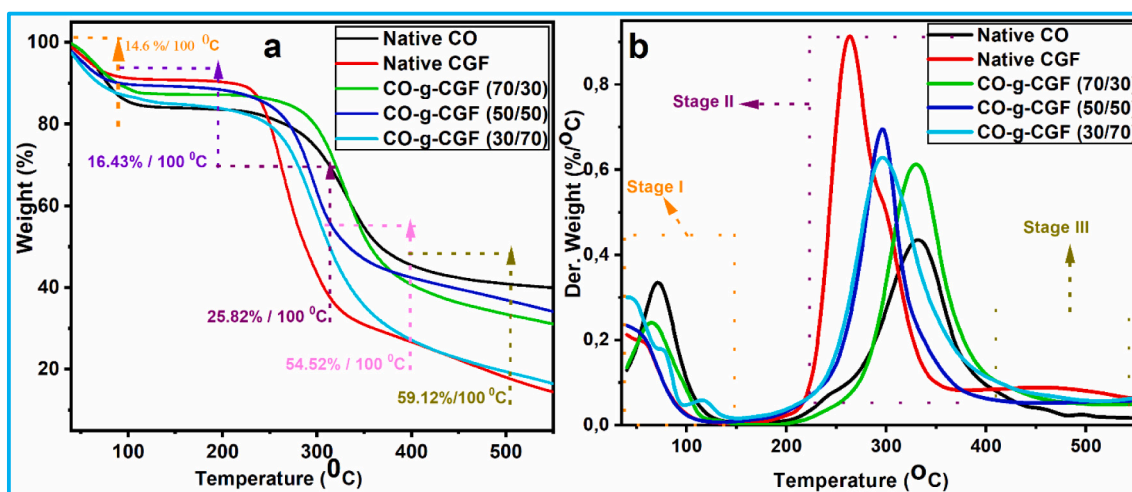**Fig. 2.** ATR-FTIR of natives CO, CGF and HBS.

Fig. 3. TG (a); DTG (b) curves of natives CO, CGF and HBS scaffolds.

degradation of CGF [28,30,41].

Hybrid scaffolds with different grafting ratios (Fig. 3a, b) exhibit peaks representing the two-stage sample destruction due to temperature. The first stage (between 25 and 75 °C) with a maximum peak at 55 °C (mass loss approx. 6%) relates to the evaporation of water absorbed to the CO-g-CGF scaffold. In the second stage (240 and 390 °C), the peak maximum at 290 °C (mass loss approx. 30.5%) corresponds to the release of water molecules attached to CO-CGF and small molecular products liberated on thermal degradation of CO. The maximum of the third peak at 300 °C (mass loss approx. 37%) was attributed to the release of water bonded to different functional groups in CGF (-OH, -NHCOCH$_3$ and -NH$_2$) CO chains and small molecular products liberated

on thermal degradation of the hybrid scaffold. From Fig. 3(a, b), we can conclude that HBS (CO-g- CGF) was thermally more stable than native CO and CGF, and the thermal stability slightly decreases with the increasing grafted ratio of the CGF in the HBS.

Fig. S3 shows the X-ray diffraction of native CO, CGF and HBS. In a neat CO scaffold, broadband-only appears at $2\theta = 15$–$25°$, corresponding to the triple helical structure of CO [58]. In CO-g-CGF (Fig. S4), different peaks appear at $2\theta = 9, 19.2, 22.5,$ and $26°$ corresponding to chitin [59], chitosan [60], and glucan [61] chemical composition of complex. Different grafting ratio of HBS (CO-g-CGF) shows the same peaks at $2\theta = 9, 19.2, 22.5,$ and $26°$ with higher intensity due to the strong interactions between different functional groups of CO (semi-crystalline) and CGF (amorphous structure). Fig. 4 shows the effect of chemical compositions of CO, CGF, and (CO-g-CGF) scaffolds on their hydrolytic stability under physiological conditions (37 °C; pH 7.5). After
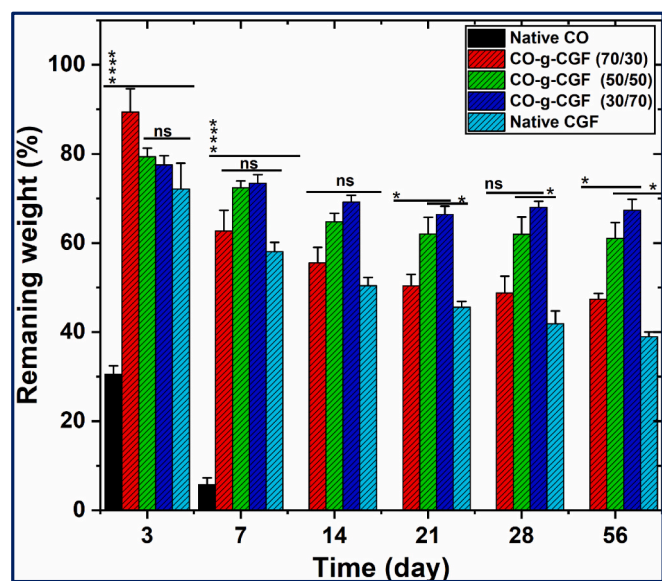

Fig. 4. Representative hydrolytic stability of CO, CGF, and HBS scaffolds.
Notes: The data were represented as the mean ± SD, n = 3; (*p<0.01, **p<0.0001, ***p<0.00001, and ****p0.000001), and ns: no significant differences. After 3 days : CO-g-CGF (70/30, 50/50, 30/70) > native CO; ns between grafted scaffold; After one week: CO-g-CGF (70/30, 50/50, 30/70) > native CO; ns between grafted scaffold; After 14 day: ns between grafted scaffold (70/30, 50/50, 30/70); After 21day: CO-g-CGF (30/70) > (70/30, 50/50, native CGF); one 30 day: ns significant differences between different HBS (CO-g-CGF) group; CO-g-CGF(50/50, 30/70) > native CGF; 56 day: CO-g-CGF (30/70) > (50/50, 30/70, native CGF).

Fig. 5. Swelling percentage of native CO, CGF and HBS scaffolds.
Notes: The data were represented as the mean ± SD, n = 3; (*p<0.01, **p<0.0001, ***p<0.00001); ns: no significant differences. At 1 min: native CO>CO-g-CGF (50/50; 30/70); 10 min: native CO>COg- CGF (30/70, 50/50, 30/70, native CGF); 30 min CO>CO-g-CGF (30/70, 50/50, 30/70, native CGF); 120 min: CO>CO-g-CGF (30/70, 50/50, 30/70, native CGF); 1440 min: CO>CO-g-CGF (30/70, 50/50, 30/70, native CGF). After 1440 min no significant differences between native CGF and all CO-g-CGF (70/30, 50/50, 30/70).
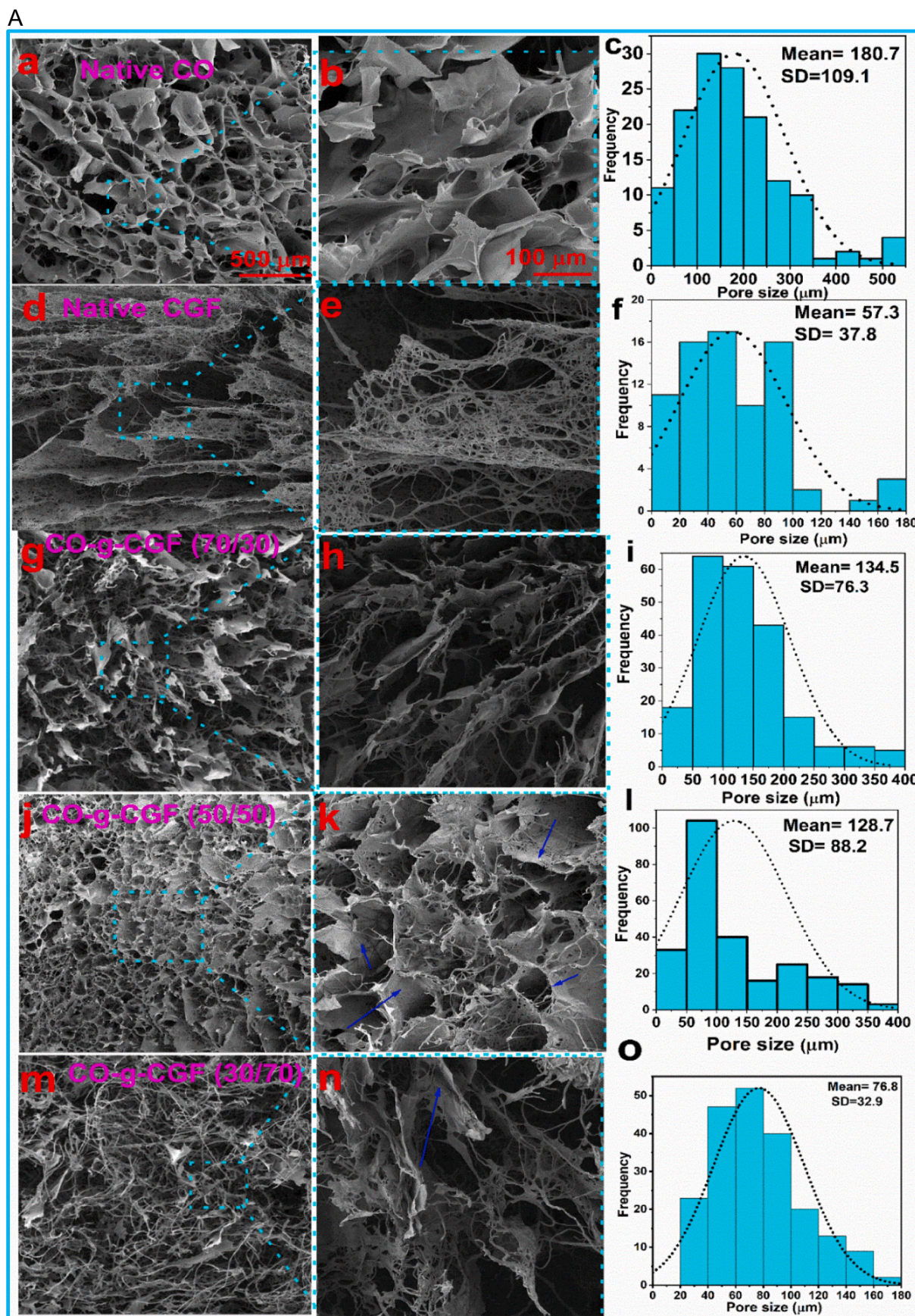
Fig. 6. Surface morphology and pore size histograms of natives CO, CGF and HBS scaffolds (A); Pore size of natives CO, CGF, and HBS scaffolds (B). Notes: The data were represented as the mean ± SD, n=3; (*p<0.01, **p<0.0001, ***p<0.00001) and ns: no significant differences. Native CO scaffold > CO-g-CGF (30/70,50/50, 70/30 > native CGF scaffold). From the porosity measurements, there were no significant changes between natives CO, CGF and grafted HBS.
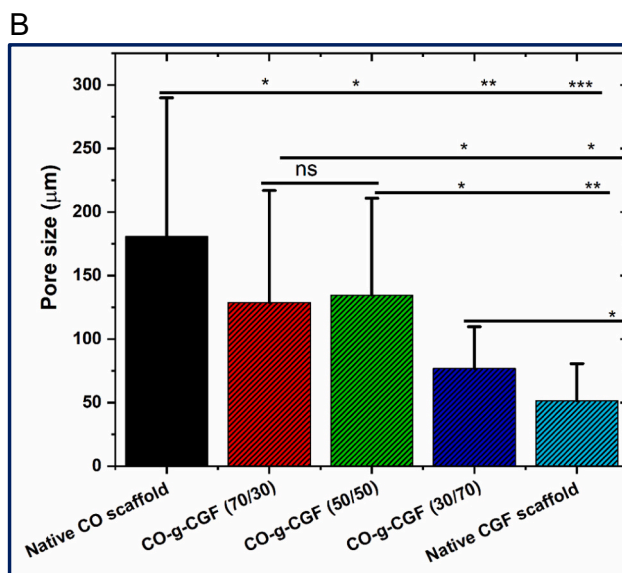
Fig. 6. (*continued*).

3 days of incubation, native CO scaffold show high degradation rate (69.5%) in comparison with native CGF (27.9 and CO-g-CGF (70/30; 50/50; 30/70) were 37.71; 27.65; 26.6%) respectively. Native CO scaffolds show significantly lower hydrolytic stability (degradation rate above 85%) after 7 days of incubation compared with native CGF and CO-g-CGF (Fig. 4).

CGF scaffold shows high weight loss compared to native CO (27.9, 41.9%) after 3 and 7 days of incubation, respectively. Interestingly, HBS (CO-g-CGF) hydrolytic degradation percentage was significantly enhanced compared with native CO and CGF after 56 days of incubation and physiological conditions. This significant improvement in the stability of CO-g-CGF, due to strong synergistic performance (chemical/physical interactions) between CO and CGF.

The scaffold's swelling percentage (SR; %) strongly depends on the scaffold's hydrophilic nature, microstructure, and chemical compositions. Native CO shows hydrophilic properties with more amphiphilic properties than CGF (Fig .5); the ability to uptake the porous scaffold structure seems to be the main explanation for the differences observed in the swelling ratio. The poor mechanical properties of native CO led to the collapse of the porous structure after it was taken out from PBS solution [28,41]. On the contrary, CGF possesses higher elasticity that was helpful for the retention of the scaffold's original porous structure. Hence, the water uptake of the scaffolds increases with the increasing ratio of CGF in HBS composition (Fig .5).

Fig .5 shows the effect of CGF different ratios (70/30; 50/50, and 30/70) on swelling percentage of HBS. CO-g-CGF (100/0) scaffold exhibits higher swelling ratio than CO-g-CGF (70:30) > (50/50) > (30/700) > (0/100). Within the first 20 min from absorption, the SR (%) was approximately the same in all native and hybrid scaffolds. Increased ratio of the CGF decreases the uptake percentage of the scaffold (0, 30, 50, and 70 wt. %). Due to the hydrophobic properties of CGF (chitin, chitosan, and glucan) and the strong chemical interaction between CO and CGF functional groups, which leads to decreased hydrophilicity of CO matrix. From the swelling values after one day of seeding the native and hybrid scaffold, the swelling percentage was significantly reduced after grafted collagen with complex fibers. Different ratios of complex fibers did not show a slight difference but were insignificant compared with the native chitosan-glucan complex scaffold. From swelling measurement, we have confirmed that the hydrophilic character left in the HBS plays a crucial role in the HBS swelling /absorption ability.

3.3. Morphology and mechanical properties of natives CO, CGF and CO-g-CGF

In tissue engineering, 3D hybrid biocomposite scaffolds (HBS) must have high porosity with interconnected pore-building block structures to enhance the compatibility and the biological activity for cell attachment, proliferation, and differentiation [10,62,63]. Fig. 6A shows the surface morphology of native CO, CGF and HBS with different grafting ratio of CGF. Fig. 6A(a-c) depicts micrographs of the 3D scaffold architecture and pore size histogram of native CO. The CO scaffold has a heterogeneous lamellar pore structure surrounded by flake-like collagen sheets with a mean pore size of $180 \pm 109\ \mu m$ (Fig. 6Ac).

Figure 6A(d-f) shows the native CGF fibers scaffold with a very smooth and homogenous fiber surface, and pore size was ($57 \pm 37\ \mu m$). The appearance of the collagen grafted chitosan-glucan fibers (CO-g-CGF) porous scaffold is shown in Fig. 6A(g-o). SEM observation clearly showed the different pore structures of the grafted CO with different ratios of CGF (70/30; 50/50; 30/70) scaffolds synthesized in the presence of EDC/NHS. The CO-g-CGF (70/30) porous scaffold with spherical pores shape ($134 \pm 76\ \mu m$; Fig. 6Ai) was smaller than the native CO scaffold (Fig. 6Aa-c). The large spherical pores were evenly distributed throughout the volume and well stacked. The CGF has adhered to the surface of collagen matrix with physical/ chemical bonds as shown in Fig. 6Ak (blue rows) and kept an open pore with an interconnected network (Fig. 6Ak). The pore size of the grafted scaffold (CO-g-CGF; 70/30; 50/50, 30/70) significantly decreased after the chemical modification of collagen (Fig. 6B). The size of the pore of the grafted scaffold decreased with an increase in the complex fiber ratio but was not significant (Fig. 6B). Chitosan-glucan complex fiber scaffold showed the smallest pore size compared with other scaffold groups (Fig. 6B). All scaffolds exhibit a highly porous structure with good adhering properties of CGF onto the surface of CO matrix. Besides, the interconnectivity of pores in the scaffold, as a significant structural property, affects the migration and proliferation of cells. The porosity of HBS was slightly decreased from 96.1 ± 0.10 (native CO) with an increase of the ratio of CGF from 30 to 70% in the hybrid scaffold (96.1 ± 0.05, 95.4 ± 0.49, and 95.2 ± 0.12), respectively (Fig. 7a). There were no significant decreases in porosity percentage from porosity measurements compared with all natives CO, CGF and grafted scaffolds with different ratios of complex fiber (70/30, 50/50, 30/70). Both pore size and porosity of HBS were slightly decreased compared with native CO due to the strong synergistic performance generating new bonds between CO and CGF

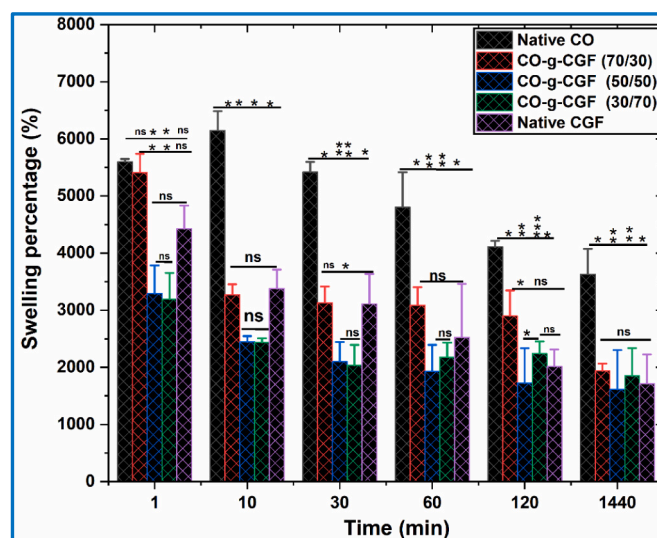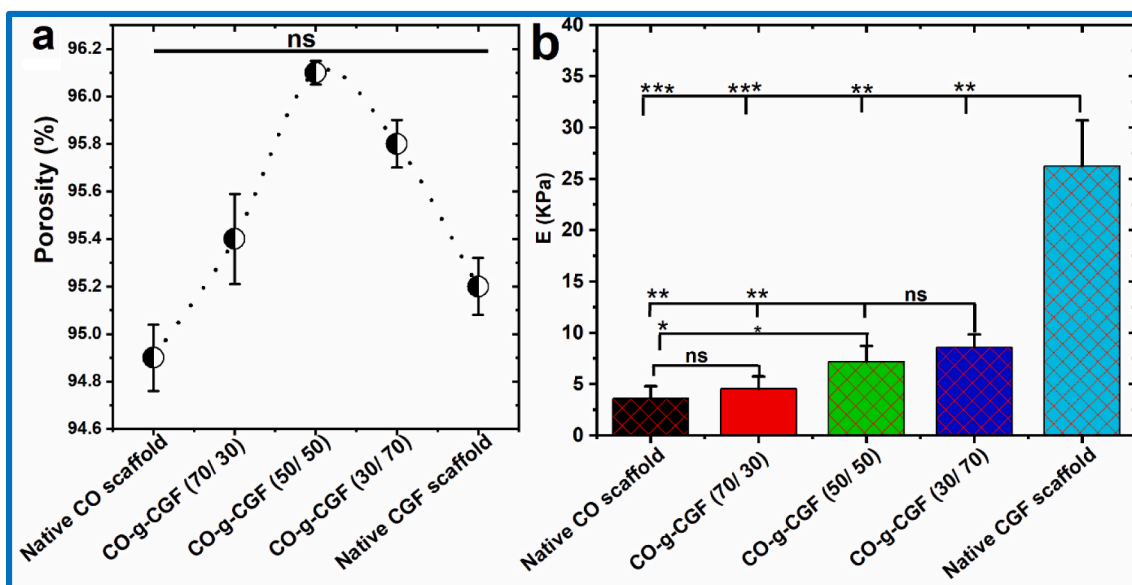**Fig. 7.** Porosity (a) and mechanical properties of native CO, CGF and HBS scaffolds (b).
Notes: The data were represented as the mean ± SD, n=3; (*p<0.01, **p<0.0001, ***p<0.00001); ns: no significant differences. Native CGF scaffold > CO-g-CGF (30/70) > CO-g-CGF (50/50) > CO-g-CGF (70/30) > native CO scaffold). From the porosity measurements, there were no significant changes between natives CO, CGF and grafted HBS.

that could weaken the interconnection network between CO fibrils and CGF [28,30,41].

The mechanical properties of the scaffold were one of the most important aspects of tissue engineering applications [64–67]. The mechanical properties of HBS in different solution media were important for scaffold seeding with different kinds of cells for a long period of time up to two months [41,68–70]. Cylindrical 3D specimens were synthesized from CO-g-CGF-HBS (100/0;70/30; 50/50; 30/70; 0/100). Interestingly, there were strong synergistic effects between the CGF concentrations and Young's modulus of HBS (Fig. 7b). The collagen scaffold shows a low young modulus of about 3.5 ± 1.2 KPa. Moreover, after chemical modification with chitosan-glucan complex fiber, the

mechanical properties of the hybrid bioscaffold increase significantly with the increased content of the complex fiber. The significant improvements of the module's values of the grafted scaffold were CO-g-CGF (30/70) > CO-g-CGF (50/50) > CO-g-CGF (70/30) > native CO scaffold. The improvement of young modulus values of grafted scaffold due to the strong physical and chemical interactions in the presence of a crosslinked agent that could generate synergetic properties between both composts. Native chitin-glucan complex fiber scaffolds showed highest modulus value compared with different grafting ratio of CO and CGF and native collagen scaffold.

Fig. 8 shows the antibacterial activity of native collagen, chitosan-glucan complex and collagen grafted by chitosanglucan complex fiber with a different grafted ratio between CO and CGF. The collagen scaffold showed the lowest antibacterial properties against both types of bacteria (Fig. 8). Chitosan-glucan complex fiber scaffold showed high antibacterial activity against both types of bacteria (-/+ G) compared with native collagen scaffold. The hybrid bioscaffold with different grafted ratios showed significantly enhanced antibacterial characteristics compared with the native collagen scaffold. The reduction rate (%) of both bacteria was increased with an increase in the complex ratio into HBS (Fig. 8). One of the main components of the complex was chitosan (DDA = 72 %), which showed the complex surface's cationic nature. From the obtained results, there was a relationship between the amount of chitosan (part of the complex) and antibacterial activity against both negative/positive gram (G-/+) of bacteria (Fig. 8). The antibacterial activity of the HBS mainly due to the presence of chitosan that could bind with negatively charged bacterial cell wall causing dispersion of the cells and disturbed the membrane permeability, followed by attaching to DNA caused inhabitation of DNA replication and subsequently cell death [28,60,62–64]. The chitosan part in hybrid grafted bioscaffold might be acting as a chelating agent that selectively binds to trace metal elements causing toxin production and inhibition of bacteria growth [28,35,60,65–69]. The HBS could also interact with bacteria's cell wall via electrostatic interaction with anionic components of the microorganism's surface (like protein and liposaccharides) that could significantly reduce the bacteria growth [62,64,70].
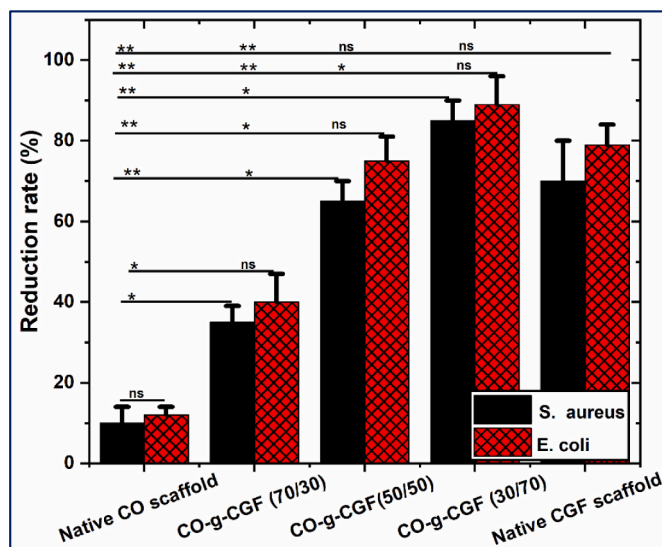

Fig. 8. Representative antibacterial properties of natives CO, CGF and HBS scaffolds.
Notes: Antibacterial activity of natives CO, CGF and HBS with different ratios of CGF against (G + -) bacteria. The data were represented as the mean ± SD, n=3; (*p<0.01, **p<0.0001); ns: no significant differences.

4. Conclusion

Chemical modification of collagen (CO) with fiber-based chitosan-glucan complex (CGF) was synthesized, and the structure was confirmed by different techniques like ATR-FTIR, TGA, SEM and X-ray diffraction. The degree of deacetylation (DDA = 72%) and fiber dimension (diameter 2.5 ± 0.5 μm and length approx. 300–500 μm) were precisely controlled during the extraction process of the complex fiber from mycelium of Aspergillus niger. The hybrid biocomposite scaffold shows a unique synergistic combination of principle and unique properties, like high swelling percentage, improved mechanical and hydrolytic stability compared with the native collagen scaffold. The obtained data shows that forming a new ester bond improved the crystallinity and thermal stability of the hybrid scaffold. The HBS exhibits significant antibacterial activity against different types of bacteria (G -/+) compared with the native collagen scaffold.

CRediT authorship contribution statement

R. M. Abdel-Rahman: Conceptualization, Methodology, Writing - original draft, Writing- review & editing; V. Vishakha: Methodology; I. Kelnar: Conceptualization, Methodology, Writing - original draft, Writing- review & editing; J. Jancar: Conceptualization, Methodology, Writing - original draft, Writing- review & editing; A. M. Abdel-Mohsen: Conceptualization, Methodology, Writing - original draft, Writing - review & editing.

Declaration of competing interest

The authors declare that they have no known competing financial interests or personal relationships that could have appeared to influence the work reported in this paper. All authors have approved the final version of the manuscript.

Appendix A. Supplementary data

Supplementary data to this article can be found online at https://doi.org/10.1016/j.ijbiomac.2022.01.004.

References

[1] J.F. Mano, G.A. Silva, H.S. Azevedo, P.B. Malafaya, R.A. Sousa, S.S. Silva, L. F. Boesel, J.M. Oliveira, T.C. Santos, A.P. Marques, N.M. Neves, R.L. Reis, Natural Origin Biodegradable Systems in Tissue Engineering and Regenerative Medicine: Present Status and Some Moving Trends, 2007.

[2] S.V. Madihally, H.W.T. Matthew, Porous chitosan scaffolds for tissue engineering, Biomaterials 20 (12) (1999) 1133–1142.

[3] Z.-M. Huang, Y.Z. Zhang, M. Kotaki, S. Ramakrishna, A review on polymer nanofibers by electrospinning and their applications in nanocomposites, Compos. Sci. Technol. 63 (15) (2003) 2223–2253.

[4] I.K. Kwon, T. Matsuda, Co-electrospun nanofiber fabrics of poly(l-lactide-co-ε-caprolactone) with type I collagen or heparin, Biomacromolecules 6 (4) (2005) 2096–2105.

[5] L. Marinucci, C. Lilli, M. Guerra, S. Belcastro, E. Becchetti, G. Stabellini, E.M. Calvi, P. Locci, Biocompatibility of collagen membranes crosslinked with glutaraldehyde or diphenylphosphoryl azide: an in vitro study, J. Biomed. Mater. Res. A 67A (2) (2003) 504–509.

[6] A. Ibara, H. Miyaji, B. Fugetsu, E. Nishida, H. Takita, S. Tanaka, T. Sugaya, M. Kawanami, Osteoconductivity and biodegradability of collagen scaffold coated with Nano-β-TCP and fibroblast growth factor 2, J. Nanomater. 2013 (2013) 11.

[7] P.A. Marone, F.C. Lau, R.C. Gupta, M. Bagchi, D. Bagchi, Safety and toxicological evaluation of undenatured type II collagen, Toxicol. Mech. Methods 20 (4) (2010) 175–189.

[8] B. Marelli, D. Le Nihouannen, S.A. Hacking, S. Tran, J. Li, M. Murshed, C.J. Doillon, C.E. Ghezzi, Y.L. Zhang, S.N. Nazhat, J.E. Barralet, Newly identified interfibrillar collagen crosslinking suppresses cell proliferation and remodelling, Biomaterials 54 (2015) 126–135.

[9] K. Merrett, W. Liu, D. Mitra, K.D. Camm, C.R. McLaughlin, Y. Liu, M.A. Watsky, F. Li, M. Griffith, D.E. Fogg, Synthetic neoglycopolymer-recombinant human collagen hybrids as biomimetic crosslinking agents in corneal tissue engineering, Biomaterials 30 (29) (2009) 5403–5408.

[10] C. Yao, M. Markowicz, N. Pallua, E. Magnus Noah, G. Steffens, The effect of cross-linking of collagen matrices on their angiogenic capability, Biomaterials 29 (1) (2008) 66–74.

[11] E. Jorge-Herrero, P. Fernández, J. Turnay, N. Olmo, P. Calero, I. Freile, J. L. Castillo-Olivares, R. García, Influence of different chemical cross-linking treatments on the properties of bovine pericardium and collagen, Biomaterials 20 (6) (1999) 539–545.

[12] K.S. Weadock, E.J. Miller, L.D. Bellincampi, J.P. Zawadsky, M.G. Dunn, Physical crosslinking of collagen fibers: comparison of ultraviolet irradiation and dehydrothermal treatment, J. Biomed. Mater. Res. 29 (11) (1995) 1373–1379.

[13] S. Dhawan, A.K. Singla, V.R. Sinha, Evaluation of mucoadhesive properties of chitosan microspheres prepared by different methods, AAPS PharmSciTech 5 (4) (2004) 122–128.

[14] J. Yang, F. Tian, Z. Wang, Q. Wang, Y.-J. Zeng, S.-Q. Chen, Effect of chitosan molecular weight and deacetylation degree on hemostasis, J. Biomed. Mater. Res. B Appl. Biomater. 84B (1) (2008) 131–137.

[15] P. Pochanavanich, W. Suntornsuk, Fungal chitosan production and its characterization, Lett. Appl. Microbiol. 35 (1) (2002) 17–21.

[16] F. Streit, F. Koch, M.C.M. Laranjeira, J.L. Ninow, Production of fungal chitosan in liquid cultivation using apple pomace as substrate, Braz. J. Microbiol. 40 (1) (2009) 20–25.

[17] A. Chen, F. Pan, T. Zhang, C. Yu, Y. Xiao, S. Li, H. Xu, X. Xu, M. Han, Z. Xu, Characterization of chitin-glucan complex from Tremella fuciformis fermentation residue and evaluation of its antibacterial performance, Int. J. Biol. Macromol. 186 (2021) 649–655.

[18] H. Kim, S. Kang, K. Li, D. Jung, K. Park, J. Lee, Preparation and characterization of various chitin-glucan complexes derived from white button mushroom using a deep eutectic solvent-based ecofriendly method, Int. J. Biol. Macromol. 169 (2021) 122–129.

[19] Y. Liu, Q. Wu, X. Wu, S.A. Algharib, F. Gong, J. Hu, W. Luo, M. Zhou, Y. Pan, Y. Yan, Y. Wang, Structure, preparation, modification, and bioactivities of β-glucan and mannan from yeast cell wall: a review, Int. J. Biol. Macromol. 173 (2021) 445–456.

[20] R. Kollár, B.B. Reinhold, E. Petráková, H.J.C. Yeh, G. Ashwell, J. Drgonová, J. C. Kapteyn, F.M. Klis, E. Cabib, Architecture of the yeast cell wall: β(1→6)-glucan interconnects mannoprotein, β(1→3)-glucan, and chitin*, J. Biol. Chem. 272 (28) (1997) 17762–17775.

[21] C. Roca, B. Chagas, I. Farinha, F. Freitas, L. Mafra, F. Aguiar, R. Oliveira, M.A. M. Reis, Production of yeast chitin–glucan complex from biodiesel industry byproduct, Process Biochem. 47 (11) (2012) 1670–1675.

[22] E. Machová, K. Kvapilová, G. Kogan, J. Šandula, Effect of ultrasonic treatment on the molecular weight of carboxymethylated chitin–glucan complex from Aspergillus niger, Ultrason. Sonochem. 5 (4) (1999) 169–172.

[23] Y.A. Skorik, A.V. Pestov, Y.G. Yatluk, Evaluation of various chitin-glucan derivatives from Aspergillus niger as transition metal adsorbents, Bioresour. Technol. 101 (6) (2010) 1769–1775.

[24] N.E. Mushi, A review on native well-preserved chitin nanofibrils for materials of high mechanical performance, Int. J. Biol. Macromol. 178 (2021) 591–606.

[25] A. Hassainia, H. Satha, S. Boufi, Chitin from Agaricus bisporus: extraction and characterization, Int. J. Biol. Macromol. 117 (2018) 1334–1342.

[26] M. Blumfield, K. Abbott, E. Duve, T. Cassettari, S. Marshall, F. Fayet-Moore, Examining the health effects and bioactive components in Agaricus bisporus mushrooms: a scoping review, J. Nutr. Biochem. 84 (2020) 108453.

[27] W.M.F.W. Nawawi, K.-Y. Lee, E. Kontturi, A. Bismarck, A. Mautner, Surface properties of chitin-glucan nanopapers from Agaricus bisporus, Int. J. Biol. Macromol. 148 (2020) 677–687.

[28] A.M. Abdel-Mohsen, J. Frankova, R.M. Abdel-Rahman, A.A. Salem, N.M. Sahffie, I. Kubena, J. Jancar, Chitosan-glucan complex hollow fibers reinforced collagen wound dressing embedded with aloe vera. II. Multifunctional properties to promote cutaneous wound healing, Int. J. Pharm. 582 (2020) 119349.

[29] R.M. Abdelrahman, A.M. Abdel-Mohsen, M. Zboncak, J. Frankova, P. Lepcio, L. Kobera, M. Steinhart, D. Pavlinak, Z. Spotaz, R. Sklenářévá, J. Brus, J. Jancar, Hyaluronan biofilms reinforced with partially deacetylated chitin nanowhiskers: extraction, fabrication, in-vitro and antibacterial properties of advanced nanocomposites, Carbohydr. Polym. 235 (2020), 115951.

[30] A.M. Abdel-Mohsen, J. Jancar, D. Massoud, Z. Fohlerova, H. Elhadidy, Z. Spotz, A. Hebeish, Novel chitin/chitosan-glucan wound dressing: isolation, characterization, antibacterial activity and wound healing properties, Int. J. Pharm. 510 (1) (2016) 86–99.

[31] D. Araújo, V.D. Alves, S.A.C. Lima, S. Reis, F. Freitas, M.A.M. Reis, Novel hydrogels based on yeast chitin-glucan complex: characterization and safety assessment, Int. J. Biol. Macromol. 156 (2020) 1104–1111.

[32] I.C. Ferreira, D. Araújo, P. Voisin, V.D. Alves, A.A. Rosatella, C.A.M. Afonso, F. Freitas, L.A. Neves, Chitin-glucan complex – based biopolymeric structures using biocompatible ionic liquids, Carbohydr. Polym. 247 (2020) 116679.

[33] J. Liao, H. Huang, Magnetic chitin hydrogels prepared from Hericium erinaceus residues with tunable characteristics: a novel biosorbent for Cu2+ removal, Carbohydr. Polym. 220 (2019) 191–201.

[34] M.H. Mohammed, P.A. Williams, O. Tverezovskaya, Extraction of chitin from prawn shells and conversion to low molecular mass chitosan, Food Hydrocoll. 31 (2) (2013) 166–171.

[35] R.M. Abdel-Rahman, R. Hrdina, A.M. Abdel-Mohsen, M.M.G. Fouda, A.Y. Soliman, F.K. Mohamed, K. Mohsin, T.D. Pinto, Chitin and chitosan from Brazilian Atlantic Coast: isolation, characterization and antibacterial activity, Int. J. Biol. Macromol. 80 (2015) 107–120.

[36] N. Nwe, T. Furuike, H. Tamura, Chapter one - isolation and characterization of chitin and chitosan from marine origin, in: K. Se-Kwon (Ed.), Advances in Food and Nutrition Research, Academic Press, 2014, pp. 1–15.

[37] S. Bartnicki-Garcia, Cell wall chemistry, morphogenesis, and taxonomy of fungi, Annu. Rev. Microbiol. 22 (1) (1968) 87–108.

[38] R.A.A. Muzzarelli, F. Tanfani, G. Scarpini, Chelating, film-forming, and coagulating ability of the chitosan–glucan complex from Aspergillus niger industrial wastes, Biotechnol. Bioeng. 22 (4) (1980) 885–896.

[39] L. Burgert R. Hrdina V. Velebny A.M. Abdel-Lattif R. Sulakova L. Sobotka J. Betak D. Smirnou Method of Preparation of Polysaccharide Fibres, Wound Covers that Contain Them, Method of Manufacturing of Wound Covers, and Apparatus for Preparation of Polysaccharide Fibres, Google Patents, 2015.

[40] B. Chagas, I. Farinha, C.F. Galinha, F. Freitas, M.A.M. Reis, Chitin–glucan complex production by Komagataella (Pichia) pastoris: impact of cultivation pH and temperature on polymer content and composition, New Biotechnol. 31 (5) (2014) 468–474.

[41] A.M. Abdel-Mohsen, R.M. Abdel-Rahman, I. Kubena, L. Kobera, Z. Spotz, M. Zboncak, R. Prikryl, J. Brus, J. Jancar, Chitosan-glucan complex hollow fibers reinforced collagen wound dressing embedded with aloe vera. Part I: preparation and characterization, Carbohydrate Polymers 230 (2020), 115708.

[42] R. Kale, A. Bajaj, Ultraviolet spectrophotometric method for determination of gelatin crosslinking in the presence of amino groups, J. Young Pharm. 2 (1) (2010) 90–94.

[43] D.V. Bax, N. Davidenko, S.W. Hamaia, R.W. Farndale, S.M. Best, R.E. Cameron, Impact of UV- and carbodiimide-based crosslinking on the integrin-binding properties of collagen-based materials, Acta Biomater. 100 (2019) 280–291.

[44] M. Nair, S.M. Best, R.E. Cameron, Crosslinking collagen constructs: achieving cellular selectivity through modifications of physical and chemical properties, Appl. Sci. 10 (19) (2020) 6911.

[45] L. Mohee, G.S. Offeddu, A. Husmann, M.L. Oyen, R.E. Cameron, Investigation of the intrinsic permeability of ice-templated collagen scaffolds as a function of their structural and mechanical properties, Acta Biomater. 83 (2019) 189–198.

[46] A. Daskalova, C.S.R. Nathala, I. Bliznakova, E. Stoyanova, A. Zhelyazkova, T. Ganz, S. Lueftenegger, W. Husinsky, Controlling the porosity of collagen, gelatin and elastin biomaterials by ultrashort laser pulses, Appl. Surf. Sci. 292 (2014) 367–377.

[47] M. Miron-Mendoza, J. Seemann, F. Grinnell, The differential regulation of cell motile activity through matrix stiffness and porosity in three dimensional collagen matrices, Biomaterials 31 (25) (2010) 6425–6435.

[48] A. Nagaraja, Y.M. Puttaiahgowda, A. Kulal, A.M. Parambil, T. Varadavenkatesan, Synthesis, characterization, and fabrication of hydrophilic antimicrobial polymer thin film coatings, Macromol. Res. 27 (3) (2019) 301–309.

[49] M. He, H. Xiao, Y. Zhou, P. Lu, Synthesis, characterization and antimicrobial activities of water-soluble amphiphilic copolymers containing ciprofloxacin and quaternary ammonium salts, J. Mater. Chem. B 3 (18) (2015) 3704–3713.

[50] T. Ristic, L. Zemljič, M.Novak Babič, M.Kralj Kuncic, S. Sonjak, N. Gunde-cimerman, S. Strnad, in: Antimicrobial Efficiency of Functionalized Cellulose Fibres as Potential Medical Textiles, 2011, pp. 37–51.

[51] L. Su, Y. Yu, Y. Zhao, F. Liang, X. Zhang, Strong antibacterial polydopamine coatings prepared by a shaking-assisted method, Sci. Rep. 6 (2016) 24420.

[52] S. Li, T. Zhu, J. Huang, Q. Guo, G. Chen, Y. Lai, Durable antibacterial and UV-protective Ag/TiO(2)@ fabrics for sustainable biomedical application, Int. J. Nanomedicine 12 (2017) 2593–2606.

[53] J.S. Pieper, T. Hafmans, J.H. Veerkamp, T.H. van Kuppevelt, Development of tailor-made collagen–glycosaminoglycan matrices: EDC/NHS crosslinking, and ultrastructural aspects, Biomaterials 21 (6) (2000) 581–593.

[54] L.-P. Yan, Y.-J. Wang, L. Ren, G. Wu, S.G. Caridade, J.-B. Fan, L.-Y. Wang, P.-H. Ji, J.M. Oliveira, J.T. Oliveira, J.F. Mano, R.L. Reis, Genipin-cross-linked collagen/chitosan biomimetic scaffolds for articular cartilage tissue engineering applications, J. Biomed. Mater. Res. A 95A (2) (2010) 465–475.

[55] N. Davidenko, J.J. Campbell, E.S. Thian, C.J. Watson, R.E. Cameron, Collagen–hyaluronic acid scaffolds for adipose tissue engineering, Acta Biomater. 6 (10) (2010) 3957–3968.

[56] A.J. van der Slot-Verhoeven, E.A. van Dura, J. Attema, B. Blauw, J. DeGroot, T.W.J. Huizinga, A.-M. Zuurmond, R.A. Bank, The type of collagen cross-link determines the reversibility of experimental skin fibrosis, Biochim. Biophys. Acta (BBA) - Mol. Basis Dis. 1740 (1) (2005) 60–67.

[57] L.H.H. Olde Damink, P.J. Dijkstra, M.J.A. van Luyn, P.B. van Wachem, P. Nieuwenhuis, J. Feijen, Cross-linking of dermal sheep collagen using a water-soluble carbodiimide, Biomaterials 17 (8) (1996) 765–773.

[58] Z. Xia, X. Yu, X. Jiang, H.D. Brody, D.W. Rowe, M. Wei, Fabrication and characterization of biomimetic collagen-apatite scaffolds with tunable structures for bone tissue engineering, Acta Biomater. 9 (7) (2013) 7308–7319.

[59] G.L. Clark, A.F. Smith, X-ray diffraction studies of chitin, chitosan, and derivatives, J. Phys. Chem. 40 (7) (1935) 863–879.

[60] A.M. Abdel-Mohsen, A.S. Aly, R. Hrdina, A. El-Aref, A novel method for the preparation of silver/chitosan-O-methoxy polyethylene glycol core shell nanoparticles, J. Polym. Environ. 20 (2) (2012) 459–468.

[61] R.H. Marchessault, Y. Deslandes, K. Ogawa, P.R. Sundararajan, X-ray diffraction data for β-(1 → 3)-D-glucan, Can. J. Chem. 55 (2) (1977) 300–303.

[62] J. Li, X. Tian, T. Hua, J. Fu, M. Koo, W. Chan, T. Poon, Chitosan natural polymer material for improving antibacterial properties of textiles, ACS Appl. Bio Mater. 4 (5) (2021) 4014–4038.

[63] P. Sahariah, B.E. Benediktssdóttir, M.Á. Hjálmarsdóttir, O.E. Sigurjonsson, K.K. Sørensen, M.B. Thygesen, K.J. Jensen, M. Másson, Impact of chain length on antibacterial activity and hemocompatibility of quaternary N-alkyl and N,N-dialkyl chitosan derivatives, Biomacromolecules 16 (5) (2015) 1449–1460.

[64] A.M. Abdel-Mohsen, R.M. Abdel-Rahman, R. Hrdina, A. Imramovský, L. Burgert, A.S. Aly, Antibacterial cotton fabrics treated with core–shell nanoparticles, Int. J. Biol. Macromol. 50 (5) (2012) 1245–1253.

[65] H. Přichystalová, N. Almonasy, A.M. Abdel-Mohsen, R.M. Abdel-Rahman, M.M.G. Fouda, L. Vojtova, L. Kobera, Z. Spotz, L. Burgert, J. Jancar, Synthesis, characterization and antibacterial activity of new fluorescent chitosan derivatives, Int. J. Biol. Macromol. 65 (2014) 234–240.

[66] A.M. Abdel-Mohsen, A.S. Aly, R. Hrdina, A.T. El-Aref, A novel method for the preparation of silver/chitosan-O-methoxy polyethylene glycol core shell nanoparticles, J. Polym. Environ. 20 (2) (2012) 459–468.

[67] A.S. Aly, A.M. Abdel-Mohsen, A. Hebeish, Innovative multifinishing using chitosan-O-PEG graft copolymer/citric acid aqueous system for preparation of medical textiles, Journal of The Textile Institute 101 (1) (2010) 76–90.

[68] A.S. Aly, A.M. Abdel-Mohsen, R. Hrdina, A. Abou-Okeil, Preparation and characterization of polyethylene glycol/dimethyl siloxane adduct and its utilization as finishing agent for cotton fabric, J. Nat. Fibers 8 (3) (2011) 176–188.

[69] S.J. Jeon, M. Oh, W.-S. Yeo, K.N. Galvão, K.C. Jeong, Underlying mechanism of antimicrobial activity of chitosan microparticles and implications for the treatment of infectious diseases, PLOS ONE 9 (3) (2014), e92723.

[70] S. Karunakaran, S. Pandit, B. Basu, M. De, Simultaneous exfoliation and functionalization of 2H-MoS2 by thiolated surfactants: applications in enhanced antibacterial activity, J. Am. Chem. Soc. 140 (39) (2018) 12634–12644.

Supporting information's

Synergistic Performance of Collagen-g-Chitosan-Glucan Fiber Biohybrid Scaffold with Tunable Properties

R. M. Abdel-Rahman[a], V. Vishakha[b], I. Kelnar[a], J. Jancar[b], A. M. Abdel-Mohsen[a,b,c*]

[a] Institute of Macromolecular Chemistry, Czech Academy of Sciences, Heyrovského nám. 2, Praha, 162 06, Czech Republic

[b] CEITEC-Central European Institute of Technology, Brno University of Technology, Purkyňova 656/123, Brno 61200, Czech Republic

[c] Department of Pretreatment and Finishing of Cellulosic Fibers, Textile Research Division, National Research Centre, 33 EL Buhouth St., Dokki, Giza 12622, Egypt

Corresponding author:

Institute of Macromolecular Chemistry, Czech Academy of Sciences, Heyrovského nám. 2, Praha, 162 06, Czech Republic. E-mail: abdellatif@imc.cas.cz

Characterization

Solid-state NMR spectroscopy: ^{13}C CP/MAS NMR spectra are recorded on a Bruker AVANCE III HD spectrometer (Larmor frequencies $\nu^{13}C$ = 125.783 MHz) using a 3.2 mm MAS probe. The spinning speed of the rotor sample is 20 kHz. The number of scans for the accumulation of ^{13}C CP/MAS NMR spectra is 2048, repetition delay of 5 s, and spinlock of 1 ms. During detection, the high-power dipolar decoupling (SPINAL 64) is used to eliminate strong hetero-nuclear dipolar couplings. The isotropic chemical shift of ^{13}C-NMR scale is calibrated with glycine as an external standard (176.03 ppm to carbonyl signal). In all cases, the dried samples are placed into the ZrO_2 rotors and all NMR experiments are performed at 303 K. Temperature calibration was performed on $Pb(NO_3)_2$. The mol (%) of chitin units was calculated according to the following Eq. **1**.

$$mol\%(N-acetyl\,gl\,u\,cos\,a\,min\,e)\ =\frac{I_{C3}}{(I_{C1}+I_{C2}+I_{C3}+I_{C4}+I_{C5}+I_{C6})/6}\times 100 \qquad (1)$$
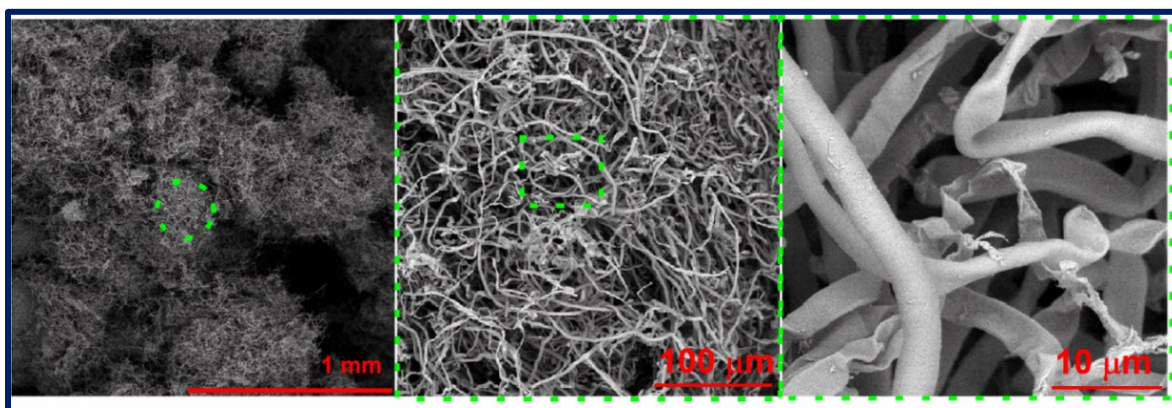

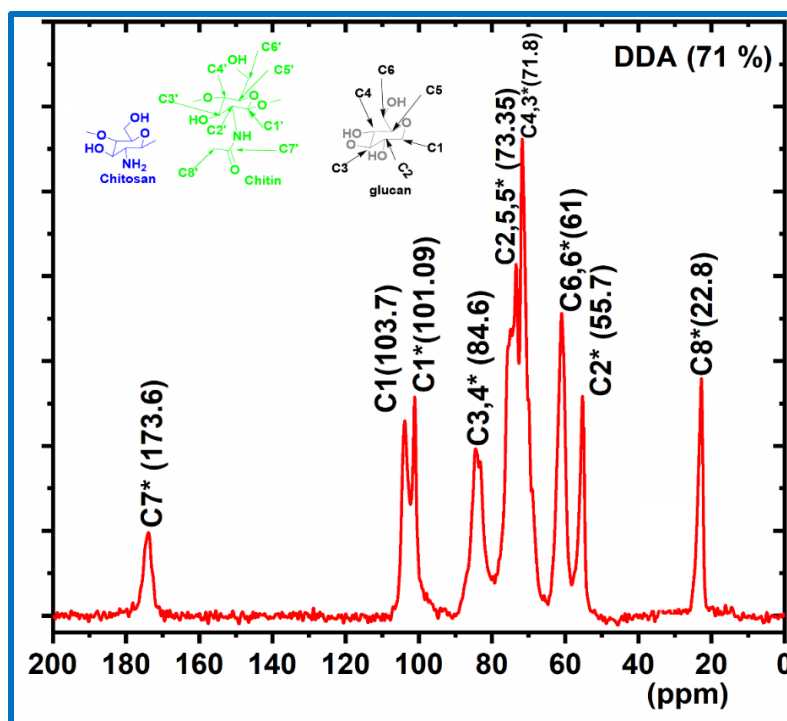**Fig.S1.** SEM of native chitosan-glucan complex fiber (CGF) before freeze-dry process.

Fig. S2. Solid ^{13}C CP/MAS-NMR spectrum of CGF with a deacetylation degree (DDA) 71 %.
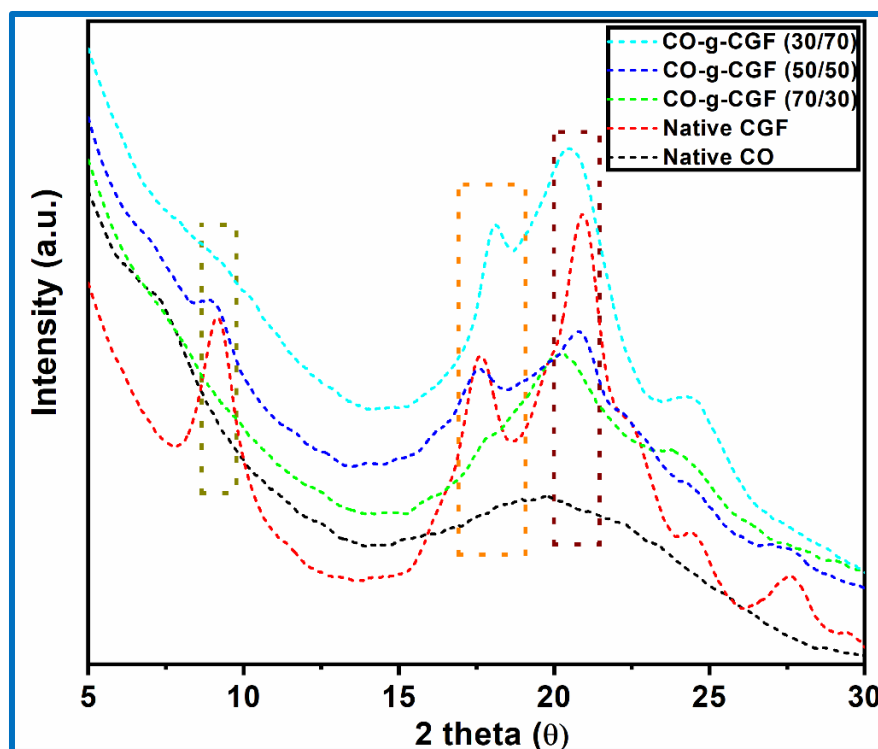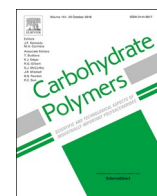

Fig. S3: X-Ray diffraction patterns of a native CO, CGF and HBS scaffolds

Publication 2

Chitosan-glucan complex hollow fibers reinforced collagen wound dressing embedded with aloe vera. Part I: Preparation and characterization

A.M. Abdel-Mohsen[a,b,c,*], R.M. Abdel-Rahman[a], I. Kubena[d], L. Kobera[e], Z. Spotz[a], M. Zboncak[a], R. Prikryl[f], J. Brus[e], J. Jancar[a,b,f]

[a] CEITEC-Central European Institute of Technology, Brno University of Technology, Purkyňova 656/123, Brno 612 00, Czechia
[b] SCITEG, a.s., Brno, Czechia
[c] Department of Pretreatment and Finishing of Cellulosic based Textiles, Textile Industries Research Division, National Research Centre, 33 EL Buhouth St., Dokki, Giza 12622, Egypt
[d] Institute of Physics of Materials, Academy of Sciences of the Czechia, Žižkova 22, CZ 61662, Brno, Czechia
[e] Institute of Macromolecular Chemistry of the Czech Academy of Sciences, HeyRovskeho Nam. 2, 162 06, Prague 6, Czechia
[f] Institute of Materials Chemistry, Faculty of Chemistry, Brno University of Technology, Purkyňova 464/118, Brno, 612 00, Czechia

A R T I C L E I N F O

A B S T R A C T

Collagen (CO)/chitosan-glucan complex (CSGC) hollow fibers encapsulated aloe vera (AV) dressing scaffold (CO/CSGC@AV) were fabricated for the first time by the freeze-dried process. Extraction process, morphology, mechanical properties, pore size, porosity, swelling ability, and degradation behavior of composites scaffold were investigated. CSGC hollow fibers were extracted from *mycelium* of *Schizophyllum commune* CSGC hollow fiber exhibited inner diameter of (600 $\pm$ 250 nm) and outer fiber diameter of (2.5 $\pm$ 0.5 μm). The results of swelling and hydrolytic degradation studies demonstrated that the physicochemical of CO/CSGC@AV was significantly enhanced by CSGC in a concentration-dependent manner. The mechanical property of the CO/CSGC@AV was improved after encapsulated AV into CSGC hollow fibers compared with native CO. The pore size and porosity of the CO/CSGC@AV were slightly decreased in the presence of AV. All these results suggested that the new dressing scaffold has a potential for clinical skin regeneration, particularly for infected chronic wounds and ulcers.

1. Introduction

Polysaccharide-protein complex, existing in different cell walls of fungi as a part of the extracellular matrix, have been investigated because of their biologically attractive functions such as antibacterial, antitumor, anti-nociceptive, anti-inflammatory, anti-oxidative, immune-stimulatory activities and healing properties (Abdel-Mohsen et al., 2016; Burkatovskaya et al., 2006). Chitin and glucan are the main components of fungi cell wall occurring in two forms, free chitin and chitin covalently bonded to β-glucan (Abdel-Mohsen et al., 2016). Intensive research efforts are concentrating on modifying the natural polymers, such as cellulose (Kontturi et al., 2018), chitin and chitosan (Abdel-Mohsen et al., 2016), (Nakashima et al., 2018; Zhao et al., 2018) and polyesters from a different type of bacteria, fungi, etc. (Irimia-Vladu, 2014). Non-animal sources reveal a huge advantage over the animal ones, due to their inherent non-allergenicity and biodegradability in the human organs (François, 2007; Kang et al., 2018).

Mycelium from *Schizophyllum commune (*non-animal source*)*, the vegetative lower part of fungi. Mycelium has been recognized as the major living organism on nature (HUMFELD, 1948; van der Linde et al., 2018). Mycelium has a porous structure composed of tubular filaments called hypha. To date, chitin microfibrils are connected next to the plasma membrane following the biosynthesis of different chains and the fibril formation process through physical hydrogen bonding (Kang et al., 2018; Ruiz-Herrera & Bartnicki-Garcia, 1974).

These micro-fibrils are covalently linked to β-1,3-glucans that extend through the cell wall and tether mannoproteins and lipids on the cell wall surface through branched networks with β-1,6-linked glucans (Duran et al., 1979; François, 2007). Chitin-glucan complex (ChGC) has been extracted from different sources of mycelium (Geißel et al., 2018) by chemical or enzymatic processes. The resultant chitosan–glucan complexes from ChGC were used as flocculants for cultivation of mammalian cells. Unfortunately, the extracted ChGC or CSGC complex is only in powder form (Skorik et al., 2010). Fibers derived from natural

---

polymer sources is an indispensable class of materials that has versatility for a wide range of structural and functional applications in the medical and environmental protection area (Kim et al., 2017).

Hollow fibers have revealed an interesting advantages due to their large surface-to-volume ratios and the ability to trap, isolate or release materials engaged in it (Yoon et al.). Coaxial and tri-axial electrospinning are an interesting methods to fabricate high-aspect-ratio hollow micro/ nanofibers with a controlled inner and outer diameter(Yin et al., 2017) (Yoon et al.). The principle is to use solvent dissolving only the core material while preserving the shell structure (Dzenis, 2004). The challenges of preparing hollow fibers include the choice of the solvent for core and shell (Halaui et al., 2017). In addition, the poor mechanical properties of the existing hollow fibers remain a great challenge (Bedford et al., 2012; Jiang et al., 2014). In our study, a novel source and a simple process were used to fabricate hollow fibers without applying any hazard solvent for extraction chitosan-glucan complex hollow fibers. The second advantage of our new hollow chitosan-glucan fiber was stability and high compatibility with human cells compared with synthetic materials such as polyacrylonitrile, polycaprolactone, acetylacetonate, and polyaniline (Bedford et al., 2012; Han et al., 2017).

Collagen is known to be one of the most promising materials and has been found in diverse applications in tissue engineering for their excellent biocompatibility (Marinucci et al., 2003), biodegradability, and non-toxicity (Marone et al., 2010). However, the fast biodegradation rate and the low mechanical strength of the native collagen scaffolds are the crucial problems that limit its broader application. Cross-linking of the collagen is an effective method to modify the biodegradation rate and to optimize its mechanical properties (Khor, 1997; Marelli et al., 2015; Merrett et al., 2009; Yao et al., 2008). Currently, there are two different kinds of crosslinking methods used in improving the chemical, physical and mechanical properties of the collagen-based scaffolds, i.e., covalent cross-links (Jorge-Herrero et al., 1999) and physical cross-links (Yunoki et al., 2003), (Saito & Marumo, 2010). The reagents used in the covalent cross-linking treatment involved traditional glutaraldehyde (GA), 1-ethyl-3-(3-dimethylaminopropyl)-carbodiimide (EDC), polyglycidyl ether, genipin and polyepoxidic resins, etc (Osborne et al., 1999; Sung et al., 1996), (Kumar et al., 2004).

Aloe vera (AV) has been used in traditional medicine for a long time and It is one of the most familiar herbs in the world. The compositions of AV include many interesting nutrients, such as amino acids, vitamins, sugars, minerals, and enzymes, that support general healthiness. In addition, it has been widely used for the treatment of burns in the last century (Paichit et al., 2012). Many studies shows various biological properties of AV including biological activity, antidiabetic, and anti-inflammatory properties (Ashraf et al., 2016). Furthermore, it has been described that aloe vera can accelerate wound healing in streptozotocin-induced diabetic rats due to their ability to stimulate fibroblasts and enhance the healing process such as collagen synthesis and maturation and wound contraction (Mijatović et al., 2018).

Different wound dressings based on collagen in combination with different polysaccharides like cellulose (Wu et al., 2017), chitosan (Kirichenko et al., 2013; Rezaii et al., 2019), hyaluronan (Rezaii et al., 2019), alginate and chitosan incorporated nanoparticles (Rezaii et al., 2019; You et al., 2017) are prepared by different techniques and applied as new wound healing have shown many disadvantages like (i) need external crosslinker agents to improve the dressing stability (Doillon & Silver, 1986; Doillon et al., 1987; Gentleman et al., 2003), (ii) many of these crosslinkers are toxic or can inhibit the cell viability, (iii) mechanical and degradation properties of the collagen-based dressing are not significant enough for long-term of applications (Ghodbane & Dunn, 2016), (iv) lack of drug control release due to deficiency of mechanical stability and fast biodegradation (Fujioka et al., 1995).

To our knowledge, hollow fibers with controlled fibers dimension extracted from *Schizophyllum commune* for the first time *and* 2/3D

structures were fabricated from it. In our study, we hypothesis that (1) CSGC hollow fibers could be trapped and encapsulate the AV, drug or any other bioactive substances inside it and controlled the release of these materials, (2) The CSGC can work as crosslinker agent, without external hazard crosslinker agent for collagen dressing scaffold, (3) New CSGC hollow fibers could improve the hydrolytic stability of collagen sponge, that could be supposed to use it in different areas of application especially in bone, cartilage or skin regeneration.

In this work, a novel dressing from collagen (CO)/chitosan-glucan complex (CSGC) hollow fiber/aloe vera (AV) composite was prepared and characterized by different techniques. They demonstrated significant enhancement swelling, suitable mechanical property, hydrolytic degradation, and controlled release.

2. Experimental part

2.1. Materials

Bovine collagen type I was supplied as an 8 wt. % of bulk material (VUP, Brno, Czechia) and then, freeze-dried (-70 °C, 48 h) obtained dry collagen (CO). Mycelium was produced from an extracellular product by *Schizophyllum commune* cultured under standard cultivation conditions. All the other chemicals were used without further purifications from commercial sources in the Czechia and were of analytical grade.

2.2. Methods

2.2.1. Cultivation of mycelium

Schizophyllum commune strain (*F-795*) Czech collection of microorganisms strain and cultivated on agar slants with potato dextrose agar (PDA) at 4 °C as described in the literature with a small modification (Mohammadi et al., 2018; Sung et al., 2018). The strain was transferred into a petri dish that was cultivated for 7 days at 30 °C. 100 ml of medium (Inoculum I) in Erlenmeyer flask was inoculated with 0.5×0.5 cm from native mycelium from the petri dishes and incubated in rotary shakers at 30 °C, for 5 days without any disruption of the cell wall bead of mycelium using homogenizer. 50 ml were used for inoculation of 1000 ml Erlenmeyer flasks with 500 ml medium. 1000 ml Erlenmeyer flasks were cultivated in rotary shakers at 30 °C, for 7 days. Medium for the seed cultures and production cultivations contained 35 g/l sucrose, 3 g/l yeast extract, 2.5 g/l disodium hydrogen phosphate, 0.5 g/l magnesium sulfate, initial pH 5.5. Mycelium (insoluble part) and *schizophyllan* yields were measured as follows: 500 ml of cultural broth were centrifuged (10 000 rpm, 25 °C, 20 min), and schizophyllan was obtained from the supernatant after. Insoluble (mycelium) was re-suspended in 250 ml of Milli-Q water, centrifuged again and discarded the supernatant. The insoluble mycelium was placed into a petri dish, freeze-dried (-70 °C, 15 Pa, 48 h) obtained dry mycelium beads.

2.2.2. Extraction of hollow fibers and AV powder preparation

Extraction of chitin-glucan (ChGC) and chitosan-glucan (CSGC) hollow fibers from mycelium beads were done by the chemical way under mild conditions. Firstly, the dry mycelium bead was treated with 5 % of sodium hydroxide (solid to liquid ratio 1/100) at 50 °C for 2 h with 200 rpm. This step was repeated many times until obtained transparent supernatant. The hollow fiber ChGC was washed with Milli-Q water until naturalized at pH 7. Finally, the hollow ChGC fibers were freeze-dried. For extraction of chitosan-glucan hollow fiber (CSGC); chitin-glucan complex (ChGC) was treated with sodium hydroxide 20 % wt.% at 40 °C for 24 h under low speed (200 rpm). The CSGC was washed with Milli-Q water until naturalized at pH 7. Finally, the hollow CSGC fibers with different degree of deacetylation (DDA) was freeze-dried for 48 h.

Aloe vera powder was prepared from fresh aloe vera leaves and the

leaves were washed well with Millli-Q water and the green part was carefully removed from the inner gel. The parenchyma part was homogenized using homogenizer then centrifuged at 15000 rpm for 30 min at 4 °C. The isolated gel was freeze-dried for 2 days, and the powder was kept in dissector to prevent the humidity.

2.3. Fabrication of dressing scaffolds

Wound dressing from collagen (CO)/chitosan-glucan complex (CSGC) hollow fibers and in the presence or absence of different concentrations of AV were fabricated by freeze-drying technique. 0.5 (wt. %) of dry CO was swelled in 10 mM of acetic acid at 4 °C for two days then, homogenized in ice bath (0 °C) for 5 min at 12000 rpm using Ultra-Turrax VD125 homogenizer (VWR International Ltd., UK). Dispersed collagen was centrifuged at 4500 rpm for 10 min (Hermle Z300, Labortechnik, Germany) removed air bubbles, cast into stainless steel molds, kept overnight at −35 °C and lyophilized at −50 °C for 48 h.

Collagen/chitosan-glucan complex hollow fiber (CO/CSGC) dressing sheet was fabricated using different ratios of CSGC to CO. CO (0.5 %) was mixed with CSGC (0.25; 0.5, 1 wt. %) in 10 mM of acetic acid and swelled at 4 °C for two days then homogenized in ice bath (0 °C) for 15 min at 12000 rpm using Ultra-Turrax VD125 homogenizer. The processing of preparation of CO-CSGC dressing scaffolds was the same as used in CO scaffold preparation. The samples coded as CO/CSGC (1/0.5); CO/CSGC (1/1); CO/CSGC (1/2) for 0.25, 0.5 and 1 wt. % of CSGC hollow fibers.

Different ratios between collagen and aloe vera (1/1, 1/2 w/w), AV was dissolved in Milli-Q (certain volume) then, blended with CO dispersed in 10 mM of acetic acid and swelled at 4 °C for two days then homogenized in ice bath (0 °C) for 15 min at 12000 rpm using homogenizer. Processing of preparation of CO/AV dressing scaffolds was the same as used in CO scaffold preparation and samples coded as CO/AV (1/1); CO/AV(1/2); for 0.5 and 1 wt. % of AV powder.

For CO/CSGC@AV dressing scaffolds were fabricated using different concentrations of AV (0.5, 1 %) the latter was dissolved in Milli-Q (certain volume) then blended with different concentrations ratios of CSGC hollow fibers (0.25, 05, 1 wt. %) then a gaited for 2 days at 4 °C, the pH of the medium was 3-4. The mixed solution was homogenized on ice bath (0 °C) for 30 min at 12000 rpm. Different ratios between CSGC@AV (0.25/0.5; 0.5/0.5; 1/0.5; 0.25/1; 0.5/1, 1/1) were mixed with net CO (0.5 wt.%) in 10 mM of acetic acid and all suspension solution (CO/CSGC@AV) were swelled at 4 °C for two days, homogenized in ice bath (0 °C) for 15 min at 12000 rpm. The air bubbles were removed from the suspension by centrifuged at 4500 rpm for 10 min. The obtained CO/CSGC@AV suspensions were poured into stainless steel molds and for a 3D scaffold the solution was poured in 48 well plates and kept overnight at −35 °C, then freeze-drier (−50 °C, 15 Pa, 48 h; CHRIST ALPHA 1-4 LSC). All the samples after freeze-dried were neutralized using phosphate buffer solution (pH 7.5) for 5 times each 30 min, kept overnight at −35 °C and lyophilized -50 °C for 48 h). The samples coded as (Table S1) CO/CSGC@AV (1/0.5/1); CO/CSGC@AV (1/1/1); CO/CSGC (1/2/1); CO/CSGC@AV (1/0.5/2); CO/CSGC@AV (1/1/2); CO/CSGC 1/2/2 for 0.25, 0.5, 1 wt. % of CSGC and 0.5, 1 wt. % of AV with constant CO concentration.

3. Scaffold characterization

Attenuated total reflectance Fourier-transformed infrared spectroscopy (ATR-FTIR): were recorded to study the chemical composition of the obtained dressing mats using Bruker Vertex80 V spectrometer equipped with the diamond crystal over the wavenumbers ranging from 4000 to 650 cm^{-1}. Each spectrum consists of 128 scans and the obtained spectra were analyzed utilizing OPUS software (version 6.5).

Transmission electron microscope (TEM) investigations were performed employing the JEOL JEM-2010 (HT) electron microscope (JEOL, Japan), with an accelerating voltage of 120 kV. The samples were dispersed in Milli-Q water with a concentration of 0.5 mg/ml, and a drop was placed on Cu grids pre-coated with carbon films and dried in air.

X-ray diffraction (XRD) was measured at 3 kW diffractometer Smart lab from Rigaku using Cu Kx radiation (λ = 1.54 Å) and detector Dtex-Ultra with Bragg-Brentano geometry. Diffraction angle 2-Theta was measured in a range from 5° to 70° with step size 0.02° at speed 4°/min. A generator was operated at the current 30 mA and voltage 40 kV.

Scanning electron microscopy (SEM, JEOL JSM-6340 F) was used to examine the morphology of the fibers and scaffold dressing. The average fiber diameter and pore size of the dressing scaffolds was determined by collecting data from 100 different locations within SEM images, and Image J software was used for subsequent measurements and analysis. The surface elemental analysis was determined by Energy Dispersive X-ray spectroscopy (EDX) (Oxford Instruments, England) and evaluated by Aztec 2.1a software. Hollow fiber diameters were measured using Image J software. Samples were then air-dried at room temperature prior to sputter coating with 20 nm of Au/Pd layer and imaged at 10 kV in SEM (Tescan, Brno, Czechia).

Thermal gravimetric analysis (TGA) in this case was used for the study of thermal stability and moisture content of the different composition of wound dressing sheets. Measurements were carried out in the inert nitrogen with a temperature rate of 10 °C/min up to 800 °C.

Mechanical properties of prepared dressing scaffolds were evaluated by Zwick/Roell-Z010 test instrument (Zwick/Roell, Germany) with a 10 N load cell at a crosshead speed of 5 mm. min^{-1} at room temperature (20 °C). All samples were cut into rectangles with dimensions of 30 mm × 5 mm. At least ten samples were tested for each type of dressing scaffold and data were averaged to get the standard deviation. The thickness of samples was measured with a micrometer (Prominent s.r.o., Czechia).

Solid-state NMR spectroscopy: ^{13}C CP/MAS NMR spectra were recorded on a Bruker AVANCE III HD spectrometer (Larmor frequencies ν^{13}C = 125.783 MHz) using a 3.2 mm MAS probe. The spinning speed of the rotor sample was 20 kHz. The number of scans for the accumulation of ^{13}C CP/MAS NMR spectra was 2048, repetition delay of 5 s, and spinlock of 1 ms. During detection, the high-power dipolar decoupling (SPINAL 64) was used to eliminate strong hetero-nuclear dipolar couplings. The isotropic chemical shift of the ^{13}C NMR scale was calibrated with glycine as an external standard (176.03 ppm to carbonyl signal). In all cases, the dried samples were placed into the ZrO$_2$ rotors and all NMR experiments were performed at 303 K. Temperature calibration was performed on Pb(NO$_3$)$_2$ using a procedure described in the literature (Brus, 2000). The mol (%) of chitin units were calculated from equation referred to in the literature (Spěváček & Brus, 2008) accord icing to Eq. (1):

$$mol\%(N-acetylglucosamine) = \frac{I_{C_3}}{(I_{C_1} + I_{C_2} + I_{C_3} + I_{C_4} + I_{C_5} + I_{C_6})/6} \times 100 \qquad (1)$$

Calcium ion measurement: The kinetics of calcium release was studied from the prepared dressing scaffold. Collagen/aloe vera (CO/AV; 1/2), collagen complex/ aloe vera (CO/CSGC@AV) with different concentration of CSGC (0.25, 0, 5, 1 wt.). The dressing scaffolds were cut into pieces in a diameter of 10 mm. These samples were then immersed in 10 ml saline buffered solution (SB, pH = 7.0) at 37 °C. 1 ml solution was taken at regular time intervals (1, 12, 24, 48, 72, 96, and 144 h) and analyzed for the amount of calcium released using Inductively Coupled Plasma Mass Spectrometry (ICP-MS), and then the same volume of fresh saline solution was added.

Degradation measurement: the wound dressing mats were cut into 1 × 1 cm strips and weight then immersed into phosphate buffer solution (PBS) solution and placed in an incubator at 37 °C to test their

hydrolytically stability at body conditions. After removing the swollen samples from the solutions at regular intervals, samples were freeze-dried until constant weight. Hydrolytic degradation was examined gravimetrically by recording weight decrements as a function of time (0, 1, 3, 5, 10, 14, and 21 days). Weight loss was calculated according to the Eq. (2).

$$Weight\ loss\ (\%) = \frac{Wi - Wf}{Wi} \times 100 \qquad (2)$$

Where W_i was the weight of dried sample and W_f was the weight of the sample in the regular time. The resulting value is an average of five measurements.

Swelling percentage: 0.5×0.5 cm dressing specimens were gravimetrically evaluated in PBS solution (pH = 7.5) at 37 °C. In regular time intervals (0.5, 1, 3, 6, 12, 24, 48, 72, 96, 120, and 168 h) swollen pieces were removed, the excess surface water was quickly swiped out by blotting paper and reweighed. The water uptake of CO; CO/CSGC; CO/CSGC@AV dressing mats were defined according to the Eq. (3).

$$Swelling\ percentage\ (\%) = \frac{Ws - Wd}{Wd} \times 100 \qquad (3)$$

Where W_s was the weight of the swollen samples at the given time and W_d is the weight of the dry sample. The resulting value is an average of 5 measurements (n = 5).

Porosity measurements: the porosity of the prepared dressing scaffold was determined by using the reported method(Liang et al., 2016). The scaffold was immersed in absolute ethyl alcohol until it was saturated. The weight of the scaffold was measured before and after the immersion. The porosity (*P*) was calculated from the following Eq. (4).

$$Porosity\ (\%) = \frac{M2 - M1}{\rho v} \times 100 \qquad (4)$$

Where, M_1 and M_2 weight of dressing before and after immersion, V was the volume of dressing before immersion, which was calculated from the formula of length × width × height. ρ the density of the alcohol. All the samples were triplicate (n = 3).

4. Results and discussion

4.1. Extraction of hollow fibers

Mycelium yield after twelve days of *Schizophyllum commune (S. commune)* cultivation varied between 12.3 ± 0.3 g/l. To prevent the deformation of the shape of the mycelium bead structure, only gentle mechanical processes had to be employed. Scheme 1 shows the sequence of extraction steps from mycelium bead. In native mycelium, the main component was the β-(1→3, 1→6)-D-glucan with different ratio between β-(1→3) and branched β-(1→6) (Scheme 1a, g) covalently bonded to proteins and lipids (Kang et al., 2018). The chitin chains were covalently connected with glucan matrix (Scheme 1a; g). After deprotenization step (DP), large amounts of lipids and proteins were removed from the mycelium matrix (Scheme 1b). By repeating the DP step 10 times, partially deacetylated chitin was obtained (DDA = 50 %). The 5 wt. % of NaOH could not remove all proteins (residual protein measured by solid-state NMR was 7 %) but it was quite enough to remove all lipids (0 %) from the mycelium matrix (DP step) (Scheme 1g). In the de-acetylation step (DA), a high concentration of sodium hydroxide (20 wt. %) was used for 24 h with changing the supernatant solution each 2 h by adding a fresh solution of NaOH. The reaction temperature was 40 °C under low mechanical stirring at 200 rpm. The chitosan-glucan complex was generated with 90 and 100 % acetylation with 0 % proteins (solid-state NMR) with the DDA depending on the reaction time (Scheme 1g). The CSGC with 90 % DDA was used to preserve a low amount of acetamide groups needed can improve the mechanical properties of the dressing scaffolds (Hsu et al., 2004; Liu

et al., 2012; Wenling et al., 2005).

The chemical structure of chitin-glucan and chitosan-glucan hollow fiber complex wasn't confirmed in literature and there weren't more details about the chemical bonds between chitin or chitosan and glucan (linear and branched chains). ^{13}C CP/MAS NMR experiments were used to confirm the chemical structure of both ChGC and CSGC and pure schizophyllan. The experimental ^{13}C CP/MAS NMR spectrum of plain glucan was confirmed the structure of β-(1→3, 1→6)-D-glucan as depicted in Scheme 1g. The peak position at 101.1 ppm corresponds with C1 atoms in the β-glycosidic bond. The peak at 84.6 ppm can be assigned to the (1→3) linked C3 carbon. The shows overlapped signal sat 71.6 ppm reflects the C5, C2 and C4 atoms of glucan units while the C6 atoms have the resonance at 60.6 ppm. From the recorded spectra C6 and C1 carbons were characterized by two signals, which could be attributed to the (1→3) and (1→6) linkage of the glycosidic bond. The ratio of linear and branched glucosidic bonds (1-3) and (1-6) was 1:1, respectively (Y.-T. Kim et al., 2000).

For the sample chitin/chitosan-glucan hollow fibers, the chitin/chitosan-glucan complex was confirmed by splitting of signal at 103.8 and 101.1 ppm, which could be assigned to C1` and C1 carbons from chitosan and glucan, respectively. The splitting of these signals (C1/C1`) indicated that the complicated bonding in the analyzed complex could be expected. It has been revealed three superimposed resonances by deconvolution (fitting) of C1/C1` signals (Scheme 1h). The resonances at 101.1 ppm and 102.7 ppm were corresponding to (1→3) and (1→6) glycosidic bonds of β-glucan, respectively. The resonance at 103.8 ppm, which was attributed to chitin/chitosan units, from the intensities of resonances at 101.7 ppm and 102.7 ppm has been revealed a dominant fraction of (1→3) glycosidic bonds (approximately 90 %). The degree of deacetylation of chitosan was 50 %, for the sample chitin-glucan hollow fiber (ChGC; DDA = 50 %). Additionally, the signal at 32.9 ppm was clearly visible in ^{13}C CP/MAS NMR spectrum of sample ChGC (Scheme 1g), which corresponds to the residual proteins and/or lipids (Roca et al., 2012; Spěváček & Brus, 2008).

The ratio of chitin/chitosan and anomeric glucan was (1:1), and the β-(1-6) glucosidic bonds approximately 10 mol % of anomeric glucan. The degree of deacetylation was 50 mol % ratio between chitin and chitosan. The spectrum of the chitosan-glucan complex (CSGC; DDA = 90 %; Scheme 1g) shows the typical pattern that was for chitosan-glucan complex polysaccharide. The characteristic peaks at 174.2, 55.3 and 22.8 ppm correspond with carbonyl (C7`), methine atoms near the nitrogen (C2`) and methylene carbons (C8`), respectively, from chitin units (Roca et al., 2012; Spěváček & Brus, 2008; Tishchenko et al., 2011). On the other hand, the absence of a peak at 33 ppm, eventually other signals, in ^{13}C CP/MAS NMR spectrum of sample CSGC (DDA = 90 %) implies the absence of impurities in chitosan-glucan complex hollow fiber (CSGC). The calculated % deacetylation degree of the hollow fiber complex was 90 %. The complex contains 15 % of chitin/chitosan units (this data was obtained from fitting of C1 signal, as in previous cases) and the degree of deacetylation of chitin/chitosan was 90 % from the chitin/chitosan weight ratio.

^{13}C-CP/MAS NMR spectrum of chitin/chitosan-glucan complex with completely deacetylated the amino groups (ChGC; DDA = 100 %) is depicted in Scheme 1g confirms the structure of β-(1→3, 1→6)-D-glucan and reflects characteristic peaks of a complex polysaccharide. The peaks appeared at 103.5, 86.1, 74.4, 68.8 and 62.1 correspond to C1-C6 carbons of anomeric β-glucan, respectively (Roca et al., 2012). However, the presence of a peak at 57.0 ppm was indicated that the polysaccharide complex also contains a certain amount of chitosan units. The mentioned resonance was typical to C2` (Scheme 1h) atoms of the chitosan structure.

Consequently, we conclude that the analyzed hollow fiber chitosan-glucan complex was β-(1→3, 1→6)-D-glucan/chitosan complex. The degree of deacetylation of chitin/chitosan was 100 % (CSGC; DDA = 100 %; Scheme 1g) and the ratio of chitosan to glucan was (95:5), respectively. Furthermore, from the considerable similarity of
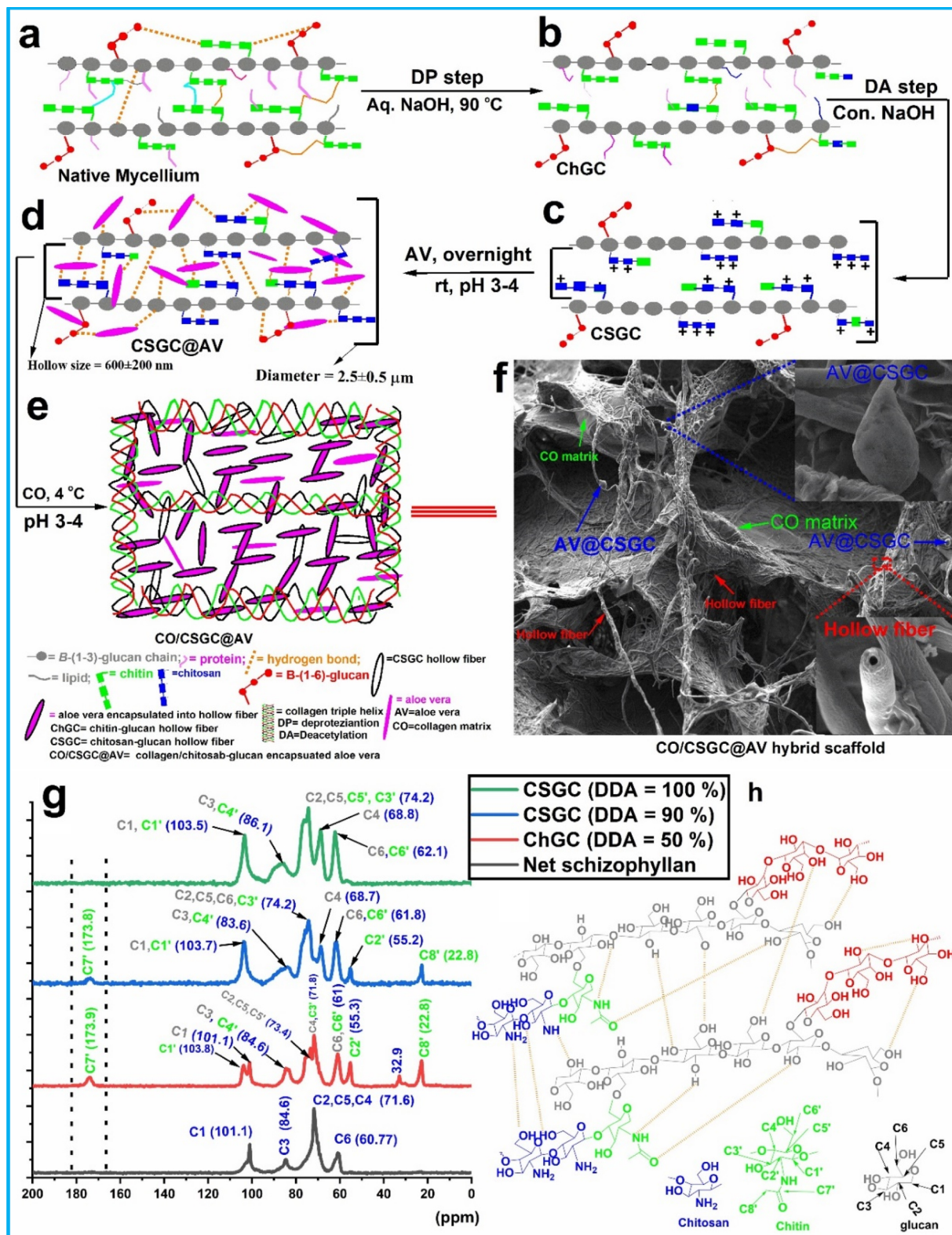
Scheme 1. Schematic illustration extracting sequence process of hollow fibers, hollow fibers encapsulated aloe vera and engineered dressing scaffolds.
Notes: (a) native mycelium beads after fermentation chemical bonded with proteins and lipids; (b) mycelium beads after deprotenization step (DP) with low proteins and lipids contents (chitin-glucan hollow fiber complex (ChGC); (c) chitosan-glucan hollow fiber after deacetylation step (CSGC) with zero proteins; (d) hollow fiber encapsulated aloe vera (CSGC@AV); (e) collagen/chitosan-glucan hollow fiber encapsulated aloe vera (CO/CSGC@AV; (f) representative SEM of CO/CSGC@AV dressing scaffold; (g) ^{13}C CP/MAS NMR spectra of native *Schizophyllum commune,* ChGC (DDA = 50 %), CSGC with different degree of deacetylation (DDA = 90, 100 %), respectively for the carbon resonance assignments and signal numbering; (h) proposed chemical structure of chitosan-glucan hollow fiber complex (DDA = 90 %).
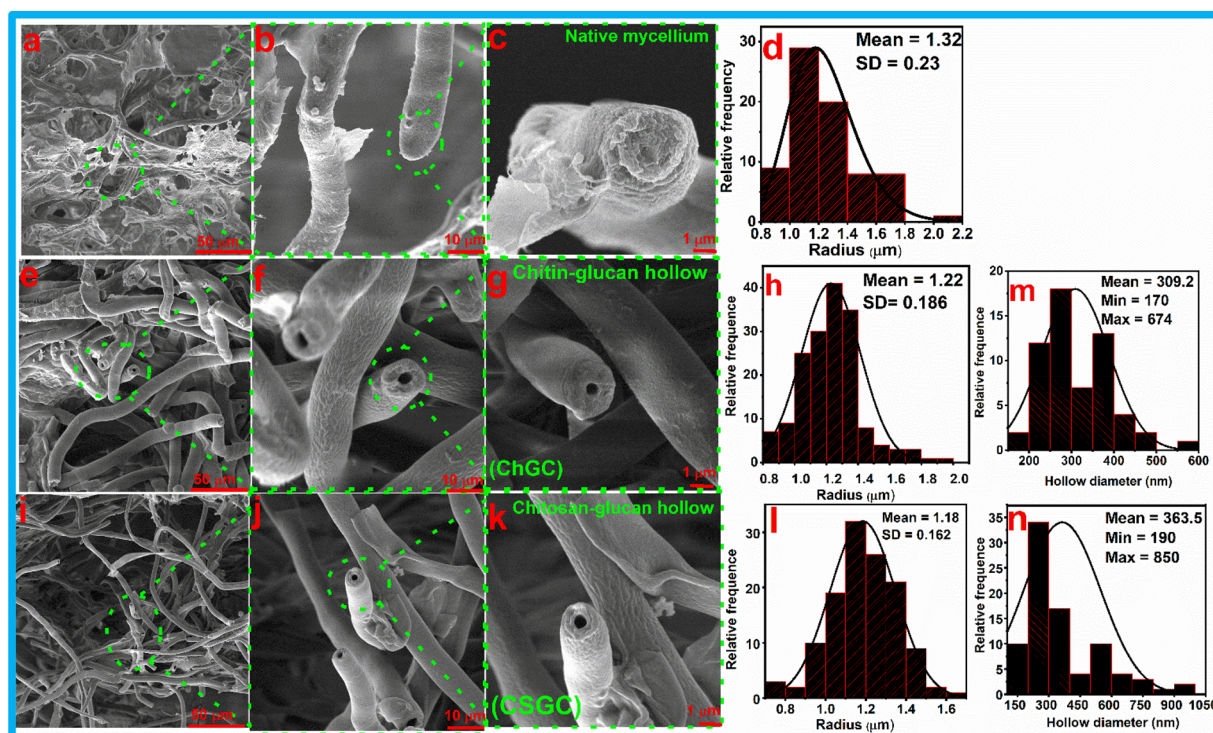
Fig. 1. Morphological visualization of native mycelium, extracted chitin-glucan (ChGC) and chitosan-glucan (CSGC) complex hollow fibers.
Notes: (a, b, c) SEM of native mycelium beads at different magnifications (scale bars were 50, 10 and 1 μm); (e, f, g) SEM of the extracted ChGC from mycelium with hollow fibers with 50 % DDA (scale bars were 50, 10 and 1 μm); (I, j, k) SEM of CSGC with 90 % DDA (scale bars were 50, 10 and 1 μm); (d, h, l) fiber radius histograms of mycelium, ChGC and CSGC, respectively; (m, n) histograms of hollow diameters of ChGC and CSGC, respectively. The histograms of fiber radius were plotted from 200 points and for hollow size was plotted from 100 points.

^{13}C CP/MAS NMR spectra of samples CSGC (DDA = 90 and 100 %; Scheme 1g) could be expected similar structure (anomeric β-glucan bonded with chitin or chitosan units) with different degree of deacetylation. The chemical structure of Ch/CSGC hollow fiber complex was not well known and need to be precisely studied and confirmed. The chemical composition depended on the source and the extraction process. From ^{13}C solid-state NMR spectroscopy (Scheme 1g) the most formed of β-(1, 3)-glucans with short branched β-(1, 6)-glucans and chitin/chitosan β-(1, 4)-*N*-acetyl glucosamine/ glucosamine connected covalently by glycosidic bonds (Scheme 1h).

Fig. 1a–c depict surface morphology and cross-section of native mycelium. The fiber diameter was 1.32 μm (Fig. 1d). The extraction of ChGC hollow fibers was done under a mild condition with low rotation speed of mechanical stirrer to prevent the destruction of the hollow fiber shape. Fig. 1e–g show the ChGC fibers after the treatment of mycelium beads with low concentrated sodium hydroxide. Fibers were well disturbed without bundled together and the surface morphology of the ChGC was more smooth, homogeneous and clear compared with native mycelium fiber (Fig. 1a). Fig. 1f explored visualization of hollow structure of ChGC appeared after mycelium beads treated with sodium hydroxide for certain time (10 h) and 50 °C with changed the alkaline aqueous medium every 2 h prevented back interactions between ChGC functional groups and proteins molecules and also to obtain pure ChGC hollow without residual of proteins or lipids that was confirmed by solid NMR and obtained clear/transparent supernatant solution.

The hollow structure was appeared, due to the extraction of proteins and pigments from the internal structure of ChGC fibers. Fig. 1g shows the cross-section of ChGC fiber with hollow shape displayed smooth surface without noticeable roughness indicated that CSGC hollow fiber has a clean surface with circular cross-section. The ChGC fiber show a radius of 1.22 0.186 ± μm (Fig. 1h) and the average inner diameter (Fig. 1m) was 674–170 nm.

Fig. 1i–k represents the CSGC after the ChGC treatment with sodium

hydroxide de-acetylated the acetamide groups on the surface and inside the hollow fibers and the extraction process was investigated and optimized at 40 °C under low mechanical stirring (200 rpm). Using high temperature (90 °C) and high speed (1000 rpm) to de-acetylate the chitin part damaged completely the fiber structure obtained (Fig. S1a,b; supporting information) and the optical morphology of the complex before and after treatment was visualized by digital camera (Fig. S1c,d). The fibers were more separated without any bundling (Fig. 1i, k) with a smooth surface and a radius of 1.18 ± 0.162 μm (Fig. 1l). The inner diameter of hollow CSGC fibers (Fig. 1n) was about 363 − 850 nm. After purifications, proteins and other impurities like pigments in native mycelium were removed successfully. Thus, the purified chitosan-glucan hollow fiber was suitable for the fabrication of biomaterials. From SEM of ChGC (Fig. 1f) and CSGC (Fig. 1j) the hollow size was increased from (400–600 nm) by increasing the degree of deacetylation from 50 % to 90 % for ChGC (Fig. 1f) and CSGC (Fig. 1j), respectively. This increase in hollow size could confirm that the majority of the chitin chains in complex macromolecule was connected inside the fiber not only on the surface of complex matrix without significant changes in surface morphology of ChGC and CSGC fibers (Fig. 1g, k). Chitosan-glucan hollow fiber (CSGC) with fiber diameters (2.5 ± 0.5 μm) and hollow size (800 nm ± 200) was prepared and used to encapsulate the AV molecule (Scheme 1d, Fig. 1n).

In the presence of CO matrix, the interactions between CSGC and AV were improved, due to the presence of different groups of CO that could be connected physically/ionically with CSGC@AV or CSGC, AV separated. In Scheme 1 shows the cross-section of collagen/hollow fibers encapsulated aloe vera (CO/CSGC@AV) and CSGC@AV well adhere and distributed onto the surface of CO matrix.

4.2. Morphological characteristics

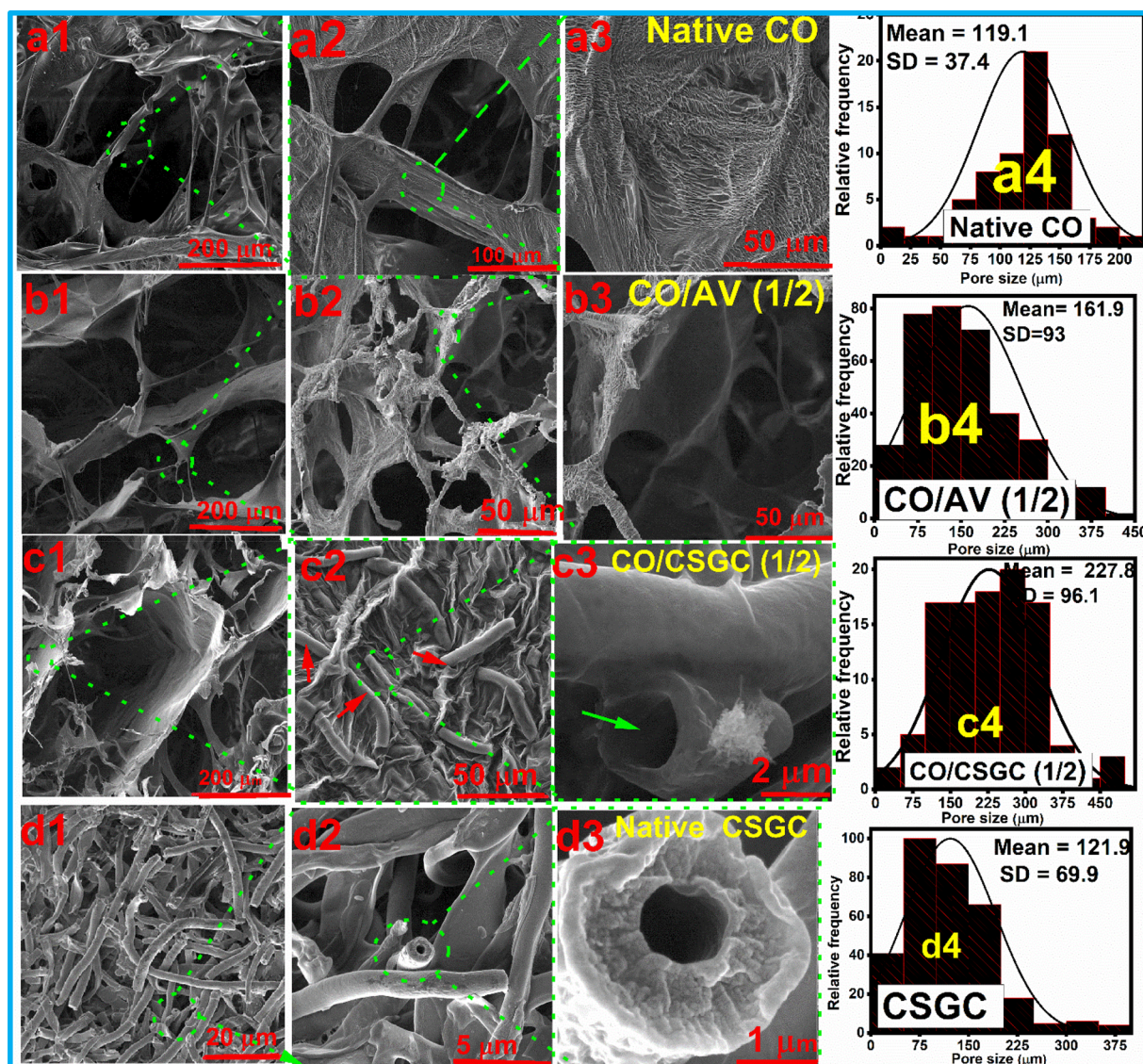The microstructure was investigated employing scanning electron

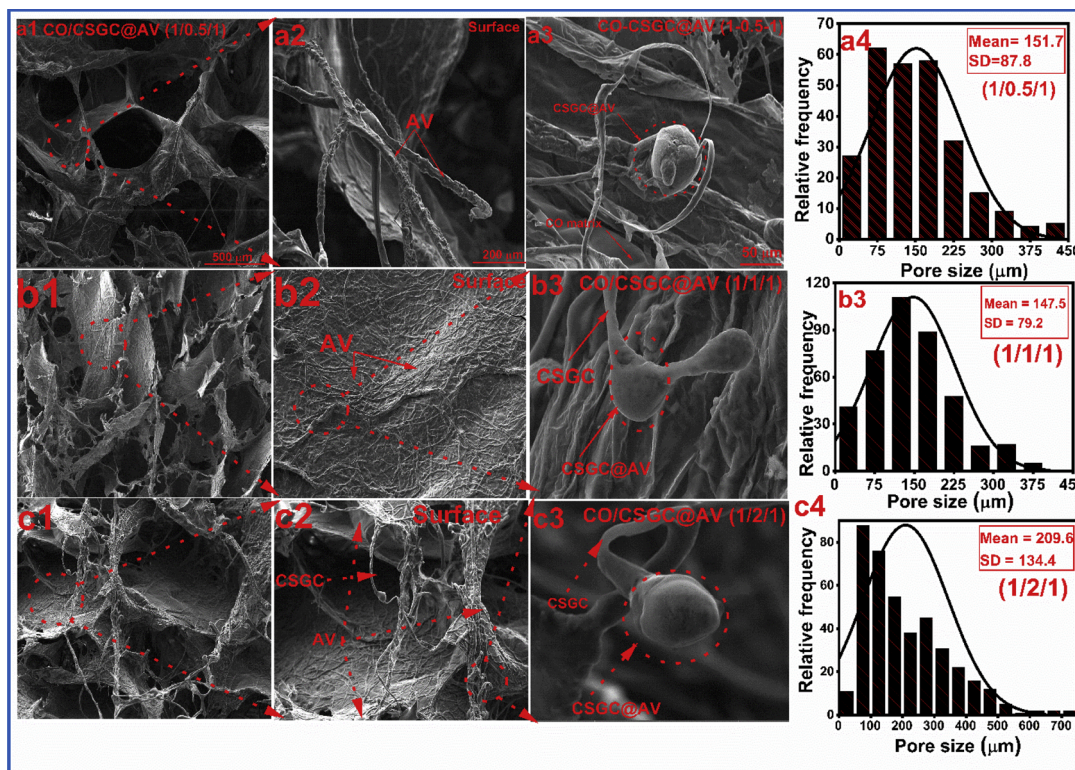**Fig. 2.** Representative SEM and pore size histograms of dressing scaffold.

Notes: (a1-a4) SEM and pore size histogram of native CO; (b1-b4) SEM photographs and pore size histogram of CO/AV (1/2); (c1-c4) SEM and pore size histogram of CO/CSGC (1/2); (d1-d4) SEM and pore size histogram of native CSGC (1/2). Scale bars of (a1, a2, a3) were 200, 100 and 50 μm, respectively for (b1, b2, b3) were 200, 100 and 50 μm, respectively for (c1, c2, c3) were 200, 50 and 2 μm, respectively. For d1(20 μm), d2 (5 μm) and d3 (200 nm). The pore size histograms were plotted from 200 points.

microscopy (SEM) as shown in Figs. 2, 3. Fig. 2a$_{1-3}$ depicts micrographs of the scaffold architecture and pore size histogram of native CO (0.5 wt. %). The CO scaffold has a heterogeneous lamellar pore structure surrounded by flake-like collagen sheets with a mean pore size of 119 ± 37 μm (Fig. 2a$_4$). At the same mass ratio between CO and AV (1:1), the pore size was increased to the average pore size of 207 ± 109 μm (Fig. S2a$_{1-3}$; Fig. S2a$_4$; supporting information). At 1:2 ratio between collagen/aloe vera presented in Fig. 2b$_{1-3}$, the pore size was decreased slightly from 207 ± 109–162 ± 93 μm, respectively (Fig. 2b$_4$). This might be due to AV acted as crosslinked agent between CO functional groups and excess of AV worked as bridge lines between CO matrix. The improvement of pore size of CO/AV, might be due to the AV molecules decreased the attraction forces between the functional groups of CO (carboxylic, hydroxyl and amino groups) and increased the pore size, as well as AV, have been reported (Rahman et al., 2017) to contain several biologically active and nutritionally compounds such as glycoproteins, saccharides, vitamins and antioxidants could interact with CO functional groups and increased the pore size.

The appearance of the collagen/chitosan-glucan (CO/CSGC) porous

scaffold is shown in Fig. 2c$_{1-3}$. SEM observation clearly showed the different pore structures of the CO/CSGC (1/2) scaffolds that were prepared in the absence of AV compared to the neat CO scaffold. The CO/CSGC (1/2) porous scaffold with large spherical pores (277 ± 96 μm; Fig. 2c$_4$) were formed in the CO/CSGC scaffold in an absence of AV (Fig. 2c$_{1-3}$). The large spherical pores evenly distributed throughout the volume and well stacked. The hollow fibers adhered to the surface of collagen matrix with physical bonds as shown in Fig. 2c$_2$, (red rows) as well as keeping open the hollow as depicted in Fig. 2c$_3$, (green row). Fig. 2d$_{1-4}$ shows the native CSGC hollow fibers scaffold with very smooth and homogenous fiber surface and pore size was (122 ± 70 μm).

Fig. 3A and B exhibits the SEM micrographs and histograms of pore size of scaffolds fabricated using different contractions of CSGC (0.25, 0.5, 1 wt.%) and AV (0.5, 1 wt. %). The surface morphology of the dressing scaffold (CO/CSGC@AV) differed from the native mycelium. The pores were interconnected, and the size was significantly increased with the increase of the CSGC concentrations (0.25–1 wt. %). Using different concentrations of CSGC as shown in Fig. 3A (a$_{1-3}$; b$_{1-3}$; c$_{1-3}$)
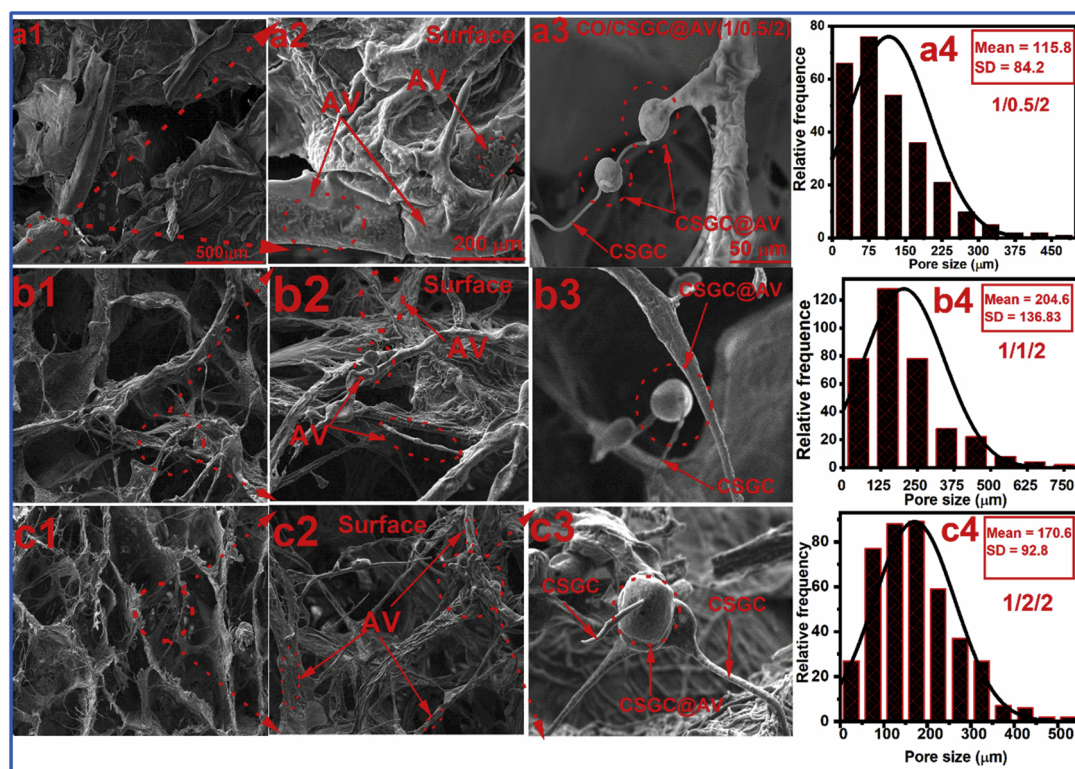
Fig. 3. (A) Representative SEM of dressing scaffolds using AV (0.5 wt.).
Notes: (a1-a4) SEM and pore size histograms of CO/CSGC@AV (1/0.5/1); (b1-b4) SEM and pore size histogram of CO/CSGC@AV (1/1/1); (c1-c4) SEM and pore size histogram of CO/CSGC@AV (1/2/1); (500 µm scale bars of (a1, b1, c1); 200 µm of (a2, b2, c2); 50 µm of (a3, b3, c3). The histograms of pore size measurements were plotted from 200 points. (B) Representative SEM of dressing scaffolds using AV (1 wt.).
Notes: (a1-a4) SEM and pore size histograms of CO/CSGC@AV (1/0.5/2); (b1-b4) SEM and pore size histogram of CO/CSGC@AV (1/1/2); (c1-c4) SEM and pore size histogram of CO/CSGC@AV (1/2/2); (500 µm scale bars of (a1, b1, c1); 200 µm of (a2, b2, c2); 50 µm of (a3, b3, c3). The histograms of pore size measurements were plotted from 200 points.
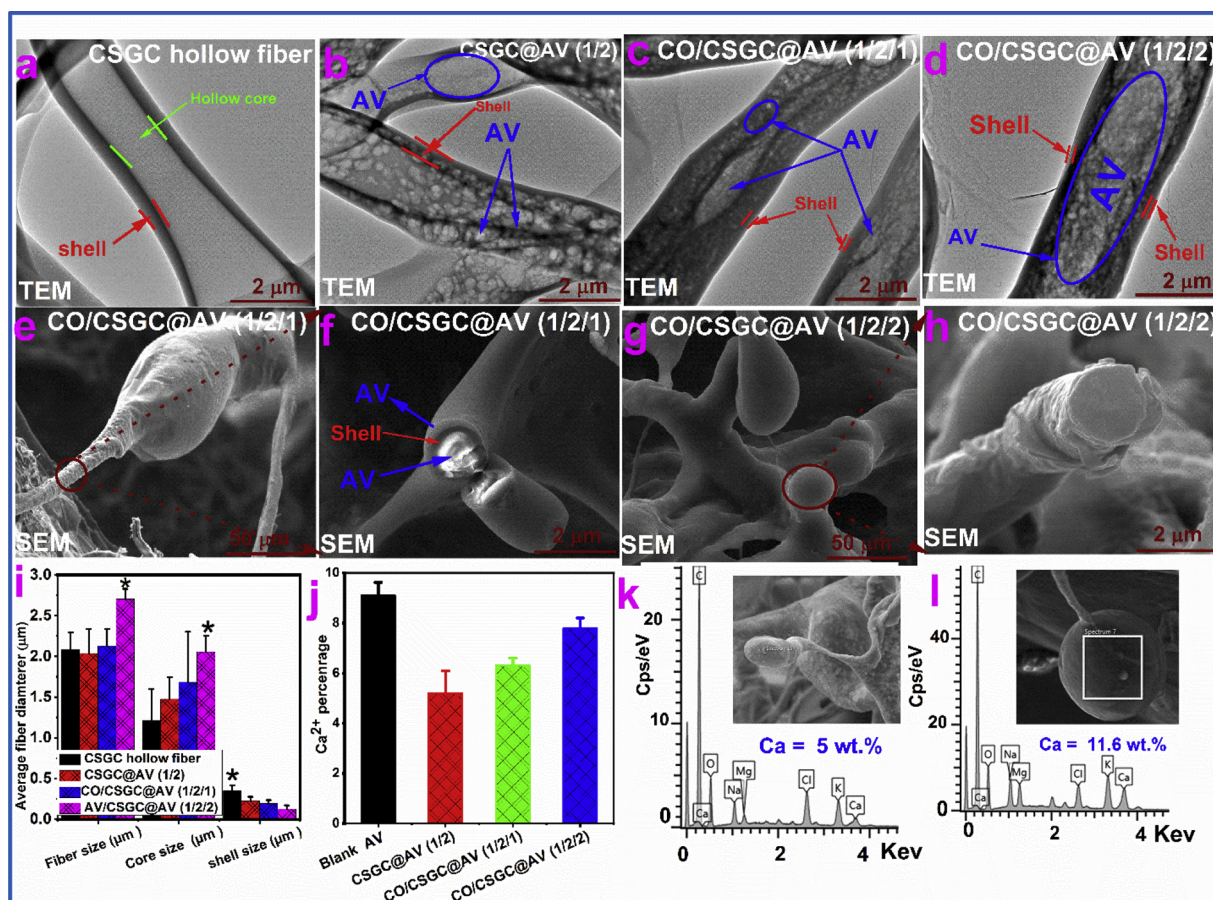
Fig. 4. TEM, SEM-EDX and cross-sectional of CO/CSGC@AV wound dressing scaffold.

Notes: (a) TEM images of native CSGC; (b) CSGC@AV (1/2); (c) CO/CSGC@AV (1/2/1); (d) CO/CSGC@AV (1/2/2). (e) SEM images of CO/CSGC@AV (1/2/1); (f) cross-section of CO/CSGC@AV (1/2/1); (g) SEM images of CO/CSGC@AV (1/2/2); (h) cross-section of CO/CSGC@AV (1/2/2); (i) Effect of AV on average size diameters of hollow fiber, core, and shell before and after encapsulation of AV; (j) Effect of hollow fibers on calcium ions percentage trapped into dressing scaffold; (k) EDX of CO/CSGC@AV (1/2/1); (l) EDX of CO/CSGC@AV (1/2/2). ($p^* > 0.01$).

the AV (0.5 wt. %) molecules were well dispersed inside (Fig. 3Aa₃,b₃,c₃) the CSGC hollow fibers (Fig. 4c) as well as on the surface of scaffold matrix (Fig. 3Aa₂,b₂,c₂). The pore size of CO/CSGC@AV (1/0.5/1; 1/1/1; 1/2/1) dressing scaffolds was 151 ± 87, 147 ± 97, 209 ± 104 μm as shown in Fig. 3Aa₄, b₄, c₄, respectively.

Fig. 3B shows the effect of 1 wt. % of AV on the surface morphology of dressing scaffold using different concentrations of CSGC hollow fibers (0.25, 0.5, 1 wt.%). Interestingly, high loaded of AV was observed (loading efficiency = 85 %; 1/2/2) into the CSGC hollow fibers. AV was encapsulated into the hollow fibers and hollow fiber size was increased slightly from 1.2 to 1.5 μm (Fig. 4i) by increased the AV concentration from 0.5 to 1 wt. %. Due to the AV was dissolved in slightly acid medium pH (4.5–5) could enhance the loading capacity of AV into CSGC and activated the amino groups in chitosan chains to absorb more AV. In addition, enhanced the adhesion properties between CO and CSGC (Fig. 3Ba₁-c₂), could create strong physical bonds between these functional groups ($-COO^-, -NH_2$) and CSGC ($-NH_2, -NHCOCH_3, -OH$ groups). From the histograms (Fig. 3Ba₄,b₄,c₄), the pore size of dressing scaffold was slightly decreased compared with 0.5 wt. % AV, but still much higher than CO dressing alone.

The hollow fiber composition was observed using transmission electron microscopy (TEM) for native chitosan-glucan complex CSGC, complex encapsulated aloe vera (CSGC@AV;1/2) and collagen/hollow encapsulated aloe vera (CO/CSGC@AV) with two different ratios of AV (1/2/1, 1/2/2). Fig. 4a depicts the plain CSGC hollow fiber with the hollow size (363 − 850 nm) and fiber radius (1.18 ± 0.162 μm). Fig. 4b shows the TEM of CSGC@ AV (1/2) without CO matrix with sharp

interface boundary after encapsulated the aloe vera into CSGC fibers. CSGC/AV (1/2) exhibited homogeneous and well distribution of AV molecules inside the hollow structure of complex with slightly decreased in shell diameter 0.22 ± 0.051 μm (Fig. 4i) compared with native CSGC (Fig. 4a,i).

Collagen did not induce any significant changes in the morphology and diameter of the CSGC fibers. Fig. 4c,d shows dressing scaffold with different concentrations of AV (1/2/1, 1/2/2). Comparing between the dressing scaffold engineered from a different concentration of AV, the CSGC exhibited more AV trapped inside the hollow fiber (Fig. 4d), due to the ionic and physical interactions between functional groups of CSGC and the AV. We can conclude that the chitosan-glucan complex hollow fibers were very interesting candidates for trapping and releasing bioactive moieties. The surface morphology and cross-section of CSGC hollow fibers were slightly changed after encapsulated the AV (Fig. 4e,g). from the cross-section, AV generated thick layer inside the CSGC fiber (Fig. 4f, h). At a higher concentration of AV, the fibers trapped more AV inside and on the surface of CSGC (Fig. 4j) with loading efficiency about 85 % compared with native AV (from Ca ions measurement). Fig. 4h suggests that the AV filled completely the hole in the CSGC fibers (1/2/2). The EDX spectra (Fig. 4k, l) captured at different locations on CO/CSGC/AV revealed 5 and 11.5 wt. % of calcium from the AV for 1/2/1 and 1/2/2 dressing scaffold, respectively.

The trapping or encapsulation mechanism of AV into CSGC hollow fibers unclear and will need more studies. Here, we proposed different mechanisms of immobilized the AV inside the CSGC fibers. (i) Under acidic conditions, amino groups of CSGC were protonated and formed

quaternary salt that could interact with components of AV generated amphiphilic property between cationic chitosan part in CSGC and anionic part of AV (acetylated mannan, anthracene derivatives), (ii) The
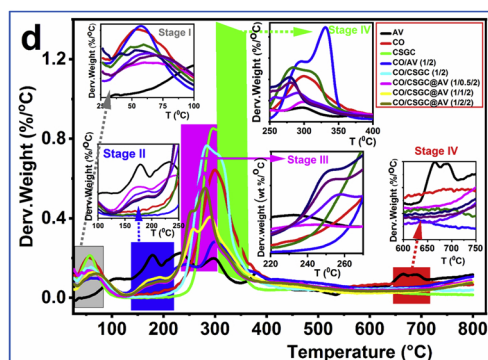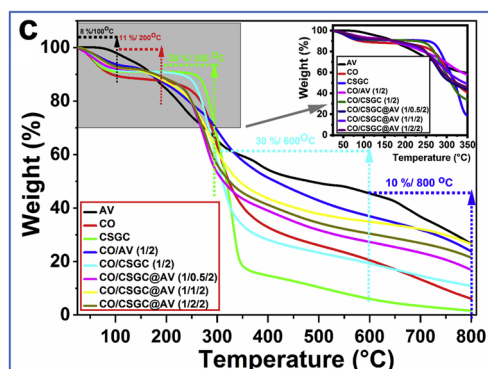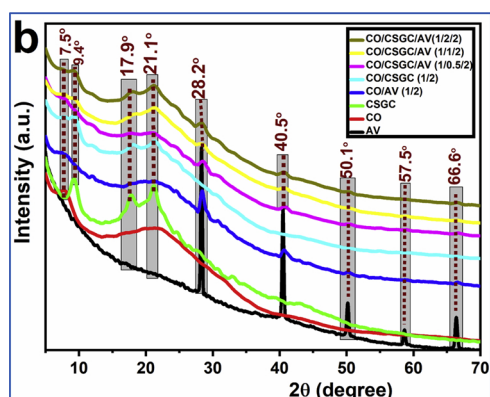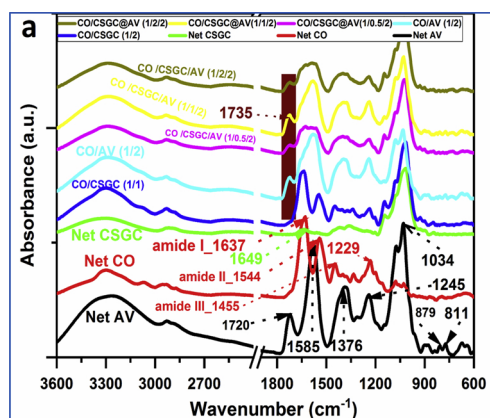

Fig. 5. FTIR of natives and hybrid scaffolds.

Notes: (a) ATR-FTIR of powder aloe vera (AV); native collagen (CO); native chitosan-glucan hollow fibers (CSGC); collagen/chitosan-glucan hollow (CO/CSGC;1/2); collagen/aloe vera (CO/AV; 1/2); collagen/chitosan-glucan hollow encapsulated Aloe Vera using different ratio of CSGC (1/0.5/2, 1/1/2, 1/2/2). (B) XRD of CO/CSGC@AV hybrid scaffolds.

Notes: (b) XR-diffraction of AV; CO; CSGC; CO/AV (1/2); CO/CSGC (1/2); CO/CSGC@AV (1/0.5/2); CO/CSGC@AV (1/1/2); CO/CSGC@AV (1/2/2). (C) TG of CO/CSGC@AV hybrid scaffolds.

Notes: (c) TG of native AV, CO; CSGC and hybrid scaffold CO/AV (1/2); CO/CSGC (1/2); CO/CSGC@AV (1/0.5/2); CO/CSGC@AV (1/1/2); CO/CSGC@AV (1/2/2), respectively. The measurement was conducted under a nitrogen atmosphere at a heating rate of 10 °C/min. (D) DTG of CO/CSGC@AV hybrid scaffolds.

Notes: (d) DTG of native AV, CO; CSGC and hybrid scaffold CO/AV (1/2); CO/CSGC (1/2); CO/CSGC@AV (1/0.5/2); CO/CSGC@AV (1/1/2); CO/CSGC@AV (1/2/2), respectively. The measurement was conducted under a nitrogen atmosphere at a heating rate of 10 °C/min.

presence of minerals like Ca and Zn ions in AC composition could form complex bridge with cationic amino groups of chitosan and attract inside the AV, (iii) The AV solution connected to the CSGC hollow fibers, a capillary force imposed on the solution, and the AV solution flowed in the hollow tube under the impact of capillary force and velocity of the fluidic depends on the concentration of AV (Fig. 2C,c,d) as well as of intermolecular forces between the AV solution and surrounding CSGC surfaces, and (iv) The size of the CSGC hollow quite sufficient bigger than the size of AV, might be surface tension of AV (caused by cohesion within the gel of AV) solution and adhesive property (Scheme 1f) between the AV solution and hollow fiber wall act to propel the solution of AV inside the hollow of CSGC. From the above hypothesis, the complex hollow fiber encapsulated the AV molecules formed ionic interactions with the protonated amino groups inside the hollow fiber.

4.3. Characterization of dressing sheets

For the dressing scaffold system composed of three different components of biomaterials, ATR-FTIR could be used as an effective technique to define the existence of each component. Fig. 5 depict ATR-FTIR, XRD, and TGA-DTG of the composite scaffold. Fig. 5a shows the ATR-FTIR of different dressing scaffold compositions compared with net CO, CSGC, and AV. Native CO scaffold displayed the characteristic absorption bands in region of 3427 cm^{-1} for υ_s stretching vibration of hydroxyl groups, 3279 cm^{-1} amide A, υ_s (NH) stretching vibration of amine group of protein, 3052 cm^{-1} amide B, overtone amide II, 2962 υ_{as} (CH$_3$), asymmetric stretching vibration of methyl group and 2924 υ_{as} (CH$_2$) asymmetric stretching vibration of methylene group in collagen chains (Fig. 5a).

The triple helix structure of collagen I show four absorption peaks at 1637,1544, 1449,1263 cm^{-1} for amide I, II, CH$_3$, and amide III, respectively. The magnitude of absorbance ratios between A$_{1235}$ and A$_{1450}$ peak intensity was 1.13 ± 0.05. from our data we conclude that after acid treatment of collagen there wasn't any denaturized and fully triple-helical confirmation of CO. Our results completely fit with reported results in literature (Gordon et al., 1974; Sylvester et al., 1989; Yannas et al., 1980).

FTIR of AV shows different peaks for amide 1 υ_s (C=O) stretching vibration bands of peptide bond were appeared at 1733 and 1248 cm^{-1} a correspond to carbonyl groups of the organic components of AV and o-acetyl esters and asymmetric and symmetric (C—H) stretching vibration band of methylene groups, respectively. These acetyl groups were necessary for the biological activity of AV, they mask hydrophilic hydroxyl groups thus make the molecule more as the main component of AV (Paichit et al., 2012). Another peak was appeared at 1585 cm^{-1} (C=C groups or from aromatic rings) in main component of AV (Logaranjan et al., 2016). A further peak at 1032 cm^{-1} could owing the

glucan units as well as glucosidic bonds (Silva et al., 2013). The pyranoside ring absorption band at 879 cm^{-1} (C–H ring vibration) and mannose absorption peak at 811 cm^{-1} were also detected for AV.

Chitosan-glucan hollow fiber complex (CSGC) shows different specific peaks at 3320 cm^{-1} correspond to hydroxyl groups on CSGC compositions, beaks at 2930 cm^{-1} related to asymmetrical stretch of methylene groups of the complex, 1649 cm^{-1} was a characteristic vibration for carbonyl groups residual in chitosan chain, 1550 cm^{-1} correspond to primary free amino groups of chitosan chains in the CSGC complex. 1070, and 1040 cm^{-1} were characteristic peaks for ether linkage (−C−O−C−) of chitosan and glucan backbone (Abdel-Mohsen et al., 2016). β-anomeric configuration was signalized by absorption at 890 and 1371 cm^{-1} (Fig. 5a). Chitosan-glucan was extracted from α-chitin form not β-form was confirmed from chitin-glucan and observed that amide I band clearly divided into two peaks at 1653 and 1638 cm^{-1} confirmed chitin-glucan complex was in α-form.

A spectrum of CO/CSGC was depicted in Fig. 5a showed characteristic absorption band in region 3310 cm^{-1} for O−H stretch (low intensity) compared with net CO, peak at 1645 cm^{-1} for CO/CSGC, with low beak intensity compared with 1645 cm^{-1} for native CO, which might be due to the physical interaction between CO and CSGC. The peak of (−C−O−C−) ether linkage at 1040 cm^{-1} was shifted to 1020 cm^{-1} with high intensity compared with net CO, due to the generation of hydrogen bonds between hydroxyl groups of CSGC and CO. The interactions between CO and CSGC might be occurred by the formation of H-bonds. The −OH groups, COO$^-$ and −NH$_2$ groups in CO were capable of forming hydrogen bonds with −OH, −NHCOCH$_3$ and −NH$_2$ groups in chitosan-glucan hollow fiber (Tamate et al., 2018). Additionally, ionic bonds might be formed between CO and CSGC. These molecules were capable of forming a complex with oppositely charged ionic polymers, and these interactions might be formed polycationic/polyanionic complexation, obviously, owing to their same main functional groups with thermal stability (Fig. 5c, d).

Spectra of collagen/chitosan-glucan/ aloe vera (CO/CSGC@AV) with different ratios of CSGC (1/0.5/2, 1/1/2, 1/2/2) were shown in Fig. 5a. CO/CSGC@AV depicted a shifting peak from 3314 cm^{-1} to 3281 cm^{-1} due to the hydrogen bonds that were generated between the functional groups of AV and (−OH, −COOH and −NH$_2$) groups in CO and/or CSGC hollow fiber. A new peak was appeared at 1735 cm^{-1} and the intensity of this peak was increased by increasing the ratio of CSGC component, could be due to the formation of amide reaction (Belbachir et al., 2009; Lee et al., 2017).

From the above results, native collagen scaffold still exhibits all the characteristic peaks of the triple helical structure of neat collagen. The spectra of CSGC Fig. 3a proved that the chitosan-glucan was extracted from α-chitin by observing that the amide I band clearly divided into two peaks at 1653 and 1638 cm^{-1}, confirming the α-form. Analysis of the ATR-FTIR spectra suggested that fabricating the 3D scaffolds did not create any significant change in the molecular structure of any of the components.

Fig. 5b shows the X-ray diffraction (XRD) patterns of dressing scaffold. The diffraction curves of all materials CO, CSGC and fabricated scaffold with different ratios of CSGC devolved exhibited mainly amorphous patterns with small crystalline fraction except native AV. Powder AV demonstrated the peaks observed for native AV at 28.2°, 40.5°, 50.1°, 57.5° and 66.6° corresponded to Ca^{2+} as well as the organic polysaccharides (glucomannan, a mannose-rich polysaccharide, and gibberellin) as the main components of AV. CO scaffold shows mainly amorphous patterned with small peak intensity at 2θ = 7.5° and other broad peak appeared at 2θ = 18–22° indicated a tendency to the structural organization of collagen triple helix structure. We further investigated the semi-crystalline structure of our new hollow fibers scaffold using X-ray diffraction (XRD). In nature, chitin occurs as supramolecular semi-crystalline and exists in two major distinct polymorphs: α-chitin (orthorhombic) and β-chitin (monoclinic). These chitin crystals have different molecular conformations (i.e., antiparallel

for α-chitin vs parallel for β-chitin) with dissimilar hydrogen-bond densities, which could be intuitively distinguished through ATR-FTIR and XRD analyses; each material presents different characteristic peaks. As revealed in the FTIR spectra (Fig. 3a), β-chitin has a single broad absorption peak at around 1630 cm^{-1} because of the intramolecular C=O···HO hydrogen bonds. Meanwhile, α-chitin was characterized by split peaks at 1653 and 1638 cm^{-1} (ATR-FTIR; Fig. 5a) which raised from the antiparallel molecular arrangement whereby the intramolecular C=O···HO hydrogen bonds were simultaneously engaged with the inter-sheet C=O···HN hydrogen bonds (Jin et al., 2016; Kim et al., 2017).

For plain CSGC scaffold exhibited mainly semi-crystalline pattern with three different phases at 2θ = 9.4, 17.9 and 21.1°, these three peaks corresponded to three components of the complex (chitin, chitosan and branched glucan). Due to the degree of deacetylation of chitosan was only 50 % (DDA = 50 %), and chitin was 50 %. These results obviously indicate that the residual chitin in the chitosan-glucan complex was in α-form structure. In collagen/aloe vera scaffold with ratio (1/2) showed only one broad beak for collagen at 2θ around 20–25° as well as two beaks related to AV in the same position compared with native AV at 2θ = 28.2, 40.3° indicated that there wasn't signification interaction between CO and AV, was only physically hydrogen bond generated between functional groups of CO and AV as well as in interaction was on the surface of collagen scaffold (Fig. 5b).

The XRD of dressing scaffold with different ratios of hollow fiber complex represented in Fig. 5b. CO/CSGC@AV (1/0.5/2; 1/1/2; 1/2/2) shows different pattern peaks related to the composition of the scaffolds. Collagen peak at 2θ = 7.5° with lower peak intensity, might be due to strong physical interaction with CSGC and/ or AV functional groups. Peak related to complex at 2θ = 9.4° (chitin part) was observed with very low intensity compared with native complex, but the intensity of this peak was raised using high ratio of the complex to CO. Amorphous two peaks of chitosan/glucan components in complex appeared 2θ = 17.9° and 21.1° were visualized in scaffold also with lower intensity. Interestingly, peaks correspond to AV were appeared in the same position in dressing scaffold with low intensity as compared with native AV.

From x-ray diffraction patterns (Fig. 5b), dressing scaffold was synthesized without significant changes in the chemical structure of the scaffold components and the interactions between collagen, chitin/chitosan-glucan hollow fibers complex and aloe vera were only on the surface and between the functional groups like (carboxylic, amino, hydroxyl) in CO, (amino, acetamide, hydroxyl) in CSGC, and (acetyl, hydroxyl, carbonyl) as well as residual metals in AV.

The thermal stability of the dressing sheets was measured using Thermogravimetric analysis (TGA) for the experimental samples CO, AV, CSGC, CO/CSGC (1/2), CO/AV (1/2), CO/CSGC@AV (1/0.5/2; 1/1/2; and ½/2) as represented in Fig. 5c, d and correspond thermal degradation values were displayed in table S2 (supporting information). From TG curves, we determined the mass loss during the heating process from 25 to 800 °C. The temperature of maximum speed process (T$_{max}$) was determined from the maximum on DTG curve (Table S2; supporting information). For CO scaffold a weight loss from room temperature to 100 °C is 4.5 % (stage I), probably resulting from the evaporation of non-bounded water absorbed into the surface of triple helix collagen structure. The second stage of collagen scaffold appeared at maximum decomposition temperature at 298 °C (stage II, Fig. 5c, d), which might be due to water bounded and small molecules liberated after degradation of helix structure of collagen to small monomer molecules (Udhayakumar et al., 2017).

The TG/DTG of chitosan-glucan hollow fiber (CSGC) was shown in Fig. 5c, d with three different decomposition stages. The first stage was appeared at 58 °C, due to the evaporation of water physically connected with a complex chain. In stage II, the complex mass loss about 29 % at 294 °C, might be due to cleaving the chain bonds β-(1-4, 1-3, 1-6) between the different components of the hollow fiber complex (chitin,

chitosan, glucan). The third stage beak was appeared at a maximum decomposing temperature about 331 °C with mass loss 66.4 %, due to the decomposition of linear and branched glucose chains, acetyl glucosamine and *N*- acetyl glucosamine (Abdel-Mohsen et al., 2016). Pure aloe vera (AV) shows five different decomposition peaks at 110, 178, 299, and 382 °C for 3.2, 11.5, 34.1, and 43.8 % mass loss, respectively.

Different decomposition stages of AV, related to the multi-components of aloe vera structure such as vitamins, enzymes, minerals, sugars, anthraquinone, fatty acid, and hormones (Silva et al., 2013; Surjushe et al., 2008). The dressing scaffold CO/CSGC@AV with different mass ratio of CSGC (0.5, 1, 2) and a constant ratio of AV (2) was shown in Fig. 5c, d and Table S2 (supporting information). Interestingly, the combination of CO, CSGC, and AV enhanced the thermal stability of scaffold compared with net CO scaffold showed weight loss only 23 % up to 250 °C that was lower compared to other scaffolds. From the

thermogravimetric data, we can conclude that different compositions of the CSGC did not show significant changes in the thermal stability of the scaffold. The addition of the AV improved the thermal stability slightly, due to the strong interaction between collagen and hollow fibers in the presence of aloe vera.

4.4. Swellability, degradability and mechanical properties of dressing sheets

Swelling rate (%) of different dressing scaffold engendered with/without aloe vera at different intervals of phosphate buffer solution (PBS) contact time was depicted in Fig. 6a. the swelling percentage (g/g) of collagen (CO) scaffold was rapidly increased up to (25 g/g) of CO in the initial 2.5 h, due to the hydrophilic character of collagen chains, then decreased up to (15 g/g) after 120 h. After 5 days of immersing of collagen in PBS buffer at 37 °C, the scaffold started to hydrolysis to
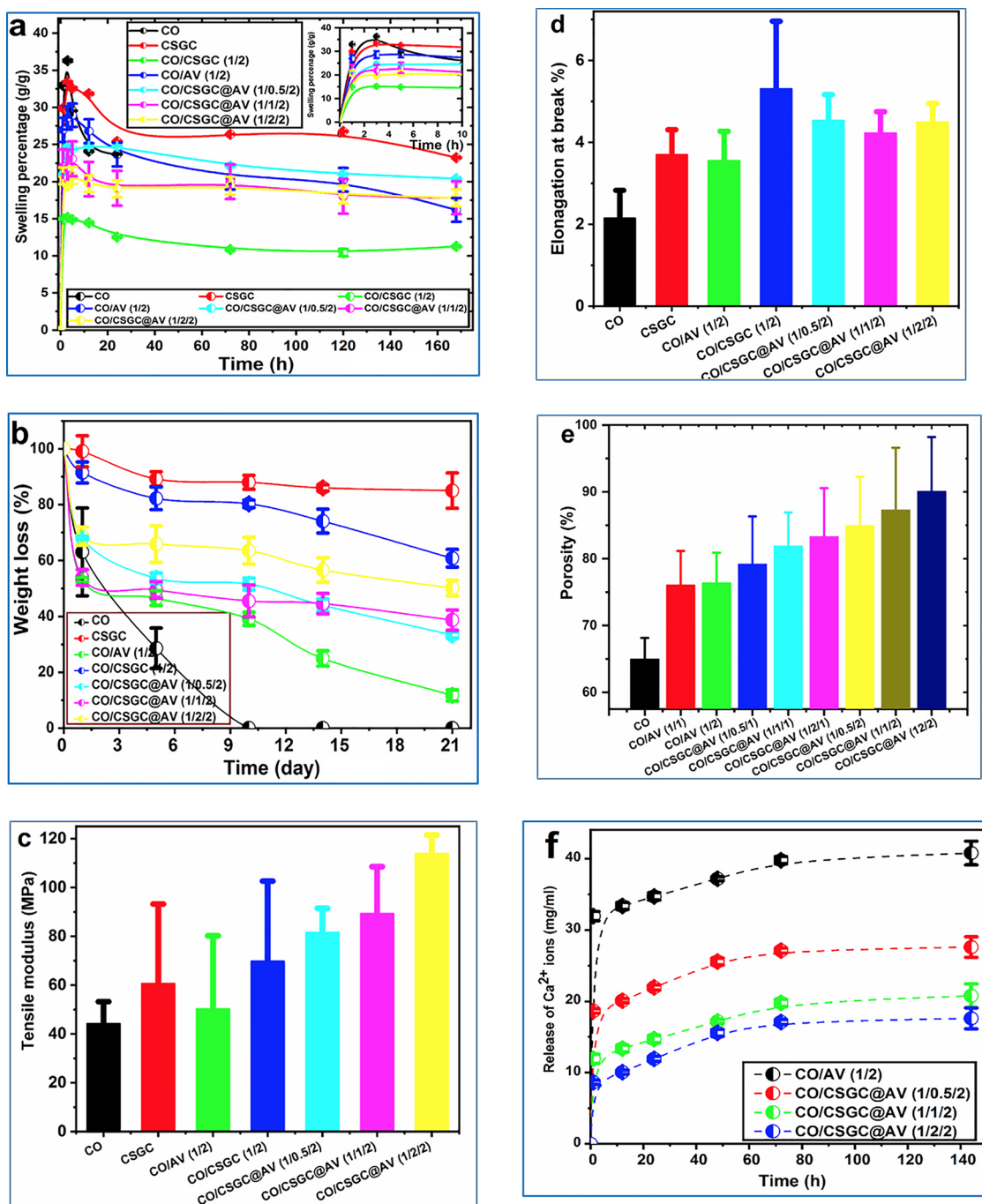
(caption on next page)

Fig. 6. (a) Swelling percentage (g/g) of dressing scaffold.

Notes: Water uptake of native collagen (CO); native chitosan-glucan hollow fibers (CSGC); collagen/aloe vera (CO/AV; 1/2); collagen/chitosan-glucan hollow (CO/CSGC; 1/2); collagen/chitosan-glucan hollow/Aloe Vera (CO/**CSGC**@AV; 1/0.5/2); collagen/chitosan-glucan hollow/aloe vera (CO/CSGC@AV; 1/1/2); collagen/chitosan-glucan hollow/Aloe Vera (CO/CSGC@AV; 1/2/2); The samples were measured three times (n = 3), using PBS at 37 ^{0}C at different time (0.5, 3, 5, 12, 24, 48, 72, 120, and after 168 h). (B) Representative hydrolytic degradation of dressing scaffold.

Notes: Weight loss percentage as a function of time for pure native CO; CSGC; CO/AV (1/2); CO/CSGC (1/2); CO/CSGC@AV; (1/0.5/2); CO/CSGC@AV (1/1/2); CO/CSGC@AV (1/2/2), the samples were measured three times (n = 3), using PBS at 37 ^{0}C at different time (1, 3, 7, 14, and 21d). (c) Tensile strength of native hybrid scaffold.

Notes: Tensile modulus of native CO; native CSGC; CO/AV (1/2); CO/CSGC (1/2); CO/CSGC@AV (1/0.5/2); CO/CSGC@AV (1/1/2); CO/CSGC@AV (1/2/2). (D) Elongation at break of native and hybrid scaffold.

Notes: Elongation at break of native (CO); native CSGC; CO/AV (1/2); CO/CSGC (1/2); CO/CSGC@AV (1/0.5/2); CO/CSGC@AV (1/1/2); CO/CSGC@AV (1/2/2), The samples were measured three times (n = 5) for (±) SD. (E) Porosity of natives and dressing scaffold.

Notes: Porosity measurements of hybrid scaffold using different concentrations of CSGC and AV. Natives collagen (CO), chitosan-glucan complex hollow fibers (CSGC), collagen/aloe vera (CO/AV; 1/1), collagen/aloe vera (CO/AV; 1/2), collagen/chitosan-glucan complex/ aloe vera (CO/CSGC@AV; 1/0.5/1), collagen/chitosan-glucan complex/ aloe vera (CO/CSGC@AV; 1/1/1), collagen/chitosan-glucan complex/ aloe vera (CO/CSGC@AV; 1/2/1), collagen/chitosan-glucan complex/ aloe vera (CO/CSGC@AV; 1/0.5/2), collagen/chitosan-glucan complex/ aloe vera (CO/CSGC@AV; 1/1/2), and collagen/chitosan-glucan complex/ aloe vera (CO/CSGC@AV; 1/2/2). (F) Representative release of calcium ions from dressing scaffold.

Notes: (f) Release measurement of calcium ions in saline solution (n = 5 for the test of Ca2$^+$ contains). collagen/aloe vera (CO/AV; 1/2), collagen/chitosan-glucan complex/ aloe vera (CO/CSGC@AV; 1/0.5/2), collagen/chitosan-glucan complex/ aloe vera (CO/CSGC@AV; 1/1/2), and collagen/chitosan-glucan complex/ aloe vera (CO/CSGC@AV; 1/2/2).

small pieces inside the solution but not completely hydrolysis. Chitosan-glucan hollow fiber scaffold show the highest water absorption scaffold and the swelling percent (SP) was rapidly increased to (30 g/g) in the initial 4 h interval and reached a saturation of (35 g/g), then was constant absorption after 25 h. after 1 day of swelling, CSGC scaffold, the SP (%) was slightly decreased but still highly water absorption capacity compared with the other scaffold. The higher swelling capacity of CSGC related to the hydrophilic properties of the complex (a lot of hydroxyl in chitin, chitosan, glucan units, and amino groups) as well as the hollow structure shape of the fiber that could trap water inside the hollow structure. Scaffold CO/CSGC (1/2) ratio was the lowest water absorption capacity compared with CO, CSGC and another scaffold, and the SP (%) increase in the first 25 h with constant swelling percent (15 g/g), after was slightly decreased up to 6 days of immersing in PBS.

The lower water absorption of CO/CSGC, related to the strong physical interactions on the surface of CO or between the matrix layers (physically interact between the different groups, −COO, NH$_2$, −OH, and −NHCOCH$_3$) prevented CO to absorb the water molecules (Fig. 6a). The swelling percentage (%) of collagen/aloe vera scaffold (1/2) was higher than the native collagen scaffold in the first 3 h (27 g/g), due to the hydrophilic properties of AV (presence of polysaccharide in the chemical composition of aloe vera). The effect of concentration of CSGC on the swelling percentage of a hybrid scaffold in the presence of AV (1 %) was depicted in Fig. 6a. increase the mass ratio of CSGC in scaffold was increased the swelling percent with a constant value up to 160 h. Due to the hydrophilic characters of CSGC, AV, and CO. At equilibrium of swelling, the composite hybrid scaffold contains (1/2/2) ratio between CO, CSGC, AV has the highest swelling percentage. Based on the above observation, the optimum concentration of CSGC to be used in the hybrid scaffold was fixed as 1 %. High water/ fluid holding capacity of such a scaffold was very important for cell adhesion, proliferation, and growths. The wide range of swelling ratios obtained for CO/CSGC@AV hybrid scaffold is advantageous for tissue engineering applications since they could finely be tuned based on their final application. In addition, the increased swelling of the scaffold at a higher ratio of CSGC can enhance their cell adherence and viability of cells *in-vivo*. For wound closure, this could greatly accelerate healing by providing high oxygen and exudate permeable and flexible wound seal (Annabi et al., 2017; Peppas et al., 2006). Results revealed that the *in-vitro* degradation rate of native and hybrid scaffolds depends on the ratio of complex to collagen

Another technical advantage of scaffold used for wound closure applications was their control degradation in wet environments. Therefore, we aimed to investigate the *in-vitro* degradation of a hybrid scaffold under physiological body application. Results revealed that the in-vitro degradation rate of native and hybrid scaffold depends on the

ratio of complex to collagen and final scaffold concentrations. Fig. 6b shows the weight loss percent (%) of different hybrid scaffolds was measured under physiological conditions (PBS pH = 7.5; 37 °C) after 1, 3, 5, 10, 14, and 21 days of immersed in PBS. Collagen scaffold was significant decrease the mass after 6 days (mass loss = 40 %), and in day ten was completely degraded in PBS (mass loss = 100 %), due to CO triple helix would be gain access to the cleavage site by binding to the metal attachment domains along the chains followed by unwinding of the triple helix and then destroyed the collagen chains (Foglia et al., 2013; Rajan et al., 2007).

Native chitosan-glucan hollow fiber scaffold was more stable with less degree of degradation compared with other scaffolds. After 1 day of immersed the mass loss was only 0.9 %, after 10 days the mass loss (%) was 12 % after incubation at 37 °C. After 21 days of seeding in PBS, the mass loss was only 15 %. This might be a strong physical and chemical interaction between the different components chain in the complex (chitin, chitosan, glucan). Scaffold engineered from CO/CSGC@AV incubated in PBS using a different ratio of CSGC exhibited lower degradability compared with native CO scaffold. In addition, the rate of degradability decreased with increased of CSGC concentration. The incorporation of AV resulted in no significant changes in the degradability rate of the composite hybrid scaffold (Fig. 6b, Table S3). In contrast, previous studies have shown that the encapsulated/ incorporations of antimicrobial agents in proteins-based biomaterials, could significantly alter the degradability percentage of the obtained biomaterials (Annabi et al., 2017; Kumar et al., 2012).

Mechanical properties of CO/CSGC@AV dressing scaffold were characterized through tensile tests. The tensile tests on the hybrid scaffold revealed that the tensile modulus (Fig. 6c) and elongation at break (Fig. 6d) of the fabricated scaffolds could be modulated by varying the collagen/ chitosan-glucan hollow fiber ratio in presence/ absence of aloe vera and the total polymer concentration. The tensile modulus of the hybrid scaffold increased consistently from 44.2 ± 8.9 kPa (native CO) to 69.7 ± 12.8 kPa (CO/CSGC; 1/2) and 50. ± 19.9 (CO/AV; 1/2) to 81.5 ± 9.8, 89.3 ± 19.2, 113.8 ± 7.6 kPa for CO/CSGC@AV (1/0.5/2; 1/1/2; 1/2/2), respectively. Elastic modulus of the scaffold was significantly increased in presence of CSGC and AV compared with native CO, due to the hydrogen/ionic interactions (presence of Ca^{2+} and Zn^{2+} in composition of AV) between their functional groups *via* hydroxyl, amino, and acetamide carboxyl of CO, CSGC and AV as well as between carboxylic groups/amino groups of CO/CSGC and metal ions (Ca^{2+} and Zn^{2+}) components of AV. These ionic interactions served as ionic cross-linker for hybrid scaffolds. In Fig. 6d, the elongation at break of hybrid scaffold (%) increased with increased concentration of CSGC (0.25, 0.5, and 1 %) in presence of AV suggested that the CSGC and AV enhanced

the elasticity of the scaffold and resulted in more stretchable scaffold.

The porosity of the engineered scaffold was shown in Fig. 6e. The porosity (%) of plain CO scaffold, CO/AV (1/2), CO/CSGC (1/2) CO/ CSGC@AV (1/0.5/1;1/1/1;1/2/2; 1/0.5/2; 1/1/2; and 1/2/2) was 65 ± 3.14, 76.1 ± 5.05, 76.4 ± 4.49, 79.2 ± 7.12, 81.9 ± 5.02, 83.3 ± 7.26, 85 ± 7.26, 87.3 ± 9.3, and 90.1 ± 8.1 (%), respectively. The porosity was slightly increased with increasing the concentrations of CSGC from 65 to 90 %, with small changes in pore size and pore architecture. Enhancement in porosity could improve the water absorption of a hybrid scaffold and could easily absorb culture medium to facility the cell migration, adhesive and proliferation into and on the surface of the hybrid scaffolds.

Since one of the aims of this study to demonstrate the possibility of different agents loaded into the hollow fiber and control release of each agent for biomedical application. Regarding our target, aloe vera was used as as a drug model and investigated the release of calcium ions (one of AV component) by using ICP-MS. CO/AV (1/2) scaffold showed high release percentage at the same time compared with scaffold contain hollow fiber (Fig. 6f). The concentration of calcium ions released in the presence of different contractions of CSGC hollow fibers was smaller without CSGC. The release of calcium ion was decreased by increasing the concentration of complex (form 0.25–1 wt. %) into the dressing scaffold. This owing to the interactions (ionic, physical, electrostatic) between calcium ions and functional groups of CSGC (amino, amide, hydroxyl) (Arias & Fernández, 2008; Li et al., 2012; Qi et al., 2018) which could reduce the release percentage of calcium from the dressing scaffold (Fig. 6f). The loading capacity of AV was increased with increasing the concentrations of CSGC (increase the encapsulated Ca^{2+}) into the hollow structure (Fig. 4 k, l). This means that the complex strongly interacts with AV components and reduced the release percentage of calcium ions. From Fig. 6 we can conclude that the presence of CSGC (different concentrations) had a significant influence on hydrogel physical properties (swelling hydrolytic degradation and porosity) mechanical properties as well as a promising material to control release different types of drugs.

5. Conclusions

A novel dressing scaffold from collagen/chitosan-glucan complex hollow fibers in presence or absence aloe vera (CO/CSGC@AV) was fabricated by freeze-dried technique for the first time with enhanced the physical, chemical and mechanical properties of collagen scaffold. CSGC hollow fibers were extracted from *Schizophyllum commune* with controlled the degree of deacetylation (DDA 50–100 %), fiber diameter (2.5 ± 0.5 μm) and hollow size (800 ± 200 nm) by green chemical treatment of native mycelium. The degree of deacetylation and surface morphology of CSGC hollow fiber was confirmed and visualized by solid-NMR and SEM spectroscopy. CO/CSGC@AV fabricated with different concentrations of CSGC (0.25, 0.5 1 wt. %) show significantly enhanced swelling percentage and stability of scaffold in the presence of AV for up to three weeks compared with native CO. The pore size and porosity of CO/CSGC@AV exhibited enhanced in the presence of high ratio f CSGC and concentration independent of AV. CSGC complex hollow fibers could control the released of calcium ions from the scaffold matrix compared with dressing scaffold in absence of CSGC. We believe that the new CO/CSGC@AV hybrid dressing scaffold opens a new approach of application in biomedical areas that could be employed for soft tissue engineering especially for skin wound healing and drug delivery application.

Authors contribution sections

Author Contributions: Conceptualization, Methodology A.M.A; R.M.A; I.K; L.K; Z.S; M.Z; R.P; J.B; J.J. Writing original manuscript, A.M.A; R.M.A; I.K; L.K; Z.S; M.Z; R.P; J.B; J.J

Writing-Review, and editing manuscript A.M.A; R.M.A; I.K; L.K; Z.S;

M.Z; R.P; J.B; J.J. Funding acquisition.

Appendix A. Supplementary data

Supplementary material related to this article can be found, in the online version, at doi:https://doi.org/10.1016/j.carbpol.2019.115708.

References

Abdel-Mohsen, A. M., Jancar, J., Massoud, D., Fohlerova, Z., Elhadidy, H., Spotz, Z., & Hebeish, A. (2016). Novel chitin/chitosan-glucan wound dressing: Isolation, characterization, antibacterial activity and wound healing properties. *International Journal of Pharmaceutics, 510*(1), 86–99.

Annabi, N., Rana, D., Shirzaei Sani, E., Portillo-Lara, R., Gifford, J. L., Fares, M. M., & Weiss, A. S. (2017). Engineering a sprayable and elastic hydrogel adhesive with antimicrobial properties for wound healing. *Biomaterials, 139*, 229–243.

Arias, J. L., & Fernández, M. S. (2008). Polysaccharides and proteoglycans in calcium carbonate-based biomineralization. *Chemical Reviews, 108*(11), 4475–4482.

Ashraf, J. M., Ansari, M. A., Khan, H. M., Alzohairy, M. A., & Choi, I. (2016). Green synthesis of silver nanoparticles and characterization of their inhibitory effects on AGEs formation using biophysical techniques. *Scientific Reports, 6*, 20414.

Bedford, N. M., Dickerson, M. B., Drummy, L. F., Koerner, H., Singh, K. M., Vasudev, M. C., & Steckl, A. J. (2012). Nanofiber-based bulk-heterojunction organic solar cells using coaxial electrospinning. *Advanced Energy Materials, 2*(9), 1136–1144.

Belbachir, K., Noreen, R., Gouspillou, G., & Petibois, C. (2009). Collagen types analysis and differentiation by FTIR spectroscopy. *Analytical and Bioanalytical Chemistry, 395*(3), 829–837.

Brus, J. (2000). Heating of samples induced by fast magic-angle spinning. *Solid State Nuclear Magnetic Resonance, 16*(3), 151–160.

Burkatovskaya, M., Tegos, G. P., Swietlik, E., Demidova, T. N., P Castano, A., & Hamblin, M. R. (2006). Use of chitosan bandage to prevent fatal infections developing from highly contaminated wounds in mice. *Biomaterials, 27*(22), 4157–4164.

Doillon, C. J., & Silver, F. H. (1986). Collagen-based wound dressing: Effects of hyaluronic acid and firponectin on wound healing. *Biomaterials, 7*(1), 3–8.

Doillon, C. J., Silver, F. H., & Berg, R. A. (1987). Fibroblast growth on a porous collagen sponge containing hyaluronic acid and fibronectin. *Biomaterials, 8*(3), 195–200.

Duran, A., Cabib, E., & Bowers, B. (1979). Chitin synthetase distribution on the yeast plasma membrane. *Science, 203*(4378), 363–365.

Dzenis, Y. (2004). Spinning continuous fibers for nanotechnology. *Science, 304*(5679), 1917–1919.

Foglia, M. L., Camporotondi, D. E., Alvarez, G. S., Heinemann, S., Hanke, T., Perez, C. J., & Desimone, M. F. (2013). A new method for the preparation of biocompatible silica coated-collagen hydrogels. *Journal of Materials Chemistry B, 1*(45), 6283–6290.

François, J. M. (2007). A simple method for quantitative determination of polysaccharides in fungal cell walls. *Nature Protocols, 1*, 2995.

Fujioka, K., Takada, Y., Sato, S., & Miyata, T. (1995). Novel delivery system for proteins using collagen as a carrier material: The minipellet. *Journal of Controlled Release, 33*(2), 307–315.

Geißel, B., Loiko, V., Klugherz, I., Zhu, Z., Wagener, N., Kurzai, O., & Wagener, J. (2018). Azole-induced cell wall carbohydrate patches kill Aspergillus fumigatus. *Nature Communications, 9*(1), 3098.

Gentleman, E., Lay, A. N., Dickerson, D. A., Nauman, E. A., Livesay, G. A., & Dee, K. C. (2003). Mechanical characterization of collagen fibers and scaffolds for tissue engineering. *Biomaterials, 24*(21), 3805–3813.

Ghodbane, S. A., & Dunn, M. G. (2016). Physical and mechanical properties of cross-linked type I collagen scaffolds derived from bovine, porcine, and ovine tendons. *Journal of Biomedical Materials Research Part A, 104*(11), 2685–2692.

Gordon, P. L., Huang, C., Lord, R. C., & Yannas, I. V. (1974). The far-infrared Spectrum of collagen. *Macromolecules, 7*(6), 954–956.

Halaui, R., Zussman, E., Khalfin, R., Semiat, R., & Cohen, Y. (2017). Polymeric microtubes for water filtration by co-axial electrospinning technique. *Polymers for Advanced Technologies, 28*(5), 570–582.

Han, D., Sherman, S., Filocamo, S., & Steckl, A. J. (2017). Long-term antimicrobial effect of nisin released from electrospun triaxial fiber membranes. *Acta Biomaterialia, 53*, 242–249.

Hsu, S.-h., Whu, S. W., Tsai, C.-L., Wu, Y.-H., Chen, H.-W., & Hsieh, K.-H. (2004). Chitosan as scaffold materials: Effects of molecular weight and degree of deacetylation. *Journal of Polymer Research, 11*(2), 141–147.

HUMFELD, H. (1948). The production of mushroom mycelium in submerged culture. *Science, 107*(2780), 373.

Irimia-Vladu, M. (2014). "Green" electronics: biodegradable and biocompatible materials and devices for sustainable future. *Chemical Society Reviews, 43*(2), 588–610.

Jiang, H., Wang, L., & Zhu, K. (2014). Coaxial electrospinning for encapsulation and controlled release of fragile water-soluble bioactive agents. *Journal of Controlled*

Release, 193, 296–303.

Jin, J., Lee, D., Im, H.-G., Han, Y. C., Jeong, E. G., Rolandi, M., & Bae, B.-S. (2016). Chitin nanofiber transparent paper for flexible green electronics. *Advanced Materials, 28*(26), 5169–5175.

Jorge-Herrero, E., Fernández, P., Turnay, J., Olmo, N., Calero, P., García, R., & Castillo-Olivares, J. L. (1999). Influence of different chemical cross-linking treatments on the properties of bovine pericardium and collagen. *Biomaterials, 20*(6), 539–545.

Kang, X., Kirui, A., Muszyński, A., Widanage, M. C. D., Chen, A., Azadi, P., & Wang, T. (2018). Molecular architecture of fungal cell walls revealed by solid-state NMR. *Nature Communications, 9*(1), 2747.

Khor, E. (1997). Methods for the treatment of collagenous tissues for bioprostheses. *Biomaterials, 18*(2), 95–105.

Kim, J.-K., Kim, D. H., Joo, S. H., Choi, B., Cha, A., Kim, K. M., & Jin, J. (2017). Hierarchical chitin fibers with aligned nanofibrillar architectures: A nonwoven-mat separator for Lithium metal batteries. *ACS Nano, 11*(6), 6114–6121.

Kim, Y.-T., Kim, E.-H., Cheong, C., Williams, D. L., Kim, C.-W., & Lim, S.-T. (2000). Structural characterization of β-d-(1→3, 1→6)-linked glucans using NMR spectroscopy. *Carbohydrate Research, 328*(3), 331–341.

Kirichenko, A. K., Bolshakov, I. N., Ali-Rizal, A. E., & Vlasov, A. A. (2013). Morphological study of burn wound healing with the use of collagen-chitosan wound dressing. *Bulletin of Experimental Biology and Medicine, 154*(5), 692–696.

Kontturi, E., Laaksonen, P., Linder, M. B., Nonappa, Gröschel, A. H., Rojas, O. J., & Ikkala, O. (2018). Advanced Materials through Assembly of Nanocelluloses. *Advanced Materials, 30*(24), 1703779.

Kumar, M. N. V. R., Muzzarelli, R. A. A., Muzzarelli, C., Sashiwa, H., & Domb, A. J. (2004). Chitosan chemistry and pharmaceutical perspectives. *Chemical Reviews, 104*(12), 6017–6084.

Kumar, P. T. S., Lakshmanan, V.-K., Biswas, R., Nair, S. V., & Jayakumar, R. (2012). Synthesis and biological evaluation of chitin Hydrogel/Nano ZnO composite bandage as antibacterial wound dressing. *Journal of Biomedical Nanotechnology, 8*(6), 891–900.

Lee, Y.-C., Chiang, C.-C., Huang, P.-Y., Chung, C.-Y., Huang, T. D., Wang, C.-C., & Reisz, R. R. (2017). Evidence of preserved collagen in an Early Jurassic sauropodomorph dinosaur revealed by synchrotron FTIR microspectroscopy. *Nature Communications, 8*, 14220.

Li, Y., Rodrigues, J., & Tomás, H. (2012). Injectable and biodegradable hydrogels: Gelation, biodegradation and biomedical applications. *Chemical Society Reviews, 41*(6), 2193–2221.

Liang, D., Lu, Z., Yang, H., Gao, J., & Chen, R. (2016). Novel asymmetric wettable AgNPs/Chitosan wound dressing: In vitro and in vivo evaluation. *ACS Applied Materials & Interfaces, 8*(6), 3958–3968.

Liu, Z., Ge, X., Lu, Y., Dong, S., Zhao, Y., & Zeng, M. (2012). Effects of chitosan molecular weight and degree of deacetylation on the properties of gelatine-based films. *Food Hydrocolloids, 26*(1), 311–317.

Logaranjan, K., Raiza, A. J., Gopinath, S. C. B., Chen, Y., & Pandian, K. (2016). Shape- and size-controlled synthesis of silver nanoparticles using Aloe vera plant extract and their antimicrobial activity. *Nanoscale Research Letters, 11*(1), 520.

Marelli, B., Le Nihouannen, D., Hacking, S. A., Tran, S., Li, J., Murshed, M., & Barralet, J. E. (2015). Newly identified interfibrillar collagen crosslinking suppresses cell proliferation and remodelling. *Biomaterials, 54*(0), 126–135.

Marinucci, L., Lilli, C., Guerra, M., Belcastro, S., Becchetti, E., Stabellini, G., & Locci, P. (2003). Biocompatibility of collagen membranes crosslinked with glutaraldehyde or diphenylphosphoryl azide: An in vitro study. *Journal of Biomedical Materials Research Part A, 67A*(2), 504–509.

Marone, P. A., Lau, F. C., Gupta, R. C., Bagchi, M., & Bagchi, D. (2010). Safety and toxicological evaluation of undenatured type II collagen. *Toxicology Mechanisms and Methods, 20*(4), 175–189.

Merrett, K., Liu, W., Mitra, D., Camm, K. D., McLaughlin, C. R., Liu, Y., & Fogg, D. E. (2009). Synthetic neoglycopolymer-recombinant human collagen hybrids as biomimetic crosslinking agents in corneal tissue engineering. *Biomaterials, 30*(29), 5403–5408.

Mijatović, S., Bramanti, A., Nicoletti, F., Fagone, P., Kaluđerović, G. N., & Maksimović-Ivanić, D. (2018). Naturally occurring compounds in differentiation based therapy of cancer. *Biotechnology Advances, 36*(6), 1622–1632.

Mohammadi, A., Shojaosadati, S. A., Tehrani, H. J., Mousavi, S. M., Saleh, T., & Khorasani, A. C. (2018). Schizophyllan production by newly isolated fungus Schizophyllum commune IBRC-M 30213: Optimization of culture medium using response surface methodology. *Annals of Microbiology, 68*(1), 47–62.

Nakashima, K., Kimura, S., Ogawa, Y., Watanabe, S., Soma, S., Kaneko, T., & Satoh, N. (2018). Chitin-based barrier immunity and its loss predated mucus-colonization by indigenous gut microbiota. *Nature Communications, 9*(1), 3402.

Osborne, C. S., Reid, W. H., & Grant, M. H. (1999). Investigation into the biological stability of collagen/chondroitin-6-sulphate gels and their contraction by fibroblasts and keratinocytes: The effect of crosslinking agents and diamines. *Biomaterials, 20*(3), 283–290.

Paichit, I., Atchariya, F., Anan, O., Anuphan, S., & Jarupa, V. (2012). Effects of the blended fibroin/aloe gel film on wound healing in streptozotocin-induced diabetic rats. *Biomedical Materials, 7*(3), 035008.

Peppas, N. A., Hilt, J. Z., Khademhosseini, A., & Langer, R. (2006). Hydrogels in biology and medicine: From molecular principles to bionanotechnology. *Advanced Materials,*

18(11), 1345–1360.

Qi, C., Lin, J., Fu, L.-H., & Huang, P. (2018). Calcium-based biomaterials for diagnosis, treatment, and theranostics. *Chemical Society Reviews, 47*(2), 357–403.

Rahman, S., Carter, P., & Bhattarai, N. (2017). Aloe Vera for tissue engineering applications. *Journal of Functional Biomaterials, 8*(1), 6.

Rajan, N., Habermehl, J., Coté, M.-F., Doillon, C. J., & Mantovani, D. (2007). Preparation of ready-to-use, storable and reconstituted type I collagen from rat tail tendon for tissue engineering applications. *Nature Protocols, 1*, 2753.

Rezaii, M., Oryan, S., & Javeri, A. (2019). Curcumin nanoparticles incorporated collagen-chitosan scaffold promotes cutaneous wound healing through regulation of TGF-β1/Smad7 gene expression. *Materials Science and Engineering C, 98*, 347–357.

Roca, C., Chagas, B., Farinha, I., Freitas, F., Mafra, L., Aguiar, F., & Reis, M. A. M. (2012). Production of yeast chitin–glucan complex from biodiesel industry byproduct. *Process Biochemistry, 47*(11), 1670–1675.

Ruiz-Herrera, J., & Bartnicki-Garcia, S. (1974). Synthesis of Cell Wall Microfibrils in vitro by a "Soluble" Chitin Synthetase from Mucor rouxii. *Science, 186*(4161), 357–359.

Saito, M., & Marumo, K. (2010). Collagen cross-links as a determinant of bone quality: A possible explanation for bone fragility in aging, osteoporosis, and diabetes mellitus. *Osteoporosis International, 21*(2), 195–214.

Silva, S. S., Popa, E. G., Gomes, M. E., Cerqueira, M., Marques, A. P., Caridade, S. G., & Reis, R. L. (2013). An investigation of the potential application of chitosan/aloe-based membranes for regenerative medicine. *Acta Biomaterialia, 9*(6), 6790–6797.

Skorik, Y. A., Pestov, A. V., & Yatluk, Y. G. (2010). Evaluation of various chitin-glucan derivatives from Aspergillus niger as transition metal adsorbents. *Bioresource Technology, 101*(6), 1769–1775.

Spěváček, J., & Brus, J. (2008). Solid-state NMR studies of polysaccharide systems. *Macromolecular Symposia, 265*(1), 69–76.

Sung, H.-W., Hsu, H.-L., Shih, C.-C., & Lin, D.-S. (1996). Cross-linking characteristics of biological tissues fixed with monofunctional or multifunctional epoxy compounds. *Biomaterials, 17*(14), 1405–1410.

Sung, K. H., Josewski, J., Dübel, S., Blankenfeldt, W., & Rau, U. (2018). Structural insights into antigen recognition of an anti-β-(1,6)-β-(1,3)-D-glucan antibody. *Scientific Reports, 8*(1), 13652.

Surjushe, A., Vasani, R., & Saple, D. G. (2008). Aloe Vera: A Short Review. *Indian Journal of Dermatology, 53*(4), 163–166.

Sylvester, M. F., Yannas, I. V., Salzman, E. W., & Forbes, M. J. (1989). Collagen banded fibril structure and the collagen-platelet reaction. *Thrombosis Research, 55*(1), 135–148.

Tamate, R., Hashimoto, K., Horii, T., Hirasawa, M., Li, X., Shibayama, M., & Watanabe, M. (2018). Self-healing micellar ion gels based on multiple hydrogen bonding. *Advanced Materials, 30*(36), 1802792.

Tishchenko, G., Šimůnek, J., Brus, J., Netopilík, M., Pekárek, M., Walterová, Z., & Lenfeld, J. (2011). Low-molecular-weight chitosans: Preparation and characterization. *Carbohydrate Polymers, 86*(2), 1077–1081.

Udhayakumar, S., Shankar, K. G., Sowndarya, S., Venkatesh, S., Muralidharan, C., & Rose, C. (2017). l-Arginine intercedes bio-crosslinking of a collagen–Chitosan 3D-hybrid scaffold for tissue engineering and regeneration: In silico, in vitro, and in vivo studies. *RSC Advances, 7*(40), 25070–25088.

van der Linde, S., Suz, L. M., Orme, C. D. L., Cox, F., Andreae, H., Asi, E., & Bidartondo, M. I. (2018). Environment and host as large-scale controls of ectomycorrhizal fungi. *Nature, 558*(7709), 243–248.

Wenling, C., Duohui, J., Jiamou, L., Gong, Y., Nanming, Z., & Zhang, X. (2005). Effects of the degree of deacetylation on the physicochemical properties and schwann cell affinity of chitosan films. *Journal of Biomaterials Applications, 20*, 157–177.

Wu, S., Applewhite, A. J., Niezgoda, J., Snyder, R., Shah, J., Cullen, B., & Treadwell, T. (2017). Oxidized regenerated Cellulose/Collagen dressings: Review of evidence and recommendations. *Advances in Skin & Wound Care, 30*(11S Suppl. 1), S1–S18.

Yannas, I. V., Burke, J. F., Gordon, P. L., Huang, C., & Rubenstein, R. H. (1980). Design of an artificial skin. II. Control of chemical composition. *Journal of Biomedical Materials Research, 14*(2), 107–132.

Yao, C., Markowicz, M., Pallua, N., Magnus Noah, E., & Steffens, G. (2008). The effect of cross-linking of collagen matrices on their angiogenic capability. *Biomaterials, 29*(1), 66–74.

Yin, L., Wang, K., Lv, X., Sun, R., Yang, S., Yang, Y., & Yu, Z. (2017). The fabrication of an ICA-SF/PLCL nanofibrous membrane by coaxial electrospinning and its effect on bone regeneration in vitro and in vivo. *Scientific Reports, 7*(1), 8616.

Yoon, J., Yang, H.-S., Lee, B.-S., & Yu, W.-R. (2019). Recent Progress in Coaxial Electrospinning: New Parameters, Various Structures, and Wide Applications. *Advanced Materials, 0*(0), 1704765.

You, C., Li, Q., Wang, X., Wu, P., Ho, J. K., Jin, R., & Han, C. (2017). Silver nanoparticle loaded collagen/chitosan scaffolds promote wound healing via regulating fibroblast migration and macrophage activation. *Scientific Reports, 7*(1), 10489.

Yunoki, S., Suzuki, T., & Takai, M. (2003). Stabilization of low denaturation temperature collagen from fish by physical cross-linking methods. *Journal of Bioscience and Bioengineering, 96*(6), 575–577.

Zhao, X., Guo, B., Wu, H., Liang, Y., & Ma, P. X. (2018). Injectable antibacterial conductive nanocomposite cryogels with rapid shape recovery for noncompressible hemorrhage and wound healing. *Nature Communications, 9*(1), 2784.

1 **Chitosan-glucan Complex Hollow Fibers Reinforced Collagen Wound Dressing Embedded**

2 **with Aloe vera. Part I: Preparation and Characterization**

3

4

5 **A.M. Abdel-Mohsen[a,b,c*], R.M. Abdel-Rahman[a], I. Kubena[d], L. Kobera[e], Z. Spotez[a], M.**

6 **Zboncak[a], R. Prikryl[f], , J. Brus[e] , J. Jancar[a,b,f]**

7

8

9 [a] CEITEC-Central European Institute of Technology, Brno University of Technology, Purkyňova

10 656/123, Brno 612 00, Czechia

11 [b] SCITEG, a.s., Brno, Czechia

12 [c] epartment of Pretreatment and Finishing of Cellulosic based Textiles, Textile Industries
13 Research Division, National Research Centre, 33 EL Buhouth St., Dokki, Giza 12622, Egypt

14 [d] Institute of Physics of Materials, Academy of Sciences of the Czech Republic, Žižkova 22, CZ

15 61662, Brno, Czechia

16 [e] Institute of Macromolecular Chemistry of the Czech Academy of Sciences, Heyrovskeho nam.

17 2, 162 06, Prague 6, Czechia

18 [f] Institute of Materials Chemistry, Facility of chemistry, Brno University of Technology,

19 Purkyňova 464/118, Brno, 612 00, Czechia

20

21 **Corresponding author**: Central European Institute of Technology (CEITEC), Brno University
22 of Technology, Purkyňova 656/123, Brno 612 00, Czechia. E-mail: abdel-
23 mohsen@ceitec.vutbr.cz; Tel: +420 773063837

24

25

26

27

28

29

30

31

32

Table S1. Wound dressing compositions and photographs of 2 and 3D dressing scaffold
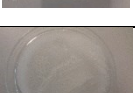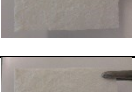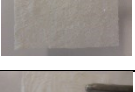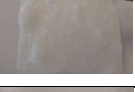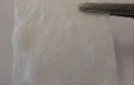
Sample No.	Sample code	Weight ratio (g/g)	CO (g)	CSGC (g)	AV (g)	3D dressing scaffold	2D dressing scaffold
1	Net CO	--	0.5	0	0		
2	CO/AV (1/1)	1/1	0.5	0	0.5		
3	CO/AV (1/2)	1/2	0.5	0	1		
4	CO/CSGC (1/0.5)	1/0.5	0.5	0.25	0		
5	CO/CSGC (1/1)	1/1	0.5	0.5	0		
6	CO/CSGC (1/2)	1/2	0.5	1	0		
7	CO/CSGC@AV (1/0.5/1)	1/0.5/1	0.5	0.25	0.5		
8	CO/CSGC@AV (1/1/1)	1/01/1	0.5	0.5	0.5		
9	CO/CSGC@AV (1/2/1)	1/02/1	0.5	1	0.5		
10	CO/CSGC@AV (1/0.5/2)	1/0.5/2	0.5	0.25	1		
11	CO/CSGC@AV (1/1/2)	1/01/2	0.5	0.5	1		
12	CO/CSGC@AV (1/2/2)	1/02/2	0.5	1	1		
13	Net CSGC	--	0	0.5	0		

Note: CO = Collagen; CSGC = chitosan-gulcan hollow fiber; AV = aloe vera; the 3D dressing was casted into 48 well plates

2
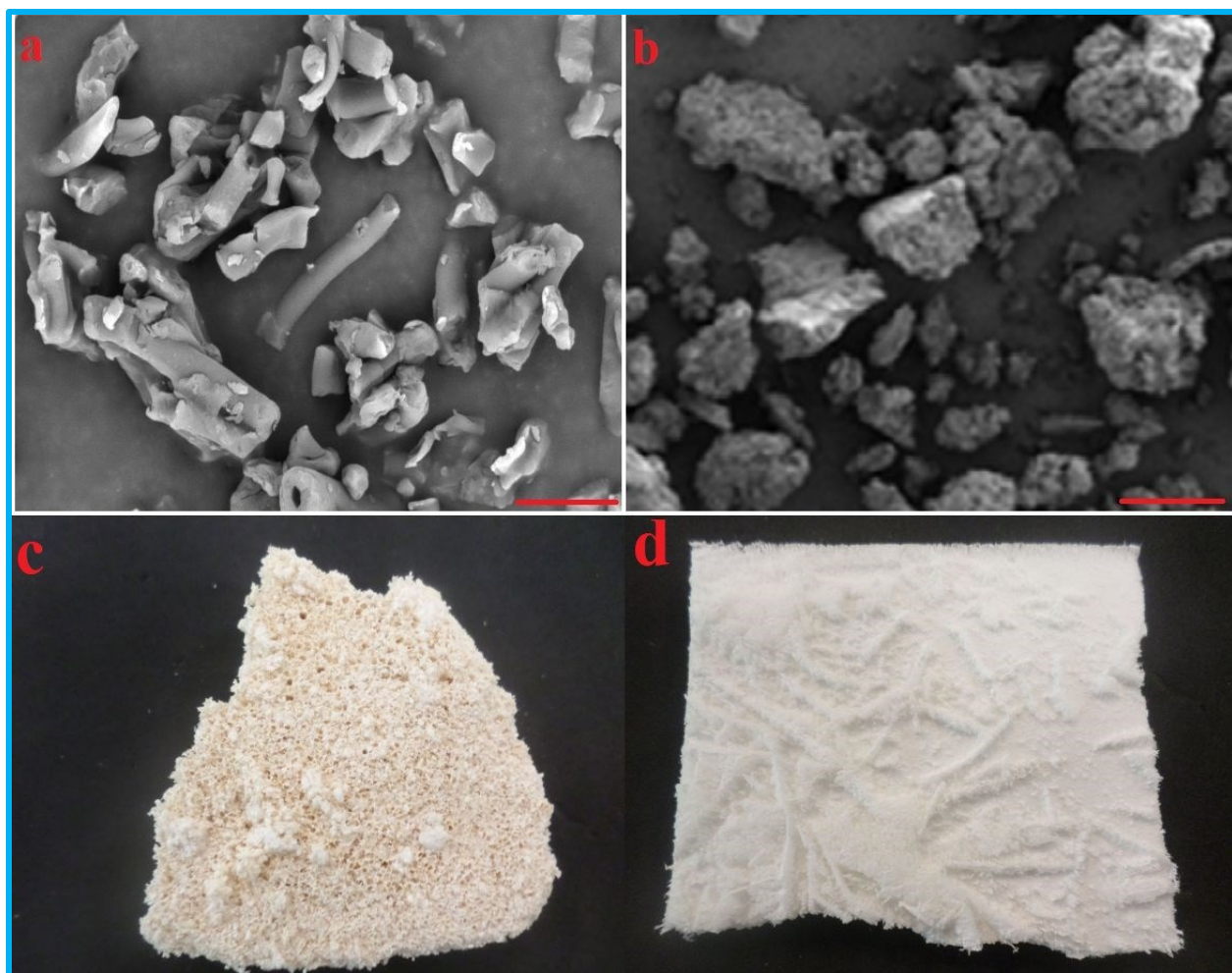
Figure S1. SEM of CSGC under high mechanical stirring **(a)**; SEM of CSGC at higher temperature treatment **(b)**; native mycelium after fermentation **(c)**; chitosan-glucan hollow fiber after purifications **(d)**.

Notes: (a) treatment was obtained at 1000 rpm ; (b) treatment was done 90 ℃; (c) beads mycelium before any treatment; (d) CSGC after purification with DDA= 90 %.
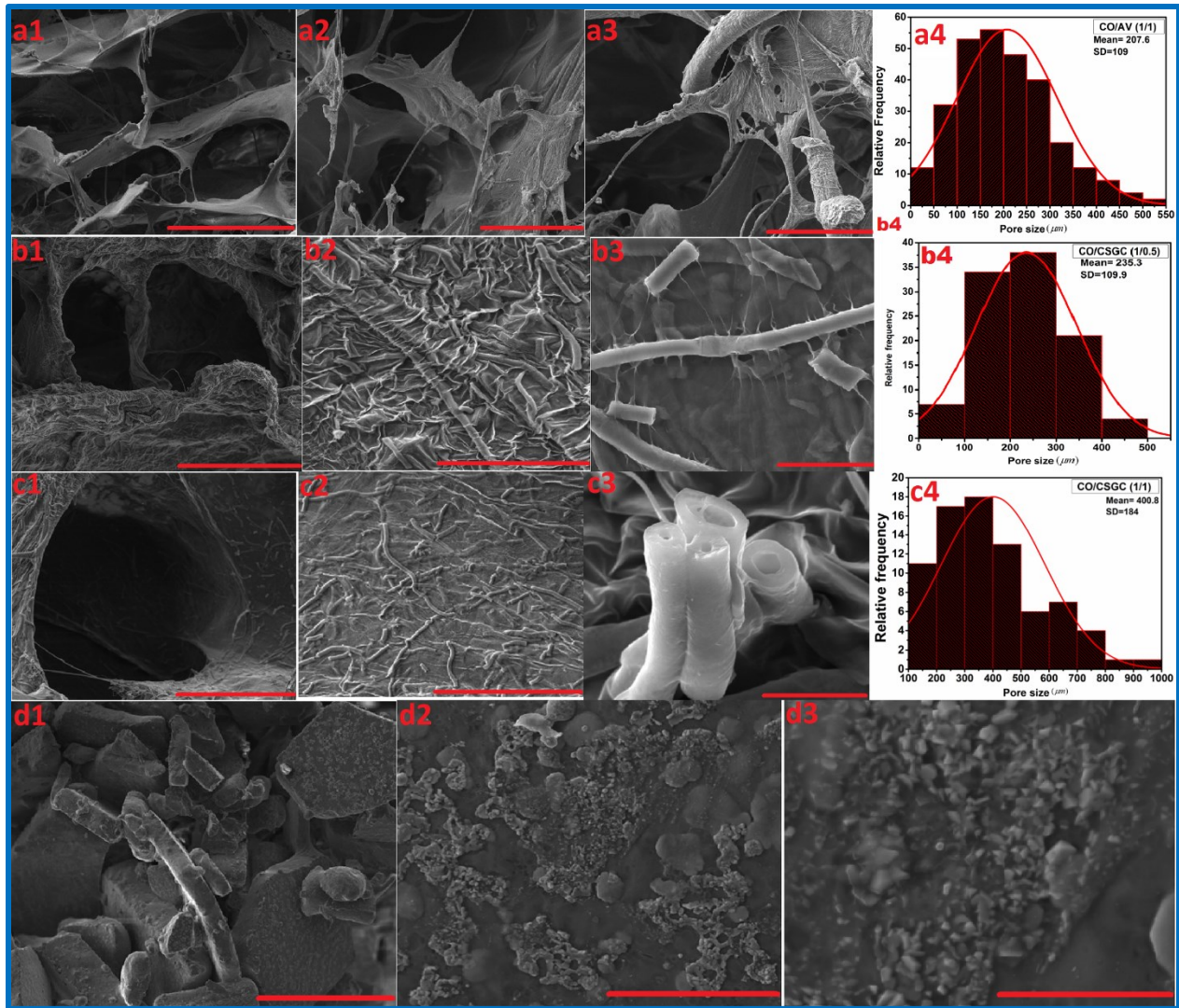
Figure S2. Scanning electron microscope and pore size histogram of dressing scaffold

Notes: (a1-a4) SEM and pore size histogram of native CO/AV (1/1); (b1-b4) SEM and pore size histogram of CO/CSGC (1/0.5); (c1-c4) SEM and pore size histogram of CO/CSGC (1/1); (d1-d3) SEM of native aloe vera (AV) Scale bars of a1, a2, a3 were 200, 100 and 5 µm, respectively for b1, b2, b3 were 200, 100 and 5 µm, respectively for c1, c2, c3 were 200, 50 and 5 µm, respectively and for d1, d2, d3 were 10 µm, 5 µm and 100 nm, respectively. The histograms of pore size measurements were plotted from 200 points.

99 **Table S2**. The stage and percentage of decomposition of unmodified CO, CSGC, AV and scaffold
100 dressing with different composition ratios under N_2 atmosphere
101

Sample code	Stage I		Stage II		Stage III		Stage IV	
	(%)	T_{max} (ºC)	(%)	T_{max} (ºC)	(%)	T_{max} (ºC)	(%)	T_{max} (ºC)
Net CO dressing	4.51	55	46.8	298				
CSGC dressing	5.5	58	29.2	294	66.4	331		
AV powder	3.2	110	11.5	178	34.1	299	43.8	382
CO/CSGC (1/2)	4.25	60	29.7	283	49.3	308		
CO/AV (1/2)	0.4	70	11.2	175	19.9	242	32.2	301
CO/CSGC/AV (1/0.5/2)	3.4	53	12.1	191	22.7	252	37	279
CO/CSGC/AV (1/1/2)	4	69	11.2	193	23.6	255	36.1	282
CO/CSGC/AV (1/2/2)	3.3	62	12.3	194	23.1	258	35.9	290

102

103

104

105

106 **Table S3:** Degradation rate percentage of native and dressing scaffolds

107

Time (days)	CO	SD	CSGC	SD	CO/AV (1/2)	SD	CO/CSGC (1/2)	SD	CO/CSGC@AV (1/0.5/2)	SD	CO/CSGC@AV (1/1/2)	SD	CO/CSGC@AV (1/2/2)	SD
0	100	0	100	0	100	0	100	0	100	0	100	0	100	0
1	63.0748	15.716	99.1	5.56	53	0.8145	91.48936	3.76431	68.13725	0.45826	53.9039	3	68.73278	3.21403
5	28.5926	7.2111	89.2	2.6	46.5	2.6058	82.23801	4.02658	53.67171	1.85203	49.483	3	65.88921	6.52865
10	0	0	88	2.5	39.1	2.3459	80.29046	1.36504	51.55196	2.15484	45.5073	6	63.52201	4.77598
14	0	0	86	1.14	24.9	2.7392	74.10208	4.27707	43.94813	2.30723	44.5619	4	56.62162	4.38216
21	0	0	85	6.33	11.7	2.0033	60.81731	3.18172	33.33333	1.09697	38.6643	4	50.13228	2.74651

108

Publication 3
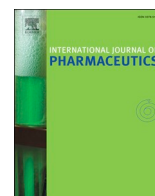
Chitosan-glucan complex hollow fibers reinforced collagen wound dressing embedded with aloe vera. II. Multifunctional properties to promote cutaneous wound healing

A.M. Abdel-Mohsen[a,b,c,*], J. Frankova[d], Rasha M. Abdel-Rahman[a], A.A. Salem[e], N.M. Sahffie[f], I. Kubena[g], J. Jancar[a,b,h]

[a] CEITEC-Central European Institute of Technology, Brno University of Technology, Purkyňova 656/123, Brno 612 00, Czechia
[b] SCITEG, a.s., Brno, Czechia
[c] Pretreatment and Finishing of Cellulosic based Textiles Department, Textile Industries Research Division, National Research Centre, 33 EL Buhouth St., Dokki, Giza 12622, Egypt
[d] Department of Medical Chemistry and Biochemistry, Faculty of Medicine and Dentistry, Palacky University, Hněvotínská 3, 775 15 Olomouc, Czechia
[e] Pharmacology Department, National Research Centre, 33 EL Buhouth St., Dokki, Giza 12622, Egypt
[f] Pathology Department National Research Centre, 33 EL Buhouth St., Dokki, Giza 12622, Egypt
[g] Institute of Physics of Materials, Academy of Sciences of the Czech Republic, Žižkova 22, CZ 61662 Brno, Czechia
[h] Institute of Materials Chemistry, Facility of Chemistry, Brno University of Technology, Purkyňova 464/118, Brno 612 00, Czechia

ARTICLE INFO

ABSTRACT

This study presents an innovative multifunctional system in fabricating new functional wound dressing (FWD) products that could be used for skin regeneration, especially in cases of infected chronic wounds and ulcers. The innovation is based on the extraction, characterization, and application of collagen (CO)/chitosan-glucan complex hollow fibers (CSGC)/aloe vera (AV) as a novel FWS. For the first time, specific hollow fibers were extracted with controlled inner (500–900 nm)/outer (2–3 μm) diameters from mycelium of *Schizophyllum commune*. Further on, research and evaluation of morphology, hydrolytic stability, and swelling characteristics of CO/CSGC@AV were carried out. The obtained FWS showed high hydrolytic stability with enhanced swelling characteristics compared to native collagen. The hemostatic effect of FWS increased significantly in the presence of CSGC, compared to native CO and displayed excellent biocompatibility which was tested by using normal human dermal fibroblast (NHDF). The FWS showed high antibacterial activity against different types of bacteria (positive/negative grams). From in vivo measurements, the novel FWS increased the percentage of wound closure after one week of treatment. All these results imply that the new CO/CSGC@AV-FWD has the potential for clinical skin regeneration and applying for controlled drug release.

1. Introduction

Skin is the largest layer of human body and provides an essential protective barrier and has several homeostatic/sensory functions that are vital to health. Its functional recovery after injury is a major task of tissue engineering. Although the skin tissue has the ability to self-heal and regenerate in case of minor injuries such as cuts and abrasions, in non-trivial injuries or in combination with additional complications (diabetes, chronic ulcers), the capacity to heal is highly reduced resulting in the occurrence of scars (Annabi et al., 2017; Bradshaw et al., 2014). Collagen type I (CO) has been extensively investigated for different biomedical purposes (Abdel-Mohsen et al., 2020a; Mano et al.,

2007). Hierarchically fibrillar structure of CO exists in different tissues (bone, cornea, skin, tendon, etc.,) and it is considered as its characteristic feature (Kwon and Matsuda, 2005). Many techniques have been used to mimic nano-fibrillar structures *in vitro* for tissue engineering, fabricated from either synthetic or native polymers such as electrospinning (Kwon and Matsuda, 2005; Liu and Ma, 2009), phase separation (Liu and Ma, 2009) and self-assembly of peptide-amphiphiles (Zhong et al., 2005) (Marone et al., 2010).

The chemical structure of a fungal cell wall is determined by chemical fractionation using a series of treatments to obtain soluble glucan and alkali-insoluble fraction consisting of linear and branched β-glucan composed of β-(1-3-) and β-(1-6-) and linked covalently to chitin

---

polymer chain (Abdel-Mohsen et al., 2020a, 2016; François, 2007). Fungal chitin is supposed to be further on linked to the plasma membrane subsequent to biosynthesis of different chains and the fibril generation process through the chemical bonds (Kang et al., 2018). The obtained chitin-glucan (ChGC) and chitosan–glucan (CSGC) complex is used as a flocculation agent for cultivating mammalian cells (Janesch et al., 2020). In addition, the CSGC is evaluated as a new absorbing material for removing heavy metals from the wastewater and industrial sectors. Unfortunately, all the extracted chitin-glucan or chitosan-glucan complexes are present only in the form of powder (Janesch et al., 2020; Singh et al., 2018; Skorik et al., 2010).

Fibers derived from the natural polymer sources are an indispensable class of materials that is versatile for a wide range of structural and functional applications in the medical and environmental sectors (Abdelrahman et al., 2020; Kim et al., 2017). Hollow fibers based on green technology display important advantages due to their large surface-to-volume ratio and show the ability to trap, isolate, or control release materials engaged in it (Yoon et al.). Coaxial and tri-axial electrospinning are progressive procedures for synthesizing high-aspect-ratio hollow micro/nanofibers with a controlled inner and outer diameter (Abdel-Mohsen et al., 2020a; Yin et al., 2017). The challenges of hollow fiber preparation from native or synthetic biomaterials lie in the selection of solvents for core and shell preparation (Halaui et al., 2017). Furthermore, the lack of mechanical characteristics, stability, compatibility, and high toxicity of the existing hollow fibers is still a great challenge (Bedford et al., 2012; Jiang et al., 2014). In our study, a novel source and a facile process were used to fabricate chitin-glucan and chitosan-glucan complex hollow fibers, using green technology and without applying any hazardous solvents in the fabrication process. The second advantage of our newly hollow chitosan-glucan complex fiber was high stability and compatibility with human cells compared to synthetic materials such as polyacrylonitrile, polycaprolactone, acetylacetonate, and polyaniline (Bedford et al., 2012; Han et al., 2017).

Innovated efficient hemostats in different shapes such as nanofibers, membrane, hydrogels, nonwoven fabrics, and 3D structure forms are a field of concern in many studies (Abdel-Mohsen et al., 2012c, 2020b; Abdel-Rahman et al., 2016; Aly et al., 2010, 2011; Liu et al., 2019; Sandri et al., 2017). Since blood clotting is a complicated procedure, functioning of mutually different hemostatic mechanisms instead of a merely morphological change would substantially improve the hemostatic performance (Du et al., 2019). After massive hemorrhage, a blood transfusion may cause possible difficulties such as anticoagulation, contamination, and many organ failures in addition to high treatment costs. Therefore, hemostasis treatment time of trauma and surgical bleeding is very important to stop the blood loss and increase the survival ratio (Li et al., 2017; Pan et al., 2018; Weisel, 2014). The postmortem reports of Iraqi and Afghan wars confirmed that more than 30% of the military war deaths could be avoided by effective hemostatic treatments (Li et al., 2017). Consequently, the innovation of effective hemostats with different shapes like two- or three-dimensional structures, nonwoven fabrics, hydrophilic adhesive hydrogel, spray, and sponge inspired many other studies (Li et al., 2017; Ryu et al., 2011).

This study reports on special multifunctional collagen (CO)/chitosan-glucan (CSGC) hollow fiber/(CO)/aloe vera (AV) composite biomaterials that were fabricated and designed to be used as a functional wound dressing (FWD). They demonstrated significant enhanced swelling, hydrolytic degradation, controlled porosity, and hemostatic characteristics. The inherent antibacterial effect and cytocompatibility of the FWD were tested on different types of bacteria and normal human dermal fibroblasts (NHDF), respectively. The healing rate and histological effects were evaluated in vivo in the full-thickness skin defect model.

2. Materials and methods

2.1. Materials

Acid-insoluble collagen type I from bovine skin was supplied as wet suspension material from VUP (Brno, Czechia), then lyophilized at −70 °C, for 48 h to obtain dry collagen (CO). *Mycelium* was produced from an extracellular product by *Schizophyllum commune* (*S. commune*) which was cultured under standard cultivation methods. Muller-Hinton agar, starch, casein hydrolase, agar, Dulbecco's Modified Eagle, fetal bovine serum (FBS), penicillin, streptomycin, and 3-(4,5-dimethylthiazol-2-yl)-2,5-diphenyltetrazolium were supplied from Sigma–Aldrich (Brno, Czechia). Moreover, glutaraldehyde was obtained by Agar Scientific (Wetzlar, Germany).

2.2. Methods

2.2.1. Extraction and fabrication of FWD

Chitin-glucan (ChGC) and chitosan-glucan (CSGC) hollow fibers were extracted from mycelium beads as described in our previous work (Abdel-Mohsen et al., 2020a). Briefly, completely dry mycelium was impregnated in a solution of sodium hydroxide (5 wt%) at 50 °C under mild mechanical stirring for 5 cycles (each 2 h) until obtained transparent supernatant. The obtained chitin-glucan complex (ChGC) hollow fibers were treated with concentrated sodium hydroxide (20%) obtained chitosan-glucan complex (CSGC) hollow fibers with a deacetylation degree about 90% (measured by ss-NMR). Aloe vera (AV) powder was extracted according to our previous work (Abdel-Mohsen et al., 2020a).

Functional wound dressings (FWD) were fabricated by the free-dry technique as described in our previous work with some modifications (Abdel-Mohsen et al., 2020a). Dry collagen (CO) of 0.5 wt% was swelled in 10 mM of acetic acid at 4 °C for two days. Then, the suspension of collagen was homogenized in ice-bath (0 °C) for 5 min using high-speed Ultra-Turrax homogenizer (12,000 rpm). The collagen solution was centrifugated at 4500 rpm for 10 min (Hermle Z300, Labortechnik, Germany), the air bubbles were removed, and then the solution was poured into stainless steel molds or into the 48-well plate to fabricate a 2- or 3-dimensional shape structure. The CO suspension was kept overnight at −30 °C and freeze-dried (−75 °C, 15 Pa, 48 h) to obtain native CO sheets.

Wound dressing without AV: Collagen/chitosan-glucan complex (CO/CSGC) dressing was fabricated by mixed collagen (CO; 0.5 wt%) with CSGC (0.25; 0.5, 1 wt%) in 10 mM of acetic acid, kept at 4 °C for 48 h. The suspensions of CO/CSGC were homogenized, centrifugated, and freeze-dried using the same protocol used for pure CO. The samples were coded as CO/CSGC (1/0.5); CO/CSGC (1/1); and CO/CSGC (1/2) for 0.25, 0.5 and 1 wt% of CSGC hollow fibers, respectively (Table 1).

Wound dressing without CSGC: AV (0.5, 1 wt%) was dissolved in Milli-Q water (5 ml), blended with CO (0.5 wt%), dispersed in 10 mM of acetic acid, and kept for two days at 4 °C. The freeze-drying process of CO/AV was done in the same manner as the native CO sheet. CO/AV wound dressings were coded as CO/AV (1/1) and CO/AV(1/2) (Table 1).

Functional wound dressing (CO/CSGC@AV): Aloe vera (0.5, 1 wt%) was dissolved in Milli-Q water (5 ml) and mixed with different ratios of CSGC hollow fibers (0.25, 05, 1 wt%) under high-speed homogenizer (12000 rpm), kept for 2 days at 4 °C. Different ratios between CSGC@AV (0.25/0.5; 0.5/0.5; 1/0.5; 0.25/1; 0.5/1, 1/1 wt./wt.) were mixed with net CO (0.5 wt%) in 10 mM of acetic acid and all suspension solutions (CO/CSGC@AV) were swelled at 4 °C for more two days. The obtained CO/CSGC@AV suspensions were poured into stainless steel molds and, for a 3D scaffold, the mixture was poured in 48 well plates

Table 1
Wound dressing codes and Formulations.

Samples codes	Weight ratio	CO (g)	CSGC (g)	AV (g)
Net CO	–	0.5	0	0
CO/AV (1/1)	1/1	0.5	0	0.5
CO/AV (1/2)	1/2	0.5	0	1
CO/CSGC (1/0.5)	1/0.5	0.5	0.25	0
CO/CSGC (1/1)	1/1	0.5	0.5	0
CO/CSGC (1/2)	1/2	0.5	1	0
CO/CSGC@AV (1/0.5/1)	1/0.5/1	0.5	0.25	0.5
CO/CSGC@AV (1/1/1)	1/01/1	0.5	0.5	0.5
CO/CSGC@AV (1/2/1)	1/02/1	0.5	1	0.5
CO/CSGC@AV (1/0.5/2)	1/0.5/2	0.5	0.25	1
CO/CSGC@AV 1/1/2)	1/01/2	0.5	0.5	1
CO/CSGC@AV (1/2/2)	1/02/2	0.5	1	1
Net CSGC	–	0	0.5	0

CO = collagen; CSGC = chitosan-glucan complex hollow fibers; AV = aloe vera.

and kept overnight at -35 °C and then freeze-dried for two days at -75 °C. All the samples, after freeze-drying, were neutralized using phosphate buffer solution (pH 7.5; 5 times each 30 min) and lyophilized for two days. All the fabricated samples were coded as CO/CSGC@AV (1/0.5/1); CO/CSGC@AV (1/1/1); CO/CSGC (1/2/1); CO/CSGC@AV (1/0.5/2); CO/CSGC@AV (1/1/2) and CO/CSGC (1/2/2) for 0.25, 0.5, 1 wt% of CSGC, 0.5, 1 wt% of AV, respectively.

3. Characterization of FWD

3.1. In vitro assays

The cell viability, proliferation, and biocompatibility assay of wound dressing were evaluated by using normal human dermal fibroblasts (NHDFs). The NHDFs were isolated during plastic surgery from the skin sections with approval from the Ethical Committee of the University Hospital Olomouc and the patient's consent. The study was performed in accordance with the Code of Ethics of the World Medical Association. The morphology and origin of the cells were authenticated in the Histology Department, University Hospital Olomouc. NHDFs were cultured in Dulbecco's Modified Eagle Medium supplemented with 10% fetal bovine serum (FBS) and 1% penicillin–streptomycin under standard culture conditions (5% CO_2, 37 °C). Cells were used between the 2nd and 3rd passages (Franková et al., 2016). When the cells reach 80% of confluence, the cells were washed with phosphate buffer saline and detached from the cultivation flasks by trypsin (0.05%), EDTA (0.2%). The cells were centrifuged (1000 rpm, 5 min) and resuspended in 5 ml of culture medium and counted cells were used for the experiment in proper concentration. The extract of the samples, which were used in MTT assay, was prepared by the incubation of the sample (1 mg/ml) in cultivation medium at 37 °C and stirring at 200 rpm for 24 h.

The cell viability was tested by MTT assay based on the reduction by metabolically active cells of tetrazolium salt 3-(4,5-dimethylthiazol-2-yl)-2,5-diphenyltetrazolium bromide to purple formazan. Briefly, the cells were seeded on 96-well microplates at the final concentration 1×10^4 cells/ml and incubated overnight then, treated with extract of tested materials at final concentrations (125, 250, 500, and 1,000 μg/ml). The cell viability was evaluated after 1, 2, 3, and 4 days. The cells cultivated only with the cultivation medium were used as a negative control and the cells treated with native CO dressing sheets were used as a positive control. After the incubation period, the medium was removed and serum-free medium supplemented with MTT (5 mg/ml) was applied to the cells for 2 h (37 °C, dark). Afterward, the solution was removed, and the crystals dissolved in DMSO with NH_3 (1%, v/v). The absorbance was measured at a wavelength of 540 nm (Sunrise, Tecan, Brno, Czechia).

In addition, live/dead staining was performed. The native CO, CSGC and dressing scaffolds (CO/CSGC, CO/AV, CO/CSGC@AV) with different ratios of CSGC in presence or absence of AV were fitted and placed on the bottom of eight well plates (chamber slide), sterilized under the UV for at least 15 min. Suspension of NHDF (0.5×10^5 cell/ml) were seeded on the top of the dressing sheets. The cells cultivated on the plastic in the cultivation medium were used as a negative control. The samples were incubated for 5 min with the staining solution (2 mg/ml of propidium iodide, 5 mg/ml of fluorescein diacetate in PBS). Finally, the dressing was rinsed with PBS before imaging with confocal microscopy and green/red colors indicated the live, dead cells, respectively. Visualization of the cell attachment/interaction with the scaffold was performed using scanning electron microscopy (SEM) analyses. Cell-seeded scaffolds were briefly and carefully rinsed in phosphate-buffered saline (1X PBS) and fixed for 1 h in 2.5% glutaraldehyde in 0.1 M Sorensen's phosphate buffer at room temperature, then followed by immersing in 10 min dehydration steps in 30, 50, 70, 90 and absolute alcohol.

3.2. In vivo measurements

All animal procedures were carried out in accordance with the Ethics Committee of the National Research Centre (Cairo, Egypt) and conformed to the "Guide for the care and use of "Laboratory Animals" published by the US National Institutes of Health. Twenty male Wister rats were used and were divided into four groups (n = 5): first group control (covered with gauze); second group (covered with native CO); third group (covered with CO/CSGC (1/2)) and fourth group (covered with CO/CSGC@AV (1/2/2)). A wound was made on the back of each rat. Five animals from each group were sacrificed on the 0th, 4th and 8th days. In each rat, the healing wound area was measured. The obtained results from the samples taken on days zero, four and eight after wounding evaluated and presented a decrease of the wound area when compared with untreated rats. After the experiment, rats were kept in separate cages. On 0th, 4th, and 8th days postoperative days and the wound was photographed. The wound area was measured by outlining the wound area. New dressings were applied to the wound sites after they were cleaned with normal saline solution and the wound changed twice a week. The rate of wound closure was determined by the following (Annabi et al., 2017; Xu et al., 2018; Zhao et al., 2017) Eq. (1),

$$\text{Wound closure percentage}(\%) = \frac{A0 - At}{A0} \times 100 \tag{1}$$

where A_0 is wound area at day 0 and A_t is wound area at a specified time of surgery, respectively. The resulting value is an average of 5 measurements (n = 5).

Specimens of all animals were dissected immediately after death and fixed in 10% neutral-buffered formal saline for 72 h at least. All the specimens were washed in tap water for half an hour and then dehydrated in ascending grades of alcohol (70, 80, and 90% and absolute alcohol), cleared in xylene, impregnated in soft paraffin wax at 55 °C and embedded in hard paraffin. Serial sections of 6 μm thick were cut and stained with Hematoxylin and eosin for histopathological investigation (Zhao et al., 2018) and the images were captured and processed using Adobe Photoshop version 8.0.

3.3. Blood clotting measurements:

The evaluation, whether the native or dressing scaffold with different ratios of CSGC or AV could increase the blood clotting, the dressing scaffold was placed into a petri dish and pre-warmed at 37 °C. Citrate whole blood 600 μl was then dispensed onto the dressing, 48 μl of calcium chloride solution was added to the dressing surface and incubated at 37 °C for 15 min. After the incubation period, the red blood cells that were not trapped in the dressing were hemolyzed with 5 ml of distilled water, and the absorbance of the resulting hemoglobin solution

was measured at 540 nm using UV/VIS spectroscopy (Ds). The absorbance of 0.2 ml whole blood hemolysis with 1 ml deionized water 540 nm was denoted as D0. The blood clotting index (BCI) was determined by the following equation (Cheng et al., 2017; Ong et al., 2008; Qu et al., 2018) Eq. (2).

$$Blood\ clotting\ index\ (BCI) = 100 \times \frac{Ds}{D0} \tag{2}$$

Statistical Analysis: All the quantitative data were expressed as mean (±) standard deviations. Statistical comparisons were performed using one-way ANOVA with *P < 0.05 considered statistically significant.

4. Results and discussions

4.1. Fabrication and characterization of FWD

The novel chitosan-glucan complex (CSGC) hollow fibers were isolated in chemical treatments as described in our previous work (Abdel-Mohsen et al., 2020a). The CSGC hollow fibers used in our study have high deacetylation degree (DDA = 90 %) and controlled outer/inner diameters of CSGC fibers. The functional Wound dressing CO/CSGC@AV-FWD was fabricated by a freeze-drying technique using different weight ratios between CSGC to CO in presence or absence of AV as described in the experimental section.

Fig. 1a shows SEM photographs of native CO dressing with heterogeneous lamellar pore structure surrounded by flake-like CO sheets with main pore size and porosity about (50 ± 20) and (65 ± 5 μm), respectively. Fig. 1b shows the surface morphology and cross-section of CSGC hollow fibers with outer size (2.5–3 μm) and inner hollow size (600–900 nm) and CSGC hollow fibers appeared without any bundle with smooth surface morphology. Wound dressing CO/CSGC (1/2) clearly displayed different surface and cross-section morphologies compared with net CO and CSGC and CSGC fibers show strong adhesion properties on CO matrix (Fig. 1c, right side). From Fig. 1c, the CO matrix did not cause any significant changes in the morphology and

diameter of the CSGC hollow fibers. The pore size and porosity of CO/CSGC (1/2) were 230 ± 100 and 76 ± 5 μm, respectively (Fig. S1, supporting information). Comparing of CO/CSGC wound dressing in presence or absence AV, the CSGC exhibited AV trapped inside the hollow fiber (Fig. 1d) due to the ionic and physical interactions between functional groups of CSGC and the AV (Abdel-Mohsen et al., 2020a). The surface morphology of hollow fibers changed after encapsulating the AV (Fig. 1d) and the pore size and porosity of the FWD in the presence of AV (CO/CSGC@AV; 1/2/2) about 204 ± 130 μm and 90 ± 9 μm, respectively (Fig. S1, supporting information). The AV has generated a thick layer inside the CSGC fiber (Fig. 1d). Transmission electron microscopy shows the AV encapsulated in to CSGC hollow fibers (Fig. 1e). Using higher concentration of AV (1 wt%), the CSGC fibers trapped more AV inside and on the surface of CSGC (Fig. 1e).

Fig. 1f shows the proposed interaction mechanism between CO, CSGC and AV. Aloe vera molecules were trapped in the hollow structure of CSGC complex by a capillary force imposed on the solution. Aloe vera molecules flowed in the hollow tube under the impact of capillary force and the velocity of the fluid depends on the concentration of AV and viscosity as well and the intermolecular forces between the AV solution and surrounding CSGC hollow surfaces (Abdel-Mohsen et al., 2020a).

The inner size of the CSGC hollow (600–900 nm) is sufficiently larger than the size of the AV molecule and might be a solution to surface tension of AV (caused by cohesion within the gel solution of AV). The adhesiveness (Fig. 1f) between the AV and hollow fibers wall further acts to propel the solution of AV inside the hollow of CSGC (Abdel-Mohsen et al., 2020a). From the above hypothesis, the CSGC complex hollow fiber could encapsulate the AV molecules and formed ionic interactions between the different functional groups of CSGC and AV. In the presence of the collagen triple helix structure (CO), the interactions between CSGC and AV improved due to the presence of different free functional groups in the CO molecules which interacted physically/ionically with CSGC@AV or CSGC, AV separated.

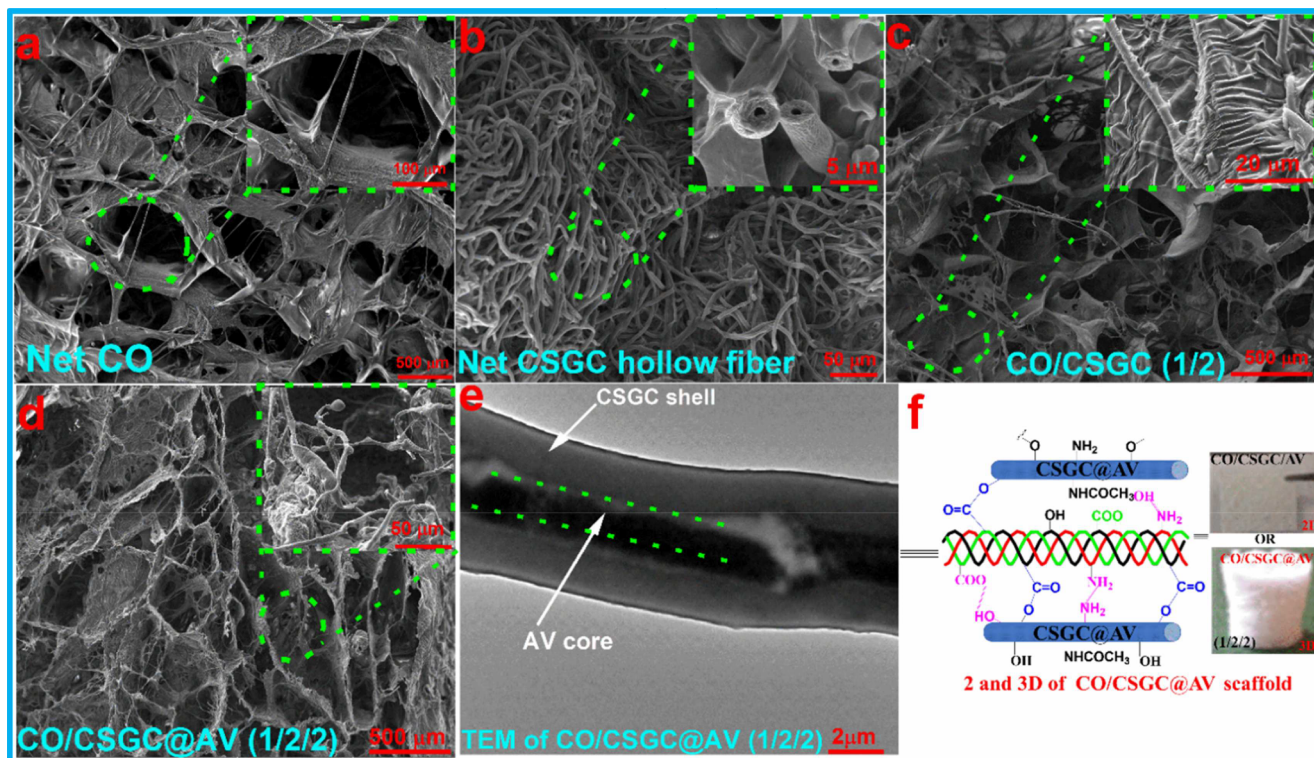Fig. 2 describes the physicochemical properties of the natives and

Fig. 1. Representative of the SEM, TEM of native, FWD and proposed chemical interaction mechanism between different components of the FWD.
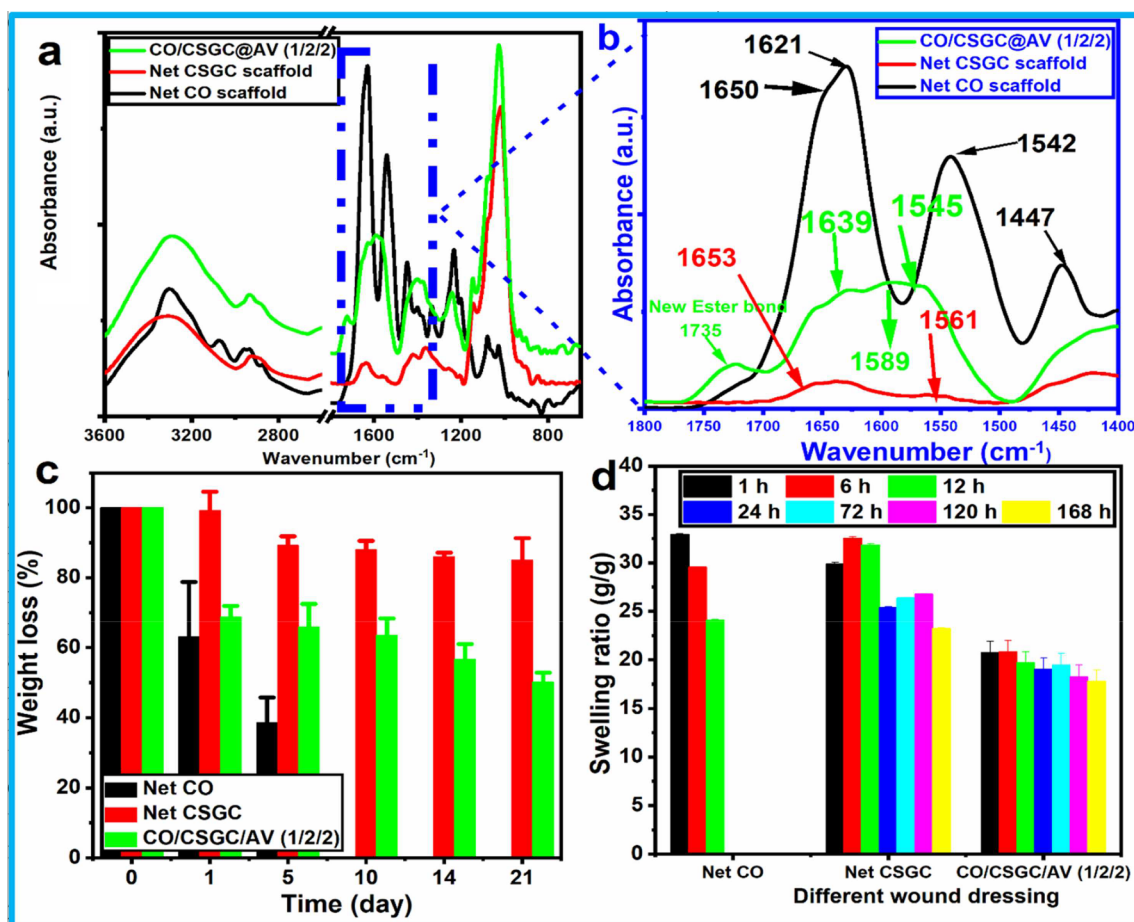
Fig. 2. Representation of the physicochemical properties of FWD.

FWD, using a higher ratio of CSGC and AV. Fig. 2a, b represented the ATR-FTIR spectra of CO, CSGC and CO/CSGC@AV-FWD (1/2/2). The characteristic peaks for collagen I appeared at 1650 cm^{-1} and 1649 cm^{-1} (Abdel-Mohsen et al., 2020a; Lee et al., 2017). Native CO still exhibits all the characteristic peaks of the collagen triple helical structure. The spectrum of CSGC (Fig. 2a) proved that the chitosan-glucan was extracted from α-chitin. The amide I band clearly divided into two peaks at 1653 and 1639 cm^{-1} and confirmed the α-form of chitin (Abdel-Rahman et al., 2016; Abdel-Rahman et al., 2015; Přichystalová et al., 2014). The FTIR spectrum of CO/CSGC@AV (1/2/2) dressing scaffold shows a new peak at 1735 cm^{-1} corresponding to the new ester bond between CO, CSGC and AV. Analysis of the ATR-FTIR spectra suggested that the fabricating of two-or three-dimensional functional wound dressing did not cause any significant change in the molecular structure of any of the components.

In thermogravimetric analysis (TGA), the thermal stability of the dressing scaffold was determined within the temperature ranging from 25 to 600 °C (Fig. S2a,b). From the thermogravimetric data, we conclude that the additive of CSGC different ratios did not show significant changes in the thermal stability of the wound dressing. The addition of the AV slightly improved the thermal slightly, due to the strong interaction between CO and CSGC hollow fibers in the presence of aloe vera. Results revealed that the *in vitro* degradation rate of native and modified wound dressing depends on the ratio of complex to collagen. Fig. 2c shows the weight loss (%) of the net Co and FWD were measured in physiological conditions (PBS, pH = 7.5; 37 °C) after 1, 3, 5, 10, 14 and 21 days. Collagen dressing was degraded after five days (mass loss = 40%) and completely degraded in PBS after 10 days of immersing in PBS. Chitosan-glucan hollow fiber scaffold was more stable compared with the other scaffolds. Incorporation of AV resulted in no

significant changes in the degradation rate (Fig. 2c). In contrast, previous studies have shown that the encapsulated/incorporations of antimicrobial agents in proteins-based biomaterials, could significantly alter the degradability percentage of the obtained biomaterials (Annabi et al., 2017; Kumar et al., 2012).

Chitosan-glucan hollow fiber scaffold showed the highest water absorption and the swelling rate rapidly increased in the initial 4 h of interval and reached saturation (35 g/g). It then kept its constant absorption after 24 h. After 1 day of swelling, the CSGC scaffold exhibited the highest water absorption capacity compared to the other scaffolds. Most probably, the higher swelling capacity of CSGC was due to the hydrophilic properties of the complex possessing different functional groups as well as the hollow shape of the fiber exposing the larger surface. The wide range of swelling ratios obtained for the hybrid scaffolds was beneficial for tissue engineering applications. In addition, the increased swelling percentage of the FWS using a higher ratio of CSGC could enhance their cell adherence and viability of cells in *in vivo* measurements. For wound closure, this could greatly accelerate the wound healing by providing high oxygen and exudate permeable and flexible wound seal (Abdel-Mohsen et al., 2014, 2013, 2017; Annabi et al., 2017; Fouda et al., 2016; Montaser et al., 2016; Peppas et al., 2006).

4.2. Hemostatic ability of CO/CSGC@AV-FWD

Traumatic bleeding is one of the leading causes of death in civil and combat trauma and affective hemostasis is the most challenging for emergency medicine (Maksym and Sikora, 2015; Millner et al., 2010; Ong et al., 2008). In order to investigate the hemostatic characteristics of net and FWD with different ratios of CSGC in the presence or absence
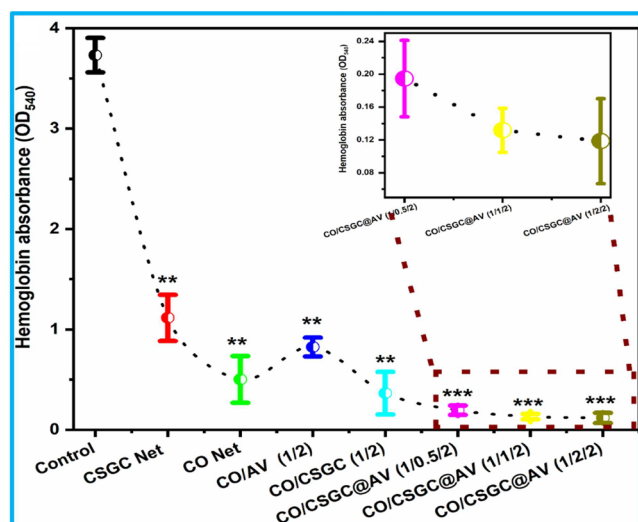
Fig. 3A. Representative *in vitro* blood clotting assay of natives and FWD using different ratios of CSGC.

of AV, net and FWS were impregnated with blood for 15 min before hemolyzing of red blood cells (Figs. 3A and 3B). The absorbance at 540 nm could reflect the concentration of hemoglobin and the amount of free red blood cells not absorbed on FWD. Lower BCI value indicates a better blood clotting capability of dressing scaffold (lower release of hemoglobin from red blood cells). In Fig. 3A, a higher absorbance value of hemoglobin solution indicated a slower clotting rate of blood. Chitosan was reported to possess a hemostatic effect and antibacterial properties (Abdel-Mohsen et al., 2012a; Zhao et al., 2017). The hemostatic capability of native CO, CSGC and CO/CSGC (1/2), CO/AV (1/2) were improved significantly ($p < 0.05$)compared with the control sample (cellulose gaze). This was due to the cationic nature of collagen (presence of amino groups), chitosan-glucan complex (amino groups) that could interact with negatively charged residues in red blood cells, as well as mucoadhesive properties of dressing scaffolds (Yuk et al., 2016; Zhao et al., 2018). The blood clotting considerably improved in the presence of aloe vera (Fig. 3A) and hemoglobin released after incubation for 15 min at 37 °C was significantly lower than native groups (CO, CSGC) and groups without AV ($p* < 0.001$). After increasing the CSGC concentration in dressing matrix (0.25 to 1 wt%), the hemostatic properties of wound dressing slightly improved (Fig. 3A, right side).

We proposed different mechanisms of hemostasis characteristics of CO/CSGC@AV-FWD in our study. First, collagen fibrils promote platelet adhesion on the surface of the dressing sheet and binding of clotting factors and could accelerate the clot formation (Jain et al., 2016). Fig. 3A shows that the blood-clotting index increased after blending CO with CSGC complex or with a complex in presence of AV. This indicates that the physical cross-linked process could improve the hemostatic property of wound dressing (CO/CSGC@AV; 1/2/2). The blood clotting capability was further enhanced after the mixing of AV due to calcium ions from AV denaturing the anticoagulating proteins (Sudheesh Kumar et al., 2012). This indicated that the novel FWD was able to significantly stop bleeding rapidly.

Fig. 3B shows the appearance and SEM of natives and FWD before and after immobilization of blood at 1 and 15 min in presence or absence of AV. Collagen/chitosan-glucan complex hollow fibers/aloe vera (CO/CSGC/AV; 1/2/2) has significantly higher blood clotting ability compared with native (CO, CSGC) or wound dressing without CSGC (Fig. 3Ba2-e3). When the blood was dripped onto the scaffold, it was rapidly absorbed by the surface and inside the porous scaffolds (Fig. 3Ba4-e5). The blood clotting ability of the dressing scaffold was further confirmed in SEM observation (Fig. 3Ba4-e5). The platelets exhibited high spread over all FWD surfaces and inside the matrix,

proposed that the new FWD could activate platelets during the wound healing process. From the results of Fig. 3A and 3B, we could conclude that the new FW-CO/CSGC@AV was the best among all wound dressings for enhancing hemostasis since it leads to the fastest blood clotting and platelet adhesion performance.

4.3. Bactericidal performance of FWD

The ideal wound dressing should also function as an antimicrobial to eliminate wound infection (Qu et al., 2018). Microbial infections can increase exudation and prolong the wound healing process (Jayakumar et al., 2011). The antibacterial activity of CO/CSGC@AV-FWD was evaluated against *Bacillus subtilis, Streptococci* (*G* +), *Klebsiella pneumoniae,* and *Escherichia coli* (*G* -) bacteria using disk diffusion method. Native CO did not show any antibacterial activity against any type of bacteria (Fig. 4). The CSGC hollow fiber wound dressing displayed antibacterial properties against gram (-/+ *G*) bacteria with no significant differences between (*G* + /-) bacteria (Fig. 4). The antibacterial activity of CSGC due to positively charged amino groups of chitosan (part of CSGC) damaged the cell walls of bacteria, releasing intracellular fluids by electrostatic adherence with cytoderm of bacteria (Abdel-Mohsen et al., 2012a, 2012b, 2016; Abdel-Rahman et al., 2016, 2015; Abdelrahman et al., 2020; Liang et al., 2016; Qu et al., 2018; Ryu et al., 2011; Zhao et al., 2017).

Collagen/chitosan-glucan hollow fiber/aloe vera (CO/CSGC@AV; 1/2/2) displayed excellent antibacterial activity against all types of bacteria with a reduction rate up to 95% compared to native CO and CSGC dressing (Fig. 4). The presence of aloe vera positively affected the antibacterial properties against a different type of bacteria, especially due to the presence of active components mainly aloin and aloe emodin (anthraquinones), and salicylic acid that could inhibit protein synthesis in bacterial cells wall (Anjum et al., 2016). The presence of calcium and magnesium ions in the main components of aloe vera improved the antibacterial characteristics of FWD (Silva et al., 2013). In addition, topical uses of aloe vera were found to be effective in the treatment of various skin problems such as burns and eczema (Silva et al., 2013). From the above results, it may be concluded that CO/CSGC@AV-FWD (1/2/2) possessed excellent bactericidal characteristics against different types of bacteria (*G* + /-). It was able to efficiently protect the wound from microorganism infection and it displayed high hemostatic characteristics that could be used as a new functional wound dressing (FWD) material for wound healing application.

4.4. Cytotoxicity measurements of FWD

Biocompatibility of wound dressing scaffold is one of the most important parameters in tissue engineering applications especially for skin regeneration purposes (Hsieh et al., 2017; Ishihara et al., 2018; Zhao et al., 2018). Fig. 5A shows the effect of different FWD on the cell viability of normal human dermal fibroblast (NHDF). Different concentrations of CO/CSGC/AV- FWD (125, 250, 500 and 1,000 μg/ml) were used first to determine the maximum concentration of FWD that could be used without any toxicity. Interestingly, increasing the concentration ratio of CSGC (0.5, 1, 2 wt%) enhanced the cell viability after one day of cells seeding and higher concertation of CSGC (1/2/2) displayed the highest viability of cells compared to lower ratio of CSGC (0.5, 1 wt%) and native CO dressing (Fig. 5A).

Fig. S3 (supporting information) explored the relationship between the native AV, CSGC and FWD-CO/AV (1/2), CO/CSGC (1/2) on cell viability at a different seeded time (24–96 h). Plain AV solution could improve cell growth using a high concentration dose (1,000 μg/ml) at a different time of seeded (24, 48, 72, 96 h). From Fig. S3 (supporting information), after 96 h of seeded with NHDF using different FWD, net AV solution displayed higher cytocompatibility than net CSGC > CO/CSGC (1/2) > CO/AV (1/2), respectively. Fig. 5B shows the cell viability of FWD at different seeding time (24, 48, 72, and 96 h) using
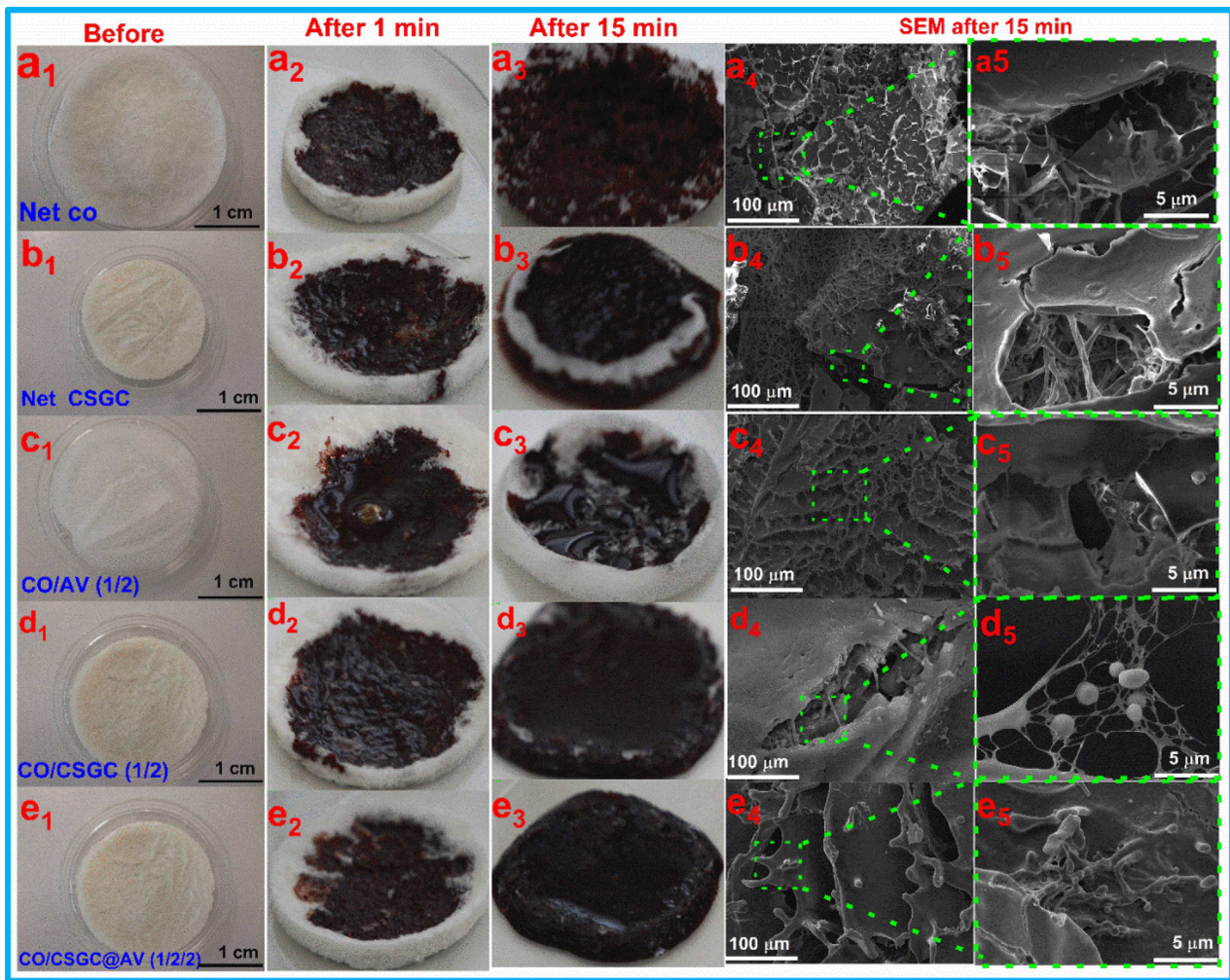
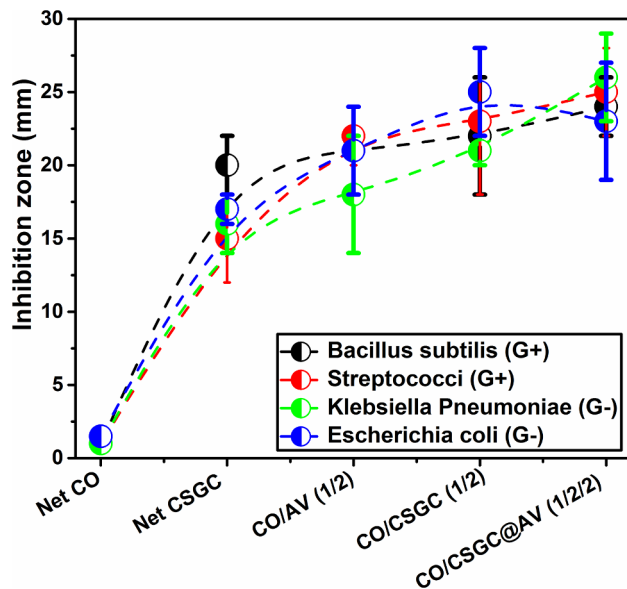**Fig. 3B.** Representative visualization of *in vitro* clotting assay of net and FWD.

Fig. 4. Representative of the bactericidal performance of natives and FWD using different ratios of CSGC in presence of AV.
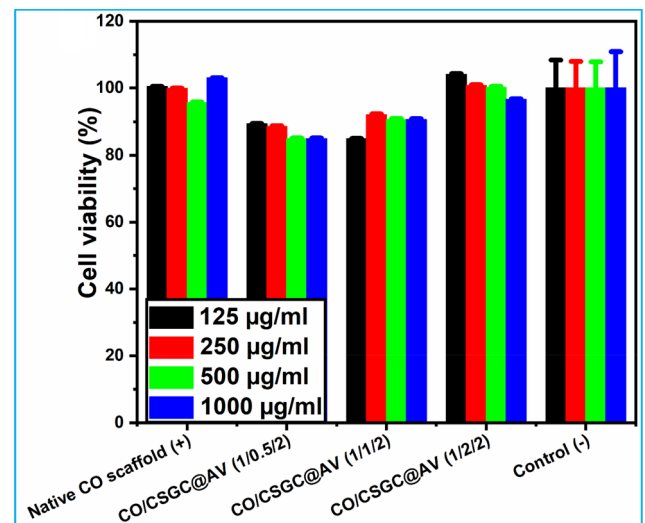

Fig. 5A. Results of MTT tests using different concentrations of CSGC after one day of seeding with NHDF cells. **Notes**: Positive control (CO sheet) and negative control (cells without samples only culture medium).
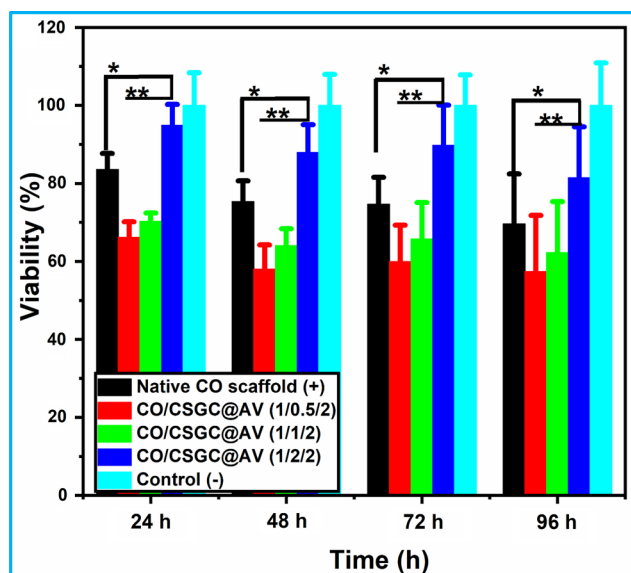
Fig. 5B. Effect of CSGC hollow fiber concentrations on cell viability of FWD at the different seeding times. **Notes:** Positive control (CO sheet) and negative control (cells without samples only culture medium). The error bar indicates the standard deviation. *P < 0.05, **P < 0.005 between groups and negative controls (native collagen only).

different ratios of CSGC (1/0.5/2; 1/1/2; 1/2/2) and a higher concentration of FWD (1000 µg/ml). A higher concentration of CSGC shows significantly improved cell viability of human fibroblast cell line compared to all incubation periods (24 to 96 h).

To visualize the live/dead cells attached to the dressing scaffold, confocal electron microscopy was used as shown in Fig. 6a–l. Fig. 6a, b provides the photographs from confocal microscopy of native CO after 1 and 5 days of seeding with NHDF with high viability of cells. After 1 day (live cells; green color), after 5 days of implantation, cells viability was decreased (dead cells; red color) compared with the first day of seeding and the cells displayed round morphology with cell bundle throughout during the study period. It might be due to the CO wound dressing that the hydrolysis started after 5 days of seeding and the cells could not proliferate in the CO matrix. AV could promote wound healing in nondiabetic and diabetic rats due to its ability to stimulate fibroblasts and reduced the wound healing closure time (Baghersad et al., 2018). Cells on the native CO sheet (Fig. 6c) showed a spherical shape morphology with an adhesive on the surface of the wound dressing (red row) and connection between cells (white row). NHDFs were able to attach and spread on the surface of the FWD, displaying different morphology dependence on the composition of FWS (Fig. 6c–m).

Fig. 6d, e shows the viability of NHDF seeded into the net CSGC dressing after one and five days, respectively. The NHDF cells distributed more on the first day of seeding with CSGC with a small number of dead cells visualized after five days of seeding. The NHDF cells were more oriented (Fig. 6d, e) with CSGC hollow fiber direction and viability was significantly improved compared with first day of seeding with NHDF. Overall, complex scaffold (Fig. 6f) shows the cells adhered to the matrix of CSGC hollow fiber.

Fig. 6g–l shows the cytocompatibility of CO/CSGC (1/2) and CO/CSGC@AV (1/2/2) after one and five days of seeding with NHDF using a high concentration of FWD (1000 µg/ml). The shape of cells slightly changed and flattened with spindle-like morphology in CO/CSGC@AV-FWD(1/2/2; Fig. 6k, l) with few dead cells (red color) which appeared in all dressings with different ratios of CSGC hollow fibers, due to cell metabolism and apoptosis. Both cell viability and live/dead staining results demonstrated that the FWD with different ratios of CSGC in the presence of AV significantly improved cell viability. There were

significant changes in cell morphology seeded with CO/CSGC (1/2; Fig. 6g, h) and cells exhibited a spherical shape morphology with small cell agglomeration throughout the study period, but the viability was enhanced during the seeded period (Fig. 6h).

Cells seeded on the CO/CSGC@AV (1/2/2) dressing scaffold showed better spreading and a higher number of cells adhered to the surface of the wound dressing. From days one to five, the NHDF cells were uniformly distributed on the surface of the FWD, exhibiting a spindle-like shape typical of fibroblasts cells, suggesting good adherence to dressing surface. CO/CSGC (1/2) shows spread and presented in round morphology with cell agglomeration and the cells covered almost by the sample surface (Fig. 6i). In CO/CSGC@AV (1/2/2), cells showed better spreading and a higher number of cells attached to the surface of scaffold (Fig. 6m) and cells exhibited a spindle-like shape typical of fibroblasts cells with good adherence to dressing surface (red row).

Cytocompatibility properties of CO/CSGC@AV depended mainly on the chemical composition of the FWD. Chitosan alone is unable to provide attachments of fibroblast cells and their proliferation. The presence of the glucan component in chitosan-glucan complex then significantly improved the hydrophilicity of complex surface. Hollow fiber complex showed excellent attaching, migration and proliferation of the NHDF cells. This was observed in comparing the water uptake of net chitosan and CSGC hollow fibers (data not shown). In turn, excellent antibacterial activity of the CO/CSGC@AV-FWD in presence of AV could also influence the physical features such as surface energy, topography and stiffness that directly influence protein adsorption and, subsequently, the cell response (Baghersad et al., 2018). Evidence illustrates that AV releases glucomannan, a mannose-rich polysaccharide connected to carbohydrate-binding, sites on two β_2 integrins called LFA-01 and Mac-1 on the fibroblast and promotes cell adhesion, migration, and proliferation (Baghersad et al., 2018; Chithra et al., 1998). In addition, the hydrophilic nature characteristic of AV could improve the attachment, adhesion and proliferation of human fibroblast cells (NHDF). Based on the above results, the multifunctional wound dressing (FWD) possessed excellent blood compatibility and cytocompatibility for wound healing application, especially in case of non-healing wounds with bacterial infection.

4.5. In vivo assays of the FWD

Figs. 7A and 7B shows the wound contractions of the control sample (gauze), natives CO, CSGC, and CO/CSGC (1/2), CO/CSGC@AV (1/2/2) groups were displayed on 0th, 4th, and 8th after the operation. On day four, all groups show wound area reduction to some extent, while the CO/CSGC@AV (1/2/2) group exhibited the largest significant wound reduction rate (area 42% (Fig. 7B); ***p < 0.0001) compared with all groups. Interestingly, on day eight, groups of CSGC, CO/CSGC (1/2) and CO/CSGC@AV (1/2/2) showed significant wound closure percentage higher (*** < 0.0001) than native CO > control sample with closure percentage 92, 68, 47, and 20 for CO/CSGC@AV (1/2/2), CO/CSGC (1/2), CSGC and CO, respectively (Fig. 7B).

One of the main aims was to use FWD to regenerate new tissues with the same functional properties of normal tissue including the re-epithelialization and orchestrated regeneration of all the skin appendages. Histological properties of wound healing for control and treated wounds by different FWD groups were investigated after eight days of surgery Fig. 7Aa4–d4. In the bare gauze control sample (Fig. 7Aa4), the wound surface appeared where the epidermal layer (black arrow) abrupt slight disappeared. Dressing CO (Fig. 7Ab4) shows restoration of epidermal thin layer and the dermal layer consists mainly of connective tissue devoid of glands or hair follicles. The higher magnification part shows swollen keratinocytes (left side). CO/CSGC (1/2) displayed intact epidermal and dermal layers that consist mainly of connective tissue that shows signs of edema (Fig. 7Ac4) as well as the higher magnification part shows thinner epidermal layer than the previous group but with distinct horny layer and edematous areas in the dermis
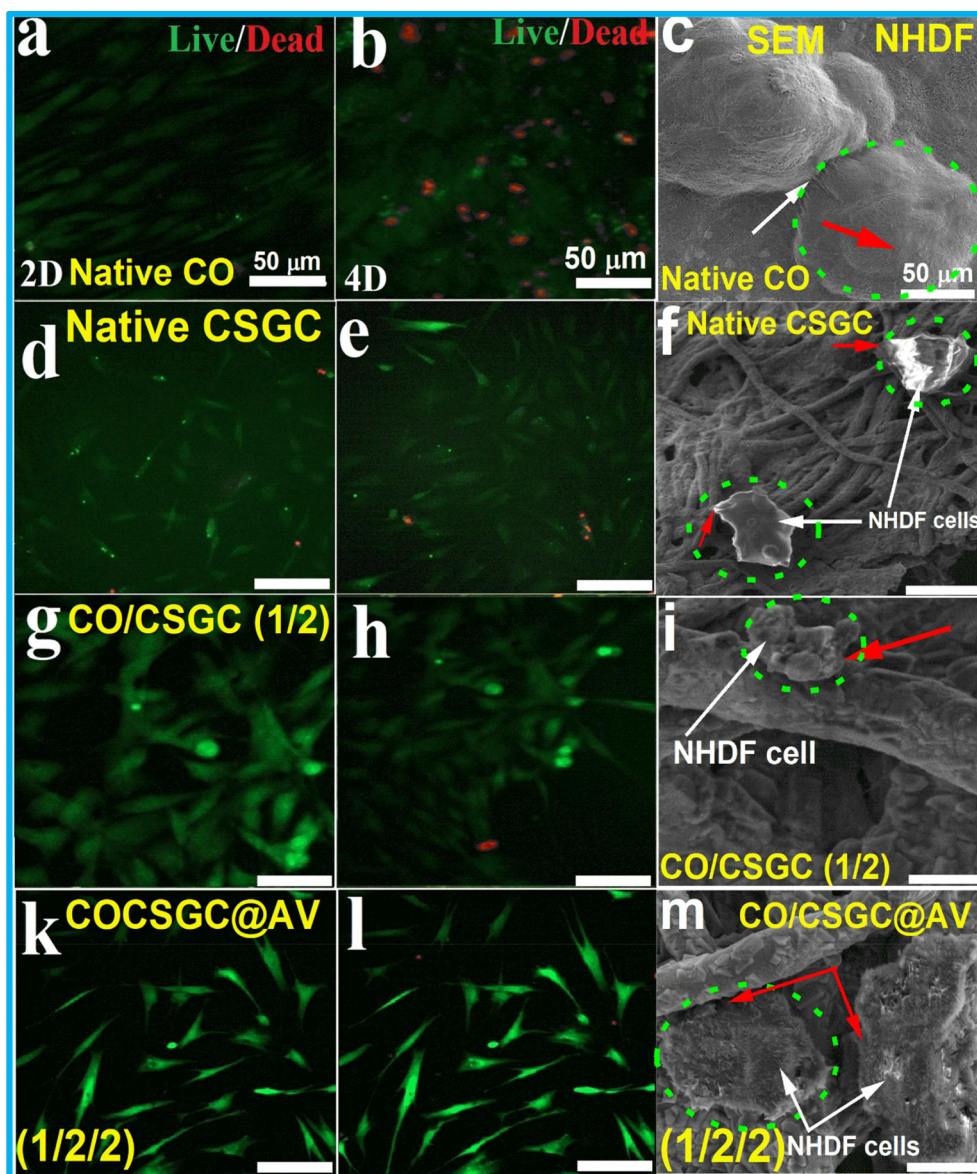
Fig. 6. Representative visualization of live/dead assay of normal human dermal fibroblast (NHDF) after 1st and 4th days of seeding (dead cells stain red and living cells stain green) using confocal and scanning electron microscopes. **Notes:** White arrows were NHDF; red arrows were adhesive points between cells and scaffold.

(left side). CO/CSGC@AV-FWD (1/2/2) shows a thick keratinized epidermal layer with an underlying dermal layer with no structure (Fig. 7Ad4) and the higher magnification part shows quite a normal epidermal layer (small right side).

CO/CSGC@AV (1/2/2; Fig. 7Ad4) demonstrated their better wound healing effect than the other groups, especially native collagen group which was attributed to the combined effect of CSGC (antibacterial, healing, hemostatic) and AV (antibacterial, healing, hemostatic properties). Functional wound dressing (CO/CSGC) encapsulated bioactive material (AV) showed the best therapeutic effect during all healing stages (inflammation, proliferation and remodeling). It increased the antioxidant enzymes around the wound environment during the inflammation phase. The FWD showed enhanced fibroblast migration (Fig. 6b) during the formation of granulation tissue, collagen and re-epithelization in proliferation phrases (Fig. 6Ag, k). Aloe vera also plays an important role in the remodeling phase, which could improve wound contraction by increasing the number of cytokines enhanced fibroblast proliferation (Maan et al., 2018; Sridhar et al., 2015; Stocco et al., 2018). Collagen/chitosan-glucan/aloe vera (CO/CSGC@AV-FWD) might maintain optimal hydration of the exposed tissues as well as

reducing wound healing time. Table S1 (Supporting information) shows compression between CO/CSGC@AV-FWD and other wound dressing reported in the literature. Interestingly, although the dressing provided satisfactory wound healing ratios, they had lower efficacy compared with the new dressing collagen/chitosan-glucan hollow fiber/aloe vera (CO/CSGC@AV; 1/2/2).

5. Conclusions

For the first time, a novel multifunctional wound dressing (FWD) based on collagen/chitosan-glucan complex hollow fibers with encapsulated aloe vera (CO/CSGC@AV) was fabricated using freeze-dried technique with significant bactericidal, biocompatibility, blood clotting efficiency and wound healing characteristics. CSGC hollow fibers were extracted with controlled fiber diameter (2–3 μm) and inner hollow size (600–900 nm) from *Schizophyllum commune*. Further on, they were used for mimicked dressing sheets in the presence of CO and AV. The FWD, in the presence of aloe vera, showed excellent antibacterial activity against different type of bacteria. CO/CSGC@AV (1/2/2) displayed significant hemostatic characteristics compared to net CO and CSGC.
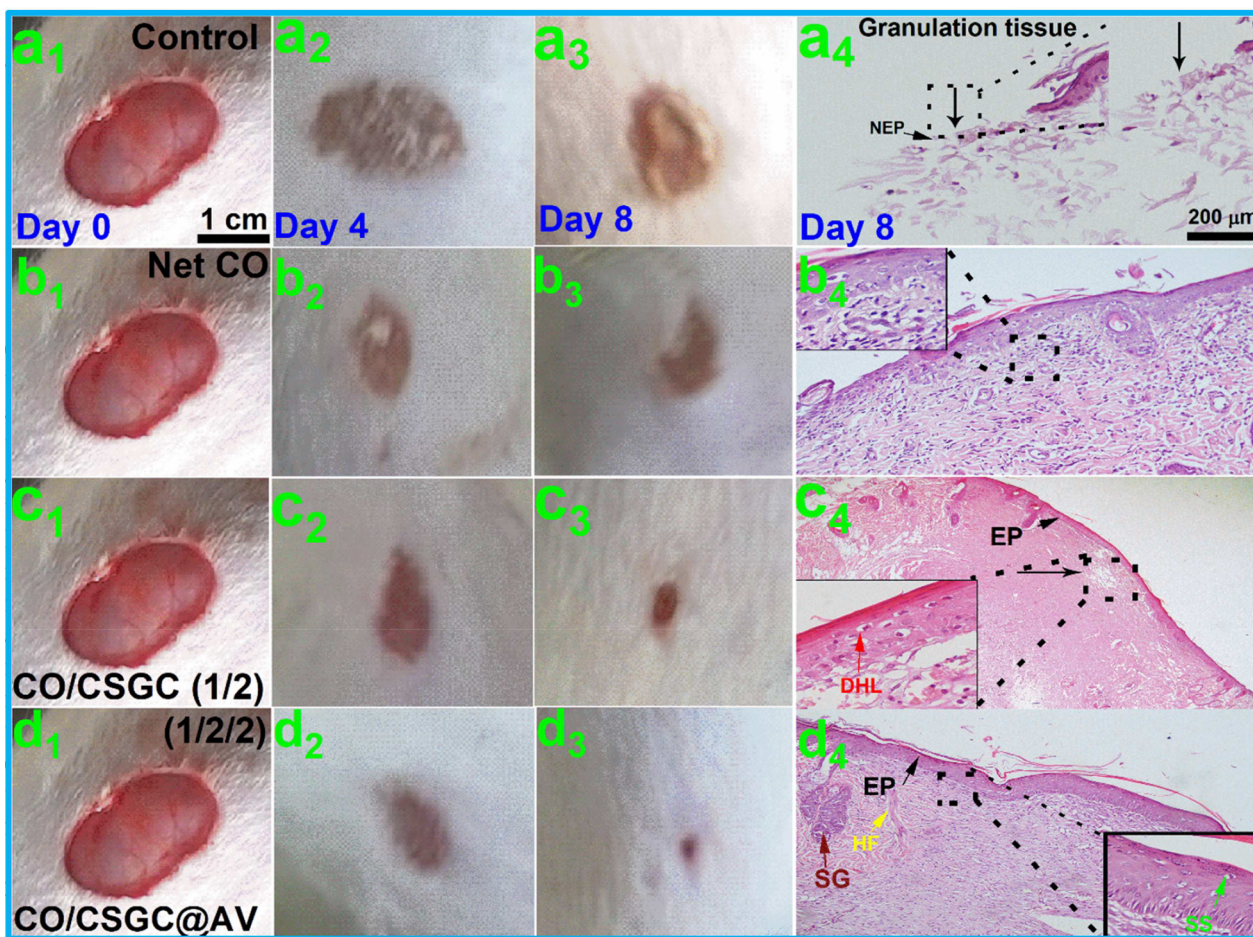
Fig. 7A. Representative digital observations of wound contraction percentage and photomicrograph of histological sections of wound area stained with hematoxylin and eosin at 8-day post wounding in control and normal rats. **Notes:** NEP = No epidermal layer, EP = epidermal layer, HF = hair follicles, GT = granulation tissue.
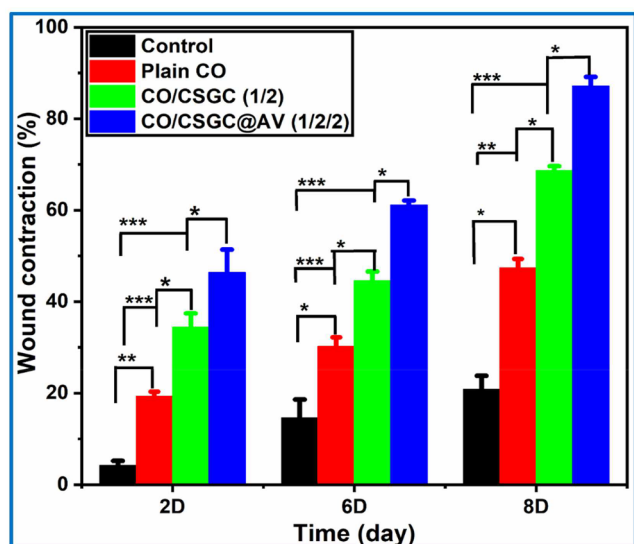
Fig. 7B. Representative wound contraction percentage using different wound dressing. Data mean ± SD (n = 4). Error bars indicated standard deviation (*p < 0.5, **p < 0.01, ***p < 0.001, ****p < 0.0001).

The hydrolytic stability and swelling behavior of the dressing scaffold were enhanced by CSGC in a concentration-dependent manner. From the obtained results, a new multifunctional dressing scaffold can be an option for wound healing of full-thickness skin. We believe that the new functional wound dressing opens new applications in biomedical fields that could be used in soft tissue engineering (FWD), especially for healing burnt skin and for drug delivery.

CRediT authorship contribution statement

A.M. Abdel-Mohsen: Conceptualization, Methodology, Writing - original draft, Writing - review & editing. **J. Frankova:** Methodology. **Rasha M. Abdel-Rahman:** Conceptualization, Methodology, Writing - original draft, Writing - review & editing. **A.A. Salem:** Methodology. **N.M. Sahffie:** Methodology. **I. Kubena:** Methodology. **J. Jancar:** Project administration, Supervision.

Declaration of Competing Interest

The authors declare that they have no known competing financial interests or personal relationships that could have appeared to influence the work reported in this paper.

Acknowledgements

Appendix A. Supplementary material

Supplementary data to this article can be found online at https://doi.org/10.1016/j.ijpharm.2020.119349.

References

Abdel-Mohsen, A.M., Abdel-Rahman, R.M., Fouda, M.M.G., Vojtova, L., Uhrova, L., Hassan, A.F., Al-Deyab, S.S., El-Shamy, I.E., Jancar, J., 2014. Preparation, characterization and cytotoxicity of schizophyllan/silver nanoparticle composite. Carbohydr. Polym. 102, 238–245.

Abdel-Mohsen, A.M., Abdel-Rahman, R.M., Hrdina, R., Imramovský, A., Burgert, L., Aly, A.S., 2012a. Antibacterial cotton fabrics treated with core–shell nanoparticles. Int. J. Biol. Macromol. 50, 1245–1253.

Abdel-Mohsen, A.M., Abdel-Rahman, R.M., Kubena, I., Kobera, L., Spotz, Z., Zboncak, M., Prikryl, R., Brus, J., Jancar, J., 2020a. Chitosan-glucan complex hollow fibers reinforced collagen wound dressing embedded with aloe vera. Part I: Preparation and characterization. Carbohydr. Polym. 230, 115708. https://doi.org/10.1016/j.carbpol.2019.115708.

Abdel-Mohsen, A.M., Aly, A.S., Hrdina, R., El-Aref, A.T., 2012b. A novel method for the preparation of silver/chitosan-O-methoxy polyethylene glycol core shell nanoparticles. J. Polym. Environ. 20, 459–468.

Abdel-Mohsen, A.M., Aly, A.S., Hrdina, R., Montaser, A.S., Hebeish, A., 2012c. Biomedical textiles through multifunctioalization of cotton fabrics using innovative methoxypolyethylene glycol-N-chitosan graft copolymer. J. Polym. Environ. 20, 104–116.

Abdel-Mohsen, A.M., Hrdina, R., Burgert, L., Abdel-Rahman, R.M., Hašová, M., Šmejkalová, D., Kolář, M., Pekar, M., Aly, A.S., 2013. Antibacterial activity and cell viability of hyaluronan fiber with silver nanoparticles. Carbohydr. Polym. 92, 1177–1187.

Abdel-Mohsen, A.M., Jancar, J., Abdel-Rahman, R.M., Vojtek, L., Hyršl, P., Dušková, M., Nejezchlebová, H., 2017. A novel in situ silver/hyaluronan bio-nanocomposite fabrics for wound and chronic ulcer dressing: in vitro and in vivo evaluations. Int. J. Pharm. 520, 241–253.

Abdel-Mohsen, A.M., Jancar, J., Kalina, L., Hassan, A.F., 2020b. Comparative study of chitosan and silk fibroin staple microfibers on removal of chromium (VI): Fabrication, kinetics and thermodynamic studies. Carbohydr. Polym. 234, 115861.

Abdel-Mohsen, A.M., Jancar, J., Massoud, D., Fohlerova, Z., Elhadidy, H., Spotz, Z., Hebeish, A., 2016. Novel chitin/chitosan-glucan wound dressing: Isolation, characterization, antibacterial activity and wound healing properties. Int. J. Pharm. 510, 86–99.

Abdel-Rahman, R.M., Abdel-Mohsen, A.M., Hrdina, R., Burgert, L., Fohlerova, Z., Pavliňák, D., Sayed, O.N., Jancar, J., 2016. Wound dressing based on chitosan/hyaluronan/nonwoven fabrics: preparation, characterization and medical applications. Int. J. Biol. Macromol. 89, 725–736.

Abdel-Rahman, R.M., Hrdina, R., Abdel-Mohsen, A.M., Fouda, M.M.G., Soliman, A.Y., Mohamed, F.K., Mohsin, K., Pinto, T.D., 2015. Chitin and chitosan from Brazilian Atlantic Coast: Isolation, characterization and antibacterial activity. Int. J. Biol. Macromol. 80, 107–120.

Abdelrahman, R.M., Abdel-Mohsen, A.M., Zboncak, M., Frankova, J., Lepcio, P., Kobera, L., Steinhart, M., Pavlinak, D., Spotaz, Z., Sklenářévá, R., Brus, J., Jancar, J., 2020. Hyaluronan biofilms reinforced with partially deacetylated chitin nanowhiskers: Extraction, fabrication, in-vitro and antibacterial properties of advanced nanocomposites. Carbohydr. Polym. 235, 115951.

Aly, A.S., Abdel-Mohsen, A.M., Hebeish, A., 2010. Innovative multifinishing using chitosan-O-PEG graft copolymer/citric acid aqueous system for preparation of medical textiles. J. Textile Institute 101, 76–90.

Aly, A.S., Abdel-Mohsen, A.M., Hrdina, R., Abou-Okeil, A., 2011. Preparation and characterization of polyethylene glycol/dimethyl siloxane adduct and its utilization as finishing agent for cotton fabric. J. Nat. Fibers 8, 176–188.

Anjum, S., Gupta, A., Sharma, D., Gautam, D., Bhan, S., Sharma, A., Kapil, A., Gupta, B., 2016. Development of novel wound care systems based on nanosilver nanohydrogels of polymethacrylic acid with Aloe vera and curcumin. Mater. Sci. Eng., C 64, 157–166.

Annabi, N., Rana, D., Shirzaei Sani, E., Portillo-Lara, R., Gifford, J.L., Fares, M.M., Mithieux, S.M., Weiss, A.S., 2017. Engineering a sprayable and elastic hydrogel adhesive with antimicrobial properties for wound healing. Biomaterials 139, 229–243.

Baghersad, S., Hajir Bahrami, S., Mohammadi, M.R., Mojtahedi, M.R.M., Milan, P.B., 2018. Development of biodegradable electrospun gelatin/aloe-vera/poly(ε-caprolactone) hybrid nanofibrous scaffold for application as skin substitutes. Mater. Sci. Eng., C 93, 367–379.

Bedford, N.M., Dickerson, M.B., Drummy, L.F., Koerner, H., Singh, K.M., Vasudev, M.C., Durstock, M.F., Naik, R.R., Steckl, A.J., 2012. Nanofiber-based bulk-heterojunction organic solar cells using coaxial electrospinning. Adv. Energy Mater. 2, 1136–1144.

Bradshaw, M., Ho, D., Fear, M.W., Gelain, F., Wood, F.M., Iyer, K.S., 2014. Designer self-assembling hydrogel scaffolds can impact skin cell proliferation and migration. Sci. Rep. 4, 6903.

Cheng, X., Shao, Z., Li, C., Yu, L., Raja, M.A., Liu, C., 2017. Isolation, characterization and evaluation of collagen from jellyfish Rhopilema esculentum Kishinouye for use in hemostatic applications. PLoS ONE 12, e0169731.

Chithra, P., Sajithlal, G.B., Chandrakasan, G., 1998. Influence of aloe vera on the healing of dermal wounds in diabetic rats. J. Ethnopharmacol. 59, 195–201.

Du, X., Liu, Y., Wang, X., Yan, H., Wang, L., Qu, L., Kong, D., Qiao, M., Wang, L., 2019. Injectable hydrogel composed of hydrophobically modified chitosan/oxidized-dextran for wound healing. Mater. Sci. Eng., C 104, 109930.

Fouda, M.M.G., Abdel-Mohsen, A.M., Ebaid, H., Hassan, I., Al-Tamimi, J., Abdel-Rahman, R.M., Metwally, A., Alhazza, I., Rady, A., El-Faham, A., Jancar, J., 2016. Wound healing of different molecular weight of hyaluronan; in-vivo study. Int. J. Biol. Macromol. 89, 582–591.

François, J.M., 2007. A simple method for quantitative determination of polysaccharides in fungal cell walls. Nat. Protoc. 1, 2995.

Franková, J., Pivodová, V., Vágnerová, H., Juráňová, J., Ulrichová, J., 2016. Effects of silver nanoparticles on primary cell cultures of fibroblasts and keratinocytes in a wound-healing model. J. Appl. Biomater. Funct. Mater. 14, 137–142.

Halaui, R., Zussman, E., Khalfin, R., Semiat, R., Cohen, Y., 2017. Polymeric microtubes for water filtration by co-axial electrospinning technique. Polym. Adv. Technol. 28, 570–582.

Han, D., Sherman, S., Filocamo, S., Steckl, A.J., 2017. Long-term antimicrobial effect of nisin released from electrospun triaxial fiber membranes. Acta Biomater. 53, 242–249.

Hsieh, H.-T., Chang, H.-M., Lin, W.-J., Hsu, Y.-T., Mai, F.-D., 2017. Poly-methyl methacrylate/polyvinyl alcohol copolymer agents applied on diabetic wound dressing. Sci. Rep. 7, 9531.

Ishihara, J., Ishihara, A., Fukunaga, K., Sasaki, K., White, M.J.V., Briquez, P.S., Hubbell, J.A., 2018. Laminin heparin-binding peptides bind to several growth factors and enhance diabetic wound healing. Nat. Commun. 9, 2163.

Jain, A., Graveline, A., Waterhouse, A., Vernet, A., Flaumenhaft, R., Ingber, D.E., 2016. A shear gradient-activated microfluidic device for automated monitoring of whole blood haemostasis and platelet function. Nat. Commun. 7, 10176.

Janesch, J., Jones, M., Bacher, M., Kontturi, E., Bismarck, A., Mautner, A., 2020. Mushroom-derived chitosan-glucan nanopaper filters for the treatment of water. React. Funct. Polym. 146, 104428.

Jayakumar, R., Prabaharan, M., Sudheesh Kumar, P.T., Nair, S.V., Tamura, H., 2011. Biomaterials based on chitin and chitosan in wound dressing applications. Biotechnol. Adv. 29, 322–337.

Jiang, H., Wang, L., Zhu, K., 2014. Coaxial electrospinning for encapsulation and controlled release of fragile water-soluble bioactive agents. J. Control. Release 193, 296–303.

Kang, X., Kirui, A., Muszyński, A., Widanage, M.C.D., Chen, A., Azadi, P., Wang, P., Mentink-Vigier, F., Wang, T., 2018. Molecular architecture of fungal cell walls revealed by solid-state NMR. Nat. Commun. 9, 2747.

Kim, J.-K., Kim, D.H., Joo, S.H., Choi, B., Cha, A., Kim, K.M., Kwon, T.-H., Kwak, S.K., Kang, S.J., Jin, J., 2017. Hierarchical chitin fibers with aligned nanofibrillar architectures: a nonwoven-mat separator for lithium metal batteries. ACS Nano 11, 6114–6121.

Kumar, P.T.S., Lakshmanan, V.-K., Biswas, R., Nair, S.V., Jayakumar, R., 2012. Synthesis and biological evaluation of chitin hydrogel/Nano ZnO composite bandage as antibacterial wound dressing. J. Biomed. Nanotechnol. 8, 891–900.

Kwon, I.K., Matsuda, T., 2005. Co-electrospun nanofiber fabrics of poly(l-lactide-co-ε-caprolactone) with type I collagen or heparin. Biomacromolecules 6, 2096–2105.

Lee, Y.-C., Chiang, C.-C., Huang, P.-Y., Chung, C.-Y., Huang, T.D., Wang, C.-C., Chen, C.-I., Chang, R.-S., Liao, C.-H., Reisz, R.R., 2017. Evidence of preserved collagen in an Early Jurassic sauropodomorph dinosaur revealed by synchrotron FTIR microspectroscopy. Nat. Commun. 8, 14220.

Li, J., Wu, X., Wu, Y., Tang, Z., Sun, X., Pan, M., Chen, Y., Li, J., Xiao, R., Wang, Z., Liu, H., 2017. Porous chitosan microspheres for application as quick in vitro and in vivo hemostat. Mater. Sci. Eng., C 77, 411–419.

Liang, D., Lu, Z., Yang, H., Gao, J., Chen, R., 2016. Novel asymmetric wettable AgNPs/chitosan wound dressing. In vitro and in vivo evaluation. ACS Appl. Mater. Interfaces 8, 3958–3968.

Liu, C., Liu, X., Liu, C., Wang, N., Chen, H., Yao, W., Sun, G., Song, Q., Qiao, W., 2019. A highly efficient, in situ wet-adhesive dextran derivative sponge for rapid hemostasis. Biomaterials 205, 23–37.

Liu, X., Ma, P.X., 2009. Phase separation, pore structure, and properties of nanofibrous gelatin scaffolds. Biomaterials 30, 4094–4103.

Maan, A.A., Nazir, A., Khan, M.K.I., Ahmad, T., Zia, R., Murid, M., Abrar, M., 2018. The therapeutic properties and applications of Aloe vera: a review. J. Herbal Med. 12, 1–10.

Maksym, P., Z. Sikora, V., 2015. Chitosan as a Hemostatic Agent: Current State.

Mano, J.F., Silva, G.A., Azevedo, H.S., Malafaya, P.B., Sousa, R.A., Silva, S.S., Boesel, L.F., Oliveira, J.M., Santos, T.C., Marques, A.P., Neves, N.M., Reis, R.L., 2007. Natural origin biodegradable systems in tissue engineering and regenerative medicine: present status and some moving trends. J. R. Soc. Interface 4, 999–1030.

Marone, P.A., Lau, F.C., Gupta, R.C., Bagchi, M., Bagchi, D., 2010. Safety and toxicological evaluation of undenatured type II collagen. Toxicol. Mech. Methods 20, 175–189.

Millner, R., Lockhart, A.S., Marr, R., 2010. Chitosan arrests bleeding in major hepatic injuries with clotting dysfunction: an in vivo experimental study in a model of hepatic injury in the presence of moderate systemic heparinisation. Ann. R. Coll. Surg. Engl. 92, 559–561.

Montaser, A.S., Abdel-Mohsen, A.M., Ramadan, M.A., Sleem, A.A., Sahffie, N.M., Jancar, J., Hebeish, A., 2016. Preparation and characterization of alginate/silver/nicotinamide nanocomposites for treating diabetic wounds. Int. J. Biol. Macromol. 92, 739–747.

Ong, S.-Y., Wu, J., Moochhala, S.M., Tan, M.-H., Lu, J., 2008. Development of a chitosan-based wound dressing with improved hemostatic and antimicrobial properties. Biomaterials 29, 4323–4332.

Pan, M., Tang, Z., Tu, J., Wang, Z., Chen, Q., Xiao, R., Liu, H., 2018. Porous chitosan microspheres containing zinc ion for enhanced thrombosis and hemostasis. Mater. Sci. Eng., C 85, 27–36.

Peppas, N.A., Hilt, J.Z., Khademhosseini, A., Langer, R., 2006. Hydrogels in biology and medicine: from molecular principles to bionanotechnology. Adv. Mater. 18, 1345–1360.

Přichystalová, H., Almonasy, N., Abdel-Mohsen, A.M., Abdel-Rahman, R.M., Fouda, M.M.G., Vojtova, L., Kobera, L., Spotz, Z., Burgert, L., Jancar, J., 2014. Synthesis, characterization and antibacterial activity of new fluorescent chitosan derivatives. Int. J. Biol. Macromol. 65, 234–240.

Qu, J., Zhao, X., Liang, Y., Zhang, T., Ma, P.X., Guo, B., 2018. Antibacterial adhesive injectable hydrogels with rapid self-healing, extensibility and compressibility as wound dressing for joints skin wound healing. Biomaterials 183, 185–199.

Ryu, J.H., Lee, Y., Kong, W.H., Kim, T.G., Park, T.G., Lee, H., 2011. Catechol-functionalized chitosan/pluronic hydrogels for tissue adhesives and hemostatic materials. Biomacromolecules 12, 2653–2659.

Sandri, G., Aguzzi, C., Rossi, S., Bonferoni, M.C., Bruni, G., Boselli, C., Cornaglia, A.I., Riva, F., Viseras, C., Caramella, C., Ferrari, F., 2017. Halloysite and chitosan oligosaccharide nanocomposite for wound healing. Acta Biomater. 57, 216–224.

Silva, S.S., Popa, E.G., Gomes, M.E., Cerqueira, M., Marques, A.P., Caridade, S.G., Teixeira, P., Sousa, C., Mano, J.F., Reis, R.L., 2013. An investigation of the potential application of chitosan/aloe-based membranes for regenerative medicine. Acta Biomater. 9, 6790–6797.

Singh, A., Dutta, P.K., Kumar, H., Kureel, A.K., Rai, A.K., 2018. Synthesis of chitin-glucan-aldehyde-quercetin conjugate and evaluation of anticancer and antioxidant activities. Carbohydr. Polym. 193, 99–107.

Skorik, Y.A., Pestov, A.V., Yatluk, Y.G., 2010. Evaluation of various chitin-glucan derivatives from Aspergillus niger as transition metal adsorbents. Bioresour. Technol. 101, 1769–1775.

Sridhar, R., Lakshminarayanan, R., Madhaiyan, K., Amutha Barathi, V., Lim, K.H.C., Ramakrishna, S., 2015. Electrosprayed nanoparticles and electrospun nanofibers based on natural materials: applications in tissue regeneration, drug delivery and pharmaceuticals. Chem. Soc. Rev. 44, 790–814.

Stocco, T.D., Bassous, N.J., Zhao, S., Granato, A.E.C., Webster, T.J., Lobo, A.O., 2018. Nanofibrous scaffolds for biomedical applications. Nanoscale 10, 12228–12255.

Sudheesh Kumar, P.T., Lakshmanan, V.-K., Anilkumar, T.V., Ramya, C., Reshmi, P., Unnikrishnan, A.G., Nair, S.V., Jayakumar, R., 2012. Flexible and microporous chitosan hydrogel/nano ZnO composite bandages for wound dressing. In vitro and in vivo evaluation. ACS Appl. Mater. Interfaces 4, 2618–2629.

Weisel, J.W., 2014. Monitoring coagulopathies in fluid resuscitation for trauma or surgery. Thromb. Res. 134, 535–536.

Xu, H., Fang, Z., Tian, W., Wang, Y., Ye, Q., Zhang, L., Cai, J., 2018. Green fabrication of amphiphilic quaternized β-chitin derivatives with excellent biocompatibility and antibacterial activities for wound healing. Adv. Mater. 30, 1801100.

Yin, L., Wang, K., Lv, X., Sun, R., Yang, S., Yang, Y., Liu, Y., Liu, J., Zhou, J., Yu, Z., 2017. The fabrication of an ICA-SF/PLCL nanofibrous membrane by coaxial electrospinning and its effect on bone regeneration in vitro and in vivo. Sci. Rep. 7, 8616.

Yoon, J., Yang, H.-S., Lee, B.-S., Yu, W.-R., Recent progress in coaxial electrospinning: new parameters, various structures, and wide applications. Adv. Mater. 1704765.

Yuk, H., Zhang, T., Parada, G.A., Liu, X., Zhao, X., 2016. Skin-inspired hydrogel–elastomer hybrids with robust interfaces and functional microstructures. Nat. Commun. 7, 12028.

Zhao, X., Guo, B., Wu, H., Liang, Y., Ma, P.X., 2018. Injectable antibacterial conductive nanocomposite cryogels with rapid shape recovery for noncompressible hemorrhage and wound healing. Nat. Commun. 9, 2784.

Zhao, X., Wu, H., Guo, B., Dong, R., Qiu, Y., Ma, P.X., 2017. Antibacterial anti-oxidant electroactive injectable hydrogel as self-healing wound dressing with hemostasis and adhesiveness for cutaneous wound healing. Biomaterials 122, 34–47.

Zhong, Teo, W.E., Zhu, X., Beuerman, R., Ramakrishna, S., Yung, L.Y.L., 2005. Formation of collagen−glycosaminoglycan blended nanofibrous scaffolds and their biological properties. Biomacromolecules 6, 2998–3004.

Chitosan-glucan Complex Hollow Fibers Reinforced Collagen Wound Dressing Embedded with Aloe vera. II. Multifunctional Properties to Promote Cutaneous Wound Healing

A.M. Abdel-Mohsen[a,b,c*], J. Frankova[d], R.M. Abdel-Rahman[a], A.A. Salem[e], N.M. Sahffie[f], I. Kubena[g], J. Jancar[a,b,h]

[a] CEITEC-Central European Institute of Technology, Brno University of Technology, Purkyňova 656/123, Brno 612 00, Czechia

[b] SCITEG, a.s., Brno, Czechia

[c] Pretreatment and Finishing of Cellulosic based Textiles Department, Textile Industries Research Division, National Research Centre, , 33 EL Buhouth St., Dokki, Giza 12622, Egypt

[d] Department of Medical Chemistry and Biochemistry, Faculty of Medicine and Dentistry, Palacky University, Hněvotínská 3, 775 15, Olomouc, Czechia

[e] Pharmacology Department, National Research Centre, , 33 EL Buhouth St., Dokki, Giza 12622, Egypt

[f] Pathology Department, National Research Centre, , 33 EL Buhouth St., Dokki, Giza 12622, Egypt

[g] Institute of Physics of Materials, Academy of Sciences of the Czech Republic, Žižkova 22, CZ 61662, Brno, Czechia

[h] Institute of Materials Chemistry, Facility of Chemistry, Brno University of Technology, Purkyňova 464/118, Brno, 612 00, Czechia

Characterization of Functional wound dressing (FWD)

Attenuated total reflectance infrared spectroscopy (ATR-FTIR): **ATR-FTIR** was performed on the fourier-transform infrared spectrometer (Bruker Tensor 27, USA) spectrometer equipped with a germanium crystal for ATR over the spectra range ranging from 4000 to 650 cm^{-1} at the resolution 4 cm^{-1} and 128 scans and the obtained spectra were analyzed utilizing OPUS software.

Transmission electron microscope (TEM): TEM investigations were performed employing the JEOL JEM-2010 (HT) electron microscope (JEOL, Japan), with an accelerating voltage of 120 kV. The dressing scaffold was dispersed in Milli-Q water with a concentration of 0.5 mg/ml, and a drop was placed on Cu grids pre-coated with carbon films and dried in air.

Scanning electron microscopy (SEM). Surface morphology and microstructure of native and dressing scaffolds were visualized using SEM (LYRA 3, Brno, Czechia). The average fiber diameter and pore size of the nat and FWD were determined by collecting data from 100 different locations within SEM images, and Image J was used for subsequent measurements and analysis. For better resolution, dressing scaffolds were dried at room temperature before sputter coating with 20 nm of Au/Pd layer and imaged at 10 kV in SEM.

Thermal gravimetric analysis (TGA): TG-DTG was used for the study of thermal stability and moisture content of the different composition of wound dressing sheets. Measurements were carried out in a nitrogen atmosphere with a temperature rate of 10 °C/min up to 600 °C and with the sample in the mass range 5-10 mg.

Degradation measurement: Wound dressing mats were cut into 1× 1 cm strips and weight then immersed into phosphate buffer solution (PBS) solution and placed in an incubator at 37 °C to test their hydrolytically stability at body conditions. After removing the swollen samples from the solutions at regular intervals, samples were freeze-dried until constant weight. Hydrolytic degradation was examined gravimetrically by recording weight decrements as a function of time (0, 1, 3, 5, 10, 14, and 21 days). Weight loss was calculated according to the Eq. (1).

$$\textit{Weight loss } (\%) = \frac{Wi - Wf}{Wi} \times 100 \qquad (1)$$

Where W_i was the weight of dried sample and W_f. was the weight of the sample in the regular time. The resulting value is an average of five measurements.

64

Swelling percentage: 0.5×0.5 cm dressing specimens were gravimetrically evaluated in PBS solution (pH=7.5) at 37 °C. In regular time intervals (0, 1, 6, 12, 24, 48, 72, 96, 120, and 168 h) swollen pieces were removed, the excess surface water was quickly swiped out by blotting paper and reweighed. The swelling percentage of native and dressing were defined according to the Eq. (2).

$$\textbf{\textit{Swelling percentage}}\ (\%) = \frac{Ws-Wd}{Wd} \times \textbf{\textit{100}} \qquad (2)$$

Where W_s was the weight of the swollen sample at the given time and W_d is the weight of the dry sample. The resulting value is an average of 5 measurements (n = 5).

Antibacterial measurements: The antibacterial activity of different dressing (net CO, CO/AV (1/2), CO/CSGC (1/2) and CO/VSGC/AV (1/2/2) scaffold were selected to evaluate the biological activity against *Bacillus subtilis, Streptococci (+ G)* and *Klebsiella Pneumoniae, Escherichia coli* (gram-negative) by disk plate method. A microbial suspension of 1×10^8 bacteria /mL was inoculated in nutrient agar plates by the spread plate method and the Muller-Hinton agar was prepared by mixing beef extract powder (3 g), starch (1.5 g), casein hydrolase (17.5), and agar (17 g) in 1 L of Milli-Q water and the pH was adjusted 7.5 the heated up to completely dissolved the medium then medium was sterilized using autoclave at 121 °C for 25 min. This nutrient agar medium was transferred into sterilized petri dishes in laminar airflow. After solidification of the media, *Bacillus subtilis, Streptococci (+ G)* and *Klebsiella Pneumoniae, Escherichia coli (- G)* cultures were streaked on the solid surface of the media. Different dressing scaffold (11 mm) was loaded into the surface of solidified medium agar. The discs (control, gauze) were incubated at 5 °C for 1 h to permit good diffusion. All the plates then incubated for 24 h at 37 °C.

Porosity measurements: the porosity of the prepared dressing scaffold was determined by using the reported method(Liang et al., 2016). The scaffold was immersed in absolute ethyl alcohol until it was saturated. The weight of the scaffold was measured before and after the immersion. The porosity (*P*) was calculated from the following Eq. (3).

$$Porosity\ (\%) = \frac{M2-M1}{\rho v} \times 100 \qquad (3)$$

91
92
93
94
95

96
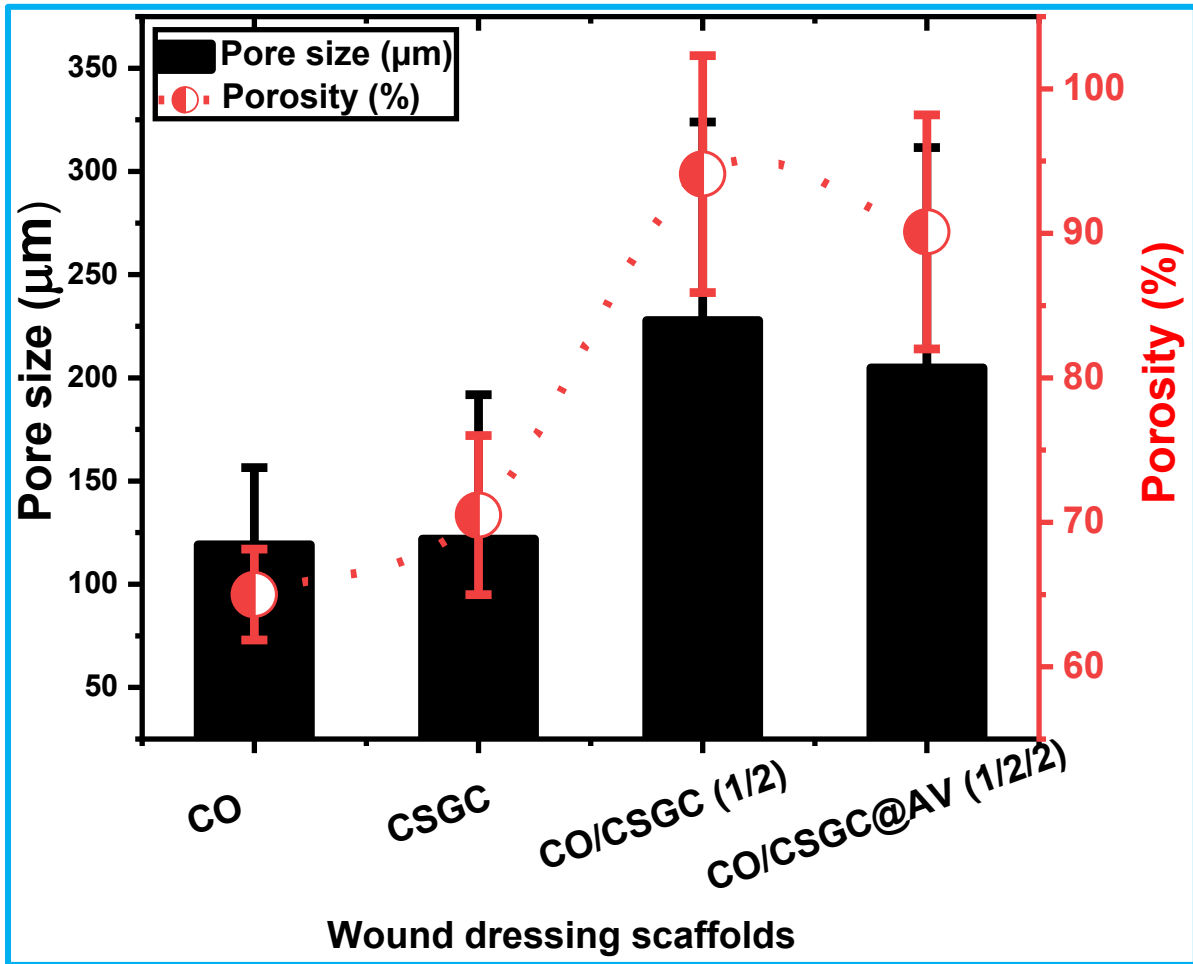
Figure S1: pore size and porosity of net and FWD

97

98

99
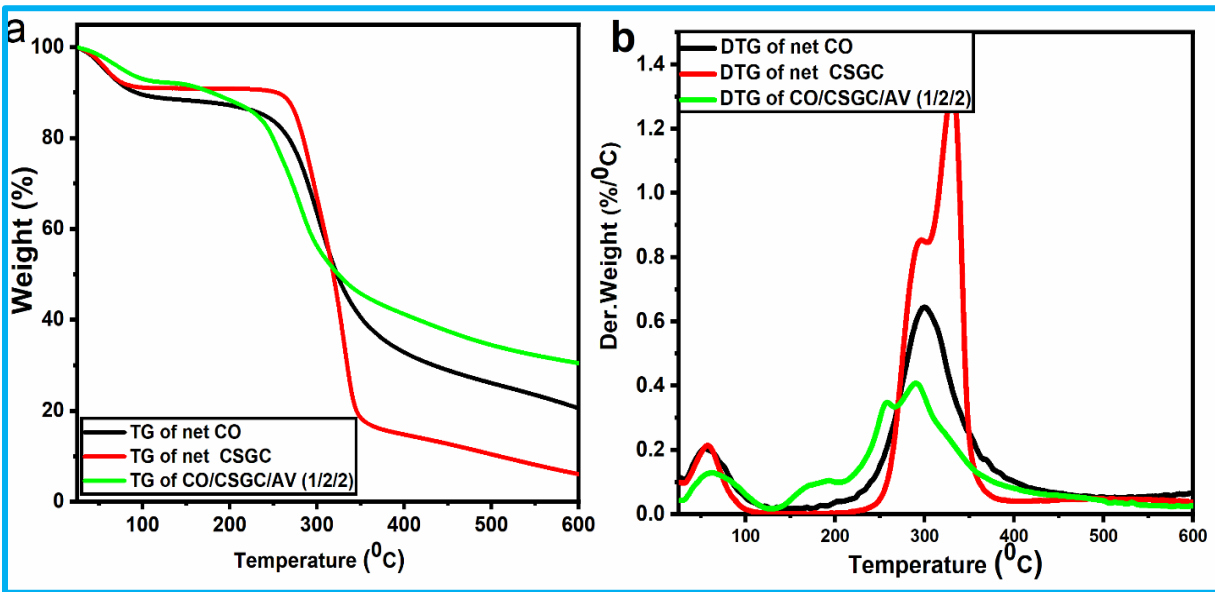
Figure S2: TG-DTG of native and FWD
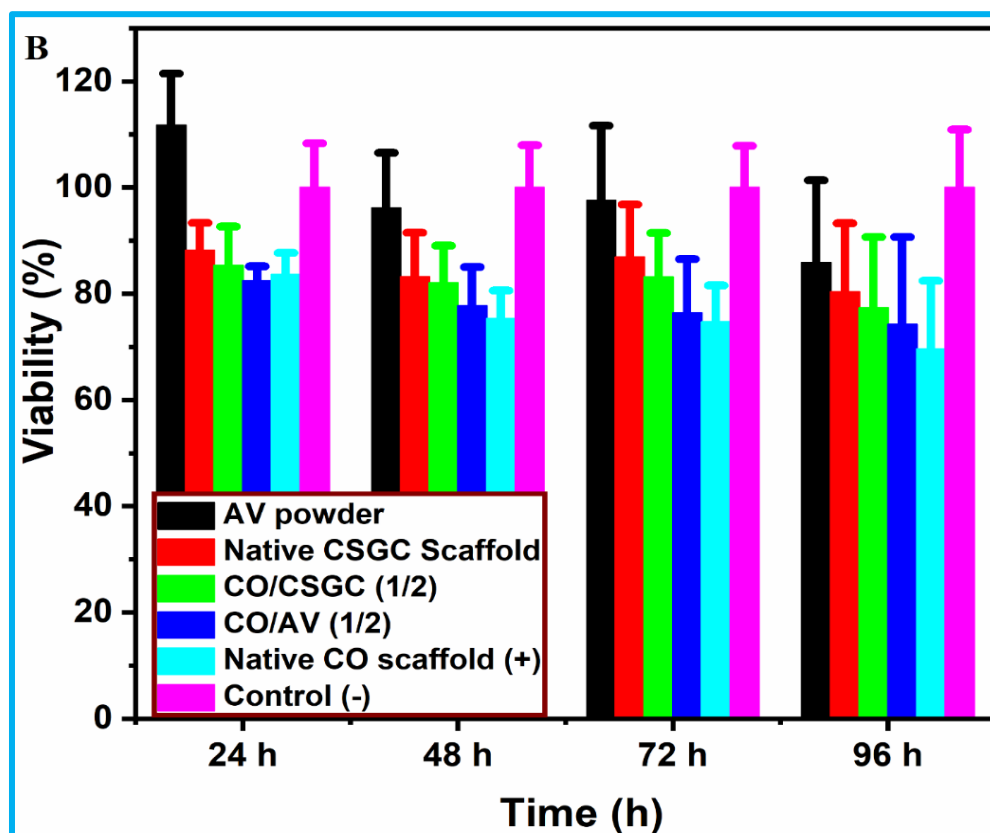
Figure S3. Cytotoxicity of natives and FWD at a different seeded time using a higher concentration of dressing scaffold (1000 mg/ml).

Notes: Positive control (CO sheet) and negative control (cells without samples only culture medium).

Table S1. Comparison between properties of CO/CSGC@AV-FWS and other dressing materials reported in the literature.

Dressing types	Days of treatments	Wound closure percent (%)	Ref.
CO/CSGC@AV	**8**	**92**	**This work**
Chitosan alginate/gentamicin	7	60	(Bakhsheshi-Rad et al., 2020)
Polyvinyl Pyrrolidone-Isatis Root	11	80	(Dong et al., 2019)
SF@Au/G	15	89	(Zhou et al., 2020)
PVA-SA hybrid hydrogel	14	86	(Kaur et al., 2019)
nanofiber sponge	21	90	(Zhang et al., 2019)
poly(ε-caprolactone)/chitosan dressings	7	77	(Zhou et al., 2017)
Nonwoven ChCSGC	15	95	(Abdel-Mohsen et al., 2016)
Silver crosslinked injectable bFGF-eluting supramolecular hydrogels	15	85	(Xuan et al., 2020)
PLLA/POSS nanofibers	24	90	(Li et al., 2018)

110   **References**

Abdel-Mohsen, A.M., Jancar, J., Massoud, D., Fohlerova, Z., Elhadidy, H., Spotz, Z., Hebeish, A., 2016. Novel chitin/chitosan-glucan wound dressing: Isolation, characterization, antibacterial activity and wound healing properties. International Journal of Pharmaceutics 510, 86-99.

Bakhsheshi-Rad, H.R., Hadisi, Z., Ismail, A.F., Aziz, M., Akbari, M., Berto, F., Chen, X.B., 2020. In vitro and in vivo evaluation of chitosan-alginate/gentamicin wound dressing nanofibrous with high antibacterial performance. Polymer Testing 82, 106298.

Dong, W.-H., Mou, X.-J., Liu, G.-S., Huang, X.-W., Yan, X., Ning, X., Russell, S.J., Long, Y.-Z., 2019. Performance of Polyvinyl Pyrrolidone-Isatis Root Antibacterial Wound Dressings Produced in situ by Handheld Electrospinner. Colloids and Surfaces B: Biointerfaces, 110766.

Kaur, P., Gondil, V.S., Chhibber, S., 2019. A novel wound dressing consisting of PVA-SA hybrid hydrogel membrane for topical delivery of bacteriophages and antibiotics. International Journal of Pharmaceutics 572, 118779.

Li, W., Wu, D., Tan, J., Liu, Z., Lu, L., Zhou, C., 2018. A gene-activating skin substitute comprising PLLA/POSS nanofibers and plasmid DNA encoding ANG and bFGF promotes in vivo revascularization and epidermalization. Journal of Materials Chemistry B 6, 6977-6992.

Liang, D., Lu, Z., Yang, H., Gao, J., Chen, R., 2016. Novel Asymmetric Wettable AgNPs/Chitosan Wound Dressing: In Vitro and In Vivo Evaluation. ACS Applied Materials & Interfaces 8, 3958-3968.

Xuan, X., Zhou, Y., Chen, A., Zheng, S., An, Y., He, H., Huang, W., Chen, Y., Yang, Y., Li, S., Xuan, T., Xiao, J., Li, X., Wu, J., 2020. Silver crosslinked injectable bFGF-eluting supramolecular hydrogels speed up infected wound healing. Journal of Materials Chemistry B.

Zhang, K., Bai, X., Yuan, Z., Cao, X., Jiao, X., Li, Y., Qin, Y., Wen, Y., Zhang, X., 2019. Layered nanofiber sponge with an improved capacity for promoting blood coagulation and wound healing. Biomaterials 204, 70-79.

Zhou, L., Yu, K., Lu, F., Lan, G., Dai, F., Shang, S., Hu, E., 2020. Minimizing antibiotic dosage through in situ formation of gold nanoparticles across antibacterial wound dressings: A facile approach using silk fabric as the base substrate. Journal of Cleaner Production 243, 118604.

Zhou, X., Wang, H., Zhang, J., Li, X., Wu, Y., Wei, Y., Ji, S., Kong, D., Zhao, Q., 2017. Functional poly(ε-caprolactone)/chitosan dressings with nitric oxide-releasing property improve wound healing. Acta Biomaterialia 54, 128-137.

Publication 4

Novel chitin/chitosan-glucan wound dressing: Isolation, characterization, antibacterial activity and wound healing properties

A.M. Abdel-Mohsen[a,b,c,*], J. Jancar[a,b,d], D. Massoud[e], Z. Fohlerova[a], H. Elhadidy[f,g], Z. Spotz[a], A. Hebeish[c]

[a] CEITEC-Central European Institute of Technology, Brno University of Technology, Brno, Czech Republic
[b] SCITEG, a.s., Brno, Czech Republic
[c] National Research Centre, Textile Research Division, Department of Pre-treatment and Finishing of Cellulosic Fibers, Dokki, Cairo, Egypt
[d] Faculty of Chemistry, Institute of Materials Chemistry, Brno University of Technology, Brno, Czech Republic
[e] Zoology Department, Faculty of Science, Fayoum University, Fayoum, Egypt
[f] CEITEC–Central European Institute of Technology, Institute of Physics of Materials, Academy of Sciences of Czech Republic, Brno, Czech Republic
[g] Faculty of Science, Physics Department, Mansoura University, Mansoura, Egypt

ARTICLE INFO

ABSTRACT

Chitin/chitosan-glucan complex (ChCsGC) was isolated from Schizophyllum commune (S. commune) and dissolved for the first time in precooled ($-15\,^{\circ}C$) 8 wt.% urea/6 wt.% NaOH aqueous solution. Novel nonwoven microfiber mats were fabricated by wet-dry-spinning technique and evaluated the mechanical of fabrics mats and surface morphology. Isolated and nonwoven mat were characterized employing FTIR-ATR, Optical microscope, TGA, DSC, H/C NMR, SEM and XRD techniques. According to the physical/chemical characterization measurements we can assumed that, the net and the novel dressing mats have the same chemical structure with slightly changes in the thermal stability for the dressing mats.The biological activity of the nonwoven ChCsGC fabric was tested against different types of bacteria exhibiting excellent antibacterial activity. Cell viability of the plain complex and nonwovens mats were evaluated utilizing mouse fibroblast cell line varying concentrations and treatment time. ChCsGC did not show any cytotoxicity against mouse fibroblast cells and the cell-fabrics interaction was also investigated using fluorescence microscope. The novel ChCsGC nonwovens exhibited excellent surgical wound healing ability when tested using rat models.

© 2016 Elsevier B.V. All rights reserved.

1. Introduction

Wounds are commonly classified as without and/or with tissue loss, acute and chronic (Lee et al., 2000) and the surgical wounds represent over 40% of all the wound cases worldwide. Wound infection is one of the primary complications of today's wound care management able to impede the healing process and can keep the wound from complete closure (Guo and DiPietro, 2010). The application of biological materials, in different form like solutions, creams, for drug delivery to the wounds are not very effective as they rapidly absorb fluid during the process and lose their physical, mechanical properties and become unstable (Boateng et al., 2008). For this reasons, the use of wound dressing mats is preferred as they provide better exudate management and prolonged residence at the wound site. The advanced wound dressing such as chitin/chitosan-glucan complex have many advantage as solid form (physical stability), antibacterial activity, healing character as well as drug carriers compared with the traditional dressing such as

gauze and cotton wool that take no active part in wound healing process. Chitosan is the second most abundant natural polysaccharide routinely obtained by deacetylation of chitin. Chitosan exhibits unique properties such as biocompatibility, biodegradability and bacteriocidity (Abdel-Mohsen et al., 2012; Abedini et al., 2013; Fan et al., 2014; Lee and Mooney, 2001) and process-ability into micro and nano-fibers. Due to the antibacterial activity, healing properties, haemostasis and anesthetic effect, it has attracted enormous attention in biomedical material research as a component of wound dressing (Angspatt et al., 2011; Arockianathan et al., 2012; Bagheri-Khoulenjani et al., 2009; Bellini et al., 2012; Boateng et al., 2008; Bueno and Moraes, 2011; Chen et al., 2015; Fan et al., 2014; Valle et al., 2014).

Fungal polysaccharides and polysaccharide-protein complexes, found in cell walls as a part of the extracellular matrix, have been investigated due to a variety of biologically attractive functions such as anti-tumor, anti-nociceptive, anti-inflammatory, anti-oxidative and immune stimulatory activities (Burkatovskaya et al., 2006; Cheng et al., 2012; Cho et al., 1999; Chorvatovičová and Šandula, 1995; Cordeiro et al., 2012; Valasques Junior et al., 2014). The β-D-glucans are polymers of D-glucose monomers linked by β-glyosidic bonds (with or without $(1 \rightarrow 6)$-β-D-glucose side chains) found in the cell walls of many bacteria, plants, fungi and yeasts (Ogawa et al., 2014; Reis et al., 2002). A variety of β-D-glucan differing in structures have been isolated from various sources and their biological activity can be regulated by various structural parameters, such as the primary structure, molecular weight, functionalization and conformation (Ogawa et al., 2014).

Chitosan and glucan are the main components of the cell walls of fungi occurring in two forms, as a free chitosan and a chitosan covalently bonded to β-glucan (Kanetsuna and Carbonell, 1970). These branched β-1,3-glucans are accompanied by different amounts of glucans with β-1,6 and β-1,3 links only or alternating β-1,3 and β-1,6 links together with chemical bonding among glucan chains. This results in forming a cross-linked network which confers rigidity to the cell wall (Mislovičová et al., 2000). The individual polysaccharide chains aggregate into micro-fibrils held together by hydrogen bonds and this, together with the cross-linked network of glucan, results a very strong and rigid cell wall structure (Dergunova et al., 2009).

Chitin–glucan complexes from Komagataella pastoris (Farinha et al., 2015), Komagataella Pichia (Chagas et al., 2014), Aspergillus niger (Skorik et al., 2010), cell wall of fungus Gongronella butleri (Nwe et al., 2008), yeast bud scars (Yamaoka et al., 1989) was isolated by chemical and enzymatic processes. The resultant chitosan–glucan complexes from chitin-glucan were used as flocculation agent and as support for cultivation of mammalian cells (Skorik et al., 2010). Moreover, chitosan–glucan complex was tested for removal of selected metal ions from waste water (Chorvatovičová and Šandula, 1995). In addition, the reduced molecular weight carboxymethylated derivative of a chitosan–glucan complex was investigated for its anti-mutagenic activity. The disadvantage of the chitin/chitosan-glucan complex is the poor solubility in water and in other types of solvents greatly reducing its applicability. The lack of applications of chitosan fibers were the poor mechanical and stability of dressing chitosan fibers/fabrics as well as to prepare 3D structure of chitosan has to be chemically cross-linked by different hazardous cross-linker (Lee et al., 2004; Schiffman and Schauer, 2007; Yang et al., 2005). Almost all studies of chitosan based wound dressing only used on form of fibers (micro/nano) (Annur et al., 2015; Schiffman and Schauer, 2007; Toivonen et al., 2015; Zhang et al., 2008), films (Ligler et al., 2001; Mi et al., 2006; Suginta et al., 2013; Yuan et al., 2007) or hydrogel (Jungst et al., 2015; Kumar et al., 2004; Suginta et al., 2013), but chitin/chitosan-glucan microfibers/nonwoven mats not been reported. Therefore, in the present research we

dissolve the complex for the first time in green solvent, and to innovate complex-based wound dressing with improved the bacteria killing and to enhance the healing properties.

In this work, we present results on isolation, physico-chemical characterization of chitin/chitosan-glucan complex (ChCsGC), and preparation of novel ChCsGC microfiber nonwoven mats using wet-spun technology. We report on using urea/sodium hydroxide aqueous solution to dissolve the complex for the first time. The surface morphology, chemical stability, biological activity and mechanical properties of a novel nonwoven mat flat wound dressing were investigated in relation to their structural variables. The antibacterial activity, cytotoxicity, in vitro and in vivo effect of this wound dressing in closing surgical wounds were assayed employing rat models.

2. Experimental

2.1. Materials

Mycelium as a source of chitin/chitosan-glucan complex was produced using Schizophyllum commune strain from collection of microorganism (Contipro Biotech Ltd., Czech Republic). Sodium hydroxide, acetic acid, ethanol, and isopropyl alcohol (IPA) were purchased from Lach-Ner, s.r.o., Czech Republic; MilliQ water was prepared by Millipore Elix instrument was used for all experiments.

2.2. Methods

2.2.1. Isolation of ChGC and ChCsGC

5 g (dry weight) mycelium fermented from Schizophyllum commune (S. commune) was treated with 1% of NaOH and stirred for 5 h at room temperature (25 °C). The biomass was treated with 2% of NaOH at 90 °C for 1–10 h, cooled down to room temperature and then diluted with distilled water to (1:100 S/L) ratio. The suspension solution of mycelium was filtered and the insoluble part was collected, washed three times in distilled water with neutral pH, washed in 75% isopropyl alcohol and pure isopropyl alcohol. The product was dried at 50 °C in oven, yielding 70% of chitin-glucan complex (ChGC). 1 g of chitin-glucan complex (ChGC) was dispersed in 25–60% sodium hydroxide, heated up to 90 °C and stirred for 5 h. The product was filtered and washed with distilled water until neutral pH, followed by drying at 50 °C. The alkali insoluble material of ChCsGC was treated with 1 M acetic acid at 50 °C for 2 h removed acid soluble chitosan, filtered, washed with distilled water until pH neutral, and then dried at 50 °C for 24 h. Increased the pH of the supernatant, chitosan started to precipitated, collected and dried at 60 °C for 5 h. The yield percent was 72% of ChCsGC and the degree of deacetylation (DDA) of the obtained chitin/chitosan-glucan complex (ChCsGC) was 71%.

2.2.2. Dissolution of ChCsGC

Chitin/chitosan-glucan complex (ChCsGC) with 71% degree of deacetylation (DDA) was used in all experiments. 6/8/86 wt.% NaOH/urea/H_2O mixture solution precooled to (−15 °C). ChCsGC sample in the desired amount was dispersed immediately in the solution under vigorous stirring for 30 min at room temperature to obtain a transparent dope of ChCsGC with different concentrations ranging from 0.1 to 5%.

2.2.3. ChCsGC fibers and nonwoven mats

ChCsGC fibers were prepared by wet-dry-spinning technique. Three grams of the complex was dissolved in urea/sodium hydroxide aqueous solution (see Section 2.2.2) until well flowing viscous and homogenous solution was obtained. The prepared solution was spun using the lab nozzle with needle diameter of

0.3 μm. The solution was extruded into coagulating solution bath containing 10% of acetic acid in isopropyl alcohol (v/v). Non-drawn fibers were obtained after 15 h of standing in coagulation bath for solidification. The solidified fibers were washed in second coagulation bath containing absolute isopropyl alcohol, and then air dried. For wound dressing mats preparation, the fibers were kept in the coagulation bath for 1 h. The long fibers were cut into small spices with length of 5 mm. The chopped fibers were suspended in isopropyl alcohol for 1 h at room temperature, then filtered using polyamide fibers as filter papers and it was hot pressed at 50 °C and a pressure of 0.1 MPa between two rubber sheets with clamp from each edge for 8 h the nonwoven wound dressing was impregnated in isopropyl alcohol two time for 1 h to remove any water residual and then hot pressed under the same above conditions. The nonwoven mats will used for all further measurements and characterizations.

2.3. Physical characterization

Optical microscope (Axiovert 200M Olympus, Japan) was used to observe the morphological changes of ChCsGC complex in precooled alkali sodium hydroxide/urea aqueous solution at room temperature. Small amounts of the ChCsGC complex solutions were taken out at different times during the dissolution process, pressed between two glass slides, and sealed with paraffin for the observations. X-ray diffraction was performed using D-8 Advance diffractometer (Bruker AXS, Germany) with Bragg-Brentano θ-θ goniometer (radius 217.5 mm) equipped with a secondary beam curved graphite mono-chromator and Na (Tl) I scintillation detector. The X-ray generator was operated at 40 kV and 30 mA. The scan was performed over the angles from 5 to 60° (2θ) in 0.02° step with a counting time of 8 s per step at room temperature.

2.3.1. Antibacterial measurements

The antibacterial activity of nonwoven ChCsGc mats were performed on different types of bacteria: *Escherichia coli* (*E. coli*; −**G**); *Klebsiella pneumoniae* (*K. pneumoniae*; −**G**), *Basillus subtilis* (*B. Subtilis*; +**G**) and *Staphylococcus aureus* (*S. aureus*; +**G**), by the disc diffusion method. Muller-Hinton was prepared by mixing beef extract powder (3 g), starch (1.5 g), Casein hydrolase (17.5), and agar (17 g) in one litter of MilliQ water and the pH was adjusted 7.5. Heated to dissolve the medium completely then the agar medium was sterilized by autoclaving at 121 °C for 15 min. This nutrient agar medium was transferred into sterilized petri dishes in a laminar air flow. After solidification of the media, *Escherichia coli*; *Klebsiella pneumoniae*, *Basillus subtilis* and *Staphylococcus aureus* cultures were streaked on the solid surface of the media. Filter paper disc (11 mm) was loaded with urea/sodium hydroxide (6:8%) aqueous solution, then left under hot air drier to complete dryness. The nonwoven ChCsGC mats were cut into discs with a diameters 11 mm, then put into surface of solidified medium agar. The discs (control, nonwoven mats) were incubated at 5 °C for 1 h to permit good diffusion. All the plates were then incubated for 24 h at 37 °C and the zones of inhibition were measured.

2.3.2. In vitro measurements

3000 (*3T3*) cells well were seeded into wells. The cells were cultured for 24 h before being treated with the plain ChCsGC and ChCsGC nonwoven mats. The cytotoxicity was measured at 0, 24, 48, and 72 h after using the 3-(4-5-dimethylthiazol-2-yl)-2.5-diphenyl tetrazolium bromide (MTT) assay (Abdel-Mohsen et al., 2014; Bobula et al., 2015, 2016). MTT stock solution was added to the cell culture medium and plates were incubated at 37 °C for 2.5 h. The supernatant was discarded and cells were lysed in a lysis solution for 30 min using a laboratory shaker. The optical density was measured employing a Versamax micro-plate reader

(Molecular devices, USA) at a wavelength of 570 nm. Mouse fibroblast cell line *NIH-3T3* (Sigma-Aldrich) was cultured till 20th passage. *NIH-3T3* cells from the10th-20th passage were grown in DMEM supplemented with 10% PBS, glutamine (0.3 mg/ml), penicillin (100 μl/ml) and streptomycin (0.1 mg/ml) in 7.5% CO_2 at 37 °C in 75 cm^2 culture flask as recommended by the supplier. Plain complex and nonwoven fabrics were prepared and used as the cell cultivation medium at different concentrations (100–1000 μg/ml). The prepared samples were autoclaved at 121 °C for 20 min and then dispersed in a sterile medium. The final concentrations of the suspension solutions were 100, 500 and 1000 μg/ml. The tested solution was added to each well so that the final concentrations of the tested solution in the well were 100–1000 μg/ml using medium as diluent. Cells were also cultured in a similar manner on tissue culture polystyrene (TCP) as a negative control.

2.3.3. Fluorescence microscope and cellular viability

In vitro qualitative analysis of cell viability as performed with live/dead assay. The samples of ChCsGC nonwoven fabrics (0.5 × 0.5 cm) were sterilized using UV light for 30 min. Before seeding with *NIH-3T3* cells, the nonwoven mats were incubated in culture medium (DMEM with ʟ-glutamine, 10% FBS, 1% penicillin/streptomycin) 1 h at 37 °C. Cells were seeded on fabrics at a density of 10^5/area in 24-well plate. Samples with seeded 3T3 cells were cultivated at 37 °C and 5% CO_2 for 3, 24, 48 and 72 h. Fluorescence microscopy and live/dead staining (calcein-AM/propidium iodide) were used to determine cell viability 3, 24, 48 and 72 h after seeding. The mixture of calcein-AM (2 μM) and propidium (1.5 μM) in PBS was added to mat fabrics containing seeded cells and incubated for 15 min at 37 °C and 5% CO_2 for live/dead cell detection. Afterwards, ChCsGC nonwoven fabrics were rinsed twice in PBS and visualized using a Zeiss Axio Imager 2 microscope.

2.3.4. In vivo biocompatibility studies

Forty eight male rats (Division of veterinary medicine, National Research Centre, Cairo, Egypt) weighing (150 ± 20 g) were used as the test animals. The animals were maintained at normal room temperature (25–29 °C) on a 12 h light/dark cycle, with free access to a commercial pellet diet and water. All experiments were conducted according to the National Communities Council directives on animal care (National Research Centre, Cairo, Egypt). The dorsal hair of control and treated rats were shaved and (2.5 × 2.5 cm) diameter full thickness wounds were created with a biopsy punch. The wounds were cleaned with normal saline and disinfected by 75% ethanol. The test wounds (n = 3) were then covered with the sterile nonwoven chitin/chitosan-glucan complex mat and fixed with sterile gauze and tapes. Similarly, control wounds (n = 3) were covered with sterile nonwoven cellulosic mat and fixed with tapes. After the treatment procedures, rats were kept in separate cages. On the 1st, 5th, 10th, and 15th postoperative day, the dressings were removed and the appearance of the wound was photographed and the wound area was measured. Then, new dressing was applied to the wound after cleaning with normal saline. The rate of wound closure was determined by the following Eq. (1):

Amount of wound healing (%) = wound area on $A_0 − A_x/A_0 × 100$(1)

where A_0—wound area at day 0, A_x—wound area at specified time of surgery, respectively.

Diabetes was induced by a single injection of freshly dissolved streptozotocin (STZ; Sigma-Aldrich, Cairo, Egypt), 50 mg/kg of body weight in a 0.1 mol L^{-1} citrate buffer (pH 4.5) into the peritoneum. Control rats were injected with citrate buffer. Seven days after STZ injection, rats were screened for serum glucose

levels. Rats with a serum glucose level ≥ 200 mg/dl after 2 h of glucose intake were considered diabetic and selected for further studies. All animals were examined daily for general health conditions and any abnormal changes were recorded. Wounds were examined at 1st, 5th, 10th and 15th post wounding. Before wound evaluation, the bandages were removed and photographs were taken. The test diabetics wounds (n = 3) were then covered with the sterile nonwoven chitin/chitosan-glucan complex mat and fixed with sterile gauze and tapes. Similarly, control diabetics wounds (n = 3) were covered with sterile nonwoven cellulosic mat and fixed with tapes. The extent of re-epithelization, granulation, tissue formation and cell migration were observed histologically during the process of wound healing. Both control and test wounds were excised at intervals of 1st, 5th, 10th and 15th day post wounding (five animals at each interval). The animals were sacrificed, and the granulation tissue formed on and around the excision wounds of the untreated and treated rats was carefully dissected with a sharp, sterile surgical knife (0.2 cm × 1.0 cm) and carefully collected without any folding. Then fixed in 10% buffered formalin solution, dehydrated with increasing alcohol concentrations, cleared with xylol, embedded in paraffin for tissue sectioning. A microtome was used to cut the tissue into 6 μm sections for staining with hematoxylin and eosin solutions. Statistical analysis for the determination of difference between the three groups was analyzed by one way ANOVA (using data analysis plugin of Microsoft Excel) in all experimental and at least three to fifth replications were analyzed from each sample of each day point. All data are presented as mean value with its standard error indicated (mean ± SE).

3. Results and discussion

3.1. Isolation of ChGC and ChCsGC

Fig. 1a shows isolation process of the complex after the fermentation step. Different concentrations of sodium hydroxide was used to remove lipids, and proteins and to deacetylate the chitin-glucan complex from the native mycelium (Farinha et al., 2015; Roca et al., 2012; Yamaoka et al., 1989). Fig. 1b depicts the effect of the reaction time on the deproteinization step of chitin-glucan complex by using NaOH. It is clear from Fig. 1b, that extending the time of reaction up to 10 h increased the percentage of isolated chitin. Fig. 1c shows the relation between the NaOH concentration and the degree of deacetylation of the chitin-glucan complex. By increasing the NaOH concentration from 25 to 60%, the degree of ChCsGC deacetylation increased from 42 to 78%, which is in agreement with what was reported of isolation of complex from different sources (Muzzarelli, 1983; Versali et al., 2009).

For the first time, the urea/NaOH aqueous solution was used for dissolution the ChCsGC. Desired concentration of the urea/NaOH aqueous solution was precooled to −15 °C, desired amount of dried ChCsGC complex was introduced in the precooled solution and stirred at the ambient temperature for 30 min. When the solution of ChCsGC became transparent and homogenous, the complex was considered completely dissolved. No solvent evaporation was observed during the dissolution of the ChCsGC at low temperature. Fig. 1d shows the photograph of freeze-dried ChCsGC (left side) and that of the complex after dissolution in urea/sodium hydroxide
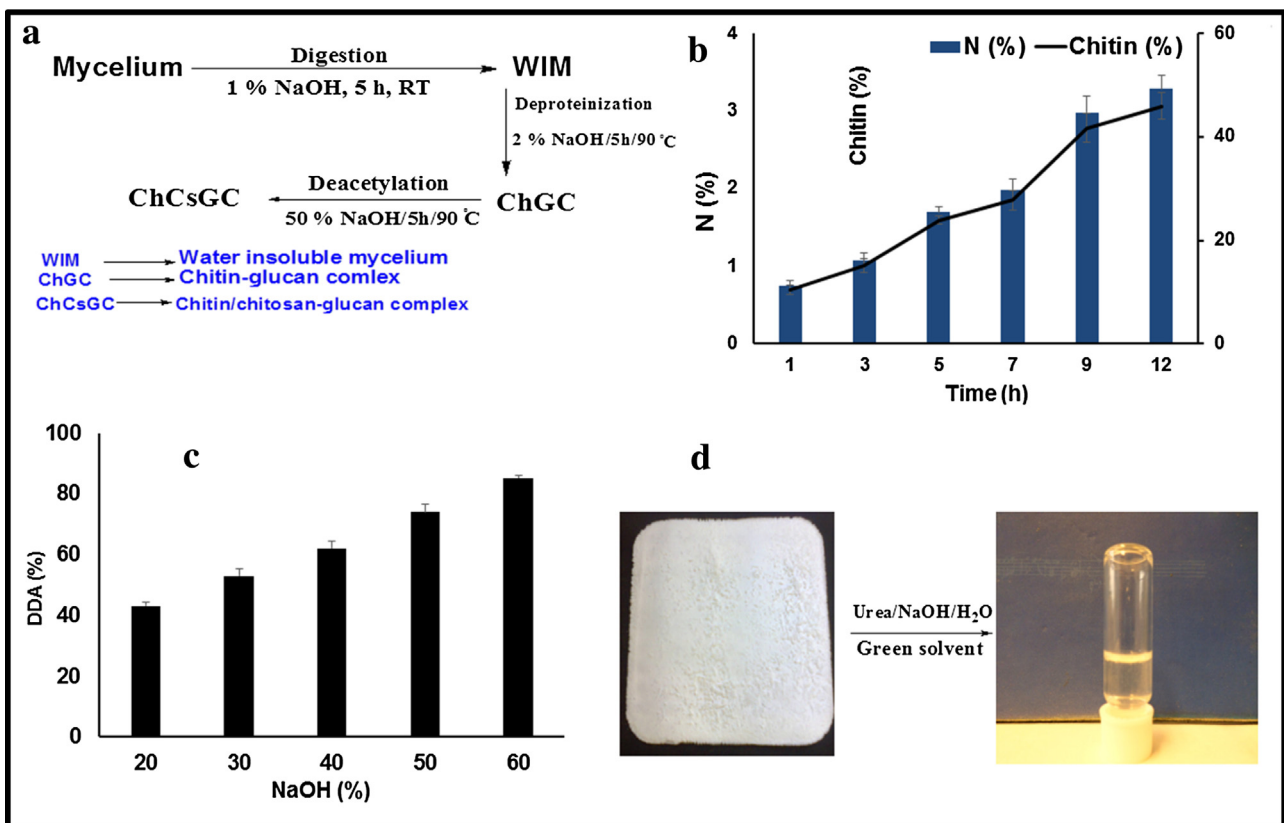

Fig. 1. Scheme of the chitin/chitosan–glucan complex isolation process from mycelium of *Schizophyllum commune* (a); effect of treatment time on the chitin and nitrogen percentage (b); sodium hydroxide concentration on the extraction of ChCsGC (c); photograph of chitin/chitosan glucan complex before and after dissolution in urea/NaOH aqueous solution (d).
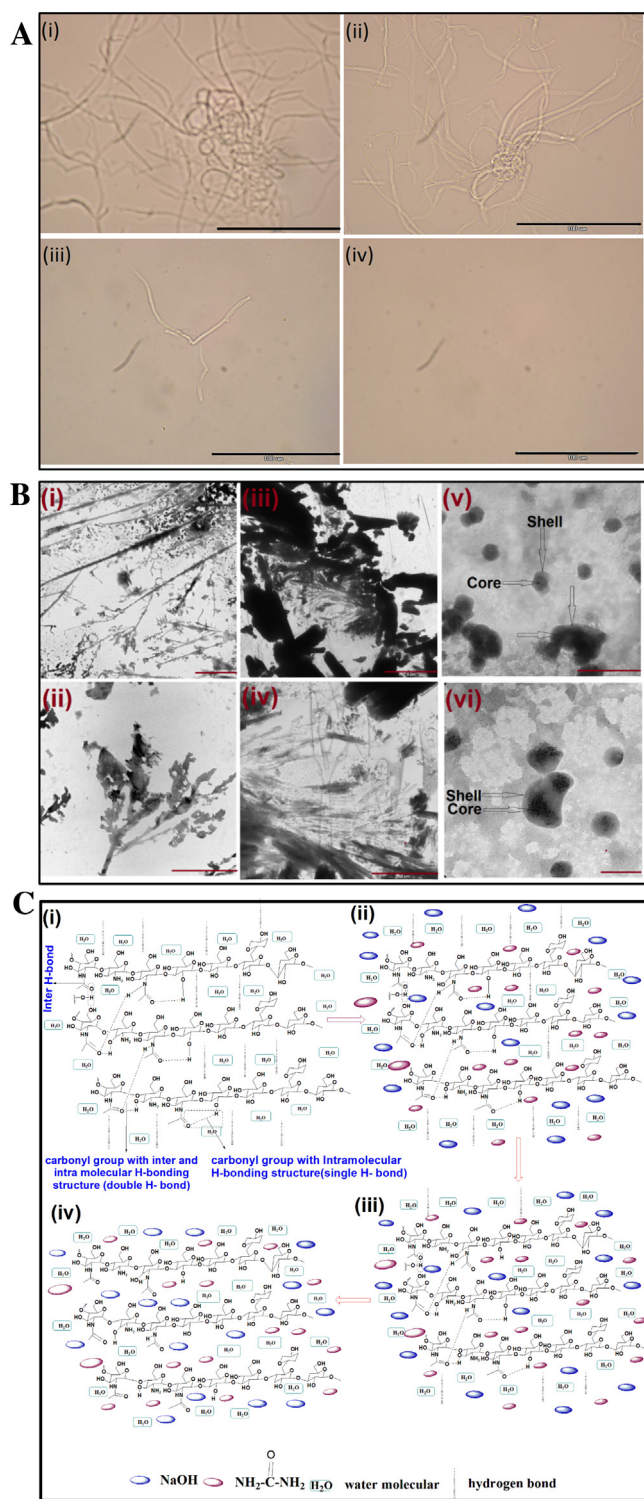
Fig. 2. (a) Optical microscope of chitin/chitosan-glucan complex in the course of dissolution at different times (i) 2 min, (ii)5 min; (iii)10 min; (iv)30 min; scale bars represent 100 μm. (b) Transmission electron microscopy of 8 wt.%urea/6 wt.% sodium hydroxide (i, ii, scale bars are 5, 2 μm); 2 wt.% ChCsGC/6 wt.% sodium hydroxide (iii, iv, scale bars are 5, 2 μm); 2 wt.% ChCsGC/8 wt.%urea/6 wt.% sodium hydroxide (v, vi; scale bars are 200, 100 nm, respectively). (c) Illustration of the dissolution process of ChCsGC; ChCsGC soaked in 6 wt.% NaOH/8 wt.% urea aqueous solution at room temperature; (i) water molecules enter into chitin molecular chain facilitated by the NaOH; (ii) water molecules freeze and expand at the freezing temperature, and break the inter-and intra-hydrogen bond; (iii) promoting solubility of the ChCsGC (iv).

aqueous solution with 2% solution of the complex (right side) exhibiting complete solubility. From the ChCsGC complex solution, various forms of this biomaterials can be prepared such as films, fibers, membranes, sheets or 3D scaffolds.

3.2. Dissolution of ChCsGC in green solvent

Fig. 2a shows the optical image microscope of the dissolution steps of the ChCsGC in urea/sodium hydroxide aqueous solution at different treatment time. Clearly, the dissolution ChCsGC in NaOH/ urea aqueous solution pre-cooled at −15 °C occurs rapidly and its time-dependent and the solubility increase with an increase of the dissolution time from 2 to 30 min, that is transparent and clear solution of ChCsGC forms above 10 min (Fig. 2a).

To provide direct evidence of the ChCsGC inclusions (ICs), transmission electron microscopy (TEM) was used (Fig. 2b). The presence of urea altered the crystalline structure of NaOH to form small crystals (Fig. 2b-i, ii), further confirming the strong association between NaOH, urea and water. As expected, the ICs associated with ChCsGC, NaOH, urea and water into spherical core-shell clusters (Fig. 2b-v, vi). The urea/NaOH solvent worked as the shell surrounding the ChCsGC molecules.

Fig. 2c shows the proposed mechanism of dissolution of ChCsGC in pre-cooled urea/sodium hydroxide aqueous solution. At first, the complex was soaked in the solvent (Fig. 2c-i) at low temperature for a short time period. The water molecules entered between the ChCsGC complex molecules assisted by sodium hydroxide molecules (Fig. 2c-ii). Freezing and expansion of the water at the freezing point broke inter/intra hydrogen bonds between the complex chains (Fig. 2c-iii), thus promoting the solubility of the complex (Fig. 2c-iv). However, above −15 °C, the freezing expansion process was shorter and the expanding effect weakened reducing the ChCsGC solubility.

3.3. Preparation of ChCsGC fibers/nonwoven mat

For the first time, the ChCsGC fibers were prepared by wet-dry-spinning technique in urea/NaOH aqueous solution. Transparent and clear viscous solution of ChCsGC was obtained and the solution was wet spun with the nozzle diameter of 0.3 mm. Fig. 3 shows SEM micrographs of the ChCsGC fibers spunned into different concentrations (2.5, 3, 3.5%) using 5% acetic acid in isopropyl alcohol as components of coagulation bath. The fibers exhibit smooth surface (Fig. 3a-i, iii, v), circular cross-section and compact inner structure (Fig. 3a-ii, iv, vi).

Nonwoven ChCsGC mat was prepared employing new wet/ hydro-spinning technique with the 3% of the ChCsGC. The viscous solution was extruded into coagulation bath and stirred at 2000 rpm/min, thus accelerating the solidification of the ChCsGC fibers compared to the spinning of long micro monofilament fibers. Moreover, this process minimized fibers sticking together into bundles (Fig. 3b). The mats were collected from the coagulation bath (Fig. 3b-i), cut into approximately 5 mm pieces and then partially fused under pressure at heating (50 °C). The fibers were bonded to each other through non-covalent interaction (electro-static bonds, hydrophilic interaction, and hydrogen bonds, and van der-Waals interactions) (Fig. 3b-iv). The treatment of neat ChCsGC with alkaline solution of NaOH in the presence of urea removed the hydrogen bonds between the functional groups of the complex components (chitin, chitosan and glucan) while and preparation of the ChCsGC in an acid solution generated the chemical interaction between the individual complex chains (Fig. 3b-ii). It seems clear that the intermolecular interactions between polysaccharide chains and water were much stronger than between polysacchar-ides and isopropyl alcohol, acetone, and ethanol, thus, biopolymers self-aggregated more easily in the presence of the relatively
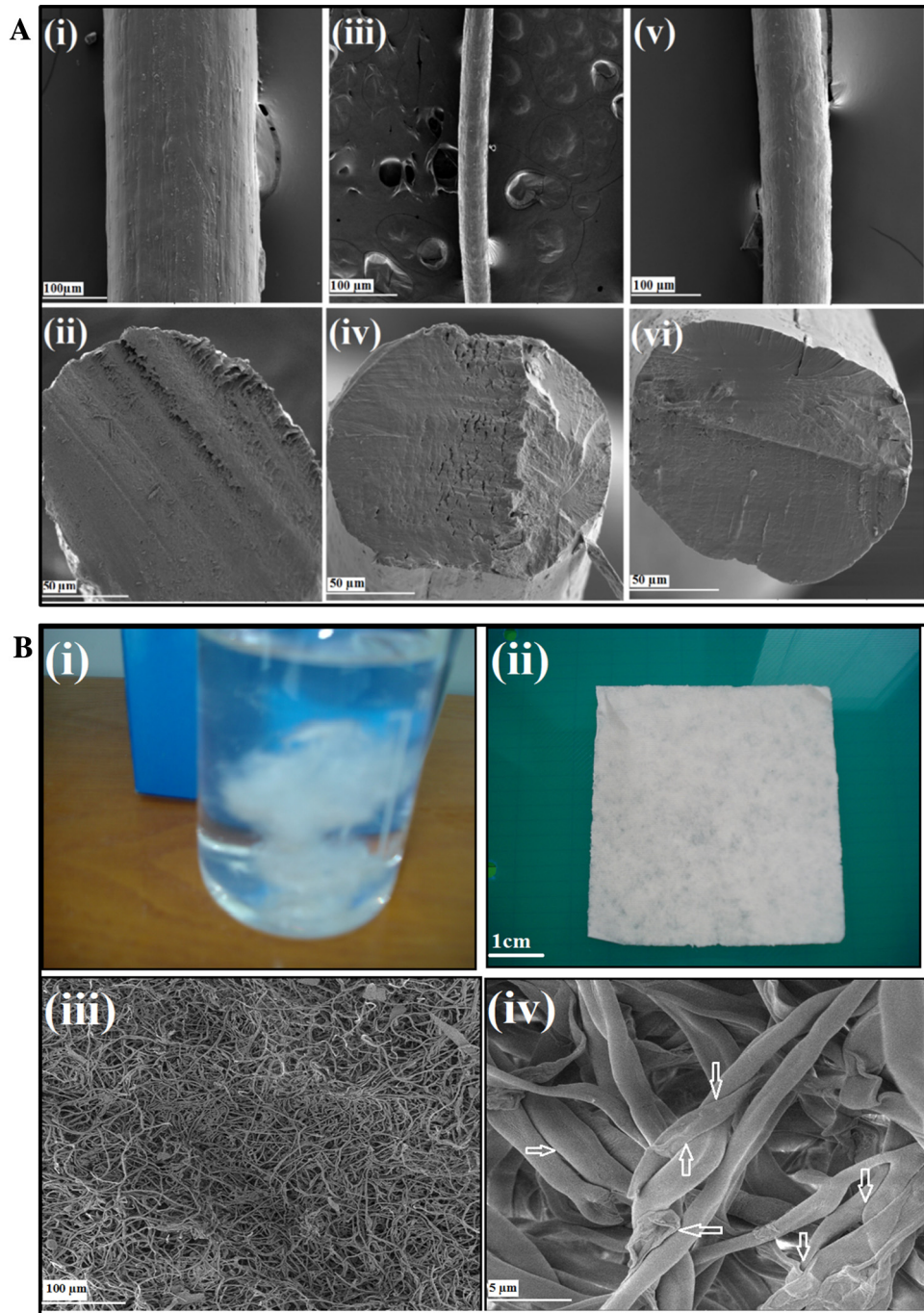
Fig. 3. (a) Scanning electron microscopy of ChCsGC fibers in different coagulation bath composition 5% acetic acid in Isopropyl alcohol (i, ii); 10% acetic acid in Isopropyl alcohol (iii, iv); 15% acetic acid in isopropyl alcohol (v, vi). (b) Photograph of short nonwoven fibers in wet-state (i); nonwoven complex sheet (ii), scale bar is 1 cm; SEM of nonwoven complex sheet with task bar 100 μm (b); SEM of nonwoven complex sheet with task bar 5 μm.

hydrophobic isopropyl alcohol than in the water (Ding et al., 2014; Duan et al., 2013; Goussé et al., 2002). Therefore, co-adhesion between ChCsGC fibers prepared in isopropyl alcohol enhanced significantly, leading to a compact chain packing after the hot pressing (Fig. 3b-iv). Interestingly, the new nonwoven fabrics show also porous structure (Fig. 3b-iv) which was also important for the supply oxygen, absorption of exudate and maintained a large amount of water and fluids (Fan et al., 2014; Wang et al., 2007). In

Table 1
Effect of coagulation bath composition on the mechanical properties of complex fibers.

Treatments	Coagulation bath composition	Tensile strength (cN/detx)	Elongiation at break (%)
I	5%(v/v)AA/IPA	1.000	1.167
II	10%(v/v)AA/IPA	1.531	6.336
III	15%(v/v)AA/IPA	1.173	3.591

AA—acetic acid, IPA—isopropyl alcohol.

Fig. 3b-iv shows more impact structure (arrows), which was able to improve the mechanical properties of the nonwoven dressing mats. Fig. S2 (Supporting information) present the photograph and scanning electron microscope of 3D ChCsGC scaffold prepared from complex microfibers by freeze-dry technique. The ChCsGC 3D scaffold show highly pore size, porosity (data not shown) and was homogeneous in shape. Comparing with plain chitosan, it's

impossible to prepare 3D scaffold structure with cross-linker agents, such structure can obtained from chitin/chitosan-glucan complex without any cross-linker. Table 1 shows the mechanical properties of the ChCsGC nonwoven mats spunned into different coagulation baths composition (5, 10 and 15% acetic acid/isopropyl alcohol solution). The tensile strength and, especially, the elongation at break of the nonwoven mats bundle was strongly
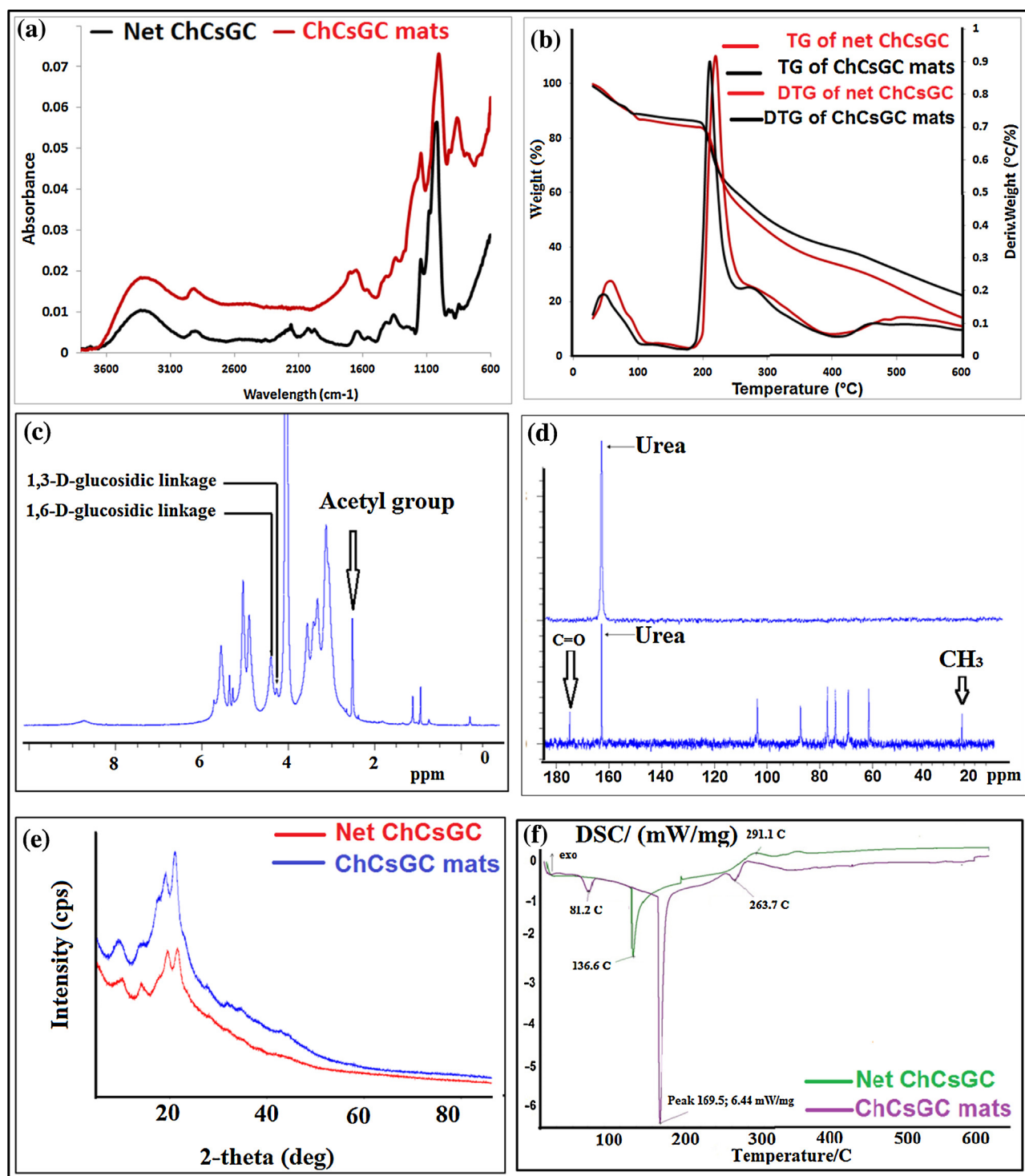
Fig. 4. FTIR-ATR of net chitin-chitosan-glucan complex (ChCsGC) and ChCsGC nonwoven mats (a); TGA and DTG of net ChCsGC and ChCsGC nonwoven mats (b); ^{1}H NMR of the ChCsGC after dissolution in urea/sodium hydroxide/D_2O solution (c); ^{13}C NMR of net urea/sodium hydroxide (upper part) and ChCsGC after dissolution in urea/sodium hydroxide/D_2O solution (d); X-ray diffraction of net ChCsGC, ChCsGC mats (e); DSC of the isolated ChCsGC, ChCsGC nonwoven mats (f).

influenced by the amount of the acetic acid in the coagulation bath. Due to the presence of the amino groups in the ChCsGC chains (Croisier and Jérôme, 2013), leads to a decreased interaction between the functional groups (amino, hydroxyl, acetamide) on the neighboring ChCsGC chains.

3.4. Physical characterization of ChCsGC nonwoven mat

Fig. 4a presents the FTIR-ATR spectra of plain ChCsGC and the nonwoven ChCsGC mats prepared by the wet/hydro-spinning technique. The chitin exhibits absorption bands at 1650, 1552 and $1376\,cm^{-1}$ corresponding to the vibrations of amide groups such (Table S1, Fig. S1, Supporting information). The presence of glucan and chitosan components was indicated by the presence of absorption bands within the wavenumber range of 3400–$2800\,cm^{-1}$. The comparison of relative intensities for absorption bands at 1653 and $1069\,cm^{-1}$ in the spectrum of chitin with corresponding absorption bands at 1650 and $1068\,cm^{-1}$ in ChCsGC spectra demonstrates that for the latter amount of the acetyl groups was lower than the amount of the pyranose rings. Moreover, the FTIR-ATR spectrum of the complex showed bands at $854\,cm^{-1}$ corresponding to the presence of β-configurations (Holan et al., 1981). In addition to these characteristic bands, the spectrum show the bands also at 1039, 1076, 1159, and $1120\,cm^{-1}$ owing to the presence of (1-3)-di-O-substituted glucose residues. Comparing the FTIR-ATR spectra of the extracted complex and nonwoven complex mats, no evidence for chemical changes in the polysaccharide structure was identified suggesting that the formed ChCsGC did not undergo any degradation in the course of processing.

Thermal degradation of the ChCsGC proceeds in three steps (Fig. 4b). The first step appearing between 50 and $130\,°C$, was attributed to the evaporation of physically adsorbed and strongly bonded water, respectively. The next two steps were related to the ChCsGC degradation. The main degradation appeared within the temperature interval from 130 to $300\,°C$ loosing approximately (46 ± 2) wt.% mass. This was caused by the depolymerization of the branched part in glucan, chitin, chitosan, and glucan chains through deacetylation and cleavage the glucosidic, and glycoside amine linkages by dehydration and deamination reactions (Fig. S3, Supporting information). For the isolated complex, the maximum decomposition was observed at $210\,°C$ and for the spun fiber mat, it was shifted to $220\,°C$ (Fig. S3, Supporting information). The second degradation stage between 300 and $600\,°C$ consisting of thermal destruction of the pyranose rings to produce formic and butyric acids. Fig. 4c shows the ^1H NMR of ChCsGC in urea/sodium hydroxide/D_2O solution. Two anomeric signals appeared at 4.2 and 4.9 ppm which was related to (1-3/1-6) linked of glucose unit in glucan in the ChCSGC. The peak at 2.2 ppm was related to the acetyl groups in chitin part of the complex and a single peak at 4.7 ppm is typical for the β-glyosidic configuration (Sonnenberg et al., 1985; Stagg and Feather, 1973). From ^{13}C NMR (Fig. 4d), one peak appearing at 162.5 ppm is related to the C=O of urea. From the ^1H and ^{13}C NMR (Fig. 4c, d) spectral analysis one can conclude that the chains in the chitin/chitosan-glucan complex were covalent bonded by β-(1-4) in linear glucose amine, N-acetyl glucose amine (chitin/chitosan chains), β-(1-4) between complex chains, linear (β-1-3/1-6) glycoside residue with branching at C-6 position of one of (1-3)-linked residue. The X-ray diffraction of extracted and processed ChCsGC (Fig. 4e) exhibits four different diffraction peaks at $2\theta = 10°$, 14°, 20°, and 21° corresponding to the inter-lattice distances of 8.5 Å, 6.2 Å, 4.5 Å and 4.2 Å respectively.

Comparing the XRD of ChCsGC nonwoven mats and mixture of urea/sodium hydroxide (Fig. S4), there was any residual of urea/sodium hydroxide beaks appeared in XRD of nonwoven mats. More conformation from nitrogen measurements, the nitrogen percent

of the nonwoven mats had the same value compared with the plain complex. That's confirmed there was any residual of urea attached the nonwoven mats. Fig. 4f presents the DSC traces of isolated and processed ChCsGC. The ChCsGC peaks at 85, 136, and $291\,°C$ were related to the removal of the non-bonded water, bonded water and decomposition of the glycosic, glucosamine units in glucan and chitin/chitosan, respectively. After processing, three different peaks appeared (Fig. 4f-ii) at 81, 169, and $263\,°C$ suggesting different phase structure of the processed ChCsGC. Structural analysis (FTIR, XRD, NMR,TGA and DSC) indicated that no measurable chemical changes occurred in the course of the ChCsGC processing and most of the structural changes evidenced by these methods were of physical nature. From the FTIR, NMR (H/C), TGA, DSC, of the net complex and wound dressing mats we can conclude that, the novel dressing keep the same chemical and thermal stability after dissolution in sodium hydroxide/urea solution and preparation new nonwoven mats (Fig. 4). The advantage of ChCsGC dressing is the solid form and the strong mechanical properties (Table 1) of the dressing material is preferred in the case of exudative wound as they provide better exudate management and extended residence at wound site. In this sense, ChCsGC wound dressing mats with high enough swelling ratio meets the requirement for effective absorption of exudate from the wound (Fig. S5, Supporting information).

3.5. Antibacterial performance of ChCsGC wound dressing

Microbial invasion is the main cause of the wound infection, which means that the antibacterial activity of the dressing should be evaluated before it is put into use the wound dressing materials. Thus, the antibacterial activity of the nonwoven ChCsGC wound dressing sheets were determined by disk diffusion method. Fig. 5 present the antibacterial activity of control (treated with urea/sodium hydroxide solution) and ChCsGC nonwoven wound dressing against gram negative bacteria Escherichia coli (donated as E. coli), Klebsiella pneumoniae (donated as K. pneumoniae) gram negative bacteria and Staphylococcus aureus (donated as S. aureus); Basillus subtilis (donated as B. subtilis) gram negative bacteria. It can be seen that wound dressing chitin/chitosan-glucan complex exhibits strong antibacterial properties against K. pneumoniae and E. coli (−G) and the inhibition zone was measured (Table S2, Supporting information). Nonwoven mats possess much better antibacterial activity against S. aureus (+G) than B. subtilis (Table S2, Supporting information). It is generally assumed that the effect of chitosan in the ChCsGC is mainly due to the interaction between positively charged chitosan molecules and negatively charged microbial cell membranes. Hence, increasing the degree of deacetylation may enhance the ChCsGC antimicrobial activity. Another proposed mechanism of action of chitin/chitosan on bacteria suggests that chitosan can penetrate the bacterial cell wall and bind to the phospholipids layer of cytoplasm membrane. In addition, the chitin/chitosan also can bind with bacteria DNA subsequently disrupting its DNA replication or it can impair the ability of ribosomes to transcribe messenger's RNA (Huang et al., 2012). Similar phenomenon was also observed and reported elsewhere (Annur et al., 2015; Inamdar and Mourya, 2014; Li et al., 2013; Rodríguez-Núñez et al., 2012; Siralertmukul et al., 2015). Glucan in chitin/chitosan-glucan complex had antibacterial activity against different types of bacteria and fungi (Al Tuwaijri et al., 1987; Bohn and BeMiller, 1995; di Luzio et al., 1979; Guyard et al., 2002; Kagimura et al., 2015; Kokoshis et al., 1978; Luzio et al., 1980; Talbott and Talbott, 2009). The antibacterial activity of the nonwoven wound dressing was only dependent on the biological activity of chitin/chitosan but also the antibacterial activity of glucan.
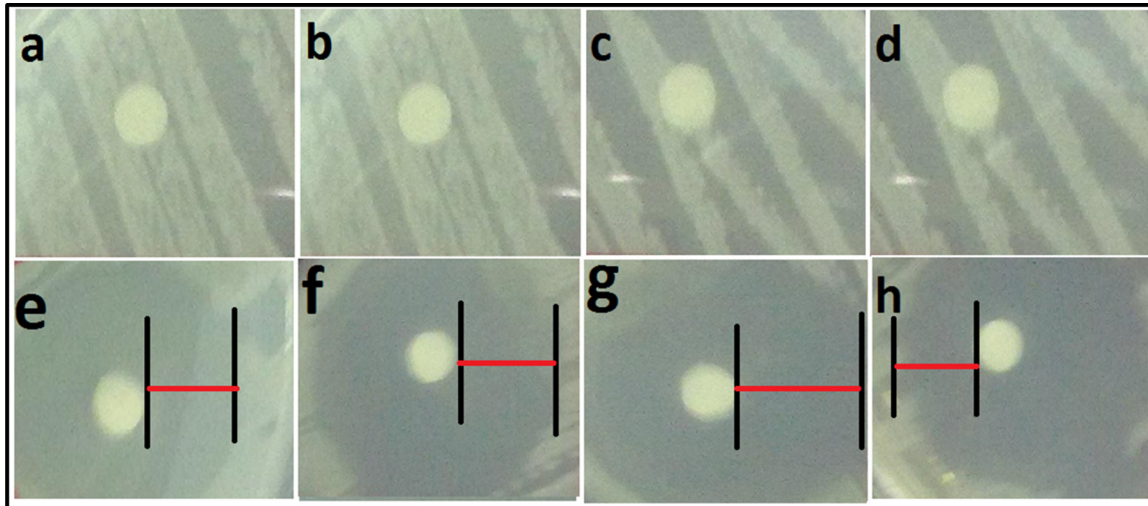
Fig. 5. Inhibition zone assays of bacillus subtilis (a), *Escherichia coli* (b); *Staphylococcus aureus* (c); *Klebsiella pneumoniae* (d) as control sample. ChCsGC nonwoven mats against bacillus subtilis (e), *Escherichia coli* (f); *Staphylococcus aureus* (g); *Klebsiella pneumoniae* (h).

3.6. In vitro measurements of ChCsGC

Fig. 6A shows the cell viability of net chitin/chitosan-glucan complex and renovated nonwoven fabrics embedded with mouse fibroblast (*NIH-3T3*) cell line. As we can see in Fig. 6a, the cell viability in plain complex was tested with mouse fibroblast (*NIH-3T3*) by using different concentrations (100–1000 μg/ml) after 24, 48 and 72 h exposition. The results showed that the isolated complex was non-toxic for mouse fibroblast cell line in the entire inverted (0–72 h) monitored comparing with the control sample. Fig. 6a presents the toxicity of nonwoven sheet tested with mouse fibroblast cell line (*NIH-3T3*). Interestingly, the nonwoven mat complex did not exhibited any measurable toxicity for the mouse fibroblast cells (*NIH-3T3*) over the all concentrations ranging (100–1000 μg/ml) after 24, 48 and 72 h of seeded with the cells. We can conclude that, urea/sodium hydroxide aqueous solution can be used as green solvent for dissolution the chitin/chitosan-glucan complex without any toxicity mentioned. The plain complex and complex nonwoven mat can be used for different medical applications especially for tissue engineering, and wound healing purposes.

The ideal wound dressing should be able to exchange air, oxygen and promote cell growth, proliferation and collagen synthesis (Leveen et al., 1973). Also the dressing material should have large absorption water capacity in order to absorb wound exudates (Wang et al., 2012). Chitin/chitosan-glucan complex wound dressing mat was soaked in physiological buffer solution (PBS; pH 7.4) for different period of times to evaluate the water absorption capacity. As shown in Fig. S5 (Supporting information), the PBS absorbing capacity of complex nonwoven sheet increases with extending soaking time and reach to equilibrium after 7 h of soaking. This indicated that, the complex sheet had large PBS absorption capacity, which is favorable to absorb a large amount of excessive exudates in a long duration. The highly swelling capacity of dressing complex due to the presence of hydrophilic glucan chain in complex structure. The equilibrium water equivalent (EWA) and air permeability present in Table S3 (Supporting information). The nonwoven mat complex has higher water uptake than plain complex, comparing with standard nonwoven viscose fabrics, due to the deformation/regeneration new bond between complex chains which could form inclusion complex (Fig. 2b). the

air permeability of the nonwoven wound dressing complex and standard nonwoven viscose fabrics were measured and nonwoven mats complex has higher air permeability (AP) percentage than standard wound dressing fabrics (Table S3). From swelling, water uptake and air permeability results makes it a favorable wound dressing material.

Cell proliferation on the wound dressing produced by ChCsGC was assessed by fluorescence microscope as shown in Fig. 6b. The viability of *3T3* cells seeded on the wound dressing mats, staining with calcein and propidium iodide was used. Fluorescence images of chitin/chitosan-glucan wound dressing mats (ChCsGC) after 3, 24, 48, and 72 h of treatments with mouse fibroblast cell lines (*NIH-3T3*). Significantly enhanced cell adhesion in the presence of ChCsGC mats after 72 h of seeding cells. The cells were appeared under fluorescence microscope well spread on the mat surface and the cells follow the mats shape and maintained as spherical shape (Fig. 6b-a, b). After 48 h of seeding fibroblast cell with novel wound dressing, the cell has spindle-shaped, confirmed that cells attached and grew on wound dressing surface (Fig. 6b-c, d; yellow arrows). The novel wound dressing mats fabricated from ChCsGC are promising materials for tissue engineering purposes especially for drug delivery and wound healing/dressing applications.

3.7. Rate of wound closure by ChCsGC nonwoven mat

Fig. 7a depicts the changes in the surgical wound area over the period of 15 days. At the date of surgery, no visible difference in the wound appearance was observed between the control and the ChCsGC treated group. Compared to the cotton gauze treated control (control nondiabetics, control diabetic) and wounds treated with ChCSGC nonwoven mat (treated non-diabetics, treated diabetics). The control nondiabetic wound closure was 18, 43, 72% after 5, 10, and 15 days of surgery, respectively (Fig. 7b). Interestingly, the nondiabetic wound rat treated with nonwoven ChCsGC mats exhibited almost 30, 68, 95% after 5, 10, and 15 days of treatment with complex nonwoven mats (Fig. 7b), respectively. ChCsGC mats enhanced and accelerated the closure percentage of diabetic rats comparing with diabetic non-treated rats (Fig. 7b). Comparing with control and treated diabetic rats, the novel wound dressing complex was accelerated and enhanced the healing process (Fig. 7b). During the healing process, chitin and chitosan
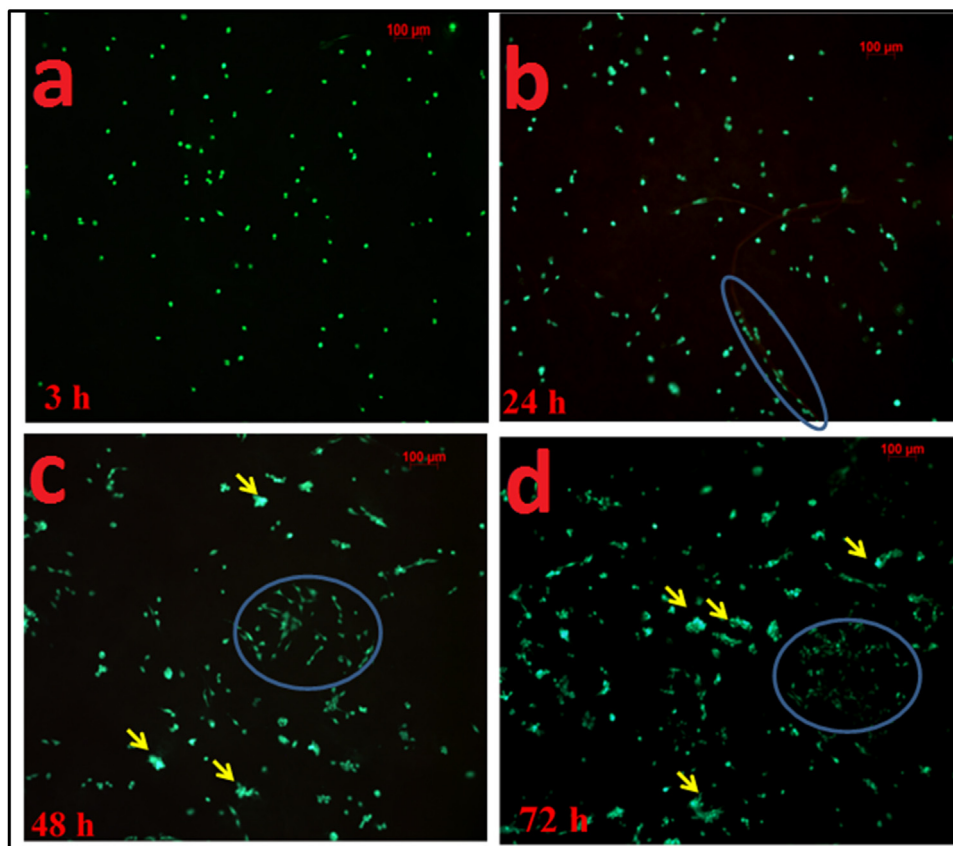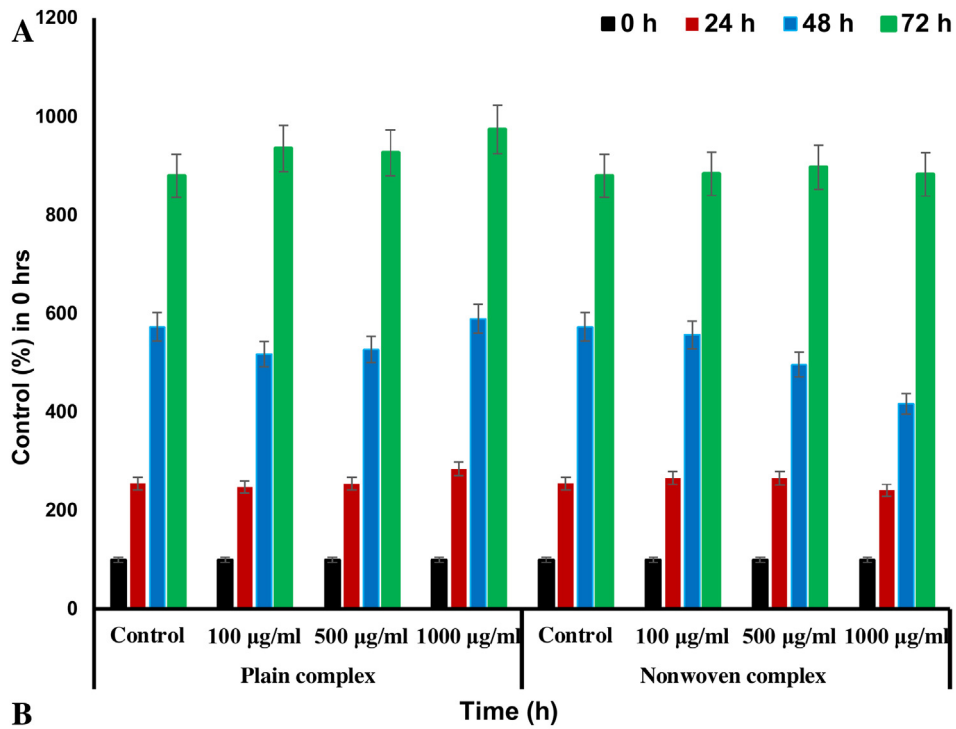
Fig. 6. (a) Cellular proliferation analysis of plain ChCsGC with different concentrations (100–1000 μg/ml), 3T3 viability, MTT, n = 4; ChCsGC nonwoven mat with different concentrations (100–1000 μg/ml), 3T3 viability, MTT, n = 4. (b) Fluorescence microscopy of nonwoven ChCsGC mats and live (green)/dead (red) staining of 3T3 cells after staining with calcein and propidium iodide after different seeding time (3, 24, 84, 72 h). (For interpretation of the references to colour in this figure legend, the reader is referred to the web version of this article.)
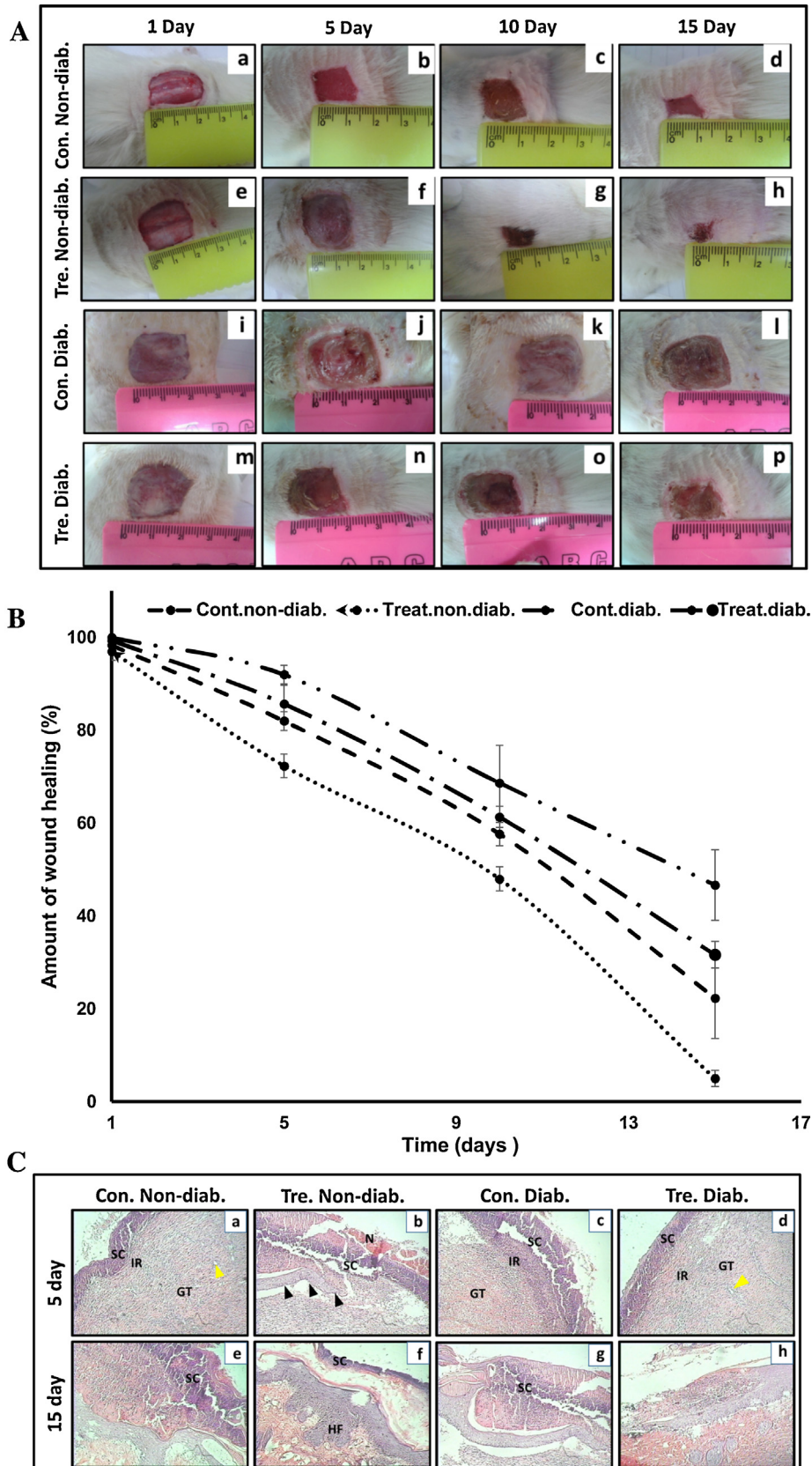
Fig. 7. (a) Macroscopic observation of the surface healing dressed with nonwoven sheet (gauze) from cellulosic material (control-non-diabetic) at 1st, 5th, 10th and 15th days after surgery (a–d), respectively; healing of wound dressed with the ChCsGC sheet (non-diabetic) at 1st, 5th, 10th and 15th days after operation (e–h), respectively; wound surface dressed with nonwoven sheet (gauze) from cellulosic material (control diabetic) at 1st, 5th, 10th and 15th days after operation (i–l), respectively; healing of wound dressed with nonwoven ChCsGC sheet (diabetic) at 1st, 5th, 10th and 15th days after operation (m–p), respectively. (b) Wound contraction as a function of post-surgery time for (non-diabetic and diabetic) wounds treated with nonwoven ChCsGC mats and the control (nonwoven cellulosic gauze), expressed as the remaining percentage of wound area. (c) Pchotomicrograph of histological sections of the wound area stained with hematoxylin and eosin at 5 the (a–d) and 15th (e–h) day post wounding in control non-

gradually depolymerize to release *N*-acetyl-glucosamine monomers, which initiate the fibroblast proliferation and helps with the ordered collagen deposition and stimulates increased level of natural hyaluronic acid synthesis at the wound site (Winter, 1962, 1965). It is generally accepted that the new epidermis grows outside in from the margin to the center of the wound, reducing the depth and area of the wounds with time. The fast wound contraction for wounds treated with ChCsGC nonwoven sheet may be attributed to the fast epidermis ingrowth due to the preserved moist wound environment, since the epithelization is accelerated for moist wounds (Winter, 1962, 1965). Furthermore, chitin and chitosan macromolecules have been reported to induce migration of inflammatory cells and fibroblasts, being activated to produced multiple cytokines (Ishihara et al., 2001; Obmińska-Mrukowicz et al., 2006; Ueno et al., 1999; Usami et al., 1998) and further accelerate the wound healing process (Ishihara et al., 2001). Furthermore, Table S4 (Supporting information) comparatively lists the wound dressing ratio of various the novel ChCsGC wound dressing ratio with those other wound dressing reported elsewhere. It is clear that, although the dressing reported provide satisfactory wound healing ratios, they are less competitive as compared with the new dressing chitin/chitosan-glucan complex. In summary, non-woven mats (ChCsGC) exhibits excellent antibacterial, no cytotoxicity, and excellent healing performance over a very short period and may find potential applications such as skin tissue regeneration and drug delivery purposes.

The final goal for the wound dressing of the skin is to restore the structural and functional properties to the levels of normal tissue, involving the re-epithelialization and orchestrated regeneration of all the skin appendages. Histologic assessment of wound closure in control and treated (diabetic and non-diabetic) groups were analyzed Fig. 7c after 5 and 15 days of surgery. After 5 day surgery in all groups, the wound consisted of a large scab covering the excision area. Acute inflammatory reaction and necrotic tissue (N) were well observed in the superficial layer, under which is the granulation tissue. A newly formed small blood vessel (angiogenesis) embedded in edematous dermis. In treated non-diabetic group (Fig. 7c-f), the epithelial tongue started to invade the underlying granulation tissue, suggesting early phase of re-epithelization and tissue regeneration. At day 15 of surgery, the wound was lined by hyper plastic epidermis, which migrate underneath the diminished scab. In treated non-diabetic group (Fig. 7c-h), the wounded area was markedly reduced in comparison to other groups; there is a complete re-epithelization with formation of new hair follicles, reflecting a higher rate of tissue remodeling and reconstruction.

4. Conclusions

A Novel wound dressing material fabricated from chitin/chitosan-glucan complex (ChCSGC) was used for the first time as wound dressing material. Micro and non-woven fiber/nonwoven sheets were prepared after dissolution of the ChCsGC in urea/sodium hydroxide aqueous solution at low temperature ($-15\,°C$). The surface morphology, crystallinity, thermal stability and mechanical properties of the fibers and nonwoven fabrics were measured and evaluated by different techniques and the complex has the same chemical structure before and after dissolution in urea/sodium hydroxide aqueous system and confirmed by FTIR-ATR, H/C NMR, TGA, and XRD. The ChCsGC has excellent antibacterial properties against different types of bacteria *Escherichia coli*, *Klebsiella pneumoniae*, *Basillus subtilis* and *Staphylococcus aureus*. Net complex/nonwoven complex mat has any cytotoxicity affect against mouse fibroblast cell line after seeded three days with different concentrations. In vivo test with rats showed excellent wound healing ability and promoted accelerated wound closure of the rat skin. We believe that the new wound dressing sheets can be used for different biomedical applications especially as new wound dressing/healing materials.

Acknowledgment

Appendix A. Supplementary data

Supplementary data associated with this article can be found, in the online version, at http://dx.doi.org/10.1016/j.ijpharm.2016.06.003.

References

Abdel-Mohsen, A.M., Aly, A.S., Hrdina, R., El-Aref, A.T., 2012. A novel method for the preparation of silver/chitosan-*O*-methoxy polyethylene glycol core shell nanoparticles. J. Polym. Environ. 20, 459–468.

Abdel-Mohsen, A.M., Abdel-Rahman, R.M., Fouda, M.M.G., Vojtova, L., Uhrova, L., Hassan, A.F., Al-Deyab, S.S., El-Shamy, I.E., Jancar, J., 2014. Preparation, characterization and cytotoxicity of schizophyllan/silver nanoparticle composite. Carbohydr. Polym. 102, 238–245.

Abedini, F., Ahmadi, A., Yavari, A., Hosseini, V., Mousavi, S., 2013. Comparison of silver nylon wound dressing and silver sulfadiazine in partial burn wound therapy. Int. Wound J. 10, 573–578.

Al Tuwaijri, A.S., Mahmoud, A.A., Al Mofleh, I.A., Al Khuwaitir, S.A., 1987. Effect of glucan on *Leishmania* major infection in BALB/c mice. J. Med. Microbiol. 23, 363–365.

Angspatt, A., Taweerattanasil, B., Janvikul, W., Chokrungvaranont, P., Sirimaharaj, W., 2011. Carboxymethylchitosan, alginate and tulle gauze wound dressings: a comparative study in the treatment of partial-thickness wounds. Asian Biomed. 5, 413–416.

Annur, D., Wang, Z.-K., Liao, J.-D., Kuo, C., 2015. Plasma-synthesized silver nanoparticles on electrospun chitosan nanofiber surfaces for antibacterial applications. Biomacromolecules 16, 3248–3255.

Arockianathan, P.M., Sekar, S., Sankar, S., Kumaran, B., Sastry, T.P., 2012. Evaluation of biocomposite films containing alginate and sago starch impregnated with silver nano particles. Carbohydr. Polym. 90, 717–724.

Bagheri-Khoulenjani, S., Taghizadeh, S.M., Mirzadeh, H., 2009. An investigation on the short-term biodegradability of chitosan with various molecular weights and degrees of deacetylation. Carbohydr. Polym. 78, 773–778.

Bellini, M.Z., Pires, A.L.R., Vasconcelos, M.O., Moraes, A.M., 2012. Comparison of the properties of compacted and porous lamellar chitosan-xanthan membranes as dressings and scaffolds for the treatment of skin lesions. J. Appl. Polym. Sci. 125, E421–E431.

Boateng, J.S., Matthews, K.H., Stevens, H.N.E., Eccleston, G.M., 2008. Wound healing dressings and drug delivery systems: a review. J. Pharm. Sci. 97, 2892–2923.

Bobula, T., Běťák, J., Buffa, R., Moravcová, M., Klein, P., Židek, O., Chadimová, V., Pospíšil, R., Velebný, V., 2015. Solid-state photocrosslinking of hyaluronan microfibres. Carbohydr. Polym. 125, 153–160.

Bobula, T., Buffa, R., Procházková, P., Vágnerová, H., Moravcová, V., Šuláková, R., Židek, O., Velebný, V., 2016. One-pot synthesis of α,β-unsaturated polyaldehyde of chondroitin sulfate. Carbohydr. Polym. 136, 1002–1009.

Bohn, J.A., BeMiller, J.N., 1995. (1→3)-β-D-Glucans as biological response modifiers: a review of structure–functional activity relationships. Carbohydr. Polym. 28, 3–14.

diabetic (a, e), Treated non-diabetic (b and f), Control diabetic (c and g) and treated diabetic rats (d and h). Note that: In day 5, complete inflammatory reaction (IR) with prominent cell proliferation beneath the scab (SC), newly formed blood vessels (yellow arrow heads) and well-formed granulation tissue (GT); In treated non-diabetic group (b), the leading epithelial tongue (black arrow heads) starts to invade the underlying granular tissue. In day 15, the epithelial lining crawl beneath the reduced scab; in treated non-diabetic group (F), a remarkable wound closure with complete re-epithelization and formation of new hair follicles (HF), suggesting accelerating phase of tissue remodeling and reconstruction. The photomicrographs were obtained at a magnification of ×100. (For interpretation of the references to colour in this figure legend, the reader is referred to the web version of this article.)

Bueno, C.Z., Moraes, A.M., 2011. Development of porous lamellar chitosan-alginate membranes: effect of different surfactants on biomaterial properties. J. Appl. Polym. Sci. 122, 624–631.

Burkatovskaya, M., Tegos, G.P., Swietlik, E., Demidova, T.N., Castano, A.P., Hamblin, M.R., 2006. Use of chitosan bandage to prevent fatal infections developing from highly contaminated wounds in mice. Biomaterials 27, 4157–4164.

Chagas, B., Farinha, I., Galinha, C.F., Freitas, F., Reis, M.A.M., 2014. Chitin–glucan complex production by *Komagataella (Pichia) pastoris*: impact of cultivation pH and temperature on polymer content and composition. New Biotechnol. 31, 468–474.

Chen, W.-Y., Chang, H.-Y., Lu, J.-K., Huang, Y.-C., Harroun, S.G., Tseng, Y.-T., Li, Y.-J., Huang, C.-C., Chang, H.-T., 2015. Self-assembly of antimicrobial peptides on gold nanodots: against multidrug-resistant bacteria and wound-healing application. Adv. Funct. Mater. 25, 7189–7199.

Cheng, N.C., Chang, H.H., Tu, Y.K., Young, T.H., 2012. Efficient transfer of human adipose-derived stem cells by chitosan/gelatin blend films. J. Biomed. Mater. Res. B 100B, 1369–1377.

Cho, Y.W., Cho, Y.N., Chung, S.H., Yoo, G., Ko, S.W., 1999. Water-soluble chitin as a wound healing accelerator. Biomaterials 20, 2139–2145.

Chorvatovičová, D., Šandula, J., 1995. Effect of carboxymethyl-chitin-glucan on cyclophosphamide induced mutagenicity. Mutat. Res. Lett. 346, 43–48.

Cordeiro, L.M.C., Reinhardt, V.d.F., Iacomini, M., 2012. Glucomannan and branched $(1\rightarrow3)(1\rightarrow6)$ β-glucan from the aposymbiotically grown *Physcia kalbii* mycobiont. Phytochemistry 84, 88–93.

Croisier, F., Jérôme, C., 2013. Chitosan-based biomaterials for tissue engineering. Eur. Polym. J. 49, 780–792.

Dergunova, M.A., Alexeenko, T.V., Zhanaeva, S.Y., Filyushina, E.E., Buzueva, I.I., Kolesnikova, O.P., Kogan, G., Korolenko, T.A., 2009. Characterization of the novel chemically modified fungal polysaccharides as the macrophage stimulators. Int. Immunopharmacol. 9, 729–733.

di Luzio, N.R., Williams, D.L., McNamee, R.B., Edwards, B.F., Kitahama, A., 1979. Comparative tumor-inhibitory and anti-bacterial activity of soluble and particulate glucan. Int. J. Cancer 24, 773–779.

Ding, F., Tang, Z., Ding, B., Xiong, Y., Cai, J., Deng, H., Du, Y., Shi, X., 2014. Tunable thermosensitive behavior of multiple responsive chitin. J. Mater. Chem. B 2, 3050–3056.

Duan, B., Chang, C., Ding, B., Cai, J., Xu, M., Feng, S., Ren, J., Shi, X., Du, Y., Zhang, L., 2013. High strength films with gas-barrier fabricated from chitin solution dissolved at low temperature. J. Mater. Chem. A 1, 1867–1874.

Fan, Z., Liu, B., Wang, J., Zhang, S., Lin, Q., Gong, P., Ma, L., Yang, S., 2014. A novel wound dressing based on Ag/graphene polymer hydrogel: effectively kill bacteria and accelerate wound healing. Adv. Funct. Mater. 24, 3933–3943.

Farinha, I., Duarte, P., Pimentel, A., Plotnikova, E., Chagas, B., Mafra, L., Grandfils, C., Freitas, F., Fortunato, E., Reis, M.A.M., 2015. Chitin–glucan complex production by *Komagataella pastoris*: downstream optimization and product characterization. Carbohydr. Polym. 130, 455–464.

Goussé, C., Chanzy, H., Excoffier, G., Soubeyrand, L., Fleury, E., 2002. Stable suspensions of partially silylated cellulose whiskers dispersed in organic solvents. Polymer 43, 2645–2651.

Guo, S., DiPietro, L.A., 2010. Factors affecting wound healing. J. Dent. Res. 89, 219–229.

Guyard, C., Dehecq, E., Tissier, J.-P., Polonelli, L., Dei-Cas, E., Cailliez, J.-C., Menozzi, F. D., 2002. Involvement of [beta]-glucans in the wide-spectrum antimicrobial activity of *Williopsis saturnus* var. mrakii MUCL 41968 killer toxin. Mol. Med. 8, 686–694.

Holan, Z., Pokorný, V., Beran, K., Gemperle, A., Tuzar, Z., Baldrián, J., 1981. The glucan–chitin complex in *Saccharomyces cerevisiae*. Arch. Microbiol. 130, 312–318.

Huang, G.-Q., Sun, Y.-T., Xiao, J.-X., Yang, J., 2012. Complex coacervation of soybean protein isolate and chitosan. Food Chem. 135, 534–539.

Inamdar, N.N., Mourya, V., 2014. Chitosan and Low Molecular Weight Chitosan: Biological and Biomedical Alications, Advanced Biomaterials and Biodevices. John Wiley & Sons, Inc., pp. 183–242.

Ishihara, M., Ono, K., Sato, M., Nakanishi, K., Saito, Y., Yura, H., Matsui, T., Hattori, H., Fujita, M., Kikuchi, M., Kurita, A., 2001. Acceleration of wound contraction and healing with a photocrosslinkable chitosan hydrogel. Wound Repair Regen. 9, 513–521.

Jungst, T., Smolan, W., Schacht, K., Scheibel, T., Groll, J., 2015. Strategies and molecular design criteria for 3D printable hydrogels. Chem. Rev. 116, 1496–1539.

Kagimura, F.Y., da Cunha, M.A.A., Barbosa, A.M., Dekker, R.F.H., Malfatti, C.R.M., 2015. Biological activities of derivatized D-glucans: a review. Int. J. Biol. Macromol. 72, 588–598.

Kanetsuna, F., Carbonell, L.M., 1970. Cell wall glucans of the yeast and mycelial forms of *Paracoccidioides brasiliensis*. J. Bacteriol. 101, 675–680.

Kokoshis, P., Williams, D., Cook, J., Di Luzio, N., 1978. Increased resistance to *Staphylococcus aureus* infection and enhancement in serum lysozyme activity by glucan. Science 199, 1340–1342.

Kumar, M.N.V.R., Muzzarelli, R.A.A., Muzzarelli, C., Sashiwa, H., Domb, A.J., 2004. Chitosan chemistry and pharmaceutical perspectives. Chem. Rev. 104, 6017–6084.

Lee, K.Y., Mooney, D.J., 2001. Hydrogels for tissue engineering. Chem. Rev. 101, 1869–1880.

Lee, Y.M., Kim, S.S., Park, M.H., Song, K.W., Sung, Y.K., Kang, I.K., 2000. beta-Chitin-based wound dressing containing silver sulfurdiazine. J. Mater. Sci. Mater. Med. 11, 817–823.

Lee, S.-H., Park, S.-Y., Choi, J.-H., 2004. Fiber formation and physical properties of chitosan fiber crosslinked by epichlorohydrin in a wet spinning system: the effect of the concentration of the crosslinking agent epichlorohydrin. J. Appl. Polym. Sci. 92, 2054–2062.

Leveen, H.H., Falk, G., Borek, B., Diaz, C., Lynfield, Y., Wynkoop, B.J., Mabunda, G.A., Rubricius, J.L., Christoudias, G.C., 1973. Chemical acidification of wounds: an adjuvant to healing and the unfavorable action of alkalinity and ammonia. Ann. Surg. 178, 745–753.

Li, B., Liu, B., Shan, C., Ibrahim, M., Lou, Y., Wang, Y., Xie, G., Li, H.-y., Sun, G., 2013. Antibacterial activity of two chitosan solutions and their effect on rice bacterial leaf blight and leaf streak. Pest Manag. Sci. 69, 312–320.

Ligler, F.S., Lingerfelt, B.M., Price, R.P., Schoen, P.E., 2001. Development of uniform chitosan thin-film layers on silicon chips. Langmuir 17, 5082–5084.

Luzio, N.R., Williams, D.L., McNamee, R.B., Malshet, V.G., 1980. Comparative evaluation of the tumor inhibitory and antibacterial activity of solubilized and particulate glucan. In: Mathé, G., Muggia, F.M. (Eds.), Cancer Chemo- and Immunopharmacology. 2. Immunopharmacology, Relations, and General Problems. Springer Berlin Heidelberg, Berlin, Heidelberg, pp. 165–172.

Mi, F.-L., Huang, C.-T., Liang, H.-F., Chen, M.-C., Chiu, Y.-L., Chen, C.-H., Sung, H.-W., 2006. Physicochemical, antimicrobial, and cytotoxic characteristics of a chitosan film cross-linked by a naturally occurring cross-linking agent, aglycone geniposidic acid. J. Agric. Food Chem. 54, 3290–3296.

Mislovičová, D., Masárová, J., Bendžálová, K.N., Šoltés, L., Machová, E., 2000. Sonication of chitin–glucan, preparation of water-soluble fractions and characterization by HPLC. Ultrason. Sonochem. 7, 63–68.

Muzzarelli, R., 1983. Chitosan–glucan complex, method for its production and end uses. Google Patents.

Nwe, N., Stevens, W.F., Tokura, S., Tamura, H., 2008. Characterization of chitosan and chitosan–glucan complex extracted from the cell wall of fungus *Gongronella butleri* USDB 0201 by enzymatic method. Enzyme Microb. Technol. 42, 242–251.

Obmińska-Mrukowicz, B., Szczypka, M., Gawęda, B., 2006. Modulatory effects of chitosan adipate on the T and B lymphocyte subsets in mice. J. Vet. Sci. 7, 157–160.

Ogawa, Y., Noda, K., Kimura, S., Kitaoka, M., Wada, M., 2014. Facile preparation of highly crystalline lamellae of $(1\rightarrow3)$-β-D-glucan using an extract of *Euglena gracilis*. Int. J. Biol. Macromol. 64, 415–419.

Reis, R.A., Tischer, C.A., Gorin, P.A.J., Iacomini, M., 2002. A new pullulan and a branched $(1\rightarrow3)$-, $(1\rightarrow6)$-linked β-glucan from the lichenised ascomycete *Teloschistes flavicans*. FEMS Microbiol. Lett. 210, 1–5.

Roca, C., Chagas, B., Farinha, I., Freitas, F., Mafra, L., Aguiar, F., Oliveira, R., Reis, M.A. M., 2012. Production of yeast chitin–glucan complex from biodiesel industry byproduct. Process Biochem. 47, 1670–1675.

Rodríguez-Núñez, J.R., López-Cervantes, J., Sánchez-Machado, D.I., Ramírez-Wong, B., Torres-Chavez, P., Cortez-Rocha, M.O., 2012. Antimicrobial activity of chitosan-based films against *Salmonella typhimurium* and *Staphylococcus aureus*. Int. J. Food Sci. Technol. 47, 2127–2133.

Schiffman, J.D., Schauer, C.L., 2007. Cross-linking chitosan nanofibers. Biomacromolecules 8, 594–601.

Siralertmukul, K., Watcharamul, S., Wicheanpaisan, N., Nuisin, R., 2015. Potential antibacterial activity of polystyrene nanoparticles/chitosan coated on cotton fabrics. Macromol. Symp. 354, 324–333.

Skorik, Y.A., Pestov, A.V., Yatluk, Y.G., 2010. Evaluation of various chitin-glucan derivatives from *Aspergillus niger* as transition metal adsorbents. Bioresour. Technol. 101, 1769–1775.

Sonnenberg, A.S.M., Sietsma, J.H., Wessels, J.G.H., 1985. Spatial and temporal differences in the synthesis of $(1\rightarrow3)$-β and $(1\rightarrow6)$-β linkages in a wall glucan of *Schizophyllum commune*. Exp. Mycol. 9, 141–148.

Stagg, C.M., Feather, M.S., 1973. The characterization of a chitin-associated D-glucan from the cell walls of *Aspergillus niger*. Biochim. Biophys. Acta 320, 64–72.

Suginta, W., Khunkaewla, P., Schulte, A., 2013. Electrochemical biosensor applications of polysaccharides chitin and chitosan. Chem. Rev. 113, 5458–5479.

Talbott, S., Talbott, J., 2009. Effect of beta 1,3/1,6 glucan on upper respiratory tract infection symptoms and mood state in marathon athletes. J. Sports Sci. Med. 8.

Toivonen, M.S., Kurki-Suonio, S., Schacher, F.H., Hietala, S., Rojas, O.J., Ikkala, O., 2015. Water-resistant, transparent hybrid nanopaper by physical cross-linking with chitosan. Biomacromolecules 16, 1062–1071.

Ueno, H., Yamada, H., Tanaka, I., Kaba, N., Matsuura, M., Okumura, M., Kadosawa, T., Fujinaga, T., 1999. Accelerating effects of chitosan for healing at early phase of experimental open wound in dogs. Biomaterials 20, 1407–1414.

Usami, Y., Okamoto, Y., Takayama, T., Shigemasa, Y., Minami, S., 1998. Chitin and chitosan stimulate canine polymorphonuclear cells to release leukotriene B4 and prostaglandin E2. J. Biomed. Mater. Res. 42, 517–522.

Valasques Junior, G.L., de Lima, F.O., Boffo, E.F., Santos, J.D.G., da Silva, B.C., de Assis, S. A., 2014. Extraction optimization and antinociceptive activity of $(1\rightarrow3)$-β-D-glucan from *Rhodotorula mucilaginosa*. Carbohydr. Polym. 105, 293–299.

Valle, M.F., Maruthur, N.M., Wilson, L.M., Malas, M., Qazi, U., Haberl, E., Bass, E.B., Zenilman, J., Lazarus, G., 2014. Comparative effectiveness of advanced wound dressings for patients with chronic venous leg ulcers: a systematic review. Wound Repair Regen. 22, 193–204.

Versali, M.F., Clerisse, F., Bruyere, J.M., Gautier, S., 2009. Cell wall derivatives from biomass and preparation thereof. Google Patents.

Wang, M., Xu, L., Hu, H., Zhai, M., Peng, J., Nho, Y., Li, J., Wei, G., 2007. Radiation synthesis of PVP/CMC hydrogels as wound dressing. Nucl. Instrum. Methods Phys. Res. Sect. B 265, 385–389.

Wang, T., Zhu, X.-K., Xue, X.-T., Wu, D.-Y., 2012. Hydrogel sheets of chitosan, honey and gelatin as burn wound dressings. Carbohydr. Polym. 88, 75–83.

Winter, G.D., 1962. Formation of the scab and the rate of epithelization of superficial wounds in the skin of the young domestic pig. Nature 193, 293–294.

Winter, G.D., 1965. A note on wound healing under dressings with special reference to perforated-film dressings. J. Investig. Dermatol. 45, 299–302.

Yamaoka, F., Kagei, Y., Tomita, S., Kondo, Y., Hirano, S., 1989. The structure of chitin–glucan complex isolated from yeast bud scars. Agric. Biol. Chem. 53, 1255–1259.

Yang, Q., Dou, F., Liang, B., Shen, Q., 2005. Studies of cross-linking reaction on chitosan fiber with glyoxal. Carbohydr. Polym. 59, 205–210.

Yuan, W., Dong, H., Li, C.M., Cui, X., Yu, L., Lu, Z., Zhou, Q., 2007. pH-controlled construction of chitosan/alginate multilayer film: characterization and application for antibody immobilization. Langmuir 23, 13046–13052.

Zhang, Y.Z., Su, B., Ramakrishna, S., Lim, C.T., 2008. Chitosan nanofibers from an easily electrospinnable UHMWPEO-doped chitosan solution system. Biomacromolecules 9, 136–141.

Supporting Information

Novel Chitin/chitosan-glucan Wound Dressing: Isolation, Characterization, Antibacterial Activity and Wound Healing Properties

A.M.Abdel-Mohsen, J. Jancar, D.F.Massoud, Z. Fohlerova, H. Elhadidy, Z. Spotz, A. Hebeish

Characterization of chitin/chitosan-glucan complex (ChCsGC)

Mechanical measurements: Universal tensile testing machine, Inston 3343 (Instron, USA) was used to measure mechanical response of specimens pre-stressed with 0.05N at cross head speed of 30 mm/min, at room temperature and relative humidity of 28 % utilizing rectangular fibrous specimens 10 cm long and 7 cm wide. Reported data represent average values from three independent measurements. The Student ($- t$) test was used to analyze the significance of the experimental data ($p \leq 0.05$).

Thermal stability: Thermal gravimetric stability of the materials was measured using thermo-gravimetric analyzer (TGA Netzsch 209 F3, Al_2O_3 crucible) at the heating rate of 5 °C/min. The heat flow was also measured employing differential scanning calorimetry (DSC, Netzsch 200 F3) in the dynamic nitrogen atmosphere with a pressure of 0.1 MPa. The sample mass for DSC was typically about 0.9 mg and the heating rate of 10 °C/min was used over the temperature range from 25 to 600 °C. Fourier transformation infrared attenuated total reflectance spectroscopy (FTIR -ATR) was performed using the Impact 400 D FTIR-ATR spectrophotometer (Nicolet, USA) equipped with a ZnSe crystal between 4000 cm^{-1} and 600 cm^{-1} with the

24 resolution of 8 cm^{-1}. Morphological observations were performed using the SEM microscope

25 Tescan VEGA II LSU (Tescan, CZ) at 5 kV, in secondary electrons with maximum resolution

26 was 3 nm. SC7620 Mini Sputter Coater (Quorum Technologies, UK) was used to deposit 15 nm

27 Au layer on the surface of non-conducting specimens.

28 **NMR measurements**: ChCsGC complex (10 mg) was dissolved in 750 µL of

29 NaOH/urea/D$_2$O, then transferred into NMR tubes and analyzed directly using Vance TM 500

30 MHz NMR (Bruker, Germany) equipped with BBFO plus probe. ^{1}H/^{13}C chemical shifts were

31 related to the 3-trimethylsilylpropanoic acid sodium salt (TSPA) used as an internal standard.

32 The elemental microanalyses of CHN were performed employing the EA 1108 (FISONS, USA).

33 **Air permeability**: Water permeability Water permeability was measured according to

34 ASTM No. D-461.

35 **Swelling measurements**: The swelling ratio of the nonwoven mat was defined as the

36 ratio of the weight increase (Ww$-$W$_d$) in the phosphate buffer saline solution (PBS, pH 7.4) at

37 room temperature to the initial weight (W$_d$). The Equilibrium water uptake was determined using

38 dry weight (Wi) of plain and nonwoven mats of chitin/chitosan-glucan complex (ChCsGC) were

39 immersed in MilliQ water at 37 ^{o}C for 12 h and allowed to completely sell. The samples were

40 removed and the excess water were wiped off with filter paper and weight (Wf). All the

41 meaurments were carried out for three times (n=3). The amount of equilibrium water uptake was

42 calculated using the following equation.

43 Equilibrium water uptake (EWA) g/g= Wf-Wi/Wi

44 **Transmission electron microscope (TEM)**: Transmission electron microscopy (TEM)

45 observation of the molecular morphology of chitin/chitosan-glucan complex (ChCsGC) in

46 aqueous sodium hydroxide /urea solution was carried out on a JEM-2010 (HT) transmission

47 electron microscope (JEOL TEM, Japan). A thin layer of the dilute ChCsGC solution (1 mg/ml)

48 was suspended on a holey carbon film, which was supported on a copper grid. The specimen was

49 dried in air at ambient temperature (22 oC) and pressure for 30 min and was then imaged at an

50 accelerating voltage of 200 kv.

51 **Scanning electron microscopy (SEM):** The images of samples were done at the electron-

52 scanning microscope Tuscan VEGA II LSU electron microscope (Tuscan USA Inc.) under the

53 following conditions: high voltage 5 kV, working distance 4.4 mm, display mode secondary

54 electrons, high vacuum room temperature. SC7620 Mini Sputter Coater (Quorum Technologies,

55 UK) applied 15 nm layers of gold particles on the sample. The samples were dusted for 120 s

56 with the current of 18 mA. The pictures were made at these conditions: voltage 2.44–10 kV,

57 detector-SE, the magnification 300–20,000 times, vacuum high, the distance between sample and

58 objective: 4–5 mm.

59

60

61

62

63

64

65

66

67

68

69

70   **Table S1.** FTIR-ATR beaks of chitin, chitosan, glucan, complex and regenerated complex.

Peaks for powder (cm-1)					Assignments
Chitin	**Chitosan**	**Glucan**	**Complex**	**Regenerated complex**	
3435					**Stretching and bending of H$_2$O**
3257	3359	3297	3309	3302	**Amide A, N-H, O-H stretching**
		2918	2925	2926	**Amide B, C-H stretching**
1654	1654		1645	1639	**Amide I, C=O stretching**
	1590		1595	1584	**Amide II, N-H bending, C=O stretching**
1425	1374	1367	1413	1412	**O-H,C-H bending, γ(CH$_2$),γ (OH)**
1375	1314	1245	1356	1335	**CH$_2$ of chitin, chitosan and glucan**
1308	1150	1200	1078	1235	**Amide III, C-H stretching, N-H bending**
1114	1060	1033	1020	1077	**C-O-C of chitin, chitosan and glucan**
1009	893		848	846	**β -anomeric configuration**

71

72

73

74   **Figure S1.** FTIR-ATR of pure chitin, chitosan and glucan

75

Figure S2. 3D structure of Chitin/chitosan-glucan complex (ChCsGC) prepared by green technology with pore size approx. 75 µm.

Figure S3. TG-DTG of chitin, chitosan and glucan

84

Figure S4: XRD of chitin (a), chitosan (b), glucan (c), and urea/sodium hydroxide powder (d)

Figure S5. Swelling percentage of ChCsGC in PBS and physiological temperature

101

Table S2. Variation of inhibition zone diameters (mm) of ChCsGC nonwoven mats against

different type of bacteria; basillus *subtilis (B. Subtilis), escherichia coli (E. coli), staphylococcus*

Sample name	Gram positive (+ve)		Gram negative (- ve)	
	K. pneumoniae	*E. coli*	*S. aureus*	*B. subtilis*
Control	0	0	0	0
Nonwoven Mats	8	12	13	11

aureus (S. aureus) and klebsiella pneumoniae (K. pneumoniae)

105

106

Table S3. Equilibrium water uptake and air permeability of plain complex, nonwoven mat

complex and nonwoven cotton fabrics

109

Samples	Equilibrium water uptake (g/g)	Air permeability cm^3/cm^2/s
Net ChCSGC	15±2	0
ChCSGC mats	22±3	110± 5
Nonwoven viscose fabrics	32±3	80±7

113

114

115

116

117

118   **Table S4.** Comparison between properties of novel wound dressing ChCsGC and wound

119   dressing materials reported elsewhere

Dressing types	Days of treatments	Wound healing percent (%)	Ref.
Nonwoven ChCsGC	15	95	This work
Chitin/alginate	14	97	(Shamshina et al., 2014)
Chitin	12	95	(Huang et al., 2014)
Cellulose/gelatin	12	85	(Pei et al., 2015)
Ag/graphene	15	95	(Fan et al., 2014)
Glucan/PVA	22	93	(Huang and Yang, 2008)
Silk/gelatin	15	83	(Kanokpanont et al., 2012)
Chitosan	14	91	(Ong et al., 2008)
Chitin/chitosan	14	87	(Murakami et al., 2010)

120

121 **References**

122 Fan, Z., Liu, B., Wang, J., Zhang, S., Lin, Q., Gong, P., Ma, L., Yang, S., 2014. A Novel Wound Dressing
123 Based on Ag/Graphene Polymer Hydrogel: Effectively Kill Bacteria and Accelerate Wound Healing.
124 Advanced Functional Materials 24, 3933-3943.
125 Huang, M.-H., Yang, M.-C., 2008. Evaluation of glucan/poly(vinyl alcohol) blend wound dressing using rat
126 models. International Journal of Pharmaceutics 346, 38-46.
127 Huang, Y., Zhong, Z., Duan, B., Zhang, L., Yang, Z., Wang, Y., Ye, Q., 2014. Novel fibers fabricated directly
128 from chitin solution and their application as wound dressing. Journal of Materials Chemistry B 2, 3427-
129 3432.
130 Kanokpanont, S., Damrongsakkul, S., Ratanavaraporn, J., Aramwit, P., 2012. An innovative bi-layered
131 wound dressing made of silk and gelatin for accelerated wound healing. International Journal of
132 Pharmaceutics 436, 141-153.
133 Murakami, K., Aoki, H., Nakamura, S., Nakamura, S.-i., Takikawa, M., Hanzawa, M., Kishimoto, S., Hattori,
134 H., Tanaka, Y., Kiyosawa, T., Sato, Y., Ishihara, M., 2010. Hydrogel blends of chitin/chitosan, fucoidan and
135 alginate as healing-impaired wound dressings. Biomaterials 31, 83-90.
136 Ong, S.-Y., Wu, J., Moochhala, S.M., Tan, M.-H., Lu, J., 2008. Development of a chitosan-based wound
137 dressing with improved hemostatic and antimicrobial properties. Biomaterials 29, 4323-4332.
138 Pei, Y., Ye, D., Zhao, Q., Wang, X., Zhang, C., Huang, W., Zhang, N., Liu, S., Zhang, L., 2015. Effectively
139 promoting wound healing with cellulose/gelatin sponges constructed directly from a cellulose solution.
140 Journal of Materials Chemistry B 3, 7518-7528.
141 Shamshina, J.L., Gurau, G., Block, L.E., Hansen, L.K., Dingee, C., Walters, A., Rogers, R.D., 2014. Chitin-
142 calcium alginate composite fibers for wound care dressings spun from ionic liquid solution. Journal of
143 Materials Chemistry B 2, 3924-3936.

144

Publication 5

CrossMark

Chitin and chitosan from Brazilian Atlantic Coast: Isolation, characterization and antibacterial activity

Rasha M. Abdel-Rahman [a,*], Radim Hrdina [a], A.M. Abdel-Mohsen [b,c,**], Moustafa M.G. Fouda [c,e], A.Y. Soliman [d], F.K. Mohamed [d], Kazi Mohsin [f], Tiago Dinis Pinto [g]

[a] Institute of Organic Chemistry and Technology, Faculty of Chemical Technology, University of Pardubice, Studentská 95, 53210 Pardubice, Czech Republic
[b] Central European Institute of Technology (CEITEC), Brno University of Technology, Technicka 3058/10, 616 00 Brno, Czech Republic
[c] Textile Research Division, National Research Centre, El Buhouth St, P.O. Box 12311, Dokki, Cairo, Egypt
[d] Chemistry Department, Faculty of Science, Fayoum University, Fayoum, Egypt
[e] Petrochemical Research Chair, Chemistry Department, College of Science, King Saud University, P.O. Box 2455, Riyadh 11451, Saudi Arabia
[f] Kayyali Chair for Pharmaceutical Industries, Department of Pharmaceutics, College of Pharmacy, POBOX-2457 King Saud University, P.O. Box 2455, Riyadh 11451, Saudi Arabia
[g] Chemistry and Development Department, VCI Brazil, Bauru, SP, Brazil

ARTICLE INFO

ABSTRACT

Chitin and chitosan were obtained by chemical treatments of shrimp shells. Different particle sizes (50–1000 μm) of the raw material were used to study their effect on size distribution, demineralization, deproteinization and deacetylation of chitin and chitosan isolation process. The particle size in the range of 800–1000 μm was selected to isolate chitin, which was achieved by measuring nitrogen, protein, ash, and yield %. Hydrochloric acid (5%, v/v) was optimized in demineralization step to remove the minerals from the starting material. Aqueous solution of sodium hydroxide (5%, w/v) at 90 °C for (20 h) was used in deproteinization step to remove the protein. Pure chitin was consequently impregnated into high concentration of sodium hydroxide (50%) for 3.5 h at 90 °C to remove the acetyl groups in order to form high pure chitosan. The degree of deacetylation (DDA) of chitosan was controlled and evaluated by different analytical tools. The chemical structure of chitin and chitosan was confirmed by elemental analysis, ATR-FTIR, H/C NMR, XRD, SEM, UV–Vis spectroscopy, TGA, and acid–base titration. The isolated chitin and chitosan from shrimp shell showed excellent antibacterial activity against Gram (−ve) bacteria (*Escherichia coli*) comparing with commercial biopolymers.

© 2015 Elsevier B.V. All rights reserved.

1. Introduction

Chitin is one of the most abundant amino polysaccharides found in nature next to cellulose; it has a wide variety of sources as exoskeleton of crustacean (crab, shrimp and crawfish, *Oniscus asellus*) [1–4], insect cuticles (*Melolontha melolontha*) [3], Orthoptera species [5,6], wings of cockroach [7], grasshopper species [8], medicinal fungus [9], larvae and adult Colorado potato beetle [10], aquatic invertebrates [11], bat guano [12], resting eggs of *Daphnia longispina* [13], spider species [14], *Daphnia magna* resting eggs [15], and cell wall of fungi and in the green algae. The chemical structure of chitin ($C_8H_{13}O_5N)_n$ is similar to cellulose, having one hydroxyl group on each monomer substituted with an acetyl amine groups. Chitin is a linear chain composed of (1–4) linked 2-acetamido-2-deoxy-D-glucosamine while chitosan (the main derivative of chitin) is obtained by removing enough acetyl groups from chitin, the actual difference between chitin and chitosan is the acetyl content of the polymer [1,2,16–21].

Both chitin and chitosan have high nitrogen content varies from 2% to 8% that make them more attractive to several industrial applications. Chitin is insoluble in water and most organic solvents, this due to its rigid structure and strong intra and inters molecular hydrogen bonds. In contrast, chitosan is readily soluble in diluted acids (as hydrochloric acid, citric acid and acetic acid) with pH below 6 [22–27]. Chitin and chitosan have great economic impact due to their biological activities and their industrial

and biomedical applications. Due to the excellent properties of chitosan such as adsorption [28], film-forming and antimicrobial properties [29]. It is used in food preservation [30], cosmetics [31,32], agriculture [33], biotechnology [34], textiles [1,17,35–37] as well as medical fields [38–40]. Shrimp shell wastes contain about 20–30% chitin which can be isolated to produce many products such as chitosan, glucosamine and their derivatives, but since chitin is closely associated with proteins, minerals, and pigments, all these components have to be removed to reach to the highest purity necessary for bio-medical applications [41–53]. The medical applications of chitin and chitosan were limited due to the allergic properties [54,55] of the both biopolymers, the phenomenon due to the presence of some impurities like proteins, pigments, and heavy metals attached into the chitin/chitosan chains. In our study, we try to study and optimized all conditions to remove the maximum amount of the hazard material [56] interacted with chitin/chitosan chains.

In this present study, the acid and base treatments of chitin is fully investigated and optimized, the particle size effect, obtained by sieving of chitin, is evaluated in term of yield % of chitin and the residual of protein % too. The isolation sequencing of chitin and chitosan is extensively studied which is considered one of the novelty of this work. In addition, the antibacterial assessment of both commercially and isolated chitin and chitosan is evaluated using a novel bioluminescence technique.

2. Experimental

2.1. Materials

Shrimp shells obtained from VCI BrasilIndústriae Commerce de Embalagens Ltda. (Brazil) were selected as a source of raw material used for the isolation of chitin/chitosan. Shrimps were captured in the Atlantic Coast of São Paulo, Brazil. Sodium hydroxide, hydrochloric acid, ethanol, isopropyl alcohol and acetone were purchased from Lach-Ner, s.r.o., Czech Republic.

2.1.1. Sample preparation

In order to remove the water-soluble impurities and soluble impurities from the raw material of shrimp, the shrimp shell wastes were washed with tap water and acetone and then dried at 60 °C overnight in dry air oven. The dried material was boiled for 5 h in distilled water and then refluxed with isopropyl alcohol for 2 h to remove impurities attached into the shrimp surface. Thus, the sample mass decreased after purification by 10–15%. The last step before the isolation process was sieved the shell to different particle sizes from less 50, 100–200, 200–300, 300–400, 400–500, 500–700, 800–1000 μm).

2.1.2. Sieving shrimp shell to different particle sizes

Particle size was determined on a duplicate 100 g sample with a Bühler laboratory siever MLU 300 (Bühler-Miag, 9240 Uzwil, Switzerland) using a set of woven-wire cloth sieves having a diameter of 26 cm (12 sieves maximum). The sieve openings were chosen according to AFNOR specifications NF X11-501 (AFNOR NF X11-501, 1970) which recommend a geometrical progression of screen sizes in a 50–1000 μm range. The sieving time was 30 min.

2.2. Isolation of chitin and chitosan from shrimp shells

The isolation of chitin and chitosan from shrimp shell begun with the preparation of the samples followed by three classical steps: demineralization (DM), deproteinization (DP) and deacetylation (DA) as described below. Demineralization was carried out by using hydrochloric acid solution. This treatment was done at

ambient temperature (25 ± 2 °C) with varying times (0.5–5 h). The emission of CO_2 gas was observed during the reaction of carbonates with diluted hydrochloric acid [6]. The resulting solid fraction of crude chitin was washed with distilled water until neutral pH was achieved, then the chitin samples were dried at 60 °C for 24 h. During this process, the effect of hydrochloric acid with different concentration on the yield, nitrogen and ash content in the product was studied.

Deproteinization (DP) was done by using aqueous sodium hydroxide. Dry crude chitin was dispersed into aqueous solution of sodium hydroxide to remove the non-bounded material like proteins, dyes, lipids and pigments [6]. Thus, crude chitin was stirred in 5% of sodium hydroxide at 90 °C for 20 h, where the alkaline solution was exchanged every 2 h with fresh solution of sodium hydroxide. The product was filtered off, washed with demineralized water until neutralization after which the sample was dried at 60 °C for 24 h. Deacetylation step was achieved by impeded the chitin sample under reflux with 20–60% of sodium hydroxide [7] at 90 °C with (1/30, w/w) solid to solvent in the time range 0.5–5 h. The product; chitosan was collected, washed to neutrality using demineralized water, rinsed with acetone, and vacuum filtered off and dried at 60 °C for 5 h to remove moisture.

2.3. Characterization of chitin and chitosan

2.3.1. Inductively coupled plasma optical emission spectrometry (ICP-OES)

Elemental analysis was carried out using the sequential, radically observed inductively coupled plasma atomic emission spectrometer INTEGRA XL-2 (GBC, Dandenong Australia), furnished with the ceramic V-groove nebulizers and the glass cyclonic spray chamber (both Glass expansion, Australia). The parameter of detection were 10 μg/L for lines 338, 289 and 328 nm, for analysis of real samples, results from both analytical lines used were averaged.

2.3.2. Scanning electron microscopy (SEM)

All sample images were taken by scanning electron microscope; Pardubice University, Tescan VEGA II LSU electron microscope (Tescan USA Inc.) under the following conditions: high voltage 5 kV, working distance 4.4 mm, display mode secondary electrons, high vacuum room temperature. SC7620 Mini Sputter Coater (Quorum Technologies, UK) applied 15 nm layers of gold particles on the sample. The samples were dusted for 120 s with the current of 18 mA. The pictures were made at these conditions: voltage 2.44–10 kV, detector-SE. The magnification 300–20,000 times, vacuum high, the distance between sample and objective: 4–5 mm.

2.3.3. Elemental analysis

The micro-analyses were performed on an apparatus of FISONS. Instruments EA 1108 C; H; N. The content of proteins (%) was calculated from the nitrogen content by using the following Eq. (1) [6,42],

$$P\ \% = [N\ \% - 6.9] * 6.25 \tag{1}$$

where P % signifies the percentage of proteins remaining in the deproteinized shell, N % represents the percentage of nitrogen calculated by elemental analysis, 6.9 corresponds to the theoretical percentage of nitrogen in fully acetylated chitin (this value was adjusted as a function of DA, the degree of acetylation), and 6.25 corresponds to the theoretical percentage of nitrogen in proteins. All the determinations were done in quadruplicate [37].

2.3.4. UV–Vis spectroscopy

UV–Vis spectroscopy was also used to determine the P %. The measurements were carried out on UV–Vis spectrophotometer UV-160A, Shimadzu, Japan using quartz cuvette with an optical

path of 1 cm. The concentration of the measured solutions was kept at 0.59 mg mL^{-1}. The protein content in supernatant was calculated from the following Eq. (2) [43,57],

$$P \ \% = 2.37 \ (A_{564}/W) \tag{2}$$

where the A_{564} was the absorbance value at 564 nm and W was the weight of sample in mg.

2.3.5. Fourier transform infrared spectroscopy-attenuated total reflection (FTIR-ATR)

Fourier transform infrared spectroscopy (FTIR) was performed by using a Nicolet Impact 400 D FTIR-ATR spectrophotometer (Nicolet CZ, Prague, Czech Republic) equipped with a ZnSe crystal for the FTIR spectroscopy. Transmittance was measured as a function of the wavenumber between 4000 and 600 cm^{-1} with the resolution of 8 cm^{-1} and the number of scans equal to 32. The degree of deacetylation of chitosan was calculated from Eq. (3) [6,34],

$$DA\% = 100 - [(A_{1655}/A_{3450}) * 100/1.33] \tag{3}$$

where A_{1655} and A_{3450} were the absorbance at 1655 cm^{-1} of the amide I. The factor 1.33 denoted the value of the ratio of A_{1655}/A_{3450} for fully N-acetylated chitosan.

2.3.6. Determinations of ash content

Chitin and chitosan ash content were determined by combustion using a constant weight crucible. Chitosan (2–5 g) was subjected to combustion at constant weight crucible in an oven at 550 ± 20 °C for 3 h. The crucible was removed, cooled in desiccators for 30 min, and re-weighed (W_1). The heating and cooling process were repeated every 1.5 h until a constant weight was established (W_2). The ash percentage was calculated by Eq. (4) [58],

$$Ash \ \% = \frac{W_2 - W_0}{W_1 - W_0} * 100 \tag{4}$$

where W_0 was the constant weight of crucible, W_1 was the weight of sample and crucible, W_2 was the weight of ash and crucible.

2.3.7. Solid NMR spectroscopy

[1]D solid-state NMR spectra were measured using a Bruker Avance 500 NMR spectrometer. Magic angle spinning (MAS) frequency of the sample was 11 kHz. Amplitude modulated cross-polarization (CP) with duration 1 ms was used to obtain ^{13}C CP/MAS NMR spectra with 5 s recycle delay. ^{13}C scale was calibrated with glycine as external standard (176.03 ppm low-field carbonyl signal).

The degree of deacetyltion of chitin and chitosan were calculated from Eq. (5) [59],

$$mol \ (\%) = \frac{I_{CH_3}}{(I_{C_1} + I_{C_2} + I_{C_3} + I_{C_4} + I_{C_5} + I_{C_6})/6} * 100 \tag{5}$$

where I_{CH_3} and I_{C_1} corresponds to the integral of the hydrogen atom in NHCOCH$_3$ groups and to the hydrogen atom of C$_1$ in glucosamine units respectively.

2.3.8. Diffusion NMR spectroscopy

NMR spectra were measured on BRUKER AV 500 MHz Ultra-shield plus with the probe BBOF plus. For all tests except for accuracy, the solutions chitosan were prepared by stirring at room temperature; 10 mg of chitosan in a solution composed of 1.96 mL of D$_2$O and 0.04 mL of DCl and waiting about 1 h to ensure complete dissolution of the polymer. The degree of deacetylation of chitosan was determined according to the following Eq. (6) [60,61],

$$DD(\%) = \frac{HID}{HID + HAc/3} * 100 \tag{6}$$

where H$_1$D was H NMR signal for proton at C-1 at deacetylation monomer; HAc was signal of acetyl group.

2.3.9. Acid–base titration

Chitosan sample (0.1 g) was dissolved in 25 mL of 0.1 M HCl aqueous solution. The sample was titrated with 0.1 M NaOH. pH meter was used for pH measurements under continues stirring at ambient temperature (25 ± 2 °C). The titrant was added until the pH value reached to 1.5. The standard solution of sodium hydroxide was added drop-wise and the pH values of the solutions were recorded and a curve with two inflection points was obtained. The degree of deacetylation of chitosan was determined by acid–base titration according to the following Eq. (7) [29,62],

$$DDA \ (\%) = C_{NaOH} \times (V_2 - V_1) \times 161/m \tag{7}$$

where C_{NaOH} was the concentration of sodium hydroxide; $(V_2 - V_1)$ was the difference between two volume values of sodium hydroxide between the two inflection points; 161 was the molecular mass unit of chitosan; m was the mass of chitosan sample. The average degree of deacetylation (DDA) of chitosan samples could be determined from elemental analysis by using the following Eq. (8) [7,10,63],

$$DDA \ (\%) = 6.857 - C/N/1.7143 \tag{8}$$

where C/N was the carbon/nitrogen ratio measured from the elemental composition of the chitosan samples.

2.3.10. X-ray diffraction (XRD)

X-ray diffraction was collected on D-8 Advance diffracto-meter (Bruker AXS, Germany) with Bragg–Brentano θ–θ goniometer (radius 217.5 mm) equipped with a secondary beam curved graphite mono-chromator and Na (Tl) I scintillation detector. The generator was operated at 40 kV and 30 mA. The scan was completed at room temperature from 5° to 100° (2θ) in 0.02° step with a counting time of 8 s per step.

2.3.11. Thermal analysis measurements

Samples were studied with regard to the kinetics of thermal decomposition, using different heating rate thermo-gravimeter (TG, Netzsch 209F3 instrument, Al$_2$O$_3$ crucible) and under heating rates of 5 (with data collecting rate of 40 points/K) and 10 °C min^{-1} (collecting rate data of 60 points/K). The test temperature range for TG was 25–600 °C with the sample mass of about 10.35–1.45 mg under 30 mL min^{-1} dynamic nitrogen atmosphere.

2.3.12. Antibacterial activity of chitin and chitosan

Antibacterial effect was examined via bioluminescent (BL) bacteria. Genetically modified Escherichia coli K-12 capable of bioluminescence were exposed to three different concentrations of the isolated chitin and chitosan (5, 10, 15 mg), which led to diminishment of bacterial viability visualized by real time BL measurement [6]. Concentrated stock bacterial suspension was prepared [6], and stored at temperature −80 °C. Final concentration of bacterial cells in applied suspension was set to approximately 380,000 cells per 100 μL. This suspension (200 μL) was mixed with 5, 10 or 15 mg of isolated chitin and chitosan partly suspended in phosphate buffer
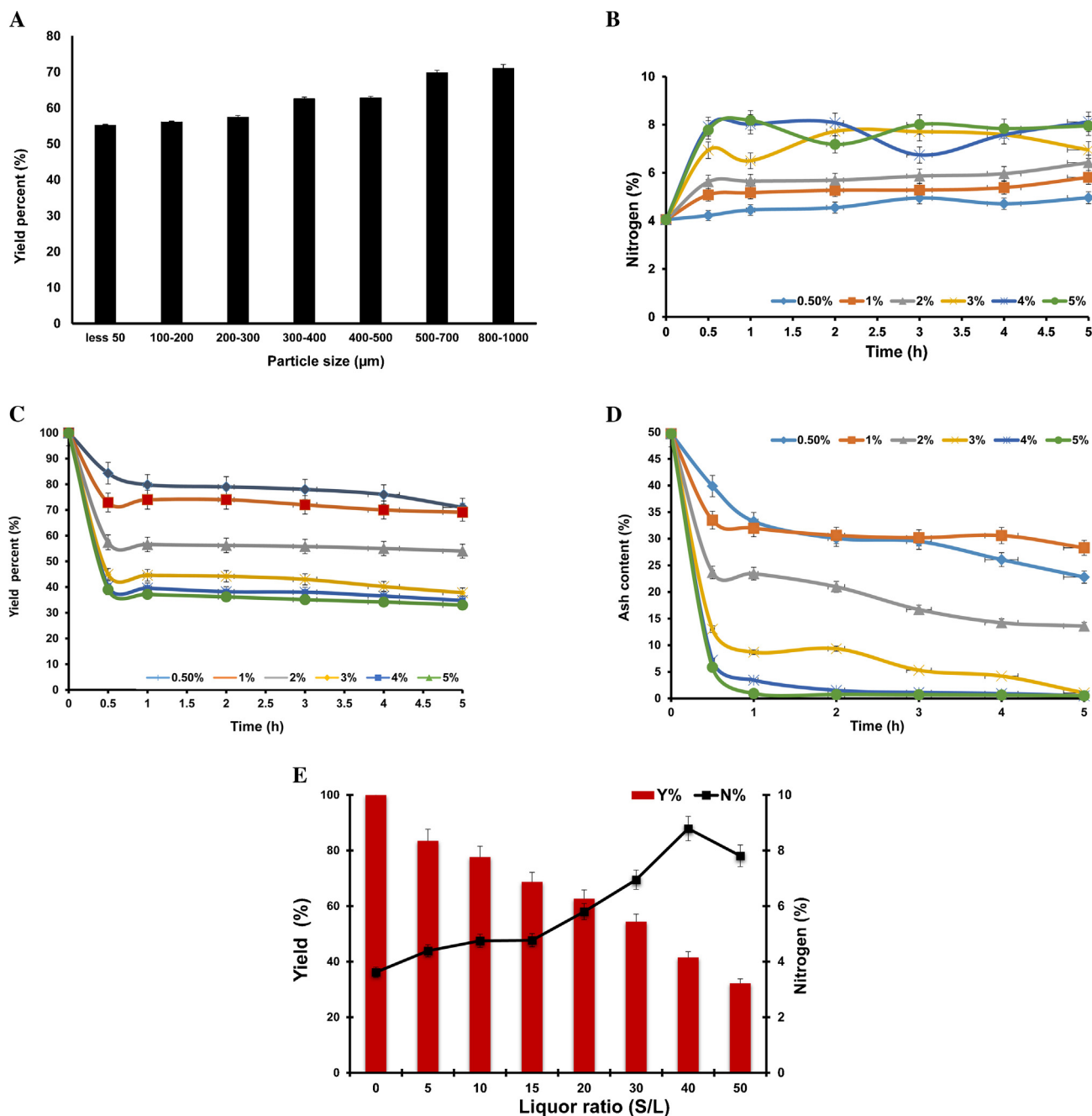
Fig. 1. (A) Relation of particle size of shrimp shell with the yield percent using aqueous solution of hydrochloric acid (5%). Experimental conditions: different sizes of dry shrimp shell, 5% aqueous hydrochloric acid, RT ($22 \pm 2\,^{\circ}$C), for 2 h. (B) Demineralization step – effect of hydrochloric acid on nitrogen percent of dry shrimp shell with particle size 800–1000 μm. Experimental conditions: shrimp shell with particle size 800–1000 μm, ratio of solid (shrimp shell) to aqueous solution of hydrochloric acid 1:20 (w/v), RT ($22 \pm 2\,^{\circ}$C). (C) Demineralization step – effect of hydrochloric acid on yield percent of shrimp shell varying with time with particle size (800–1000). Experimental conditions: shrimp shell with particle size 800–1000 μm, ratio of solid (shrimp shell) to aqueous solution of hydrochloric acid 1:20 (w/v), RT ($22 \pm 2\,^{\circ}$C). (D) Demineralization step – effect of hydrochloric acid on ash content of shrimp shell with particle size 800–1000 μm. Experimental conditions: shrimp shell with particle size 800–1000 μm, ratio of solid (shrimp shell) to aqueous solution of hydrochloric acid 1:20 (w/v), RT ($22 \pm 2\,^{\circ}$C). (E) Effect of liquor ratio of hydrochloric acid on yield percent and nitrogen percent of shrimp shell with particle size 800–1000 μm. Experimental conditions: 5% hydrochloric acid, shrimp shell with particle size 800–1000 μm, RT ($22 \pm 2\,^{\circ}$C).

(100 μL) in wells of a white flat-bottom 96-well μL plates (Thermo Scientific, Czech Republic). MC cellulose samples (5–15 mg) were used as an appropriate control. Light (490 nm) generated by enzymatic reaction in bioluminescent bacteria was measured continuously during 60 min by luminometer LM-01T (Immunotech, Czech Republic) at laboratory temperature ($25 \pm 2\,^{\circ}$C). Results are expressed in relative light units (RLU). Average integral under the kinetic curve was compared with control and the percentage of bacterial killing was calculated. Experiments were repeated independently three times.

2.3.13. Statistical analysis

All experiments were carried out in triplicate and the results were expressed with SD (standard deviation).

3. Results and discussion

The present data represents the first attempt to investigate various physicochemical and functional properties of chitin and chitosan from shrimp shell. The shrimp shells were collected from Brazilian Atlantic Coast, washing with water, acetone and isopropyl
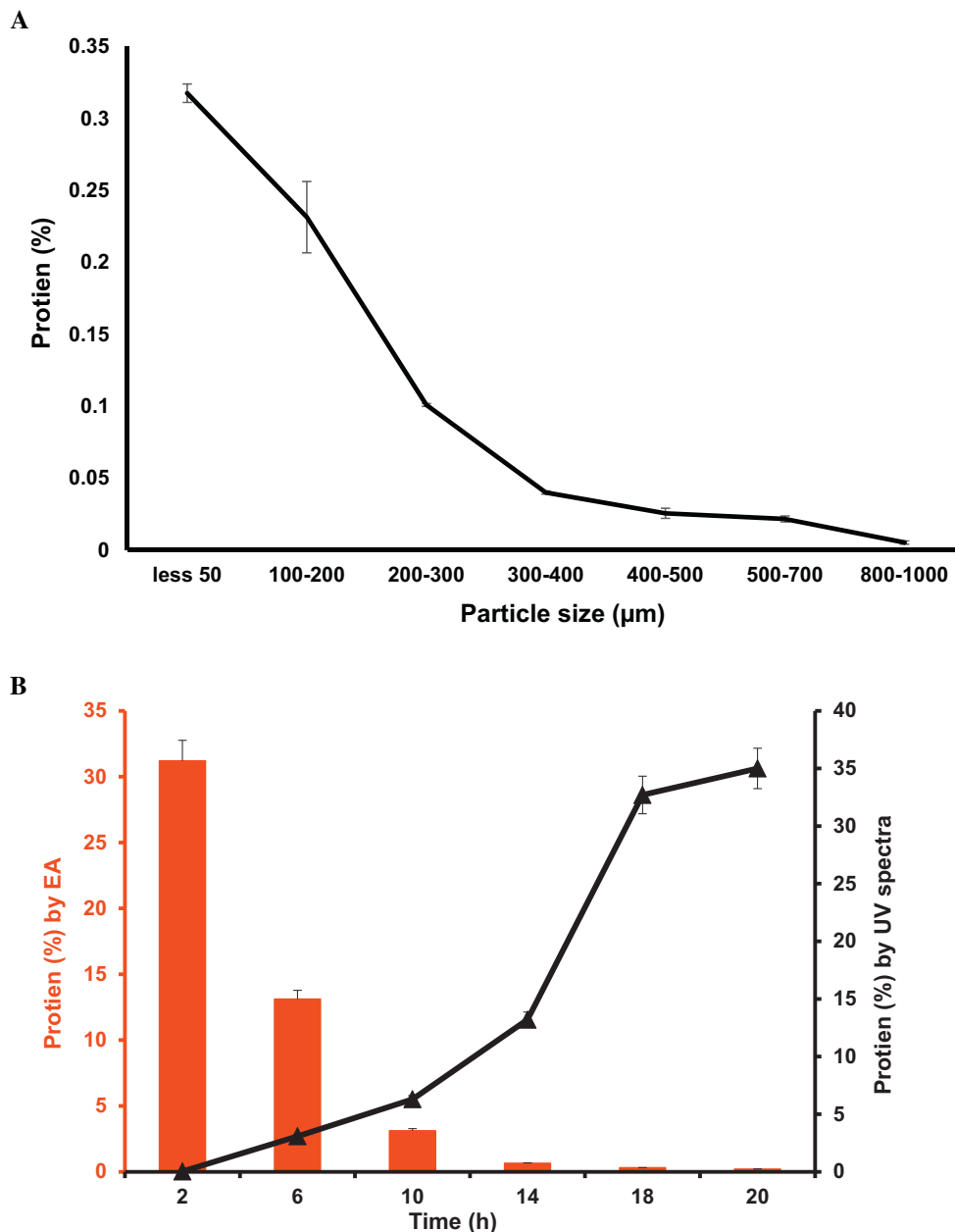
Fig. 2. (A) Effect of particle size of demineralized shell on protein percent of demineralized shell. *Experimental conditions*: ratio of solid of demineralized shell to solvent (aqueous NaOH) 1:20 (w/v), RT (22 ± 2 °C), 2 h. (B) Relation between time of treatment of demineralized shell and protein percentages of demineralized shell; *Experimental conditions*: DM-demineralization: 5% hydrochloric acid, 2 h, RT (22 ± 2 °C), solid to liquid (1:20, w/v); DP-deprotenization: 5% sodium hydroxide, 90 °C, solid to liquid (1:20, w/v).

alcohol then dried at oven at 60 °C overnight (as mentioned before in sample preparation) followed by sieving the shrimp shell to different particle sizes from (less 50, 100–200, 200–300, 300–400, 400–500, 500–700, 800–1000 μm) using sieving machine. The variation in chemical, physical, physicochemical and functional properties of isolated biopolymers in the three sequential processes (DP, DM, DA) of the isolation process were investigated.

3.1. Isolation of chitin

In shrimp shell, chitin is found as a part of a complex based on proteins and minerals as calcium carbonate and calcium phosphate deposit to form the rigid shell [64,65]. Thus the isolation of chitin from Atlantic shrimp shell is summarized in two major steps:

removal of calcium salts in demineralization step using diluted hydrochloric acid and second step: removal of proteins in deproteinization process using sodium hydroxide [65].

3.1.1. Demineralization step (DM)

Shrimp shell contains about 25–40% of minerals and the huge amount of these minerals are calcium carbonate and calcium phosphate [8,47]. Hydrochloric acid was used as a reagent in demineralization step in order to remove the minerals (as calcium carbonate) from the shell. In this process, minerals were hydrolysed into highly water soluble salts which could be separated by filtration and washing with deionized water for several times. Various concentrations of HCl were used at room temperature with
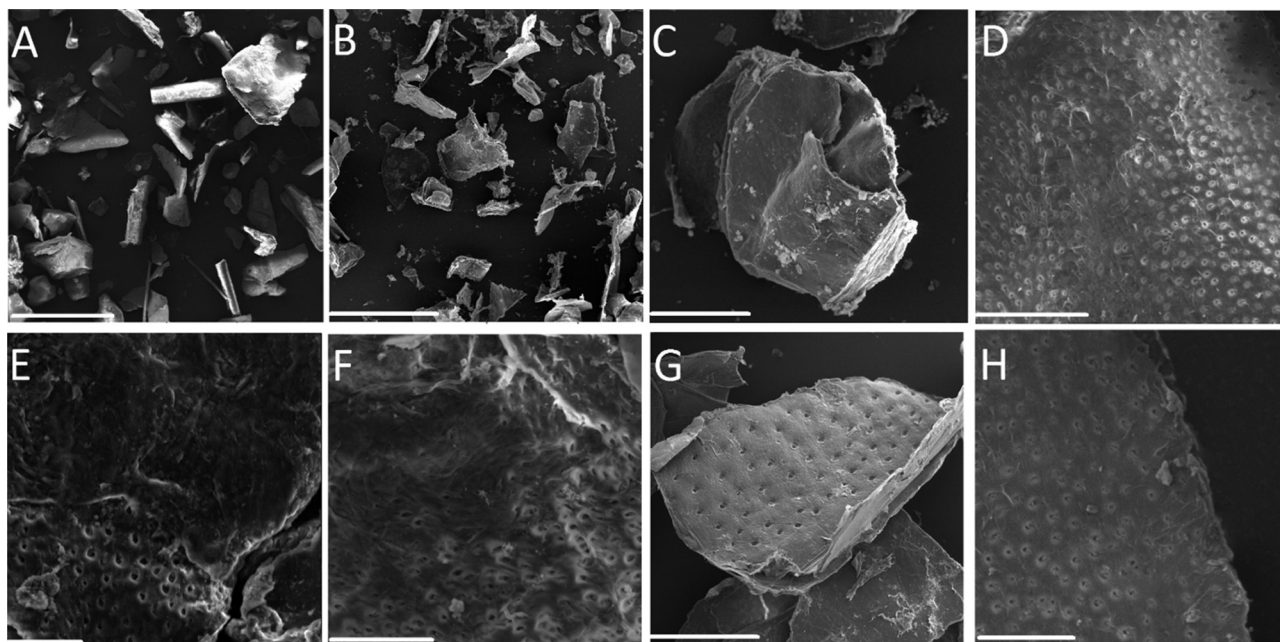
Fig. 3. Scanning electron microscope of shrimp shell and different particle sizes (sieving process) of chitin after deproteinization and demineralization steps. *Experimental conditions*: DM-demineralization: 5% hydrochloric acid, 2 h, RT ($22 \pm 2\,^\circ$C); DP-deproteinization: 5% sodium hydroxide; 20 h, 90 $^\circ$C. (A) Raw material of shrimp shell bar 500 μm; (B) less 50 (bar 20 μm); (C) 100–200 (bar 20 μm); (D) 200–300 (bar 200 μm); (E) 300–400 (bar 200 μm); (F) 400–500 (bar 200 μm); (G) 500–700 (bar 200 μm); (H) 800–1000 μm (bar 200 μm).

agitation to detect their effects on nitrogen percent, the yield and ash content [66].

In the beginning, studying on the best yield that obtained from different particle sizes (less 50–1000 μm) of shrimp shell by using aqueous solution of hydrochloric acid (5%) was performed as in Fig. 1A; as expected the yield increased with increasing the size of shell. It was improved slightly with increasing the size of shell from less 50 to 1000 μm, and it could be returned to the bigger size bonded lower impurities. So, the particle size 800–1000 μm, was chosen to study the influence of the isolated chitin and chitosan through isolation sequence process. Fig. 1B reveals the effect of different concentration of hydrochloric acid (0.5–5%) on nitrogen percentage. The treatments were carried out at room temperature with various time intervals (0.5–5 h). At zero time treatment, the nitrogen percent was about 4, and increased slowly by increased the concentration of HCl (0.5–2%) and there was no significant differences in the treatment time (Fig. 1B). By increased the concentration of hydrochloric acid from 2% to 5%, the nitrogen percent value was raised from 6 to 8.5 and this could be attributed to the increase in nitrogen percent which confirm the presence of large amount of chitin. Thus, the 5% of hydrochloric acid produced higher percent of chitin.

Fig. 1C shows the effect of concentrations of hydrochloric acid on the yield percent during the treatment of the shrimp shell under different time. It is obviously clear that, the yield percentage decreased with increasing the concentration of hydrochloric acid; this is due to the removal higher percentage of mineral salts (calcium carbonate and/or phosphate) during the treatment [8]. The yield percentage decreased rapidly in the first 1 h then the rate became constant as the composition of minerals decreased with demineralization time.

Fig. 1D shows the effect of different concentrations of hydrochloric acid on ash content varying with treatment time. Based on the obtained results, the ash content was decreased rapidly with increasing the concentration of hydrochloric acid, then it started to be more constant, this can be explained in term the fast

treatment and fast removal of the impurities and the metal salts in the first hour. The decrease of ash content percentage reflect the purity of chitin. The ratio of solid to solvent was an important factor affecting in yield percent and nitrogen percent of shrimp shell. In Fig. 1E, the demineralization of shrimp shell with 5% hydrochloric acid for 2 h at room temperature with different liquor ratio between solid to solvent 1:5, 1:10, 1:15, 1:20, 10:30, 1:40, and 1:50 (w/v) were effective in decreasing the yield % and nitrogen % by increasing the liquor ratio between solid to solvent. According to our result the mineral content obtained from Atlantic Ocean shrimp shell had lower percentage yield (8–10) which was lower when comparing with the different sources of chitin in the previous literature as shown in Table S2 [24,67–70].

3.1.2. Deproteinization step (DP)

In deproteinization step the chemical treatment is used to destroy the covalent chemical bonds between the chitin–protein complexes (proteins are bound by covalent bonds to the chitin through aspartyl or histidyl residues or both forming stable complexes such as glycoproteins) [71,72]. Alkaline solution from sodium hydroxide was used to remove the proteins, lipids and pigments from the crawfish shell [8,73]. Effect of particle sizes and the time of chemical deproteinization process influence the properties of the chitin product. Fig. 2A shows the effect of different particle sizes of the shell on the yield percentage and the residual protein percent. The particle sizes play an important role in the purity of chitin. Fig. 2A reveals the relation between particle size and protein content. The amount of protein percent decreased sharply at higher particle size of the shell. In addition; bigger particle size effects the reaction efficiency of shell with hydrochloric acid (demineralization step) and/or with sodium hydroxide (deproteinization step). Based on Fig. 2A the protein content decreased to 0.005 for particle size 800–1000 μm in comparing with 0.317 for particle size less 50 μm. Fig. 2B shows the relation of treatment time with the protein percent measured by various two methods. In Fig. 2B, the protein percent decreased in the shell by increasing the time of

treatments from 2 to 20 h confirmed by elemental analysis. In the same time the percentage of protein increased in the supernatant by increasing the time of treatment from 2 to 20 h confirmed by UV–Vis spectroscopy. The reason of protein decrease, was the reaction of sodium hydroxide with the residual impurities [74]. It our finding result, the protein percent was very low comparing with different sources of shrimp shell in previous literature as shown in Table S1 [24,64,68–70].

3.1.2.1. Scanning electron microscopy of pure chitin. To better understand of chitin morphology, some chitin flakes were isolated from different places of the exoskeleton and were observed by SEM. Fig. 3A shows scanning electron microscopy of the raw material of shrimp shell after washing and drying process. As shown (Fig. 3A), there was heterogeneous in particle size, beside some impurities are attached on the shrimp surface. Also, a roughness surface of the raw material without porosity was observed which might be related to their high molecular packing, with inter- or intramolecular hydrogen bonds, imparting a high crystalline degree to chitin. Fig. 3B–H shows the different particle sizes (less 50–1000 μm) of chitin after deproteinization and demineralization treatments. It is observed that, independent of part of the shrimp exoskeleton, the isolated chitin retains its fibrils character. After separation, different particle sizes (Fig. 3B–H), the surface morphology of the chitin was changed due to the treatment with acid and basic agents. The mobility or diffusion of the acid or basic inside chitin structure is crucial and inhabited by low porosity and high crystallinity of chitin. Due to the sieving process, each sample has approximately the same particle size, and it easy to detect the surface changes due to the treatment process. Different sizes of chitin has porous structure after the Isolation process which somehow can significantly reduce the time of treatments. The surface of the isolated chitin from shrimp shell was found to have smooth surface structure similar to morphology of chitin isolated from spider species [14]. It's very clear that the particle size 800–1000 μm gave the best clear morphology, smooth, and high porosity than other sizes. Therefore to perform all experiments in our study.

3.2. Isolation of chitosan from chitin (deacetylation step)

Chitosan was isolated from chitin by removing the acetyl groups from the chain of chitin using strong concentration of sodium hydroxide in process called deacetylation. Different parameters could be effect the deacetylation step like concentration of sodium hydroxide, time and temperature of the reaction medium. In order to determine the effect of sodium hydroxide on the degree of deacetylation of chitosan (DDA % calculated by Solid NMR), different concentrations of sodium hydroxide solution (30%, 40%, 50%, 60%) were used to replace the acetyl group of chitin with free amino groups. Fig. 4A, demonstrated the great influence of NaOH in removing the acetyl groups along the chitin Chain. The DDA values of chitosan increased gradually as the sodium hydroxide concentration increased up to 30% and increased rapidly when the concentration was higher than 50%. The DDA of chitosan was lower than 45% when the concentration of NaOH was lower than 30%. However, the DDA of chitosan increased dramatically up to 95.5 when the concentration of NaOH was between 50% and 60%. Fig. 4B shows the influence of time on the DDA of chitosan (calculated by elemental analysis). Chitin was refluxed with 50% of sodium hydroxide at 90 °C for different treatment time (0.5–4 h). In the first hour of the treatment the degree of DDA reached to 40%; then increased gradually with the time till 3.5 h and then the DDA became 95%.
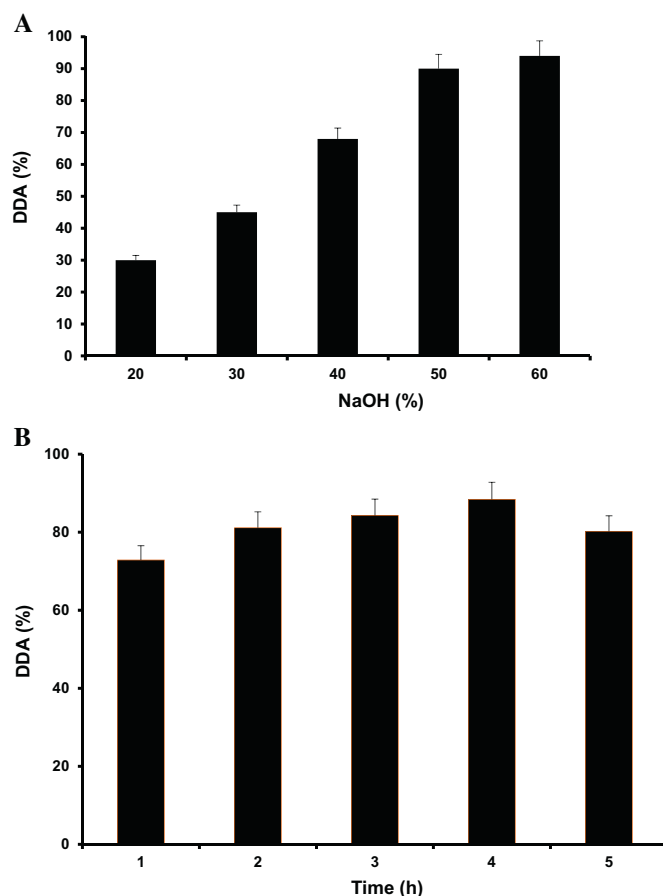
Fig. 4. (A) DA-deacetylation step – effect of the sodium hydroxide concentration on the degree of deacetylation of formed chitosan (DDA). *Experimental conditions*: DM-demineralization: 5% hydrochloric acid, 2 h, RT (22 ± 2 °C), solid to liquid (1:20, w/v); DP-deproteinization: 5% sodium hydroxide, 20 h, 90 °C, solid to liquid (1:20, w/v); DA-deacetylation: 2 h, 90 °C, chitin to aqueous NaOH (1:30, w/v). (B) DA-deacetylation step – effect of time on the degree of deacetylation of chitosan. *Experimental conditions*: DM-demineralization: 5% hydrochloric acid, 2 h, RT (22 ± 2 °C), solid to liquid (1:20, w/v); DP-deproteinization: 5% sodium hydroxide, 20 h, 90 °C, solid to liquid (1:20, w/v); DA-deacetylation: 50% sodium hydroxide, 90 °C, solid to liquid (1:30, w/v).

3.3. Isolation sequences of chitin and chitosan

Fig. 5 shows the Isolation sequence process of the isolated chitin and chitosan by demineralization (DM), deproteinization (DP) and deacetylayion steps (DA). AS shown in Fig. 5, in obviously clear the sequence treatment steps effect on the yield percent of chitin and chitosan. The yield percent of chitin and chitosan was higher by the following sequence DMPA > DPMA > DAPM > DAMP, respectively. From Fig. 5, we conclude that demineralization, deproteinization, and deacetylayion were the best sequence for isolation of pure and high yield percent of chitin and chitosan from shrimp shell. These results differ from the reported results [75,76].

3.4. Thermal stability of chitin and chitosan

Thermal gravimetric analysis of chitin and chitosan has been used to investigate the thermal degradation and crystallization of the polymers. Fig. 6A shows the TGA curves and the corresponding derivate-grams (DTG) of the isolated chitin and chitosan. The isolated chitin (Fig. 6A) shows two major peaks on the DTG curves. The first, which appeared around 50–100 °C, could be explained as the evaporation of physically adsorbed and strongly hydrogen boned water to the complex and alcohol solvent, respectively [14,15,77].
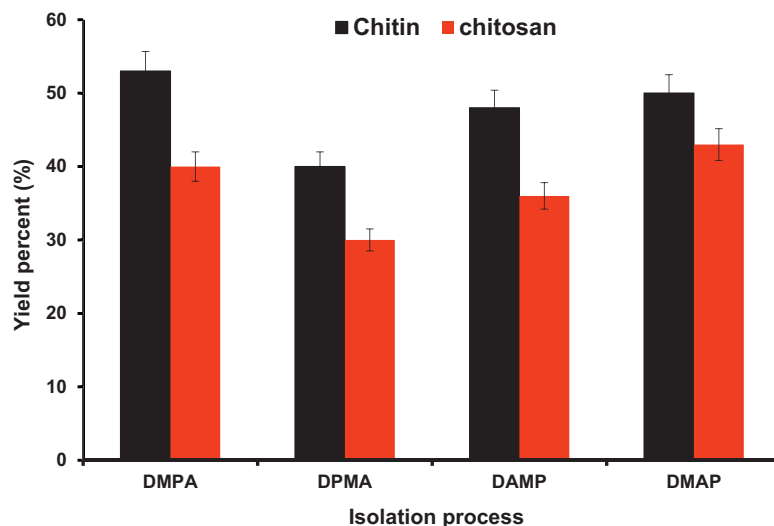
Fig. 5. Isolation sequence of chitin and chitosan from shrimp shell of particle size (800–10000 μm). *Experimental conditions for chitin*: DM-demineralization: 5% hydrochloric acid, 2 h, RT (22 ± 2 °C), solid to liquid (1:20, w/v); DP-deproteinization: 5% sodium hydroxide, 20 h, 90 °C, solid to liquid (1:20, w/v). *Experimental conditions for chitosan*: DM-demineralization: 5% hydrochloric acid, 2 h, RT (22 °C), solid to liquid (1:20, w/v); DP-deproteinization: 5% sodium hydroxide, 20 h, 90 °C, solid to liquid (1:20, w/v); DA-deacetylation: 50% sodium hydroxide, 3.5 h, 90 °C, solid to liquid (1:30, w/v), degree of deacetylation DDA (95%, measured by NMR).
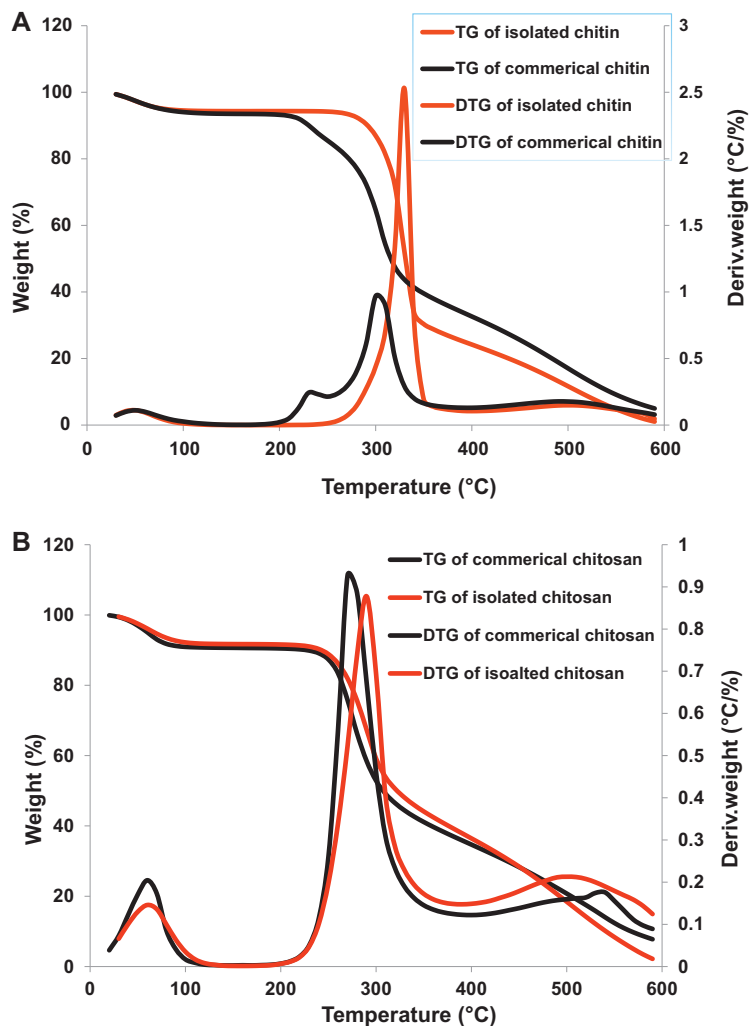
Fig. 6. (A) TGA and DTG of chitin. *Experimental conditions*: DM-demineralization: 5% hydrochloric acid, 2 h, RT (22 ± 2 °C); DP-deproteinization: 5% sodium hydroxide, 20 h, 90 °C. Degree of deacetylation DDA (5%, measured by FTIR). (B) TGA and DTG of chitosan. *Experimental conditions*: DM-demineralization: 5% hydrochloric acid, 2 h, RT (22 ± 2 °C); DP-deproteinization: 5% sodium hydroxide, 20 h, 90 °C; DA-deacetylation: 50% sodium hydroxide, 3.5 h, 90 °C, degree of deacetylation DDA (95%, measured by NMR).

Second peaks appeared at 330 °C is related to cleavage of glyosidic amine units by dehydration or deamination. Commercial chitin had three peaks on the DTG curve. At 50–100 °C, could be explained as the evaporation of physically adsorbed and strongly hydrogen boned water to the chitin [77]. The second peaks were appeared at 230 °C, which may corresponding to the residual of proteins, pigments encored to chitin chains. The third peak appeared at 300 °C, related to cleavage of glyosidic amine units by dehydration or deamination [78]. From the TGA and DTG data of both isolated and commercial chitin we can conclude that, the isolated chitin from Brazilian Atlantic Ocean was more pure and more thermal stable than the commercial chitin. Fig. 6B showed the TGA and DTG of isolated and commercial chitosan. The isolated chitosan had two different beaks appeared in DTG curve. The first peak appeared at 50–90 °C, which was related to the evaporation of residual of water [12]. The second decomposition peak was appeared at 290 °C, may be related to decomposition of glucosamine and residual acetyl glucosamine in chitosan chain [79]. In commercial chitosan,

there was two different peaks appear at 50–80 °C and at 270 °C for evaporated water and decomposition of the glucosamine and residual of acetyl glucose amine units in chitosan chains [79]. From the comparison data between isolated chitin, chitosan and commercial product chitin, chitosan, we can see that, isolated chitin and chitosan were more thermal stable than commercial products.

3.5. ATR-FTIR of chitin and chitosan

Fig. 7 shows the FTIR-ATR of the isolated biopolymers (chitin, chitosan) comparing with the commercial one. Fig. 7A shows the FTIR-ATR of chitin isolated from shrimp shell and commercial chitin, respectively; we can see that both commercial and isolated chitin showed similar beak there are not identical. Different peaks appeared at 3470–3390 cm^{-1} for stretching vibration of hydroxyl and secondary amine groups and at 2880 cm^{-1} for methylene groups in chitin. Within the FTIR-ATR spectrum of
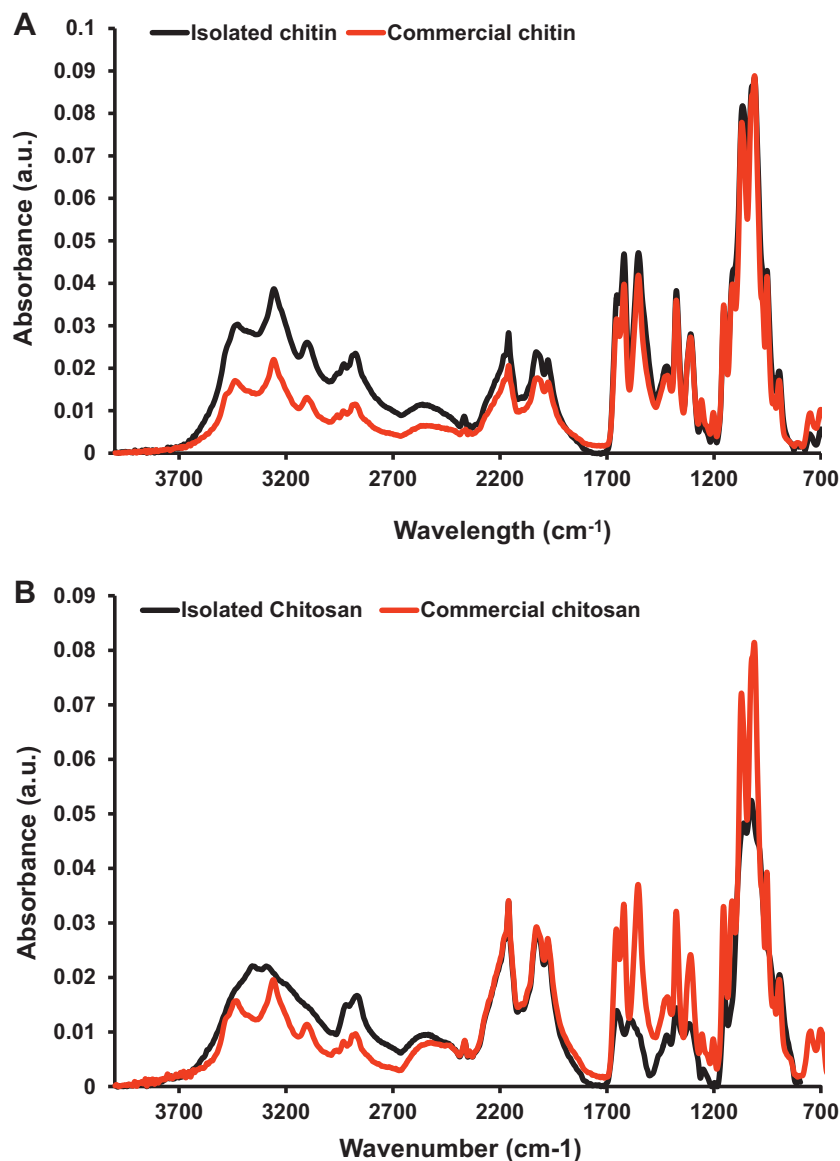
Fig. 7. (A) FTIR-ATR of chitin. *Experimental conditions*: DM-demineralization: 5% hydrochloric acid, 2 h, RT (22 ± 2 °C); DP-deproteinization: 5% sodium hydroxide, 20 h, 90 °C, solid to liquid (1:20, w/v), degree of deacetylation DDA (5%, measured by FTIR). (B) FTIR-ATR of chitosan. *Experimental conditions*: DM-demineralization: 5% hydrochloric acid, 2 h, RT (22 ± 2 °C); DP-deproteinization: 5% sodium hydroxide, 20 h, 90 °C; DA deacetylation: 50% sodium hydroxide, 3.5 h, 90 °C, solid to liquid (1:30, w/v), degree of deacetylation DDA (95%, measured by FTIR).

isolated β-chitin, bands are observed at 1650 and 1550 cm^{-1} [6], the peaks were appeared at 1620 cm^{-1} and 1590 cm^{-1} for amide I and amide II, respectively [6,7]. Beak at 1050 cm^{-1} correspond to the C—O—C in chitin chain. Isolated chitosan (Fig. 7B) has a broad band about 3200–3374 cm^{-1} for stretching vibration of OH and NH groups, 1661 cm^{-1} for (amide I), 1595 cm^{-1} for (amide II), 1380 cm^{-1} for (amide III) [5,7]. The intensity of the absorption band at 1595 cm^{-1} for very short due to the highly degree of deacetylation of the isolated chitosan (95%) comparing with the commercial chitosan. Asymmetric stretching of (C—O—C bridge) and 1080 cm^{-1} for (C—O stretching) [11] characteristic of its polysaccharide structure (Fig. 7B) in comparing with the commercial chitosan. Higher similarity was recorded between the commercial and the chitin and chitosan isolated from Brazilian Atlantic Ocean.

3.6. Solid NMR of chitin and chitosan

Solid-state NMR spectroscopy has been identified as the most useful and accurate tool for structurally analyzing insoluble complex biomaterial [80]. Fig. 8 shows solid-NMR spectra of different deacetylated products prepared from chitin with various time using sodium hydroxide. The deacetylation temperature and concentration of sodium hydroxide were consistently set at 90 °C 50%, respectively. Each spectrum included seven well-defined resonances of C1–C6 and acetyl. They are $\varepsilon = 173.7$, ppm for C=O, $\varepsilon = 102.8$ ppm for C1, $\varepsilon = 82.5$ ppm for C4, $\varepsilon = 74.5$ ppm for C5, $\varepsilon = 61.3$ ppm for C6, $\varepsilon = 56.1$ ppm for C2, and $\varepsilon = 23.2$ ppm for CH$_3$. In highly deacetylated chitosan, there no any appearance for $\varepsilon = 73.7$, and 23.2 for carbonyl and acetyl groups in chitin, respectively. The DDA increase by increasing the treatment times, DDA (%) = 30%, 67%, 93% and 95% after 1, 2, 3, and 4 h. treated with 50% sodium hydroxide at 90 °C, respectively, were illustrated in Fig. 8. Different peaks were related to protein residual appeared at ~181.5, 128.7, 32.9, 30.0 and 14.2 ppm [81–83] which were not appeared in our products spectra this indicated that there was no any residual of protein interconnected to Atlantic source of purified chitin and chitosan compared with different other sources [81,84–86].

3.7. Residual of metals on chitin and chitosan after isolation process

Fig. 9 shows the amount of minerals of the isolated chitin and chitosan in comparison to their source (shrimp shell). The concentrations of calcium, potassium, sodium, magnesium, aluminum, copper, manganese and titanium was decreased after the treatment with hydrochloric acid in demineralization step and sodium hydroxide in deproteinization and deacetylation steps of the Isolation chitin and chitosan from the shrimp shell. Comparing with commercial different sources of chitin and chitosan, the metal residual in commercial products were 20 times higher than the isolated chitin and chitosan, indicated that the Brazilian Atlantic Ocean biopolymers were more pure than the commercial biopolymers (Table S1).

3.8. X-ray diffraction of chitin and chitosan

The XRD spectra of the isolated chitin and chitosan comparing with commercial biopolymers were shown in Fig. 10. Diffraction pattern of isolated chitin (Fig. 10a) exhibits ten markable diffraction peaks on angle $2\theta = 9.3°$, 19.3°, 20.9°, 23.5°, 26.5°, 34.8°, 38,9°, positions of peaks corresponds to inter-planar distances 9.5, 4.6, 4.2, 3.8, 3.4, 2.3 Å which in accordance with the literature data from different sources of chitin and chitosan [69,87–89]. The commercial chitin exhibits also 10 remarkable diffraction peaks on the same position peaks comparing with isolated one. Only one more beaks at $2\theta = 12.7°$ corresponds to inter-planar distances 7 Å which was corresponding to residual of impurities in commercial chitin like protein and pigments [90]. Some recent studies also reported similar crystalline peaks in the XRD measurements of β-chitin [75,91]. From comparable intensities of corresponding peaks concluded that the crystallinity of isolated chitin and commercial chitin were similar. The diffraction patterns of the isolated and commercial chitosan (Fig. 9b) shows comparable data. Isolated chitosan and commercial chitosan had two broad beaks at $2\theta = 9.5°$, and 21.5° corresponded to inter-lattice distances 4.6 and 2.6 Å [6]. From XRD data both isolated and commercial chitin and chitosan (shrimp shell sources) had the same crystalline and amorphous properties.
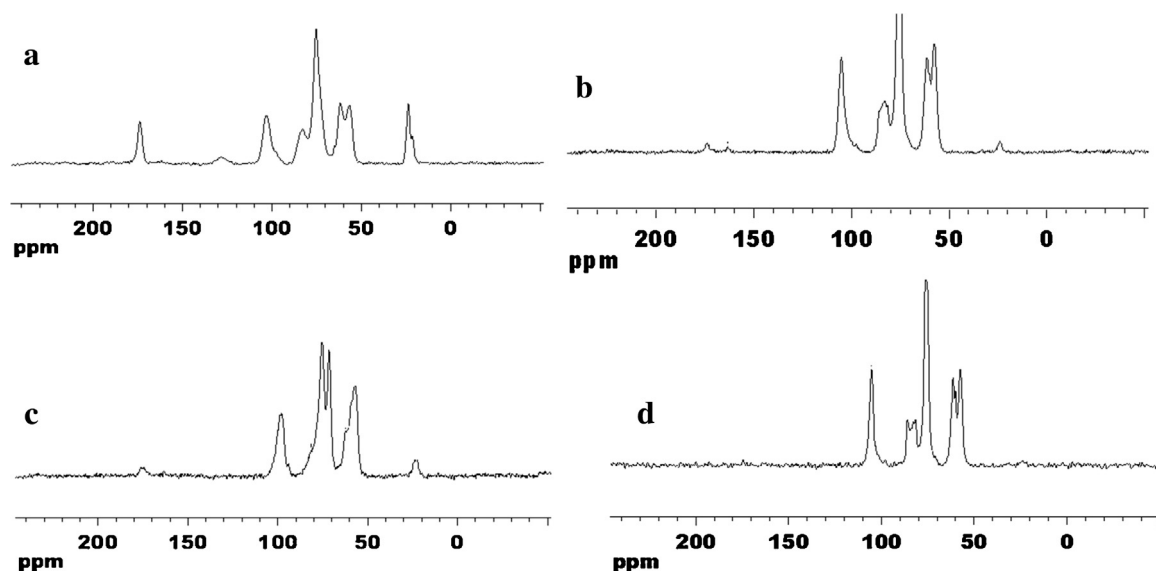

Fig. 8. Solid ^{13}C CP/MAS NMR spectra of chitin and chitosan with different degree of deacetylation after various time. (a) DDA 30% after 1 h; (b) DDA 67% after 2 h; (c) DDA 93% after 3 h; (d) DDA 95% after 4 h. *Experimental conditions*: DM-demineralization: 5% hydrochloric acid, 2 h, RT (22 ± 2 °C); DP-deproteinization: 5% sodium hydroxide, 20 h, 90 °C.
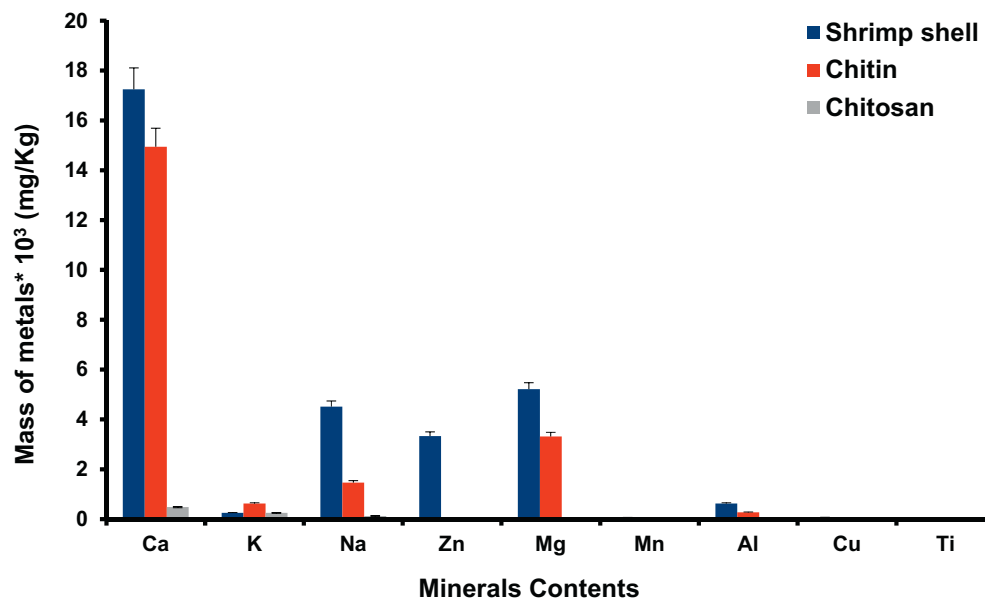
Fig. 9. Residual metals in the isolated chitin and chitosan in the comparison with shrimp shell. *Experimental conditions*: DM-demineralization: 5% hydrochloric acid, 2 h, RT (22 °C ± 2); DP-deproteinization: 5% sodium hydroxide, 20 h, 90 °C; DA-deacetylation: 50% sodium hydroxide, 3.5 h, 90 °C, solid to liquid (1:30, w/v), degree of deacetylation DDA (95%, measured by NMR).
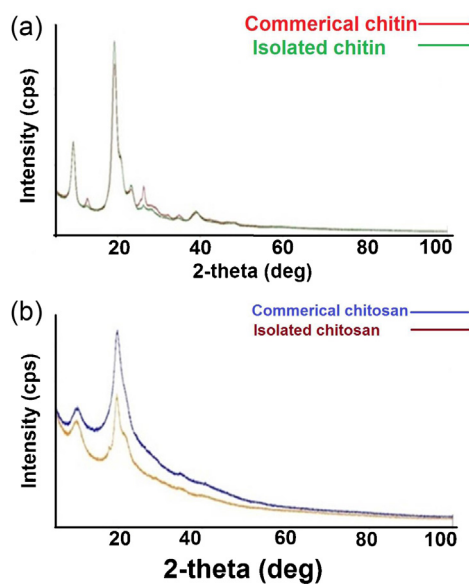
Fig. 10. XRD of chitin and chitosan. (a) *Experimental conditions*: DM-demineralization: 5% hydrochloric acid, 2 h, RT (22 ± 2 °C); DP-deproteinization: 5% sodium hydroxide, 20 h, 90 °C. (b) *Experimental conditions*: DM-demineralization: 5% hydrochloric acid, 2 h, RT (22 °C ± 2). DP-deproteinization: 5% sodium hydroxide, 20 h, 90 °C; DA-deacetylation: 50% sodium hydroxide, 3.5 h, 90 °C, degree of deacetylation DDA (95%, measured by NMR).

3.9. Scanning electron microscopy of chitosan

The morphology of the isolated chitosan sample was studied using a scanning electron microscope. SEM images with different magnifications 1000, 500, 200, 50 μm (Fig. 11A–D), respectively; of chitosan sample were presented in Fig. 11. It was observed that the biopolymer surface became very smooth as comparing with the chitin sample before deacetylation step [92,93].

3.10. Deacetylation degree (DDA) measurements of chitosan by different techniques

Chitosan was obtained from chitin using high concentrated sodium hydroxide solution. The degree of deacetylation (DDA), was an important parameter that indicated the molar % of monomeric units that have amino groups and vary from zero (chitin) to 100 (fully deacetylated) chitosan. DDA of chitosan was measured and compared between the data as described in Table 1. As shown in Table 1 the DDA of chitin was very low after treatment with 5% of sodium hydroxide for 20 h. DDA was 35, 30, 23, and 25 by ATIR-FTIR, H/C NMR, elemental analysis and acid–base titration, respectively. After removing the acetyl groups from chitin by using high concentration of sodium hydroxide for 3.5 h at 90 °C, the degree of deacetylation was measured and confirmed by ATR-FTIR, H/C NMR, elemental analysis, and acid–base titration and it was 65, 95, 85, 75, respectively. From the data in Table 1, we could conclude that, the DDA of chitosan have different variable values due to the different techniques used.

3.11. Antibacterial activity of chitin and chitosan

Fig. 12 shows the antibacterial activity of chitin and chitosan isolated from shrimp shell by chemical treatments. The biological activity of chitin and chitosan was evaluated against Gram negative bacteria (*E. coli*) by chemo-luminescence technique. This technique

Table 1
Determination of degree of deacetylation (DDA) by different analytical techniques.

	Degree of deacetylation (%)			
	FTIR	NMR	Elemental analysis	Acid–base titration
Chitin	35 ± 2[a]	30	23 ± 5	25 ± 1.5
Chitosan	65 ± 3	95	85 ± 3	75 ± 2.5

[a] Mean (standard deviation).
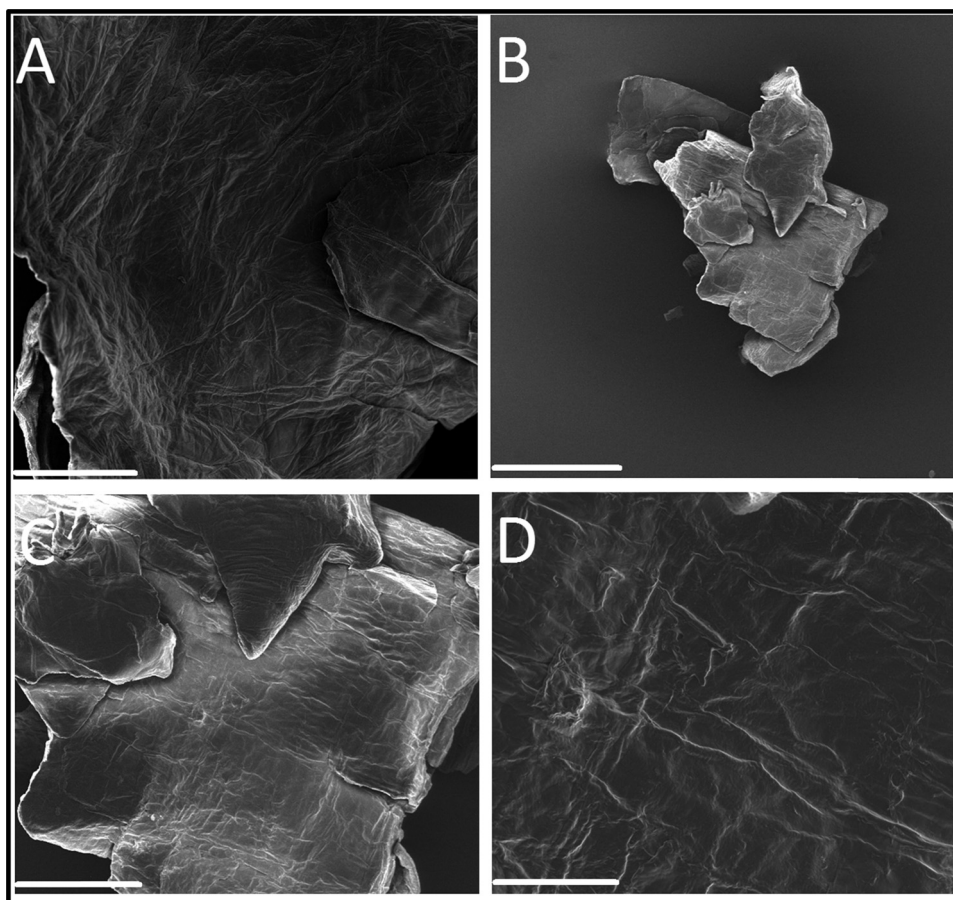
Fig. 11. Scan electron microscope of pure chitosan isolated from shrimp shells with particle size 800–1000 μm at different magnification. (A) 1000 μm; (B) 500 μm; (C) 200 μm; (D) 50 μm, respectively. *Experimental conditions*: DM-demineralization: 5% hydrochloric acid, 2 h, RT (22 ± 2 °C); DP-deproteinization: 5% sodium hydroxide, 20 h, 90 °C; DA-deacetylation: 50% sodium hydroxide, 3.5 h, 90 °C, degree of deacetylation DDA (95%, measured by NMR).
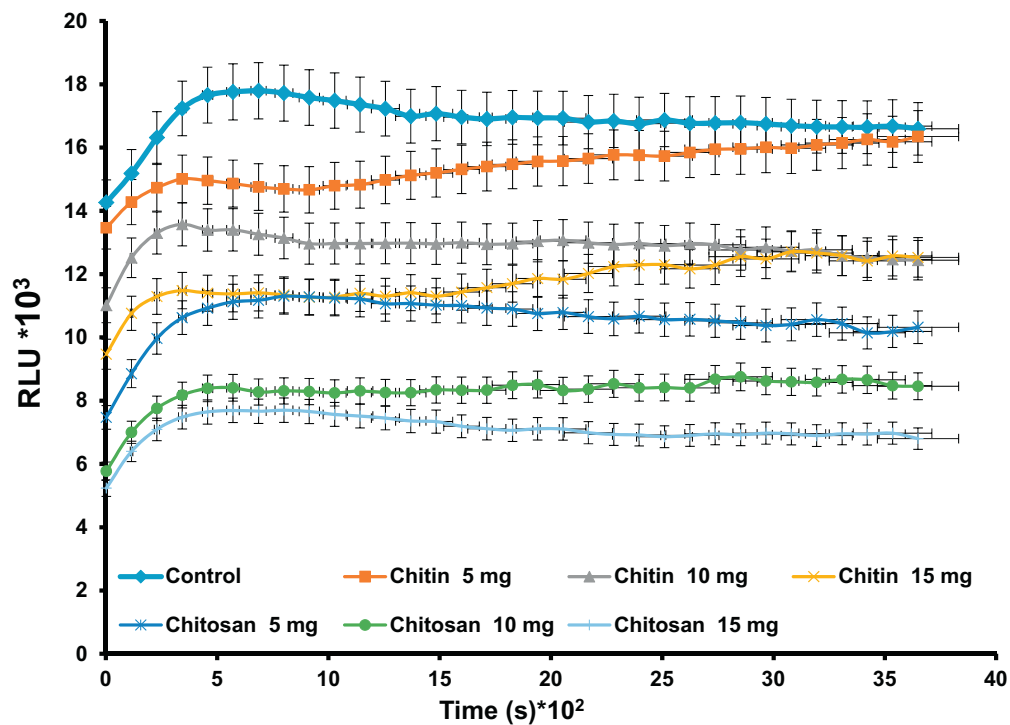

Fig. 12. Kinetic curve of the bioluminescence of *E. coli* within 60 min in the presence of isolated chitin and chitosan. *Experimental conditions for chitin*: DM-demineralization: 5% hydrochloric acid, 2 h, RT (22 ± 2 °C); DP-deproteinization: 5% sodium hydroxide, 20 h, 90 °C. *Experimental conditions for chitosan*: DM-demineralization: 5% hydrochloric acid, 2 h, RT (22 °C); DP-deproteinization: 5% sodium hydroxide, 20 h, 90 °C; DA-deacetylation: 50% sodium hydroxide, 3.5 h, 90 °C; degree of deacetylation DDA (95%, measured by NMR).

is more accurate comparing with the other techniques like disc diffusion method. As described in (Fig. 12), three different concentrations (5, 10, 15 mg) of chitin, chitosan, isolated from Atlantic Ocean and commercial were measured and evaluated to compare the biological activity of both material. As shown in Fig. 12, the antibacterial activity of the isolated chitin increased by increasing the concentration of chitin (5, 10, 15 mg). However, with lower reduction rate value (10%, 15%, and 20%, respectively). This can be explained by the blocking of the amino groups (low deacetylation degree, DDA = 5% confirmed by NMR data). On the other hand the antibacterial activity of isolated chitosan increased (reduction rate; 60%, 80%, 90%) dramatically by increasing the concentration of chitosan (5, 10, 15 mg), since in this case chitosan had highly DDA = 95% confirmed by NMR data. There was relations between the antibacterial activity of chitosan and the free amino groups (DDA). The mechanism of the antibacterial activity of chitin and chitosan are still well unknown. The antibacterial activity of chitin and chitosan has been correlated with its degree of deacetylation (DDA), purity and molecular weight [1,13,18,21,94–96]. The antibacterial or antifungal activity of chitosan depends on the presence of positive charge numbers created on chitosan chains by DDA step, could be expected to have a more potent antibacterial activity. From the obtained results, this concluded that the biological activity of both chitin and chitosan isolated from Atlantic ocean as a source after DM, DP, DA steps had very high antibacterial activity in comparison with biopolymers (chitin and chitosan) from different other sources [97–100].

4. Conclusion

Highly pure chitin and chitosan were isolated from Brazilian Atlantic Coast shrimp shell by the chemical treatment method. Furthermore, chitosan of different DDA and zero % of protein is obtained by alkali treatment. The isolated biopolymers were characterized and confirmed by different analytical tools like ATR-FTIR, TGA, XRD, elemental analysis, NMR, SEM, acid–base titration and compared with the commercial available chitin and chitosan. DMPA > DPMA > DAPM > DAMP had the heights value of chitin and chitosan. The isolated chitin and chitosan showed excellent antibacterial activity against Gram-negative bacteria (E. coli). In addition, the high pure chitin and highly DDA of chitosan were obtained by demineralization, deproteinization and deacetylation sequences steps. Finally we can conclude that, chitin and chitosan from Brazilian Atlantic Ocean had low protein, minerals percentage, high DDA, thermal stable as well as excellent antibacterial activity compared with the other sources of chitin and chitosan. According to this finding, Atlantic chitin and chitosan can be used for different medial application especially for tissue engineering and drug carrier purposes.

Acknowledgments

Appendix A. Supplementary data

Supplementary data associated with this article can be found, in the online version, at http://dx.doi.org/10.1016/j.ijbiomac.2015.06.027

References

[1] A.M. Abdel-Mohsen, R.M. Abdel-Rahman, R. Hrdina, A. Imramovský, L. Burgert, A.S. Aly, Int. J. Biol. Macromol. 50 (2012) 1245–1253.
[2] A.M. Abdel-Mohsen, A.S. Aly, R. Hrdina, A.S. Montaser, A. Hebeish, J. Polym. Environ. 20 (2012) 104–116.
[3] M. Kaya, V. Baublys, E. Can, I. Šatkauskienė, B. Bitim, V. Tubelytė, T. Baran, Zoomorphology 133 (2014) 285–293.
[4] A. Busilacchi, A. Gigante, M. Mattioli-Belmonte, S. Manzotti, R.A.A. Muzzarelli, Carbohydr. Polym. 98 (2013) 665–676.
[5] M. Kaya, S. Erdogan, A. Mol, T. Baran, Int. J. Biol. Macromol. 72 (2015) 797–805.
[6] M. Kaya, T. Baran, M. Asan-Ozusaglam, Y. Cakmak, K. Tozak, A. Mol, A. Mentes, G. Sezen, Biotechnol. Bioprocess Eng. 20 (2015) 168–179.
[7] M. Kaya, T. Baran, Int. J. Biol. Macromol. 75 (2015) 7–12.
[8] M. Kaya, E. Lelešius, R. Nagrockaitė, I. Sargin, G. Arslan, A. Mol, T. Baran, E. Can, B. Bitim, PLOS ONE 10 (2015) e0115531.
[9] M. Kaya, I. Akata, T. Baran, A. Menteş, Food Biophys. (2014) 1–7.
[10] M. Kaya, T. Baran, S. Erdoğan, A. Menteş, M. Aşan Özüsağlam, Y.S. Çakmak, Mater. Sci. Eng. C 45 (2014) 72–81.
[11] M. Kaya, T. Baran, A. Mentes, M. Asaroglu, G. Sezen, K. Tozak, Food Biophys. 9 (2014) 145–157.
[12] M. Kaya, O. Seyyar, T. Baran, T. Turkes, Front. Zool. 11 (2014) 1–10.
[13] M. Kaya, Y. Cakmak, T. Baran, M. Asan-Ozusaglam, A. Mentes, K. Tozak, Biotechnol. Bioprocess Eng. 19 (2014) 58–69.
[14] M. Kaya, O. Seyyar, T. Baran, S. Erdoğan, M. Kar, Int. J. Biol. Macromol. 65 (2014) 553–558.
[15] M. Kaya, I. Sargin, K.Ö. Tozak, T. Baran, S. Erdogan, G. Sezen, Int. J. Biol. Macromol. 61 (2013) 459–464.
[16] A.M. Abdel-Mohsen, R.M. Abdel-Rahman, R. Hrdina, A. Imramovsky, L. Burgert, A.S. Aly, Int. J. Biol. Macromol. 50 (2012) 1245–1253.
[17] A.S. Aly, A.M. Abdel-Mohsen, A. Hebeish, J. Text. Inst. 101 (2010) 76–90.
[18] A.M. Abdel-Mohsen, A.S. Aly, R. Hrdina, A. El-Aref, J. Polym. Environ. 20 (2012) 459–468.
[19] A.S. Aly, A.M. Abdel-Mohsen, R. Hrdina, A. Abou-Okeil, J. Nat. Fibers 8 (2011) 176–188.
[20] H. Přichystalová, N. Almonasy, A.M. Abdel-Mohsen, R.M. Abdel-Rahman, M.M.G. Fouda, L. Vojtova, L. Kobera, Z. Spotz, L. Burgert, J. Jancar, Int. J. Biol. Macromol. 65 (2014) 234–240.
[21] A.M. Abdel-Mohsen, A.S. Aly, R. Hrdina, A.S. Montaser, A. Hebeish, J. Polym. Environ. 19 (2011) 1005–1012.
[22] M.R. Kasaai, Carbohydr Polym 71 (2008) 497–508.
[23] E.S. de Alvarenga, C. Pereira de Oliveira, C. Roberto Bellato, Carbohydr. Polym. 80 (2010) 1155–1160.
[24] M.S. Benhabiles, R. Salah, H. Lounici, N. Drouiche, M.F.A. Goosen, N. Mameri, Food Hydrocolloids 29 (2012) 48–56.
[25] D. Tahtat, C. Uzun, M. Mahlous, O. Güven, Nucl. Instrum. Methods Phys. Res. B 265 (2007) 425–428.
[26] R. Jayakumar, M. Prabaharan, P.T. Sudheesh Kumar, S.V. Nair, H. Tamura, Biotechnol. Adv. 29 (2011) 322–337.
[27] I. Younes, O. Ghorbel-Bellaaj, R. Nasri, M. Chaabouni, M. Rinaudo, M. Nasri, Process Biochem. 47 (2012) 2032–2039.
[28] Z.M. dos Santos, A.L.P.F. Caroni, M.R. Pereira, D.R. da Silva, J.L.C. Fonseca, Carbohydr. Res. 344 (2009) 2591–2595.
[29] Y. Zhang, X. Zhang, R. Ding, J. Zhang, J. Liu, Carbohydr. Polym. 83 (2011) 813–817.
[30] H.K. No, S.P. Meyers, W. Prinyawiwatkul, Z. Xu, J. Food Sci. 72 (2007) R87–R100.
[31] S. Hirano, K. Hirochi, K.-I. Hayashi, T. Mikami, H. Tachibana, Cosmetic and pharmaceutical uses of chitin and chitosan, in: C. Gebelein, T. Cheng, V. Yang (Eds.), Cosmetic and Pharmaceutical Applications of Polymers, Springer, US, 1991, pp. 95–104.
[32] A.M. Abdel-Mohsen, R.M. Abdel-Rahman, M.M.G. Fouda, L. Vojtova, L. Uhrova, A.F. Hassan, S.S. Al-Deyab, I.E. El-Shamy, J. Jancar, Carbohydr. Polym. 102 (2014) 238–245.
[33] D. Zeng, X. Luo, R. Tu, Int. J. Carbohydr. Chem. 2012 (2012) 5.
[34] N.R. Sudarshan, D.G. Hoover, D. Knorr, Food Biotechnol. 6 (1992) 257–272.
[35] A. Hebeish, F.A. Abdel-Mohdy, M.M.G. Fouda, Z. Elsaid, S. Essam, G.H. Tammam, E.A. Drees, Carbohydr. Polym. 86 (2011) 1684–1691.
[36] M.M.G. Fouda, E. Fahmy, Carbohydr. Polym. 86 (2011) 625–629.
[37] M. Hashem, M.H. Elshakankery, S.M. Abd El-Aziz, M.M.G. Fouda, H.M. Fahmy, Carbohydr. Polym. 86 (2011) 1692–1698.
[38] S. Şenel, S.J. McClure, Adv. Drug Deliv. Rev. 56 (2004) 1467–1480.
[39] J. Zhang, W. Xia, P. Liu, Q. Cheng, T. Tahi, W. Gu, B. Li, Mar. Drugs 8 (2010) 1962–1987.
[40] A. Przekora, G. Ginalska, Cent. Eur. J. Biol. 9 (2014) 634–641.
[41] R. Ramya, J. Venkatesan, S.K. Kim, P.N. Sudha, J. Biomater. Tissue Eng. 2 (2012) 100–111.
[42] P.-B. Céline, V. Antoine, B. Denis, V. Laurent, D. Laurent, F. Catherine, J. Appl. Polym. Sci. 128 (2013) 2945–2953.
[43] H.S. Kas, J. Microencapsul. 14 (1997) 689–711.
[44] R. Mukhopadhyay, D. Talukdar, B.P. Chatterjee, A.K. Guha, Process Biochem. 39 (2003) 381–385.
[45] M.Z. Albanna, T.H. Bou-Akl, O. Blowytsky, H.L. Walters Iii, H.W.T. Matthew, J. Mech. Behav. Biomed. Mater. 20 (2013) 217–226.

[46] A. Qurashi, Chitin and chitosan polymer nanofibrous membranes and their biological applications, in: Handbook of Bioplastics and Biocomposites Engineering Applications, John Wiley & Sons, Inc., 2011, pp. 357–370.

[47] I. Aranaz, M. Mengibar, R. Harris, I. Panos, B. Miralles, N. Acosta, G. Galed, A. Heras, Curr. Chem. Biol. 3 (2009) 203–230.

[48] C.E. Tanase, I. Spiridon, Mater. Sci. Eng. C 40 (2014) 242–247.

[49] S. Chandrasekar, S. Vijayakumar, R. Rajendran, Biomed. Aging Pathol. 4 (2014) 59–64.

[50] L. Casettari, D. Vllasaliu, E. Castagnino, S. Stolnik, S. Howdle, L. Illum, Prog. Polym. Sci. 37 (2012) 659–685.

[51] V. Balan, L. Verestiuc, Eur. Polym. J. 53 (2014) 171–188.

[52] M. Larsson, W.-C. Huang, M.-H. Hsiao, Y.-J. Wang, M. Nydén, S.-H. Chiou, D.-M. Liu, Prog. Polym. Sci. 38 (2013) 1307–1328.

[53] F. Croisier, C. Jérôme, Eur. Polym. J. 49 (2013) 780–792.

[54] C.G. Lee, Yonsei Med. J. 50 (2009) 22–30.

[55] Z. Zhu, T. Zheng, R.J. Homer, Y.-K. Kim, N.Y. Chen, L. Cohn, Q. Hamid, J.A. Elias, Science 304 (2004) 1678–1682.

[56] A.F. Hassan, A.M. Abdel-Mohsen, M.M.G. Fouda, Carbohydr. Polym. 102 (2014) 192–198.

[57] A. Percot, C. Viton, A. Domard, Biomacromolecules 4 (2003) 1380–1385.

[58] G. Chaussard, A. Domard, Biomacromolecules 5 (2004) 559–564.

[59] L. Heux, J. Brugnerotto, J. Desbrières, M.F. Versali, M. Rinaudo, Biomacromolecules 1 (2000) 746–751.

[60] J. Kumirska, M.X. Weinhold, S. Steudte, J. Thöming, K. Brzozowski, P. Stepnowski, Int. J. Biol. Macromol. 45 (2009) 56–60.

[61] M. Lavertu, Z. Xia, A.N. Serreqi, M. Berrada, A. Rodrigues, D. Wang, M.D. Buschmann, A. Gupta, J. Pharm. Biomed. Anal. 32 (2003) 1149–1158.

[62] Y. Boonsongrit, B.W. Mueller, A. Mitrevej, Eur. J. Pharm. Biopharm. 69 (2008) 388–395.

[63] M.R. Kasaai, J. Agric. Food Chem. 57 (2009) 1667–1676.

[64] M.S. Benhabiles, N. Drouiche, H. Lounici, A. Pauss, N. Mameri, J. Food Meas. Character. 7 (2013) 215–221.

[65] A. Sila, N. Mlaik, N. Sayari, R. Balti, A. Bougatef, J. Polym. Environ. 22 (2014) 78–87.

[66] I. Younes, M. Rinaudo, Mar. Drugs 13 (2015) 1133–1174.

[67] S.-L. Wang, T.-W. Liang, Y.-H. Yen, Carbohydr. Polym. 84 (2011) 732–742.

[68] S. Hajji, I. Younes, O. Ghorbel-Bellaaj, R. Hajji, M. Rinaudo, M. Nasri, K. Jellouli, Int. J. Biol. Macromol. 65 (2014) 298–306.

[69] F.A.A. Sagheer, M.A. Al-Sughayer, S. Muslim, M.Z. Elsabee, Carbohydr. Polym. 77 (2009) 410–419.

[70] E.S. Abdou, K.S.A. Nagy, M.Z. Elsabee, Bioresour. Technol. 99 (2008) 1359–1367.

[71] Y.S. Nakagawa, M. Kudo, J.S.M. Loose, T. Ishikawa, K. Totani, V.G.H. Eijsink, G. Vaaje-Kolstad, FEBS J. 282 (2015) 1065–1079.

[72] S.J. Hamodrakas, J.H. Willis, V.A. Iconomidou, Insect Biochem. Mol. Biol. 32 (2002) 1577–1583.

[73] B. John, G. Louis, T.W. Mark, A. Chitin, Protein complexes, in: Biological Activities of Polymers, American Chemical Society, 1982, pp. 149–162.

[74] Y. Yuan, B.M. Chesnutt, W.O. Haggard, J.D. Bumgardner, Materials 4 (2011) 1399–1416.

[75] G.T. Kjartansson, S. Zivanovic, K. Kristbergsson, J. Weiss, J. Agric. Food Chem. 54 (2006) 5894–5902.

[76] A. Einbu, S.N. Naess, A. Elgsaeter, K.M. Vårum, Biomacromolecules 5 (2004) 2048–2054.

[77] M.-K. Jang, B.-G. Kong, Y.-I. Jeong, C.H. Lee, J.-W. Nah, J. Polym. Sci. A 42 (2004) 3423–3432.

[78] I. Uzun, G. Topal, J. Chem. 2013 (2013) 8.

[79] G.L. Clark, A.F. Smith, J. Phys. Chem. 40 (1935) 863–879.

[80] K. Van de Velde, P. Kiekens, Carbohydr. Polym. 58 (2004) 409–416.

[81] B. Chagas, I. Farinha, C.F. Galinha, F. Freitas, M.A.M. Reis, New Biotechnol. 31 (2014) 468–474.

[82] I. Farinha, P. Duarte, A. Pimentel, E. Plotnikova, B. Chagas, L. Mafra, C. Grandfils, F. Freitas, E. Fortunato, M.A.M. Reis, Carbohydr. Polym. 130 (2015) 455–464.

[83] Y.A. Skorik, A.V. Pestov, Y.G. Yatluk, Bioresour. Technol. 101 (2010) 1769–1775.

[84] B. Chagas, F. Freitas, L. Mafra, J. Cortez, R. Oliveira, M.A.M. Reis, J. Biotechnol. 150 (Suppl.) (2010) 381–382.

[85] N. Nwe, W.F. Stevens, S. Tokura, H. Tamura, Enzyme Microb. Technol. 42 (2008) 242–251.

[86] A.S.M. Sonnenberg, J.H. Sietsma, J.G.H. Wessels, Exp. Mycol. 9 (1985) 141–148.

[87] S. Kumari, P. Rath, A. Sri Hari Kumar, T.N. Tiwari, Environ. Technol. Innov. 3 (2015) 77–85.

[88] M.H. Mohammed, P.A. Williams, O. Tverezovskaya, Food Hydrocolloids 31 (2013) 166–171.

[89] S. Kumari, P.K. Rath, Proc. Mater. Sci. 6 (2014) 482–489.

[90] A. Watthanaphanit, P. Supaphol, T. Furuike, S. Tokura, H. Tamura, R. Rujiravanit, Biomacromolecules 10 (2009) 320–327.

[91] A. Yoshifuji, Y. Noishiki, M. Wada, L. Heux, S. Kuga, Biomacromolecules 7 (2006) 2878–2881.

[92] K.D. Trimukhe, A.J. Varma, Carbohydr. Polym. 71 (2008) 698–702.

[93] A. Montilla, E. Casal, F. Javier Moreno, J. Belloque, A. Olano, N. Corzo, Int. Dairy J. 17 (2007) 459–464.

[94] H.K. No, S.H. Kim, S.H. Lee, N.Y. Park, W. Prinyawiwatkul, Carbohydr. Polym. 65 (2006) 174–178.

[95] R.C. Goy, D.d. Britto, O.B.G. Assis, Polímeros 19 (2009) 241–247.

[96] C. Clasen, T. Wilhelms, W.M. Kulicke, Biomacromolecules 7 (2006) 3210–3222.

[97] X. Zhu, H. Wu, J. Yang, J. Tong, J. Yi, Z. Hu, J. Hu, T. Wang, L. Fan, React. Funct. Polym. 91–92 (2015) 71–76.

[98] Z. Shariatinia, M. Fazli, Food Hydrocolloids 46 (2015) 112–124.

[99] K. Song, A. Gao, X. Cheng, K. Xie, Carbohydr. Polym. 130 (2015) 381–387.

[100] L. Fan, J. Yang, H. Wu, Z. Hu, J. Yi, J. Tong, X. Zhu, Int. J. Biol. Macromol. 79 (2015) 830–836.

Supporting Information

Novel Chitin/chitosan-glucan Wound Dressing: Isolation, Characterization, Antibacterial Activity and Wound Healing Properties

A.M.Abdel-Mohsen, J. Jancar, D.F.Massoud, Z. Fohlerova, H. Elhadidy, Z. Spotz, A. Hebeish

Characterization of chitin/chitosan-glucan complex (ChCsGC)

Mechanical measurements: Universal tensile testing machine, Inston 3343 (Instron, USA) was used to measure mechanical response of specimens pre-stressed with 0.05N at cross head speed of 30 mm/min, at room temperature and relative humidity of 28 % utilizing rectangular fibrous specimens 10 cm long and 7 cm wide. Reported data represent average values from three independent measurements. The Student ($-t$) test was used to analyze the significance of the experimental data ($p \leq 0.05$).

Thermal stability: Thermal gravimetric stability of the materials was measured using thermo-gravimetric analyzer (TGA Netzsch 209 F3, Al_2O_3 crucible) at the heating rate of 5 °C/min. The heat flow was also measured employing differential scanning calorimetry (DSC, Netzsch 200 F3) in the dynamic nitrogen atmosphere with a pressure of 0.1 MPa. The sample mass for DSC was typically about 0.9 mg and the heating rate of 10 °C/min was used over the temperature range from 25 to 600 °C. Fourier transformation infrared attenuated total reflectance spectroscopy (FTIR -ATR) was performed using the Impact 400 D FTIR-ATR spectrophotometer (Nicolet, USA) equipped with a ZnSe crystal between 4000 cm^{-1} and 600 cm^{-1} with the

24   resolution of 8 cm^{-1}. Morphological observations were performed using the SEM microscope

25   Tescan VEGA II LSU (Tescan, CZ) at 5 kV, in secondary electrons with maximum resolution

26   was 3 nm. SC7620 Mini Sputter Coater (Quorum Technologies, UK) was used to deposit 15 nm

27   Au layer on the surface of non-conducting specimens.

28   **NMR measurements**: ChCsGC complex (10 mg) was dissolved in 750 µL of

29   NaOH/urea/D$_2$O, then transferred into NMR tubes and analyzed directly using Vance TM 500

30   MHz NMR (Bruker, Germany) equipped with BBFO plus probe. ^{1}H/^{13}C chemical shifts were

31   related to the 3-trimethylsilylpropanoic acid sodium salt (TSPA) used as an internal standard.

32   The elemental microanalyses of CHN were performed employing the EA 1108 (FISONS, USA).

33   **Air permeability**: Water permeability Water permeability was measured according to

34   ASTM No. D-461.

35   **Swelling measurements**: The swelling ratio of the nonwoven mat was defined as the

36   ratio of the weight increase (Ww−W$_d$) in the phosphate buffer saline solution (PBS, pH 7.4) at

37   room temperature to the initial weight (W$_d$). The Equilibrium water uptake was determined using

38   dry weight (Wi) of plain and nonwoven mats of chitin/chitosan-glucan complex (ChCsGC) were

39   immersed in MilliQ water at 37 $^{\circ}$C for 12 h and allowed to completely sell. The samples were

40   removed and the excess water were wiped off with filter paper and weight (Wf). All the

41   meaurments were carried out for three times (n=3). The amount of equilibrium water uptake was

42   calculated using the following equation.

43   Equilibrium water uptake (EWA) g/g= Wf-Wi/Wi

44   **Transmission electron microscope (TEM)**: Transmission electron microscopy (TEM)

45   observation of the molecular morphology of chitin/chitosan-glucan complex (ChCsGC) in

46   aqueous sodium hydroxide /urea solution was carried out on a JEM-2010 (HT) transmission

47 electron microscope (JEOL TEM, Japan). A thin layer of the dilute ChCsGC solution (1 mg/ml)

48 was suspended on a holey carbon film, which was supported on a copper grid. The specimen was

49 dried in air at ambient temperature (22 oC) and pressure for 30 min and was then imaged at an

50 accelerating voltage of 200 kv.

51 **Scanning electron microscopy (SEM):** The images of samples were done at the electron-

52 scanning microscope Tuscan VEGA II LSU electron microscope (Tuscan USA Inc.) under the

53 following conditions: high voltage 5 kV, working distance 4.4 mm, display mode secondary

54 electrons, high vacuum room temperature. SC7620 Mini Sputter Coater (Quorum Technologies,

55 UK) applied 15 nm layers of gold particles on the sample. The samples were dusted for 120 s

56 with the current of 18 mA. The pictures were made at these conditions: voltage 2.44–10 kV,

57 detector-SE, the magnification 300–20,000 times, vacuum high, the distance between sample and

58 objective: 4–5 mm.

59

60

61

62

63

64

65

66

67

68

69

70   **Table S1.** FTIR-ATR beaks of chitin, chitosan, glucan, complex and regenerated complex**.**

Peaks for powder (cm-1)					Assignments
Chitin	Chitosan	Glucan	Complex	Regenerated complex	
3435					Stretching and bending of H_2O
3257	3359	3297	3309	3302	Amide A, N-H, O-H stretching
		2918	2925	2926	Amide B, C-H stretching
1654	1654		1645	1639	Amide I, C=O stretching
	1590		1595	1584	Amide II, N-H bending, C=O stretching
1425	1374	1367	1413	1412	O-H,C-H bending, $\gamma(CH_2)$,γ (OH)
1375	1314	1245	1356	1335	CH_2 of chitin, chitosan and glucan
1308	1150	1200	1078	1235	Amide III, C-H stretching, N-H bending
1114	1060	1033	1020	1077	C-O-C of chitin, chitosan and glucan
1009	893		848	846	β -anomeric configuration

71

72

73

74   **Figure S1.** FTIR-ATR of pure chitin, chitosan and glucan

75

4

Figure S2. 3D structure of Chitin/chitosan-glucan complex (ChCsGC) prepared by green technology with pore size approx. 75 µm.

Figure S3. TG-DTG of chitin, chitosan and glucan

84

Figure S4: XRD of chitin (a), chitosan (b), glucan (c), and urea/sodium hydroxide powder (d)

Figure S5. Swelling percentage of ChCsGC in PBS and physiological temperature

101

Table S2. Variation of inhibition zone diameters (mm) of ChCsGC nonwoven mats against

different type of bacteria**;** basillus *subtilis (B. Subtilis), escherichia coli (E. coli), staphylococcus*

Sample name	Gram positive (+ve)		Gram negative (- ve)	
	K. pneumoniae	*E. coli*	*S. aureus*	*B. subtilis*
Control	0	0	0	0
Nonwoven Mats	8	12	13	11

aureus (S. aureus) and klebsiella pneumoniae (K. pneumoniae)

105

106

Table S3. Equilibrium water uptake and air permeability of plain complex, nonwoven mat

complex and nonwoven cotton fabrics

109

Samples	Equilibrium water uptake (g/g)	Air permeability cm^3/cm^2/s
Net ChCSGC	15±2	0
ChCSGC mats	22±3	110± 5
Nonwoven viscose fabrics	32±3	80±7

113

114

115

116

117

118 **Table S4.** Comparison between properties of novel wound dressing ChCsGC and wound

119 dressing materials reported elsewhere

Dressing types	Days of treatments	Wound healing percent (%)	Ref.
Nonwoven ChCsGC	15	95	This work
Chitin/alginate	14	97	(Shamshina et al., 2014)
Chitin	12	95	(Huang et al., 2014)
Cellulose/gelatin	12	85	(Pei et al., 2015)
Ag/graphene	15	95	(Fan et al., 2014)
Glucan/PVA	22	93	(Huang and Yang, 2008)
Silk/gelatin	15	83	(Kanokpanont et al., 2012)
Chitosan	14	91	(Ong et al., 2008)
Chitin/chitosan	14	87	(Murakami et al., 2010)

120

121 **References**

122 Fan, Z., Liu, B., Wang, J., Zhang, S., Lin, Q., Gong, P., Ma, L., Yang, S., 2014. A Novel Wound Dressing

123 Based on Ag/Graphene Polymer Hydrogel: Effectively Kill Bacteria and Accelerate Wound Healing.

124 Advanced Functional Materials 24, 3933-3943.

125 Huang, M.-H., Yang, M.-C., 2008. Evaluation of glucan/poly(vinyl alcohol) blend wound dressing using rat

126 models. International Journal of Pharmaceutics 346, 38-46.

127 Huang, Y., Zhong, Z., Duan, B., Zhang, L., Yang, Z., Wang, Y., Ye, Q., 2014. Novel fibers fabricated directly

128 from chitin solution and their application as wound dressing. Journal of Materials Chemistry B 2, 3427-

129 3432.

130 Kanokpanont, S., Damrongsakkul, S., Ratanavaraporn, J., Aramwit, P., 2012. An innovative bi-layered

131 wound dressing made of silk and gelatin for accelerated wound healing. International Journal of

132 Pharmaceutics 436, 141-153.

133 Murakami, K., Aoki, H., Nakamura, S., Nakamura, S.-i., Takikawa, M., Hanzawa, M., Kishimoto, S., Hattori,

134 H., Tanaka, Y., Kiyosawa, T., Sato, Y., Ishihara, M., 2010. Hydrogel blends of chitin/chitosan, fucoidan and

135 alginate as healing-impaired wound dressings. Biomaterials 31, 83-90.

136 Ong, S.-Y., Wu, J., Moochhala, S.M., Tan, M.-H., Lu, J., 2008. Development of a chitosan-based wound

137 dressing with improved hemostatic and antimicrobial properties. Biomaterials 29, 4323-4332.

138 Pei, Y., Ye, D., Zhao, Q., Wang, X., Zhang, C., Huang, W., Zhang, N., Liu, S., Zhang, L., 2015. Effectively

139 promoting wound healing with cellulose/gelatin sponges constructed directly from a cellulose solution.

140 Journal of Materials Chemistry B 3, 7518-7528.

141 Shamshina, J.L., Gurau, G., Block, L.E., Hansen, L.K., Dingee, C., Walters, A., Rogers, R.D., 2014. Chitin-

142 calcium alginate composite fibers for wound care dressings spun from ionic liquid solution. Journal of

143 Materials Chemistry B 2, 3924-3936.

144

Publication 6

Wound dressing based on chitosan/hyaluronan/nonwoven fabrics: Preparation, characterization and medical applications

Rasha M. Abdel-Rahman [a,*,1], A.M. Abdel-Mohsen [b,c,d,**,1], R. Hrdina [a], L. Burgert [e], Z. Fohlerova [b], D. Pavliňák [f], O.N. Sayed [g], J. Jancar [b,c,h]

[a] Institute of Organic Chemistry and Technology, Faculty of Chemical Technology, University of Pardubice, Pardubice, Czech Republic
[b] CEITEC—Central European Institute of Technology, Brno University of Technology, Brno, Czech Republic
[c] National Research Centre, Textile Research Division, Pre-Treatment and Finishing of Cellulosic Fibers, Dokki, Cairo, Egypt
[d] SCITEG,a.s., Brno, Czech Republic
[e] Institute of Chemistry and Technology of Macromolecular Compounds, Faculty of Chemical Technology, University of Pardubice, Pardubice, Czech Republic
[f] Department of Physical Electronics, Masaryk University, Brno, Czech Republic
[g] Chemistry Department, Faculty of Science, Fayoum University, Fayoum, Egypt
[h] Faculty of Chemistry, Institute of Materials Chemistry, Brno University of Technology, Brno, Czech Republic

ARTICLE INFO

ABSTRACT

Thin layers of chitosan (positively charged)/sodium hyaluronate (negatively charged)/nonwoven fabrics were constructed by polyelectrolyte multilayer pad-dry-cure technique. Pure chitosan (CS) was isolated from shrimp shell and immobilized onto nonwoven fabrics (NWFs) using citric acid (CTA) as cross linker and solvent agents through a pad-dry-cure method. The prepared thin layer of chitosan citrate/nonwoven fabrics (CSCTA/NWFs) were consequently impregnated with hyaluronan (CSCTA/HA/NWFs) in the second path through a pad-dry-cure method. Chitosan/hyaluronan/nonwoven fabrics wound dressing was characterized by different techniques such as FTIR-ATR, TGA and SEM. The antibacterial activity and the cytotoxicity of the dressing sheets were evaluated against *Escherichia coli* (*E. coli*) and *Streptococcus aureus* (*S. aureus*), mouse fibroblast (*NIH-3T3*) and keratinocytes (*HaCaT*) cell lines, respectively. The cell-fabrics interaction was also investigated using fluorescence microscope, based on live/dead staining assay of *3T3* cells. The healing properties of the new wound dressing were evaluated and compared with the control sample.

© 2016 Elsevier B.V. All rights reserved.

1. Introduction

Healing of wound is a complicated process of restoring cellular structures and epidermal tissue in damaged part to its normal condition as closely as possible [1]. This dynamic process consisting of three continuous, overlapping phases, the first phase is the inflammation phase which occurs immediately after wounding and continue for 24–48 h, hemostasis is the beginning of this phase which leads to the inflammation. Platelet-derived growth factors are released into the wound that promote the chemotaxis and proliferation of neutrophils in order to clean the wounds from bacteria, dead tissues or debris [2–6]. The second phase is fibroblast proliferation; in this phase, collagen is produced in order to supply the structure to wounds and replaces the fibronectin–fibrin matrix. The last phase is the remodeling which approximately starts after two or three weeks and can take more than two years. In this phase, new collagen forms and wound strength gradually increases. Many factors affecting on healing process as the type of damage, the ability of the tissue to repair and the general state of the host's health [7–9]. Layer-by-layer (LbL) assembly is a technique that was used in large scale due to its extraordinary advantages in the preparation of multilayer films [10–14]. Multilayer films were formed as the result of impregnation procedure, different alternating polyelectrolyte layers of oppositely charged was successfully assembled on flat surfaces. Also, these films were easy synthesized on different substrates. On other hand, these layers had varies features as uniform,

* Corresponding author at: Institute of Organic Chemistry and Technology, Faculty of Chemical Technology, University of Pardubice, Pardubice, Czech Republic.
** Corresponding author at: CEITEC—Central European Institute of Technology, Brno University of Technology, Brno, Czech Republic. Tel.: +420773063837.
E-mail addresses: rmmar2008@yahoo.com (R.M. Abdel-Rahman), abdel-mohsen@ceitec.vutbr.cz, abdo_mohsennrc@yahoo.com (A.M. Abdel-Mohsen).
[1] These authors contribute equally to these work.

continuous, easily tailored, and resistant to protein adsorption in especial cases [15–27].

Chitosan is a cationic biopolymer, owing to its characteristic as nontoxicity, biodegradability, biocompatibility, antimicrobial activity and improving the healing of wounds; chitosan has been widely used as topical dressing in wound management [28–35]. Chitosan is characterized by three functional groups, an amino, acetamido and hydroxyl groups. Cationic character of amino group (after its potentization) gives good opportunities for it to react with other compounds, and the key properties of chitosan includes that it is bactericidal, fungicidal, and has immune-enhancing properties [28,36,37]. Also, chitosan is water soluble in acidic media due to the protonation of amino group on the second carbon of glucosamine [37]. Recently, chitosan has received extensive attention because it is a promising natural substances used in the biomedical, food, and chemical industries [36]. Chitosan and its derivatives have been shown an excellent antimicrobial activities towards most of living microorganisms as yeast, fungi and bacteria, this make many scientists be attention by this biopolymers [38,39]. The anti-bactericidal activity of chitosan is related to its cationic character with high affinity for the microbial cell wall [28,38,40–42].

Hyaluronic acid (HA) is a natural biopolymer found in all living organisms; the major component in the extracellular of many organs in all body fluids as eyes, skin, joints and hyaline cartilage [43,44]. HA has various applications especially in medical field, it can be used as tumor marker in different types of cancer such as prostate and breast cancer. Also, it's used in wound healing repair and improve the biomechanical properties of tissues. HA interact with many cell surface receptor as CD44, and ICAM-1 causing cellular processess including morghogensis, wound repair, inflammation and metastasis [45–47]. Furthermore, HA has a main role in the viscoelasticity of bio-fluids, it can control the hydration of tissue and transport of water [48–50]. The characteristic of hyaluronic acid as the biocompatibility and the hydrophobicity make it an excellent component in cosmetics [50]. Nowadays HA has been used as drug delivery agent in various fields as ophthalmic, topical and parental [51].

This paper describes the preparation of novel wound dressing sheets based on chitosan/hyaluronan/nonwoven fabrics and their physical, chemical and biological properties were evaluated.

2. Experimental

2.1. Materials

Chitosan (CS) was isolated from shrimp shell of Brazilian Atlantic Ocean obtained from VCI Brasil Indústria e Comércio de Embalagens Ltda. (Brazil). Citric acid (CTA) was purchased from Sigma Aldrich (Germany) and sodium hyaluronate (HA) high molecular mass (1.5–1.7 MDa, determined by SEC-MAALS) was purchased from Contipro Biotech Ltd., Dolni Dobrouč, Czech Republic. Viscose (100-%, 40 g/m^2) nonwoven cotton fabrics and samples (produced by random distribution for web and spun bonded thermally) were used in this study and kindly provided from El-Nasr Company for Spinning, Weaving and Dyeing–El-Mahalla El-Kubra, Egypt. These fabrics were cut into identical sheets (10 × 10 cm) and used for all experiments as described below.

2.2. Isolation of chitosan from shrimp shell

Pure chitosan (CS) was isolated from Brazilian Atlantic ocean according to our previous work with small modification [28]. Briefly, shrimp shells were washed with water, acetone and isopropyl alcohol to remove sand, salts and other impurities. Washing was followed by three classical steps: the first step was deminer-

alization which was carried out by 5-% hydrochloric acid solution for 2 h; the second step was deproteinization step (DP) which was done by the use of 5-% aqueous sodium hydroxide for 20 h; finally, the crude chitin was stirred in 50-% sodium hydroxide for 3.5 h to obtain pure chitosan (deacetylation step). The isolated chitosan was fully characterized by FTIR, X-ray diffraction, NMR, TGA-DTG and elemental analysis. The deacetylation degree of chitosan was 95% [28] (determined by NMR and FTIR-ATR techniques).

2.2.1. Immobilization of chitosan citrate/hyaluronan onto nonwoven cotton fabrics

Cotton nonwoven fabrics (NWFs) were used as substrates for immobilization of chitosan citrate (CSCTA) and sodium hyaluronate (HA). Firstly, cotton nonwoven fabrics were washed with hot water for 30 min then with 0.1% sodium bicarbonate to activate the fabric surface. The nonwoven fabrics (10 × 10 cm) were immersed in chitosan citrate (CTA was 5 wt.%) of 0.5, 1, 2 wt.% solutions for 30 min, then squeezed at constant pressure using padding machine. The chitosan citrate/nonwoven fabrics with different concentration of chitosan (0.5, 1, 2 wt.%) (coded as $CS_{0.5}CTA/NWFs$, $CS_1CTA/NWFs$ and $CS_2CTA/NWFs$) were dried at 80 °C for 10 min by-thermal fixation machine. The CSCTA/NWFs were dried at 80 °C for 10 min in thermal fixation machine. The CSCTA/NWFs were rinsed for three times with ultrapure water to remove nonattached (non-bonded) materials from the surface of nonwoven sheets and then dried at 80 °C for 10 min. The washing step was repeated three times to obtain layers of chitosan citrate onto non-woven cotton fabrics (CSCTA/NWFs).

The CSCTA/NWFs (coded as $CS_{0.5}CTA/NWFs$, $CS_1CTA/NWFs$, $CS_2CTA/NWFs$) were immersed in the second bath contained 0.5 wt.% of sodium hyaluronate (HA), then $CS_{0.5}CTA/HA/NWFs$, $CS_1CTA/HA/NWFs$, $CS_2CTA/HA/NWFs$ were dried at 80 °C for 10 min, rinsed with demineralized water to remove non-attached (non-bonded) materials. The washing step was repeated three times obtained layer of hyaluronan onto chitosan citrate layers. Keep the wet pick up 100% in immersing step in each step. All non-woven fabrics were dried at 150 °C for 5 min. The CSCTA/HA/NWFs were code as $CS_{0.5}CTA/HA/NWFs$, $CS_1CTA/HA/NWFs$ and $CS_2CTA/HA/NWFs$.

2.3. Wound dressing characterization

Attenuated total reflectance fourier transforms infrared spectroscopy (ATR-FTIR) was performed by the spectrophotometer Nicolet Impact 400 D FTIR-ATR (Nicolet CZ, Prague, Czech Republic) equipped with a ZnSe crystal for the ATR-FTIR spectroscopy. Absorbance was measured as a function of the wavenumber (cm^{-1}) between 4000 cm^{-1} and 650 cm^{-1} with the resolution of 8 cm^{-1} and the number of scans equal to 128. Thermal decomposition was measured on thermogravimetric TG, Netzsch 209F3 instrument (Al$_2$O$_3$ crucible) with the heating rate 10 °C min^{-1} (with data collecting rate 40 points per Kelvin), which was performed in the dynamic nitrogen atmosphere with the pressure of 0.1 MPa. The sample mass for TGA was about 0.9 mg, TGA temperature range 25–800 °C. The morphology of nonwoven fabrics was studied by the scanning electron microscopy (SEM). The nonwoven dressing sheets were cut with a razor scalpel after being frozen in liquid nitrogen for 10 min. X-Ray diffraction (XRD) data were collected utilizing the D8 Advance diffractometer (Bruker AXS, Germany) with Bragg-Brentano θ-θ goniometer (radius 217.5 mm) equipped with a secondary beam curved graphite mono-chromator and Na(Tl) I scintillation detector. The generator was operated at 40 kV and 30 mA and the scan was performed at room temperature from 2 to 50° (2θ) in 0.02° steps with a counting time of 8 s per step.

The antibacterial activity of the wound dressing nonwoven fabrics was performed as follow [54,55]; 1 cm of each wound dress-

ing nonwoven fabric were-sterilized by autoclave at 120 °C for 20 min. Each sample was placed in a sterile vial and the dressing nonwoven fabrics were pre-treated with I ml distilled water for 30 min. Tryptone soy broth (3 ml). 10 μl of *Escherichia coli* (*E. coli*) and *Staphylococcus aureus* (*S. aureus*) suspension was added to each nonwoven dressing fabric-containing vial (1.6×10^3/ml). Control agar with/without bacterial inoculation was also included. The vials were incubated with agitation at 37 °C at 500 rpm. Aliquots of 10 μl broth were sampled at 24 h and serial dilution for the aliquots was prepared in broth. Duplicate aliquots (50 μl) of the serially diluted samples were spread onto plates. The plates were incubated at 37 °C and bacterial counts were performed. The dressing nonwoven fabrics were divided into three groups. The first group was control group (CTA/NWFs; treated with 5 wt.% of citric acid). The second group was nonwoven fabrics (NWFs) treated with 0.5%, 1% and 2 wt.% of chitosan citrate forming CSCTA/NWFs (coded as (CS0.5CTA/NWFs, CS1CTA/NWFs, CS2CTA/NWFs). The third group was CSCTA/NWFs immersed in 0.5 wt.% sodium hyaluronate (HA) solution forming CSCTA/HA/NWFs assembly (coded as (CS0.5CTA/HA/NWFs, CS1CTA/HA/NWFs, CS2CTA/HA/NWFs). The bactericidal activity was evaluated after 24 h and the reduction rate percentage (RD%) was calculated by the following Eq. (1);

$$\text{Reduction rate percentage (RD\%)} = (A - B)A \times 100 \qquad (1)$$

where, A = the number of bacterial colonies from untreated nonwoven fabrics, and B = the number of bacterial colonies from treated wound dressing nonwoven fabrics. Each measurement was carried out in triplicate and the arithmetic means are reported for all experiments.

The swelling ratio of nonwoven fabrics (NWFs), fabrics were-immobilized with chitosan citrate (CSCTA/NWFs), and fabrics immobilized with chitosan citrate/sodium hyaluronate (CSCTA/HA/NWFs) was measured under the physiological conditions. Thus, the samples were immersed in phosphate buffer solution (pH 7.5) at 37 °C for different times (0.5–72 h). The swelling percentage (%) of the wound dressing was calculated by the following Eq. (2);

$$\text{Swelling percentage(\%)} = (Wf - Wi)/Wi \times 100 \qquad (2)$$

where, Wf is weight of sample after certain swelling time and Wi is weight of sample in the dry state.

Cell viability assays are commonly used to measure the response of cells to toxic substances. Mouse fibroblast cell line (*NIH-3T3*) was cultured till 20th passage. Cells of 5th–20th passage were used in the following experiments. *NIH-3T3* were grown in DMEM (Dulbecco's Modified Eagle Medium) supplemented with 10% FBS, glutamine (0.3 mg/ml), penicillin (100 μg/ml) and streptomycin (0.1 mg/ml) in 7.5-% CO_2 at 37 °C in 75 cm^2 culture flask as recommended by the supplier. Spontaneously immortalized human keratinocyte cell line (*HaCaT*) was grown in DMEM supplemented with 10-% FBS, glutamine, and gentamycin in 5% CO_2 at 37 °C as described previously [56–59]. All nonwoven cotton fabric (NWFs) treated with citric acid 5-wt.% (CTA/NWFs), nonwoven cotton fabric (NWFs) treated with chitosan citrate 1-% (CS_1CTA/NWFs) and nonwoven cotton fabric treated with 1% chitosan citrate then treated with 0.5-% hayluronan (CS_1CTA/HA/NWFs) samples were sterilized by autoclave at 120 °C for 20 min.

3000 (3T3) and 4000 (*HaCaT*) cells/well were seeded to wells of 96-well test plates. The cells were cultured for 24 h before treated with the suspended solutions. Then, the suspended solutions were added to each well using as diluent medium. Cell viability was measured 0, 24, 48, 72 h after treatment using the 3-(4.5-dimethylthiazol-2-yl)-2.5-diphenyl tetrazolium bromide (*MTT*) assay. In the assay, *MTT* is reduced by viable cells to a colored formazan salt, which is later released from the cells

and determined spectrophotometric [59,60]. When cells die, they lose the ability to convert *MTT* into formazan, thus color formation express of only the viable cells [61]. *MTT* stock solution was added to the cell culture medium and plates were incubated at 37 °C for 2.5 h. The supernatant was discarded and cells were lysed in lysis solution for 30 min on a shaker. The optical density was measured in 96-well plate in triplicate by a versamax microplate reader at a wavelength of 570 nm. All experiments were carried out at least in four independent repeats. Relative cell viability was determined by the following Eq. (3);

$$\text{Relative cell viability (\%)} = OD_1\text{-}OD_3/OD_2\text{-}OD3 \times 100 \qquad (3)$$

where, OD is the optical density of cell culture with sample (OD_1), without sample (OD_2) and of the medium (OD_3) measured by a microplate reader (Bio-Rad 550, Hercules) at 570 nm.

In vitro qualitative analysis of cell viability as performed with live/dead assay. The samples of differently treated nonwoven fabrics (0.5×0.5 cm) were sterilized using UV light for 30 min. Before seeding with *NIH-3T3* cells, the fabrics were incubated in culture medium (DMEM with L-glutamine, 10-% FBS, 1-% penicillin/streptomycin) 1 h at 37 °C. Cells were seeded on fabrics at a density of 10^5/area in 24-well plate. Samples with seeded *3T3* cells were cultivated at 37 °C and 5-% CO_2 for 3, 24, 48 and 72 h. Fluorescence microscopy and live/dead staining (calcein-AM/propidium iodide) were used to determine cell viability 3, 24, 48 and 72 h after seeding. The mix of calcein-AM (2 μM) and propidium (1,5 μM) in PBS was added to fabrics containing seeded cells and incubated for 15 min at 37 °C and 5% CO_2 for live/dead cell detection. Afterwards, fabrics were rinsed twice in PBS and visualized using a Zeiss Axio Imager 2 microscope.

Fifty male rats (National Research Centre, Cairo, Egypt) weighing (150 ± 20 g) were used as the test animals. The animals were maintained at normal room temperature (25–29 °C) on a 12 h. Light/dark cycle, with free access to a commercial pellet diet and water. After the wound procedure, the animals were kept in individual cages. All experiments were conducted according to the National Communities Council directives on animal care. The dorsal hair of control and treated rats were shaved and (2.5×2.5 cm) diameter full thickness wounds were created with a biopsy punch. The wounds were cleaned with normal saline and disinfected by 75-% ethanol. The test wounds (n = 3) were then covered with the sterile chitosan/hyaluronan nonwoven fabrics and fixed with sterile gauze and plasters. Similarly, control wounds (n = 3) were covered with sterile nonwoven cotton fabrics and fixed with plasters. On 0, 3rd, 7th, and 14th, postoperative days, the dressings were removed and the appearance of the wound was photographed. The wound area was estimated by outlining the wound area. New dressings were applied to the wound sites after they were cleaned with normal saline. Photographs of wounds were taken every one to three days. If the bandage was applied, photographs were taken at each bandage change. When photographing the wound, a millimeter ruler was placed approximately 5 mm from the wound edge. Wound surface and ruler were in one plane. The images of the wound were open in Image J software. The image calibrated using a known length (2–4 cm): The rate of wound closure was determined by the following Eq. (4);

$$\text{Amount of wound healing (\%)} = A_0 - A_X/A_0 \times 100 \qquad (4)$$

Where, A_0 – wound area at day 0, Ax wound area at specified time of surgery, respectively.
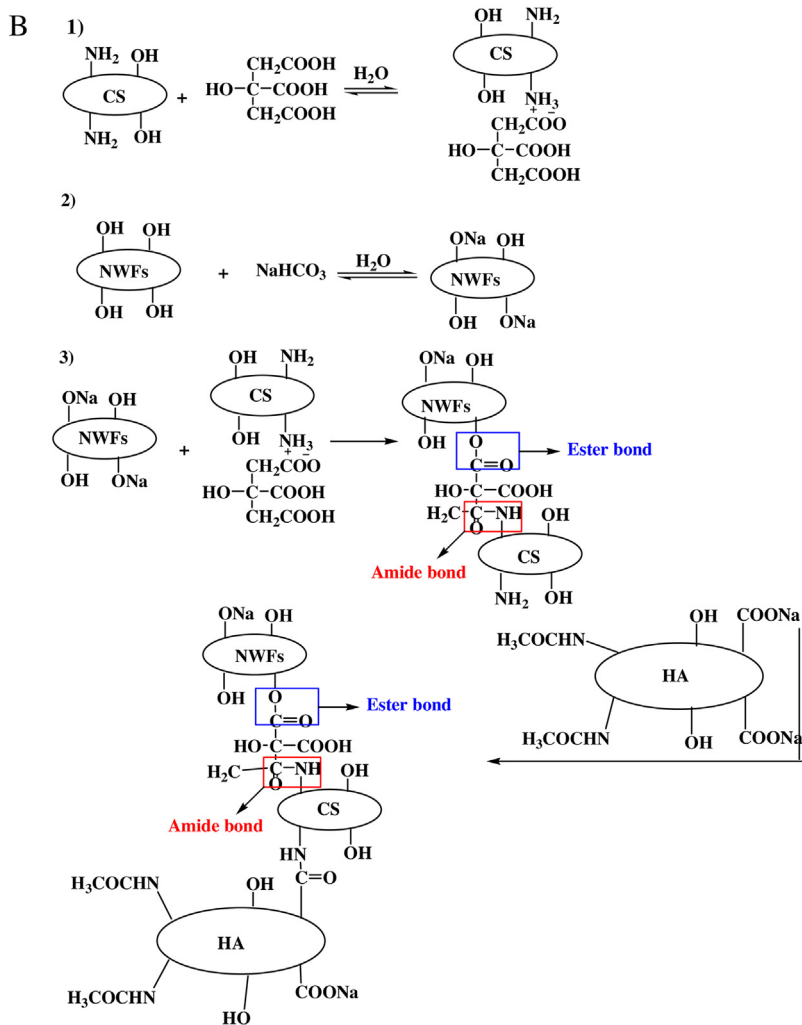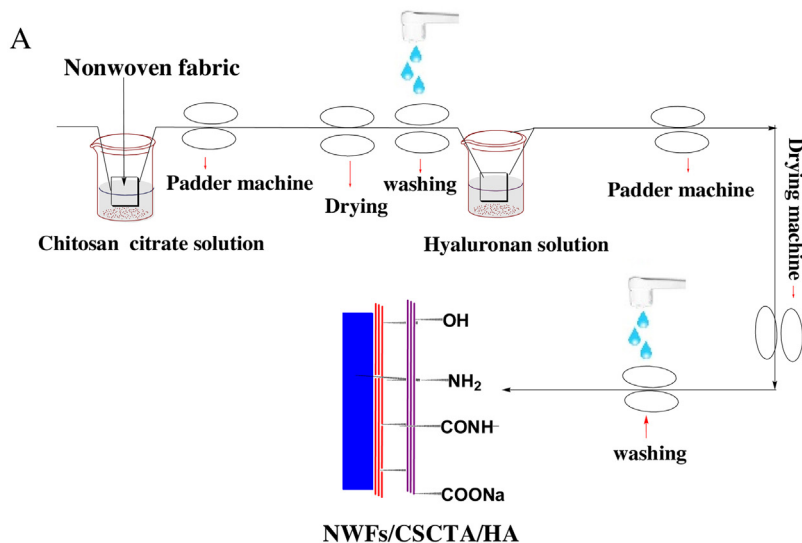
Fig. 1. (A) Immobilization of chitosan citrate and sodium hyaluronate onto nonwoven fabrics. (B) Proposed mechanism of interaction between chitosan citrate/sodium hyaluronate/nonwoven fabrics.
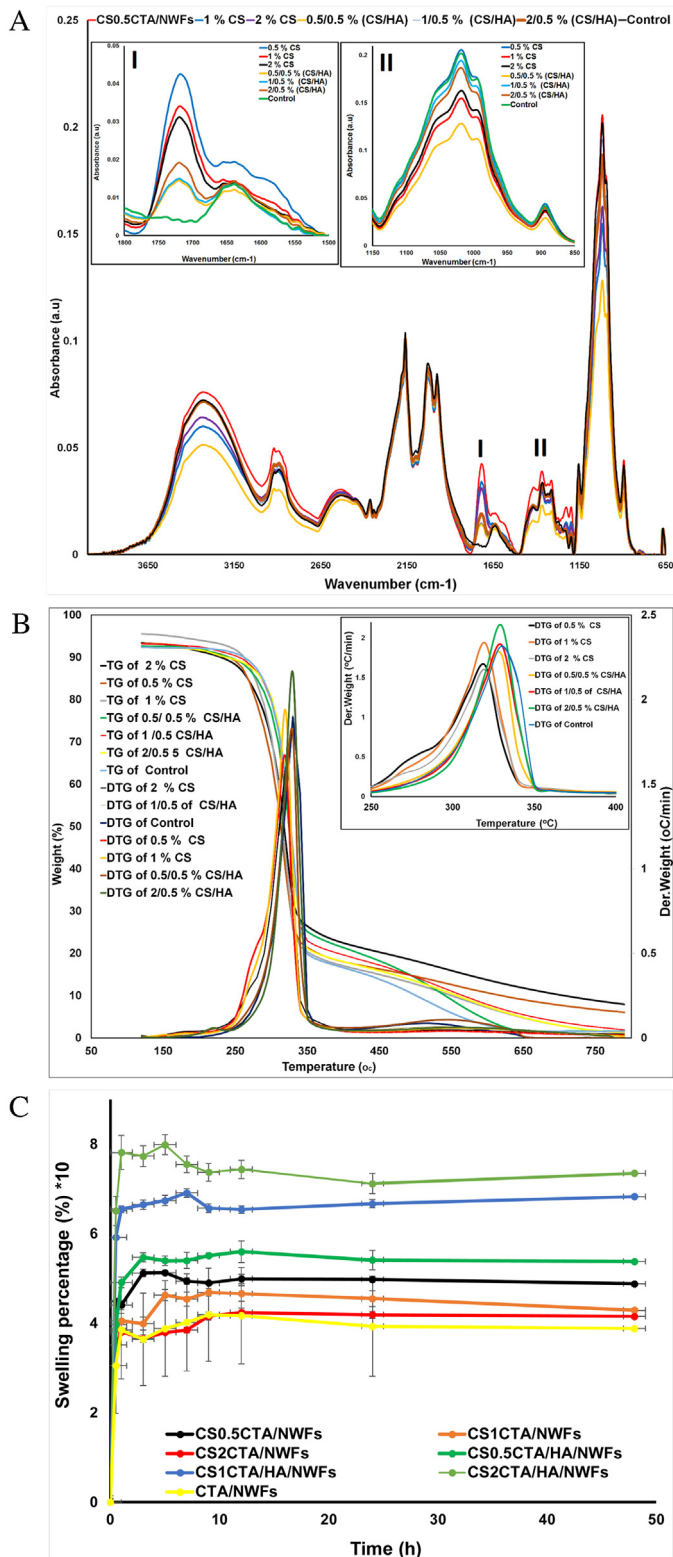
Fig. 2. (A) ATR-FTIR of chitosan citrate/nonwoven fabrics ($CS_{0.5}CTA/NWFs$, $CS_1CTA/NWFs$, $CS_2CTA/NWFs$); chitosan citrate/sodium hyaluronate/nonwoven fabrics ($CS_{0.5}CTA/HA/NWFs$, $CS_1CTA/HA/NWFs$, $CS_2CTA/HA/NWFs$), nonwovens fabrics (CTA/NWFs), respectively. (B) TGA-DTG of chitosan citrate/nonwoven fabrics ($CS_{0.5}CTA/NWFs$, $CS_1CTA/NWFs$, $CS_2CTA/NWFs$); chitosan citrate/sodium hyaluronate/nonwoven ($CS_{0.5}CTA/HA/NWFs$, $CS_1CTA/HA/NWFs$, $CS_2CTA/HA/NWFs$), nonwovens (CTA/NWFs), respectively. (C) Swelling percentage of wound dressing was fabricated from chitosan citrate/nonwoven fabrics without/with hyaluronan ($CS_{0.5}CTA/NWFs$, $CS_1CTA/NWFs$, $CS_2CTA/NWFs$); ($CS_{0.5}CTA/HA/NWFs$, $CS_1CTA/HA/NWFs$, $CS_2CTA/HA/NWFs$), and nonwovens (CTA/NWFs) under physiological conditions (PBS, pH 7.5; 37 °C).

3. Results and discussion

3.1. Immobilization of chitosan citrate/hyaluronan onto nonwoven cotton fabrics

Pure chitosan (particle size 800–1000 μm) was used in this work by the method described in our previous work-[28]. Thus, the isolation of chitosan (CS) was done by four consequent steps. Firstly, shrimp shells were washed for many hours under reflux with hot water to kill some microorganisms and to remove the organic and inorganic impurities. Demineralization process (second step) the shrimp shell was treated with aqueous hydrochloric acid (5-% v/v) for 2 h at room temperature (22 °C) to remove the minerals (mainly $CaCO_3$) from the shells. The third step was deproteinization step which was done by aqueous solution of sodium hydroxide (5-% w/v) at 90 °C for 20 h in order to remove the proteins. The last step was deacetylation, where highly concentrated sodium hydroxide (50-%) was used for 3.5 h at 90 °C in order to hydrolyze the acetamido groups obtained high pure chitosan with high degree of deacetylation (DDA). The chemical structure and degree of deacetylation of chitosan were measured and confirmed by different techniques like ATR-FTIR, TG-DTG, XRD, NMR (Fig. S1; supporting information). The degree of deacetylation of chitosan was found 95-%. Citric acid was used as dual functional material for dissolution of chitosan and as cross-linker agent between nonwoven fabrics (NWFs)/chitosan (CS) and/or chitosan/nonwoven fabrics (CSCTA/NWFs)/hyaluronan (HA). Citric acid have three carboxylic groups which was prepared anhydride cycle under higher temperature [30]. Layer by layer (LbL) assembly is mainly occurred by the electrostatic interactions. This process consist of adsorption and deposition of different charged constituents and washing step removed the non-reacted specimens [62]. Citrate was improved the solubility of chitosan compared with other organic solvent for LbL assembled with sodium hyaluronate. Layer by layer technique itself was an effective way produced functionalized materials. In fact, both CSCTA and HA are pH-sensitive. It can be expected that the multilayers agglomerated of CSCTA–HA also responsive to the change of environmental pHs.

Nonwoven cotton fabrics (NWFs; 10 × 10 cm, 0.45 g) were first impregnated in a solution of chitosan citrate solutions ($CS_{0.5}CTA$, CS_1CTA, CS_2CTA) prepared chitosan citrate layers onto NWFs surface coded as $CS_{0.5}CTA/NWFs$, $CS_1CTA/NWFs$, $CS_2CTA/NWFs$ and the molar ratio between CS and CTA was (1:8;1:4; 1:2), respectively (Fig. 1A). During the activated step of NWFs surface, the hydroxyl groups in cellulosic fabrics converted to salt forms (O-Na^+), which could easily interact with carboxylic anhydride in the citric acid generated during the increased the reaction temperature in curing step [32,33]. Citric acid/anhydride citric acid was used as cross-linker between NWFs and CS by amidation or esterification reactions. $CS_{0.5}CTA/NWFs$, $CS_1CTA/NWFs$, and $CS_2CTA/NWFs$ were dried at 80 °C for 10 min in thermal fixation machine. The samples were rinsed for three times with ultrapure water to remove non-attached (non-bonded) materials from the surface of nonwoven sheets, then dried at 80 °C for 10 min this step was repeated three times to obtain LBL (multi-layer) of chitosan citrate. The $CS_{0.5}CTA/NWFs$, $CS_1CTA/NWFs$, $CS_2CTA/NWFs$ were immersed in the second bath contained 0.5 wt.% of sodium hyaluronate, coded as $CS_{0.5}CTA/HA/NWFs$, $CS_1CTA/HA/NWFs$, $CS_2CTA/HA/NWFs$ (molar ratio between CS0, 5, 1, 2%) and HA was 2:1, 4:1, 8:1, respectively. The dressing materials were dried, washed with water to remove the non-bonded hyaluronan then immersed again in HA solution, then dried at 80 °C for 10 min. Finally, all the prepared nonwoven fabrics were dried at 150 °C for 5 min. Different layers of hyaluronan were generated on the surface of CSCTA/NWFs by pad-dry cure technique. Fig. 1B shows the proposed mechanism of interactions between NWFs, CS and CTA. CTA could interact with hydroxyl groups on NWFs surface formed ester bond as well
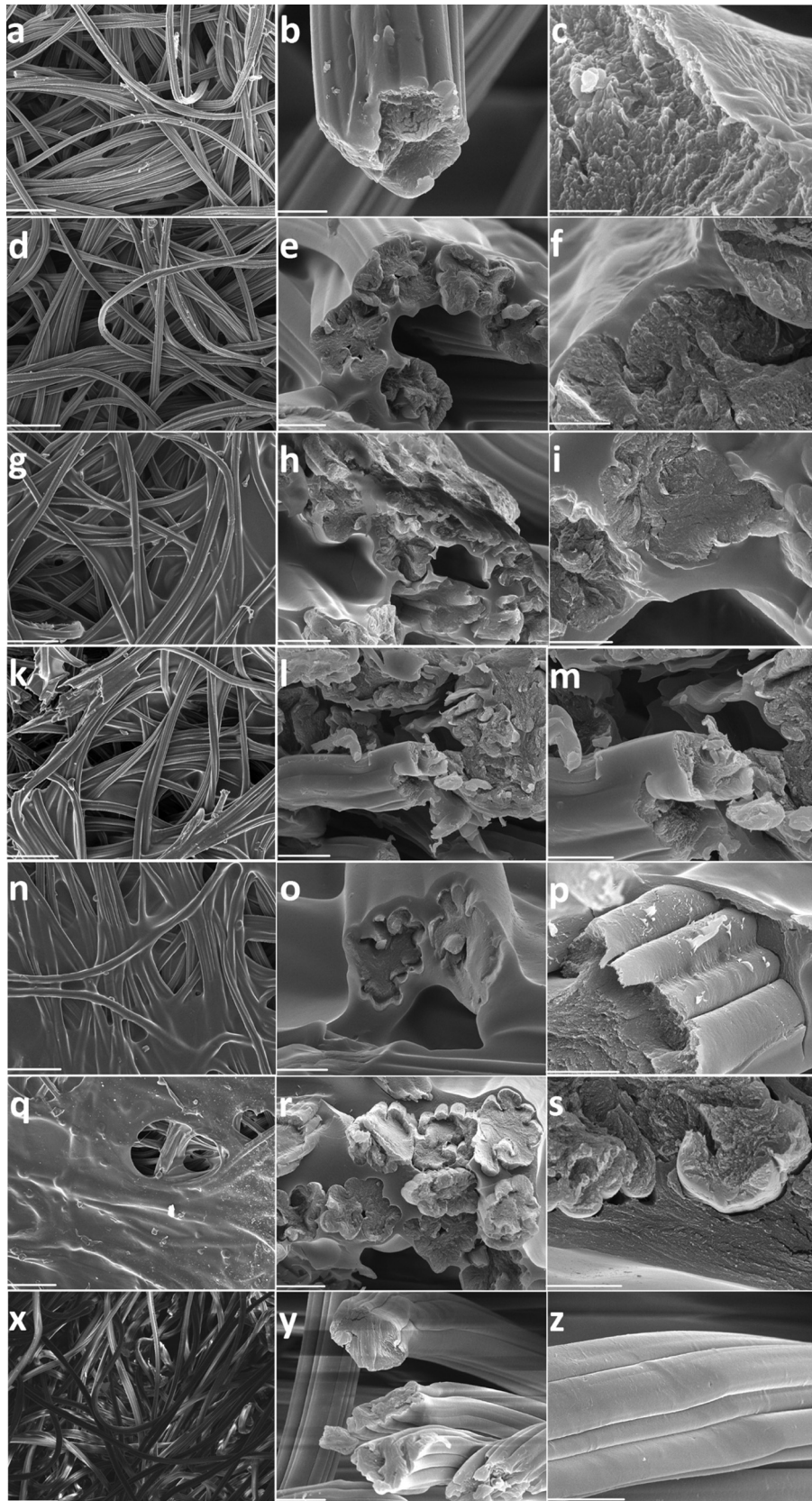
Fig. 3. Scanning electron microscopy of chitosan/hyaluronan wound dressing nonwoven fabrics.
CS$_{0.5}$CTA/NWFs (a–c); CS$_1$CTA/NWFs (d–f); CS$_2$CTA/NWFs (g–i); CS$_{0.5}$CTA/HA/NWFs (k–m); CS$_1$CTA/HA/NWFs (n–p); CS$_2$CTA/NWFs (q–s); CTA/NWFs (t–z). (a, d, g, k, m, q, t) scale bars are 100 μm; (b, e, h, l, o, r, z) scale bars are 10 μm; (c, f, i, n, p, s, z) scale bars are 5 μm.

Table 1
Antibacterial activity of the wound dressing nonwoven fabrics.

Nonwoven dressing fabrics	Reduction rate RD (%)	
	E. coli	*S. aureus*
CTA/NWFs	0	0
CS$_{0.5}$CTA/NWFs	85	80
CS$_1$CTA/NWFs	95	92
CS$_2$CTA/NWFs	90	75
CS$_{0.5}$CTA/HA/NWFs	88	84
CS$_1$CTA/HA/NWFs	98	92
CS$_2$CTA/HA/NWFs	80	70

CTA/NWFs: Nonwoven cotton fabric (NWFs) treated with citric acid (5%); CS$_{0.5}$CTA/NWFs: nonwoven cotton fabric (NWFs) treated with chitosan citrate (0.5%); CS$_1$CTA/NWFs: nonwoven cotton fabric (NWFs) treated with chitosan citrate (1%); CS$_2$CTA/NWFs: nonwoven cotton fabric (NWFs) treated with chitosan citrate (2%); CS$_{0.5}$CTA/HA/NWFs: chitosan citrate (0.5%) nonwoven cotton fabric (NWFs) treated with hayluronan (0.5%); CS$_1$CTA/HA/NWFs: chitosan citrate (1%) nonwoven cotton fabric (NWFs) treated with hayluronan (0.5%); CS$_2$CTA/HA/NWFs: chitosan citrate (2%) nonwoven cotton fabric (NWFs) treated with hayluronan (0.5%).

as with CS formed ester/and or amide bonds with hydroxyl and amino groups of chitosan chains under higher temperature. During the layers preparations efficiency of interactions was improved. Hyaluronan layer was generated during the impregnated process of CS$_{0.5}$CTA/NWFs, CS$_1$CTA/NWFs, and CS$_2$CTA/NWFs into sodium hyaluronan solution. Hyaluronan have different functional groups like coo— and —OH which could interact and/or assembled with the chitosan layers on the surface of nonwoven fabrics formed new ester or amide bonds between CSCTA/NWFs and HA (Fig. 1B). During dissolution of hyaluronan in alkaline solution, the deacetylation process was partially done and few free amino groups [57,63] were generated, and the pH of final product was 4.7.

Fig. 2A shows ATR-FTIR-spectra of nonwoven fabrics (NWFs), chitosan citrate/nonwoven (CS$_{0.5}$CTA/NWFs, CS$_1$CTA/NWFs, CS$_2$CTA/NWFs), and chitosan/hyaluronan/nonwoven fabrics (CS$_{0.5}$CTA/HA/NWFs, CS$_1$CTA/HA/NWFs, CS$_2$CTA/HA/NWFs) sheets prepared by layer by layer assembled technique. Polycarboxylic acid such as citric acid (CTA), butane-tetrcarboxylic acid (BUTCA) can form a five member cyclic anhydride as reactive intermediate by dehydrate of two carboxylic groups bound to adjacent carbons in its backbone, which can react with a hydroxyl groups in nonwoven cellulosic fabrics and/or hydroxyl/amino groups in the backbone of chitosan chains [30,32,64–67]. New band was appeared at 1715–1720 cm^{-1} due to the overlapping bands between carbonyl, carboxyl and ester bonds formed between cellulosic nonwoven fabrics (hydroxyl groups) and chitosan (hydroxyl groups). The intensity of the carbonyl/carboxylic/ester decreased by increase the concentrations of chitosan citrate [68–70]. Due to the presence of chitosan (free hydroxyl, amino groups) was easy interacted with a cyclic anhydride of citric acid and prevented appearance of anhydride cyclic ester band at 1852 and 1785 cm^{-1}, respectively [64]. It was seen in Fig. 2AI that the intensity of amide bond at 1650 cm^{-1} was slightly increase by increased of chitosan concentrations (0.5–2 wt.%). by addition of hyaluronan layers interacted with chitosan/nonwoven fabrics layers (CSCTA/CNFs), the intensity of the band 1715 cm^{-1} was slightly increased due to the formation of ester bonds between chitosan citrate and hyaluronan (carboxyl, hydroxyl) groups. (Fig. 2A). It was seen in Fig. 2AII that the intensity of amide bond at 1650 cm^{-1} was slightly increased by increase of chitosan concentrations (0.5–2 wt.%) after addition of hyaluronan layer generated. From Fig. 2, we could conclude that citric acid can work as cross-linking agent between nonwoven cellulosic fabrics/chitosan, and sodium hyaluronate generated ester amide, and/or electrostatic hydrogen bonds between the different functional groups of the biomaterial and fabric matrix.

Fig. 2B shows the thermogravimetric analysis (TGA-DTG) of wound dressing chitosan/hyaluronan/nonwoven fabrics pre-

pared by layer by layer technique. Three different concentrations of chitosan citrate were used (CS$_{0.5}$CTA/NWFs, CS$_1$CTA/NWFs, CS$_2$CTA/NWFs) for preparation different layers on the surface of nonwoven fabrics. Chitosan citrate/nonwoven fabrics layers has three different stage appeared. The first stage was related to evaporate the non-bonded and/or bonded water/solvent solution at decomposition at 75 °C and the second stage around 250 °C corresponded to decomposition stage of chitosan citrate. The last stage around 320 °C was associated with the oxidative degradation of chitosan backbone [30,32,71].

Hyaluronan layer was generated onto chitosan citrate/nonwoven fabrics (Fig. 2B) only two different stages were appeared after CSCTA/NWFs was impregnated with HA solution and formed HA layers (CS$_{0.5}$CTA/HA/NWFs, CS$_1$CTA/HA/NWFs, CS$_2$CTA/HA/NWFs). There were two different stages were distinguished, the first stage was appeared in the same area of chitosan citrate layers at 75 °C related to the evaporations of non/bonded water and solvent from the dressing sheets. The stage was appeared when NWFs was treated with CSCTA solution, it means the hyaluronan assembled on the surface of chitosan layers improved the stability of wound dressing layers. Furthermore, the second stage (appeared at 330 °C) was related to decomposition of chitosan/hyaluronan layers it was shifted comparing with only chitosan layers. Thus, an assembled of chitosan citrate and hyaluronan layers provide strong chemical interactions reflected in improved thermal stability of the new wound dressing sheet.

Fig. 2C shows the swelling percentage of nonwoven fabrics (NWFs), chitosan citrate/nonwoven fabrics with different concentrations of chitosan (CS$_{0.5}$CTA/NWFs, CS$_1$CTA/NWFs, CS$_2$CTA/NWFs) and chitosan citrate/sodium hyaluronate/nonwoven fabrics with different chitosan concentrations (CS$_{0.5}$CTA/HA/NWFs, CS$_1$CTA/HA/NWFs, CS$_2$CTA/HA/NWFs). As we can see, the layers of chitosan citrate (CSCTA) improved the swelling percentage of nonwoven fabrics (NWFs) compared with the non-treated sample. The swelling percentage of nonwoven fabrics was increased with the decrease the concentration of chitosan from CS$_{0.5}$CTA/NWFs to CS$_2$CTA/NWFs. This decreasing may be due to the hydrophobicity of chitosan chains, affecting the swelling of NWFs. After layers of sodium hyaluronate were immobilized onto chitosan citrate/nonwoven fabrics (CSCTA/NWFs) surface, the swelling percentage (Fig. 2C) was increased comparing with CSCTA/NWFs and plain NWFs and the percentage of swelling was raised by the increase the concentrations of chitosan (CS$_{0.5}$CTA/HA/NWFs to CS$_2$CTA/HA/NWFs). Due to the amphiphilic properties (hydrophobic of chitosan and hydrophilic of hyaluronan) of the immobilized layers onto NWFs, the swelling percentage was improved.

Fig. 3 shows scanning electron microscopy of wound dressing nonwoven fabrics impregnated with chitosan citrate different concentrations (0.5, 1, 2 wt.%) and sodium hyaluronate solution (0.5 wt.%). Layer thickness of chitosan citrate onto the nonwoven fabrics surface was increased by increase the chitosan concentration for 0.5 % (a–c), 1 % for (d–f) and 2 wt.% for (g–h). From the cross-section (Fig. 3c,f,i), the chitosan citrate coated the nonwoven fabrics and homogenous layer with aggregations appeared on the monofilament surface and between the fabrics matrix. The hyaluronan layer was assembled on the chitosan/nonwoven fabrics surface by chemical/physical interactions (Fig. 3k–s). The hyaluronan solution was coated the chitosan citrate layer onto nonwoven fabrics and the coated layers thickens was increased and CSCTA concentration increase. From the cross-section of CS$_{0.5}$CTA/HA/NWFs (Fig. 3m), CS$_1$CTA/HA/NWFs (Fig. 3p), CS$_2$CTA/HA/NWFs (Fig. 3s), the layers of chitosan/hyaluronan were surrounded the monofilament formed coated layer on fiber surface. Fig. 3t–z, the plain nonwoven fabrics with clean surface and circular shape from cross-section, respectively.
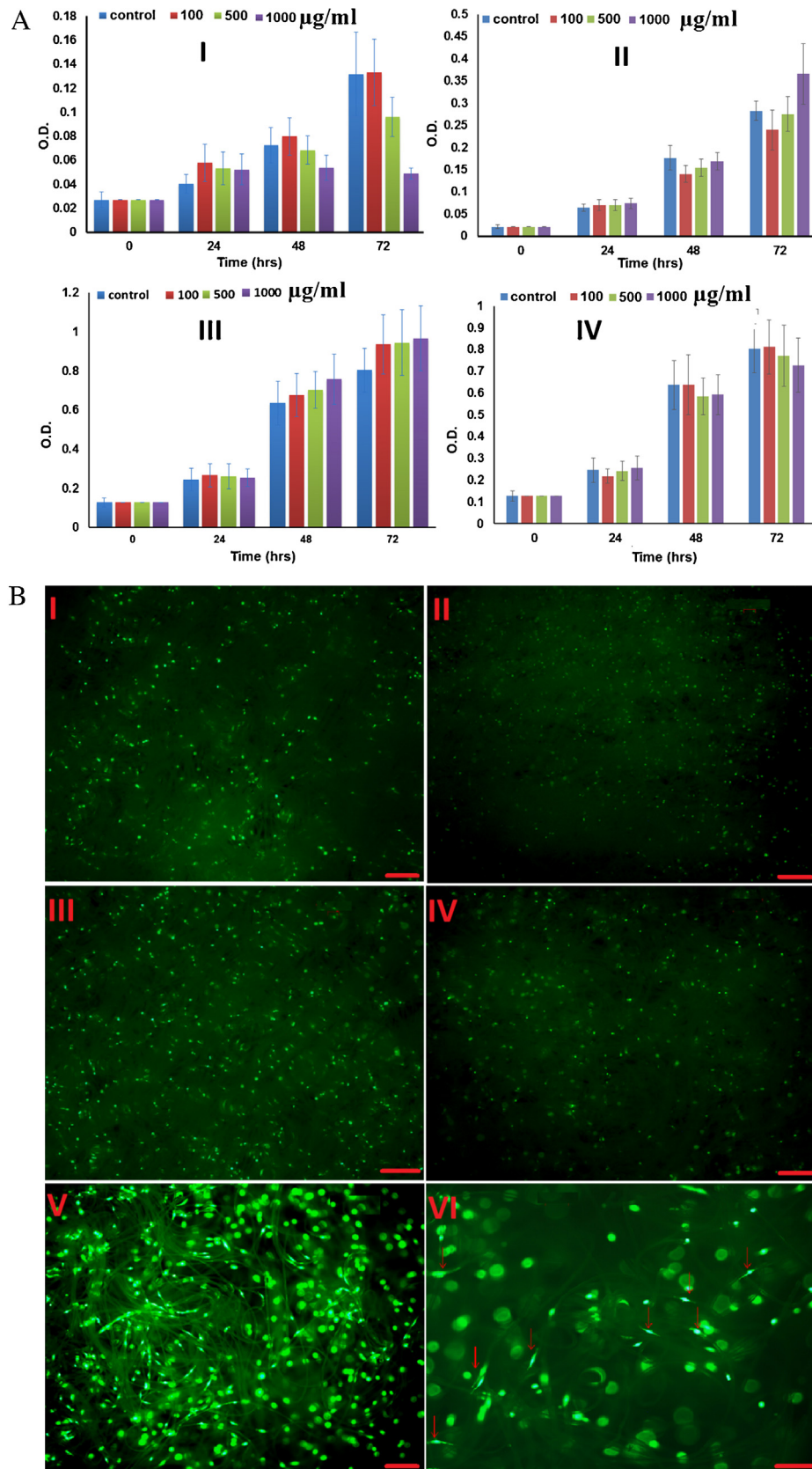
Fig. 4. (A) Cytotoxicity of chitosan/hyaluronan nonwoven wound dressing fabrics (I) chitosan citrate/nonwoven fabrics (CS1CTA/NWFs) against mouse fibroblast cell line (NIH-3T3) with different concentrations (100–1000 μg/ml), 3T3 viability, *MTT*, n = 6. (II) chitosan citrate/nonwoven fabrics (CS1CTA/NWFs) against kerationcytes cell line (HaCaT) with different concentrations (100–1000 μg/ml), 3T3 viability, *MTT*, n = 6. (III) chitosan citrate/hyalurionan/nonwoven fabrics (CS1CTA/HA/NWFs) against mouse fibroblast cell line (*NIH-3T3*) with different concentrations (100–1000 μg/ml), 3T3 viability, MTT, n = 6. (IV) chitosan citrate/hyalurionan/nonwoven fabrics (CS1CTA/HA/NWFs) against kerationcytes cell line (*HaCaT*) with different concentrations (100–1000 μg/ml), 3T3 viability, MTT, n = 6. Cell viability was measured at-0, 24, 48, 72 hrs. The data

Fibers and fabrics materials are carriers of different microorganism like pathogenic bacteria, odor-producing bacteria, and fungi due to the adhesion of these microorganisms to the fibers/fabric surface. Most nonwoven fabrics recently used in operation rooms and hotels are good environment to cross-infection or transfer of diseases occurred by microorganisms. Bacteria attached on fabrics tend to pass through fabric, especially the fabric is wet [32]. Research revealed that ordinary hospital textiles could not prevent bacterial transmission from person in surgical rooms [30]. The innovate of new wound healing dressing products (dressing) fabricated from immobilization of antibacterial and highly healing materials on nonwoven fabrics have recently increasing the importance to both the research and production sectors. Nowadays, a huge range of biological materials with different chemical structures were immobilized on the fibers/fabrics, bringing new unique performance to the final fibers/fabrics products [72,73]. Chitosan, was used as an antimicrobial agent, have recently received renewed interest [72,73].

The antibacterial activity of chitosan, chitosan/hyaluronan immobilized onto nonwoven cotton fabrics against different types of bacteria was evaluated as shown in Table 1. The antibacterial activities of chitosan were remarkably affected by the concentration of it, ($CS_{0.5}CTA/NWFs$, $CS_1CTA/NWFs$, and CS2CTA/NWFs) and the type of bacteria (-G,+G). $CS_1CTA/NWFs$ has high reduction rate (RD% = 95, 92 for −G and +G) than $CS_{0.5}CTA/NWFs$ (RD% = 85, 80 for −G and +G) and for CS2CTA/NWFs (RD (%) = 90, 75 for −G + G) on the growth of both types of bacteria *Staphylococcus aureus* (*S. aureus*) as Gram positive bacteria (+G) and *Escherichia coli* as Gram negative bacteria (-G), respectively. The antibacterial activity of chitosan clearly decreased with low concentration of its solution and it higher concentrations of chitosan ($CS_2CTA/NWFs$) the diffusion of chitosan inside the medium was hard and inhibited the interaction of chitosan and bacteria. Chitosan/hyaluronan/nonwoven cotton fabrics have also highly antibacterial activity (Table 1) against *E. coli* and *S. aureus* compared with plain chitosan coated nonwoven fabrics. The reduction rate was 88, 84% for $CS_{0.5}CTA/HA/NWFs$, 98, 92% for $CS_1CTA/HA/NWFs$, and 80, 70% for $CS_2CTA/HA/NWFs$ against *E. coli* and *S. aureus*, respectively. The antibacterial activity of chitosan/hyaluronan was higher than plain chitosan against both types of bacteria due to hyaluronan has antibacterial activity against different types of microorganisms [72,74].

In Table 1, chitosan possess high antibacterial activity against both types of bacteria especially with gram-negative bacteria; and the mechanisms were proposed that, the chemical interaction between positively charged chitosan and negatively charged microbial cell membranes this could be explain as the electrostatic forces between the protonated $^+NH_3$ groups and the negative residues or the positively charged $^+NH_3$ in glucosamine unit inhibit the growth of bacteria and this was occurred by binding the negatively charged cell wall [9,75,76].

Viability assays were studies aimed to detect the cellular response to a toxic materials. From the evaluation of cytotoxicity, the information about metabolic activity and the death of cell can be obtained from it [77]. There are many of helpful assay technologies that use to evaluate metabolic markers to estimate the number of viable cells. The *MTT* 3-(4.5-dimethylthiazol-2-yl)-2.5-diphenyl tetrazolium bromide has been widely used to detect the viable cells; and this assay is based on the reduction of tetrazolium salt (yellow color) to insoluble formazan crystals (purple color) by metabolically viable cells [60,61]. The *MTT* viability test was carried out to obtain the main information about

the metabolism and proliferation influenced by $CS_1CTA/NWFs$ and $CS_1CTA/HA/NWFs$ wound dressing. This assay is rapid and very effective method for testing for both *NIH-3T3* and *HaCaT* cell line activity [78,79]. On the basis of obtained results (Fig. 4) CS1CTA/NWFs did not induce any changes in the cell growth for both *NIH-3T3* and *HaCaT* cell line and the cell viability of tested CS1CTA/NWFs demonstrating the nontoxic effect (Fig. 4AI,II). The viability of cells after the treatment with CS1CTA/NWFs had small decrease increases changed in whole tested time 0–72 h (Fig.4AI) but still in safe values. Fig. 4AIII,IV shows the toxicity of sodium hyaluronate immobilized into CS1CTA/NWFs with different concentrations (100–1000 μg/ml) under different time treatments.. Interestingly, chitosan/hyaluronan nonwoven fabrics ($CS_1CTA/HA/NWFs$) enhanced, and accelerated the cell growth with all concentrations ranges (100–1000 μg/ml) and with different treatment times (0–3 days). This result agrees very well with the good biocompatibility properties of chitosan/hyaluronan with different types of cells.

Fig. 4B shows fluorescence images of CS1CTA/NWFS(I,II), CS1CTA/HA/NWFS(III,IV) and cell-wound dressing fabrics interaction (V,VI) after 3, and 72 h of treatments with mouse fibroblast cell lines (*NIH-3T3*). From our observation it is clear that the cells prefer treated fabrics without any evident differences between CS1CTA/NWFs and CS1CTA/HA/NWFs treated surfaces. That could be due to more biocompatible treatment of fabrics for cell adhesion. However, it seems that the cells did not show the character of well spread cells. By contrast, they were round, captured in the fibers and just a couple of cells were spread and interact with the surface of fabrics. This interaction was observed only for CS1CTA/HA/NWFs wound dressing treated fabrics (Fig. 4BV,VI) higher magnification of interacting cells in Fig. 4BVI marked with red arrows in CS1CTA/HA/NWFs and detailed cell-fiber interaction. The low spreading density could be the reason why the cells did not exhibit extensive proliferation as just a slight increasing number of cells is evident for treated fabrics and a constant number for the control. Further, for all samples the decreasing number of cells was observed 72 h of cultivation. This could imply the washing cells out from the fabrics due to the poorer adhesion in time. In summary, the treatment of nonwoven fabrics with different concentrations of chitosan and chitosan/hyaluronan ratio are promising as new wound dressing/healing materials and correspond with our results obtained from the cytotoxicity assay.

Wound healing is stepwise process which consists of various phases as inflammation, proliferative and remodeling [7,9,80]. The genetic response regulating (normal state) cellular resistance mechanisms contributes to the wound and its repair. The damaged tissues requires biocompatible materials like chitosan on which cells may adhere and proliferate. Chitosan prepared from natural biopolymer chitin has been tested as wound dressing at the skin-shaving site in rats [7,81–83]. Fig. 5AI induced the results of nondiabetics rats wounds treated with control nonwoven fabric (without any treatment with chitosan or chitosan/hyaluronan) at 0, 3, 7, and 14 days and for wounds treated. There was slightly evident effect of non-treated nonwoven fabrics (control sample) onto nondiabetic rats after two weeks of treatments and the wound closer percentage was 40% (Fig. 5B). Comparing with chitosan/hyaluronan composite wound dressing, the healing properties of nondiabetic rates (Fig. 5AII) was enhanced and accelerated after wound treated with biomaterials and the wound closer rate after two week was 95% (Fig. 5B).

were expressed as mean ± SEM (n = 6). (B) Fluorescence microscopy of live/dead mouse fibroblast cell line seed with chitosan/hyaluronan/nonwoven fabrics dressing. (I,II) live/dead cell of CS1CTA/NWFs after 3 and 72 hrs, respectively. (III,IV) live/dead cell of CS1CTA/NWFs after 3 and 72 hrs, respectively. (V,V) cell-nonwoven dressing interaction of CS1CTA/NWFs after 72 hrs, at 100, 20 μm respectively.

Fig. 5. (A) Visual observation of the surface healing dressed with wound dressing sheet (control non-diabetic) at 0th, 3th, 7th and 14th days after operation (I), (one of three same cases in each group was shown); healing dressed with chitosan/hyaluronan nonwoven dressing sheet (non-diabetic rats) at 0th, 3th, 7th and 14th days after operation (II); surface healing dressed with nonwoven sheet (gauzy) from cellulosic material (control diabetic rats) at 0th, 3th, 7th and 14th days after operation (III); (one of three same cases in each group was shown); healing dressed with chitosan/hyaluronan/nonwoven fabrics sheet (diabetic rats) at 0th, 3th, 7th and 14th days after operation (IV). (B) Wound contraction as a function of postoperative time for (non-diabetic and diabetics rats) wounds treated with chitosan/hyaluronan nonwoven fabric ($CS_1CTA/HA/NWFs$) sheets and control (nonwoven cellulosic fabrics-gauze), indicated by the percentage of wound size vs healing dates.

In Fig. 5AIII control diabetics rat treated with nonwoven cotton fabrics (treated with 5 wt.% CTA). The closer percentage after two week of treatments was 25% comparing with control diabetic rats. Fig. 5AIV present the CS1CTA/HA/NWFs treated the diabetic rats. The wound closure was 60% after 14 days of the treatment. It was suggested that their wound-healing properties of chitosan were due to their ability to stimulate fibroblast production by affecting the fibroblast growth factor [39,84–88]. From Fig. 5A, B we can conclude that, chitosan/hyaluronan was highly efficient accelerated and enhancement the healing properties of diabetics and nondiabetics rats comparing with control sample. Chitosan/hyaluronan composite had very high healing properties compared between plain chitosan or plain hyaluronan (data not shown), due to healing properties of both chitosan and hyaluronan together. Enhanced tissue repair ability of CS/HA immobilized into nonwoven cotton fabrics in the early phase of inflammatory response could be reasonably ascribed to the recapitulation of induction signals exerted by HA. Indeed, HA naturally interacts with signaling receptors (primarily CD44) to initiate inflammatory response, to maintain structural cell integrity and to promote recovery from tissue injury [89]. Furthermore, a possible activity of HA on peroxisome proliferator-activated receptors (PPARs) during wound healing could not be excluded [90]. The formation of a highly hydrated HA-rich matrix could be supposed to facilitate cell migration into the provisional wound matrix fostering proliferation and in turn regeneration process [91]. Although wound contraction is the primary mechanism underlying healing process of closure in the murine model adopted, re-epithelialization of the wound site, which is prevalent in human skin, and suggested by in vitro results, can well take place and contribute to wound closure as observed elsewhere [92].

4. Conclusions

New wound dressing materials based on chitosan/hyaluronan composite/nonwoven fabrics were prepared and evaluated. Pure chitosan was isolated from shrimp shell with high degree of deacetylation (95-%) and non-protein residual percent. Nonwoven viscose fabrics were used for immobilization of biologically active biopolymers (chitosan, hyaluronan) by pad-dry-cure method. Chitosan/hyaluronan/composite showed well distribution of chitosan and hyaluronan on the surface of nonwoven fibers confirmed by scanning electron microscope. The prepared wound dressing material showed excellent antibacterial activity against two types of bacterial *E. coli* and *S. aureus* as gram negative and positive, respectively. The cytotoxicity of the new dressing materials was revealed by using mouse fibroblast cell line (*NIH-3T3*) and keratinocytes cell lines (*HaCaT*) with different times and concentration of treatments and showed that there was not any toxicity of the prepared dressing material. From the healing measurements, chitosan/hyaluronan nonwoven fabrics composite accelerated and enhanced the healing properties of diabetics and nondiabetics rats compared with control sample. In summary, this novel-chitosan/hyaluronan/nonwoven fabrics wound dressing will open new doors for realizing potential using the dressing as carrier of drugs to better treat wound defects and promote the wound healing.

Acknowledgments

Appendix A. Supplementary data

Supplementary data associated with this article can be found, in the online version, at http://dx.doi.org/10.1016/j.ijbiomac.2016.04.087.

References

[1] T. Dai, M. Tanaka, Y.-Y. Huang, M.R. Hamblin, Expert Rev. Anti Infect. Ther. 9 (2011) 857–879.
[2] M.J. Portou, D. Baker, D. Abraham, J. Tsui, Vasc. Pharmacol. 71 (2015) 31–36.
[3] T.R. Dargaville, B.L. Farrugia, J.A. Broadbent, S. Pace, Z. Upton, N.H. Voelcker, Biosens. Bioelectron. 41 (2013) 30–42.
[4] S.A. Kramer, J. Vasc. Nurs. 17 (1999) 17–23.
[5] S. Rawat, R. Singh, P. Thakur, S. Kaur, A. Semwal, Asia. Pac. J. Trop. Biomed. 2 (2012) S1910–S1917.
[6] T. Kaufman, J. Wesley Alexander, B.G. MacMillan, Burns 9 (1983) 169–173.
[7] R. Jayakumar, M. Prabaharan, P.T. Sudheesh Kumar, S.V. Nair, H. Tamura, Biotechnol. Adv. 29 (2011) 322–337.
[8] T. Velnar, T. Bailey, V. Smrkolj, J. Int. Med. Res. 37 (2009) 1528–1542.
[9] P. Zahedi, I. Rezaeian, S.-O. Ranaei-Siadat, S.-H. Jafari, P. Supaphol, Polym. Adv. Technol. 21 (2010) 77–95.
[10] J.H. Choi, Y.W. Park, T.H. Park, E.H. Song, H.J. Lee, H. Kim, S.J. Shin, V. Lau Chun Fai, B.-K. Ju, Langmuir 28 (2012) 6826–6831.
[11] G. Decher, J. Schmitt, Fine-Tuning of the film thickness of ultrathin multilayer films composed of consecutively alternating layers of anionic and cationic polyelectrolytes, in: C. Helm, M. Lösche, H. Möhwald (Eds.), Trends in Colloid and Interface Science VI, Steinkopff, Berlin, Germany, 1992, pp. 160–164.
[12] L. Chen, K. Liu, J.-R. Ye, Q. Shen, Mater. Sci. Eng.: C 56 (2015) 518–521.
[13] J. Hernández-Montelongo, V.F. Nascimento, D. Murillo, T.B. Taketa, P. Sahoo, A.A. de Souza, M.M. Beppu, M.A. Cotta, Carbohydr. Polym. 136 (2016) 1–11.
[14] P. Kujawa, G. Schmauch, T. Viitala, A. Badia, F.M. Winnik, Biomacromolecules 8 (2007) 3169–3176.
[15] E.C. Dreaden, S.W. Morton, K.E. Shopsowitz, J.-H. Choi, Z.J. Deng, N.-J. Cho, P.T. Hammond, ACS Nano 8 (2014) 8374–8382.
[16] A. Schneider, C. Picart, B. Senger, P. Schaaf, J.-C. Voegel, B. Frisch, Langmuir 23 (2007) 2655–2662.
[17] B. Thierry, P. Kujawa, C. Tkaczyk, F.M. Winnik, L. Bilodeau, M. Tabrizian, J. Am. Chem. Soc. 127 (2005) 1626–1627.
[18] L. Bui, S. Abbou, E. Ibarboure, N. Guidolin, C. Staedel, J.-J. Toulmé, S. Lecommandoux, C. Schatz, J. Am. Chem. Soc. 134 (2012) 20189–20196.
[19] L. Richert, F. Boulmedais, P. Lavalle, J. Mutterer, E. Ferreux, G. Decher, P. Schaaf, J.-C. Voegel, C. Picart, Biomacromolecules 5 (2004) 284–294.
[20] T. Salditt, U.S. Schubert, Rev. Mol. Biotechnol. 90 (2002) 55–70.
[21] H.E. Emam, A.P. Manian, B. Široká, H. Duelli, P. Merschak, B. Redl, T. Bechtold, Surf. Coat. Technol. 254 (2014) 344–351.
[22] H.E. Emam, M.H. El-Rafie, H.B. Ahmed, M.K. Zahran, Fibers Polym. 16 (2015) 1676–1687.
[23] H.E. Emam, M.K. Zahran, Int. J. Biol. Macromol. 75 (2015) 106–114.
[24] H.E. Emam, N.H. Saleh, K.S. Nagy, M.K. Zahran, Int. J. Biol. Macromol. 78 (2015) 249–256.
[25] H.E. Emam, H.B. Ahmed, Carbohydr. Polym. 135 (2016) 300–307.
[26] H.B. Ahmed, H.E. Emam, Fibers Polym. 17 (2016) 418–426.
[27] H.E. Emam, N.H. Saleh, K.S. Nagy, M.K. Zahran, Int. J. Biol. Macromol. 84 (2016) 308–318.
[28] R.M. Abdel-Rahman, R. Hrdina, A.M. Abdel-Mohsen, M.M.G. Fouda, A.Y. Soliman, F.K. Mohamed, K. Mohsin, T.D. Pinto, Int. J. Biol. Macromol. 80 (2015) 107–120.
[29] H. Přichystalová, N. Almonasy, A.M. Abdel-Mohsen, R.M. Abdel-Rahman, M.M.G. Fouda, L. Vojtova, L. Kobera, Z. Spotz, L. Burgert, J. Jancar, Int. J. Biol. Macromol. 65 (2014) 234–240.
[30] A.M. Abdel-Mohsen, R.M. Abdel-Rahman, R. Hrdina, A. Imramovský, L. Burgert, A.S. Aly, Int. J. Biol. Macromol. 50 (2012) 1245–1253.
[31] A.M. Abdel-Mohsen, A.S. Aly, R. Hrdina, A. El-Aref, J. Polym. Environ. 20 (2012) 459–468.
[32] A.M. Abdel-Mohsen, A.S. Aly, R. Hrdina, A.S. Montaser, A. Hebeish, J. Polym. Environ. 20 (2012) 104–116.
[33] A.M. Abdel-Mohsen, A.S. Aly, R. Hrdina, A.S. Montaser, A. Hebeish, J. Polym. Environ. 19 (2011) 1005–1012.
[34] Y. Yuan, B.M. Chesnutt, W.O. Haggard, J.D. Bumgardner, Materials 4 (2011) 1399.
[35] S. Kuppusamy, J. Karuppaiah, Asian Pac. J. Trop. Dis. 2 (2012) S769–S773.
[36] M.S. Benhabiles, R. Salah, H. Lounici, N. Drouiche, M.F.A. Goosen, N. Mameri, Food Hydrocolloids 29 (2012) 48–56.
[37] S. Şenel, S.J. McClure, Adv. Drug Deliv. Rev. 56 (2004) 1467–1480.
[38] M.-M. Lou, B. Zhu, I. Muhammad, B. Li, G.-L. Xie, Y.-L. Wang, H.-Y. Li, G.-C. Sun, Carbohydr. Res. 346 (2011) 1294–1301.

[39] W. Wang, S. Lin, Y. Xiao, Y. Huang, Y. Tan, L. Cai, X. Li, Life Sci. 82 (2008) 190–204.

[40] N. Nwe, W.F. Stevens, S. Tokura, H. Tamura, Enzyme Microb. Technol. 42 (2008) 242–251.

[41] G. Muñoz, C. Valencia, N. Valderruten, E. Ruiz-Durántez, F. Zuluaga, React. Funct. Polym. 91–92 (2015) 1–10.

[42] A.A. Tayel, S.H. Moussa, W.F. El-Tras, N.M. Elguindy, K. Opwis, Int. J. Biol. Macromol. 49 (2011) 241–245.

[43] X. Zheng Shu, Y. Liu, F.S. Palumbo, Y. Luo, G.D. Prestwich, Biomaterials 25 (2004) 1339–1348.

[44] T. Segura, B.C. Anderson, P.H. Chung, R.E. Webber, K.R. Shull, L.D. Shea, Biomaterials 26 (2005) 359–371.

[45] B.P. Toole, Nat. Rev. Cancer 4 (2004) 528–539.

[46] S. Cai, Y. Xie, T.R. Bagby, M.S. Cohen, M.L. Forrest, J. Surg. Res. 147 (2008) 247–252.

[47] J. Cell Biol. 116 (1992) 1055–1062.

[48] J. Kim, I.S. Kim, T.H. Cho, K.B. Lee, S.J. Hwang, G. Tae, I. Noh, S.H. Lee, Y. Park, K. Sun, Biomaterials 28 (2007) 1830–1837.

[49] Y. Luo, K.R. Kirker, G.D. Prestwich, J. Controlled Release 69 (2000) 169–184.

[50] J.L. Drury, D.J. Mooney, Biomaterials 24 (2003) 4337–4351.

[51] J.A. Burdick, G.D. Prestwich, Adv. Mater. 23 (2011) H41–H56.

[54] M. Liong, B. France, K.A. Bradley, J.I. Zink, Adv. Mater. 21 (2009) 1684–1689.

[55] S. Chen, S. Chen, S. Jiang, M. Xiong, J. Luo, J. Tang, Z. Ge, ACS Appl. Mater. Interfaces 3 (2011) 1154–1162.

[56] A.M. Abdel-Mohsen, R.M. Abdel-Rahman, M.M.G. Fouda, L. Vojtova, L. Uhrova, A.F. Hassan, S.S. Al-Deyab, I.E. El-Shamy, J. Jancar, Carbohydr. Polym. 102 (2014) 238–245.

[57] A.M. Abdel-Mohsen, R. Hrdina, L. Burgert, R.M. Abdel-Rahman, M. Hašová, D. Šmejkalová, M. Kolář, M. Pekar, A.S. Aly, Carbohydr. Polym. 92 (2013) 1177–1187.

[58] A. Limat, F.K. Noser, J. Invest. Dermatol. 87 (1986) 485–488.

[59] L. Vistejnova, J. Dvorakova, M. Hasova, T. Muthny, V. Velebny, K. Soucek, L. Kubala, Neuro Endocrinol. Lett. 30 (Suppl 1) (2009) 121–127.

[60] H. Wang, H. Cheng, F. Wang, D. Wei, X. Wang, J. Microbiol. Methods 82 (2010) 330–333.

[61] A. Lojek, L. Kubala, H. Cížová, M. Cíž, Luminescence 17 (2002) 1–4.

[62] M. Srivastava, J. Singh, M. Yashpal, D.K. Gupta, R.K. Mishra, S. Tripathi, A.K. Ojha, Carbohydr. Polym. 89 (2012) 821–829.

[63] A.M. Abdel-Mohsen, R. Hrdina, L. Burgert, G. Krylová, R.M. Abdel-Rahman, A. Krejčová, M. Steinhart, L. Beneš, Carbohydr. Polym. 89 (2012) 411–422.

[64] C.Q. Yang, D. Chen, J. Guan, Q. He, Ind. Eng. Chem. Res. 49 (2010) 8325–8332.

[65] C.Q. Yang, Q. He, B. Voncina, Ind. Eng. Chem. Res. 50 (2011) 5889–5897.

[66] C.Q. Yang, Lan Xu, Shiqi Li, Yanqiu Jiang, Text. Res. J. 68 (1998) 457–464.

[67] V.A. Dehabadi, H.-J. Buschmann, J.S. Gutmann, Text. Res. J. 83 (2013) 1974–1995.

[68] S.P. Rowland, C.M. Welch, M.A.F. Brannan, D.M. Gallagher, Text. Res. J. 37 (1967) 933–941.

[69] N. Morris, E. Catalano, B.A.K. Andrews, Cellulose 2 (1995) 31–39.

[70] Weilin Xu, Yi Li, Text. Res. J. 70 (2000) 588–592.

[71] H. Přichystalová, N. Almonasy, A.M. Abdel-Mohsen, R.M. Abdel-Rahman, M.M.G. Fouda, L. Vojtova, L. Kobera, Z. Spotz, L. Burgert, J. Jancar, Int. J. Biol. Macromol. 65 (2014) 234–240.

[72] P. Pirnazar, L. Wolinsky, S. Nachnani, S. Haake, A. Pilloni, G.W. Bernard, J. Periodontol. 70 (1999) 370–374.

[73] I. Perelshtein, G. Applerot, N. Perkas, G. Guibert, S. Mikhailov, A. Gedanken, Nanotechnology 19 (2008) 245705.

[74] I.F. Radaeva, G.A. Kostina, S.G. Il'ina, R.N. Kostyleva, Zh. Mikrobiol. Epidemiol. Immunobiol. (2001) 74–75.

[75] E.I. Rabea, M.E.T. Badawy, C.V. Stevens, G. Smagghe, W. Steurbaut, Biomacromolecules 4 (2003) 1457–1465.

[76] Y.C. Chung, Y.P. Su, C.C. Chen, G. Jia, H.L. Wang, J.C. Wu, J.G. Lin, Acta Pharmacol. Sin. 25 (2004) 932–936.

[77] N. Nwe, T. Furuike, H. Tamura, Materials 2 (2009) 374.

[78] P. Šedová, R. Buffa, S. Kettou, G. Huerta-Angeles, M. Hermannová, V. Leierová, D. Šmejkalová, M. Moravcová, V. Velebný, Carbohydr. Res. 371 (2013) 8–15.

[79] S.M. Luna, S.S. Silva, M.E. Gomes, J.F. Mano, R.L. Reis, J. Biomater. Appl. 26 (2011) 101–116.

[80] B. Viollet, B. Guigas, N. Sanz Garcia, J. Leclerc, M. Foretz, F. Andreelli, Clin. Sci. (Lond. Engl.: 1979) 122 (2012) 253–270.

[81] J. Somboonwong, M. Kankaisre, B. Tantisira, M.H. Tantisira, BMC Complement. Altern. Med. 12 (2012).

[82] A. O'Loughlin, M. Kulkarni, E.E. Vaughan, M. Creane, A. Liew, P. Dockery, A. Pandit, T. O'Brien, Stem Cell Res. Ther. 4 (2013), 158–158.

[83] S.-Y. Ong, J. Wu, S.M. Moochhala, M.-H. Tan, J. Lu, Biomaterials 29 (2008) 4323–4332.

[84] P. Ramasamy, N. Subhapradha, V. Shanmugam, A. Shanmugam, Int. J. Biol. Macromol. 64 (2014) 202–212.

[85] K. Murakami, H. Aoki, S. Nakamura, S.-i. Nakamura, M. Takikawa, M. Hanzawa, S. Kishimoto, H. Hattori, Y. Tanaka, T. Kiyosawa, Y. Sato, M. Ishihara, Biomaterials 31 (2010) 83–90.

[86] H. Ueno, H. Yamada, I. Tanaka, N. Kaba, M. Matsuura, M. Okumura, T. Kadosawa, T. Fujinaga, Biomaterials 20 (1999) 1407–1414.

[87] J.-P. Chen, C.-Y. Kuo, W.-L. Lee, Appl. Surf. Sci. 262 (2012) 95–101.

[88] Y.-W. Cho, Y.-N. Cho, S.-H. Chung, G. Yoo, S.-W. Ko, Biomaterials 20 (1999) 2139–2145.

[89] H. Zhu, N. Mitsuhashi, A. Klein, L.W. Barsky, K. Weinberg, M.L. Barr, A. Demetriou, G.D. Wu, Stem Cells 24 (2006) 928–935.

[90] M. Fronza, G.F. Caetano, M.N. Leite, C.S. Bitencourt, F.W.G. Paula-Silva, T.A.M. Andrade, M.A.C. Frade, I. Merfort, L.H. Faccioli, PLoS One 9 (2014) e112297.

[91] G. Abatangelo, R. Cortivo, M. Martelli, P. Vecchia, Exp. Cell Res. 137 (1982) 73–78.

[92] Y. Liu, M. Durand, B. Zhou, A. Houard, B. Prade, A. Mysyrowicz, In: Lasers and Electro-Optics 2009 and the European Quantum Electronics Conference. CLEO Europe —EQEC, 2009. European Conference on, 2009, pp. 1–1.

Supporting Information's

Novel Wound Dressing based on Chitosan/hyaluronan Nonwoven Fabrics: Preparation, Characterization and Medical Applications

Rasha M. Abdel-Rahman, A. M. Abdel-Mohsen, R. Hrdina, L. Burgert, Z. Fohlerova, D. Pavliňák, Ola N. Sayed, J. Jancar

Sample codes	Treatment code
CTA/NWFs	Nonwoven cotton fabric (NWFs) treated with citric acid (5%).
CS$_{0.5}$CTA/NWFs	Nonwoven cotton fabric (NWFs) treated with chitosan citrate (0.5 %).
CS$_1$CTA/NWFs	Nonwoven cotton fabric (NWFs) treated with chitosan citrate (1 %).
CS$_2$CTA/NWFs	Nonwoven cotton fabric (NWFs) treated with chitosan citrate (2 %).
CS$_{0.5}$CTA/HA/NWFs	Chitosan citrate (0.5 %) nonwoven cotton fabric (NWFs) treated with hayluronan (0.5 %).
CS$_1$CTA/HA/NWFs	Chitosan citrate (1 %) nonwoven cotton fabric (NWFs) treated with hayluronan (0.5 %).
CS$_2$CTA/HA/NWFs	Chitosan citrate (2 %) nonwoven cotton fabric (NWFs) treated with hayluronan (0.5 %).

Table S1. Code of treated and untreated cotton fabrics with different chitosan citrate/hyaluronan concentrations.
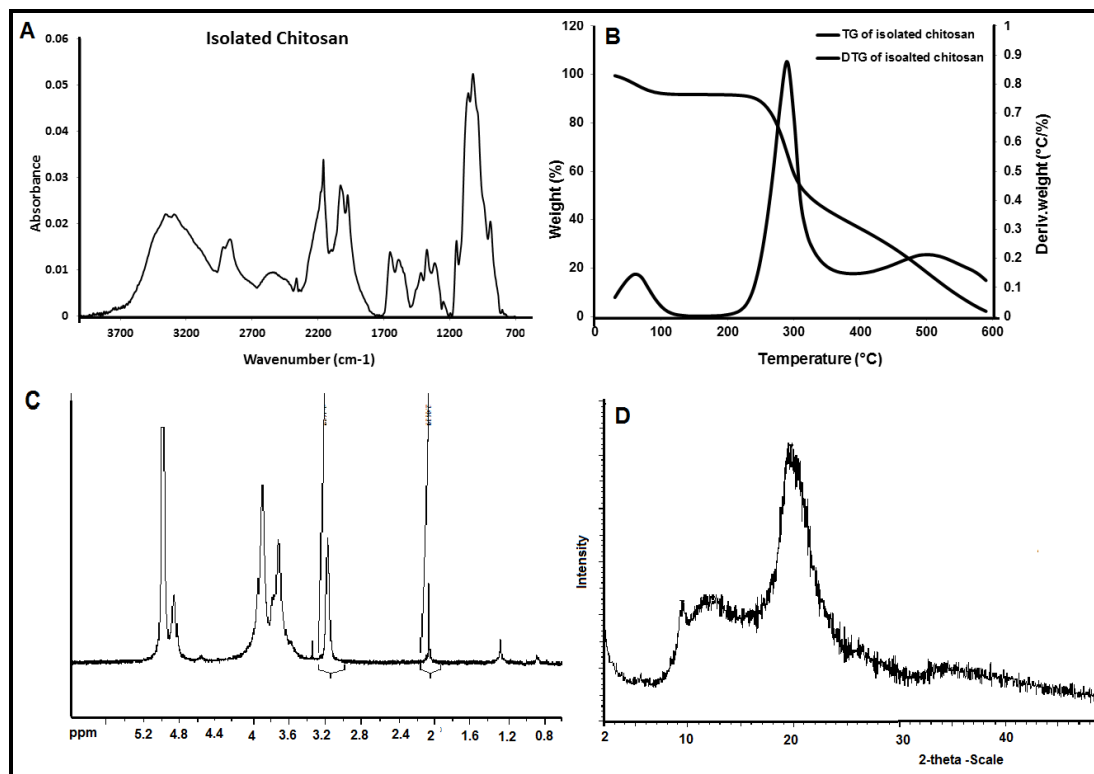
Fig.S1. FTIR-ATR (A); TGA-STG (B); H-NMR (C); XRD (D) of the isolated chitosan from shrimp shell.

Publication 7

Synthesis, characterization and antibacterial activity of new fluorescent chitosan derivatives

Hana Přichystalová [a,b], Numan Almonasy [a,b,*], A.M. Abdel-Mohsen [c,g,**],
Rasha. M. Abdel-Rahman [a], Moustafa M.G. Fouda [d,g], L. Vojtova [c], Libor Kobera [e],
Zdenek Spotz [c], Ladislav Burgert [b], J. Jancar [c,f]

[a] Institute of Organic Chemistry and Technology, Faculty of Chemical Technology, University of Pardubice, Studentská 573, Pardubice CZ-532 10, Czech Republic
[b] Institute of Polymeric Materials, Faculty of Chemical Technology, University of Pardubice, Studentská 573, Pardubice CZ-532 10, Czech Republic
[c] Central European Institute of Technology (CEITEC), Brno University of Technology, Brno, Czech Republic
[d] Petrochemical Research Chair, Chemistry Department, College of Science, King Saud University, P.O. Box 2455, Riyadh 11451, Saudi Arabia
[e] Institute of Macromolecular Chemistry, Academy of Sciences of the Czech Republic, Heyrovského nám. 2, 162 06 Praha 6, Czech Republic
[f] Institute of Materials Chemistry, Brno University of Technology, Czech Republic
[g] Textile Research Divisions, National Research Centre, Dokki, Cairo, Egypt

ARTICLE INFO

ABSTRACT

The present work aims to the development of innovative new derivatives of chitosan that can be used for medical applications. This innovation is based on the synthesis and characterization of chitosan-g-aminoanthracene derivatives. Thus, *N-(anthracen-9-yl)-4,6-dichloro-[1,3,5]-triazin-2-amine* (AT) reacted with chitosan by the following steps: at first, cyanuric chloride reacted with 9-aminoanthracene to obtain *N-(anthracen-9-yl)-4,6-dichloro-[1,3,5]-triazin-2-amine* (AT), then the AT reacted with chitosan to obtain (CH-g-AT). The final product of CH-g-AT was separated, purified and re-crystallized by dioxane. The structure of the prepared chitosan derivatives was confirmed by FTIR-ATR, solid-NMR, TGA, X-RD, and DSC. The new chitosan derivatives showed fluorescence spectra in liquid and in solid state as well. CH-g-AT showed also high antibacterial activity against gram −ve species (*Escherichia coli*).

© 2014 Elsevier B.V. All rights reserved.

1. Introduction

The term modification of polymers is understood as the changes in terms of physical and chemical transformations of polymers. The chemical modification is based on the chemical reactions of active substances with functional groups of that polymer. A great attention is paid to such modification as well as to the preparation of synthetic polymers in order to obtain new potential biocompatible materials [1,2]. Considerable attention in recent years is paid also to the study of the preparation and properties of photoactive polymers. The interest of such modified polymers is connected with their wide range of applications in electronic and optoelectronic devices. Such polymers have great potential application in holographic recording, data storage, light-emitting diodes and solar systems, etc. [3]. Although most previously studied, fluorescent polymers are of synthetic origin. Recently, this research is focused on natural polymers having similar applications [4–7]. The advantages of natural polymers, compared to synthetic ones, represent in safety, biocompatibility, biodegradability, easy availability and relatively low cost. Chitosan is one of the natural and attractive polymers that exhibits a variety of biological activities with a wide potential of different applications.

Chitosan (CH) (β-1-4)-D-glucosamine) is the deacetylated structure of chitin, which is the second famous polymer found in nature after cellulose, that isolated from crabs, shrimps and other crustaceans [21,22]. Chitosan have unique properties like nontoxic, biodegradability, biocompatibility that has long been used as a natural polymer or a crude material in medicine, textile and food industry [8–12,23]. Due to the polycationic nature, chitosan has antimicrobial activity against several bacteria and fungi [10,24]. From the previous work [10,24] chitosan, can inhibit the growing of bacteria and fungi by inhibiting the normal metabolism of through the ionic interactions at cell surfaces and consequently leading at the end to the cell death [11]. The presence of a large number of primary amine and hydroxyl groups on the chitosan molecule

---

* Corresponding author at: Institute of Organic Chemistry and Technology, Faculty of Chemical Technology, University of Pardubice, Studentská 573, Pardubice CZ-532 10, Czech Republic. Tel.: +420 466038500; fax: +420 466038004.
** Corresponding author at: Central European Institute of Technology (CEITEC), Brno University of Technology, Brno, Czech Republic. Tel.: +420 773063837.
E-mail addresses: almonasy@gmail.com (N. Almonasy), abdel-mohsen@ceitec.vutbr.cz, abdo_mohsennrc@yahoo.com (A.M. Abdel-Mohsen).
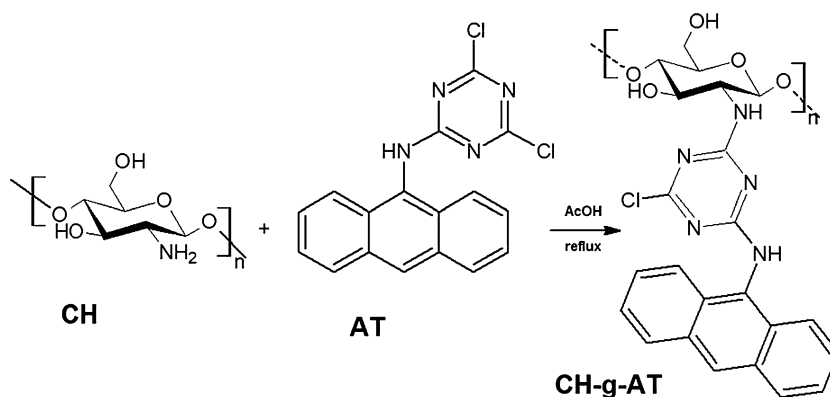
Scheme 1. Preparation of CH-g-AT.

gives a possibility for many chemical modifications, by obtaining a new class of biomaterials. Recently, a large number of publications dealing with the labeling of chitosan by the introduction of a fluorophore in its molecule can be found, mostly via the primary amino group. Hence, fluorescent polymer could be obtained [13–15].

The present work aims to the synthesis, characterization and fluorescence measurements of new chitosan derivatives (CH-g-AT). The final product was confirmed using FTIR-ATR, solid NMR, TGA, X-RD, DSC, and fluorescence spectra. The antibacterial activity was also evaluated by using gram −ve bacteria (*Escherichia coli*).

2. Experimental

2.1. Materials

Chitosan extracted from the Crawfish shell with the degree of deacetylation (95%, MW 100 kDa), 9-aminoanthracene, cyanuric chloride (Sigma–Aldrich), other solvents were used for the synthesis are received without further purification.

2.2. Methods

2.2.1. Preparation of N-(anthracen-9-yl)-4,6-dichloro-[1,3,5]-triazin-2-amine (AT)

The label N-(anthracen-9-yl)-4,6-dichloro-[1,3,5]-triazin-2-amine (AT) was prepared by the reaction of cyanuric chloride with 9-aminoanthracenes according to the procedure described in the previous work [16]. Briefly, cyanuric chloride (5 g, 27 mmol) was dissolved in 100 mL of acetone, sodium carbonate was added and the mixture was cooled to −5 °C. The solution of 9-aminoanthracene (5 g, 26 mmol) in 100 mL of acetone was added drop-wise under nitrogen atmosphere. The temperature of the reaction mixture was maintained between −5 to 10 °C and the reaction was continuously monitored by TLC. After 4 h, the reaction mixture was poured into 100 mL water and the precipitated crude product was filtered off and dried. The crude product was re-crystallized by using toluene.

2.2.2. Preparation of fluorescent chitosan-g-(anthracen-9-yl)-4,6-dichloro-[1,3,5]-triazin-2-amine (CH-g-AT)

Chitosan (0.2 g) was dissolved in 30–60 ml of 2% aqueous solution of acetic acid. Then, a solution of AT (10 mg, 0.0293 mmol, 20 mg, 0.0586 mmol, and 40 mg, 0.117 mmol) in 1,4-dioxane (10–25 ml) was added. The reaction mixture was heated under reflux for 3 h. Then, the heating was turned off and the reaction mixture was stirred at room temperature overnight, a mixture of

250 ml of acetone and 150 ml 1,4-dioxane was added. After addition of acetone the sample precipitate start to appear, filtered through pleated filter-papers, washed with acetone and dried at 50 °C, the crude product was purified and recrystallized by 1,4-dioxane.

2.3. Characterization of CH-g-AT

2.3.1. UV/vis spectroscopy

The absorption spectra were measured on a UV/vis spectra-Perkin-Elmer Lambda 35 spectrophotometer at room temperature. The instrument provides corrected excitation spectra directly.

2.3.2. Fluorescence spectra

Very weakly absorbing solutions (optical density ~0.05 at the excitation wavelength in 1 cm cell) were used. The fluorescence spectra were recorded by excitation at the wavelengths of the most intensive absorption vibronic band; the optical density at this wavelength was about 0.05 in a 1 cm cell. The fluorescence quantum yields in solution were measured using quinine sulphate ($q_F = 0.54$ in 0.5 mol/L H_2SO_4) [19] as the standard. The fluorescence spectra in solid phase were recorded from the surface of the pressed powder in special commercial cuvettes for spectrophotometer PE LS 55. Fluorescence spectra were corrected for the characteristics of the emission mono-chromator and for the photomultiplier response.

2.3.3. Solid-NMR spectroscopy

[1]D solid-state NMR spectra were measured using a Bruker Avance III HD 500 NMR spectrometer. Magic angle spinning (MAS) frequency of the sample was 11 kHz. Amplitude modulated cross-polarization (CP) with a duration of 1 ms was used to obtain ^{13}C CP/MAS NMR spectra. The applied recycle delay was 5 s. The ^{13}C NMR scale was calibrated with glycine as an external standard (176.03 ppm – low-field carbonyl signal). To compensate for frictional heating of the spinning samples, all NMR experiments were measured under active cooling. The sample temperature was maintained at 298 K, and the temperature calibration was performed on Pb $(NO_3)_2$ using a calibration procedure described in the literature [20].

2.3.4. XRD diffraction

X-ray diffraction were collected on a device namely; D-8 Advance diffractometer (Bruker AXS, Germany) with Bragg–Brentano θ–θ goniometer (radius 217.5 mm) equipped with a secondary beam curved graphite mono-chromator and Na (Tl) I scintillation detector. The generator was operated at 40 kV and 30 mA. The scan was completed at room temperature from 5 to 60° (2θ) in 0.02° step with a counting time of 8 s per step.
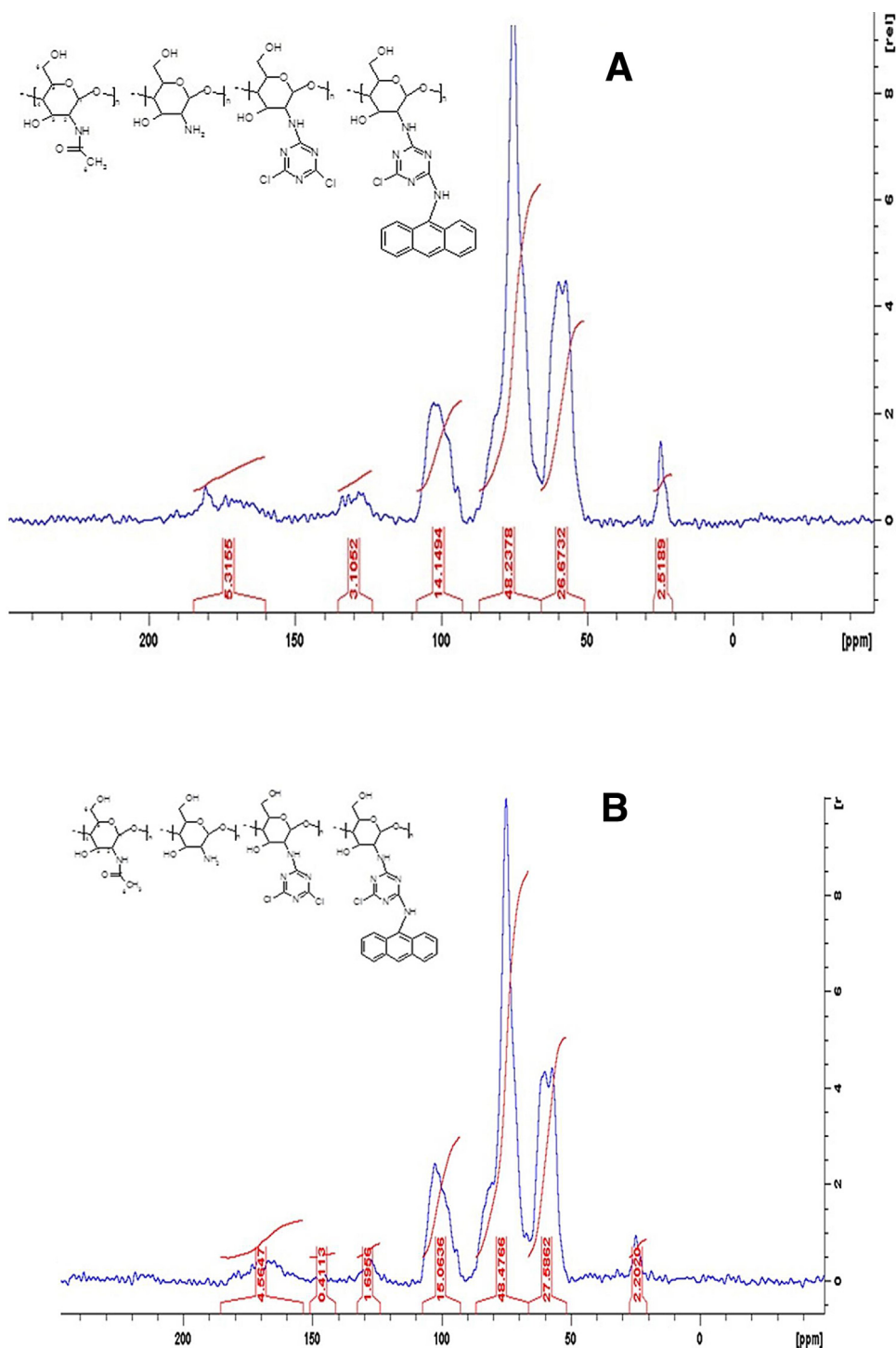
Fig. 1. (A) NMR of CH-g-AT1. (B) NMR CH-g-AT2.

2.3.5. Thermal analysis spectra

The thermal analysis was evaluated by using different heating rate using the device; (TG, Netzsch 209F3 instrument, Al_2O_3 crucible) and under heating rate; $5\,°C\,min^{-1}$. The heat flow properties of the samples were also measured by the differential scanning calorimetry; (DSC, Netzsch 200 F3 instrument, aluminum pans with a pin hole cover), which was completed in a dynamic nitrogen atmosphere under a pressure of 0.1 MPa. The samples mass for DSC was about 0.9 mg with a heating rate of $10\,°C\,min^{-1}$ and temperature range $50–600\,°C$.

2.3.6. Attenuated total reflectance Fourier transforms infrared spectroscopy

FTIR-ATR spectroscopy was measured using a device namely; Nicolet Impact 400 D FTIR-ATR |spectrophotometer (Nicolet CZ, Prague, Czech Republic) equipped with a ZnSe crystal for the ATR-FTIR spectroscopy. The absorbance bands were measured as a function of wave numbers in between 4000 and $400\,cm^{-1}$.

2.3.7. Antibacterial test

The antibacterial activity of chitosan derivatives was measured by using a luminometer Microtiter Plate Luminometer CM3X

Fig. 2. ATR-FTIR of CH (a); CH-g-AT2 (b).

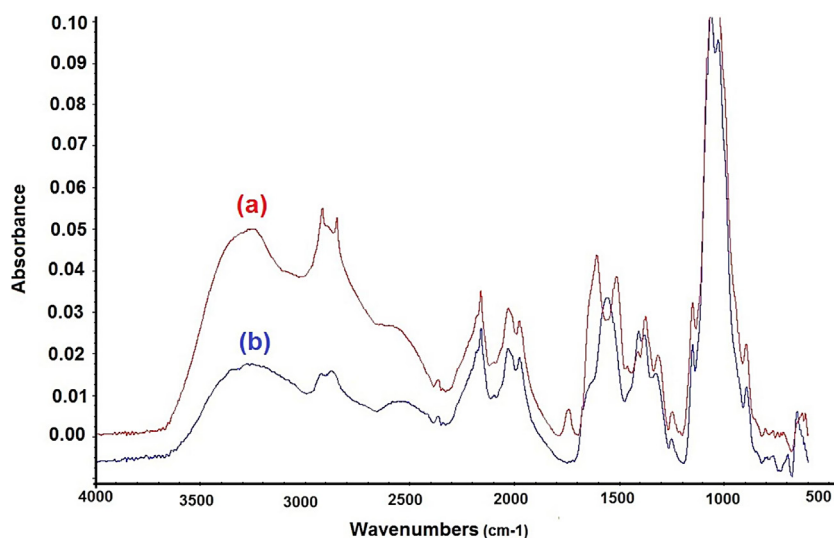(Dynex Technologies Inc., USA). 5, 10, 15 mg of the chitosan derivatives were used for testing the biological activity of the fluorescence chitosan against gram −ve *E. coli*. In 96 well plates, 5, 10 and 15 mg of chitosan derivatives were inserted in each hole together with 200 μL bacterial suspension (bacterial strain K12 with the optical density of OD at 600 = 0.251). The control sample was only prepared with bacteria strain without chitosan derivatives samples. Each concentration was performed at least three times.

3. Results and discussion

3.1. Preparation of CH-g-AT

It is well known that, the chlorine atoms of triazinyl ring are sufficiently reactive. Therefore the fluorescent label *N-(anthracen-9-yl)-4,6-dichloro-[1,3,5]-triazin-2-amine* (AT) having two reactive chlorine atoms on 1,3,5-triazine moieties and was used for the grafting of chitosan; and thereby the fluorescent chitosan-g-*(anthracen-9-yl)-4,6-dichloro-[1,3,5]-triazin-2-amine* was prepared. Chitosan has two different active groups (amino and hydroxyl groups) and both could react with the chlorine atoms in the triazine ring of AT by substitution reaction. However, with a high confidence, it could be stated that the reaction takes place mainly via the amino group of CH (Scheme 1). The fluorescent chitosan derivatives were prepared by using different molar ratio between CH and AT under acidic conditions CH-g-AT (10:0.2, 10:0.5, 10:1, and 1:1); the corresponding products were designated as CH-g-AT1, CH-g-AT2, CH-g-AT3, and CH-g-AT4, respectively. The isolation of the product was completed after diluting the reaction mixture with acetone–dioxane mixture and subsequent filtration of the product.

3.2. Solid state NMR analysis of CH and CH-g-AT samples

Fig. 1 shows the ^{13}C CP/MAS NMR spectra of the compounds CH-g-AT1 (Fig. 1A) and CH-g-AT2 (Fig. 1B). It has been found that the ^{13}C CP/MAS NMR spectra obtained with a contact time of 1 ms lead to an approximately correct representation of the relative intensities of the CH/AT resonances. In the following it will be considered that the substitution of chitosan can be measured by integration of the corresponding peaks and calculated from Eqs. (1)–(3).

The recorded ^{13}C CP/MAS NMR spectrum of prepared samples (Fig. 1) confirms the presence of substituted chitosan. The assignment of signals to various carbon types of chitosan follows the data found in the literature [17,18]. Following the fact that chitosan is

also polymer of glucose derivative, the range of the resonances 30–110 ppm is similar in both systems, however both systems are not identical. Additionally, for the compound CH-g-AT1 the signals from anthracene group (ca. 130 ppm, Fig. 1A) and from heterocyclic ring (ca. 170–160 ppm) were detected. The amount of residual acetyl group calculated according Eq. (1) is about 19%. The amount of anthracene groups in the system was estimated from Eq. (2) to be ca. 1.5% and the amount of heterocyclic rings was calculated by Eq. (3) to ca. 13%. For the sample CH-g-AT2 the signals corresponding to the anthracene groups (ca. 130 ppm) and to the heterocyclic rings (ca. 170–160 ppm, Fig. 1B) were also detected. The amount of residual acetyl group calculated according Eq. (1) is, however, reduced to be ca. 14%. The amount of anthracene groups in the system was estimated from Eq. (2) to be less than 1% and the amount of heterocyclic rings estimated form Eq. (3) seems to be about 10%.

$$\text{mol\%}(\text{acetyl groups}) = \frac{I_{CH_3}}{(I_{C1} + I_{C2} + I_{C3} + I_{C4} + I_{C5} + I_{C6})/6} \times 100 \quad (1)$$

$$\text{mol\%}(\text{antracene}) = \frac{(I_{C_{antr}})/14}{(I_{C1} + I_{C2} + I_{C3} + I_{C4} + I_{C5} + I_{C6})/6} \times 100 \quad (2)$$

$$\text{mol\%}(\text{heterocycle}) = \frac{(I_{C_{heteroc}})/3}{(I_{C1} + I_{C2} + I_{C3} + I_{C4} + I_{C5} + I_{C6})/6} \times 100 \quad (3)$$

3.3. FTIR-ATR of spectra of CH-g-AT2

FTIR-ATR spectrum of both CH and CH-g-AT2 graft copolymer shows the characteristic absorption band of both pure chitosan and fluorescent copolymer (Fig. 2). Chitosan shows a broad band about 3200–3374 cm^{-1} that corresponding to a stretching vibration of OH and NH groups, 1661 cm^{-1} is corresponding to (amide I), 1593 cm^{-1} is corresponding to (amide II) and 1380 cm^{-1} is corresponding to (amide III). The absorption band at 1158 cm^{-1} for asymmetric stretching of (C—O—C Bridge) and 1080 cm^{-1} for (C—O stretching) are corresponding to the structure of polysaccharide (Fig. 2a). For CH-g-AT2 (Fig. 2b), the peaks of hydroxyl and amino groups of chitosan was slightly shifted and their intensity is significantly reduced because of the grafting of *N*(anthracen-9-yl)-4,6-dichloro-[1,3,5]-triazin-2-amine. In Comparison with the peak of amide I at 1661 cm^{-1}, the peak intensity of (amide II) at 1593 cm^{-1} is decreased significantly. This resulted spectrum shows that the amino groups of chitosan were grafted with AT2. If all chitosan chains are grafted, the peaks corresponding to NH$_2$ of chitosan at 1593 cm^{-1} disappear and form a single peak after
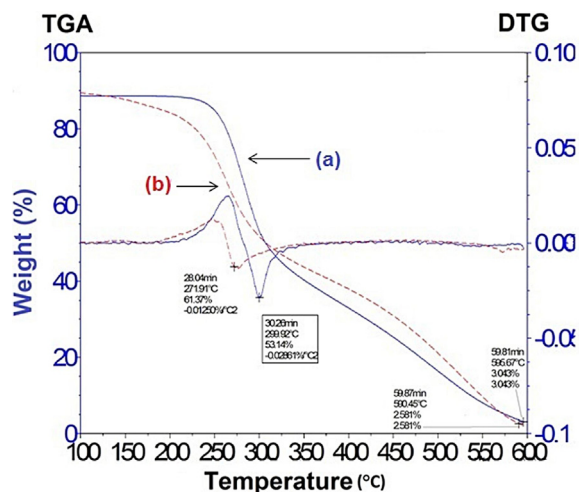
Fig. 3. TGA of CH (a); CH-g-AT2 (b).

Fig. 5. XRD of CH (a); CH-g-AT2 (b).

completion of the reaction. The peaks at 2882 cm^{-1} and 1108 cm^{-1} in CH-g-AT2 were attributed to the superposition of C—H stretching vibration of chitosan and AT.

3.4. Thermal stability of CH and CH-g-AT2

The thermal gravimetric analysis (TGA) of CH and CH-g-AT2 is explained in Fig. 3. It is clear in Fig. 3a that the weight-loss of chitosan was slow; starting from 88 °C i.e. (12.5%). This weight-loss is caused by the presence of non-bonded and bonded water, which can be removed at low temperature, followed by more weight-loss starting from 300 °C that could be caused by a complex process including the dehydration of acetylated and deacetylated saccharide rings. CH-g-AT2 (Fig. 3b) exhibits two-stage thermal decomposition process: the first one with 91 °C (10%) weight-loss due to the presence of residual water bonded and un bonded in chitosan chain, and the second one at 285 °C that corresponds to the decomposition of chitosan back-bone. The TGA curves
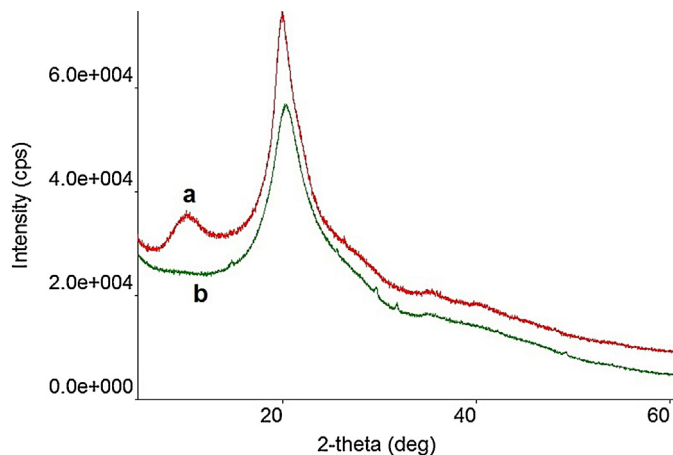
indicated that CH-g-AT2 is less thermally stable than the original chitosan.

3.5. Differential scanning calorimetric of CH and CH-g-AT2

Fig. 4 shows the differential scanning calorimetry (DSC) of CH and CH-g-AT2. The thermal spectrum of CH (Fig. 4a) shows two sharp endothermic peaks at 45 °C and 190 °C. The former peak may be due to the water present in chitosan while the second peak may attributed to the decomposition of chitosan chain. The thermal spectra of CH-g-AT2 (Fig. 4b) show two sharp endothermic peaks at 45 °C and 162 °C which corresponding to the structure arrangements and its degree of substituted changes. This results show that the chemical structure of CH have been changed due to its grafting with AT.

3.6. XRD of chitosan and CH-g-AT2

Fig. 5 shows the X-RD of pure chitosan (CH; Fig. 5a) and chitosan-g-*N*(anthracen-9-yl)-4,6-dichloro-[1,3,5]-triazin-2-amine (CH-g-AT2; Fig. 5b). Fig. 5a shows that chitosan has reflection

Fig. 4. DSC of CH (a); CH-g-AT2 (b).

Fig. 6. Absorption (A) spectrum of AT (left), absorption (A) spectrum and fluorescence spectra in solution (F) and in the solid phase (Fs) of CH-g-AT1.

peaks at $2\theta = 10.7^{O}$, and 22.2^{O}. In Fig. 5b only one peak appears at $2\theta = 22.2^{O}$ after grafting of the *N-(anthracen-9-yl)-4,6-dichloro-[1,3,5]-triazin-2-amine* into chitosan and preparation of fl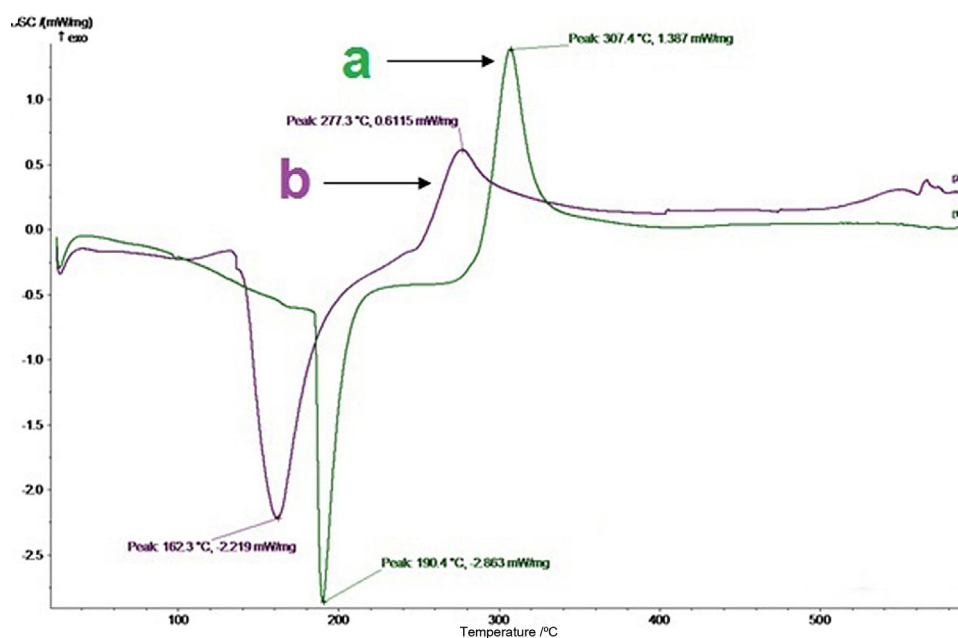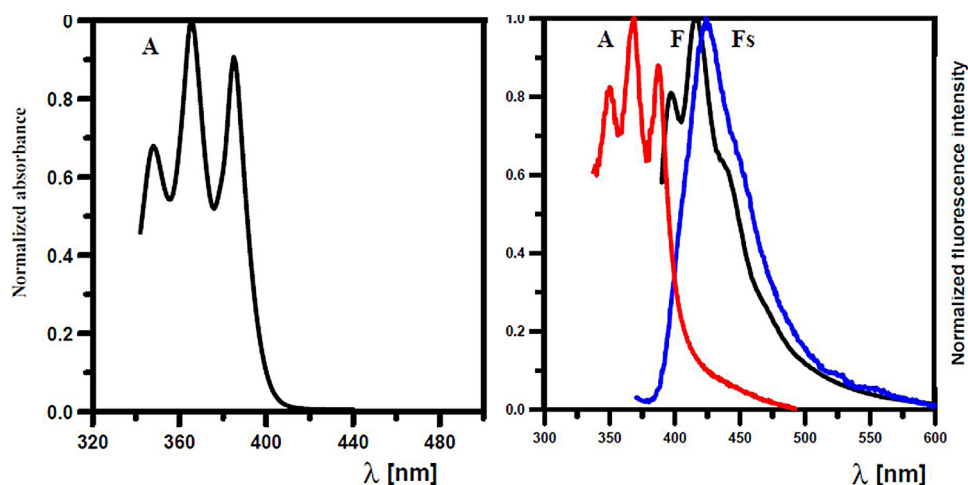orescence chitosan derivatives. We can conclude that after the grafting of the AT onto chitosan chains, the crystallinity of chitosan changed due to the grafting process.

3.7. Absorption and fluorescence spectra of CH-g-AT2

The shape and position of the absorption spectra of CH-g-AT2 in solution are practically the same as that for the AT (Fig. 6A). The fluorescence spectra of CH-g-AT2 in solutions are almost identical with that for *N*-triazinyl derivatives of 9-aminoanthracene [16]. The fluorescent label AT shows no fluorescence in solution and only a weak fluorescence in solid phase. However, the fluorescence was observed in both the solid and in solution phases after the binding of the fluorescent label to the chitosan chain by a covalent bond (Figs. 6B and 7A and B). The fluorescent phenomena was appeared due to the substitution reaction of mono or di chlorine atoms on triazinyl ring of AT by the amino group in chitosan chains. From the previous work [16], the influences of electronic excited states

leading to dramatic increase of the fluorescence quantum yield of the corresponding compounds.

The fluorescence spectra of CH-g-AT in solution exhibit a vibronic structure and are approximately mirror symmetric to the first absorption band. Unlike the fluorescence spectra in solution, the fluorescence spectra in solid phase show a broad and structure less band. The fluorescence maxima in solid phase are shifted by about 8 nm bath chronically compared with the maximum in solution (Fig. 6). By comparison of the fluorescence intensity of CH-g-AT 1–3 in solid phase, only insignificant difference was observed. The fluorescence quantum yields in solution are identical ($q_F = 0.046 \pm 0.002$). Relative fluorescence intensities of CH-g-AT 4 in solid phase are about ten times lower compared with the maximum intensity of CH-g-AT1-3. At the same time, in contrast with CH-g-AT1-3, CH-g-AT4 exhibits no fluorescence in solution.

3.8. Antibacterial activity of chitosan derivatives

Three different concentrations of chitosan derivative; CH-g-AT2 (5, 10, and 15 mg), were used to determine the antibacterial activity of the prepared new fluorescence chitosan. Fig. 8 shows the antibacterial activity of chitosan derivative comparing with control sample. As shown in (Fig. 8), as the concentration of CH-g-AT2 (5, 10, and 15 mg), the antibacterial activity increases. However, the reduction rate was less than 100%, which is due to the blocking/masking of the amino groups in chitosan chain by *N-(anthracen-9-yl)-4,6-dichloro-[1,3,5]-triazin-2-amine*, in addition to the acetylation of amino groups of chitosan (which is confirmed
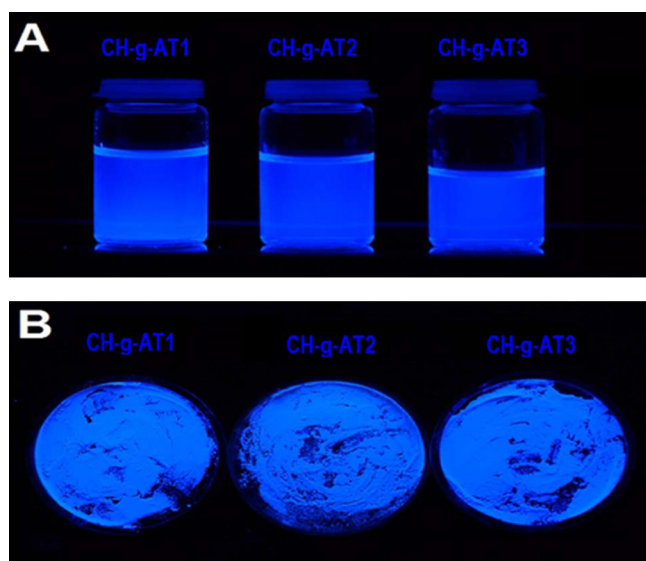

Fig. 7. CH-g-AT1-3 in aqueous solution (A); and in solid phase under irradiation of UV light (B).
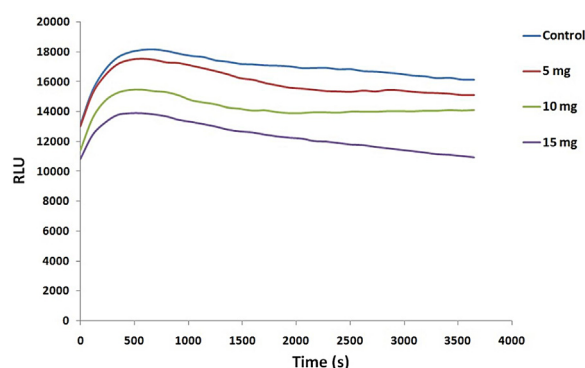

Fig. 8. Antibacterial activity of CH-g-AT2 against gram (−ve) bacteria (*E. coli*).

by NMR data; Section 3.2), both reasons lead to decreasing the antibacterial activity of chitosan derivatives.

4. Conclusions

The fluorescent chitosan-g-*(anthracen-9-yl)-4,6-dichloro-[1,3,5]-triazin-2-amine* (CH-g-AT) was successfully prepared via the nucleophilic substitution reaction of chlorine atom of triazinyl ring of the label *N-(anthracen-9-yl)-4,6-dichloro-[1,3,5]-triazin-2-amine* with the amino group of chitosan. The structure of chitosan derivatives were confirmed by FTIR-ATR, solid ^{13}C NMR, TGA, and DSC. To confirm the change in fluorescence intensity, four different samples of fluorescent polymer were prepared by using different molar ratios of the reactants. The UV/vis absorption and fluorescence spectra, as well as the fluorescence quantum yields of the prepared samples were measured in 2% of acetic acid. Moreover, the fluorescence spectra were measured in solid phase. It was found that the polymer with very high fluorescence intensity could be obtained already using a molar ratio of chitosan/label 1:0.3. The fluorescent chitosan shows higher antibacterial activity against gram (−ve) bacteria. We believe that the new derivatives of chitosan can be used for different medical applications especially for diagnostic, and magnetic resonance imaginations.

Acknowledgements

References

[1] D. Ozdal, S. Asir, J.B. Bodapati, H. Icil, Photochemical & Photobiological Sciences 12 (2013) 1927–1938.
[2] W.L. Meyer, Y. Liu, X.W. Shi, X. Yang, W.E. Bentley, G.F. Payne, Biomacromolecules 10 (2009) 858–864.
[3] M. Nowakowska, L. Moczek, K. Szczubiałka, Biomacromolecules 9 (2008) 1631–1636.
[4] Q. Yang, L. Shuai, X. Pan, Biomacromolecules 9 (2008) 3422–3426.
[5] B.R. Qaqish, M.M. Amiji, Carbohydrate Polymers 38 (1999) 99–107.
[6] Ch. Gentile, P. Boccafoschi, F. Carmagnola, I. Ninov, M. Georgieva, V.G. Georgiev, G. Ciardelli, Biomacromolecules 11 (2010) 309–315.
[7] F.L. Mi, Biomacromolecules 6 (2005) 975–987.
[8] A.M. Abdel-Mohsen, A.S. Aly, R. Hrdina, Journal of Polymers and the Environment 20 (2012) 459–468.
[9] A.M. Abdel-Mohsen, A.S. Aly, R. Hrdina, A.S. Montaser, A. Hebeish, Journal of Polymers and the Environment 19 (2011) 1005–1012.
[10] A.M. Abdel-Mohsen, A.S. Aly, R. Hrdina, A.S. Montaser, A. Hebeish, Journal of Polymers and the Environment 20 (2012) 104–116.
[11] A.M. Abdel-Mohsen, M.A. Rasha, R. Hrdina, A. Imramovský, L. Burgert, A.S. Aly, International Journal of Biological Macromolecules 50 (2012) 1245–1253.
[12] A.S. Aly, A.M. Abdel-Mohsen, R. Hrdina, A. Abou-Okeil, Journal of Natural Fibers 8 (2011) 176–188.
[13] C. Cunha-Reis, A.J. El Haj, X. Yang, Y. Ying, Journal of Tissue Engineering and Regenerative Medicine 7 (2013) 39–50.
[14] Ch. Kaewsaneha, P. Opaprakasit, D. Polpanich, S. Smanmoo, P. Tangboriboonrat, Journal of Colloid and Interface Science 377 (2012) 145–152.
[15] Q. Nie, W.B. Tan, Y. Zhang, Nanotechnology 17 (2006) 140–144.
[16] H. Prichystalova, N. Almonasy, M. Nepraš, F. Bureš, M. Dvořák, M. Michl, J. Čermák, L. Burgert, Journal of Fluorescence 23 (2013) 425–437.
[17] F.S. Tanner, H. Chanzy, M. Vincendon, J.C. Roux, F. Gaill, Macromolecules 23 (1990) 3576.
[18] M.H. Ottey, K.M. Vårum, O. Smidsrød, Carbohydrate Polymers 29 (1996) 17–24.
[19] J.B. Birks, D.J. Dyson, Proceedings of the Royal Society A 275 (1963) 135–148.
[20] J. Brus, Solid State Nuclear Magnetic Resonance 16 (2000) 151–160.
[21] M.M.G. Fouda, M.R. El-Aassar, S.S. Al-Deyab, Carbohydrate Polymers 92 (2013) 1012–1017.
[22] R.M. Abdel-Rahman, A.M. Abdel-Mohsen, M.M.G. Fouda, S.S. Al Deyab, A.S. Mohamed, Life Science Journal 10 (4) (2013) 834–839.
[23] M.M.G. Fouda, R. Wittke, D. Knittel, E. Schollmeyer, International Journal of Diabetes Mellitus (IJDM) 1 (1) (2009) 61–64.
[24] A.M. El-Shafei, M.M.G. Fouda, D. Knittel, E. Schollmeyer, Journal of Applied Polymer Science 110 (3) (2008) 1289–1296.

Publication 8

Hyaluronan/Zinc Oxide Nanocomposite-Based Membrane: Preparation, Characterization, and *In Vitro* and *In Vivo* Evaluation

R. M. Abdel-Rahman, J. Frankova, R. Sklenarova, L. Kapralkova, I. Kelnar, and A. M. Abdel-Mohsen*

Cite This: *ACS Appl. Polym. Mater.* 2022, 4, 7723−7738

Read Online

ACCESS | Metrics & More | Article Recommendations | SI Supporting Information

ABSTRACT: Hyaluronic acid (HA) has attracted the attention of scientists for its application in many medical fields owing to its intrinsic properties such as biodegradability, biocompatibility, and nontoxicity. Poor stability and antibacterial activity are the most significant drawbacks of using HA in preparing a wound dressing. The wound dressing should be able to swell and absorb exudates from the wound, as well as possess antibacterial activity. Herein, we successfully prepared an HA-based antibacterial wound dressing that can swell more than 500 times and with good mechanical properties. HA was used both as reducing and stabilizing agents, and zinc oxide nanoparticles (ZnO-NPs) were incorporated via *in situ* synthesis. The uniform spherical shape of ZnO-NPs (50 ± 10 nm) was synthesized and assembled on a hyaluronan/polyvinyl alcohol matrix (HA/PVA), forming stable and evenly distributed ZnO-NPs, which interacted with the HA/PVA. Such a hybrid nanostructure prevented ZnO-NPs from dropping off the PVA/HA network and thus minimized the toxicity of NPs. Concerning the slow release of NPs, the nanocomposite membrane still exhibited significant antibacterial activity against different types of bacteria (G+/−). The ZnO-NPs/HA/PVA composite membrane allows the attachment and growth of normal human dermal fibroblasts and human primary osteogenic sarcoma (Saos-2) without exhibiting toxicity. *In vivo* measurements showed that the nanocomposite PVA/HA/ZnO-NP membrane promoted infected wound healing compared with the control sample. The results obtained suggest that the investigated nanocomposite has reasonable potential as an antibacterial wound dressing material.

KEYWORDS: hyaluronan membrane, zinc oxide nanoparticles, mechanical properties, biocompatibility, wound healing
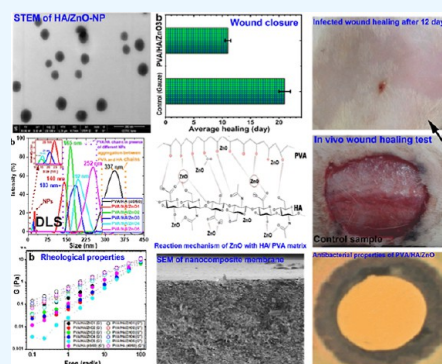
1. INTRODUCTION

Nanocomposites, combining two phases of different materials, are at the forefront of materials exploited in medical and nanotechnology applications.[1−4] The improved properties of nanocomposites depend on the individual properties of each substance. Several polymers have been used to develop nanocomposite properties that could be improved by adding reinforcing organic/inorganic compounds as a filler.[5−9]

Hyaluronan (HA) is widely used in various applications.[10−13] Abundant in human tissues and fluids, hyaluronan is a non-immunogenic biopolymer that contains alternating *N*-acetyl-D-glucosamine units, linked by alternating β-(1 → 4) and β-(1 → 3) glycosidic bonds.[14−17] The role of in the human body depends on its dimensions, which can vary from a few oligosaccharides (one disaccharide is 400 Da and corresponds to ~1 nm size) to up to 25×10^3 disaccharide units (10 MDa, 25 μm).[18,19] Due to its physicochemical properties, healing ability, high biodegradability, thermal/hydrolytic stabilities, and biological characteristics, hyaluronan has been revealed to contribute to a range of biomedical applications, such as tissue engineering, drug delivery, and wound dressing applications.[8,12,17,19,20] However, the poor mechanical properties of uncross-linked hyaluronan, the fast

degradation rate, and the rapid clearance *in vivo* limit its use.[21,22] To improve all these disadvantages and generate a mechanically and chemically robust HA-based system while maintaining the biocompatibility and biodegradability, an aqueous solution of HA can be chemically modified or cross-linked to form an insoluble form of hyaluronan.[23,24]

It exhibits a high-water content and high porosity, is degradable by hyaluronidase, and is resistant to cell adhesion. These unsatisfactory shortcomings can be compensated for by implementing a chemical cross-linking approach. Today, a frequently used method for crosslinking HA is the reaction with butanediol diglycidyl ether, glutaraldehyde, and 1-ethyl-3-(3-dimethylaminopropyl)carbodiimide/*N*-hydroxysuccinimide under alkaline conditions to obtain a stable covalent ether linkage between HA and the cross-linker.[25,26] Unfortunately,
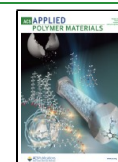
Scheme 1. Representative *In Situ* Synthesis of ZnO-NPs Using HA and PVA[a]
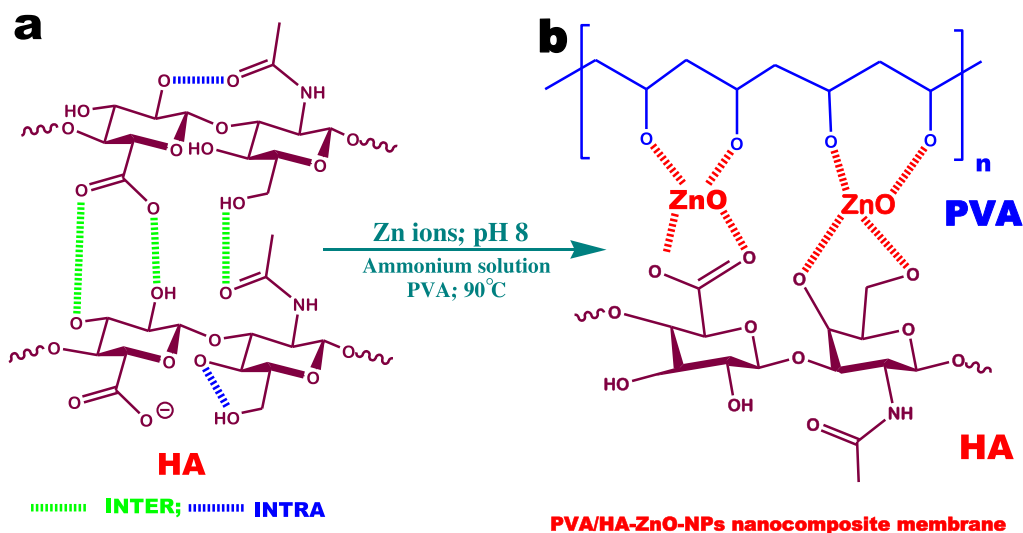
[a]Chemical structure of hyaluronan with intra- and interhydrogen bonds, (b) *in situ* synthesis of ZnO-NPs using hyaluronan/PVA.

the materials obtained after the cross-linking process affect the biocompatibility and viability of hyaluronan.[27,28]

Zinc oxide nanoparticles (ZnO-NPs) have emerged as interesting substances with physical and chemical characteristics that can be used as suitable fillers in polymer nanocomposites.[29] Because of their limited size and high surface area-to-volume ratio, they are able to have a volume ratio, low toxicity, and good antimicrobial properties. ZnO-NPs are especially attractive with respect to applications in catalysis, sensing, energy storage, solar cells, and biomedicine.[30−32]

Polyvinyl alcohol (PVA) is a synthetic material with desirable characteristics, such as biocompatibility, water solubility, and robust mechanical, chemical, thermal, and hydrolytic stabilities.[33−35] PVA exhibits a high degree of swelling in physiological solutions under physiological conditions, are noncytotoxic, non-carcinogenic, and biocompatible with our human body.[4,36] In aqueous solutions with a polymer concentration greater than 1% by weight, entangled aggregates of strongly hydrogen-bonded[4] PVA molecules are generated due to the formation of high crystalline regions.[2]

Only three studies in the literature have described the formation of a hyaluronan/ZnO composite in different forms (scaffold, nanofibers mats, hydrogels).[37] Unfortunately, there were many drawbacks during the preparation of ZnO-NPs, such as the use of an external reducing agent (4-diglycidyl ether) to protect carboxylic groups of HA during the preparation of ZnO-NPs (losing the healing efficiency of HA) causing difficulty in removing the residual cross-linker agent from the hydrogel matrix, high aggregation of NPs, low stability of ZnO-NPs, and harmful effects of NPs on mechanical properties of the prepared matrix.[37]

To the best of our knowledge, an *in situ* process in the ZnO/ hyaluronan system has not yet been reported. *In situ* synthesis of ZnO-NPs can offer a large surface area, low bulk density, and high hydrophilicity. ZnO-NPs can penetrate the HA chain and cross-link the hyaluronan macromolecule and improve the stability of HA in aqueous solution. The existence of ZnO-NPs in HA-based membranes can offer an enhancement in terms of their tensile strength and dimensional stability when used under externally applied forces. The combination of ZnO-NPs

and HA is expected to improve the properties of hyaluronan (chemical, physical, and mechanical) while increasing the duration of HA in the human body or wound dressing site.

In the present work, wound dressings based on the hyaluronan/ZnO/NP nanocomposite membrane to enhance the antibacterial activity and stability of hyaluronan by avoiding the rapid release of ZnO-NPs and avoid the addition of any hazardous external reducing agent to synthesize ZnO-NPs. ZnO was synthesized *in situ* through the reaction of zinc ions with hyaluronan acting as both reducing and stabilizing agents. Such a reaction resulted in a stable and robust interaction between uniformly distributed spherical ZnO-NPs and hyaluronan, as evidenced by the well-controlled ZnO-NP release. The surface morphology, structural, mechanical, and thermal response differences in HA/ZnO-NP composite membranes were analyzed using different techniques like scanning electron microscopy (SEM), X-ray diffraction (XRD), attenuated total reflectance-Fourier transform infrared spectroscopy (ATR-FTIR), thermogravimetric analysis (TGA), dynamic light scattering (DLS), scanning transmission electron microscopy (STEM), and energy-dispersive X-ray spectroscopy (EDX). Improvements in Young's modulus, water retention capacity, and hydrolytic stability have been observed compared to those of the native membrane without it.

In vitro ZnO release properties of PVA/HA/ZnO-NP and control samples were measured under physiological conditions. Antibacterial activities of PVA/HA/ZnO-NPs against *Staphylococcus aureus* (*S. aureus*), *Escherichia coli* (*E. coli*), and *Enterobacter aerogenes* (*E. aerogenes*) were demonstrated by the disk diffusion test method. Furthermore, the effect of the PVA/ HA/ZnO-NP nanocomposite membrane on cell growth was investigated using normal human dermal fibroblasts (NHDFs) and human primary osteogenic sarcoma (Saos-2) and facilitated the development of both cells and demonstrates their low toxicity. Furthermore, it was found that the nanocomposite membrane PVA/HA/ZnO-NPs significantly promoted antimicrobial healing of infected wounds, which was never investigated previously.

2. EXPERIMENTAL PART

2.1. Materials. Sodium hyaluronate (HA; average molecular weight, 1.75 MDa) from *Streptococcus pneumoniae* was provided by Contipro a.s., Czech Republic. PVA (weight-average molecular weight, 85−99 kDa) and Zn(II) acetate dihydrate was procured from Sigma-Aldrich. Sodium hydroxide (>98%), hydrochloric acid (>35%), absolute ethanol (Et; > 98%), and isopropyl alcohol [IPA; (>99.9%)] were purchased from Lachner sro., Czech Republic. All chemicals and materials for cell cultivation were obtained from Sigma-Aldrich.

2.2. Methods. *2.2.1. Preparation of the PVA/HA Membrane.* Five grams of PVA was added to 100 mL of Milli-Q water and dissolved at 80 °C for 5 h to obtain a homogenous and transparent solution from PVA. After being cooled to 25 °C, the PVA solution was mixed with hyaluronan (1%) and stirred for 5 h at 25 °C to obtain a homogeneous solution of two polymers. Solutions with different PVA/HA ratios were prepared by varying the compositions (100/0; 90/10; 80/20; 60/40; 50/50; 40/60; 20/80; 10/90; and 0/100). Then, the solutions were poured into Petri dishes at 25 °C at different intervals of time to obtain PVA/HA composite membranes without ZnO-NPs.

2.2.2. In Situ Synthesis of Zinc Oxide Nanoparticles. ZnO-NPs were prepared by the *in situ* process using hyaluronan (HA) as stabilizing and capping agents to prevent the aggregation of ZnO-NPs during the preparation process. Different concentrations of Zn-(CH₃COO)₂·2H₂O were added to 1% sodium hyaluronate (HA) and stirred for 5 h at 80 °C. Then, a certain amount of 5% PVA solution was added to the mixture and stirred at 80 °C to obtain a completely homogeneous solution from PVA/HA/Zn acetate. The pH of the reaction mixture was increased to 8 using an ammonium hydroxide solution. The solution turned from transparent to a white homogeneous solution without precipitation, depending on the concentration of zinc ions, indicating the formation of ZnO-NPs into the PVA/HA matrix. NPs were synthesized according to eqs 1−3.

$$NH_3 + H_2O \rightarrow NH_4^+ + {}^-OH \tag{1}$$

$$Zn(CHOO)_2 + 2{}^-OH + HA \rightarrow HA/Zn(OH)_2 + H_2O \tag{2}$$

$$HA/Zn(OH)_2 + {}^-OH + PVA$$
$$\rightarrow PVA/HA/ZnO - NPs + {}^-OH \tag{3}$$
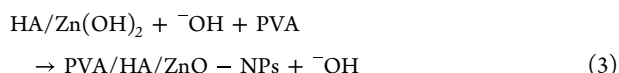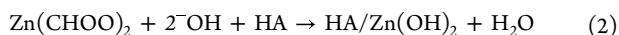
The nanocomposite membrane (PVA/HA/ZnO-NP) was fabricated using different concentrations of zinc acetate, as shown in Table S1 and Scheme 1. The solution of PVA/HA/ZnO-NPs was centrifuged at 1000 rpm for 30 min at rt to remove air bubbles. Nanocomposite PVA/HA/ZnO-NP solutions were casted into Petri dishes at room temperature for 2 days to obtain transparent membranes.

3. CHARACTERIZATION OF NANOCOMPOSITE MEMBRANES

Swelling Percentage (%). The membranes were cut into small pieces (1 × 1 cm), weighed, and then placed in glass vials immersed in water or phosphate-buffered saline (PBS) solutions and incubated at 37 °C. At regular time intervals (1, 3, 6, 12, 24, 48, 72, 96, and 120 h),[11] the PVA/HA/ZnO-NP membranes were removed, and the membranes were dried with a filter paper to remove excess water or PBS from the membrane surface. The percentage of swelling (%) of the PVA/HA/ZnO-NP nanocomposite membrane was calculated from eq 4.

$$\text{swelling ratio} = \frac{W_s - W_d}{W_d} \times 100 \tag{4}$$

where W_s is the weight of the swollen membrane and W_d is the weight of the dry membrane; each value is averaged from three parallel measurements.

Hydrolytic Stability. The weight loss of the nano-composite membranes was determined gravimetrically under physiological conditions (PBS, water, pH = 7.5, 37 °C). After different times (0.4, 0.5, 1, 2, 4, 6, 15, 21, and 30 days), the immersed membranes were removed and washed well with Milli-Q water to remove any attached salts from the membrane surface and then freeze-dried for 2 days at − 90 °C. The weight loss of the composite membranes was calculated according to eq 5.

$$\text{Weight loss} = \frac{W_i - W_f}{W_i} \times 100 \tag{5}$$

where W_i is the weight of the membrane after various times and W_f is the weight of the starting dry membrane. Each value was averaged from three parallel measurements.

***In Vitro* Measurement.** The biocompatibility and cell viability of the membranes were measured using NHDFs and human primary osteogenic sarcoma (Saos-2). NHDF was isolated from skin sections of plastic surgery with the approval of the Ethics Committee of the University Hospital Olomouc and the consent of the patient, Olomouc, Czech Republic. The study was carried out according to the Code of Ethics of the World Medical Association. The morphology and origin of the cells were authenticated in the Histology Department of the University Hospital Olomouc. NHDFs were grown in Dulbecco's modified Eagle's medium supplemented with 10% fetal bovine serum (FBS) and 1% penicillin−streptomycin under standard culture conditions (37 °C, 5% CO₂, and 95% humid air). Cells were used between the second and third passages.[38,39]

The Saos-2 cell line was obtained from the European Collection and Authenticated Cell Culture (ECACC) and cultivated according to the protocol in McCoys 5A (modified) medium supplemented with 10% FBS and 10% penicillin−streptomycin under standard culture conditions (5% CO₂, 37 °C).[40] Reduction of the tetrazolium salt, 3-(4-dimethylthiazol-2-yl)-2,5-diphenyltetrazolium bromide (MTT) was used as a parameter for cytotoxicity assessment. MTT was reduced by intracellular dehydrogenases of viable living cells that led to the formation of purple formazan crystals, which are insoluble in aqueous solutions. After the solution in an organic solvent, the absorbance was monitored. Cells in 96-well microplates were treated with tested materials extracted on a final membrane of 62.5, 125, 250, 500, and 1000 μg/mL and quantified after 24 h. As a control, cells were used with only the cultivation medium.

After the incubation period, the medium was removed and a serum-free medium supplemented with MTT (5 mg/mL) was applied directly to the cells for 2 h (37 °C, dark). The solution was removed, and the crystals were dissolved again in dimethyl sulfoxide with −NH₃ (1%, v/v). The absorbance was measured at a wavelength of 540 nm (Tecan, Czech Republic). Furthermore, live/dead staining was performed on NHDF cells. The selected membranes were fitted and placed on the bottom of eight well plates (Chamber slide), sterilized under UV-light for at least 15 min, and NHDFs were added. The samples were incubated for 5 min with a staining solution (2 mg/mL propidium iodide, 5 mg/mL fluorescein diacetate in PBS). Finally, before imaging with fluorescent microscopy, it was rinsed with PBS.

***In Vitro* Antibacterial Measurement.** The antibacterial activity of PVA, PVA/HA (40/60), and PVA/HA/ZnO3 was measured by the Kirby−Bauer disk diffusion assay under standard conditions.[13,14,39] The antibacterial properties of different membranes were measured using different types of bacteria (G +/−). *S. aureus* (as a model-positive bacterium), *E. coli* (as a model-negative bacterium), and *E. aerogenes* (as a model-negative bacterium) maintained at 37 ° C for 1 day during the incubation period. 1×10^6 colony formation units (CFU)/mL was utilized for the antibacterial assay. Both strains of bacteria were first inoculated in the Mueller−Hinton broth[14,38] and incubated in a shaking incubator at 37 ° C at an agitation speed of 500 rpm. After 12 h, the bacterial suspensions were diluted to achieve an OD_{600} value of 0.05. The medium was poured into sterilized Petri dishes and 200 μL of bacterial species was spread on the agar surface after solidification and each sample [control, native PVA, PVA/HA (40/60), and PVA/HA/ZnO3] was immersed for 1 h at 5 ° C to allow good diffusion and then incubated for 24 h under optimal conditions in an incubator at 37 °C. The diameters of the inhabitation zone (as indicated by the area surrounding the dressing where no bacterial growth is observed) were measured.

***In Vivo* Measurements.** The wound closure efficacy of the nanocomposite membrane (HA/ZnO-NPs) was evaluated in rats weighing 200 to 250 g. PVA/HA membranes (40/60), PVA/HA/ZnO1, and PVA/HA/ZnO3 membranes were used and compared with the control sample (cellulose gauze). All rats were randomly divided into four groups: *S. aureus-infected* [control; PVA/HA (40/60); PVA/HA/ZnO1; and PVA/HA/ZnO3] groups. After anesthetization with ketamine (50 mg/kg) and xylazine (15 mg/kg) by intraperitoneal injection,[12,38,41] the dorsal region of the rats was shaved and the back hair was completely removed using a sodium sulfide solution (10%) for 10 min. The area was then antiseptically prepared with a 2% Betadine solution and 60% ethyl alcohol. Round full-thickness skin wounds (3 cm in diameter) were created in the dorsum of each rat for the optical observation of wound healing. 500 μL of *S. aureus* or suspension (1.0×10^6 CFU/mL) was applied to create infected wounds. On the following day, the infected wounds were divided into four groups ($n = 4$) that were topical, group I with cellulose gauze dressing, group II with PVA/HA (40/60), group III treated with (PVA/HA/ZnO1), and group IV treated with PVA/HA/ZnO3. The wounds became severely infected 48 h after the addition of the bacterial suspensions. For the first 2 days, all wounds were covered with sterile gauze. Then, when the infection groups became infected, the rats in each group were covered with different membranes [PVA/HA (40/60); PVA/HA/ZnO1, and PVA/HA/ZnO3]. All materials were covered and fixed with elastic adhesive tape. The dressings were changed and the wound sizes were measured every 3 days. The wound closure rate was determined by eq 6.

$$\text{Degree of wound contraction (\%)} = \frac{A_0 - A_x}{A_0} \qquad (6)$$

where A_0 is the wound area on day 0 and A_x is the wound area at the specified time of surgery.

Statistical analysis for the determination of the difference between the three groups was analyzed by one-way ANOVA (using the Microsoft Excel data analysis plugin) in all experimental samples, and at least three to three replications

from each sample of each day point were analyzed. All data are presented as mean values with their standard error indicated (mean ± SE).

4. RESULTS AND DISCUSSION

4.1. Preparation of Nanocomposite Membranes. The nanocomposite membranes were fabricated *via* a casting−evaporating method. Zinc oxide (NPs) nanofillers were used in the mixture of the PVA/HA composite matrix. Scheme 1a shows the chemical structure of hyaluronan with intra- and inter-hydrogen bonds between the functional groups of HA. First, zinc ions interacted with HA carboxylic groups through the coordination interaction, and then increasing the pH of the reaction medium to 8. Zinc ions (Zn^{2+}) were chemically attached through coordination bonds with COO^- of HA and $-OH$ of PVA (Scheme 1b). In the last step, the reaction temperature was increased up to 80 °C to facilitate the nucleation and growth of ZnO-NPs. The particle size of the NPs was approximately 50 ± 10 nm with a spherical shape and a high polydispersity. Table S1 shows the chemical composition of the membranes with and without *in situ* synthesis of ZnO-NPs using different ratios of volume fraction (V_f) of NPs.

4.2. Physiochemical Properties of Nanocomposite Membranes. Figures 1a and S1 show the FTIR spectra of native PVA, HA, and PVA/HA/ZnO-NP membranes. The spectrum of native PVA showing a high broadband at 3282 cm^{-1} was related to hydroxyl stretching vibration modes of $-OH$ of PVA chain.[4,42−45] In native PVA, the 1657 cm^{-1} band was attributed to COO^- groups because residual acetate groups remained after PVA manufacturing due to the hydrolysis of polyvinyl acetate (the degree of hydrolysis of native PVA was about 95%). Different peaks at 2940−2901 cm^{-1} were related to the PVA backbone's symmetrical and asymmetrical methylene groups.[4,10,12,46] The native HA membrane shows a broad peak at 3390 cm^{-1} related to the vibrational modes of $-OH$ and $-NH$.[22,47] However, in the HA membrane, this band appeared to be broader and less intense than PVA because it participated in intra/intermolecular hydrogen bonding between hyaluronan chains (Scheme 1b). The bands between 1734 and 1595 cm^{-1} that appeared in the native HA membrane correspond to the superposition of the amide I and II bands and the various carbonyl and carboxyl groups.[11,13,48,49] The PVA/HA composite membrane (40/60) shows a broad peak at 3331 cm^{-1} with less intensity than PVA and HA indicating that the intensity of the OH group was decreased due to the physical interaction between PVA and HA chains in the composite matrix (Figures 1a and S1). Moreover, the peaks at 2938 and 2907 cm^{-1} were shifted to 2887 and 2859 cm^{-1}; after *in situ* preparation of ZnO-NPs, due to the intermolecular hydrogen bond between PVA/HA functional groups and ZnO-NPs. Interestingly, the band related to the carboxylic groups of HA disappeared after *in situ* syntheses of ZnO-NPs indicating the strong coordination bonds between $-COO^-$ of HA and NPs (Figures 1a and S1). The amide I absorption peaks at 1653 cm^{-1}, amide II peaks at 1560 cm^{-1}, and amide III peaks at 1300 cm^{-1} were characteristic of the hyaluronan macromolecular chain structure.[13,23,50]

XRD patterns for membranes PVA/HA and PVA/HA/ZnO-NPs are shown in Figures 1b and S2. Native HA and PVA membranes show only broad scattering peaks at $2\theta = 15-25°$ for HA and slightly sharp peaks at 19.82° for the PVA chain.
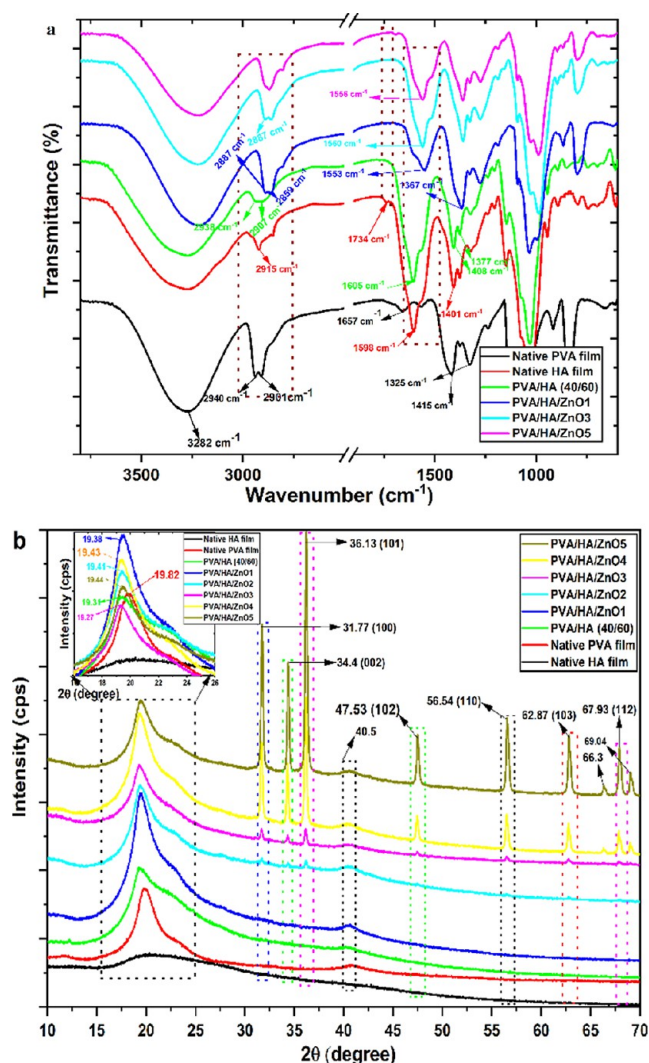
Figure 1. ATR-FTIR spectra of the nanocomposite membrane (a) and XRD patterns of PVA/HA membranes in the presence and absence of ZnO-NPs (b). (a) Native PVA film (black); native HA film (red); PVA/HA (40/60) film (green); PVA/HA/ZnO1(blue); PVA/HA/ZnO3 (aqua); PVA/HA/ZnO5 (pink). (b) native PVA film (black); native HA film (red); PVA/HA (40/60) film (green); PVA/HA/ZnO1(blue); PVA/HA/ZnO2 (aqua); PVA/HA/ZnO3 (pink); PVA/HA/ZnO4 (yellow); and PVA/HA/ZnO5 (Shada).

The composite membranes of PVA/HA (40/60) with different ratios between PVA and HA show a characteristic pattern of an amorphous phase with a typical prominent peak between $2\theta = 16-26°$ and a peak related to PVA that slightly shifted after being mixed with HA (Figures 1b, and S2), due to the synergistic performance between PVA and HA macro-molecular chains.[13,23,51] Figure 1b shows XRD of nano-composite membranes with different peaks appearing at $2\theta = 31.77, 34.4, 36.13, 47.53, 56.5, 62.87, 66.3, 69.04,$ and $67.93°$ corresponds to the ZnO-NP lattice. There was no new peak or peak shift compared to native PVA and PVA/HA (40/60) indicating that the PVA/HA/ZnO-NPs nanocomposite membranes consisted of two-phase structures, that is, composite and nanoparticles. The peak intensity of NPs in PVA/HA/ZnO NPs increased with an increase in the V_f content of NPs (Figures 1b and S2). These results indicated that *in situ* synthesis of ZnO-NPs using polyvinyl alcohol (PVA)/HA did not change the structural uniformity of the

matrix polymer blend but improved the molecular ordering in the amorphous polymer blend matrix, as shown in Figures 2a,b and S3, explored the swelling properties of PVA/HA composite membranes in the presence and absence of *in situ* ZnO-NPs under physiological conditions (PBS, pH 7.5, 37 °C). The native PVA membrane shows a lower swelling percentage compared to the native HA membrane. The swelling rate was increased by increasing the amount of HA in the membrane matrix. Maximum swelling was obtained in a 40/60 ratio between PVA and HA, respectively (Figure 2a). With a higher percentage of HA (20/80; 10/90; 0/100), the membranes were completely hydrolyzed in a short time. PVA/HA (40/60) was selected to prepare ZnO-NPs *in situ* (Figure 2b). The nanocomposite membrane (PVA/HA/ZnO-NPs) exhibited a high swelling percentage compared to the PVA/HA composite membrane without ZnO-NPs, due to the strong coordination interaction between the NPs, the HA, and PVA chains (Scheme 1). The swelling behavior of the nano-composite membranes decreased with an increase in the volume fraction of NPs but was still higher than that of the membrane with a ratio of 40/60 (Figure 2b).

Figure 2c,d shows the percentage of weight loss of the native PVA membrane and the membranes with different chemical compositions. Native PVA illustrations show that the lowest hydrolytic degradation rate after 30 days of incubation and weight loss was approximately 10%. Increasing the HA composition in the PVA/HA membrane decreased the stability of the membrane during the incubation time (Figure 2c). Figure 2d illustrates the effect of ZnO-NPs with different V_f on the hydrolytic stability of nanocomposite membranes. The hydrolytic stability of the PVA/HA/ZnO-NPs was improved in the presence of NPs, and the weight loss percentage decreased as the V_f of the NPs increased compared to that of PVA/HA alone. The improvement in hydrolytic stability of the membrane could be due to the coordination interaction between ZnO-NPs and different functional groups ($-COO^-$, $-OH$, and $-NH-CO-CH_3$) of the hyaluronan-PVA matrix (Scheme 1b).

The TGA curves of native PVA, HA, PVA/HA membrane, and nanocomposite PVA/HA/ZnO-NPs with different V_f values of NPs are shown in Figure S4 and Table S2. The native PVA membrane shows two stages of mass loss: stage I at 50−100 °C, which prescribes the evaporation of moisture (approximately 5.2%) and the decomposition stage, and the second prescribes the release of the PVA backbone of bonded water.

The native PVA membrane lost about 70% of the weight up to 300 ° C (Figure S4a,b). At the end of the decomposition of native PVA membrane, the solid residue was approximately 9.7% (Table S2). Wound dressing membranes of PVA/HA with different ratios between PVA and HA show more thermal stability with a lower amount of HA (10, 20%). At a higher content of HA (50, 60%), the stability of the membrane decreased slightly (Figure 4a,b and Table S2) due to a partial breakage of the high molecular structure of hyaluronan in the range of 200−300 ° C. The PVA/HA membranes also show different weight loss events (Table S2) due to the dehydration of the −OH groups in the PVA and HA backbone chains, followed by the generation of volatile organic compounds and the formation of a conjugated unsaturated polyene compound structure.[4,10] At higher temperatures above 500 °C, another stage of degradation predominates by producing lesser amounts of hydrocarbon-related products, such as alkenes,
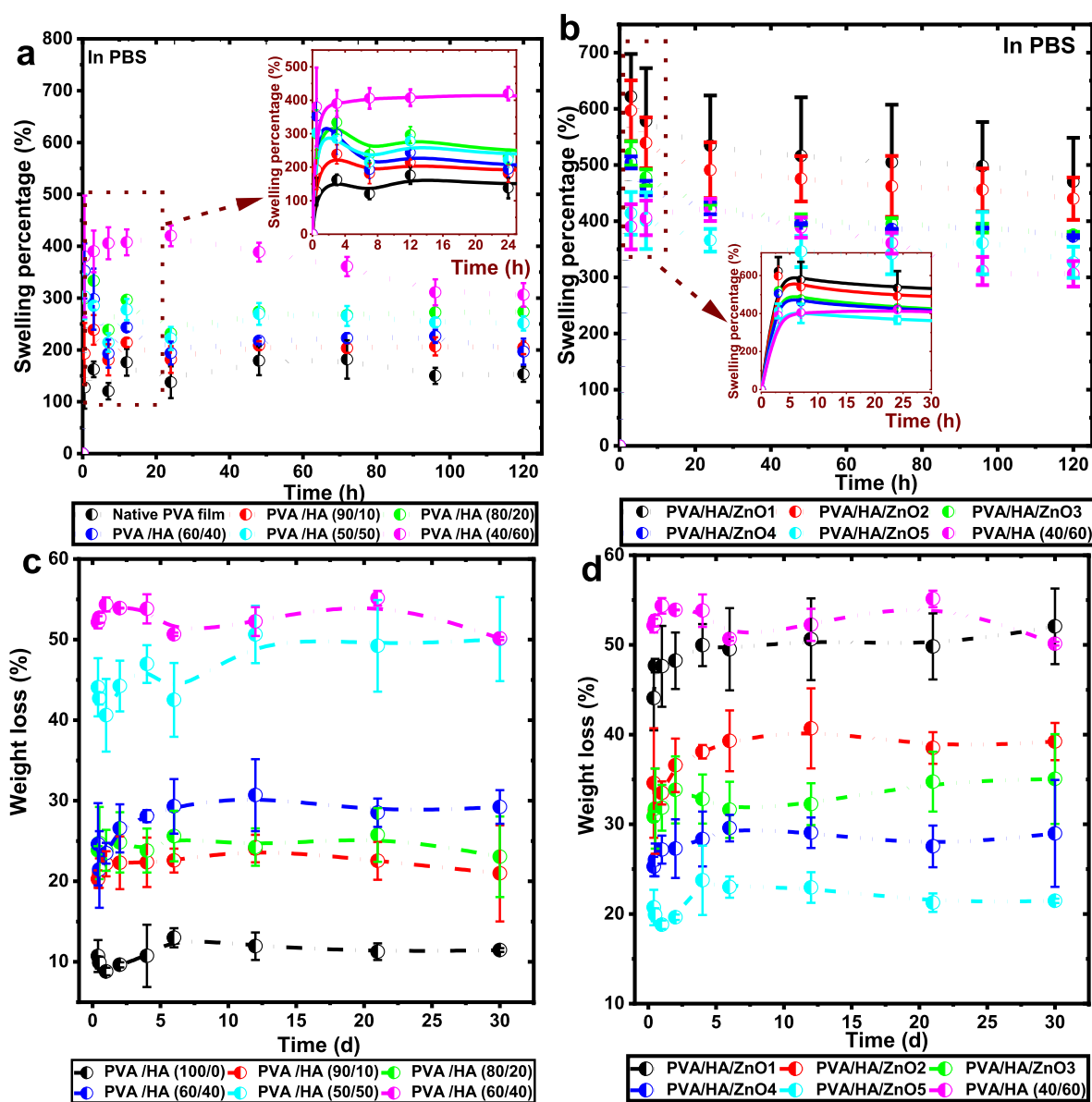
Figure 2. Representative swelling percentage of native PVA and different ratio between PVA/HA in the absence of ZnO-NPs (a); swelling percentage of native PVA/HA (40/60) in the presence of different volume fractions of ZnO-NPs (b); weight loss percentage of native PVA and different ratios between PVA/HA in the absence of ZnO-NPs (c); and weight loss percentage of native PVA/HA (40/60) in the presence of different volume fractions of ZnO-NPs (d).

alkanes, and aromatic compounds (Figure S4a,b and Table S2).

In situ synthesis of ZnO-NPs using PVA/HA exhibited composition stages different from those of native PVA/HA membranes. The presence of NPs shows an improvement in nanocomposite membrane stability compared to native PVA, HA, and PVA/HA matrixes (Figure S4c,d, and Table S2). The residual percentage in the presence of NPs is much higher than in the membranes without NPs (Table S2). This weight retention revealed the presence of ZnO-NPs and the inorganic portion of metal traces in the nanocomposite composition.

4.3. Optical, Rheological, and Mechanical Properties of Nanocomposite Membranes. Figure 3a explores the optical transmittance of native PVA, HA, and PVA/HA composite membranes and PVA/HA/ZnO-NP nanocomposite membranes. The native PVA membrane shows high optical transmittance compared to HA and other composite

membranes (Figure 3a). The optical transmittance of the composite membrane decreased with increasing HA content due to the physical interaction between PVA and HA chains.[51,52] In the PVA/HA/ZnO-NP nanocomposite membrane, optical transmittance was decreased due to the white color behavior generated after the synthesis of the NPs compared to PVA/HA (40/60) (Figure 3a).

Figure 3b illustrates DLS of the composite using different V_f values of the NPs. All NP ratios show small particles with a range of 50 ± 10 nm. The DLS of PVA/HA (40/60) exhibited more aggregation (size approximately 300−450 nm) between the molecular chains of PVA and HA due to the interaction of the macromolecular chains of PVA and HA. In PVA/HA/ZnO-NPs, the chain size decreased compared to PVA/HA (40/60) due to a strong coordination between the matrix chain (PVA/HA) and ZnO-NPs that destroys the physical interaction between the polymeric chain of both polymers
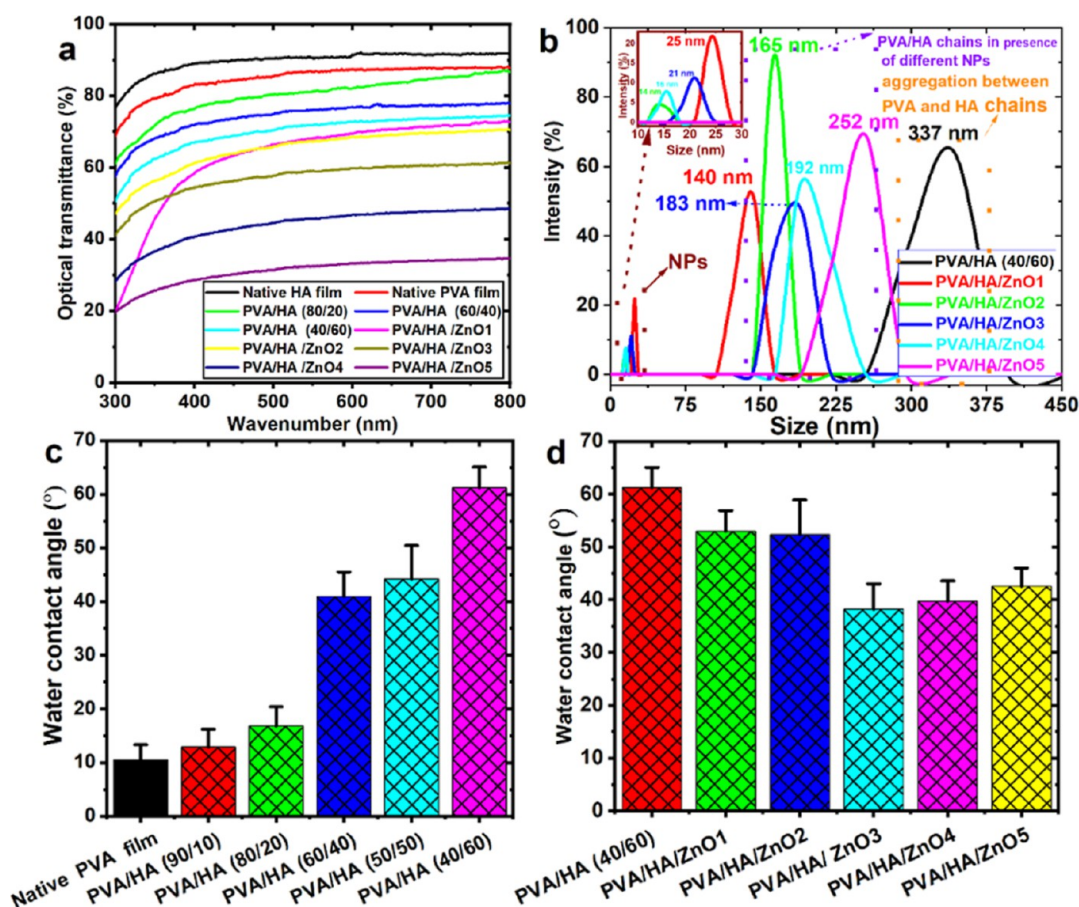
Figure 3. Optical transmittance, dynamic light scattering, and water CA of nanocomposite membrane in the presence and absence of different volumes of ZnO-NPs. (a) Optical transmittance of PVA/HA membrane with and without ZnO-NPs; (b) DLS of PVA/HA (40/60) with different volume fractions of ZnO-NPs; (c) water CA of native PVA and PVA/HA different ratios; and (d) water CA of PVA/HA with different volume fractions of ZnO-NPs.

(Figure 3b and Scheme 1). The storage stability of HA/ZnO-NP nanocomposite dispersion stabilized using sodium hyaluronate was checked after storage for 2 weeks. From the DLS measurements (data not shown), the size of ZnO-NPs in all V_f of NPs was the same as the initial size of ZnO-NPs. The keeping size of NPs due to hyaluronan worked as the keeping agent preventing the agglomeration of ZnO-NPs.

Figure 3c,d explores the water contact angle (CA) (°) of native PVA, PVA/HA (100/0, 90/10, 80/20, 60/40, 50/50, and 40/60), and PVA/HA/ZnO-NPs and V_f of NP (ZnO1, ZnO2, ZnO3, ZnO4, and ZnO5). The CA was slightly increased by increasing the HA ratio in the membrane matrix. An increase in the CA may cause the particle to flocculate from the dispersion or to float over to the surface. The native hyaluronan membrane did not stabilize for a longer time in water and above the 40/60 ratio all composite membranes completely hydrolyzed in a few minutes. Figure 3d illustrates the CA of the membrane with different concentrations of NPs. The CAs of PVA/HA/ZnO NPs was decreased slightly with an increase in V_f due to the hydrophobic behavior of the NPs and chemical and physical interactions between the functional groups of the functional groups PVA, HA, and ZnO NPs (Figure 1a). A decrease in the CA may increase dispersibility of ZnO-NPs inside the PVA/HA matrix.

Figures 4 and S5 show STEM photos of PVA/HA solution in the presence and absence of ZnO-NPs. Composite PVA/HA exhibited higher aggregation behavior than nanocomposite

PVA/HA/ZnO-NPs due to the supramolecular structure between both backbone chains (Figures 4a−c & 3b). In the presence of a small volume fraction of NPs (V_f 0.001), a strong interaction between the NPs and the composite matrix was visualized, and the NPs were surrounded and attached within the composite matrix PVA/HA (Figures 4d−f and S5). At a higher volume fraction (0.01), the nanoparticles show a well-organized structure, and the NPs generate rod structures connected with a polymer matrix (Figure 4g−i, red ring). The nanocomposite PVA/HA/ZnO5 shows strong adhesion between the NPs and the polymer matrix with a good distribution of the NPs within the surface of the matrix. Small agglomeration was observed (Figure 3b) due to the high-volume fraction of NPs used (Figure 4k−m). The STEM results show that the ratio between PVA/HA compound to NPs with V_f (0.01) indicates a good distribution of NPs within the polymer matrix without aggregations and can be used for further biological studies.

Figure 5a shows the effect of the angular frequency (rad/s) on the storage modulus (G') and the loss modulus (G') of native PVA, HA, and membranes PVA/HA without NP. The storage modulus (G') and the loss modulus (G'') correspond to the elasticity and viscosity of the materials, respectively. The storage modulus (G') was a much larger value than the loss modulus (G') for all ratios of the blend solution and native PVA and HA, indicating a typical true solution nature. Native PVA shows the lowest viscosity compared to different PVA/
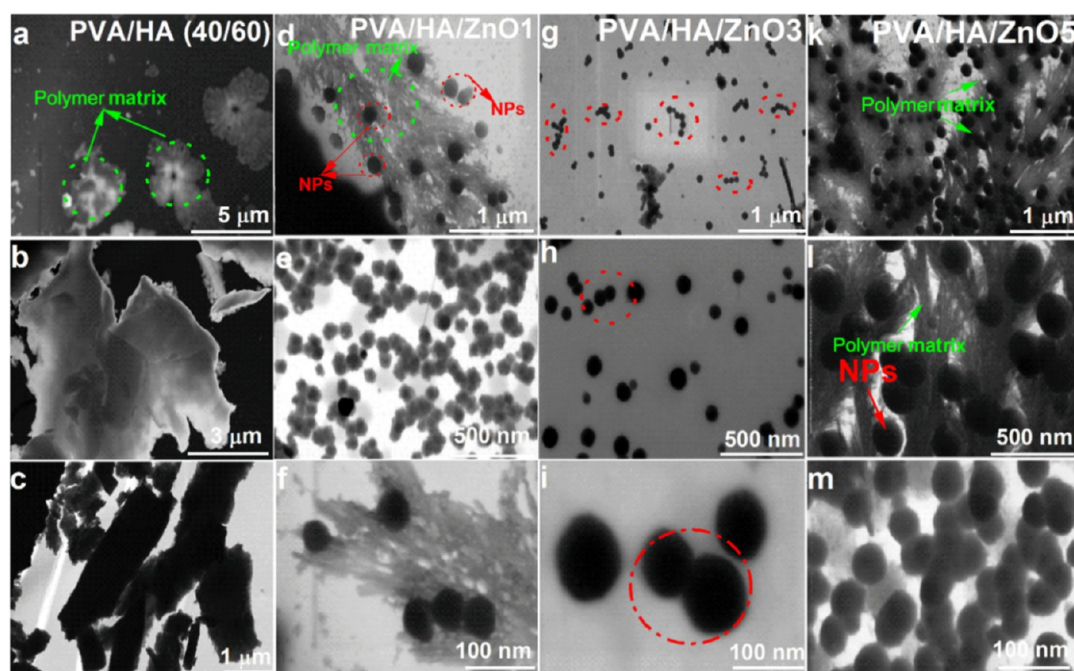
Figure 4. STEM of PVA/HA (40/60) membrane and PVA/HA/ZnO-NPs nanocomposite membranes with different volume fractions of NPs (V_f 0.001, 0.01, and 0.1). (a−c) STEM of PVA/HA (40/60) with different magnifications (5, 3, 1 μm); (d−f) STEM of PVA/HA (40/60)/ZnO1 with different magnifications (1000, 500, and 100 nm); (g−i) STEM of PVA/HA (40/60)/ZnO3 with different magnifications (1000, 500, and 100 nm); and (k−m) STEM of PVA/HA (40/60)/ZnO5 with different magnifications (1000, 500, and 100 nm).

HA composites. The viscosity of PVA/HA increased with increasing HA ratio from 10 to 80% (Figure 5a). In nanocomposite PVA/HA/ZnO-NPs with lower V_f (0.001), the viscosity increased at a lower frequency than in PVA/HA alone. At a higher V_f of NP (0.005−0.1), the viscosity decreased slightly from 9.8 to 8.4 Pa in PVA/HA/ZnO5 (Figure 5b). The decrease in viscosity at higher V_f of NPs is due to the NP−NP interaction ratio compared with that of the NP−polymer interaction. From the viscosity measurements, we can conclude that the NP filler show more physical interaction than those that are chemically bonded between the NPs and the PVA/HA matrix. An increase in the viscosity after the NPs are generated by the *in situ* process might improve the formation of networks within the membrane matrix. From the water CA, optical transmittance, and rheological measurements, the PVA/HA membrane with (40/60) was selected to continue with our studies.

Tensile testing was used to investigate the effect of the PVA/HA blend ratio on the mechanical properties of nanocomposite membranes. Furthermore, different NPs were also studied to evaluate the efficiency of improving the compatibility between the two polymers in the presence of *in situ* synthesis NPs. Figures 5c,d, S6, and S7 show the mechanical properties of native HA, PVA, and PVA/HA membranes and PVA/HA/ZnO-NP nanocomposite membranes with different V_f values of NP. The native HA membrane shows poor mechanical properties with Young's modulus of only 0.07 ± 0.01 MPa with elongation at break (EB) of 160.4 ± 7.4%. The native PVA membrane shows Young's modulus of 21.4 ±2 MPa and EB of about 462.8 ± 32.1% (Figure 5c). Young's modulus and tensile strength of PVA/HA membranes decreased with the increase of the HA ratio compared to the native PVA membrane (Figure S6). However, the EB of PVA/HA (40/60) increased slightly compared to another ratio of PVA and HA (Figures 5d and S6). In nanocomposite membranes with

different V_f of NPs, the Young's modulus and strength were enhanced from 4.8 ± 0.2 MPa for the PVA/HA membrane (40/60) to 13.1 ± 0.7 for PVA/HA/ZnO3 (Figure 5c). The Young's modulus was slightly decreased in PVA/HA/ZnO5 but still significantly higher by 250% than in the PVA/HA (40/60) matrix alone. The EB (%) of PVA/HA/ZnO was increased compared to the PVA/HA membrane (Figures 5d and S7). Improvement in ductility properties of PVA/HA/ZnO membranes in a high-volume fraction (V_f) of NPs (ZnO1− ZnO3) due to the superior flexibility exhibited through the physical and chemical interactions between matrix chains (PVA/HA) and NPs. The lack of improvement in elongation in a higher ratio of NPs-(ZnO4 and ZnO5) was attributed to the small aggregation with less uniform dispersion/distribution of the NP clusters interacted with the PVA/HA composite (Figure 4g−m).

Rheological properties of composite without (a) and with ZnO-NPs (b). Young's modulus and tensile strength of PVA/HA (40/60) membrane with different volume fractions (V_f) of ZnO-NPs (c); and EB of PVA/HA (40/60) with and without ZnO-NPs (d).

Figures 6 and S8 illustrates the fractured cross section of native PVA, HA, PVA/HA, and PVA/HA/ZnO-NP membranes with different V_f of NPs at different magnifications. The surface morphology of different ratios of PVA and HA shows high homogeneity, is flat and smooth, with no defects or pores appearing on the surface. The native PVA membrane shows a parallel compact structure from the cross section (Figure 6a−c) with aggregated heterogeneous formation particles that may have also influenced topography.

This behavior underlines the excellent processability and membrane-forming ability of PVA during the solvent-casting process. Small cracks without any particular order were observed on the native surface of HA (Figure 6d−f) caused by the uneven shrinkage of the hyaluronan biopolymer during
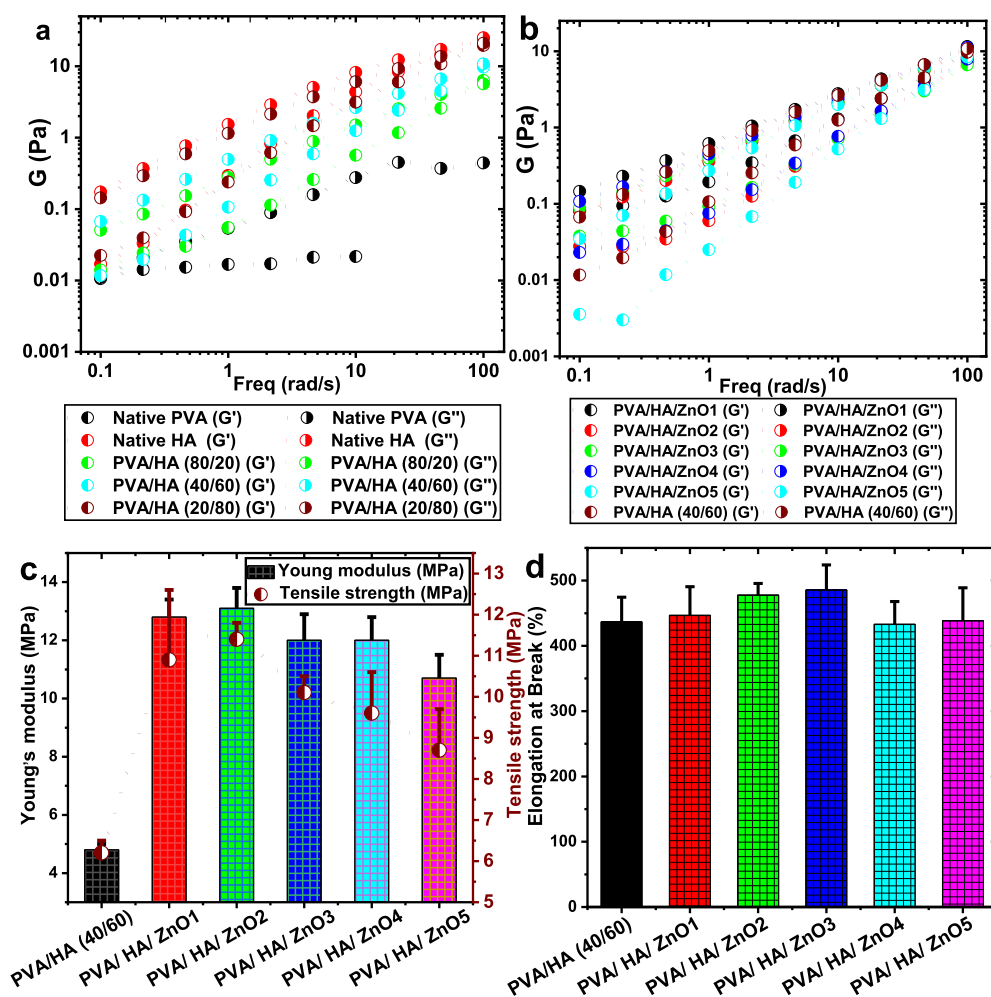
Figure 5. Rheological and mechanical properties of composite membranes with and without ZnO-NPs.

drying processes. Different blend ratios between PVA and HA (Figures 6g−I and S8) and PVA/HA with a ratio (40/60) showed flat and smooth surfaces without the surface defect (Figure 6g−i) and in the cross section, a porous structure appeared with a pore size of less than 1 μm and heterogeneous sizes (Figure 7h).

PVA/HA membranes with different ratios show a dense surface structure without fibrous forms (Figure S8). In general, the homogeneous and dense network of the mixed composite membrane suggested a high miscibility between the PVA and HA solutions. Figure 6g−o shows the fracture surface of the nanocomposite membranes with different V_f of ZnO-NPs (V_f 0.001, 0.1). At lower V_f 0.001 (Figure 6g−i), the NPs were well disturbed and strongly attached within the polymer composite matrix (Figure 4d−f) without appearing agglomerated. ZnO-NPs show a highly uniform dispersion in the polymer matrix at a lower concentration of NPs (ZnO1−ZnO3, Figures 4a−I and S8). At high V_f of NPs (ZnO4 and ZnO5) with small aggregation into a polymer matrix (Figures 4k−m and S8). The weight percent of Zn inside the nanocomposite membranes increased with increasing concentration of ZnO-NPs (Figure S9).

Figure S10 shows the EDX mapping distribution of NPs within the polymer composite matrix. The overall element compositions of the hybrid nanocomposite confirmed the homogeneous distribution of the ZnO-NPs into a composite matrix. The concentration of NPs increased with an increase in the concentration of zinc ions (Figure S10).

Figure S11 shows the release of ZnO-NPs from nano-composite membranes under physiological conditions (PBS, pH 7.5, 37 °C). The ideal release profile of bioactive composite or drugs was a combination of rapid initial release and slower sustained release over a longer period.[53,54]

In the first interval, the release of NPs was slow at a lower concentration of NPs and increased significantly with increased V_f. After 6 h, the higher V_f exhibited a fast release of NPs compared to the low V_f. The increases of ZnO released as a result of the partial NPs−NPs and low physical bonding between NPs and polymers could reduce the interaction between the NPs and functional groups of the polymer matrix. After 24 h of incubation, NP release was stable. In the first stage, a slight increase might be due to the dissociation of the physical bond (non-bonded NPs) within the polymer matrix. After 24 h, the coordination of NPs with the polymer matrix started to dissociate (Figure S11).

The XPS measurements confirm and explain the interaction between the HA and ZnO-NPs. The XPS measurements were carried out to obtain more detailed information about elemental compositions and chemical states of pure native HA, PVA/HA (40/60), and PVA/HA (40/60)/ZnO3, and the results are presented in Figure S12. Figure S12a shows the survey scan of native HA, PVA/HA (40/60), and PVA/HA (40/60)/ZnO3. In Figure S12b,c, the peaks at 1022.1 and
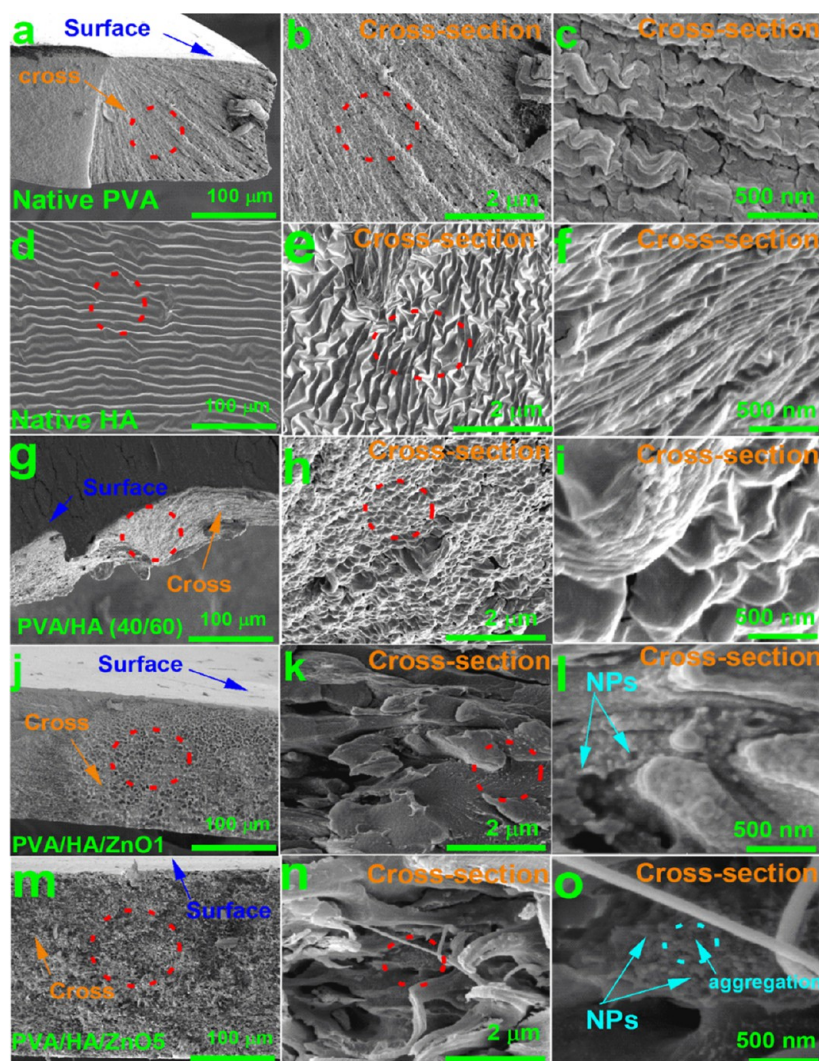
Figure 6. SEM of the fractured cross section of native PVA and nanocomposite membrane at different magnifications. (a−c) SEM of native PVA membrane at different magnifications (100 μm, 2 μm, 500 nm); (d−f) SEM of native HA membrane at different magnifications (100 μm, 2 μm, 500 nm); (g−i) SEM of PVA/HA (40/60) at different magnifications (100 μm, 2 μm, 500 nm); (j−l) SEM of PVA/HA (40/60)/ZnO1 at different magnifications (100 μm, 2 μm, 500 nm); and (m−o) SEM of PVA/HA (40/60)/ZnO5 at different magnifications (100 μm, 2 μm, and 500 nm).

1045.1 eV correspond to the binding energy of Zn $2p_{3/2}$ and Zn $2p_{1/2}$, respectively, indicating the presence of Zn^{2+} in the ZnO wurtzite structure and implying the successful incorporation of ZnO-NPs in the HA backbone. Figure S12c−e shows typical C 1s peaks of native HA, PVA/HA (40/60), and PVA/HA (40/60)/ZnO3, respectively, which have been deconvoluted into five peaks by Gaussian distribution. The high-resolution C1s spectrum of pure HA (Figure S12c) reveals that there were five main components arising from the C/C/H, C/O, C−N, C=O, and O−C=O groups. The five peaks of PVA/HA (40/60)/ZnO3 (Figure S12e) were shifted compared to the native membrane of PVA/HA (Figure S12d), indicating the substantial introduction of ZnO-NPs into the HA chain. The typical O 1s peaks of three different samples (pure native HA, PVA/HA (40/60), and PVA/HA (40/60)/ZnO3 are depicted in Figure S12f−h), which have been deconvoluted into four peaks for HA and PVA/HA (40/60) and five peaks for PVA/HA/ZnO3 by Gaussian distribution. The binding energy peaks of PVA/HA/ZnO3 are shifted compared to the native HA and PVA/HA peaks, as shown in

Figure S15h. A new peak appeared at 528.13 eV was assigned to the O^{2-} ions in the ZnO lattice and the second peak located at around 531.13 eV was related to OH$^-$ groups attached on the surface of ZnO-NPs. These results (Figure S12) further indicated that HA was the product of ZnO-NPs that was successfully bound to functional groups of hyaluronan chains.

4.4. Biocompatibility, Antibacterial Activity, and Healing Properties of Nanocomposite Membranes. We evaluated the biocompatibility of the nanocomposite membranes using the primary culture of NHDF and Saos-2 cell lines. Figure 7a−c shows the cell viability of different membrane compositions without and with NPs. Different concentrations of PVA/HA membranes (40/60) (62.5, 125, 250, 500, and 1000 μg/mL) were used to confirm the maximum membrane concentration that could be applied without showing toxicity. Cell viability was enhanced (Figure 7a) using high concentrations of composite membranes (1000 μg/mL) at high HA content in the PVA/HA composite matrix. Figure 7b illustrates the biocompatibility of nanocomposite membranes in the presence of different V_f of NP. Different
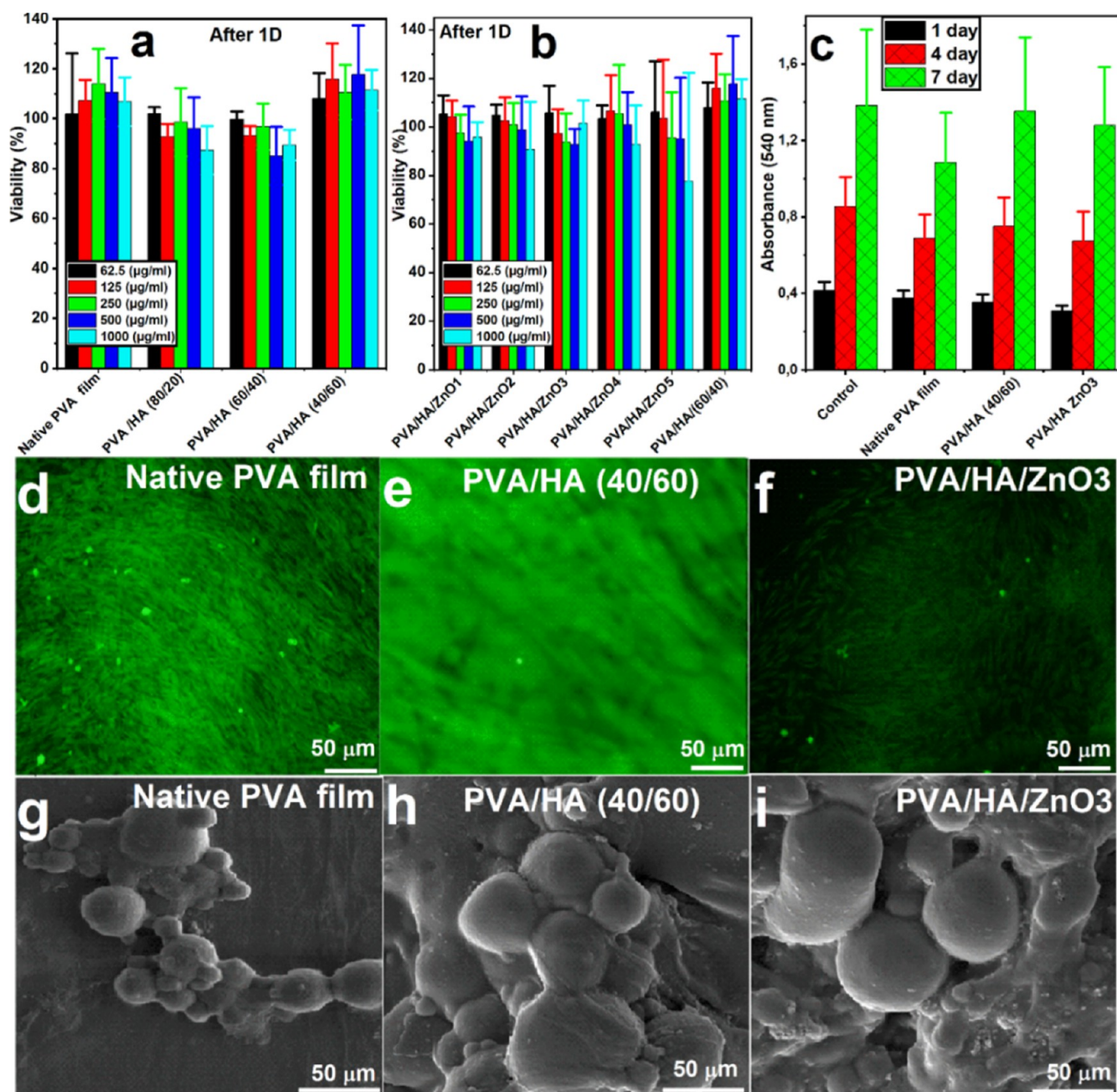
Figure 7. *In vitro* live/dead biocompatibility study of the membranes in the presence and absence of ZnO-NPs incorporated with NHDF (green: live cells, red: dead cells). (a) Results of NHDF viability using different membrane compositions without NPs; (b) effect of different NP V_f (62.5− 1000 µg/mL) on cell viability after 1 day of seeding; (c) cell viability of the selected membranes in the presence and absence of NP after 7 days of seeding with NHDF; (d−f) confocal images of cell-laden membranes [native PVA; PVA/HA (40/60) and PVA/HA/ZnO3] after seeding with NHDF for 1 week. (g−i) SEM images of seeding composite membranes with NHDF after 1 week of seeding.

concentrations (62.5, 125, 250, 500, and 1000 µg/mL) of the nanocomposite membranes were used to select the optimal concentrations without cytotoxicity.

In Figure 7b, the PVA/HA/ZnO3 nanocomposite membrane with 500 µg/mL shows high cell compatibility with NHDF. At a higher concentration of 1000 µg/mL, the nanocomposite membrane was slightly toxic, and the percentage of cell viability was reduced by 20% compared to the concentration of 500 µg/mL. Figure 7c shows the relationships between cell compatibility and the chemical composition of the membranes at different seeding times (1−7 days) with a concentration of 500 µg/mL compared to the

control sample. The presence of high V_f of NPs did not show any cytotoxicity against NHDF cells. A higher concentration of ZnO-NPs (0.05−0.1) improved NHDF cell viability compared to all incubation periods (1−7 days). The biocompatibility of the nanocomposite membranes in the presence of NPs confirms that the membrane was safe, and the procedures used to synthesize the nanocomposite membrane were completely eco-friendly for different cells (Figure 7c). Figure S13 shows the cytotoxicity of the native PVA membrane and nanocomposite membranes with different V_f of NP after 1 day of seeding with Saos-2 cells. Native PVA shows non-toxic properties against Saos-2 cells after seeding compared to the

control sample. The membrane of PVA/ZnO3 without HA has improved biocompatibility using Saos-2 cells compared to the native PVA membrane (Figure S13). The PVA/HA membrane (40/60) shows good biocompatibility with high cell viability compared to the control and native PVA membrane (Figure S13).

Figure S13 explores the effect of V_f NP on the viability of Saos-2 cells of different membrane concentrations (62.5 to 1000 μg/mL). The nanocomposite shows high biocompatibility against Saos-2 cells. Cell viability decreased with a high V_f of PVA/HA/ZnO5 and a high concentration (1000 μg/mL) compared to the lower V_f of NP and control samples. Confocal electron microscopy was used to visualize live/dead cells attached to the nanocomposite membranes, as shown in Figure 7d–i. Figure 7d–f provides the photographs from confocal microscopy of native PVA, PVA/HA (40/60), and nanocomposite PVA/HA/ZnO3 after 7 days of seeding with NHDF with high cell viability. NHDF cells show around morphology with the cell bundle during the study period after 1 week. Figure 7g–i shows the SEM photos of adhered NHDF cells in native PVA and PVA/HA and PVA/HA/ZnO-NP3 membranes. NHDF shows a spherical morphology with strong adhesion on the surface of composite membranes and a good connection between cell–cell interactions.

Figures S14 and S15 show the antibacterial activity and inhibition zone of control sample, PVA membrane, PVA/HA (40/60) membrane, and the PVA/HA/ZnO3 nanocomposite membrane against a different type of bacteria ($\pm$ G). The native PVA membrane did not show antibacterial activity against ($\pm$ G) bacteria. Composite membrane PVA/HA (40/60) indicates slightly antibacterial activity against *E. aerogenes* bacteria and *E. coli* and zero inhabitation zone against *S. aureus*. The antibacterial activity of PVA/HA against *E. aerogenes* and *E. coli* membranes was due to the bacteriostatic properties of hyaluronan against different types of bacteria.[32,55,56] The nanocomposite PVA/HA/ZnO3 membrane (Figure S15) shows high antibacterial properties against various types of bacteria (*E. aerogenes*, *E. coli*, *S. aureus*). Antibacterial properties of the nanocomposite membranes due to the synergistic properties between PVA/HA and ZnO-NPs. Different mechanisms explain the antimicrobial properties of ZnO-NPs.[13,57]

The electron and positively charged holes of ZnO-NPs undergo a series of relaxation reactions with oxygen and water on the surface of the NPs to generate reactive oxygen species (ROS) with high surface reactivity and then the ROS penetrated the cell membrane of the bacteria, causing cell membrane destruction.[32] Hydrogen peroxide could penetrate the cell bacteria membrane, causing DNA and protein destruction in the cell membrane.[58,59] The antibacterial activity of composite membranes (PVA/HA/ZnO3) was due to the release of zinc ions from the matrix in a wet environment that penetrates the cell membrane of bacteria-produced protein denaturation. In the meantime, penetration of zinc ions through the cell walls of bacteria results in loss of cell proliferation and disorder of energy metabolism of bacterial substances caused by the internalization of ZnO-NPs.[60–63] Cellulose dressing gauzes that are now widely used in clinical practice could act as a physical barrier and have no antimicrobial performance. Therefore, the wound healing performance of PVA/HA nanocomposite membranes in the presence and absence of ZnO-NPs was further investigated by an *in vivo* test that included four groups: *S. aureus*-infected wounds [control, PVA/HA (40/60), PVA/HA/ZnO-1, and PVA/HA/ZnO-1].

To the best of our knowledge, this study is the first use of PVA/HA/ZnO-NP-based membranes as dressings in animal wound healing experiments. Representative photographs of the healing process are shown in Figures 8 and 9. In each group,
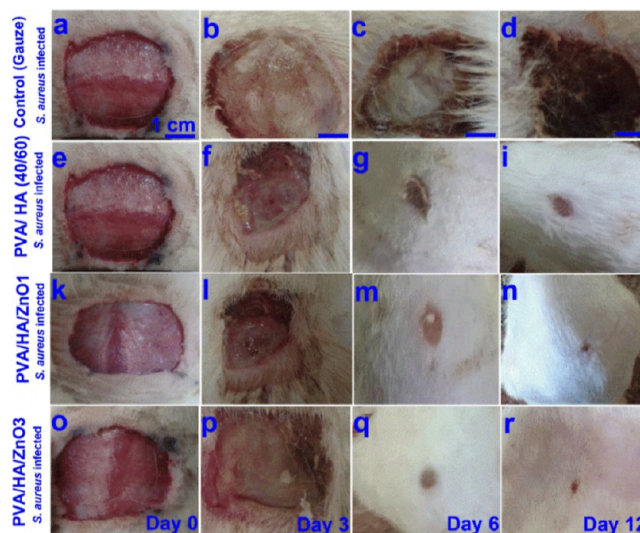
Figure 8. Photographs of the healing process of an infected wound with *E. coli* bacteria after 3, 6, and 12 days of treatments. Infected wound treated with the control (gauze), native PVA/HA without NP, and PVA/HA/ZnO with two different concentrations of NP (ZnO1 and ZnO3). (a–d) Control infected sample treated with a gauze at different treatment times (0, 3, 6, and 12); (e–i) PVA/HA (40/60) wound dressing membrane-treated infected wound at different treatment times (0, 3, 6, and 12); (k–n); PVA/HA (40/60)/ZnO1 wound dressing membrane-treated infected wound at different treatment times (0, 3, 6, and 12); and (o–r) PVA/HA (40/60)/ZnO5 wound dressing membrane-treated infected wound at different treatment times (0, 3, 6, and 12).
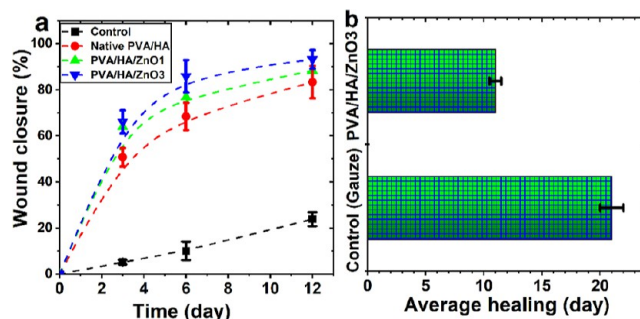
Figure 9. Effect of native and nanocomposite membranes on the closure percentage of infected wounds on the skin of rats. (a) Average percentages of wound healing per day and (b) increased wound closure revealed by nanocomposite membranes.

significant differences were observed between wounds treated with PVA/HA and PVA/HA/ZnO-NPs and with cellulosic gauzes. The wound infected with the *S. aureus* showed accelerated wound closure after treatment with PVA/HA and PVA/HA/Zn-O-NP. Throughout the treatment period, the wound size measurements and the average healing time are quantitatively illustrated in Figure 9a,b. PVA/HA (40/60) significantly improved the wound healing percentage (12 days; closure rate 55%) compared to the control sample (gauze).

Wound healing in the presence of ZnO-NPs (PVA/HA/ZnO1 and PVA/HA/ZnO3) was significantly promoted and the closure percentage increased with increasing volume fraction of zinc oxide within the matrix, demonstrating its excellent antibacterial effect on the infected wound of *S. aureus*. This was due to the interaction between the ZnO-NPs and the bacterial cell walls in the infected wounds. Furthermore, Table S3 comparatively lists the wound dressing ratio of HA/ZnO-NPs/PVA nanocomposite membrane with different wound dressing reported elsewhere. It was clear that, although the reported dressing provides satisfactory wound healing ratios, they are less efficient as compared with the membranes based on the HA/ZnO-NPs/PVA nanocomposite. The mechanism of how HA can support the migration of the cells is explained below. Briefly, HA signals in stem cells *via* CD44: HA binding to CD 44 leads to a conformational change in the receptor, which results in the activation of the intracellular fragments that phosphorylate cellular components such as calmodulin kinase (CaMK). Upon activation, the intracellular domains of CD44 form complexes with cytoplasmic proteins, such as merlin, Src, and PKC, which can trigger downstream signaling pathways, including the Raf/MEK/ERK pathway, which results in enhanced cell proliferation. In addition, activation through ankyrin, ERM, or Vav2/Tiam1 results in the activation of F-actin, which is involved in cellular migration, membrane ruffling, and stem cell differentiation. Furthermore, HA-CD44 binding can lead to cell migration through the regulation of focal adhesion complexes.[64] In conclusion, HA/ZnO-NPs/PVA nanocomposite membrane exhibits excellent antibacterial, no cytotoxicity, and excellent healing performance against an infected wound over a very short period (12 days) and may find potential applications for skin tissue regeneration and drug delivery purposes.

CONCLUSIONS

A series of hyaluronan/ZnO-NP (HA/ZnO-NPs) composite membranes could be prepared using an *in situ* approach. The strong coordination interaction between ZnO-NPs and HA was proven to prevent any leaking of NPs from the PVA/HA network and, therefore, minimize potential nanoparticle toxicity. PVA/HA/ZnO-NP hybrid nanostructure membranes offered excellent and sustainable contractibility of ZnO-NPs with an exponent depending on the zinc content. Regardless of the slow release of ZnO-NPs, PVA/HA/ZnO-NPs still exhibited significant antibacterial rates with more than 95% reduction against different types of bacteria. The nanocomposite significantly promoted infected wound healing compared to gauze from the control sample. Additionally, hybrid nanocomposite membranes HA/ZnO-NPs allowed the adhesion and growth of the fibroblast cell line (NHDF) and human primary and osteogenic sarcoma (Saos-2) with a high-volume fraction of NPs without cytotoxicity emerging in cocultures with two cell lines. In conclusion, the current study showed that PVA/HA with in situ synthesis of loaded ZnO-NPs can be produced and possesses the desired properties for wound dressing applications.

ASSOCIATED CONTENT

Supporting Information

The Supporting Information is available free of charge at https://pubs.acs.org/doi/10.1021/acsapm.2c01296.

Instruments and characterizations; preparation and chemical compositions of PVA/HA/ZnO-NPs with different volume fractions; ATR-FTIR of PVA/HA biofilm fabricated using different ratios between PVA and HA; XRD of biofilm (PVA/HA) without ZnO-NPs; swelling percentage of PVA/HA membrane without ZnO-NPs in water; TG-DTG of PVA/HA membranes without ZnO-NP and with ZnO-NPs; steps of decomposition of native PVA, HA, PVA/HA membranes and nanocomposite membranes (PVA/HA/ZnO-NPs) with different ratios of NPs; STEM of PVA/HA/ZnO-NPs nanocomposite with different volume fraction with NPs; mechanical properties of the PVA/HA composite membrane in the absence of ZnO-NPs; EB of the PVA/HA composite biofilms in the absence of ZnO-NPs; SEM of fractured cross-section of composite membrane in the absence and presence of ZnO-NPs at different magnifications; representative concentration of ZnO-NPs from cross section of the nanocomposite membrane; EDX with mapping of native PVA, HA, PVA/HA (different ratios) and nanocomposite membrane (PVA/HA/ZnO-NPs) with different concentrations of NPs; release profile of ZnO-NPs from nanocomposite membranes; XPS survey of native HA, PVA/HA (40/60) and PVA/HA (40/60)/ZnO3 nanocomposite; cytocompatibility of native PVA and nanocomposite membranes in the absence and presence of ZnO-NPs using Saos-2 cells; antibacterial performance of nanocomposite membranes against different types of bacteria; bar graph showing the effect of ZnO-NP concentration on the diameter of the zone of inhibition against Gram-positive and Gram-negative bacteria; and comparison between properties of wound dressing membranes based on HA/ZnO-NPs/PVA and different wound dressing materials reported elsewhere (PDF)

AUTHOR INFORMATION

Corresponding Author

A. M. Abdel-Mohsen − *Institute of Macromolecular Chemistry, Czech Academy of Sciences, Praha 162 06, Czech Republic; Department of Pretreatment and Finishing of Cellulosic Fibers, Textile Research Institute, National Research Centre, Giza 12622, Egypt;* orcid.org/0000-0003-1872-9425; Email: abdellatif@imc.cas.cz

Authors

R. M. Abdel-Rahman − *Institute of Macromolecular Chemistry, Czech Academy of Sciences, Praha 162 06, Czech Republic*

J. Frankova − *Department of Medical Chemistry and Biochemistry, Faculty of Medicine and Dentistry, Palacký University, Olomouc 775 15, Czech Republic*

R. Sklenarova − *Department of Medical Chemistry and Biochemistry, Faculty of Medicine and Dentistry, Palacký University, Olomouc 775 15, Czech Republic;* orcid.org/0000-0001-7877-555X

L. Kapralkova − *Institute of Macromolecular Chemistry, Czech Academy of Sciences, Praha 162 06, Czech Republic*

I. Kelnar − *Institute of Macromolecular Chemistry, Czech Academy of Sciences, Praha 162 06, Czech Republic;* orcid.org/0000-0002-2334-3319

Complete contact information is available at:
https://pubs.acs.org/10.1021/acsapm.2c01296

Notes

The authors declare no competing financial interest.

■ REFERENCES

(1) Toor, A.; So, H.; Pisano, A. P. Improved Dielectric Properties of Polyvinylidene Fluoride Nanocomposite Embedded with Poly-(vinylpyrrolidone)-Coated Gold Nanoparticles. *ACS Appl. Mater. Interfaces* **2017**, *9*, 6369−6375.

(2) Zhang, C.; Liang, K.; Zhou, D.; Yang, H.; Liu, X.; Yin, X.; Xu, W.; Zhou, Y.; Xiao, P. High-Performance Photopolymerized Poly-(vinyl alcohol)/Silica Nanocomposite Hydrogels with Enhanced Cell Adhesion. *ACS Appl. Mater. Interfaces* **2018**, *10*, 27692−27700.

(3) Gam, S.; Meth, J. S.; Zane, S. G.; Chi, C.; Wood, B. A.; Seitz, M. E.; Winey, K. I.; Clarke, N.; Composto, R. J. Macromolecular Diffusion in a Crowded Polymer Nanocomposite. *Macromolecules* **2011**, *44*, 3494−3501.

(4) Abdel-Mohsen, A. M.; Aly, A. S.; Hrdina, R.; Montaser, A. S.; Hebeish, A. Eco-Synthesis of PVA/Chitosan Hydrogels for Biomedical Application. *J. Polym. Environ.* **2011**, *19*, 1005−1012.

(5) Chen, S.; Han, Y.; Huang, J.; Dai, L.; Du, J.; McClements, D. J.; Mao, L.; Liu, J.; Gao, Y. Fabrication and Characterization of Layer-by-Layer Composite Nanoparticles Based on Zein and Hyaluronic Acid for Codelivery of Curcumin and Quercetagetin. *ACS Appl. Mater. Interfaces* **2019**, *11*, 16922−16933.

(6) Pramanik, N.; Ranganathan, S.; Rao, S.; Suneet, K.; Jain, S.; Rangarajan, A.; Jhunjhunwala, S. A Composite of Hyaluronic Acid-Modified Graphene Oxide and Iron Oxide Nanoparticles for Targeted Drug Delivery and Magnetothermal Therapy. *ACS Omega* **2019**, *4*, 9284−9293.

(7) Ates, B.; Koytepe, S.; Ulu, A.; Gurses, C.; Thakur, V. K. Chemistry, Structures, and Advanced Applications of Nanocomposites from Biorenewable Resources. *Chem. Rev.* **2020**, *120*, 9304−9362.

(8) Bhattacharya, S.; Samanta, S. K. Soft-Nanocomposites of Nanoparticles and Nanocarbons with Supramolecular and Polymer Gels and Their Applications. *Chem. Rev.* **2016**, *116*, 11967−12028.

(9) Yu, C.; Schimelman, J.; Wang, P.; Miller, K. L.; Ma, X.; You, S.; Guan, J.; Sun, B.; Zhu, W.; Chen, S. Photopolymerizable Biomaterials and Light-Based 3D Printing Strategies for Biomedical Applications. *Chem. Rev.* **2020**, *120*, 10695−10743.

(10) Abdel-Mohsen, A. M.; Pavliňák, D.; Čileková, M.; Lepcio, P.; Abdel-Rahman, R. M.; Jančář, J. Electrospinning of hyaluronan/polyvinyl alcohol in presence of in-situ silver nanoparticles: Preparation and characterization. *Int. J. Biol. Macromol.* **2019**, *139*, 730−739.

(11) Abdel-Rahman, R. M.; Abdel-Mohsen, A. M.; Hrdina, R.; Burgert, L.; Fohlerova, Z.; Pavliňák, D.; Sayed, O. N.; Jancar, J. Wound dressing based on chitosan/hyaluronan/nonwoven fabrics: Preparation, characterization and medical applications. *Int. J. Biol. Macromol.* **2016**, *89*, 725−736.

(12) Abdel-Mohsen, A. M.; Jancar, J.; Abdel-Rahman, R. M.; Vojtek, L.; Hyršl, P.; Dušková, M.; Nejezchlebová, H. A novel in situ silver/hyaluronan bio-nanocomposite fabrics for wound and chronic ulcer dressing: In vitro and in vivo evaluations. *Int. J. Pharm.* **2017**, *520*, 241−253.

(13) Abdelrahman, R. M.; Abdel-Mohsen, A. M.; Zboncak, M.; Frankova, J.; Lepcio, P.; Kobera, L.; Steinhart, M.; Pavlinak, D.; Spotaz, Z.; Sklenářévá, R.; Brus, J.; Jancar, J. Hyaluronan biofilms reinforced with partially deacetylated chitin nanowhiskers: Extraction, fabrication, in-vitro and antibacterial properties of advanced nanocomposites. *Carbohydr. Polym.* **2020**, *235*, 115951.

(14) Abdel-Mohsen, A. M.; Hrdina, R.; Burgert, L.; Krylová, G.; Abdel-Rahman, R. M.; Krejčová, A.; Steinhart, M.; Beneš, L. Green synthesis of hyaluronan fibers with silver nanoparticles. *Carbohydr. Polym.* **2012**, *89*, 411−422.

(15) Suo, H.; Hussain, M.; Wang, H.; Zhou, N.; Tao, J.; Jiang, H.; Zhu, J. Injectable and pH-Sensitive Hyaluronic Acid-Based Hydrogels with On-Demand Release of Antimicrobial Peptides for Infected Wound Healing. *Biomacromolecules* **2021**, *22*, 3049−3059.

(16) Wang, Y.; Cheng, L.; Wen, S.; Zhou, S.; Wang, Z.; Deng, L.; Mao, H.-Q.; Cui, W.; Zhang, H. Ice-Inspired Superlubricated Electrospun Nanofibrous Membrane for Preventing Tissue Adhesion. *Nano Lett.* **2020**, *20*, 6420−6428.

(17) Spadea, A.; Rios de la Rosa, J. M.; Tirella, A.; Ashford, M. B.; Williams, K. J.; Stratford, I. J.; Tirelli, N.; Mehibel, M. Evaluating the Efficiency of Hyaluronic Acid for Tumor Targeting via CD44. *Mol. Pharm.* **2019**, *16*, 2481−2493.

(18) Yang, L.; Pijuan-Galito, S.; Rho, H. S.; Vasilevich, A. S.; Eren, A. D.; Ge, L.; Habibović, P.; Alexander, M. R.; de Boer, J.; Carlier, A.; van Rijn, P.; Zhou, Q. High-Throughput Methods in the Discovery and Study of Biomaterials and Materiobiology. *Chem. Rev.* **2021**, *121*, 4561−4677.

(19) Xue, J.; Wu, T.; Dai, Y.; Xia, Y. Electrospinning and Electrospun Nanofibers: Methods, Materials, and Applications. *Chem. Rev.* **2019**, *119*, 5298−5415.

(20) Ran, X.; Du, Y.; Wang, Z.; Wang, H.; Pu, F.; Ren, J.; Qu, X. Hyaluronic Acid-Templated Ag Nanoparticles/Graphene Oxide Composites for Synergistic Therapy of Bacteria Infection. *ACS Appl. Mater. Interfaces* **2017**, *9*, 19717−19724.

(21) Mittal, A. K.; Bhardwaj, R.; Arora, R.; Singh, A.; Mukherjee, M.; Rajput, S. K. Acceleration of Wound Healing in Diabetic Rats through Poly Dimethylaminoethyl Acrylate-Hyaluronic Acid Polymeric Hydrogel Impregnated with a Didymocarpus pedicellatus Plant Extract. *ACS Omega* **2020**, *5*, 24239−24246.

(22) Lee, J. S.; Cho, J. H.; An, S.; Shin, J.; Choi, S.; Jeon, E. J.; Cho, S.-W. In Situ Self-Cross-Linkable, Long-Term Stable Hyaluronic Acid Filler by Gallol Autoxidation for Tissue Augmentation and Wrinkle Correction. *Chem. Mater.* **2019**, *31*, 9614−9624.

(23) Dienes, J.; Browne, S.; Farjun, B.; Amaral Passipieri, J.; Mintz, E. L.; Killian, G.; Healy, K. E.; Christ, G. J. Semisynthetic Hyaluronic Acid-Based Hydrogel Promotes Recovery of the Injured Tibialis Anterior Skeletal Muscle Form and Function. *ACS Biomater. Sci. Eng.* **2021**, *7*, 1587−1599.

(24) Yang, S.; Zhu, B.; Yin, P.; Zhao, L.; Wang, Y.; Fu, Z.; Dang, R.; Xu, J.; Zhang, J.; Wen, N. Integration of Human Umbilical Cord Mesenchymal Stem Cells-Derived Exosomes with Hydroxyapatite-Embedded Hyaluronic Acid-Alginate Hydrogel for Bone Regeneration. *ACS Biomater. Sci. Eng.* **2020**, *6*, 1590−1602.

(25) Seo, J.; Park, S. H.; Kim, M. J.; Ju, H. J.; Yin, X. Y.; Min, B. H.; Kim, M. S. Injectable Click-Crosslinked Hyaluronic Acid Depot To Prolong Therapeutic Activity in Articular Joints Affected by Rheumatoid Arthritis. *ACS Appl. Mater. Interfaces* **2019**, *11*, 24984−24998.

(26) Johansson, J. Å.; Halthur, T.; Herranen, M.; Söderberg, L.; Elofsson, U.; Hilborn, J. Build-up of Collagen and Hyaluronic Acid Polyelectrolyte Multilayers. *Biomacromolecules* **2005**, *6*, 1353−1359.

(27) Zhou, D.; Li, S.; Pei, M.; Yang, H.; Gu, S.; Tao, Y.; Ye, D.; Zhou, Y.; Xu, W.; Xiao, P. Dopamine-Modified Hyaluronic Acid Hydrogel Adhesives with Fast-Forming and High Tissue Adhesion. *ACS Appl. Mater. Interfaces* **2020**, *12*, 18225−18234.

(28) Domingues, R. M. A.; Silva, M.; Gershovich, P.; Betta, S.; Babo, P.; Caridade, S. G.; Mano, J. F.; Motta, A.; Reis, R. L.; Gomes, M. E. Development of Injectable Hyaluronic Acid/Cellulose Nanocrystals Bionanocomposite Hydrogels for Tissue Engineering Applications. *Bioconjugate Chem.* **2015**, *26*, 1571−1581.

(29) Bao, Z.; Yuan, Y.; Leng, C.; Li, L.; Zhao, K.; Sun, Z. One-Pot Synthesis of Noble Metal/Zinc Oxide Composites with Controllable Morphology and High Catalytic Performance. *ACS Appl. Mater. Interfaces* **2017**, *9*, 16417−16425.

(30) Kumankuma-Sarpong, J.; Tang, S.; Guo, W.; Fu, Y. Naphthoquinone-Based Composite Cathodes for Aqueous Rechargeable Zinc-Ion Batteries. *ACS Appl. Mater. Interfaces* **2021**, *13*, 4084−4092.

(31) Wu, W.; Huang, X.; Li, S.; Jiang, P.; Toshikatsu, T. Novel Three-Dimensional Zinc Oxide Superstructures for High Dielectric Constant Polymer Composites Capable of Withstanding High Electric Field. *J. Phys. Chem. C* **2012**, *116*, 24887−24895.

(32) Dong, Y.; Argaiz, M.; He, B.; Tomovska, R.; Sun, T.; Martín-Fabiani, I. Zinc Oxide Superstructures in Colloidal Polymer Nanocomposite Films: Enhanced Antibacterial Activity through Slow Drying. *ACS Appl. Polym. Mater.* **2020**, *2*, 626−635.

(33) Posoknistakul, P.; Tangkrakul, C.; Chaosuanphae, P.; Deepentham, S.; Techasawong, W.; Phonphirunrot, N.; Bairak, S.; Sakdaronnarong, C.; Laosiripojana, N. Fabrication and Characterization of Lignin Particles and Their Ultraviolet Protection Ability in PVA Composite Film. *ACS Omega* **2020**, *5*, 20976−20982.

(34) Gao, T.; Yang, Z.; Chen, C.; Li, Y.; Fu, K.; Dai, J.; Hitz, E. M.; Xie, H.; Liu, B.; Song, J.; Yang, B.; Hu, L. Three-Dimensional Printed Thermal Regulation Textiles. *ACS Nano* **2017**, *11*, 11513−11520.

(35) Aly, A. S.; Abdel-Mohsen, A. M.; Hrdina, R.; Abou-Okeil, A. Preparation and Characterization of Polyethylene Glycol/Dimethyl Siloxane Adduct and Its Utilization as Finishing Agent for Cotton Fabric. *J. Nat. Fibers* **2011**, *8*, 176−188.

(36) Aly, A. S.; Abdel-Mohsen, A. M.; Hebeish, A. Innovative multifinishing using chitosan-O-PEG graft copolymer/citric acid aqueous system for preparation of medical textiles. *J. Text. Inst.* **2010**, *101*, 76−90.

(37) Rao, K. M.; Suneetha, M.; Zo, S.; Duck, K. H.; Han, S. S. One-pot synthesis of ZnO nanobelt-like structures in hyaluronan hydrogels for wound dressing applications. *Carbohydr. Polym.* **2019**, *223*, 115124.

(38) Abdel-Mohsen, A. M.; Frankova, J.; Abdel-Rahman, R. M.; Salem, A. A.; Sahffie, N. M.; Kubena, I.; Jancar, J. Chitosan-glucan complex hollow fibers reinforced collagen wound dressing embedded with aloe vera. II. Multifunctional properties to promote cutaneous wound healing. *Int. J. Pharm.* **2020**, *582*, 119349.

(39) Fouda, M. M. G.; Abdel-Mohsen, A. M.; Ebaid, H.; Hassan, I.; Al-Tamimi, J.; Abdel-Rahman, R. M.; Metwalli, A.; Alhazza, I.; Rady, A.; El-Faham, A.; Jancar, J. Wound healing of different molecular weight of hyaluronan; in-vivo study. *Int. J. Biol. Macromol.* **2016**, *89*, 582−591.

(40) Pivodova, V.; Frankova, J.; Dolezel, P.; Ulrichova, J. The Response of Osteoblast-Like SaOS-2 Cells to Modified Titanium Surfaces. *Int. J. Oral Maxillofac. Implants* **2013**, *28*, 1386.

(41) Montaser, A. S.; Abdel-Mohsen, A. M.; Ramadan, M. A.; Sleem, A. A.; Sahffie, N. M.; Jancar, J.; Hebeish, A. Preparation and characterization of alginate/silver/nicotinamide nanocomposites for treating diabetic wounds. *Int. J. Biol. Macromol.* **2016**, *92*, 739−747.

(42) Ma, S.; Wang, S.; Li, Q.; Leng, Y.; Wang, L.; Hu, G.-H. A Novel Method for Preparing Poly(vinyl alcohol) Hydrogels: Preparation, Characterization, and Application. *Ind. Eng. Chem. Res.* **2017**, *56*, 7971−7976.

(43) Hou, Y.; Chen, C.; Liu, K.; Tu, Y.; Zhang, L.; Li, Y. Preparation of PVA hydrogel with high-transparence and investigations of its transparent mechanism. *RSC Adv.* **2015**, *5*, 24023−24030.

(44) Thakur, K.; Rajhans, A.; Kandasubramanian, B. Starch/PVA hydrogels for oil/water separation. *Environ. Sci. Pollut. Res.* **2019**, *26*, 32013−32028.

(45) Kudo, K.; Ishida, J.; Syuu, G.; Sekine, Y.; Ikeda-Fukazawa, T. Structural changes of water in poly(vinyl alcohol) hydrogel during dehydration. *J. Chem. Phys.* **2014**, *140*, 044909.

(46) Abdel-Mohsen, A. M.; Abdel-Rahman, R. M.; Fouda, M. M. G.; Vojtova, L.; Uhrova, L.; Hassan, A. F.; Al-Deyab, S. S.; El-Shamy, I. E.; Jancar, J. Preparation, characterization and cytotoxicity of schizophyllan/silver nanoparticle composite. *Carbohydr. Polym.* **2014**, *102*, 238−245.

(47) Burdick, J. A.; Prestwich, G. D. Hyaluronic Acid Hydrogels for Biomedical Applications. *Adv. Mater.* **2011**, *23*, H41−H56.

(48) Lopez, K. M.; Ravula, S.; Pérez, R. L.; Ayala, C. E.; Losso, J. N.; Janes, M. E.; Warner, I. M. Hyaluronic Acid-Cellulose Composites as Patches for Minimizing Bacterial Infections. *ACS Omega* **2020**, *5*, 4125−4132.

(49) Abdel-Mohsen, A. M.; Hrdina, R.; Burgert, L.; Abdel-Rahman, R. M.; Hašová, M.; Šmejkalová, D.; Kolář, M.; Pekar, M.; Aly, A. S. Antibacterial activity and cell viability of hyaluronan fiber with silver nanoparticles. *Carbohydr. Polym.* **2013**, *92*, 1177−1187.

(50) Chen, S.; Sun, C.; Wang, Y.; Han, Y.; Dai, L.; Abliz, A.; Gao, Y. Quercetagetin-Loaded Composite Nanoparticles Based on Zein and Hyaluronic Acid: Formation, Characterization, and Physicochemical Stability. *J. Agric. Food Chem.* **2018**, *66*, 7441−7450.

(51) Lewandowska, K. Miscibility Studies of Hyaluronic Acid and Poly(Vinyl Alcohol) Blends in Various Solvents. *Materials* **2020**, *13*, 4750.

(52) Nakano, Y.; Kurokawa, T.; Du, M.; Liu, J.; Tominaga, T.; Osada, Y.; Gong, J. P. Effect of Hyaluronan Solution on Dynamic Friction of PVA Gel Sliding on Weakly Adhesive Glass Substrate. *Macromolecules* **2011**, *44*, 8908−8915.

(53) Zhao, Y.-Z.; Lin, M.-T.; Lan, Q.-H.; Zhai, Y.-Y.; Xu, H.-L.; Xiao, J.; Kou, L.; Yao, Q. Silk Fibroin-Modified Disulfiram/Zinc Oxide Nanocomposites for pH Triggered Release of Zn2+ and Synergistic Antitumor Efficacy. *Mol. Pharm.* **2020**, *17*, 3857−3869.

(54) Zheng, X.; Su, Y.; Chen, Y.; Wan, R.; Liu, K.; Li, M.; Yin, D. Zinc Oxide Nanoparticles Cause Inhibition of Microbial Denitrification by Affecting Transcriptional Regulation and Enzyme Activity. *Environ. Sci. Technol.* **2014**, *48*, 13800−13807.

(55) Wang, Y.-W.; Cao, A.; Jiang, Y.; Zhang, X.; Liu, J.-H.; Liu, Y.; Wang, H. Superior Antibacterial Activity of Zinc Oxide/Graphene Oxide Composites Originating from High Zinc Concentration Localized around Bacteria. *ACS Appl. Mater. Interfaces* **2014**, *6*, 2791−2798.

(56) Hatamie, A.; Khan, A.; Golabi, M.; Turner, A. P. F.; Beni, V.; Mak, W. C.; Sadollahkhani, A.; Alnoor, H.; Zargar, B.; Bano, S.; Nur, O.; Willander, M. Zinc Oxide Nanostructure-Modified Textile and Its Application to Biosensing, Photocatalysis, and as Antibacterial Material. *Langmuir* **2015**, *31*, 10913−10921.

(57) Abdel-Rahman, R. M.; Vishakha, V.; Kelnar, I.; Jancar, J.; Abdel-Mohsen, A. M. Synergistic performance of collagen-g-chitosan-glucan fiber biohybrid scaffold with tunable properties. *Int. J. Biol. Macromol.* **2022**, *202*, 671−680.

(58) Ibrahim, D. M.; Sani, E. S.; Soliman, A. M.; Zandi, N.; Mostafavi, E.; Youssef, A. M.; Allam, N. K.; Annabi, N. Bioactive and Elastic Nanocomposites with Antimicrobial Properties for Bone Tissue Regeneration. *ACS Appl. Bio Mater.* **2020**, *3*, 3313−3325.

(59) Elbourne, A.; Cheeseman, S.; Wainer, P.; Kim, J.; Medvedev, A. E.; Boyce, K. J.; McConville, C. F.; van Embden, J.; Crawford, R. J.; Chapman, J.; Truong, V. K.; Della Gaspera, E. Significant Enhancement of Antimicrobial Activity in Oxygen-Deficient Zinc Oxide Nanowires. *ACS Appl. Bio Mater.* **2020**, *3*, 2997−3004.

(60) Aditya, A.; Chattopadhyay, S.; Jha, D.; Gautam, H. K.; Maiti, S.; Ganguli, M. Zinc Oxide Nanoparticles Dispersed in Ionic Liquids Show High Antimicrobial Efficacy to Skin-Specific Bacteria. *ACS Appl. Mater. Interfaces* **2018**, *10*, 15401−15411.

(61) Wang, D.-C.; Yu, H.-Y.; Song, M.-L.; Yang, R.-T.; Yao, J.-M. Superfast Adsorption-Disinfection Cryogels Decorated with Cellulose Nanocrystal/Zinc Oxide Nanorod Clusters for Water-Purifying Microdevices. *ACS Sustainable Chem. Eng.* **2017**, *5*, 6776−6785.

(62) Liu, J.; Cheng, W.; Wang, Y.; Fan, X.; Shen, J.; Liu, H.; Wang, A.; Hui, A.; Nichols, F.; Chen, S. Cobalt-Doped Zinc Oxide Nanoparticle-MoS2 Nanosheet Composites as Broad-Spectrum Bactericidal Agents. *ACS Appl. Nano Mater.* **2021**, *4*, 4361−4370.

(63) Wang, J.; Zhou, H.; Guo, G.; Tan, J.; Wang, Q.; Tang, J.; Liu, W.; Shen, H.; Li, J.; Zhang, X. Enhanced Anti-Infective Efficacy of ZnO Nanoreservoirs through a Combination of Intrinsic Anti-Biofilm Activity and Reinforced Innate Defense. *ACS Appl. Mater. Interfaces* **2017**, *9*, 33609−33623.

(64) Fang, Y.; Shi, L.; Duan, Z.; Rohani, S. Hyaluronic acid hydrogels, as a biological macromolecule-based platform for stem cells

delivery and their fate control: A review. *Int. J. Biol. Macromol.* **2021**, *189*, 554−566.

📖 Recommended by ACS

Hyaluronan/zinc oxide nanocomposite-based Membrane: Preparation, Characterization, In vitro and In vivo Evaluation

R. M. Abdel-Rahman[1], J. Frankova[2], R. Sklenarova[2], L. Kapralkova[1], I. Kelnar[1], A. M. Abdel-Mohsen[1,3*]

[1] Institute of Macromolecular Chemistry, Czech Academy of Sciences, Heyrovského nám. 2, Praha, 162 06, Czech Republic,

[2] Department of Medical Chemistry and Biochemistry, Faculty of Medicine and Dentistry, Palacký University, Hněvotínská 3, 775 15, Olomouc, Czech Republic

[3] Department of Pretreatment and Finishing of Cellulosic Fibers, Textile Research Institute, National Research Centre, 33 EL Buhouth St., Dokki, Giza 12622, Egypt

Corresponding author:

Institute of Macromolecular Chemistry, Czech Academy of Sciences, Heyrovského nám. 2, Praha, 162 06, Czech Republic. E-mail: abdellatif@imc.cas.cz;

Characterization of nanocomposite membrane

Scanning electron microscope (SEM): Mira3 XM (Tescan, Czech Republic) was used to visualize the morphology of the membranes and further analyze the size and diameters of the zinc oxide nanoparticles in transmission mode (STEM). All samples were coated with a thin conductive metallic layer of Pd/Au alloy (thickness 10-20 nm) to achieve better resolution and prevent overcharging. **Mechanical Measurements:** Tensile testing was used to investigate the strength of the nanocomposite membrane (PVA/HA-ZnO-NPs), which was necessary for sampling handling. It was carried out with Universal testing equipment Z010 from Zwick–Roell (Germany) with a 1 kN measuring cell. The samples are cut in a dog bone shape with a parallel specimen length of 12 mm. Testing rate was 10^{-3} $s^{-1,}$ and the tests were performed at laboratory temperature.

XRD: X-ray diffraction is measured on a Smart lab 3 kW diffractometer (Rigaku, Japan) using Cu Kα radiation (λ = 1.54) and the Dtex Ultra detector with Bragg-Brentano geometry. The difraction angle 2θ (XRD) was measured in the range of 5 ° to 50 ° with a step size of 0.02 ° at a speed of 4°/min. A generator was operated at a current of 30 mA and a voltage of 40 kV.

ATR-FTIR: Attenuated total reflectance Fourier transforms infrared spectroscopy (ATR-FTIR) is performed using a Nicolet Impact 400 D FTIR-ATR spectrophotometer (Nicolet CZ, Prague, Czech Republic) equipped with a ZnSe crystal for the ATR-FTIR spectroscopy. The absorbance was measured as a function of the wavenumber (cm^{-1}) between 4000 cm^{-1} and 600 cm^{-1} with a resolution of 8 cm^{-1}. **TG-DTG:** Thermal decomposition evaluated using thermogravimetric (TG, Entsch 209F3 instrument, Al_2O_3 crucible) and at heating rates of 10 °C/ min (with data collection rate of 40 points per Kelvin). X-ray photoelectron spectroscopy **(XPS)** was carried out with Kratos Analytical Axisc Ultra DLD system using a monochromatic Al Kα (hν = 1486.7 eV) X-ray source operating at 75 W (5 mA, 15 kV). The spectra were obtained using an analysis area of ∼300 × 700 μm. The Kratos charge neutralizer system was used for all analyses. The high-resolution spectra were measured with the step size 0.1 eV and 20 eV pass energy. Instrument base pressure was $2×10^{-8}$ Pa. Spectra were analyzed using CasaXPS software (version 2.3.15).

Table S1. Preparation and chemical compositions of PVA / HA / ZnO-NPs with different volume fraction (V_f)

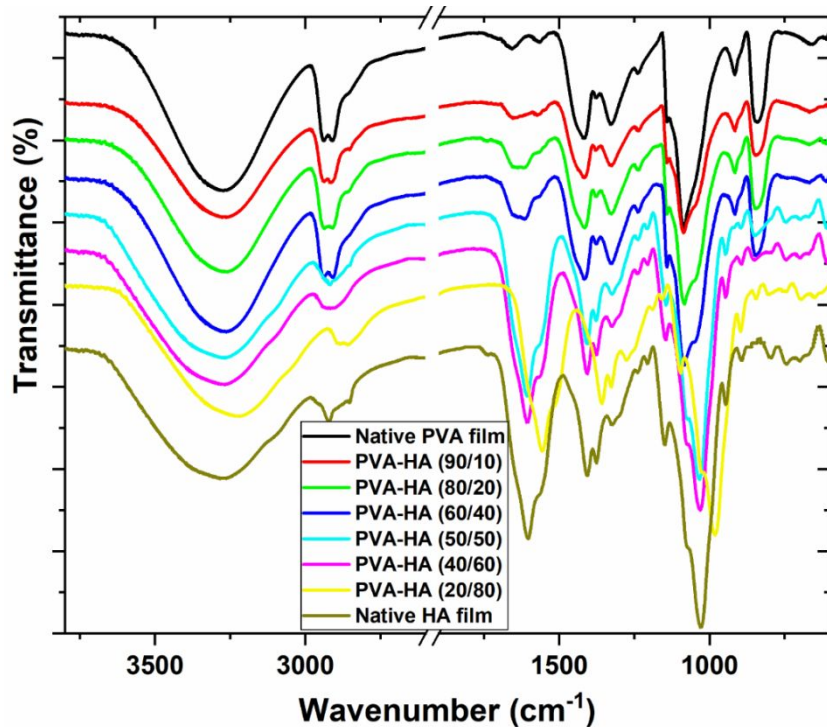| Chemical composition	Ratio between PVA to HA	Volume fraction of ZnO-NPs (V_f)
Native PVA membrane	100/ 0	0
Native HA (90/10)	90/10	0
PVA/HA (80/20)	80/20	0
PVA/HA (60/40)	60/40	0
PVA/HA (50/50)	50/50	0
PVA/HA (40/60)	40/60	0
PVA/HA (20/80)	20/80	0
PVA/HA (10/90)	10/90	0
Native HA membrane	0/100	0
PVA/HA/ZnO 1	40/60	0.001
PVA/HA/ZnO 2	40/60	0.005
PVA/HA/ZnO 3	40/60	0.01
PVA/HA/ZnO 4	40/60	0.05
PVA/HA/ZnO 5	40/60	0.1

Figure S1. ATR-FTIR of PVA/HA membrane fabricated using different ratio between PVA and HA.
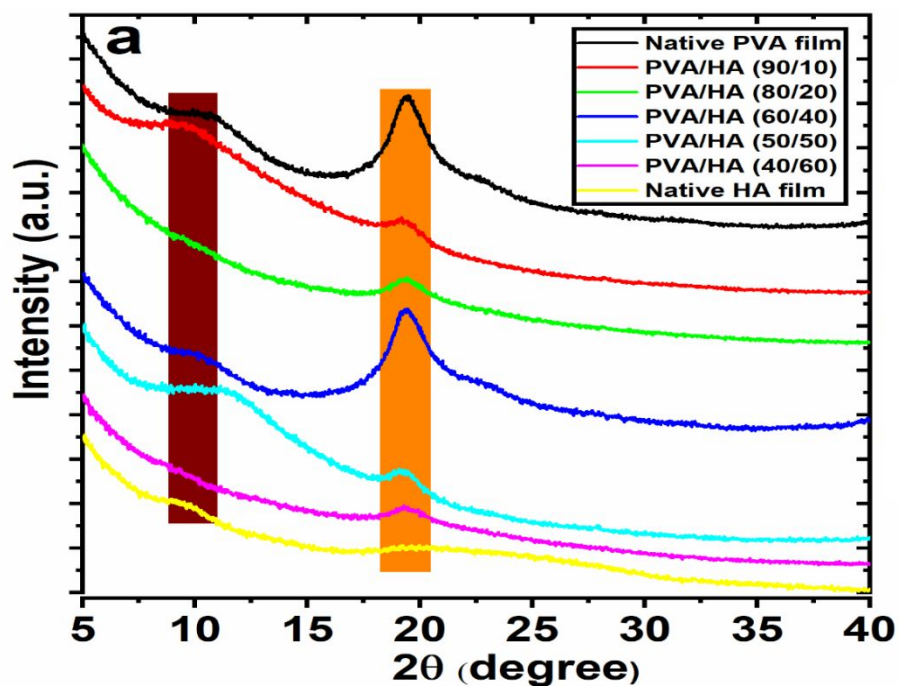
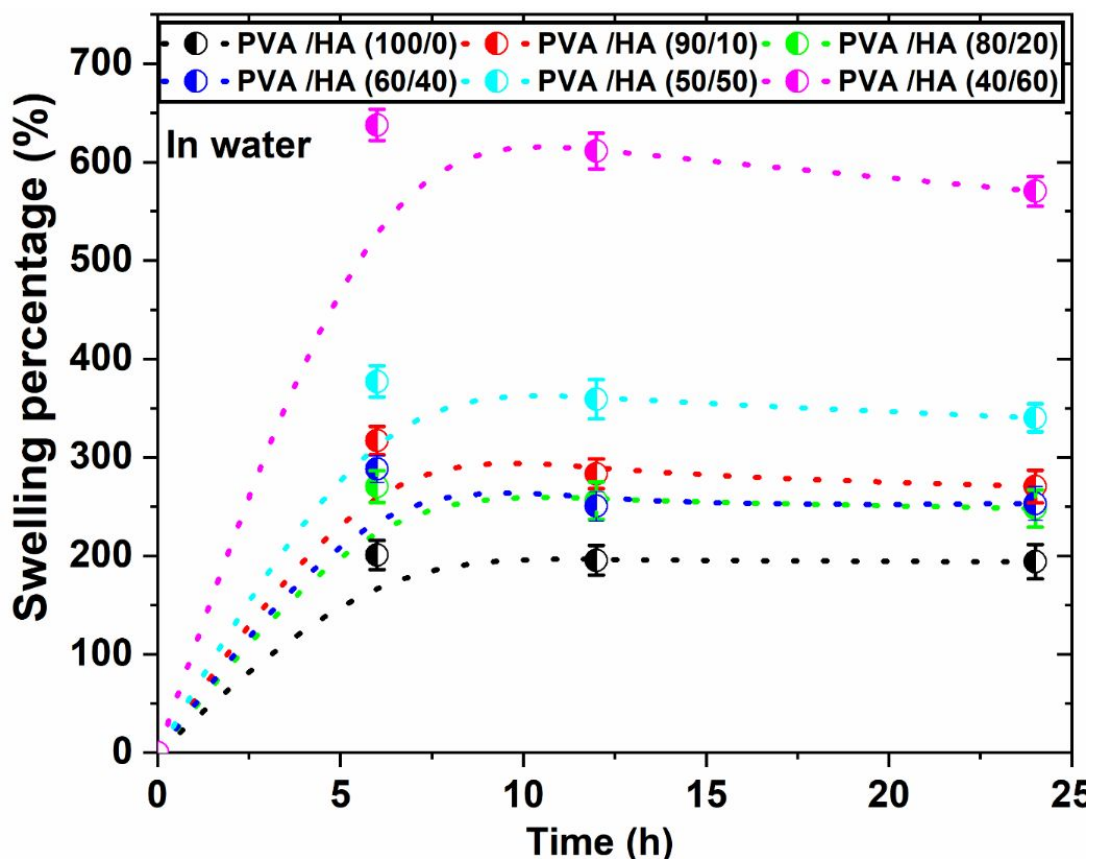**Figure S2.** XRD of membrane (PVA/HA) without ZnO-NPs

Figure S3: Swelling percentage of PVA/HA membrane without ZnO-NPs in water at 37 °C.
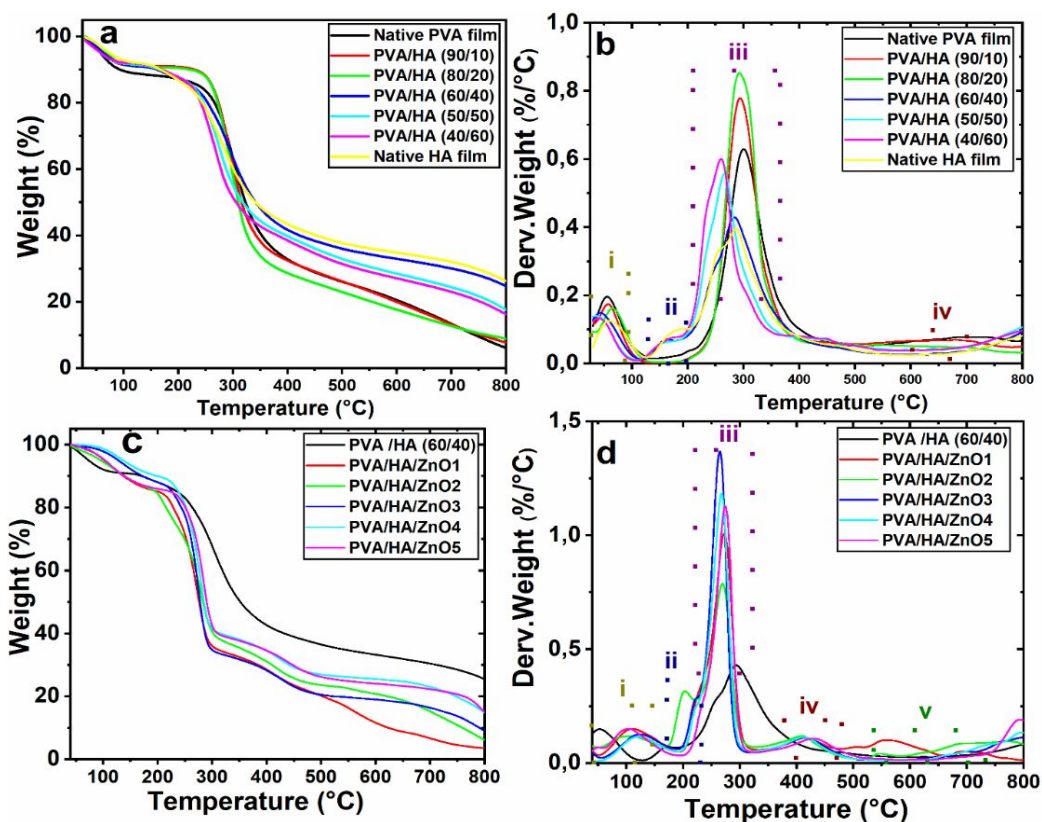
Figure S4. TG-DTG of PVA/HA membranes without ZnO-NP (a, b) and with ZnO-NP (c, d)

Table S2. Steps of decomposition of native PVA, HA, membranes (PVA / HA) and nanocomposite membranes (PVA / HA / ZnO-NPs) with different ratios of NPs

Samples	Δ_1		Δ_2		Δ_3		$\Delta4$		$\Delta5$		$\Delta6$		Residue
	Δ_{W1} (%)	T_{d1} (°C)	Δ_{W2} (%)	T_{d2} (°C)	Δ_{W3} (%)	T_{d3} (°C)	Δ_{W4} (%)	T_{d4} (°C)	Δ_{W5} (%)	T_{d5} (°C)	Δ_{W6} (%)	T_{d6} (°C)	(%)
PVA membrane	5.2	100	0.18	160	64.3	300	6.3	450	7.7	700	6.6	800	9.7
PVA/HA (90/10)	2.8	100	0.35	160	77.2	300	6.2	450	6.6	700	4.9	800	1.9
PVA/HA (80/20)	2.3	100	0.35	160	83.7	300	4.3	450	4.7	700	3.2	800	1.4
PVA/HA (60/40)	2.2	100	7.4	160	37.5	300	5	450	3.6	700	9.2	800	64.9
PVA/HA (50/50)	6.2	100	6.2	160	27.6	300	6.7	450	4.7	700	1.6	800	47
PVA/HA (40/60)	0.9	100	6.6	160	22.1	300	7.4	450	4.9	700	9.6	800	48.5
HA membrane	7.5	100	7.5	160	34.3	300	5.6	450	3.5	700	8.1	800	31.4
PVA/HA/ZnO1	14.4	100	8.9	160	13.5	300	11.2	410	10	550	1.3	800	40.6
PVA/HA/ZnO2	11.7	100	7.6	160	11	300	12.1	410	4.1	550	8.2	800	45.3
PVA/HA/ZnO3	9.5	100	8.8	160	5.9	300	11.2	410	1.7	550	1.1	800	61.8
PVA/HA/ZnO4	9.2	100	7.3	160	7	300	11.5	410	1.1	550	1.3	800	62.2
PVA/HA/ZnO5	15.2	100	6.1	160	9.3	300	9.5	410	2	550	1.8	800	56.1

Weight loss in each step (Δ_{WN}, %), the temperature of the fastest weight loss in each stage (Td, (°C)), and the percentage of residence (%).
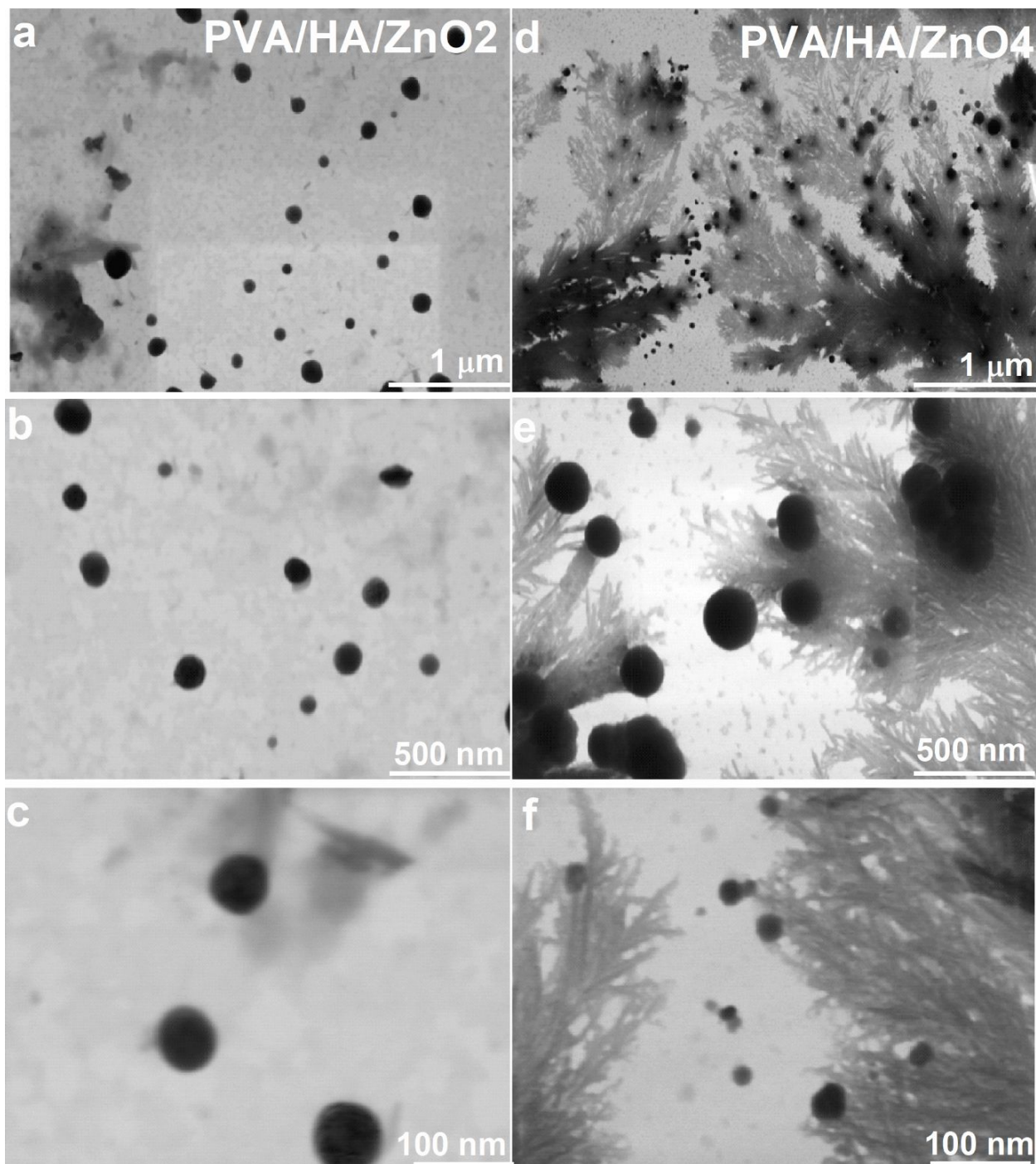
Figure S5. STEM of PVA/HA/ZnO-NPs nanocomposite with different volume fraction with NPs (V_F 0.005 and 0.5).
(a-c) STEM of PVA/HA (40/60)/ZnO2 with different magnifications (1000, 500, 100 nm); (d-f) STEM of PVA/HA (40/60)/ZnO4 with different magnifications (1000, 500, 100 nm).
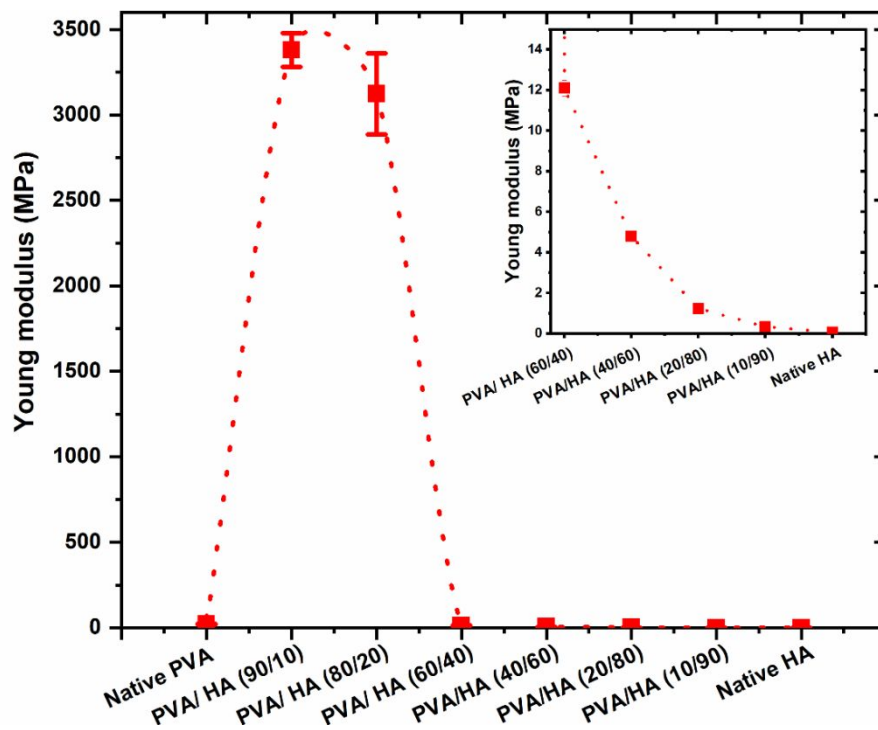
Figure S6. Mechanical properties of the PVA/HA composite membrane in absence of ZnO-NPs
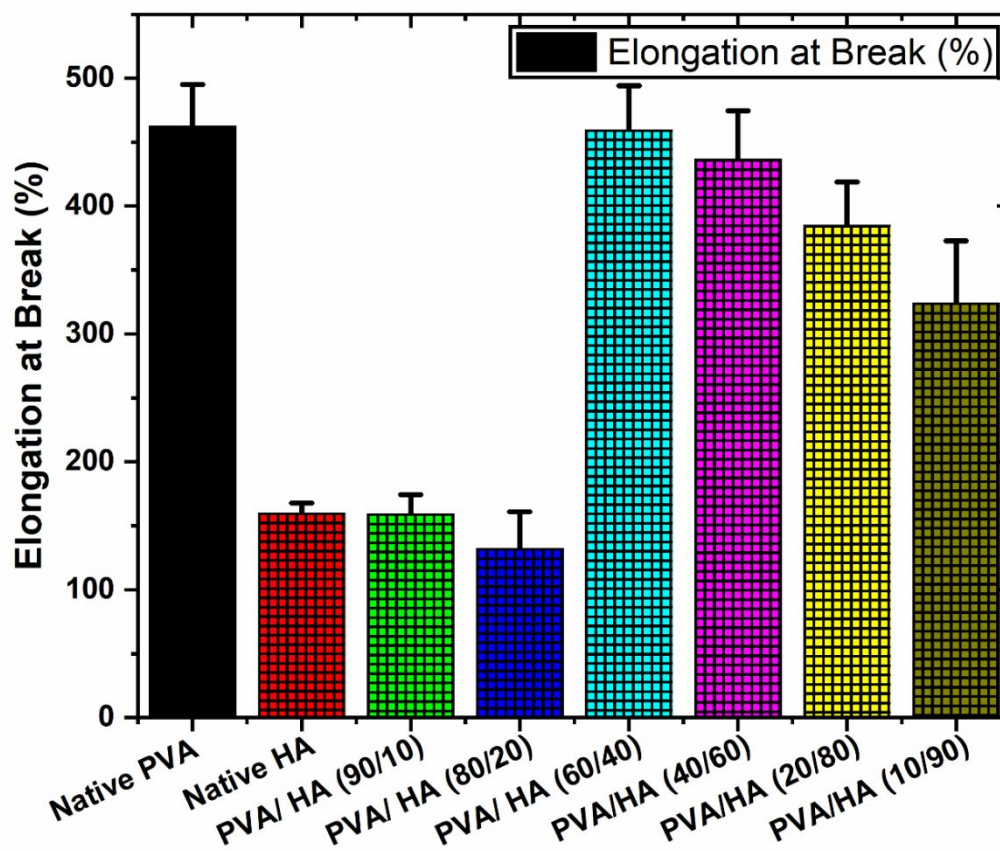
Figure S7. Elongation at break of the PVA/HA composite membrane in absence of ZnO-NPs
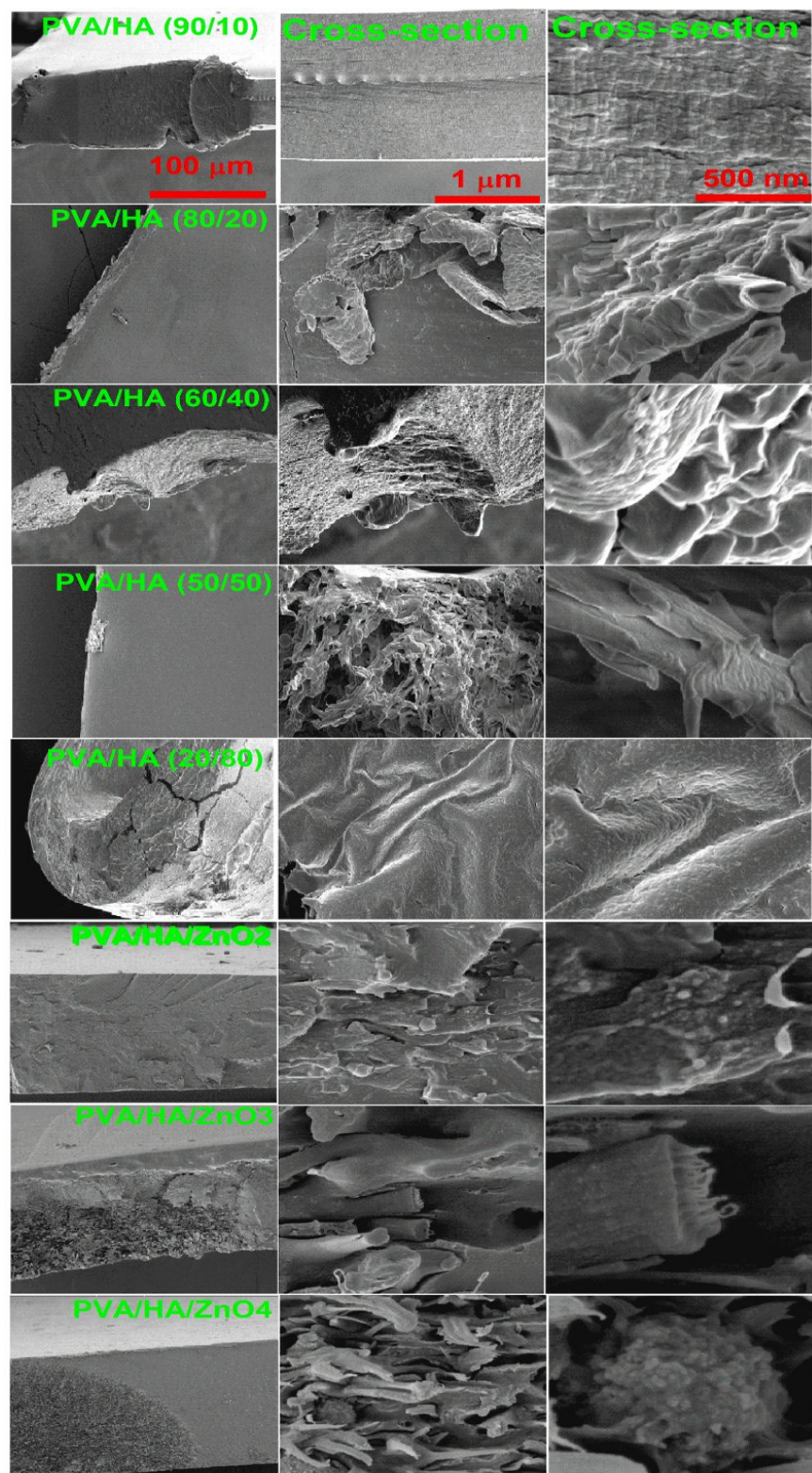
Figure S8. SEM of fractured cross-section of composite membrane in absence and presence of ZnO-NPs at different magnifications.
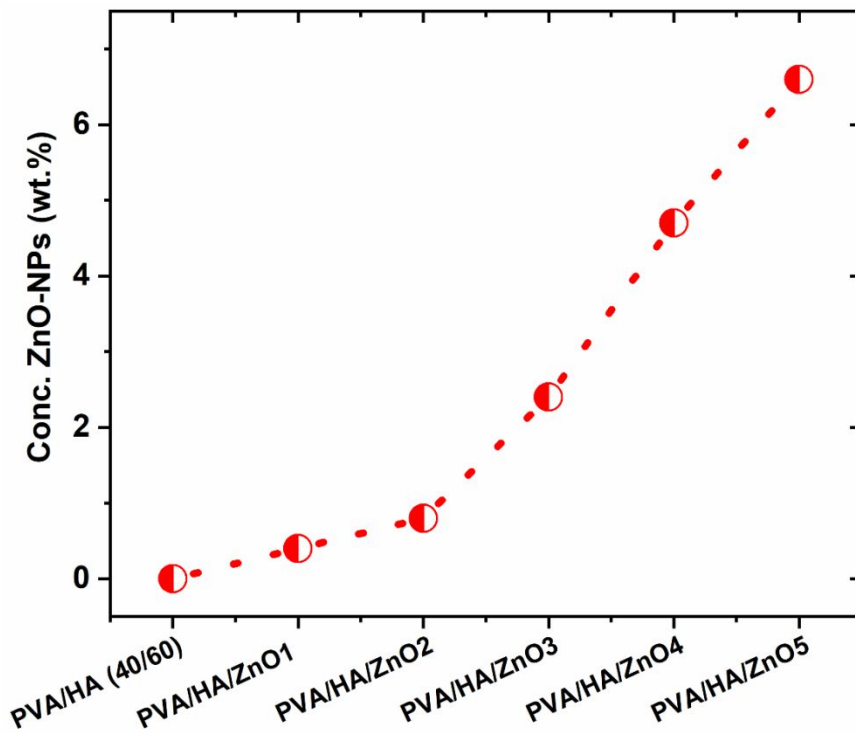
Figure S9. Representative concentration of ZnO-NPs from cross-section of the nanocomposite membrane
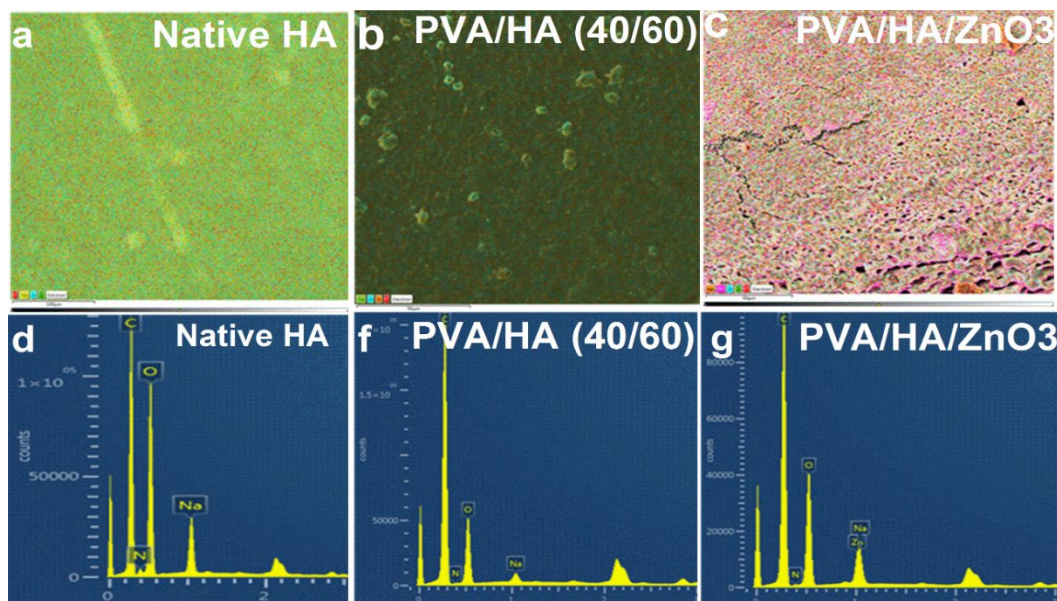
Figure S10 mapping with EDX of native, HA, PVA/HA (40/60) and nanocomposite membrane of (PVA/HA/ZnO3).
Map (a) and EDX of native HA (d); Map (b) and EDX of PVA/HA (40/60) (f); Map a (c) and EDX of PVA/HA/ZnO3 (g).
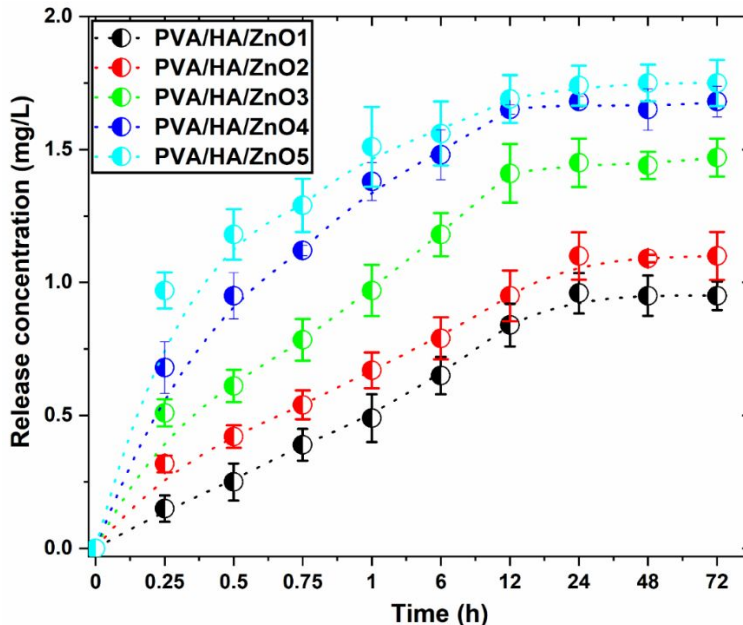
Figure S11. Release profile of ZnO-NPs from nanocomposite membranes
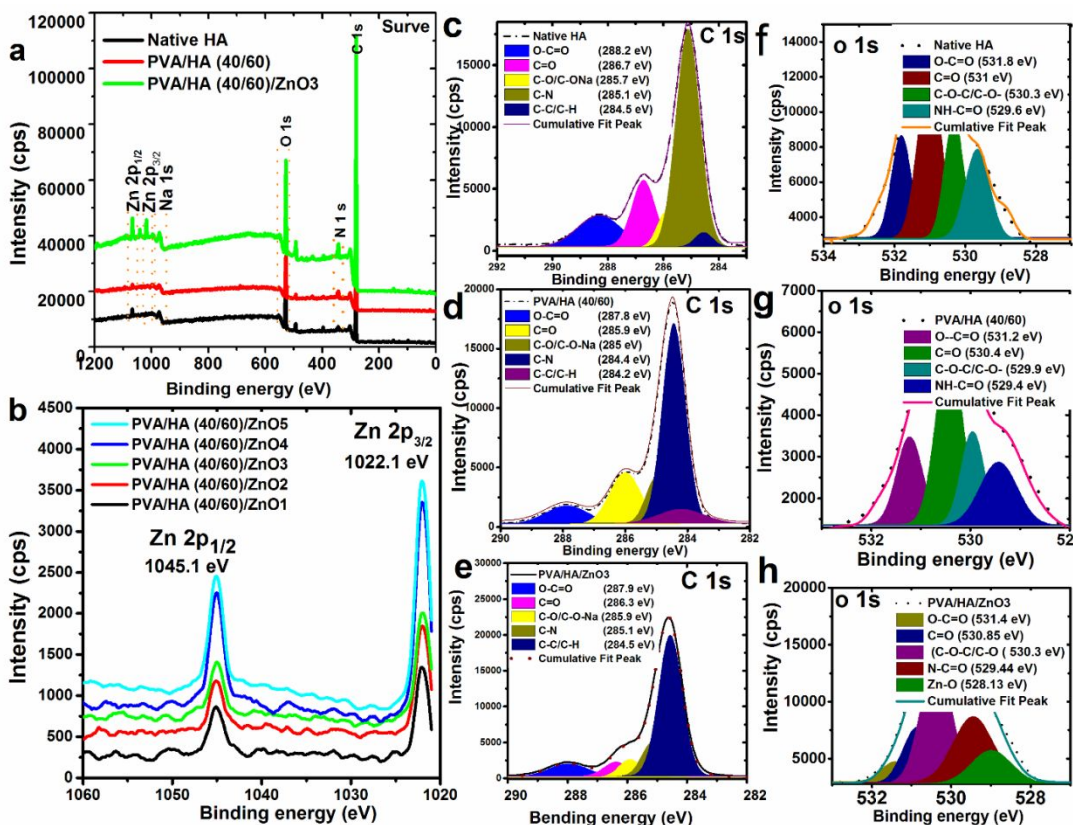
Figure S12. XPS survey of native HA, PVA/HA (40/60) and PVA/HA (40/60)/ZnO3 nanocomposite (a); high resolution of zinc oxide nanoparticles (b); C 1s of native HA film (c); C 1s of native PVAHA (40/60) membrane (d); C 1s of native PVAHA (40/60)/ZnO3 nanocomposite membrane (e); O 1s of native HA film (f); C 1s of native PVAHA (40/60) membrane (g); C 1s of native PVAHA (40/60)/ZnO3 nanocomposite membrane (h).
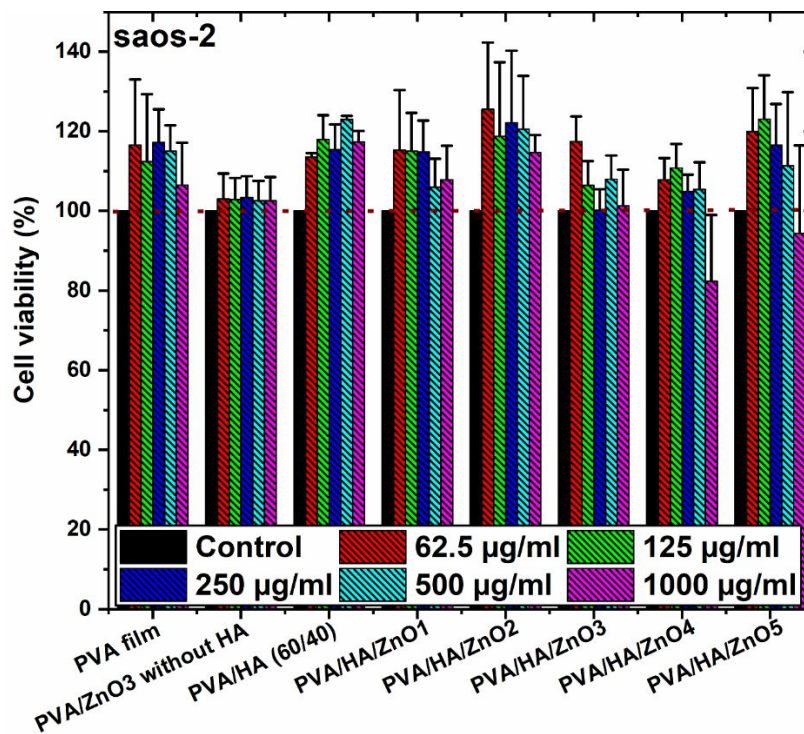
Figure S13. Representative the cytocompatibility of native PVA and nanocomposite membrane in absence and presence of ZnO-NPs using Saos-2 cells.
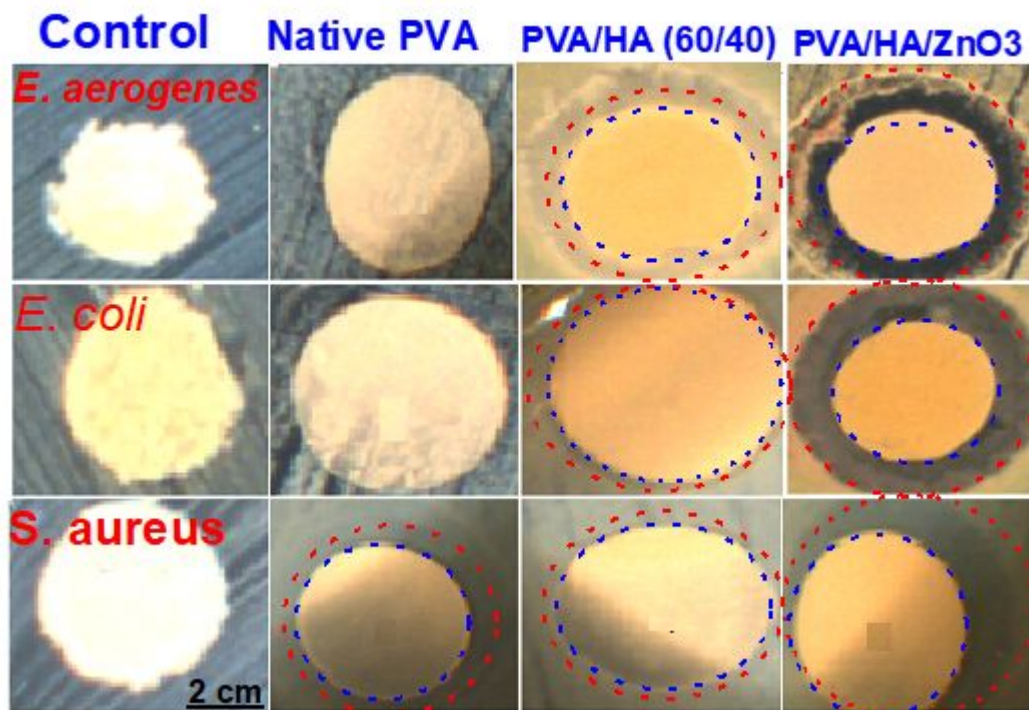
Figure S14. Antibacterial performance of nanocomposite membranes against different type of bacteria. Blue and red dotted circles represent the inhibition zone area
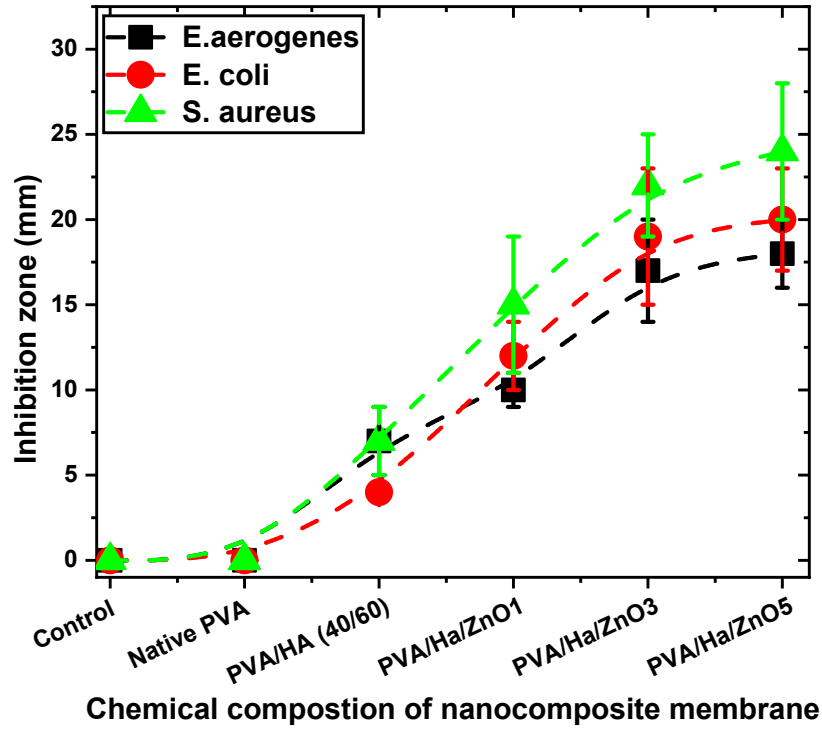
Figure S15. Bar graph showing the effect of zinc oxide nanoparticles concentration in diameter of the zone of inhibition against gram positive and gram-negative bacteria

Table S3. Comparison between properties of PVA/HA/ZnO membrane and different wound dressing materials reported elsewhere.

Wound dressing types	Healing types	Wound size (cm²)	Wound closure time (day)	Closure percentage (%)	Ref.
Hyaluronan/PVA/Zinc oxide membrane	Infected Wound	3	12	96	This work
Hyaluronan/ silver nanoparticles composite	Diabetic wound	3	7	92	1
hyaluronic acid-corn starch-propolis film	Nondiabetic	2	14	82	2
Hyaluronan/ Bisphosphonate/Silver Hydrogel	Nondiabetic	3	10	80	3
Hyaluronic Acid/PLGA Core/Shell Fiber	Diabetic wound	1	14	85	4
Chitin/calcium alginate fibers	Nondiabetic	3	10	93	5
Hyaluronan/gelatin nanofibers mats	Diabetic wound	3	14	92	6
Carboxymethyl Chitosan/Cellulose Nanocrystal	Infected wound	2	12	85	7
chitosan-silica wound dressing	Nondiabetic	3	8	82	8
cellulose/gelatin sponges	Infected wound	4	12	95	9
Hyaluronan/collagen hydrogel	Nondiabetic	3	12	85	10
hyaluronic acid/paeoniflorin	Diabetic wound	2.5	12	85	11
Hyaluronic acid sustains platelet Hydrogel	Diabetic wound	3	15	100	12
Hyaluronan injectable hydrogel	Infected wound	3	13	95	13
hyaluronic acid/carboxymethyl starch hydrogel	Diabetic wound	3	12	99	14
Hyaluronic Acid /Poly Dimethylaminoethyl Acrylate–Polymeric Hydrogel	Nondiabetic	2	14	90	15
Silver-doped zinc oxide and silver oxide nanocomposites	Diabetic wound	1.5	21	83	16
Micro/nanofibrous scaffolds incorporated with curcumin and zinc oxide nanoparticles	Diabetic wound	1	15	75	17
Pullulan Electrospun / ZnO-NPs mats	Nondiabetic	3	12	85	18
Chitosan-Modified ZnO Nanoparticles film	Infected wound	2.5	14	92	19
Hyaluronan/curcumin/iron oxide NPs	Nondiabetic	2.5	21	100	20
Hyaluronic acid /Polygalacturonic/ AgNPs nanofibers mats	Nondiabetic	2.5	14	100	21

References

1. Moustafa M.G.Fouda, A.M.Abdel-Mohsen, Hossam Ebaid, Iftekhar Hassan, Rasha M.Abdel-Rahma, Ali Metwalli, Ibrahim Alhazza, Ahmed Rady, Ayman El-Faham, J.Jancar,Wound healing of different molecular weight of hyaluronan; *in-vivo* study. <u>International Journal of Biological Macromolecules</u> <u>89</u>, 2016, Pages 582-591.

2. Amirhosein Kefayatb, Maria Agheb, SepehrNavid, Karim Ebrahimpour.Cornstarch-based wound dressing incorporated with hyaluronic acid and propolis: *In vitro* and *in vivo* studies. Carbohydrate Polymers, 216, 2019, 25-35.

3. Liyang Shi, Yannan Zhao, Qifan Xie, Caixia Fan, Jöns Hilborn, Jianwu Dai, and Dmitri. A. Ossipo. Moldable Hyaluronan Hydrogel Enabled by Dynamic Metal–Bisphosphonate Coordination Chemistry for Wound Healing. Adv. Healthcare Mater. 7, 2018, 1700973.

4. Yong Cheol Shin, Dong-Myeong Shin, Eun Ji Lee, Jong Ho Lee, Ji Eun Kim, Sung Hwa Song, Dae-Youn Hwang, Jun Jae Lee, Bongju Kim, Dohyung Lim, Suong-Hyu Hyon, Young-Jun Lim and Dong-Wook Han. Hyaluronic Acid/PLGA Core/Shell Fiber Matrices Loaded with EGCG Beneficial to Diabetic Wound Healing. Adv. Healthcare Mater. 5, 2016, 3035–3045.

5. J. L. Shamshina,ab G. Gurau,ab L. E. Block,a L. K. Hansen,c C. Dingee,c A. Waltersc and R. D. Rogers. Chitin–calcium alginate composite fibers for wound care dressings spun from ionic liquid solution. J. Mater. Chem. B, 2014, 2, 3924.

6. So Yun Lee, Sangheon Jeon, Young Woo Kwon , Mina Kwon1\ , Moon Sung Kang , Keum-Yong Seong , Tae-Eon Park , Seung Yun Yang , Dong-Wook Han , Suck Won Hong , Ki Su Kim. Combinatorial wound healing therapy using adhesive nanofibrous membrane equipped with wearable LED patches for photobiomodulation. Sci. Adv. 8, eabn1646 (2022).

7. Weijuan Huang, Yixiang Wang, Zhiqiang Huang, Xiaolan Wang, Lingyun Chen, Lina Zhang. On-Demand Dissolvable Self-Healing Hydrogel Based on Carboxymethyl Chitosan and Cellulose Nanocrystal for Deep Partial Thickness Burn Wound Healing. *ACS Appl. Mater. Interfaces* 2018, 10, 48, 41076–41088.

8. Jun-SungOhaEun-JungLee. Engineered dressing of hybrid chitosan-silica for effective delivery of keratin growth factor and acceleration of wound healing. Materials Science and Engineering: C 103, October 2019, 109815.

9. Ying Pei, Dongdong Ye, Qi Zhao, Xueying Wang, Chun Zhang, Weihua Huang, Nu Zhang, Shiqing Liu and Lina Zhang. Effectively promoting wound healing with cellulose/gelatin sponges constructed directly from a cellulose solution. J. Mater. Chem. B, 2015, 3, 7518.

10. Huiyan YingJuan ZhouMingyu WangDandan SuQiaoqiao MaGuozhong LvJinghua Chen. In situ formed collagen-hyaluronic acid hydrogel as biomimetic dressing for promoting spontaneous wound healing. Materials Science and Engineering: C 101, 2019, 487-498

11. Hao Yang Liu Song Bingxue Suna, Leilei Yanga Meng Lia Huan Lia Yun Daib ZhuoYuc Jianfeng Guo. Modulation of macrophages by a paeoniflorin-loaded hyaluronic acid-based hydrogel promotes diabetic wound healing, Materials Today Bio 12, 2021, 100139

12. Sneha S.Rao, Ashwini Prabhua Jagadish Kudkulia Suprith Suryab P.D.Rekha. Hyaluronic acid sustains platelet stability with prolonged growth factor release and accelerates wound healing by enhancing proliferation and collagen deposition in diabetic mice. Journal of Drug Delivery Science and Technology 67, 2022, 102898

13. Suo, Mubashir Hussain, Hua Wang, Nuoya Zhou, Juan Tao, Hao Jiang, and Jintao Zhu. Injectable and pH-Sensitive Hyaluronic Acid-Based Hydrogels with On-Demand Release of Antimicrobial Peptides for Infected Wound Healing. Biomacromolecules 2021, 22, 3049−3059.

14. YiqingZhanga1YongjunZheng,FutingShub1RenjieZhouaBingkunBaocShichuXiaobKaiLiaQiuningLincLin yongZhuacZhaofanXi. In situ-formed adhesive hyaluronic acid hydrogel with prolonged amnion-derived conditioned medium release for diabetic wound repair. Carbohydrate Polymers, 276, 15 2022, 118752.

15. Rohit Bhardwaj, Riya Arora, Aarti Singh, Monalisa Mukherjee, and Satyendra K. Rajput. Acceleration of Wound Healing in Diabetic Rats through Poly Dimethylaminoethyl Acrylate–Hyaluronic Acid Polymeric Hydrogel Impregnated with a Didymocarpus pedicellatus Plant Extract. ACS Omega 2020, 5, 38, 24239–24246

16. Francyelle Borges Rosa de Moura. Antioxidant, anti-inflammatory, and wound healing effects of topical. silver-doped zinc oxide and silver oxide nanocomposites International Journal of Pharmaceutics 617, 5 2022, 121620.

17. TingYing, Jinxiu, LibYafengXuab Ruiqi Wangb QinfeiKeb,ve G.F.Shenac, HeXub. Hierarchical micro/nanofibrous scaffolds incorporated with curcumin and zinc ion eutectic metal organic frameworks for enhanced diabetic wound healing via anti-oxidant and anti-inflammatory activities. Chemical Engineering Journal 402, 2020, 126273

18. Mina Shahriari-Khalaji, Feng F. Hong. Functionalization of Aminoalkylsilane-Grafted Bacterial Nanocellulose with ZnO-NPs-Doped Pullulan Electrospun Nanofibers for Multifunctional Wound Dressing. *ACS Biomater. Sci. Eng.* 2021, 7, 8, 3933–3946.

19. Ana M. Díez-Pascual, Angel L. Díez-Vicente. Wound Healing Bionanocomposites Based on Castor Oil Polymeric Films Reinforced with Chitosan-Modified ZnO Nanoparticles. *Biomacromolecules* 2015, 16, 9, 2631–2644.

20. Hao Yang, Liu Song, Yifang Zou, Dandan Sun, Limei Wang, Zhuo Yu and Jianfeng Guo. Role of Hyaluronic Acids and Potential as Regenerative Biomaterials in Wound Healing. *ACS Appl. Bio Mater.* 2021, 4, 1, 311–324

21. M.R.El-Aassar1Omar M.Ibrahim, 1Moustafa M.G.Fouda, dNagham G.El-Beheri, bMona M.Agwae Wound healing of nanofiber comprising Polygalacturonic/Hyaluronic acid embedded silver nanoparticles: In-vitro and in-vivo studies. Carbohydrate Polymers, 238, 15 2020, 116175

Publication 9
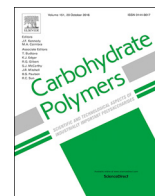
Hyaluronan biofilms reinforced with partially deacetylated chitin nanowhiskers: Extraction, fabrication, *in-vitro* and antibacterial properties of advanced nanocomposites

R.M. Abdelrahman[a,*,1], A.M. Abdel-Mohsen[a,b,c,*,1], M. Zboncak[a], J. Frankova[d], P. Lepcio[a], L. Kobera[e], M. Steinhart[e], D. Pavlinak[f], Z. Spotaz[a], R. Sklenářévá[d], J. Brus[e], J. Jancar[a,b,g]

[a] *CEITEC-Central European Institute of Technology, Brno University of Technology, Purkynova 656/123, Brno 61200, Czechia*
[b] *SCITEG, a.s., Brno, Czechia*
[c] *Department of Pretreatment and Finishing of Cellulosic based Textiles, Textile Industries Research Division, National Research Centre, 33 EL Buhouth St., Dokki, Giza 12622, Egypt*
[d] *Department of Medical Chemistry and Biochemistry, Faculty of Medicine and Dentistry, Palacky University Olomouc, Czechia*
[e] *Institute of Macromolecular Chemistry of the Czech Academy of Sciences, Heyrovskeho Nam. 2, 162 06, Prague 6, Czechia*
[f] *Department of Physical Electronics, Masaryk University, Kotlářská 267/2, Brno, 611 37, Czechia*
[g] *Institute of Materials Chemistry, Facility of Chemistry, Brno University of Technology, Purkyňova 464/118, Brno 61200, Czechia*

ARTICLE INFO

ABSTRACT

Fabrication of nanocomposite biofilms with enhanced mechanical and antibacterial properties was successfully achieved from hyaluronan (HA) and partially deacetylated chitin nanowhiskers (ChNWs) by a casting-evaporation method. The hydrolysis process of chitin showed an important role in the dimensions, stability, and the crystallinity of extracted ChNWs in a time-dependent manner. The volume fraction of ChNWs nanofiller varying from (0.001 to 0.5) exhibited a great influence on the mechanical properties of the biofilms (young modulus, strength) was enhanced by the high load-bearing capacity of NWs compared with net HA film. The antibacterial activity of the nanocomposite biofilms exhibited significant bactericidal activity against different types of bacteria ($-/+$ gram). HA/ChNWs Nanocomposite biofilms did not show any toxicity against normal human dermal fibroblasts (NHDF) and human primary osteogenic sarcoma (Saos-2) cell lines. The new biofilms with unique properties like edibleness, environmental friendliness, high mechanical properties, antibacterial performance, and non-cytotoxicity that could be used in skin tissue regenerations, and drug delivery applications.

1. Introduction

Polymers filled with nanoscale reinforcement such as inorganic or organic nano-objects attracted an unprecedented interest of the scientific and engineering community due to the large potential of these nanosized objects to substantially modify the properties of polymers beyond the capabilities of their microsized alternatives (Jancar et al., 2010; Kumar, Benicewicz, Vaia, & Winey, 2017). For example, antibacterial, cell growth acceleration or inhibition, thermal resistance, electric or magnetic actuation, or mechanical robustness can be added into the portfolio of polymer properties via the addition of nanoparticles with desired properties and their organization into defined structures. While modification of the function-aimed properties is a little bit more straightforward and more successful, the full potential of

nanoparticles for modification of the mechanical properties remain rather dormant.

The development of nanocomposites based on natural polymers has attracted great interest of scientists due to several features of polymers such as resource renewability, easy extraction, lightweight and multifunction properties. Nevertheless, natural polymers such as starch, cellulose, chitosan, chitin, and hyaluronic acid have lacked in several parameters such as low modulus, poor mechanical performance, and rapid degradation. Therefore, combining a polymeric matrix with polymeric nanoparticles as reinforcement into a nanocomposite could enhance the performance of those materials such as the mechanical strength and the degradation properties.

Hyaluronan (HA) is a glycosaminoglycan, an anionic polysaccharide made up of glucuronic acid and *N*-acetylglucosamine disaccharide units

having one carboxyl group on each disaccharide unit (Abdel-Mohsen et al., 2017). Nowadays, HA is widely used due to its unique features of biocompatibility, nontoxicity, healing properties. It can be prepared in various forms such as a hydrogel (David et al., 2008), fibers (Abdel-Mohsen, Hrdina et al., 2012, 2019), or a scaffold (Tan, Wu, Lao, & Gao, 2009). However, hyaluronan showed poor mechanical stability, rapid degradation (Lou et al., 2018) and itself does not possess antimicrobial properties; therefore, it often provides a favorable environment for colonization by microorganisms, which cause infection and delay healing (Ao et al., 2019; Lequeux, Ducasse, Jouenne, & Thebault, 2014).

Chitin, a long polymer chain of *N*-acetyl glucosamine and its partly deacetylated form chitosan represent huge natural resources of polysaccharides found in many places throughout the natural world, possessing various parameters such as biocompatibility, biodegradability, nontoxicity and it is potential to be converted into nanofibrils (Abdel-Rahman et al., 2015). By acid hydrolysis, a stiff rod-like chitin nanowhisker (ChNWs) can be prepared with many advantages including the good mechanical performance (Zhu et al., 2019), low density (Zeng, He, Li, & Wang, 2012), high surface area (Li et al., 2016) and the nano-reinforcement ability in polymeric structures (Morganti et al., 2014). All these properties render ChNWs a prospective candidate for use as a nanofiller or nano-reinforcement additive for high-performance nanocomposite materials. Chitin acid hydrolysis using hydrochloric acid is the best choice to extract chitin nanowhiskers without any chemical modification compared to the analogical methods using sulfuric acid (Roman & Winter, 2004) or phosphoric acid (Suryanegara, Okumura, Nakagaito, & Yano, 2011) (generate sulphate and phosphate groups, respectively.

The combination of hyaluronan and chitosan shows a synergic effect in the characterestic of the final nanocomposite. Biopolymer nanocomposites from the combination of HA and chitosan is their capability to form a polyelectrolyte complex (PEC) via ionic interactions. It was concluded that the carboxylate moieties on HA polymer will ionically interact with the free amino groups on chitosan counterparts to generate a matrix, known as a physically cross-linked hydrogel (Bongaerts, Cooper-White, & Stokes, 2009). Due to these opposite charges, a homogeneous solution of hyaluronan and chitosan solutions would readily coagulate or form gels (Boddohi, Moore, Johnson, & Kipper, 2009), leading to unfeasible production of the hyaluronan/chitosan membrane/fiber/film from the mixed dope solutions of the biopolymers.

3D scaffolds are fabricated using α-Chitin-whisker-reinforced hyaluronan–gelatin nanocomposite by freeze-drying technique (Hariraksapitak & Supaphol, 2010) without information about the DDA of chitin nanowhiskers and bacterial properties of the prepared scaffold and reinforced properties of ChNWs on the hyaluronan-gelation scaffold (Hariraksapitak & Supaphol, 2010). Nanocomposite films from α-Chitin nanowhiskers reinforced Poly(vinyl alcohol) are fabricated by solution impregnation method (Peng & Chen, 2018). Partially chitin nanowhiskers films are prepared first then immersed in PVA solution and heat-treated for a different time and temperature to improve the solubility of PVA/ChNWs in water. Unfortunately, there are no available data about the DDA of chitin, the stability, distribution of nanowhiskers in the film matrix.

In the current study, for the first time, we focus on a novel method for Synthesizing nanocomposite biofilms from hyaluronan and partially deacetylated chitin nanowhiskers (HA/ChNWs) by a casting-evaporation method of a dope suspension synthesized from a direct mixing of a hyaluronan and nanowhiskers solutions. Briefly, ChNWs suspension (without agglomerations) was subsequently added into the HA solution under vigorous stirring to obtain a homogeneous HA/ChNWs dope suspension.

The advantage of the described method here is the homogenization of the target materials prior to processing, thus homogeneity and composition of the substances could be controlled. In addition, it is confirm that all the ingredients in the dope solution still in the biofilm and this process is convenient and facile to scale-up for large-scale production. Therefore, the overall goals of this investigation were (i) to investigate a new process of nanocomposite preparation from cationic/anionic biopolymers and maximize the nanofiller content (to provide sufficient beneficial properties of NWs) by simply prevent the direct interactions between functional groups, while retaining the film-processing ability of hyaluronan, (ii) to investigate altered characteristic of the obtained HA/ChNWs nanocomposite biofilms thereby obtained and (iii) to improve the mechanical, antibacterial properties, stability and biocompatibility of the nanocomposites biofilms.

2. Experimental part

2.1. Materials and methods

Shrimp shells were selected as a source for chitin (Ch) extraction and partially deacetylated chitin nanowhiskers (ChNWs). Sodium hydroxide, hydrochloric acid, ethanol, isopropyl alcohol, and acetone were acquired from Lach-Ner, s.r.o., Czechia. Commercial sodium hyaluronate (HA) with weight molecular (Mw = 500 000 g/mol; Mw/Mn = 1.5) was provided by Contipro a.s. (Dolni Dobrouc, Czechia) and assigned using SEC-MALLS technique. All chemicals were used as obtained without further purification.

2.2. Extraction and partially deacetylated ChNWs

Extraction of pure chitin from shrimp shell was done according to our previous works with minor modifications (Abdel-Rahman et al., 2015, 2016), in brief, shrimp shells were refluxed with absolute ethanol removed soluble impurities and then, dried at 60 °C overnight in the air-dry oven. The extraction process of chitin (Ch) and chitosan (Cs) consisted of three main steps: demineralization (DM), deprotenization (DP) and deacetylation (DA). The DM step was carried out using aqueous hydrochloric acid (HCl) at ambient temperature (25 ± 2 °C) for 24 h. The obtained solid fraction of crude chitin was washed with Milli-Q water until neutral pH was achieved, then dried at 60 °C for 24 h. In the deproteinization (DP) step, aqueous NaOH was used to remove the non-bounded materials like proteins, dyes, lipids, and pigments. The crude chitin was stirred in 5 % of NaOH at 90 °C for 24 h, where the alkaline solution was exchanged each 2 h with a fresh solution of NaOH. The product was filtered off, washed with Milli-Q water until achieved neutral pH, dried at 60 °C for 12 h.

Chitin nanowhiskers suspension was fabricated by acid-hydrolysis using different concentrations of hydrochloric acid (1, 3, 5 M) at 90 °C for a variable time (1–6 h) under mechanical stirring. The solid-liquid ratio of the chitin suspension was (1/100). After the acid hydrolysis, the suspension was diluted with Milli-Q water and centrifuged at 4000 rpm. The process was repeated five times (each 10 min) until achieved pH 4. The suspension of chitin Nws were transferred into a cellulose dialysis bag (molecular cut 12 − 14 kDa) and dialyzed in Milli-Q water until t neutral pH (6–6.5). Part of the ChNWs suspension was preserved by storing in sealed vessels placed in a refrigerator at 4 °C. The suspension was cast into a plastic petri dish and kept at − 20 °C. Afterward, lyophilized at – 80 °C for 2 days. The partial deacetylation chitin nanowhiskers (ChNWs) was achieved by refluxing chitin with (5–60 % w/v) of sodium hydroxide solution at 90 °C with solid to solvent ratio (1/30 w/w) in the time range of 0.5 − 5 h. Partially deacetylated ChNWs were collected, washed by Milli-Q water until neutral pH was achieved, rinsed with ethanol, vacuum filtered and dried at 60 °C for 12 h to remove moisture.

2.3. Preparation of nanocomposite biofilms (HA/ChNWs)

Partially deacetylated chitin nanowhiskers with DDA 27 % was selected to prepare nanocomposite biofilms from hyaluronan and

different ratio of chitin nanowhiskers by casting-evaporation method. Certain amount of HA (3 %) was dissolved into Milli-Q water at room temperature (rm), then different volume fraction (V$_f$) ratios from partially deacetylated ChNWs (27 % DDA) was added drop by drop into HA solution with smooth mechanical stirrer at rm for 5 h. the nanocomposite solutions were centrifuged at 5000 rpm for 30 min then, casted into petri dishes, dried at 50 °C for 24 h. The obtained biofilms were hydrothermally crosslinked by placing into an oven at 125 °C for 10 min. All prepared samples with different volume fraction (V$_f$) between HA and ChNWs (27 % DDA) are listed in Table S1.

3. Characterization

Native hyaluronan and hyaluronan/chitin nanowhiskers biofilms were measured by a UV/Vis spectrophotometer (JASCO-V550) in the wavelength range of 200–800 nm. MTensile testing was used to investigate the strength of HA/ChNWs biofilms, which was important when it comes to sample handling. It was carried out by Universal testing equipment Z010 from Zwick–Roell (Germany) with 1 kN measuring cell. Samples were cut into a dog bone shape with a parallel specimen length of 12 mm. Testing rate was $10-3$ s-1 and the tests were performed at laboratory temperature.ira3 XM (Tescan, Czechia) was used for imaging of biofilm morphology and further analysis of the diameter of nanowhiskers in transmission mode (STEM). In order to achieve better resolution and prevent overcharging, the samples were coated with a thin conductive metallic layer of Pd/Au alloy (thickness of 20 nm). The morphology imaging was obtained at different magnifications in the resolution regime with the accelerating voltage of 10 kV, using secondary emission detector. TeRheological characterization was executed on nanocomposite solutions prior the film preparation using ARES G2 rheometer (TA Instruments, USA) with cone-plate 40 mm, 2° geometry at 25 °C. Frequency sweep measurements were performed in the range from 0.05–100 Hz at 0.5 and 1 % strain amplitude. The linear viscoelastic region was detected by strain sweeps from 0.05–10 % strain amplitude at 1 Hz. Flow tests were performed by ramping the shear rate from 0.1–100 s^{-1} at logarithmic rate. Prior to the flow test, each sample was pre-sheared at 0.1 s^{-1} for 60 s. Evaporation of the solvent was prevented by a solvent trap.nsile testing was used to investigate the strength of HA/ChNWs biofilms, which was important when it comes to sample handling. It was carried out by Universal testing equipment Z010 from Zwick–Roell (Germany) with 1 kN measuring cell. Samples were cut into a dog bone shape with a parallel specimen length of 12 mm. Testing rate was 10^{-3} s^{-1} and the tests were performed at laboratory temperature.

Cytotoxicity, proliferation and biocompatibility assay of the biofilms was done by using normal human dermal fibroblasts (NHDF) and cell line human primary osteogenic sarcoma (Saos-2). NHDF were isolated from plastic surgery skin sections with the approval of the Ethical Committee of the University Hospital Olomouc and the patient's consent. The study was performed in accordance with the Code of Ethics of the World Medical Association. The morphology and origin of the cells were authenticated in the Histology Department, University Hospital Olomouc. NHDFs were cultured in Dulbecco's Modified Eagle Medium supplemented with 10 % fetal bovine serum (FBS) and 1 % penicillin-streptomycin under standard culture conditions (5 % CO$_2$, 37 °C). Cells were used between the 2nd and 3rd passages (Franková, Pivodová, Vágnerová, Juráňová, & Ulrichová, 2016). The saos-2 cell line was obtained from European Collection and Authenticated Cell Culture (ECACC) and cultivated according to the protocol in McCoys´5A (modified) medium supplemented with 10 % of FBS and % penicillin-streptomycin under (5 % CO$_2$, 37 °C) standard culture conditions (Tomšíčková, Frankova, Dolezel, & Ulrichova, 2013).

Reduction of tetrazolium salt, 3-(4,5-dimethylthiazol-2-yl)-2,5-diphenyltetrazolium bromide (MTT) was used as a parameter for cytotoxicity assessment. MTT was reduced by intracellular dehydrogenases of viable living cells that lead to the formation of purple formazan

crystals, insoluble in aqueous solutions. After dissolution in an organic solvent, the absorbance is monitored. The cells on 96-well microplates were treated with extract of tested materials at a final concentration of biofilm 125, 250, 500 and 1000 µg/ml and it was quantified after 24 h. As a control, cells were used only with the cultivation medium. After the incubation period, the medium was removed and serum-free medium supplemented with MTT (5 mg/ml) was applied to the cells for 2 h (37 °C, dark). The solution was removed, and the crystals were dissolved in DMSO with NH$_3$ (1 %, v/v). The absorbance was measured at a wavelength of 540 nm (Tecan, Czechia). In addition, live/dead staining was performed. The selected biofilms were fitted and placed on the bottom of 8 well plates (Chamber slide), sterilized under the UV for at least 15 min and NHDFs and Saos-2 were added. The samples were incubated 5 min with the staining solution (2 mg/ml of propidium iodide, 5 mg/ml of fluorescein diacetate in PBS). Finally rinsed with PBS before imaging with fluorescent microscopy.

4. Results and discussions

4.1. Extraction of partially de-acetylated ChNWs

Chitin is a part of the matrix (chitin-protein-minerals) deposit which forms the rigid shell of shrimps (Abdel-Rahman et al., 2015; Chaussard & Domard, 2004). The extraction process of chitin could be summarized by two main steps: removal of minerals (demineralization step; DM) using diluted HCl and removal of proteins (deproteinization step; DP) using NaOH (Fig. 1a). Residual proteins after 24 h of treatment with NaOH were less than 0.005 (Fig.1b), measured by the standard method (Chaussard & Domard, 2004). Low residual protein content was very important for the potential medical applications of chitin and chitosan biopolymers.

Effects of acid concentrations (1, 3, 5 M) on the degree of deacetylation (DDA) of pure ChNWs were monitored using solid-state NMR spectroscopy (Fig. 1c). The DDA of ChNWs slightly increased from 8.3 % for native chitin to 12.2 % when the hydrolysis was done for 6 h at 90 °C using different acid concentrations (1, 3, 5 M). From Fig. 1c, we could conclude that the strong acid treatment affected the surface of chitin chains with no significant changes in the skeleton structure of chitin (in DDA percentage). ^{13}C CP/MAS NMR experiments were used to elucidate the chemical structure of ChNWs (i) treated with different acid concentrations (HCl) and (ii) treated with different concentrations of NaOH. The results were compared with the purified raw material (5 % NaOH; Fig. 1c, d– black lines). The assignment of signals in ^{13}C CP/MAS NMR spectra was based on data from literature (David et al., 2008; Ottey, Vårum, & Smidsrød, 1996), and depicted in Fig. 1c and d.

All ^{13}C CP/MAS NMR spectra of the neat and treated chitosan systems show relatively narrow peaks (half-width ca. 300 Hz), which indicates their well-ordered structure in all cases. Furthermore, no signal was detected at ca. 33 ppm in ^{13}C CP/MAS NMR spectra (Fig. 1c, d), which indicated the absence of any residual proteins and/or lipids in all systems (Roca et al., 2012). Typically, the chitin/chitosan samples are defined by a degree of deacetylation, using Eq. 3 from the ^{13}C CP/MAS NMR spectra.

Our system, denoted as neat chitin, contains 9.0 ± 0.5 mol % of chitosan units. In cases of acid-treated samples, the content of chitosan units is almost independent of the acid concentration and was defined as 12.8 ± 0.5 mol % for all three samples. However, the concentration of the alkaline solution had a strong influence on the final chitin/chitosan ratio. The number of chitosan units increased at higher concentrations of NaOH. After the treatment in 10, 20, 30 and 40 % solution of NaOH, the deacetylation process was promoted and the chitosan content was 17.6, 18.8, 23.9 and 27.8 ± 0.5 mol. %, respectively.

Fig. 1d shows ^{13}C CP/MAS NMR spectra of partially deacetylated ChNWs (3 M HCl, 6 h, 90 °C) was prepared using different concentrations of NaOH (5, 10, 20, 30, 40, and 50 w/v.%) for 5 h at 70 °C. The degree of deacetylation (DDA %) slightly increased from 8.3 to 27 %
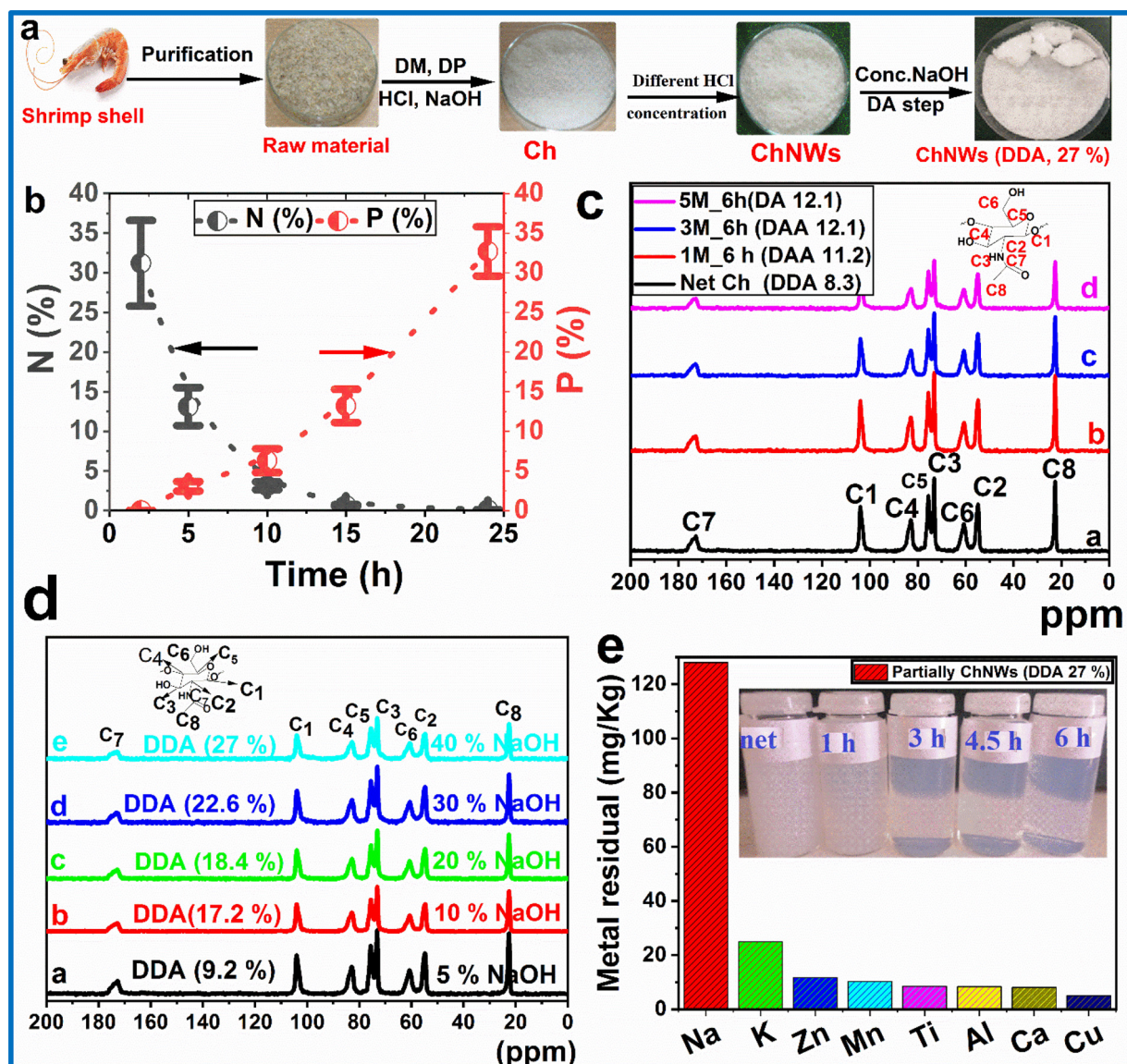
Fig. 1. Representative extraction sequence of partially deacetylated chitin nanowhiskers. **(a)** Extraction sequence of partially ChNWs; **(b)** Relation between treatment time and residual protein content of demineralized shrimp shell measured by elemental analysis and UV/VIS spectroscopy; **(c)** ^{13}C-CP/MAS NMR spectra of net Ch and ChNWs treated with different HCl concentrations (1, 3, 5 M) at 90 ℃ for 6 h; **(d)** Effect of NaOH concentrations (5, 10, 20, 30, 40, 50 %) on the DDA of ChNWs at 90 ℃; **(e)** Residual metal ions content in partially deacetylated ChNWs (27 %), photos in the upper right corner shows the samples of partially deacetylated ChNWs suspension using different treatment time (1 − 6 h).

upon increasing NaOH concentration from 5 to 40 %, respectively. Chitin nanowhiskers with 27 % DDA were used for all experiments and preparation of nanocomposite biofilms. Fig. 1e explores the residual metal ions after nanowhiskers preparation (DDA 27 %). This residual amount of metal ions completely meets the criteria of European pharmacopeia for medical application materials. The upper right corner of the Fig. 1e shows the effect of time on the extraction of partially deacetylated ChNWs from chitin using 40 % NaOH, 3 M HCl at different treatment time (1 − 6 h). The net Ch shows dense shape after 1 h of sonication at room temperature and after acid treatment (1, 3, 4.5, 6 h) the partially deacetylated ChNWs nanowhiskers solution had a high homogenous distribution.

Net shrimp shell has a flat surface morphology with compact structure and small particles on the shrimp surface (Fig. S1a, supporting information). After the demineralization step (DM) for 24 h using 10 % HCl at room temperature (Section 2.2), shrimp shell had a micro-fibrillose structure with length more than 10 μm and porous surface structure with the pore size of about 500 nm. This shape of shrimp after

the acid treatment might be caused by destroying the matrix of the complex chitin/protein/minerals composition and generating by decomposition of the mineral salts (Fig. S1b, supporting information). After basic treatment (5 % NaOH) for 24 h, more micro-fibrils of chitin were observed with much bigger pore size (700 nm) of the porous surface structure pore size (Fig. S1b, supporting information). Low concentration of hydrochloric acid acted on the surface of chitin chains and caused intra-chain hydrolysis destroying the chemical bonds between proteins and chitin functional groups which gave rise to more fibrillose chitin structure (Fig. S1c, supporting information).

Figure 2Aa shows the effect of acid treatment time using partially deacetylated chitin (DDA 27 %) on the length, width, and morphology of NWs. STEM of ChNWs (27 % DDA) was obtained after 1, 3, 4.5 and 6 h using 3 M HCl at 90 ℃ were shown in Fig. 2A(a–d). STEM showed (Fig. 2a,b; white circle) highly agglomerated sections of nanowhiskers after 1 and 3 h of acid hydrolysis, and SEM (Fig. 2Ae, f; 1 h, 3 h) revealed that nanowhiskers formed strong bundle network between single nanowhiskers. After longer treatment time using HCl (3 M), i.e. 4.5 and
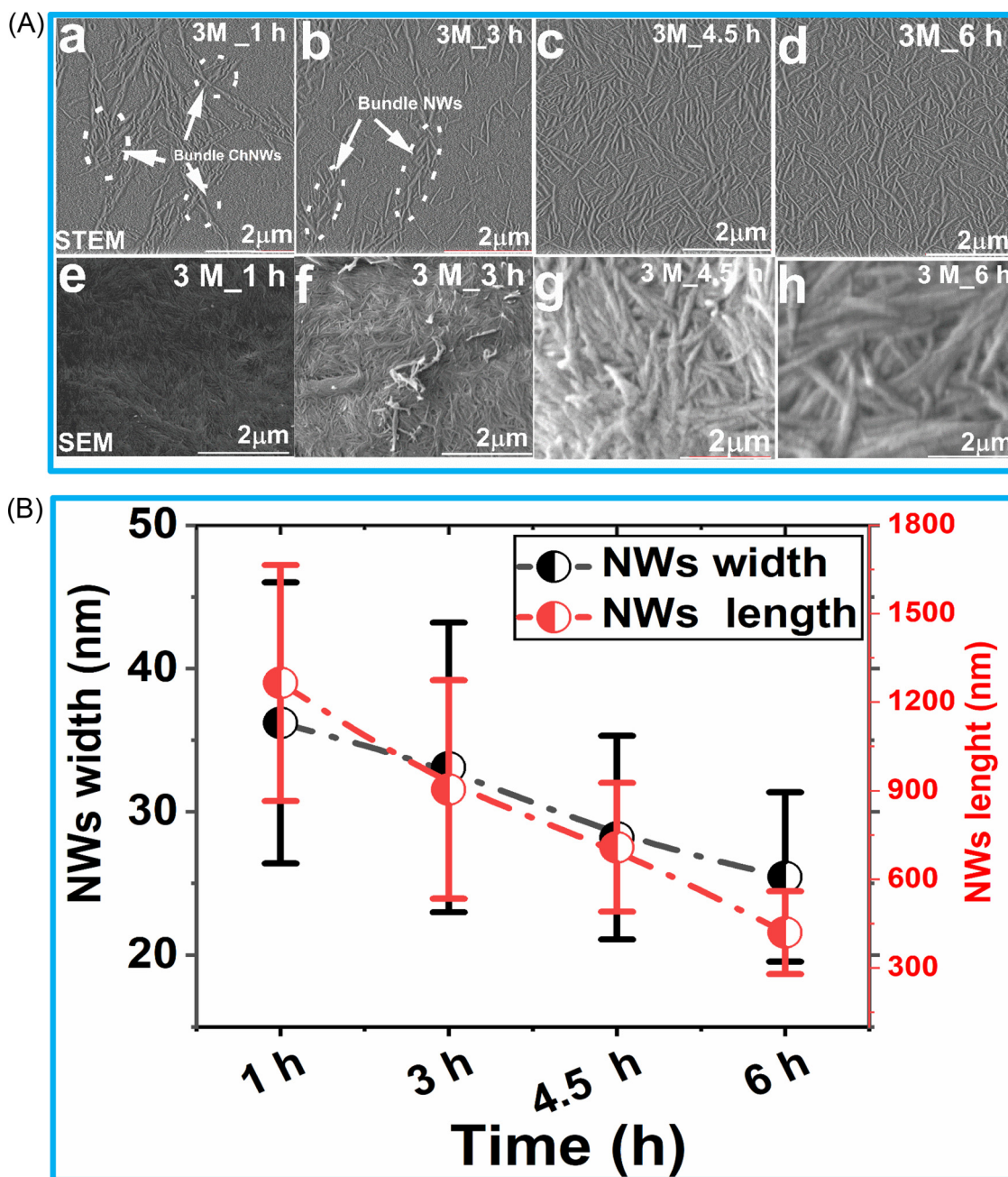
Fig. 2. A: Representative STEM and SEM images of partially deacetylated ChNWs (27 % DDA) at different treatment time by acid (1–6 h). **B:** Representative effect of time of acid treatments on the length and width of partially deacetylated chitin nanowhiskers (27 % DDA). (For interpretation of the references to color in this figure legend, the reader is referred to the web version of this article.)

6 h (Fig. 2Ac,d), more single fibrils appeared with lesser aggregation without a network structure generated between ChNWs. After 6 h of treatment with HCl, single chitin nanowhiskers were obtained without any aggregation/agglomeration between NWs (Fig. 2Ad,h).

Fig. 2B shows the effects of time treatment using hydrochloric acid (3 M) at 90 °C on length and width of partially deacetylated ChNWs with 27 % degree of deacetylation. From Fig. 2B and histograms of widths (Fig. S2a-d, supporting information) and length (Fig. S2e-h, supporting information) of ChNWs (DDA 27 %), the length of the NWs was decreased significantly with the increasing time of acid treatment from 1, 3, 4.5, to 6 h and took the value of 1265, 904, 709 and 419 nm, respectively. The width of NWs decreased with the increasing treatment time from 36.4 to 19.7 nm (Figs. 2B, S2 Supporting information). The decrease in width and length of the nanowhiskers during the extended

time of acid treatment might be caused by the hydrolysis of the amorphous part of the chitin chains while the crystalline part was retained intact.

Fig. 3 shows the XRD, crystallinity index and yield percent of the ChNWs extracted after different hydrolysis time varying from 1 to 6 h using 3 M of HCl. XRD measurements were employed to reveal detailed information about the crystallographic structure of the native and partially deacetylated chitin nanowhiskers (ChNWs) using different treatment time (Fig. 3a, b). All of the native chitin and partially deacetylated chitin nanowhiskers exhibited six diffraction peaks at $2\theta = 9.2°, 12.7°, 19.4°, 20.7°, 23.4°,$ and $26.5°$ indexed as (020), (021), (110), (120), (130), and (013), respectively (Fig. 3a, b), proposed a crystalline structure of the α-chitin (Noishiki et al., 2003; Zhu et al., 2019).
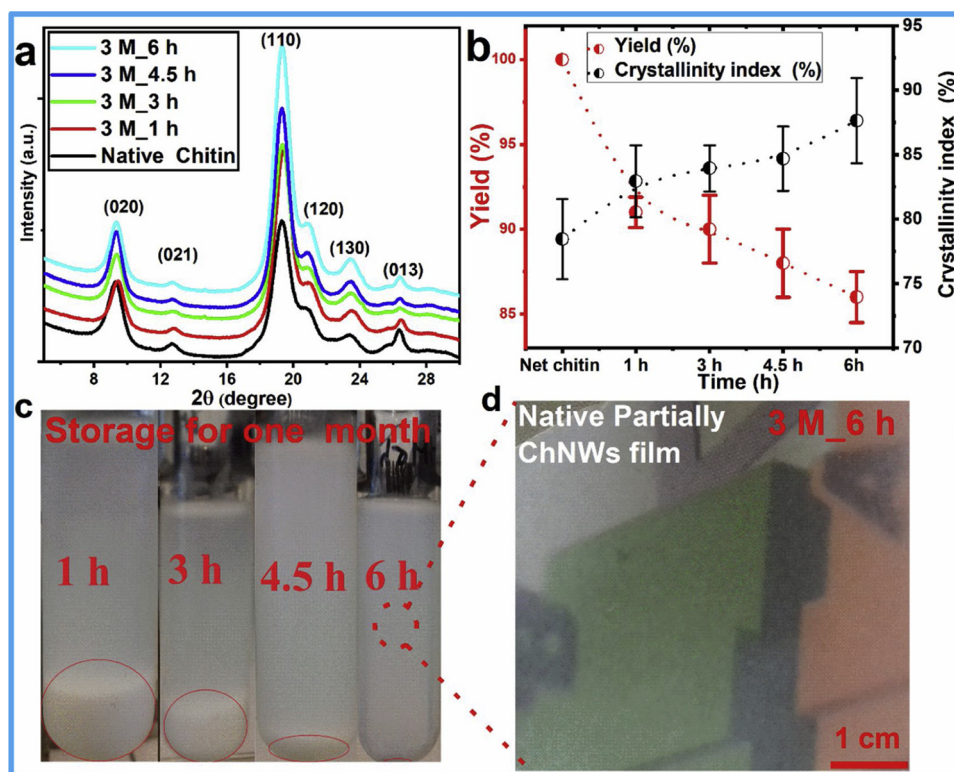
Fig. 3. Representative XRD, crystallinity yield percent, and stability of the extracted partially deacetylated ChNWs.

The diffraction peaks of the native Ch were much broader and weaker than that of the partially deacetylated ChNWs, indicated a decrease in crystallinity (Fig. 3b). Meanwhile, the crystallinity content was slightly increased from 78.45 ± 3.1–87.63 ± 3.3 % with the increasing time of acid hydrolysis from 1 h to 6 h. In the view of these results, the partially deacetylated ChNWs retained the intrinsic structure and the property of the native α-chitin. The yield percent of NWs was slightly decreased with the prolonged acid treatment time with the loss percent of about 15 % from the dry weight due to, the smaller size of NWs which was difficult to collect during the purification steps (Fig. 3b).

Fig. 3c shows the stability of colloids solutions of NWs was extracted at different treatment time after one month of storage at room temperature (20 ± 3 °C) with pH of the solution of about (4.5–5). After one month of storage, at shorter treatment time, the NWs were highly aggregated into a bulk structure due to the electrostatic interaction between the charges on the surface of the partially deacetylated NWs (free amino groups). This phenomenon was also confirmed in Fig. 1a using STEM (Fig. 2Aa). At longer treatment time above 3 h and 4.5, lower quantities of NWs precipitated (compared with 1 h treatment). Partially deacetylated ChNWs was extracted after 6 h of treatment with 3 M of HCl were highly dispersed without precipitations after one month of storage at room temperature (Fig. 3c). Fig. 3d show the biofilm of net ChNWs after (6 h, 3 M HCl, one-month storage at RT), with high transmittance properties and uniform surface morphology with highly oriented nanowhiskers in the film matrix.

4.2. Fabrication of HA/ChNWs biofilms

Scheme 1a shows the skeleton structure of shrimp shell matrix before and after chemical treatment and generated chitin microfibrils (Fig. S1b,c, Supporting information). Chitin microfibrils were generated after the DM and DP with highly interconnected and porous structure (Fig. S1b,c, Supporting information). Partially deacetylated chitin nanowhiskers (DDA 27 %) with controlled dimensions of short nanofibrils

with the width and length of 19 nm, and 410 nm, respectively (Scheme 1b), were generated as a result of acid hydrolysis (3 M; 6 h). Partially deacetylated ChNWs with DDA 27 % interacted with hyaluronan (negative charge surface) via the physical and chemical interactions (ionic, hydrogen bonds, van der Waals) between the functional groups of NWs and HA (Scheme 1b, c). During hydrothermal treatment of nanocomposite biofilm at high temperature, ester and amide bonds could be partially formed between the functional groups of hyaluronan ($-OH$, $-COONa$) and partially chitin nanowhiskers ($-OH$, $-NH2$, $-NHCOCH_3$) (Scheme 1c). In Scheme 1d, it is apparent that the NWs were well dispersed and oriented within the HA matrix with no agglomeration observed between the nano-fibrils with the same size of single nanowhiskers.

Rheology is an important parameter of polymer processing and, due to its sensitivity to structural features, might be used as indirect evidence of the structural changes. The rheological properties were altered by the presence of partially deacetylated NWs compared to the net HA solution (Fig. 4). All samples show significant shear thinning behavior and conforms well to both the Herschel-Bulkley and the power-law viscosity models. The values and meaning of the fitting parameters are discussed in supplementary info (Fig. S3, Supporting information). Moreover, the 1/25, 1/35 and 1/50 HA/ChNWs solutions were slightly thixotropic, the remaining samples showed no thixotropy. The flow viscosity drops from the initial 6.9–17.2 Pa s (measured after pre-shear) to 0.8–1.3 Pa s at high shear rates (Fig. 4a). All nanocomposites with different ratios of HA/ChNWs (1–50) showed higher viscosity compared to the net HA, which increased nearly linearly up to 17.2 Pa·s with the increase of the volume fraction of NWs content with the exception of 1:50 HA/NW sample (Fig. 4c). Provided the viscosity of the net nanowhisker suspension was as low as 9.7 mPa·s, the observed increase in viscosity is far higher than would be expected from a simple flow distortion caused by solid obstacles. However, a similar increase in viscosity was previously reported due to formation of nanoparticle/polymer structure induced by nanoparticle interaction with polymer chains (Lepcio et al., 2018). As the structure was destroyed upon
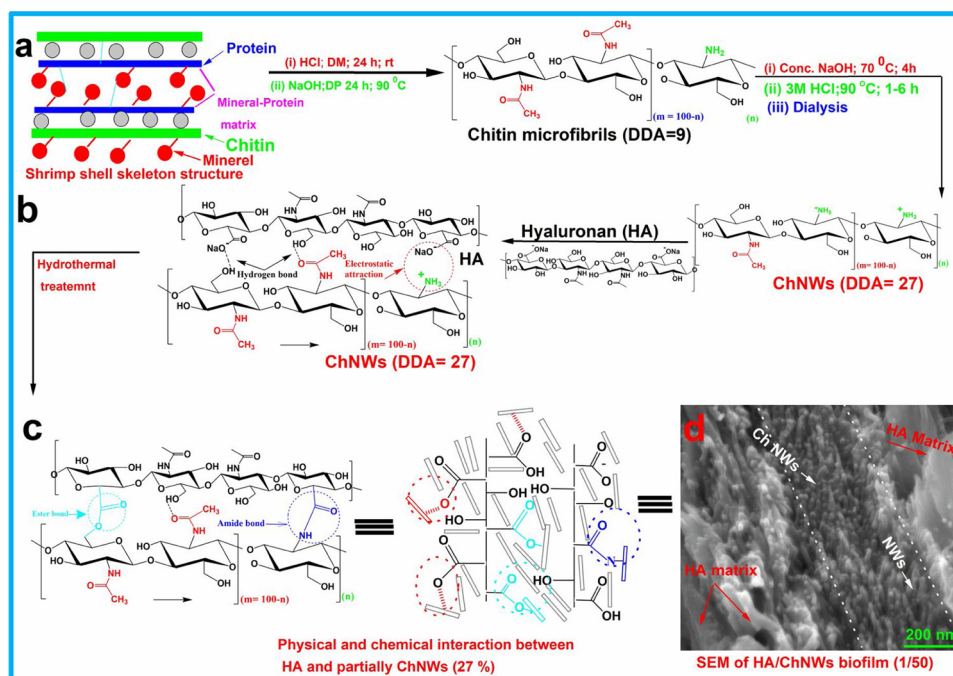
Scheme 1. Arepresentative mechanism of extraction of partially deacetylated chitin nanowhiskers and interactions between hyaluronan (HA) and partially deacetylated chitin nanowhiskers (ChNWs).

shearing, the increase in viscosity of nanocomposite solutions diminished and for most samples dropped below the viscosity of the net HA at higher shear rates. Furthermore, regarding the rheological data, the structuring tendency reached a threshold between 1/35 and 1/50 HA/NW and the 1/50 HA/NW sample was qualitatively dissimilar to the rest of the samples. An analogical situation was observed for the

oscillatory tests.

Fig. 4d shows the dependence of storage and loss moduli, loss factor tan δ and complex viscosity of HA/NW solutions on the frequency at 1 % strain amplitude. We note that the 1 % (Fig. 4d) strain amplitude lies on the very edge of the linear viscoelastic region (LVR) for some samples (Fig. 4b), however, comparison with 0.5 % strain amplitude
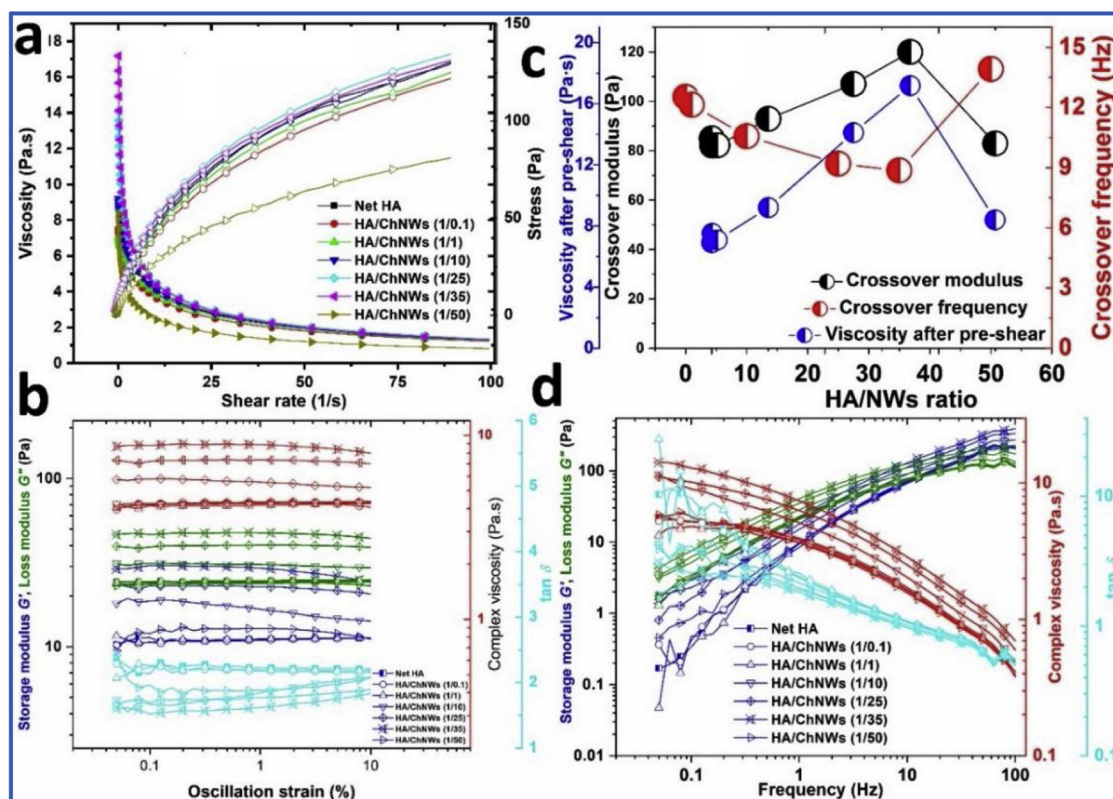

Fig. 4. Rheological properties of net HA and HA/ChNWs nanocomposites.

measurements (data not shown) revealed no significant hints of non-linear effects at the higher strain amplitude. Since the 1 % strain amplitude oscillatory tests provided a better signal-to-noise ratio, we chose to present this data. Clearly, the effect of NW on the rheological response of HA solution is more apparent at lower shear rates/frequencies. This finding was consistent with the previous reports on behavior of nanoparticles in polymer fluids (Akhlaghi, Menceloglu, & Akbulut, 2016; Cassagnau, 2008; Jung, Lee, & Shin, 2014; Mahallati, Hassanabadi Hojjat, Wilhelm, & Rodrigue, 2016; Patras, Qiao, & Solomon, 2001).

The reason for that was that the reputation dynamics of polymer chains was slowed down by nanoparticles, contrary to Rouse dynamics that remains unaffected. The dependence of crossover modulus on HA/NW ratio showed a nearly linear increase from 82 Pa to 120 Pa with the increasing NWs content up to 1/35 HA/NWs, followed by an immense drop to the value of 83 Pa for the 1/50 HA/NWs sample. Crossover frequency, on the other hand, decreased from 12.5 Hz for the net HA to 8.9 Hz for 1/35 HA/NW, followed by an increase to 13.9 Hz for the 1/50 HA/NWs sample. The higher crossover frequency corresponds to shorter relaxation time and vice versa. Polymer relaxation is slowed down by attractively interacting nanoparticles (Jancar et al., 2010). Therefore, lower crossover frequency might indicate attractive interaction between the HA and ChNWs.

4.3. Physicochemical properties of HA/ChNWs biofilms

Fig. 5 shows the ATR-FTIR spectra of net HA, partially deacetylated ChNWs and biofilms of HA/ChNWs with different ratio of ChNWs to HA, confirming the evaluation of the chemical interactions and formations of a polymeric structure (Fig. 5). The ATR-FTIR spectra for HA/ChNWs biofilms in the fingerprint region from 900 cm^{-1} to 1800 cm^{-1} evidenced the presence of ionic interactions. In α-chitin, two absorption peaks are observed at 1655 and 1622 cm^{-1} corresponding to α-chitin phase. β-chitin is characterized by only one peak at 1656 cm^{-1}. Accordingly, the two peaks around 1655 and 1622 cm^{-1} observed in the

FTIR spectrum (Fig. 5) confirmed that the chitin from shrimp shells was in α-crystalline form (Abdel-Rahman et al., 2015). For high DDA chitosan, the band of amide I at 1655 cm^{-1} had a higher intensity than the band of amide II at 1557 cm^{-1}, which suggests efficient deacetylation. When the deacetylation of chitin occurs, the absorption band assigned to amide II decreases, while the increased intensity of the amide I band indicates the formation of NH_2 groups. However, in our case, only low DDA showed (27 %) the peak at 1557 cm^{-1} stronger than the peak at 1655 cm^{-1}. The positively charged amino group of the partially deacetylated ChNWs as observed with the NH_3^+ bending vibrations (1557 cm^{-1}) interacted with the negatively charged COO^- of HA (1622 cm^{-1}).

The formation of polyelectrolyte complex PEC and crosslinking resulted in a reduced absorption for the OH and NH stretching vibration peaks. In addition, the presence of new peak at 1702 cm^{-1} region indicated the esterification reaction between carboxylic groups of HA and hydroxyl groups of NWs and peak intensity ws increased by increase the ratio of NWs into the matrix. The peak of net HA film at 1744 cm^{-1} corresponded to the physical ester bond between COOH and OH groups of HA and disappeared after the addition of NWs, this could be due to the interaction between COOH of HA and NH_2 and $-OH$ of the partially deacetylated ChNWs (Fig. 5) (Abdel-Mohsen et al., 2016; Abdel-Rahman et al., 2016). The peak intensity of free amino groups at 1557 cm^{-1} weakened at higher nanofiller loading in the HA matrix due to the strong ionic interaction between the amino and the carboxylic groups of the partially deacetylated Ch and HA matrix, respectively (Fig. 5).

The microstructures of the HA/ChNWs nanocomposite biofilms were investigated by X-ray diffraction. As shown in Fig. S4 (Supporting information), neat HA film exhibited a wide diffraction peak around 2θ = 20–22°, indicated the amorphous state of the hyaluronan matrix. Partially deacetylated chitin nanowhiskers (DDA = 27 %) exhibited six diffraction peaks at 2θ = 9.4°, 12.9°, 19.3°, 20.8°, 23.5°, and 26.5° indexed as (020 plane), (021 plane), (110 plane), (120 plane), (130 plane), and (013 plane) (Ifuku et al., 2009; Zhu et al., 2019),
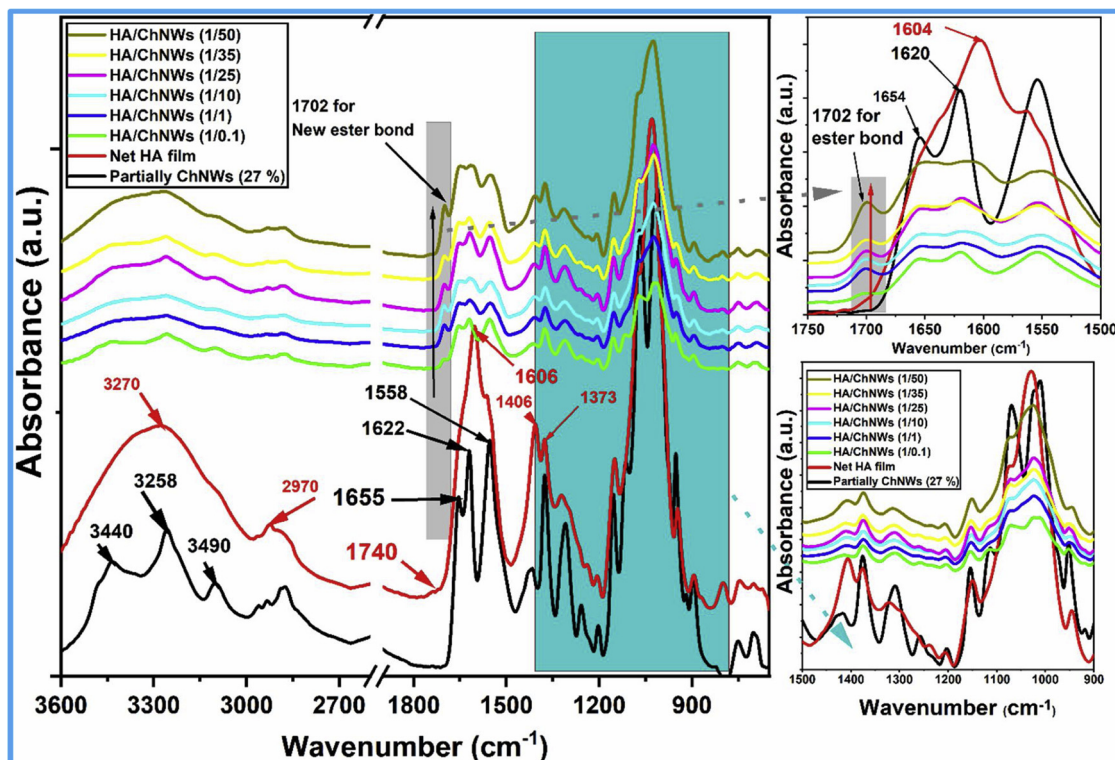

Fig. 5. ATR-FTIR of native hyaluronan and hyaluronan/partially deacetylated chitin nanowhiskers (DDA = 27 %) nanocomposite biofilms.

respectively (Fig. 3a). This was consistent with the diffraction peak of native chitin, suggesting that the acidolysis process did not affect the crystalline structure of the purified chitin. When the ratio of HA/ChNWs was less than (1/1) V_f. (0.012), there was no peak assigned to ChNWs. Afterward, a small peak around 9.42° assigned to 020 planes of CNCs gradually appeared in the nanocomposite. Furthermore, the intensity of peaks at 9.42° and 19.34° was increased with the increase of the ratio between the HA and the ChNWs from 1 to 50 and slight shifted, indicating that no intercalation of NWs into the interlayer of the HA matrix occurred as well as a partial orientation of NWs took place in the HA matrix biofilm via the interfacial interactions with ChNWs. The partially deacetylated chitin nanowhiskers chains with large molecular size might be blocked by strong physical and partially chemical bonds among the sheets of the HA matrix. Because the XRD pattern was a statistical result, higher ChNWs loading strengthened the peak intensities and the crystallinity of nanocomposite biofilms were enhanced with the increased volume fraction (V_f) ratios between HA and ChNWs (Fig. S4, Supporting information). The XRD results suggest that ChNWs were successfully incorporated into the hyaluronan matrix (Fig. S4, Supporting information). Based on the XRD results, it could be concluded that ChNWs could be uniformly distributed and partially oriented in the HA biofilm, but their layer space remained unchanged.

Fig. S5 (Supporting information) shows the light transmittance spectra of the nanocomposite biofilms from net HA, HA/ChNWs with a different ratio, and net ChNWs. The transmittance of net HA film was high (82 %) in the visible light range from (400–750 nm). The transmittance properties of biofilms were decreased by increasing the weight ratio between hyaluronan and nanowhiskers from (1/1 to 1/50). At lower ratios (0.1–10) the optical transmittance was decreased slightly, up to 1/35 and 1/50 wt ratio. This result suggests that the nanowhiskers content had a little influence on the transparency of nanocomposite biofilms. Therefore, due to the small diameter of NWs, it was possible to prepare high-strength HA/ChNWs nanocomposite with a high-volume fraction of nanowhiskers combined with a preserved transparency. The partially deacetylated ChNWs showed a large surface area and small dimensions, which provided a higher probability of their mutual interaction with the hyaluronan matrix, leading to the strong adhesion between HA and ChNWs. According to the results of FTIR, X-RD, SEM, and optical transmittance, the partially deacetylated ChNWs were dispersed homogeneously and embedded very well in the HA matrix.

The swelling percentage (SP) of the nanocomposite biofilms were evaluated in water and phosphate buffer solution under physiological conditions (PBS, pH 7.5 at 37 °C). All nanocomposite films showed a high swelling percentage after 1 h (Figs. S6$_{a,b}$, S7, Supporting information). After 3 h of immersed in water and PBS, the SP was decreased in both water and PBS medium and showed no significant differences between immersed samples in water and PBS after 24 h (Fig. S7, Supporting information). The stability of nanocomposite biofilms due to physical and chemical bonds generated between HA and ChNWs functional groups as confirmed by FTIR measurements (Fig. 5). Fig. 6c shows the weight loss of nanocomposites biofilm after 24 h of immersed in water and PBS solution at 37 °C. As shown in figure S6c, increase the volume fraction ratio of NWs in HA matrix improved the hydrolytic stability of biofilms. In the first 1 h, the non-bonded HA fast leached than ChNWs (Fig. S6d) and after 24 h of immersed more NWs was leached from the matrix (Fig. S6d).

4.4. Mechanical properties of nanocomposite biofilms

Mechanical robustness, namely tensile modulus and stress were enhanced considerably with an addition of ChNWs into HA matrix. The modification of property in relative units linearly scales with the volume fraction of ChNWs (Fig. 6a,b). Yield and further plastic deformation of nanocomposites were evident at lower volume fraction however, up to 25 vol. % of ChNWs. Yield and further plastic deformation of polymer nanocomposites diminish at high volume

fractions 35 and 50 vol. % and samples brittle fracture. Tensile modulus and yield stress of the HA matrix were measured as 2.58 ± 0.16 GPa and 69.64 ± 3.71 MPa, respectively. With an addition of 50 vol. % of ChNWs in HA matrix, tensile modulus and stress was enhanced considerably to 4.54 ± 0,18 GPa (+76 % increase compared to neat HA) and 80.54 ± 10.02 MPa (+31 % increase compared to neat HA), respectively (Fig. 6b). On the other hand, ductility of the films decreases with an addition of ChNWs (Fig. 6b). This embrittlement of the system can be caused due to the addition of stiff reinforcing phase and increased number of NWs ends and their aggregation decreasing their reinforcing effectivity at higher loadings. It is mentioned that a similar behavior to what has been seen here was also observed for natural and synthetic films reinforced with α-chitin whiskers, in which the Tensile modulus and yield stress of the films initially were increased with increasing chitin whisker content and leveled off when the whisker contents was about 20 wt.% or greater (Chen, Liu, Chang, Cao, & Anderson, 2009; Gopalan Nair & Dufresne, 2003; Hariraksapitak & Supaphol, 2010; Lu, Weng, & Zhang, 2004; Peng & Chen, 2018). The mechanical and viscoelastic response of such hybrid nanocomposite systems is not well understood yet but common theories in the field of polymer nanocomposites include immobilization of polymer chains adsorbed on the surface of nanosized filler while altering relaxations of the chains and thus their time-temperature dependent mechanical properties (Jancar & Recman, 2010; Jancar, 2008). Strong cationic-anionic interfacial interactions between ChNWs and HA arise a formation of strong interphase which can be a couple of nanometers thick. HA chains have altered relaxations. This was supported via our rheological and FTIR measurements suggesting attractive interactions and possible esterification between HA and ChNWs affecting the relaxation of HA which might be responsible for modification of nanocomposites properties.

The surface fracture after the mechanical experiments were explored in Fig. 7. SEM images of fracture surface of native HA film (Fig. 7a–c) and nanocomposite biofilms with different NWs ratios HA/ChNWs (1/1, Fig. 7d–f), HA/ChNWs (1/10, Fig. S8a-c; supporting information), HA/ChNWs (1/25, Fig. S8d-f, supporting information), HA/ChNWs (1/35, Fig. S8g-I, supporting information), HA/ChNWs (1/50, Fig. 7g–i). The modeling results demonstrated that the HA/ChNWs biofilms with different ratios exhibited superior mechanical performance over the net HA film. It was well known that the mechanical performance of polymer nanocomposites is directly associated with the dispersion state of the reinforcing agents and interfacial adhesion between the reinforcing agent and polymer matrix. Therefore, to interpret the observed distinctive reinforcing efficiency of the partially deacetylated chitin nanowhiskers with DDA of 27 % in the HA matrix, their fracture surface morphology was observed using SEM, as shown in Figs. 7, S8 (Supporting information). The neat HA film showed a very smooth fracture surface (Fig. 7a–c). The incorporation of partially deacetylated ChNWs from 0.1 to 50-volume fraction (V_f) generated a very distinctive fracture morphology. For HA/ChNWs biofilm (Fig. 7d–f), a homogeneous fracture surface (1/1), including smooth phase (corresponding to the unfilled matrix) and relatively rough phase (corresponding to the ChNWs-filled matrix), was clearly observed.

The formation of ChNWs clusters and a highly entangled network (Fig. 7e, f) were responsible for the poor dispersion state. However, no microsized fibers could be seen on the fracture surface, suggesting that the ChNWs were still distributed at nanoscale in the HA matrix at this loading level. At the ratio of (1/10, Fig. S8a–c, Supporting information) of HA to ChNWs, the fracture surface became rougher with the presence of a considerable number of voids and nanowhiskers (Fig. S8a–c, Supporting information). It was postulated that at this loading level, the ChNWs aggregated in the form of microsized fibers, which were further pulled out under an external force, leaving the observed voids. With the further increase in the concentration of the ChNWs to (1/10), more significant ChNWs distrusted and without holes were clearly found on the fracture surface (Fig. S8a–c, Supporting information). Fig. S8g–i
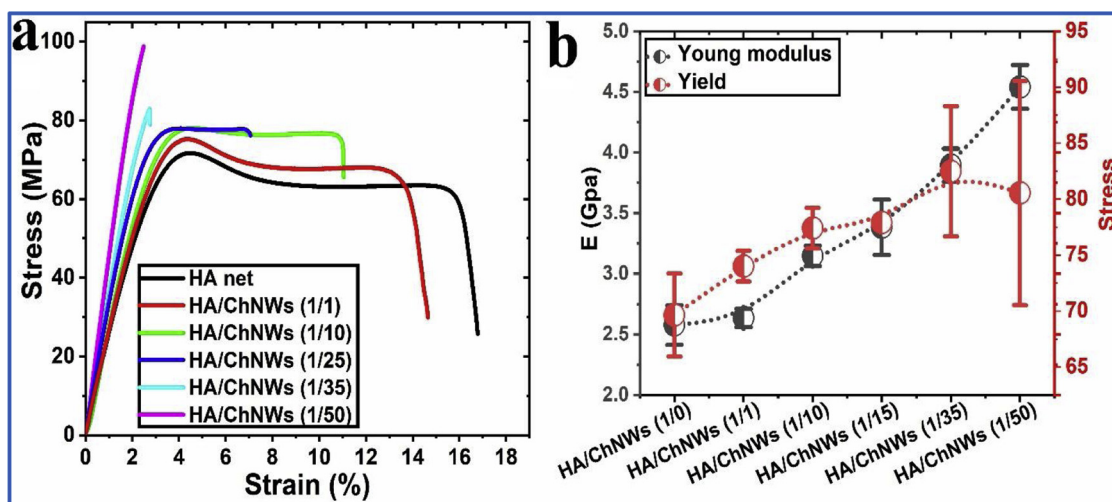
Fig. 6. Representative stress-strain curves for nanocomposites biofilm with different content of ChNWs in HA matrix **(a)**. A plot of change of mechanical properties (tensile modulus and yield/maximum stress) in relative units (divided by properties of the neat matrix) as a function of ChNWs volume fraction **(b)**.

(Supporting information) visualizes a layered morphology reminiscent of a surface fracture of HA/ChNWs (1/35) with a high distribution of nanowhiskers within the HA matrix without holes in the fracture morphology with highly oriented ChNWs in the matrix. At the high-volume fraction (V_f) of nanowhiskers (1/50), the morphology of nanocomposites showed high orientation with well-distributed nanowhiskers in the HA matrix and without microsized fibers from NWs

(Fig. 7g–i).

4.5. Bactericidal and toxicity properties of biofilms

Antibacterial properties are another important issue for food packaging as well as for wound dressing and skin regeneration application. The antibacterial activities of HA/ChNWs nanocomposite

Fig. 7. SEM of fracture surface morphologies of HA/ChNWs nanocomposite biofilms.

Fig. 8. Bactericidal properties of nanocomposite biofilm against different types of bacteria.

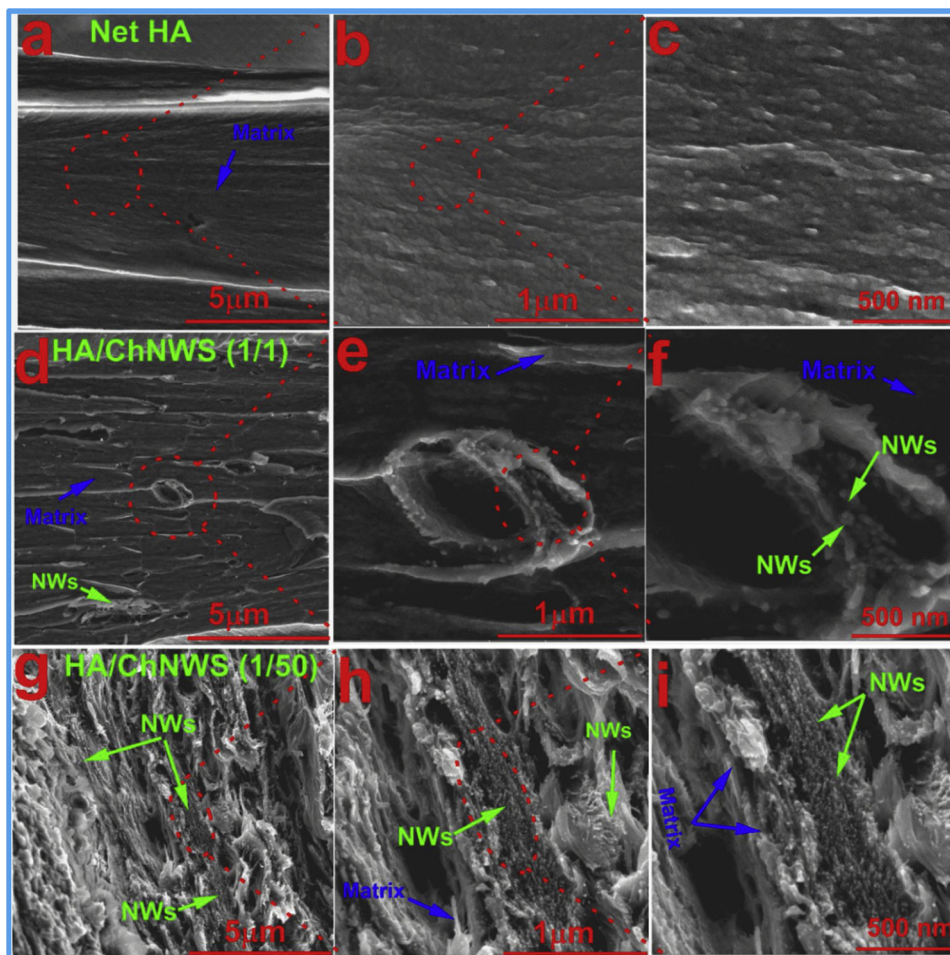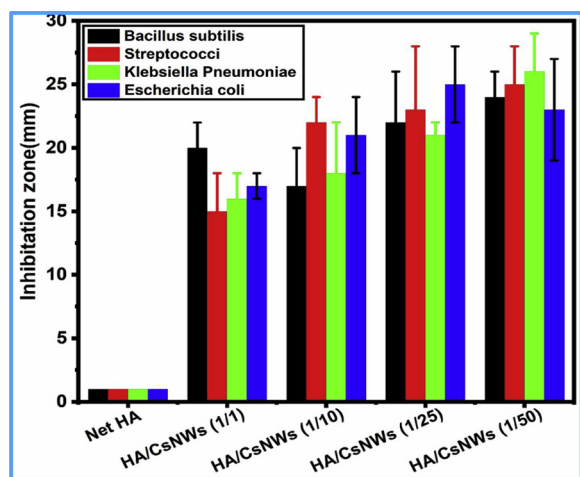biofilms with different ratios against both the gram-negative (*Escherichia coli, Klebsiella pneumoniae)* and gram-positive (*Bacillus subtilis, Streptococci*) were examined, as shown in Figs. 8, S9, Supporting information). In the net HA biofilm, there was no inhabitation zone visulized around the specimens, indicating that the native HA biofilm had no antibacterial properties against type types of bacteria (Figs. 8, S9, Supporting information). The inhibition zone gradually increased upon increasing the concentration of CHNWs in the biofilm matrix from 1 to 50 % (Figs. 8) Furthermore, the antibacterial properties of the biofilms against gram-negative slightly better than against gram-positive bacteria. The antimicrobial performance of CS against gram-negative/positive bacteria has been reported in the recent years

(Krajewska, Wydro, & Jańczyk, 2011; Li et al., 2016; Sahariah et al., 2015).

The antibacterial mechanisms of partially deacetylated chitin nanowhiskers (ChNWs) were suggested and could be concludedas follows: (i) Presence of partially amino groups on partially deacetylated chitin nanowhiskers might be interact with the anionic groups on the cell membrane of gram-negative bacteria, lading the leakage of intracellular constitutes (Abdel-Mohsen et al., 2016); (ii) ChNWs with nano-size (less than 40 nm width) penetrated into the cell nucleus, hindering the synthesis of RNA and proteins (Přichystalová et al., 2014); and (iii) ChNWs could act as a adsorbing agent, which bound metals to inhibit the bacterial growth and toxin production (Abdel-Mohsen, Aly, Hrdina, & El-Aref, 2012).

In the presented article, it was evaluated that the cytotoxicity and biocompatibility of HA/ChNWs nanocomposite biofilms in different ration using Saos-2 cells and NHDFs with highly comparable results. These cells were chosen to respect the future application of the nano-composite biofilms as a wound dressing or the drug delivery system. Based on the MTT test, it was determined that none of the prepared nanocomposite biofilms in all the tested concentrations were toxic to the cells (the viability higher than 80 %, Fig. 9a,b). Similar results were obtained by Zubareva et al. (Zubareva, Shagdarova, Varlamov, Kashirina, & Svirshchevskaya, 2017) who postulated that positively charged chitosan did not cause the toxicity of the variety of cells as well as Haridas et al. (Haridas & Rosemary, 2019) who declared that HA containing hydrogel showed almost 100 % viability. The rate of increase in the cell viability confirmed the suitability of proper HA and ChNWs combination for further applications. This material was used for further examination, fluorescent visualization of the live cells (Fig. 9b,d). In the culture treatment with these items, no lysis of cells was observed and demonstrated the number of live cells (green cells).
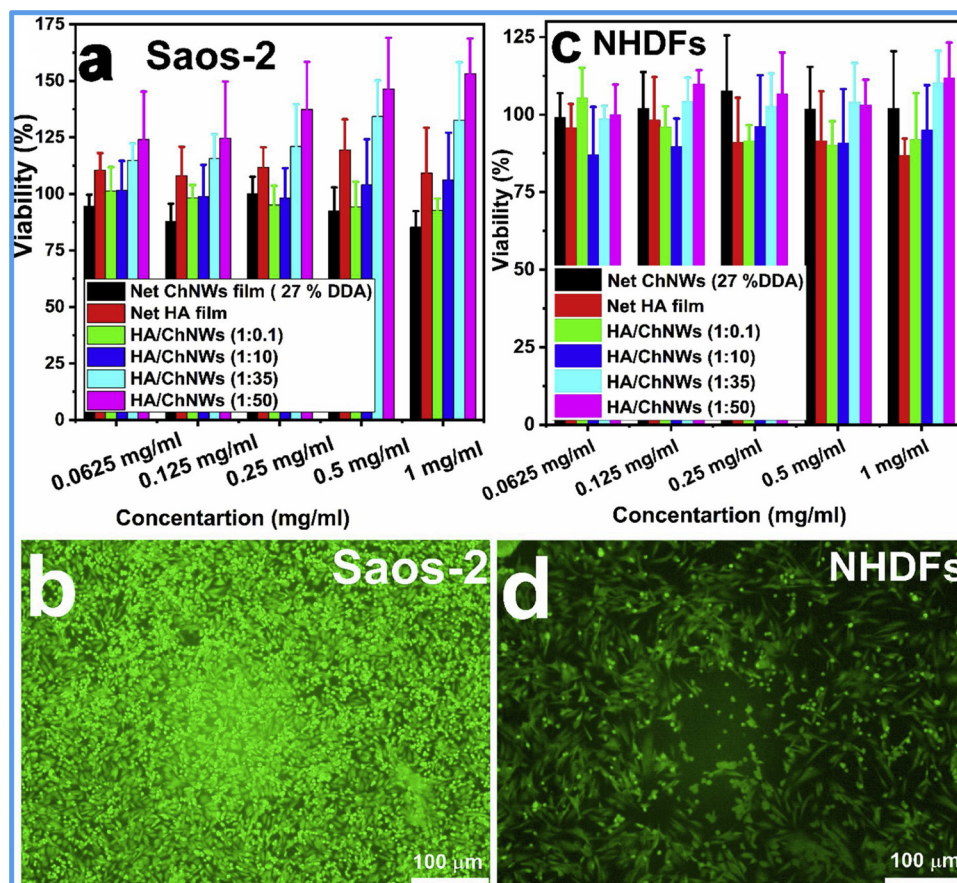

Fig. 9. Representative cytotoxicity of nano-composite biofilms using primary human fibroblast cells (NHDFs) and Human Osteogenic Sarcoma cells (Saos-2 cells) and visualized cell lines using fluorescent microscope. (For interpretation of the references to color in this figure legend, the reader is referred to the web version of this article.)

5. Conclusions

Partially deacetylated chitin nanowhiskers (ChNWs) were successfully prepared from shrimp shells with different lengths and diameters by investigating the effect of treatment time by hydrochloric acid on dimensions of NWs after extraction of pure chitin by the demineralization, deproteinization and partially deacetylated steps. The obtained NWs after acid treatment were investigated and characterized by XRD, SEM, TEM, and ^{13}C-ssNMR. The results showed that there were no significant effects of time of acid treatment on the DDA of the NWs, but there were significant changes on the dimensions of the NWs. The width and length of NWs were decreased from 36 and 1265 nm to 20 and 420 nm, with increased in the treatment time from 1 to 6 h using 3 M HCl, respectively. The nanocomposite biofilms (HA-ChNWs) showed enhanced mechanical properties over net HA films with high volume fraction of the NWs. Results of the mechanical and fracture morphology visualized using SEM showed that the enhanced interfacial bonding via the formation of a stronger electrostatic and chemical attractions at the ChNWs-HA interface. Nanocomposite biofilms exhibited good antibacterial properties against different types of bacteria (-/+ G) which was improved with the increasing volume fraction of the NWs loaded into the HA matrix. The novel biofilms significantly enhanced the viability of cells (NHDF, Saos-2) without any toxicity using different concentrations of nanocomposite biofilm extracts (0.0625–1 mg/ml). It was expected, that the present work would not only enrich the high-value of sea food wastes utilized but also provide an alternative way to synthesize edible, renewable, eco-friendly, mechanically enhancement, and antibacterial biofilms for the active food packaging application, drug-carrier applications as well as for skin tissue regeneration purposes.

CRediT authorship contribution statement

R.M. Abdelrahman: Conceptualization, Methodology. **A.M. Abdel-Mohsen:** Conceptualization, Methodology. **M. Zboncak:** Methodology. **J. Frankova:** Formal analysis. **P. Lepcio:** Methodology. **L. Kobera:** Methodology. **M. Steinhart:** Methodology. **D. Pavlinak:** Methodology. **Z. Spotaz:** . **R. Sklenářévá:** Methodology. **J. Brus:** Methodology. **J. Jancar:** Conceptualization, Supervision, Funding acquisition.

Acknowledgments

Appendix A. Supplementary data

Supplementary material related to this article can be found, in the online version, at doi:https://doi.org/10.1016/j.carbpol.2020.115951.

References

Abdel-Mohsen, A. M., Jancar, J., Abdel-Rahman, R. M., Vojtek, L., Hyršl, P., Dušková, M., & Nejezchlebová, H. (2017). A novel in situ silver/hyaluronan bio-nanocomposite fabrics for wound and chronic ulcer dressing: In vitro and in vivo evaluations. *International Journal of Pharmaceutics, 520*(1), 241–253.

Abdel-Mohsen, A. M., Jancar, J., Massoud, D., Fohlerova, Z., Elhadidy, H., Spotz, Z., & Hebeish, A. (2016). Novel chitin/chitosan-glucan wound dressing: Isolation, characterization, antibacterial activity and wound healing properties. *International Journal of Pharmaceutics, 510*(1), 86–99.

Abdel-Mohsen, A. M., Pavliňák, D., Čileková, M., Lepcio, P., Abdel-Rahman, R. M., & Jančář, J. (2019). Electrospinning of hyaluronan/polyvinyl alcohol in presence of in-situ silver nanoparticles: Preparation and characterization. *International Journal of Biological Macromolecules, 139*, 730–739.

Abdel-Mohsen, A. M., Aly, A. S., Hrdina, R., & El-Aref, A. T. (2012). A novel method for the preparation of silver/chitosan-*O*-methoxy polyethylene glycol core shell nanoparticles. *Journal of Polymers and the Environment, 20*(2), 459–468.

Abdel-Mohsen, A. M., Hrdina, R., Burgert, L., Krylová, G., Abdel-Rahman, R. M., Krejčová, A., ... Beneš, L. (2012). Green synthesis of hyaluronan fibers with silver nanoparticles. *Carbohydrate Polymers, 89*(2), 411–422.

Abdel-Rahman, R. M., Abdel-Mohsen, A. M., Hrdina, R., Burgert, L., Fohlerova, Z., Pavliňák, D., ... Jancar, J. (2016). Wound dressing based on chitosan/hyaluronan/nonwoven fabrics: Preparation, characterization and medical applications. *International Journal of Biological Macromolecules, 89*, 725–736.

Abdel-Rahman, R. M., Hrdina, R., Abdel-Mohsen, A. M., Fouda, M. M. G., Soliman, A. Y., Mohamed, F. K., & Pinto, T. D. (2015). Chitin and chitosan from Brazilian Atlantic Coast: Isolation, characterization and antibacterial activity. *International Journal of Biological Macromolecules, 80*, 107–120.

Akhlaghi, O., Menceloglu, Y. Z., & Akbulut, O. (2016). Rheological behavior of poly(acrylonitrile) concentrated solutions: Effect of Sb_2O_3 nanoparticles on shear and extensional flow. *Colloid and Polymer Science, 294*(9), 1463–1473.

Ao, H., Yang, S., Nie, B. E., Fan, Q., Zhang, Q., Zong, J., & Tang, T. (2019). Improved antibacterial properties of collagen I/hyaluronic acid/quaternized chitosan multilayer modified titanium coatings with both contact-killing and release-killing functions. *Journal of Materials Chemistry B, 7*(11), 1951–1961.

Boddohi, S., Moore, N., Johnson, P. A., & Kipper, M. J. (2009). Polysaccharide-based polyelectrolyte complex nanoparticles from chitosan, heparin, and hyaluronan. *Biomacromolecules, 10*(4), 1402–1409.

Bongaerts, J. H. H., Cooper-White, J. J., & Stokes, J. R. (2009). Low biofouling chitosan-hyaluronic acid multilayers with ultra-low friction coefficients. *Biomacromolecules, 10*(5), 1287–1294.

Cassagnau, P. (2008). Melt rheology of organoclay and fumed silica nanocomposites. *Polymer, 49*(9), 2183–2196.

Chaussard, G., & Domard, A. (2004). New aspects of the extraction of chitin from squid pens. *Biomacromolecules, 5*(2), 559–564.

Chen, Y., Liu, C., Chang, P. R., Cao, X., & Anderson, D. P. (2009). Bionanocomposites based on pea starch and cellulose nanowhiskers hydrolyzed from pea hull fibre: Effect of hydrolysis time. *Carbohydrate Polymers, 76*(4), 607–615.

David, L., Dulong, V., Le Cerf, D., Cazin, L., Lamacz, M., & Vannier, J.-P. (2008). Hyaluronan hydrogel: An appropriate three-dimensional model for evaluation of anticancer drug sensitivity. *Acta Biomaterialia, 4*(2), 256–263.

Franková, J., Pivodová, V., Vágnerová, H., Juráňová, J., & Ulrichová, J. (2016). Effects of silver nanoparticles on primary cell cultures of fibroblasts and keratinocytes in a wound-healing model. *Journal of Applied Biomaterials & Functional Materials, 14*(2), 137–142.

Gopalan Nair, K., & Dufresne, A. (2003). Crab shell chitin whisker reinforced natural rubber nanocomposites. 2. Mechanical behavior. *Biomacromolecules, 4*(3), 666–674.

Haridas, N., & Rosemary, M. J. (2019). Effect of steam sterilization and biocompatibility studies of hyaluronic acid hydrogel for viscosupplementation. *Polymer Degradation and Stability, 163*, 220–227.

Hariraksapitak, P., & Supaphol, P. (2010). Preparation and properties of α-chitin-whisker-reinforced hyaluronan–gelatin nanocomposite scaffolds. *Journal of Applied Polymer Science, 117*(6), 3406–3418.

Ifuku, S., Nogi, M., Abe, K., Yoshioka, M., Morimoto, M., Saimoto, H., & Yano, H. (2009). Preparation of chitin nanofibers with a uniform width as α-chitin from crab shells. *Biomacromolecules, 10*(6), 1584–1588.

Jancar, J. (2008). Review of the role of the interphase in the control of composite performance on micro- and nano-length scales. *Journal of Materials Science, 43*(20), 6747–6757.

Jancar, J., & Recman, L. (2010). Particle size dependence of the elastic modulus of particulate filled PMMA near its T-g. *Polymer, 51*(17), 3826–3828.

Jancar, J., Douglas, J. F., Starr, F. W., Kumar, S. K., Cassagnau, P., Lesser, A. J., ... Buehler, M. J. (2010). Current issues in research on structure–property relationships in polymer nanocomposites. *Polymer, 51*(15), 3321–3343.

Jung, J., Lee, B.-K., & Shin, S. (2014). Yield shear stress and disaggregating shear stress of human blood. *Korea-Australia Rheology Journal, 26*(2), 191–198.

Krajewska, B., Wydro, P., & Jańczyk, A. (2011). Probing the modes of antibacterial activity of chitosan. Effects of pH and molecular weight on chitosan interactions with membrane lipids in Langmuir films. *Biomacromolecules, 12*(11), 4144–4152.

Kumar, S. K., Benicewicz, B. C., Vaia, R. A., & Winey, K. I. (2017). 50th anniversary perspective: are polymer nanocomposites practical for applications? *Macromolecules, 50*(3), 714–731.

Lepcio, P., Ondreas, F., Zarybnicka, K., Zboncak, M., Caha, O., & Jancar, J. (2018). Bulk polymer nanocomposites with preparation protocol governed nanostructure: The origin and properties of aggregates and polymer bound clusters. *Soft Matter, 14*(11), 2094–2103.

Lequeux, I., Ducasse, E., Jouenne, T., & Thebault, P. (2014). Addition of antimicrobial properties to hyaluronic acid by grafting of antimicrobial peptide. *European Polymer Journal, 51*, 182–190.

Li, M.-C., Wu, Q., Song, K., Cheng, H. N., Suzuki, S., & Lei, T. (2016). Chitin nanofibers as reinforcing and antimicrobial agents in Carboxymethyl cellulose films: Influence of partial deacetylation. *ACS Sustainable Chemistry & Engineering, 4*(8), 4385–4395.

Lou, J., Liu, F., Lindsay, C. D., Chaudhuri, O., Heilshorn, S. C., & Xia, Y. (2018). Dynamic hyaluronan hydrogels with temporally modulated high injectability and stability using a biocompatible catalyst. *Advanced Materials, 30*(22), 1705215.

Lu, Y., Weng, L., & Zhang, L. (2004). Morphology and properties of soy protein isolate thermoplastics reinforced with chitin whiskers. *Biomacromolecules, 5*(3), 1046–1051.

Mahallati, P., Hassanabadi Hojjat, M., Wilhelm, M., & Rodrigue, D. (2016). Rheological characterization of thermoplastic elastomers (Tpe) based on pp and recycled epdm. *Applied Rheology, 26*, 32.

Morganti, P., Palombo, M., Tishchenko, G., Yudin, V. E., Guarneri, F., Cardillo, M., ... Fabrizi, G. (2014). Chitin-hyaluronan nanoparticles: A multifunctional carrier to deliver anti-aging active ingredients through the skin. *Cosmetics, 1*(3), 140–158.

Noishiki, Y., Takami, H., Nishiyama, Y., Wada, M., Okada, S., & Kuga, S. (2003). Alkali-induced conversion of β-chitin to α-chitin. *Biomacromolecules, 4*(4), 896–899.

Ottey, M. H., Vårum, K. M., & Smidsrød, O. (1996). Compositional heterogeneity of heterogeneously deacetylated chitosans. *Carbohydrate Polymers, 29*(1), 17–24.

Patras, G., Qiao, G. G., & Solomon, D. H. (2001). Controlled formation of micro-heterogeneous polymer networks: Influence of monomer reactivity on gel structure. *Macromolecules, 34*(18), 6396–6401.

Peng, C., & Chen, G. (2018). Preparation and assessment of heat-treated α-chitin nano-whiskers reinforced poly(viny alcohol) film for packaging application. *Materials, 11*(10), 1883.

Přichystalová, H., Almonasy, N., Abdel-Mohsen, A. M., Abdel-Rahman, R. M., Fouda, M. M. G., Vojtova, L., & Jancar, J. (2014). Synthesis, characterization and antibacterial activity of new fluorescent chitosan derivatives. *International Journal of Biological Macromolecules, 65*, 234–240.

Roca, C., Chagas, B., Farinha, I., Freitas, F., Mafra, L., Aguiar, F., & Reis, M. A. M. (2012). Production of yeast chitin–glucan complex from biodiesel industry byproduct. *Process Biochemistry, 47*(11), 1670–1675.

Roman, M., & Winter, W. T. (2004). Effect of sulfate groups from sulfuric acid hydrolysis on the thermal degradation behavior of bacterial cellulose. *Biomacromolecules, 5*(5), 1671–1677.

Sahariah, P., Benediktssdóttir, B. E., Hjálmarsdóttir, M.Á., Sigurjonsson, O. E., Sørensen, K. K., Thygesen, M. B., & Másson, M. (2015). Impact of chain length on antibacterial activity and hemocompatibility of quaternary *N*-alkyl and *N,N*-dialkyl chitosan derivatives. *Biomacromolecules, 16*(5), 1449–1460.

Suryanegara, L., Okumura, H., Nakagaito, A. N., & Yano, H. (2011). The synergetic effect of phenylphosphonic acid zinc and microfibrillated cellulose on the injection molding cycle time of PLA composites. *Cellulose, 18*(3), 689–698.

Tan, H., Wu, J., Lao, L., & Gao, C. (2009). Gelatin/chitosan/hyaluronan scaffold integrated with PLGA microspheres for cartilage tissue engineering. *Acta Biomaterialia, 5*(1), 328–337.

Tomšíčková, V., Frankova, J., Dolezel, P., & Ulrichova, J. (2013). *The response of osteoblast-like SaOS-2 cells to modified titanium surfaces*.

Zeng, J.-B., He, Y.-S., Li, S.-L., & Wang, Y.-Z. (2012). Chitin whiskers: An overview. *Biomacromolecules, 13*(1), 1–11.

Zhu, K., Tu, H., Yang, P., Qiu, C., Zhang, D., Lu, A., & Zhang, L. (2019). Mechanically strong chitin fibers with nanofibril structure, biocompatibility, and biodegradability. *Chemistry of Materials, 31*(6), 2078–2087.

Zubareva, A., Shagdarova, B., Varlamov, V., Kashirina, E., & Svirshchevskaya, E. (2017). Penetration and toxicity of chitosan and its derivatives. *European Polymer Journal, 93*, 743–749.

Supporting information's

Hyaluronan Biofilms Reinforced with Partially Deacetylated Chitin Nanowhiskers: Extraction, Fabrication, *In-vitro* and Antibacterial Properties of Advanced Nanocomposites

R. M. Abdelrahman[a,1*], A. M. Abdel-Mohsen[a,b,c,1], M. Zboncak[a], J. Frankova[d], P. Lepcio[a], L. Kobera[e], M. Steinhart[e], D. Pavlinak[f], Z. Spotaz[a], R. Sklenářévá[d], J. Brus[5], J. Jancar[a,b,g]**

[a] CEITEC-Central European Institute of Technology, Brno University of Technology, Purkynova 656/123, Brno, Czechia

[b] SCITEG, a.s., Brno, Czechia

[c] Department of Pretreatment and Finishing of Cellulosic based Textiles, Textile Industries Research Division, National Research Centre, 33 EL Buhouth St., Dokki, Giza 12622, Egypt

[d] Department of Medical Chemistry and Biochemistry, Faculty of Medicine and Dentistry, Palacky University Olomouc, Czechia

[e] Institute of Macromolecular Chemistry of the Czech Academy of Sciences, Heyrovskeho nam. 2, 162 06, Prague 6, Czechia

[f] Department of Physical Electronics, Masaryk University, Brno, Czechia

[g] Institute of Materials Chemistry, Facility of chemistry, Brno University of Technology, Brno, Czechia

Corresponding author: CEITEC-Central European Institute of Technology, Brno University of Technology, Brno, Czech Republic. Mail: Rasha.Abdelrahman@ceitec.vutbr.cz; abdel-mohsen@ceitec.vutbr.cz.

[1]These authors contributed equally to this work

Biofilms characterization

X-ray diffraction was measured at 3 kW diffractometer Smart lab (Rigaku, Japan) using Cu Kα radiation (λ = 1.54 Å) and detector Dtex Ultra with Bragg-Brentano geometry. Diffraction angle 2θ (XRD) was measured in the range from 5° to 50° with a step size of 0.02° at speed 4°/min. A generator was operated at the current of 30 mA and the voltage of 40 kV. The crystallinity index (%) of materials was determined using Eq. (1)

$$Cr.I = \frac{I_{110}}{I_{110} + I\ am} * 100 \tag{1}$$

where Cr.I is the crystallinity index, I110 is the maximum intensity of the diffraction from the plane at 2θ = 19.6°, and I_{am} was the intensity of the background scatter measured at 2θ = 16° using Scherrer's equation (Fan, Saito, & Isogai, 2008).

The microanalysis was performed by the FISONS Instruments EA 1108 C, H, N apparatus (Thermo scientific, USA). Firstly, the elemental analysis was performed, where the total protein content was calculated from the nitrogen content (Chaussard & Domard, 2004) by using the following Eq. (2)

$$P\ (\%) = [N\% - 6.9] * 6.25 \tag{2}$$

where P (%) represents the percentage of proteins remaining in the deproteinized shell, N % represents the percentage of nitrogen measured by elemental analysis, 6.9 corresponds to the theoretical percentage of nitrogen in a fully acetylated chitin (this value was adjusted as a function of DA, the degree of acetylation), and 6.25 corresponds to the theoretical percentage of nitrogen in proteins. All the determinations were done in quadruplicate. UV/Vis spectroscopy was used to determine the P %. The measurements were carried out on UV/VIS 160A, Shimadzu, Japan using a quartz cuvette with an optical path of 1 cm. The concentration of the measured solutions was kept at 0.59 mg/ml. The protein content in the supernatant (Chaussard & Domard, 2004). was calculated from the following Eq. (3)

$$P\ (\%) = 2.37\ (A_{564}/W) \tag{3}$$

where the A_{564} was the absorbance value at 564 nm and W was the weight of sample in mg.

The antibacterial activity of net HA and HA-ChNWs biofilms with different ratios were selected to evaluate the biological activity against *Bacillus subtilis, Streptococci* (gram-positive) *and Klebsiella Pneumoniae, Escherichia coli* (gram-negative) by the disk plate method. A bacterial suspension of 1×10^8 cells/mL was inoculated in nutrient agar plates by the spread plate

62 method and the Muller-Hinton agar was prepared by mixing beef extract powder (3 g), starch

63 (1.5 g), casein hydrolase (17.5 g), and agar (17 g) in 1 liter of Milli-Q water. pH was adjusted to

64 7.5, the mixture was heated up to completely dissolved the medium and the medium was then

65 sterilized in an autoclave at 121 °C for 25 min. This nutrient agar medium was transferred into

66 sterilized petri dishes in laminar airflow. After solidification of the media, *Bacillus subtilis,*

67 *Streptococci* (gram-positive) and *Klebsiella Pneumoniae, Escherichia coli* (gram-negative)

68 cultures were streaked on the solid surface of the media. Different biofilms (11 mm) were loaded

69 on the surface of the solidified agar medium. Discs (control, gauze) were incubated at 5 °C for 1

70 h to allow good diffusion. All the plates were then incubated for 24 h at 37 °C. The positive

71 control (streptomycin disc) was tested in the same way to compare antibacterial activities. The

72 plates with discs were monitored and each zone of clearance was measured.

73 Solid-state NMR spectroscopy*:* ^{13}C CP/MAS NMR spectra were recorded on a Bruker

74 AVANCE III HD spectrometer (Larmor frequencies $v^{13}C = 125.783$ MHz) using a 3.2 mm MAS

75 probe. The spinning speed of the rotor sample was 20 kHz. The number of scans for the

76 accumulation of ^{13}C CP/MAS NMR spectra was 2048, a repetition delay of 5 s, and a spinlock of

77 1 ms (Heux, Brugnerotto, Desbrières, Versali, & Rinaudo, 2000). During detection, the high-

78 power dipolar decoupling (SPINAL 64) was used to eliminate strong hetero-nuclear dipolar

79 couplings. The isotropic chemical shift of the ^{13}C-NMR scale was calibrated with glycine as an

80 external standard (176.03 ppm to carbonyl signal). In all cases, the dried samples were placed

81 into the ZrO$_2$ rotors and all NMR experiments were performed at 303 K. Temperature calibration

82 was performed on Pb(NO$_3$)$_2$ using a procedure described in the literature (Brus, 2000). The mol.

83 (%) of chitin units were calculated from equation referred to in the literature (Spěváček & Brus,

84 2008) according to Eq. (4).

85 $$mol\%(N-acetyl\,g\,l\,u\,co\,s\,a\,\min e) = \frac{I_{C8}}{(I_{C1}+I_{C2}+I_{C3}+I_{C4}+I_{C5}+I_{C6})/6} \times 100 \qquad \textbf{(4)}$$

86

87 The swelling percentage of biofilms was carried out in water and phosphate buffer solution

88 (PBS). The biofilms were cut into small pieces (1× 1 cm), weight, put into glass vials, immersed

89 in water or PBS and incubated at 37 °C. At regular interval time (1, 3, 6, 12, 24 h). The

90 HA/CHNWs biofilms were removed, dried with filter paper to eliminate the excess of water or

91 PBS from the biofilm surface. The swelling percentage was calculated according to equation (5).

92 $$\text{Swelling ratio} = Ws - \frac{Wd}{Wd} \times 100 \qquad (5)$$

93 Where Ws was the weight of swollen biofilm and Wd was the weight of dry biofilm, each value
94 was averaged from three parallel measurements

95   The weight loss of nanocomposite biofilms was determined gravimetrically under
96 physiological conditions (PBS, pH= 7.5, 37 °C). After 1 day of immersed biofilms were removed
97 and washed well with Milli-Q water to remove any attached salts from the biofilm surface and
98 then freeze-dried for two days at – 50 °C. The weight loss was calculated according to equation
99 6.

100 $$\text{Weight loss} = Wi - \frac{Wf}{Wi} \times 100 \qquad (6)$$

101 Where Wi was the weight of biofilm after 24 h and Wf was the weight of starting dry biofilm,
102 each value was averaged from three parallel measurements.

103   Rheological evaluation: The fitting parameters of the Herschel-Bulkley and power-law
104 viscosity models are presented in Fig. S3, the rate index n was obtained independently for both
105 models. For n < 1, the fluid is shear-thinning, whereas, for n > 1, the fluid is shear-thickening.
106 Both models showed that the shear-thinning tendency strengthened with the presence of ChNWs
107 up to the HA/ChNWs ratio of 1/35 while it was weakened for the highest ChNWs content. The
108 Herschel-Bulkley model features an additional fitting parameter of yield stress which was
109 estimated negative for all measurements. Negative yield stress has no physical meaning and was
110 likely caused as an artifact caused by residual stress after pre-shear. It correlated well with the
111 relaxation times though, with the fastest relaxing samples showing the least negative value of
112 yield stress and the slowest relaxing samples providing the largest negative values.

113

114

115

116

117

118

119

120

Table S1: Different volume fractions ratios of the hyaluronan (HA) and partially deacetylated chitin nanowhiskers (ChNWs) investigated in this study.

123

Sample Codes	ChNWs/ HA ratio (wt/wt)	V_f of ChNWs to HA
Net HA	0	0
HA/ChNWs (1/0.1)	0.1	0.00125
HA/ChNWs (1/1)	1	0.012
HA/ChNWs (1/10)	10	0.111
HA/ChNWs (1/15)	15	0.159
HA/ChNWs (1/25)	25	0.239
HA/ChNWs (1/35)	35	0.312
HA/ChNWs (1/50)	50	0.386

124

Notes: HA= hyaluronan; ChNWs = partially deacetylated chitin nanowhiskers (DDA 27 %); V_f = Volume fraction, HA concentration was 3 %.

127

128

129
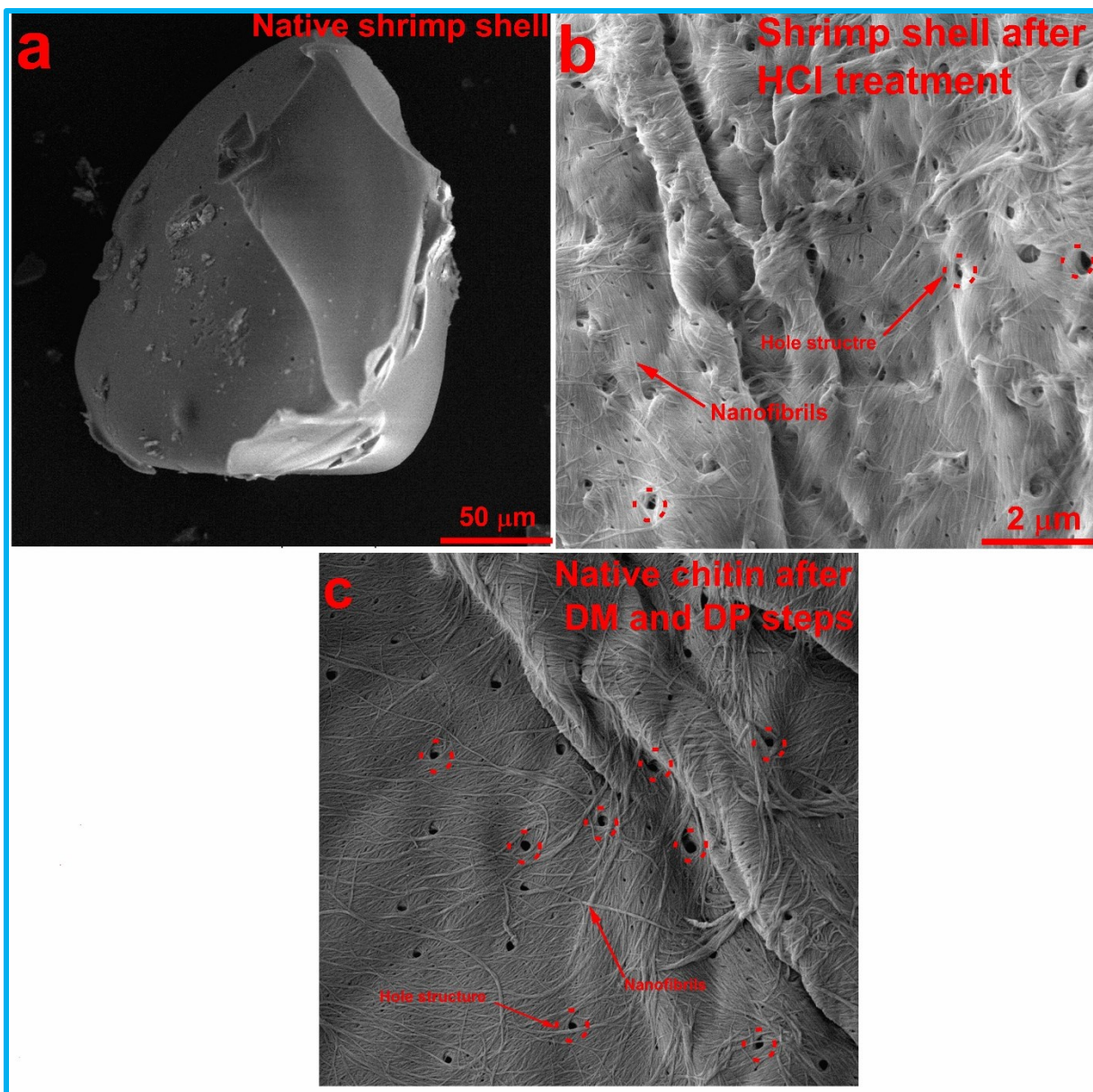
Fig. S1: SEM of native shrimp shells (a) and shrimp shells after demineralization (b) and deproteinization steps (c).
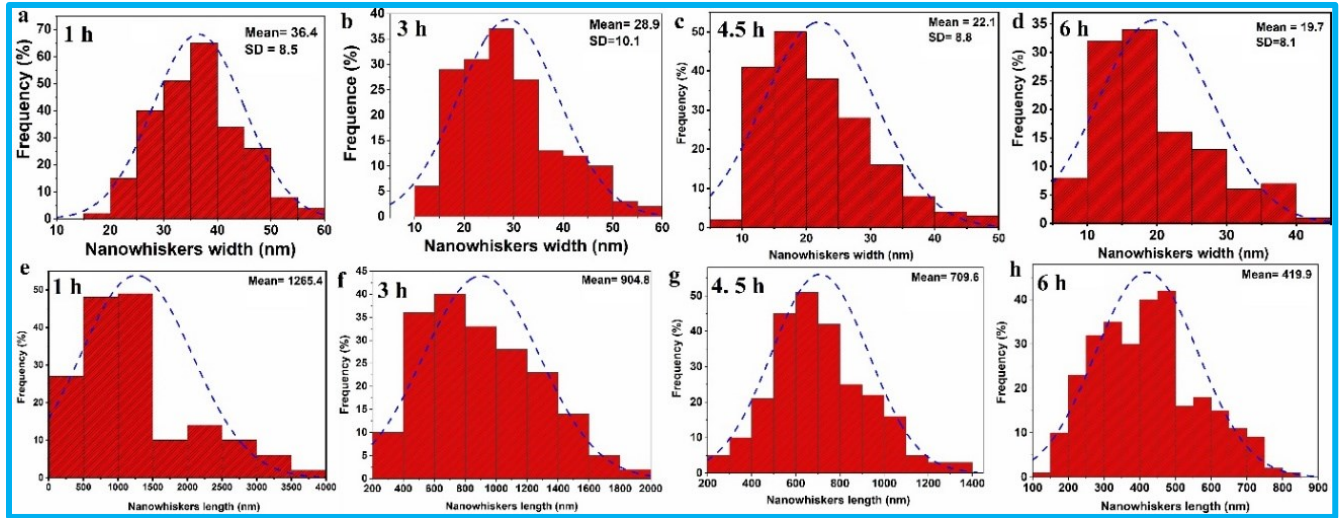
Fig. S2: Histograms of widths and lengths of partially chitin nanowhiskers after acid treatment (3 M) at different treatment times (1-6 h). Length and width histograms were plotted from 300 points.
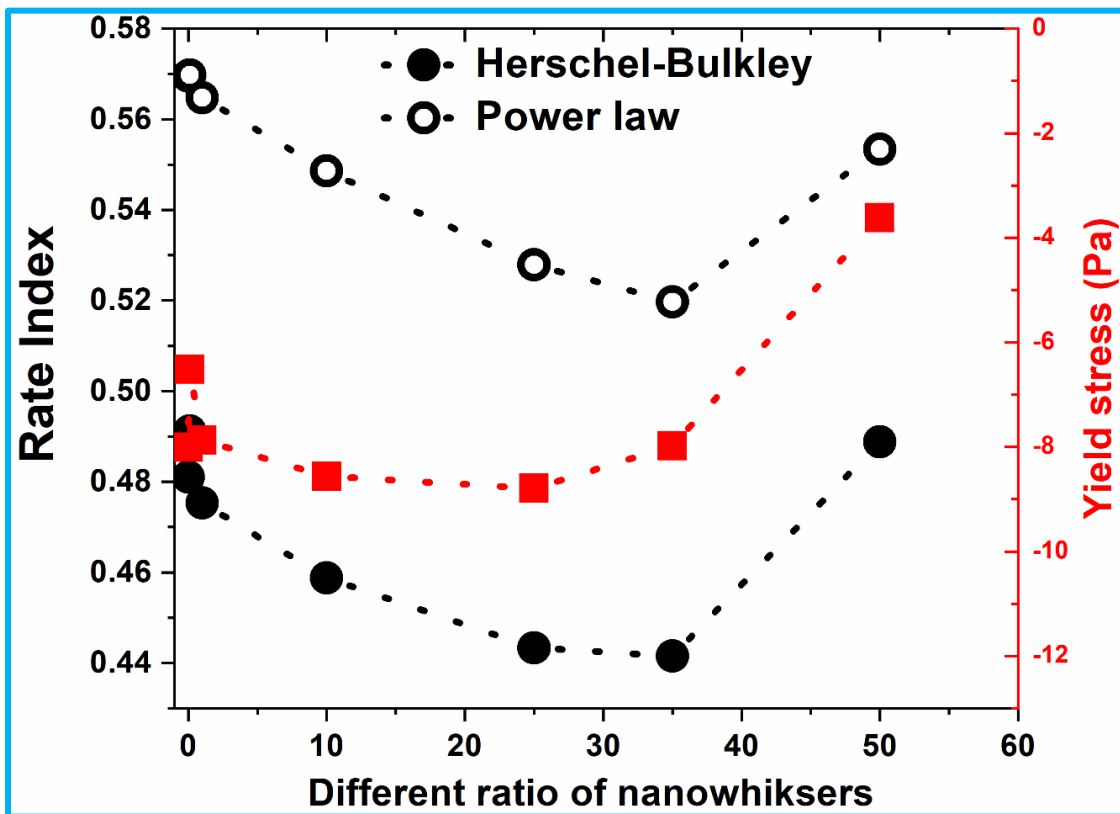
Fig. S3. Dependence of the Herschel-Bulkley and Power-law viscosity models fitting parameters on the HA/ChNWs ratio of the nanocomposite solutions.

140
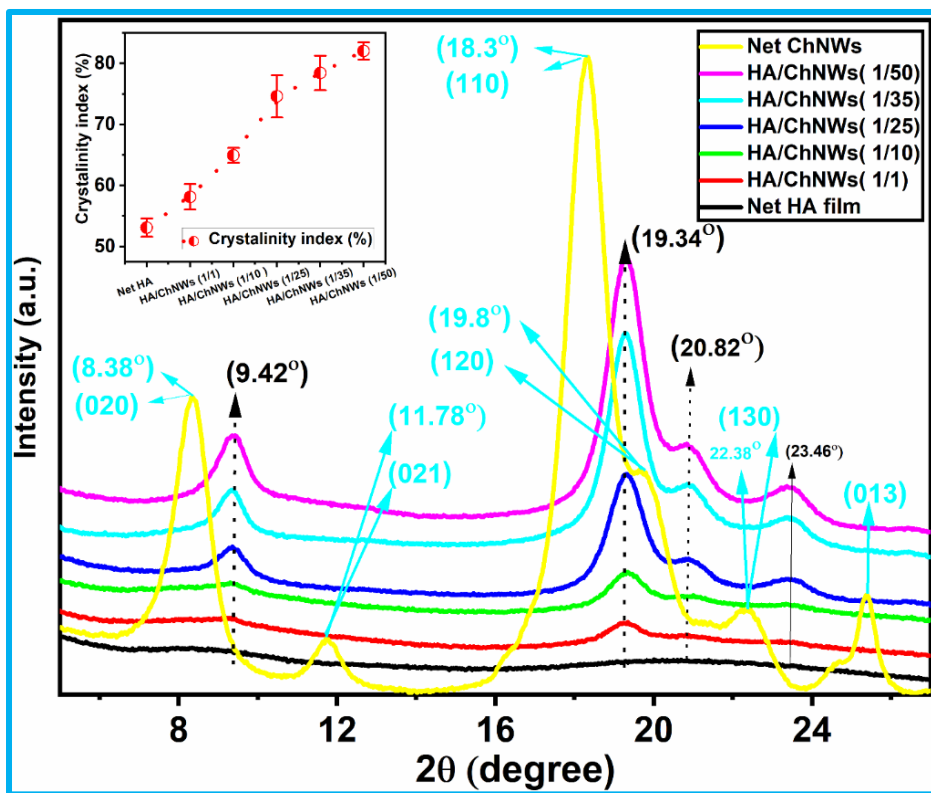
Fig.S4: XRD and crystallinity index of nanocomposite biofilms

142
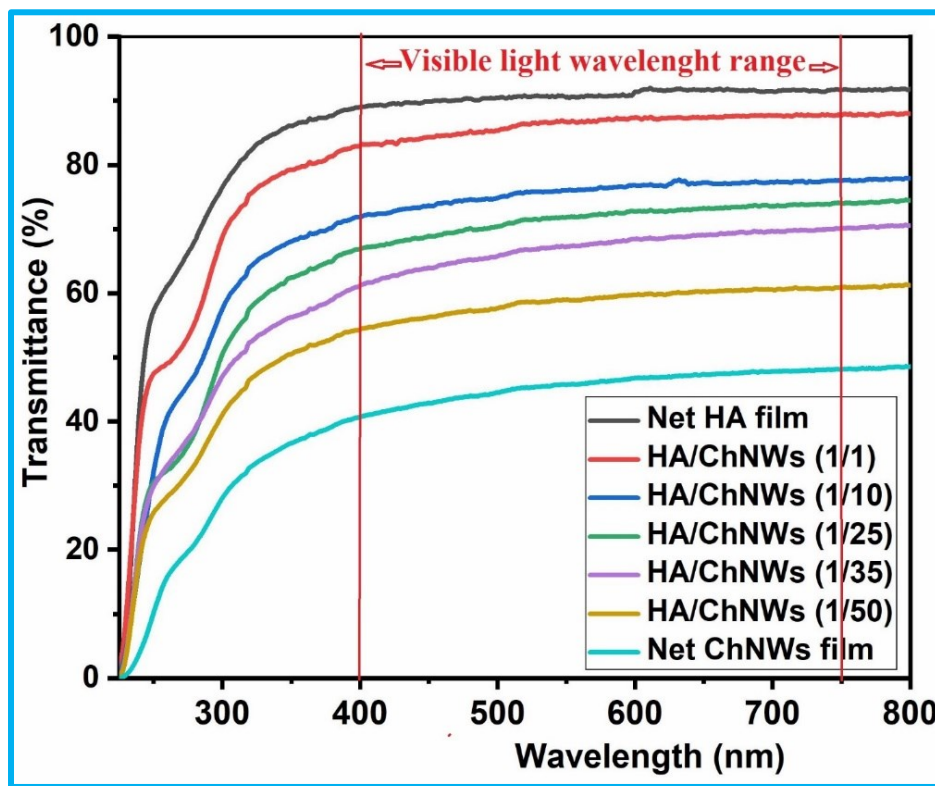
Fig. S5: Optical transmittance of native HA and HA/ChNWs nanocomposite biofilms

8

144
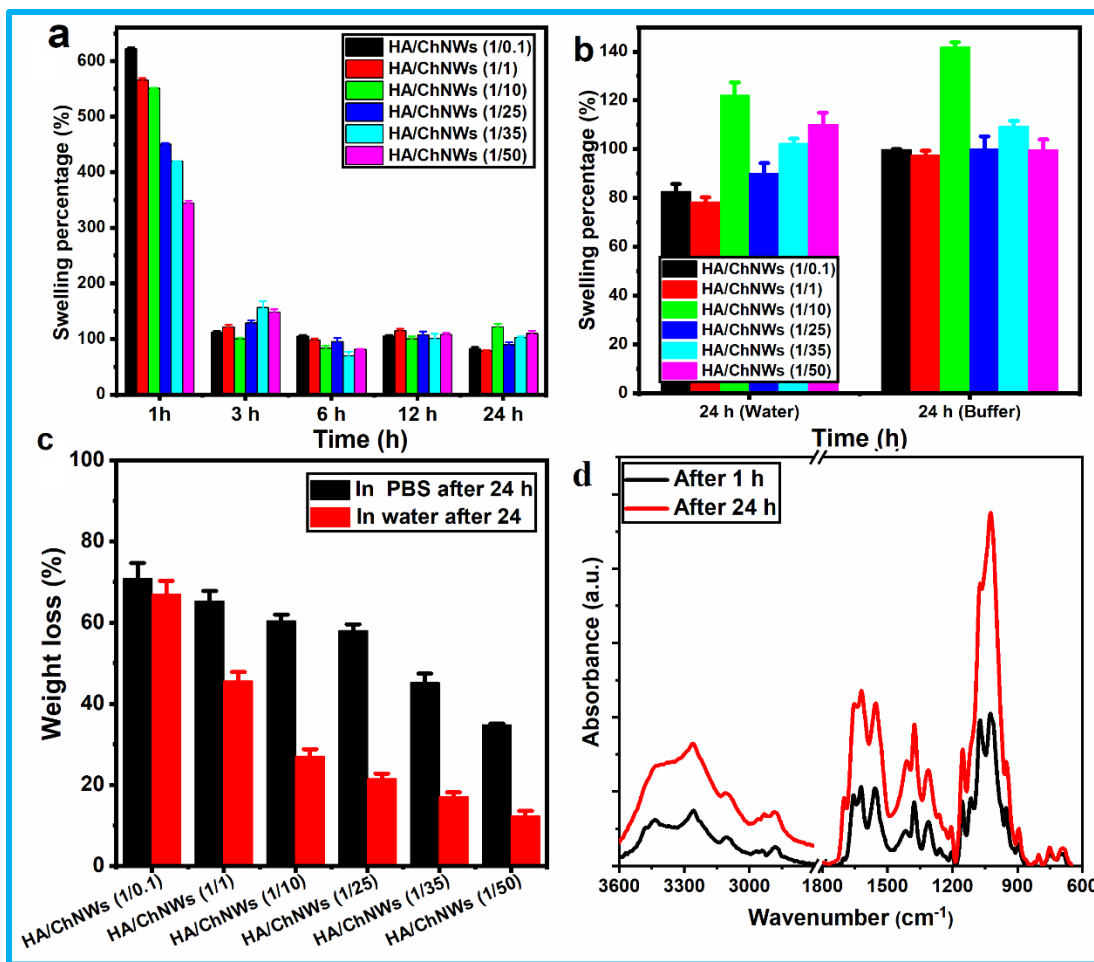
Fig. S6. Swelling and hydrolytic degradation of HA/ChNWs nanocomposite biofilms

146
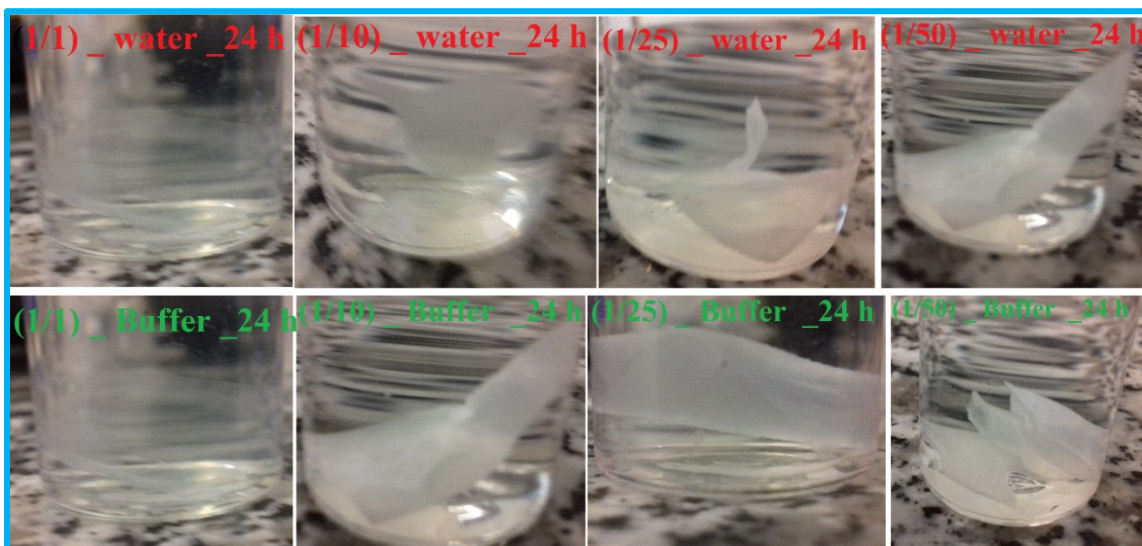
Fig. S7. Representative the Swelling behavior of nanocomposite biofilms with different ratios in water and PBS solutions after incubated for one day at 37°C.
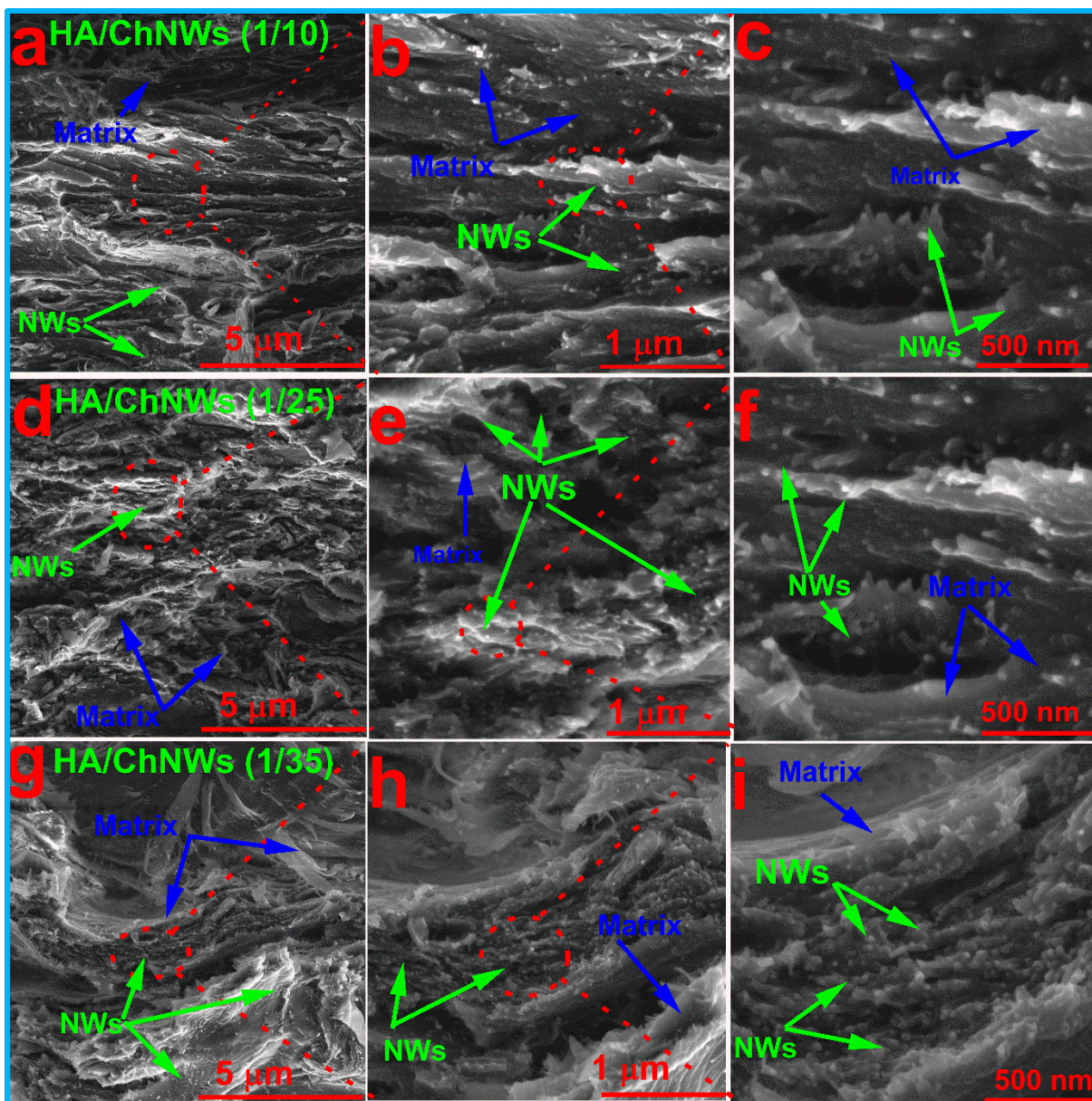
Fig. S8. SEM of fracture surface morphologies of HA/ChNWs nanocomposite biofilms.
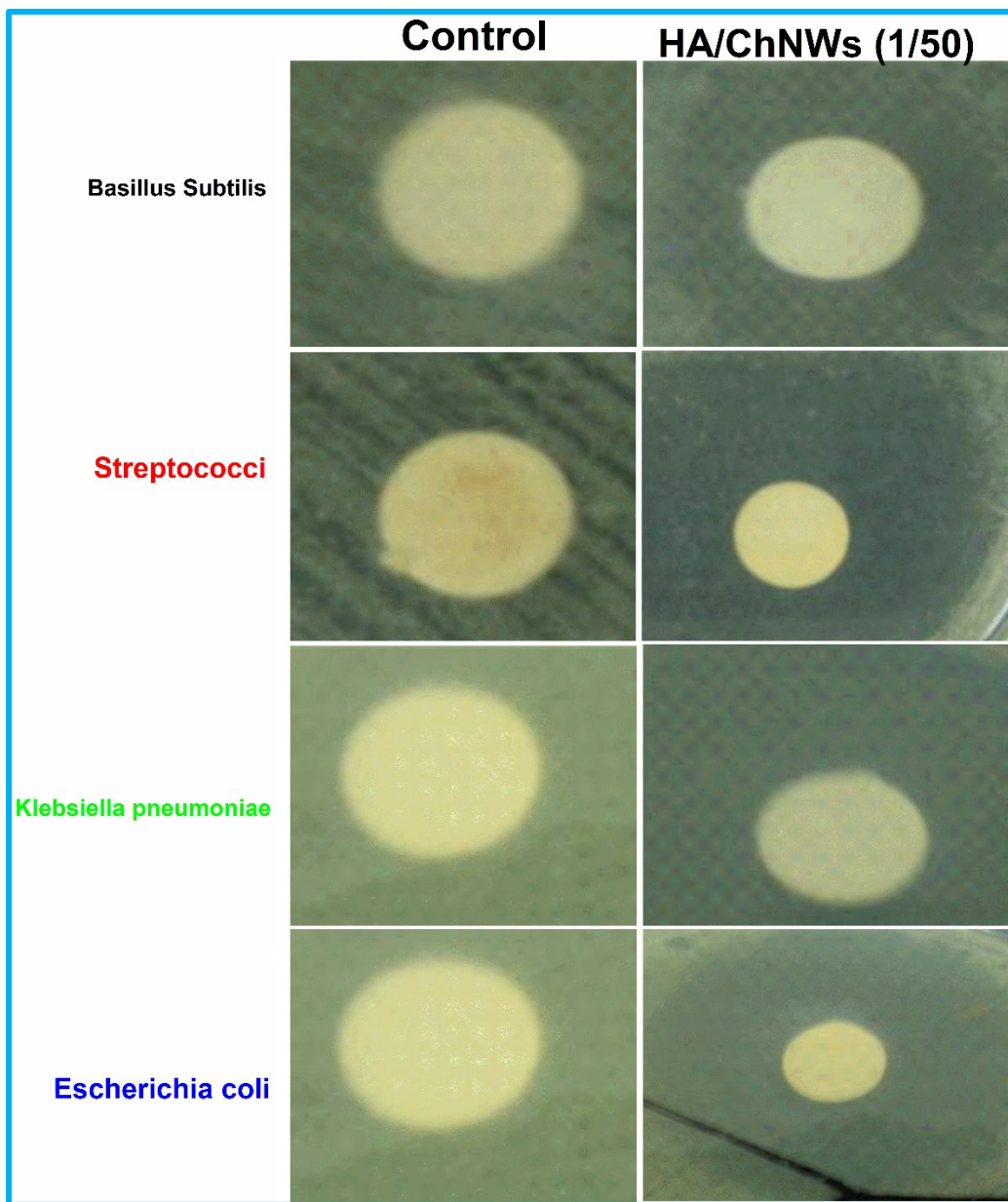
Fig. S9. Inhabitation zones of different biofilms measured using different bacteria types

References

Brus, J. (2000). Heating of samples induced by fast magic-angle spinning. *Solid state nuclear magnetic resonance,* 16(3), 151-160.

Chaussard, G., & Domard, A. (2004). New Aspects of the Extraction of Chitin from Squid Pens. *Biomacromolecules,* 5(2), 559-564.

Fan, Y., Saito, T., & Isogai, A. (2008). Preparation of Chitin Nanofibers from Squid Pen β-Chitin by Simple Mechanical Treatment under Acid Conditions. *Biomacromolecules,* 9(7), 1919-1923.

Heux, L., Brugnerotto, J., Desbrières, J., Versali, M. F., & Rinaudo, M. (2000). Solid State NMR for Determination of Degree of Acetylation of Chitin and Chitosan. *Biomacromolecules,* 1(4), 746-751.

Spěváček, J., & Brus, J. (2008). Solid-State NMR Studies of Polysaccharide Systems. *Macromolecular Symposia,* 265(1), 69-76.

Publication 10
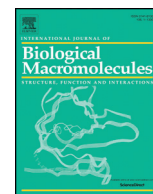
Electrospinning of hyaluronan/polyvinyl alcohol in presence of *in-situ* silver nanoparticles: Preparation and characterization

A.M. Abdel-Mohsen [a,b,*], D. Pavliňák [c], M. Čileková [d], P. Lepcio [a], R.M. Abdel-Rahman [a], J. Jančář [a,d]

[a] *CEITEC-Central European Institute of Technology, Brno University of Technology, Purkynova 123, Brno, 612 00, Brno, Czechia*
[b] *Pretreatment and Finishing of Cellulosic Fibers, Textile Research Division, National Research Centre, Dokki, Cairo, Egypt*
[c] *Department of Physical Electronics, Masaryk University, Brno, Czechia*
[d] *Institute of Materials Chemistry, Faculty of Chemistry, Brno University of Technology, Purkynova 118, Brno 612 00, Czechia*

ABSTRACT

Novel nanofibers mats were fabricated by electrospinning of polyvinyl alcohol/hyaluronan (PVA/HA) solutions in the presence of silver nanoparticles (AgNPs). The AgNPs were synthesized by *in-situ* chemical reduction of silver ions (Ag^+) using HA as a reducing and stabilizing agent. Narrow size distribution and spherical shape of AgNPs were achieved by optimizing the initial silver nitrate concentration (0.01 to 1 M) and reaction time (10–60 min). HA-AgNPs nanocomposite and PVA/HA-AgNPs nanofibrous mats were fabricated by electrospinning technique from aqueous solution containing a different mass ratio of PVA and HA-AgNPs and characterized by UV/Vis spectroscopy, SEM, TEM, DLS, XRD, TGA, and ATR-FTIR. Mechanical and rheological properties were also investigated and discussed. The novel nanofibrous mats show great potential in skin regeneration and drug carrier applications.

© 2019 Elsevier B.V. All rights reserved.

1. Introduction

Hyaluronan (HA) is a naturally generated biopolymer with various molecular weights. It consists of *N*-acetyl-*D*-glucosamine connected with *D*-glucuronic acid unit *via* alternating β-1,4, β-1,3 glycosidic links [1,2]. Hyaluronan is found widely in human organs, *e.g.* eye, cartilage or skin [3–5]. Hyaluronan has different functional groups such as hydroxyl, carboxyl, and acetamide groups that can be used for chemical modification of HA surface. Unique physicochemical properties of HA including biodegradability [6], biocompatibility, oxidative degradation [7], and viscoelasticity [2], make it an attractive biopolymer for an extensive range of pharmaceutics, medical, textile and cosmetic applications [8–10].

Hyaluronan composites and, especially those with inorganic metal nanoparticles (Ag, Au, ZnO-NPs), has attracted a wide interest primarily due to their potential suitability for medical applications [11–15]. Significant effort has been devoted to generating silver nanoparticles (AgNPs) with controlled shape and size of NPs and excellent distribution [1,16,17]. The current challenge investigated by multiple research group is to develop "green" eco-friendly processing technology of AgNPs without any toxic agents using polysaccharides such as hyaluronan [18], chitosan [14,19], schizophyllan [20], alginate [21,22],

cellulose [23,24], starch [25], and their derivatives [26–30]. Nevertheless, in all studies known to the authors, the AgNPs were prepared using hazardous reducing agents. In our previous study, we reported on preparation and further development of hyaluronan/silver nanoparticles composite (HA/AgNPs) which was originally invented as wound dressing with antitumor effect [16]. Due to the unique physicochemical and optical properties of the novel HA/AgNPs composite as well as its nontoxicity, small spherical NPs, and long term stability, HA/AgNPs was used as a new marker for micro/nano-X-ray computed tomography [31] and, within the scope of this study, new materials that can be used as a drug delivery system comprising of function-specific drugs for application as an efficient tumor-theranostic agent were fabricated [32–34].

Electrospinning is a simple process capable of producing fine fibers from nano-dimension (approx. tens of nanometers) to several micrometers [35–37]. Electrospun nanofibrous mats have very small pore size and high overall porosity; their specific surface area exceeds that of casted films or microfibers [38–40]. Different natural and synthetic materials, such as collagen, dextran, silk fibroin, poly-lactic acid (PLA), lignin [41], and polycaprolactone (PCL), have been successfully electrospun to generate nanofibrous scaffolds for different medical and environmental purposes [42–44]. As a main component of the extracellular matrix (ECM), hyaluronan also attracts great interest in electrospinning. However, electrospinning of net HA represents an unsolved challenge, since hyaluronan is a polyelectrolyte with high conductivity and surface tension [45]. The repulsive force among the

---

polyanions is the key factor complicating the electrospinning of hyaluronan [46]. Moreover, the unusually high viscosity of HA solutions even at low concentrations and its strong concentration dependence represents another major issue hindering the generation of electrospun nanofibers. To the best of our knowledge, we are the first to report on fabrication of electrospun composite nanofibers based on HA/PVA with *in-situ* synthesized AgNPs of controlled size and shape. We hypothesize that HA could work as a capping and reducing agent for synthesizing AgNPs by the *in-situ* way. We further hypothesize that the HA could control the dimensions of the AgNPs and prevent their agglomerations and separation during the electrospinning of nanofibrous mats. Proving our hypotheses would lead to develop of a novel nanofibrous mats from HA/AgNPs accompanied by PVA using a green process. Compared to net PVA mats, these materials would offer enhanced mechanical and thermal properties.

The current study focuses on our attempts to prepare the HA/AgNPs nanocomposite with controlled size and shape of NPs and fabricate electrospun HA-AgNPs/PVA nanofibrous mats according to the above-mentioned concept of our hypothesis. Moreover, the nanocomposite and nanofibers were fully characterized using different techniques such as UV/Vis spectroscopy, SEM, TEM, ATR-FTIR, TGA, XRD, and rheological and mechanical investigation.

2. Experimental procedure

2.1. Materials

Hyaluronan (HA) with a molecular weight of (150 to 170) kDa was purchased from CPN Ltd., (Czech Republic). Sodium hydroxide, acetic acid, isopropyl alcohol purchased from Lach-Ner (Czech Republic), silver nitrate from Sigma-Aldrich (Germany). Milli-Q water was used for all the experiments.

2.2. Methods

2.2.1. Synthesis of hyaluronan/silver nanocomposite

Nanocomposite HA-AgNPs was prepared by *in-situ* chemical reduction method using HA as a reducing and capping agent. Different concentration of $AgNO_3$ (0.0 to 1 M) was used as a source of AgNPs. 1 wt% of HA was used at varying reaction duration (10–60 min) at 90 °C. Firstly, Hyaluronan (1 g) was dissolved in milli-Q water (95 ml). After its complete dissolution, 1 ml of $AgNO_3$ solution with different concentrations of Ag^+ was added dropwise for 5 min while the temperature continually rose up to 90 °C. The pH of the reaction was then optimized to be 11 by adding an appropriate amount of sodium hydroxide (0.2–0.5 ml, 0.5 M). The reaction went on for time varying from 10 to 60 min, then the reaction was stopped and the reaction mixture (HA-AgNPs) was stored at 4 °C.

2.2.2. Fabrication of nanofibers dressing mats

Nanofibers mats were prepared from PVA and HA-AgNPs. Firstly, the PVA powder was dissolved in water (16 wt%) at 90 °C for 5 h. After cool-down to room temperature (approx. 25 °C), different weight ratio (w/w) of PVA and HA-AgNPs (100/0; 95/5; 90/10; 80/20; 60/40; 50/50) was homogeneously blended together by a magnetic stirrer. Elmarco Nanospider™ NSLAB 500 unit equipped with a fully controlled HV generator up to 80 kV/>1 mA applied voltage and current limiter was used for the preparation of the nanofibers. The PVA/HA-AgNPs solutions were electrospun under following conditions: distance between the electrodes was fixed to 130 mm, applied voltage to 58 kV, and rotating speed of the 10 cm wire-working electrode to 4 rpm. The actual current was limited to the maximum range and it was only observed as a sign of well proceeding electrospinning process. Nanofibrous layer was continuously collected on a nonwoven polypropylene fabric (nanofiber carrier) for approximately 30 min.

3. Characterization of nanocomposite and nanofibrous dressing mats

Ultraviolet/visible (UV/Vis) spectroscopy measurement was carried out at (25 ± 2) °C using the UV-160A, (Shimadzu, Japan) equipped with quartz cuvettes with an optical path of 1 cm. The measured solutions were diluted 10 times and the concentration was kept constant for all the UV/Vis spectra measurements. Nanostar dynamic light scattering unit (Wyatt Technology) was used to measure the diameter of AgNPs produced under different conditions. Quartz and disposable polystyrene cuvettes were used for the measurement. Every sample was measured three times, a single measurement typically consisted of 10 acquisitions, the duration of each acquisition was 15 s. The average diameter and standard deviation were evaluated in the supplied Dynamics software.

Rheology was measured in order to investigate changes in viscosity related to the different ratios between HA/AgNPs and PVA, as the viscosity of the solution was an important parameter for electrospinning. Viscosity of PVA/HA-AgNPs nanocomposite blend was measured by ARES G2 Rheometer (TA Instruments) and results were processed in the supplied Trios software. Cone-plate geometry with cone angle 2° and cone diameter of 40 mm was used. Samples were diluted to the concentration of 1.8 mg/ml, approximately 0.62 ml of sample was used for a single measurement. Both flow and oscillatory tests were carried out for each sample and the results were directly compared according to the semi-empirical Cox-Merz rule.

Transmission electron microscope (TEM) investigations were performed employing the JEOL JEM-2010 (HT) electron microscope (JEOL, Japan), with the accelerating voltage of 120 kV. The sample was dissolved in milli-Q water with a concentration of 0.5 mg/ml, then one drop was placed on a pre-coated carbon Cu grid and air dried. X-ray diffraction was measured at 3 kW diffractometer Smart lab (Rigaku) using Cu Kα radiation ($\lambda = 1.54$ Å) and detector Dtex Ultra with Bragg-Brentano geometry. The spectrum was collected at a diffraction angle 2-Theta ranging from 10° to 80° with the step size 0.02° at the rate of 4°/min. The generator was operated at current of 30 mA and voltage of 40 kV. Scanning electron microscope (SEM) was used to visualize the morphology of nanofibrous sheets and further analysis of the nanofiber diameter. To achieve better resolution and prevent overcharging, samples were coated with a thin conductive metallic layer of Pd/Au alloy (thickness 20 nm). The images of nanocomposite surface and morphology were obtained at various magnifications in the *depth* regime at 5 kV, using secondary emission detector. Thermal gravimetric analysis (TGA) was used to study thermal stability and moisture content of the nanofibrous mats. Measurement was carried out in the inert nitrogen atmosphere up to 800 °C, at a heating rate of 10 °C/min. The initial weight of the samples was approx. 5 μg and alumina pan was used for all samples. Tensile testing was used to investigate the strength of nanofibrous sheets, which is an important parameter when it comes to handling the wound dressings. It was carried out by Universal testing equipment ZWICK Z 010 (Zwick–Roell) with 10 N measuring cell. Samples were cut to the dog-bone shape with parallel specimen length of 10 mm. Testing rate was set to 5 mm/min.

4. Results and discussions

4.1. Characterization of HA-AgNPs nanocomposite

AgNPs were prepared by *in-situ* green way using HA as a reducing and capping agent at the same time. We would like to highlight that no toxic reducing agent for AgNPs preparation was used in our study, which is a mandatory condition for the potential use in medical applications [47,48]. Fig. 1 shows the effect of the reaction time (5, 10, 20, 40, 60 min) using different concentrations of Ag^+ on the preparation of AgNPs as evidenced by the UV/VIS spectroscopy. It was noted that (i) at the early stages of the reaction using 0.01 M Ag^+ (5 min; data
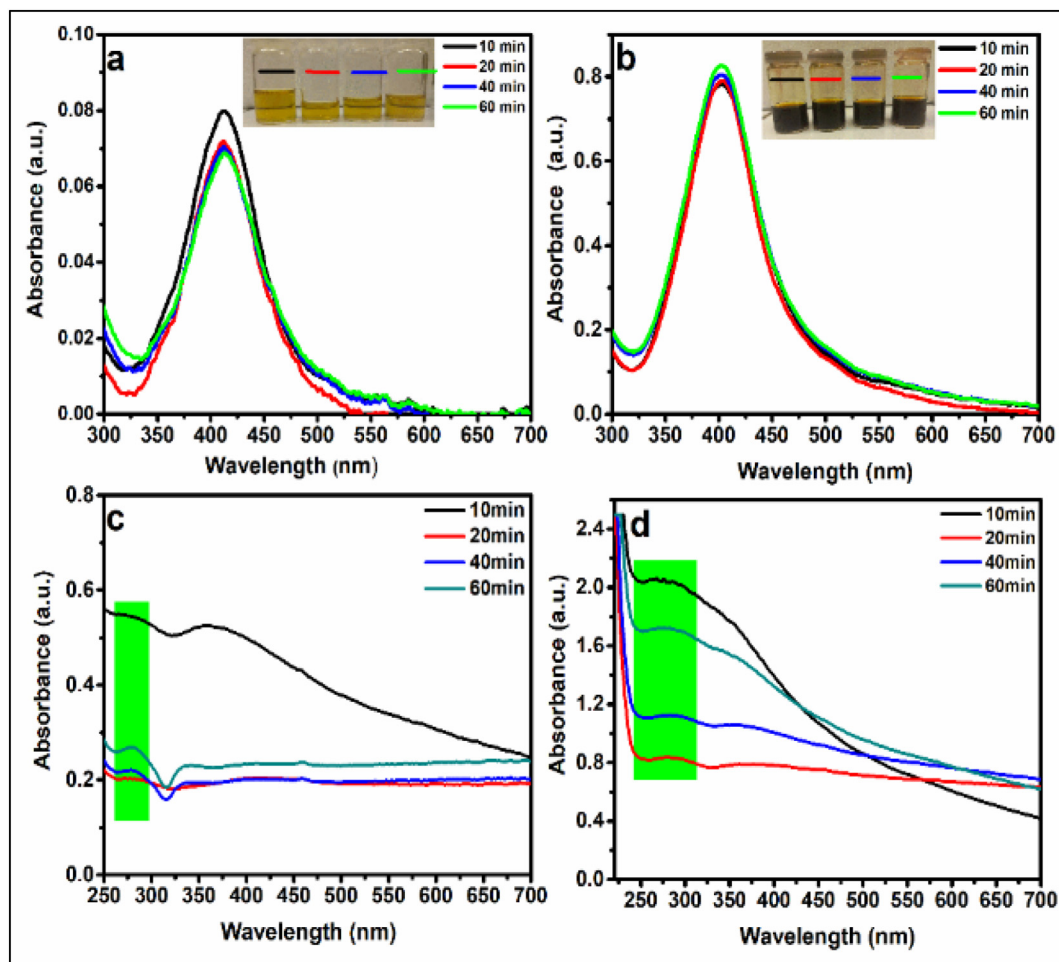
Fig. 1. Effect of time and concentration of silver nitrate on preparation of HA-AgNPs nanocomposite. Experimental conditions: 10 times diluted after different reaction duration (10, 20, 40, and 60 min); solution composition: 1% HA, (0.01–1 M) AgNO$_3$, 1 ml NaOH, 90 °C; **(a)** 0.01 M AgNO$_3$, **(b)** 0.1 M AgNO$_3$, **(c)** 0.5 M AgNO$_3$, **(d)** 1 M AgNO$_3$.

not shown), the plasmon band broadens and a simple test for silver ions using NaCl solution indicates low conversion of Ag$^+$ to the metallic AgNPs [49]; (ii) extending the reaction time to 10 min leads to a new absorption peak around 410 nm related to Ag^0 [50–52], the absorption intensity of Ag^0 decreased slightly upon increasing the reaction time from 10 to 60 min. The dependence of absorption intensity on reaction time is shown in Fig. S1 (supporting information). Photographs in the right upper corner (Fig. 1a), shows the effect of reaction time on the color of HA/AgNPs solutions. The hue of the yellowish color increased slightly upon increasing the reaction time. The same behavior was observed using 0.1 M Ag$^+$ (Fig. 1b). The intensity of the absorption peak at 410 nm corresponding to Ag^0 was 10 times higher compared to 0.01 M Ag$^+$. Absorption intensity of Ag^0 increased slightly by increasing the reaction time from 10 to 60 min. Higher initial concentration of Ag$^+$ ions also caused a color change of the solutions from the pale yellow (Fig. 1a) to the dark brown (Fig. 1b). Fig. 1(c, d), shows the UV/Vis spectra using higher initial concentrations of Ag$^+$, *i.e.*, 0.5 and 1 M, respectively. Interestingly, there was no peak related to Ag^0 when higher initial concentrations of Ag$^+$ were used, which might be caused by insufficiently low concentration of hyaluronan that could reduce the Ag$^+$ to Ag^0.

Fig. 2 shows the transmission electron spectra (TEM) and particle size histograms of HA-AgNPs synthesized using different Ag$^+$ concentrations and reaction duration. The particle size distribution histograms in the insets of Fig. 2a–d were obtained by image analysis of TEM snapshots. Fig. 2a shows the TEM image of nanocomposite (HA/AgNPs; 0.1 M Ag$^+$) formed after 10 min. The average particle size was 2–6 nm. This was possibly due to the formation of silver seeds with spherical and homogenous shapes during the first 10 min of the reaction, after which the growth steps started. Fig. 2b–d shows the TEM and particle size distribution histograms after 20, 40 and 60 min of reaction, respectively. The reaction time neither had a significant effect on the particle size of AgNPs nor it caused aggregation up to 60 min of reaction (Fig. 2b). Interestingly, the particles of AgNPs featured the same size and shape up to 60 min of the reaction. Fig. 2(e, f) shows the size distribution of the AgNPs prepared from two different concentrations of silver ions (0.01 and 0.1 M) recorded by dynamic light scattering (DLS). As we can see, there was no significant change in particle size of AgNPs. The size distribution of AgNPs (Fig. 2e, f) is very narrow and the average was found between 3 and 8 nm. According to Fig. 2, we could conclude that the particle size of AgNPs was time independent, and that higher concentration of Ag$^+$ could be prepared without agglomeration after 20 min of reaction. Literature results report on preparing AgNPs using hyaluronan only in the presence of harsh external reducing agents such as xylose [53], ammonia [54], gamma irradiation [55], glutamic acid [56], UV irradiation [57] or glucose [58], which may render such nanocomposite problematic for use in medical applications. Compared to another study where AgNPs coated with HA molecule were fabricated as a nanoplatform for *in vivo* imaging applications using hyaluronan as only the capping agent while sodium borohydride was used as the reducing agent [34], our results show higher homogeneity, smaller particle size (2–6 nm compared to 10–30 nm) and avoids the necessity of hazardous reducing agent.

The fabrication of the electrospun nanofibrous mats can be affected by many variables, such as the rheological properties of the polymer solution and the spinning parameters [59,60]. Fig. S2 (supporting
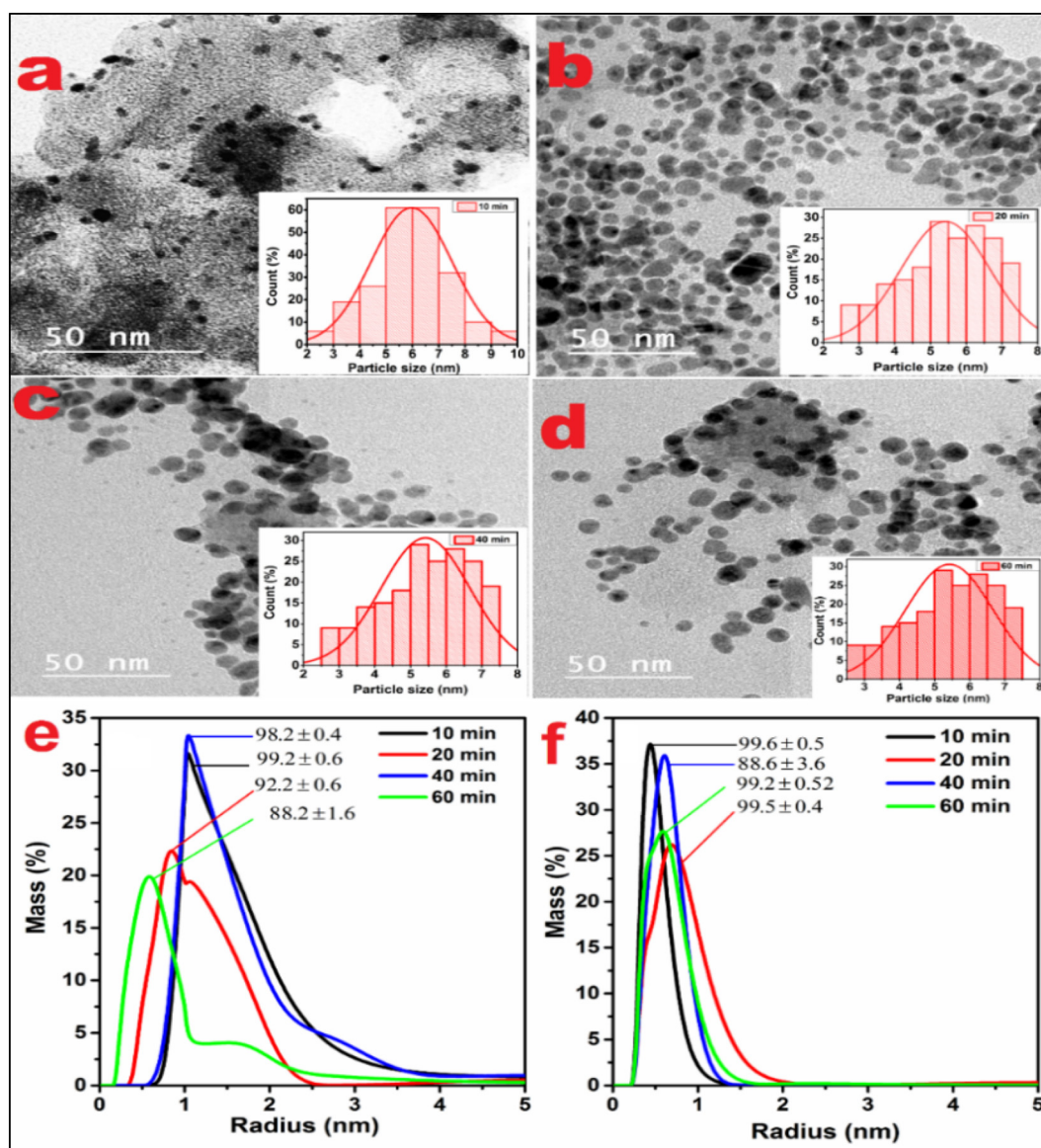
Fig. 2. TEM and DLS of HA-AgNPs nanocomposite. Experimental conditions: (a) 1 % HA, 0.1 M Ag$^+$, 1 ml NaOH, 10 min; histogram of 1 % HA, 0.1 M Ag$^+$, 1 ml NaOH, 10 min; (b) 1 % HA, 0.1 M Ag$^+$, 1 ml NaOH, 20 min; histogram of 1 % HA, 0.1 M Ag$^+$, 1 ml NaOH, 20 min, (c) 1 % HA, 0.1 M Ag$^+$, 1 ml NaOH, 40 min; histogram of 1 % HA, 0.1 M Ag$^+$, 1 ml NaOH, 40 min; (d) 1 % HA, 0.1 M Ag$^+$, 1 ml NaOH, 60 min; histogram of 1 % HA, 0.1 M Ag$^+$, 1 ml NaOH, 60 min. (e) DLS of HA-AgNPs, 1 % HA, 0.01 M Ag$^+$; (f) DLS of HA-AgNPs; 1 % HA, 0.1 M Ag$^+$ at different reaction time (10, 20, 40, 60 min).

information) illustrates the effect of the PVA concentration on the viscosity of PVA/HA-AgNPs solution. The viscosity of PVA/HA increased with the increasing ratio of HA to PVA (data not shown) due to the high viscosity of the hyaluronan as well as the intermolecular interactions between the polyvinyl alcohol and hyaluronan, such as hydrogen bonding between functional groups of PVA (-OH) and hyaluronan (COO$^-$, -OH, -CONHCH$_3$) (Fig. 3). Viscosity was decreased in the case of PVA/HA-AgNPs blends (different mass ratio), which might be attributed to the preparation procedure of Ag^0: During the preparation, in the reduction step of Ag$^+$, HA may undergo degradation to a certain extent due to the redox reaction and the heat treatment under alkaline condition (Fig. S2; supporting information) [34,61]. From Figs. 1 and 2, the first and second hypothesis of our studied were proved, i.e., (i) hyaluronan could reduce the Ag$^+$ to Ag^0 as well as prevent the Ag^0 agglomeration under certain reaction condition such as concentration of Ag$^+$ and HA, and reaction duration, (ii) HA could control the size and shape of Ag^0 and assure good dispersion of AgNPs in the HA matrix.

Experimental conditions: (a) 1% HA, 0.1 M Ag$^+$, 1 ml NaOH, 10 min; histogram of 1% HA, 0.1 M Ag$^+$, 1 ml NaOH, 10 min; (b) 1% HA, 0.1 M

Ag$^+$, 1 ml NaOH, 20 min; histogram of 1% HA, 0.1 M Ag$^+$, 1 ml NaOH, 20 min, (c) 1% HA, 0.1 M Ag$^+$, 1 ml NaOH, 40 min; histogram of 1% HA, 0.1 M Ag$^+$, 1 ml NaOH, 40 min; (d) 1% HA, 0.1 M Ag$^+$, 1 ml NaOH, 60 min; histogram of 1% HA, 0.1 M Ag$^+$, 1 ml NaOH, 60 min. (e) DLS of HA-AgNPs, 1% HA, 0.01 M Ag$^+$; (f) DLS of HA-AgNPs; 1% HA, 0.1 M Ag$^+$ at different reaction time (10, 20, 40, 60 min).

4.2. Fabrication of nanofiber dressing mats

The best preparation conditions of nanocomposite (HA-AgNPs) were used to produce nanofibrous mats via electrospinning technique. Net hyaluronan nanofibers were difficult to fabricate via the electrospinning process using the green solvents (water) because of its polyanionic nature and its viscosity. To overcome this shortcoming of HA, many researchers have sought to improve its electrospinning ability by mixing hyaluronan with other polymers such as gelatin [62,63], poly(ethylene oxide) [45], collagen [64], chitosan [65,66] and hyaluronan [67,68] or from different molecular weight hyaluronan [69]. The last mentioned polymer has been also extensively investigated
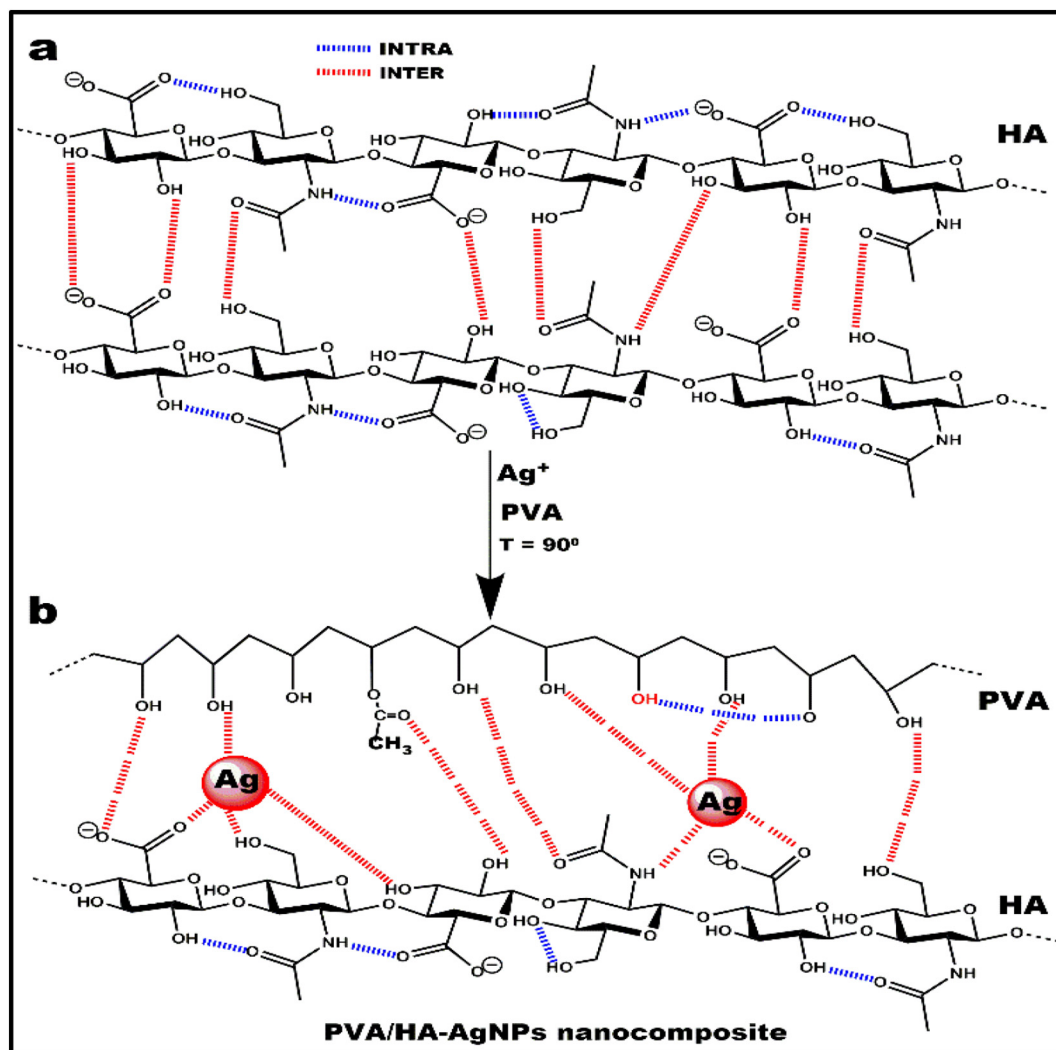
Fig. 3. Proposed scheme of interaction between polyvinyl alcohol (PVA) and hyaluronan silver nanoparticle composite (HA-AgNPs).

in our previous research to generate electrospun fiber mats with high mechanical integrity [70]. Therefore, polyvinyl alcohol (PVA) was dissolved in distilled water at a concentration of 16 wt%, then blended with hyaluronan-based AgNPs at various mass ratios between PVA and HA-AgNPs (100/0; 95/5 90/10; 80/20; 60/40; 50/50 and 40/60). The list of samples is summarized in Table 1.

A study reported fabrication of nanofibrous mats from PVA/PEI which were treated with different concentrations of low molecular weight hyaluronan after the fabrication. However, it did not clarify if the treatment of nanofiber with HA can improve the mechanical properties of the mats or not as well as whether the carboxylic groups of

HA were completely blocked by covalent bonding using a cross-linker between amino groups of PEI and carboxylic group of HA that could lose the unique properties of HA like the healing ability [71]. In another study, HA nanofibers were prepared by electrospinning technique in the presence of (dimethylformamide/ammonia) mixture as solvent [72]. Unfortunately, there is no available discussion about the DMF residues, mechanical and thermal properties in both articles. We, for the first time, fabricated nanofibrous mats from HA/PVA nanocomposite with *in-situ* synthesized AgNPs without surface modification of HA or blocking carboxylic groups of HA and, moreover, using a green solvent (water). Fig. 3 shows a proposed scheme of interactions between HA, AgNPs, and PVA. According to the scheme, inter/intra hydrogen bonds between HA units (Fig. 3a) were spontaneously destroyed/generated due to the higher pH of the reaction mixture [16,73]. AgNPs were connected with functional groups of HA (-OH, -NHCOCH$_3$, and -COO$^-$) (Fig. 3a) as well as the functional groups of PVA (-OH, residual of -COCH$_3$). The AgNPs were surrounded by the HA and PVA functional groups [74]. AgNPs acted as physical cross-linking agents between the HA and PVA chains (Fig. 3b).

4.3. Surface morphology of nanofibrous mats

SEM images, diameter distribution and average diameter of PVA/HA-AgNPs nanocomposite nanofibrous mats with different mass ratios between PVA and HA-AgNPs were shown in Fig. 4. As documented by

Table 1
Compositions of nanofibers mats and suitable mass ratio used for electrospinning preparation.

Sample labeling	Ratio of PVA to HA-AgNPs	Products
PVA/HA-AgNPs	100/0	Nanofibers
PVA/HA-AgNPs	95/05	Nanofibers
PVA/HA-AgNPs	90/10	Nanofibers
PVA/HA-AgNPs	80/20	Nanofibers
PVA/HA-AgNPs	60/40	Nanofibers
PVA/HA-AgNPs	50/50	Nanofibers/beads
PVA/HA-AgNPs	40/60	No nanofibers

Experimental conditions: 16 wt% PVA; 1% HA; 0.1 M Ag$^+$; 20 min; mixed at RT, Distance = 130 mm, voltage 58 kV, and different mass ratio between PVA and HA-AgNPs.
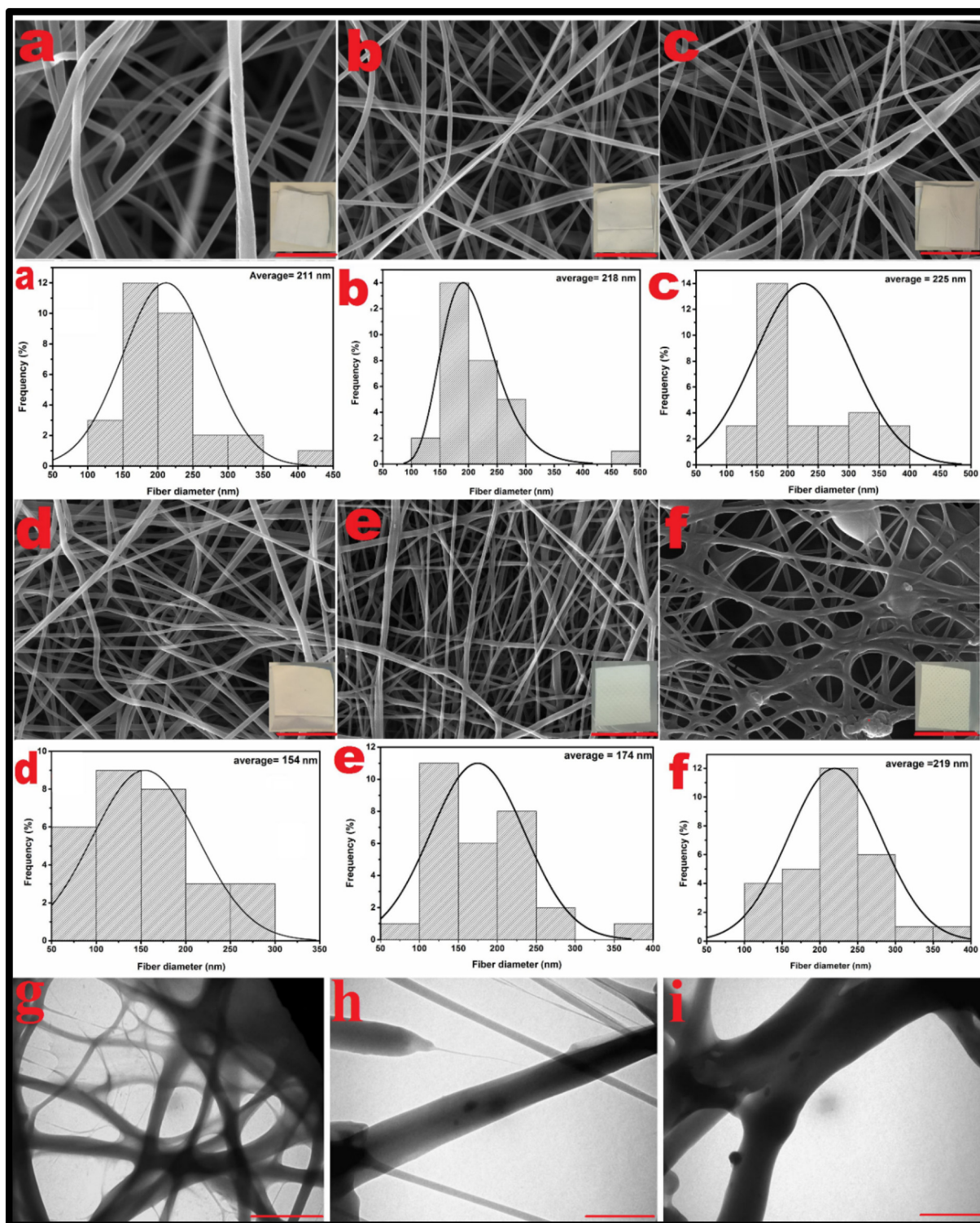
Fig. 4. Representative scanning, transmission electron micrographs and histograms of electrospun mats. Experimental conditions: nanofibers fabricated from neat polyvinyl alcohol and hyaluronan/silver nanoparticle composite (PVA/HA-AgNPs) blend e-spin at different weight ratios between PVA and HA-AgNPs. **(a)** SEM and histograms of PVA/HA-AgNPs (100/0); **(b)** SEM and histograms of PVA PVA/HA-AgNPs (95/5); **(c)** SEM and histograms of PVA/HA-AgNPs (90/10); **(d)** SEM and histograms of PVA/HA-AgNPs (80/20); **(e)** SEM and histograms of PVA/HA-AgNPs (60/40); **(f)** SEM and histograms of PVA/HA-AgNPs (50/50). SEM scale bars were 2-μm, TEM SEM scale bars were 500 nm, and histograms were done using 200 points.

the SEM images in Fig. 4(a–c), defect-free nanofibers were observed in neat PVA and PVA/HA-AgNPs (95/5; 90/10) with the increasing average size of nanofibers. Histogram of diameter distribution is shown in Fig. 4 (a–c) from 211, 218 and 225 nm (Fig. S3a), respectively. Simultaneously, as the HA-AgNPs ratio in the mixture increased from 20 to 40 wt%, the average diameters of PVA/HA-AgNPs electrospun nanofibers decreased from 211 nm to 174 nm (Fig. S5a; supporting

information), and the diameter distribution of nanofibrous mats become slightly narrower. This was probably caused by the increasing hyaluronan content in the solution which led to the increased charge on the surface of the ejected jet formed during the electrospinning [69]. The silver nanoparticles were observed on the surface of the nanofibrous mats using SEM (Fig. S3b; supporting information) without aggregations or agglomerations, and the content of AgNPs in the

nanofibrous mats was increased by increasing the mass ratio between HA-AgNPs as we confirmed using SEM-EDX (Table SI; supporting information). Unfortunately, at lower HA-AgNPs to PVA ratios (95/5; 90/10), there were no AgNPs detected on the surface/inside the nanofibrous mats (Table S1). Fig. 4(g, h, i) shows the TEM of net PVA/HA and PVA/HA-AgNPs with different ratio of PVA to HA-AgNPs (60/40; 50/50), respectively. In PVA/HA nanofibers, there was no AgNPs observed on the surface/inside the nanofibers. In PVA/HA-AgNPs (60/40; 50/50), AgNPs were observed on the surface/inside the nanofibers, with a high content of nanocomposite with spherical AgNPs shape without aggregation.

4.4. Characterization of nanofibrous mats

Fig. 5a shows the ATR-FTIR spectra of pure PVA nanofibrous mats and PVA/HA-AgNPs with different weight ratios between PVA and HA-AgNPs (95/5; 90/10; 80/20; 60/40 and 50/50). In neat PVA, the broadband at $3353\ cm^{-1}$ was associated with —OH vibration, $2935-2905\ cm^{-1}$ could be assigned to the asymmetric stretching of —CH$_2$ group, similarly the vibration at $1426\ cm^{-1}$ can be assigned as

CH$_2$ bending. Residual part of acetyl group is shown as a vibration band around $1730\ cm^{-1}$, $1605\ cm^{-1}$ indicates on the presence of OH vibration of water molecules, (Fig. 5aI) [45,46]. Interestingly, the vibration of amide I ($1616\ cm^{-1}$) [75] of pure hyaluronan was shifted to $1580\ cm^{-1}$ when HA-AgNPs was blended with PVA, and the intensity of the shifted peak was increased upon increasing the mass content of HA-AgNPs in the PVA/HA-AgNPs (Fig. 5aII). The band at $1044\ cm^{-1}$ on plain hyaluronan was ascribed to C—O flex vibration of carbonyl, and was not sharp when HA was mixed with PVA, which might result from the helix structure formed by hydrogen bonding inside the HA molecule or between HA and AgNPs as well as with PVA chain [76]. The intensity of peak at $2935-2905\ cm^{-1}$ corresponding to –CH$_2$– of PVA increased with increasing the HA-AgNPs ratio of the nanofibrous mats. Nevertheless, ATR-FTIR provided reasonably conclusive evidence that both hyaluronan and hyaluronan silver nanoparticles composite and polyvinyl alcohol were successfully incorporated into the electrospun nanofibrous mats. Fig. 5b shows the X-ray diffraction of dressing mats fabricated using different PVA to HA-AgNPs weight ratios. PVA shows only broad reflection peak at $2\theta = 20°$, due to a semi-crystalline character of the PVA. Moreover, the XRD peaks for the
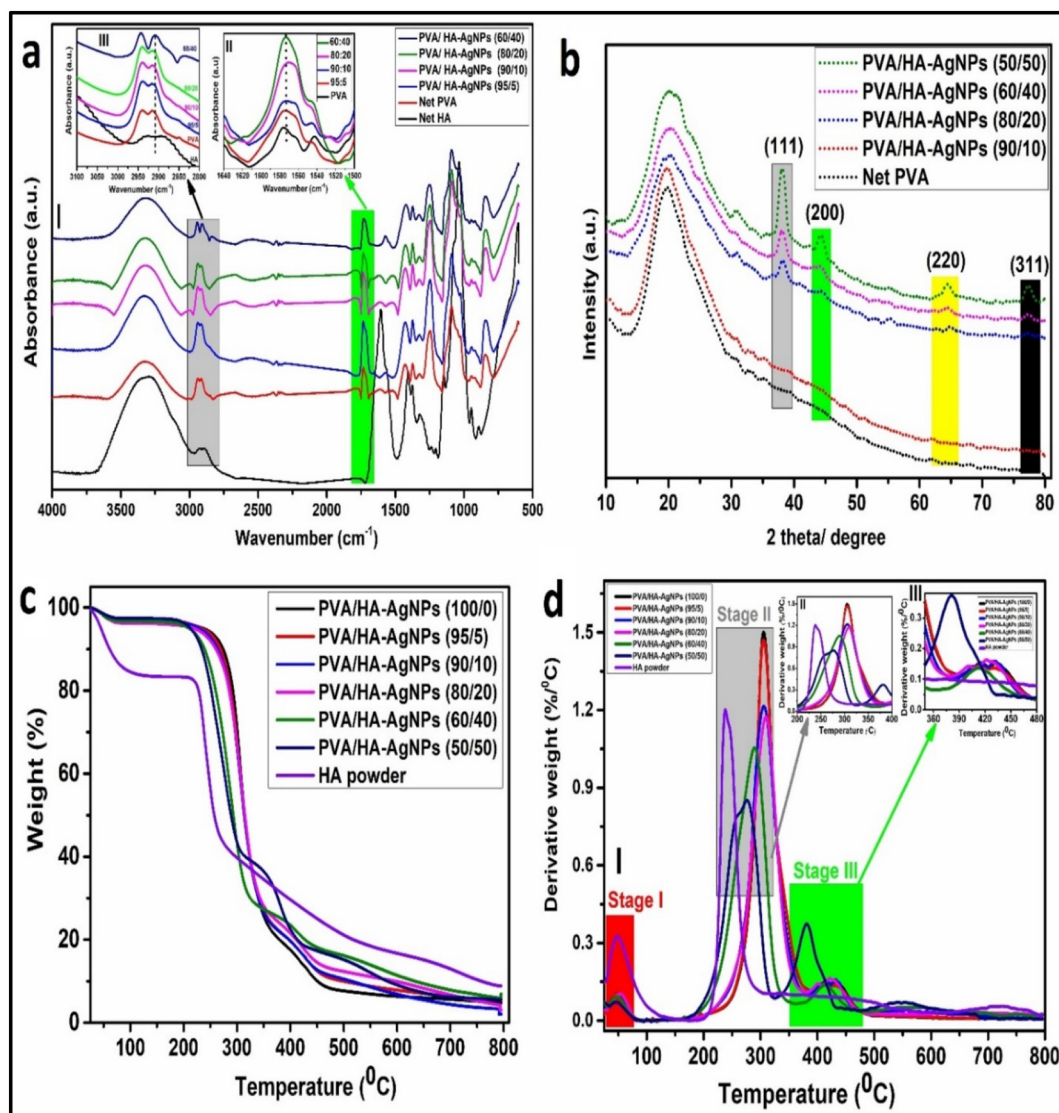
Fig. 5. Characterization of PVA/HA-AgNPs nanofibrous mats. Experimental conditions: (a) ATR-FTIR spectra of nanofiber dressing mats with different chemical compositions; Experimental conditions: 1% HA, 0.1 M Ag$^+$, 1 ml NaOH, 20 min, a) HA powder; b) PVA; c) ratio 95:5; d) ratio 90:10; e) ratio 80:20; f) ratio 60:40. (b) X-ray diffraction of wound dressing mats with different ratio between PVA and HA-AgNPs; Experimental conditions: 1% HA, 0.1 M Ag$^+$, 1 ml NaOH, 20 min, and different ratio between nanofibrous mats compositions. (c) TGA of nanofibrous mats (PVA/HA-AgNPs); (d) DTG of nanofibrous mats (PVA/HA-AgNPs); Experimental conditions: 1% HA, 0.1 M Ag$^+$, 1 ml NaOH, 20 min, and different ratio between nanofibrous mats compositions.

AgNPs were found at 2θ of 38.2°, 44.6°, 64.6° and 78.9°, which were related to the (111), (200), (220), and (311) planes with cubic symmetry, respectively. This confirmed that the fabricated AgNPs crystals were stabilized in these samples by hyaluronan without any further post-processing due to the existence of HA/PVA molecules, even for the ultra-small ones [57,58]. The intensity of the AgNPs peaks increased with increasing the PVA to HA-AgNPs ratio (Fig. 5b). However, the peaks of the silver nanocrystals from the PVA/HA-AgNPs mats, which contained the lowest content of AgNPs (95/5 and 90/10 weight ratio), could hardly be detected due to the resolution limit of XRD analysis.

TGA thermograms shown in Fig. 5(c, d) for net PVA mats, PVA with different mass ratios of HA (95/5; 90/10; 80/20; 60/40 and 50/50) and net HA. Fig. 5c indicates that the nanofibrous mats with various PVA/HA-AgNPs mass ratios showed different decomposition temperatures. Fig. 5c shows the DTG of nanofibrous mats, PVA and plain HA. As shown in Fig. 5c, about 5% of the mass of the nanofibrous mat was lost at 100 °C, and for HA powder, the mass loss was 18% at 100 °C (stage I), primarily due to the evaporation of the moisture in nanofibrous mats and the HA powder and the water physically adsorbed in the material. The thermal decomposition of the HA occurs mainly at temperatures between 200 and 300 °C with a corresponding mass loss of nearly 50.0%. At 245 °C, the rate of decomposition reaches the maximum (Fig. 5c). DTG of different PVA to HA-AgNPs mass ratios (Fig. 5d), 95/5; 90/10; 80/20 showed the maximum decomposition temperature between 280 and 310 °C (stage II) with lower decomposition rate compared to the net PVA nanofibers. At higher PVA to nanocomposite ratio, 60/40 and 50/50, the maximum decomposition rate was shifted to 250–270 °C, due to

the increase of the HA content in e-spun nanofiber. After the major degradation step, there was another mass loss present (Fig. 5cII) which was represented by different mass ratios (stage III) in the DTG curve at 400 and at 460 °C, while the net PVA nanofibers, did not show any at this region, due to degradation of hyaluronan oligomers generated in the preparation of AgNPs step. This 5% mass loss between 500 and 600 °C might be caused by the elemental composition like silver nanoparticles, residual calcium, and magnesium, which was present in the original samples. The small mass loss at 700 °C was caused by the decomposition of polysaccharide chains. However, with the increasing content of HA-AgNPs nanoparticles, the temperature at which the PVA weight loss related to the nanofibrous mats occurred shifted to a lower temperature range (stage II). This was mainly due to the formation of hydrogen bonds between the hyaluronan/silver nanoparticles and PVA molecules. From the results of TGA-DTG, we could conclude that nanocomposite (HA/AgNPs) enhanced the thermal stability of dressing mats compared to the net PVA and proved one of the hypotheses of this study.

The mechanical properties of the nanofibers play a very important role in using the material in different medical applications [77]. Fig. 6 shows the stress-strain curve of pure PVA mats and PVA/HA-AgNPs nanofibrous mats with different ratios between PVA and HA-AgNPs (95/5; 90/10 and 80/20). Interestingly, the addition of nanocomposite (HA-AgNPs) as a reinforced material into PVA caused a significant enhancement on the mechanical properties of the electrospun nanofibrous mats (Fig. 6a). Tensile strength significantly improved with increasing the ratio of HA-AgNPs (5, 10, and 20 wt%) (4×) compared with the neat PVA mats. The reinforcing effect of HA-AgNPs on
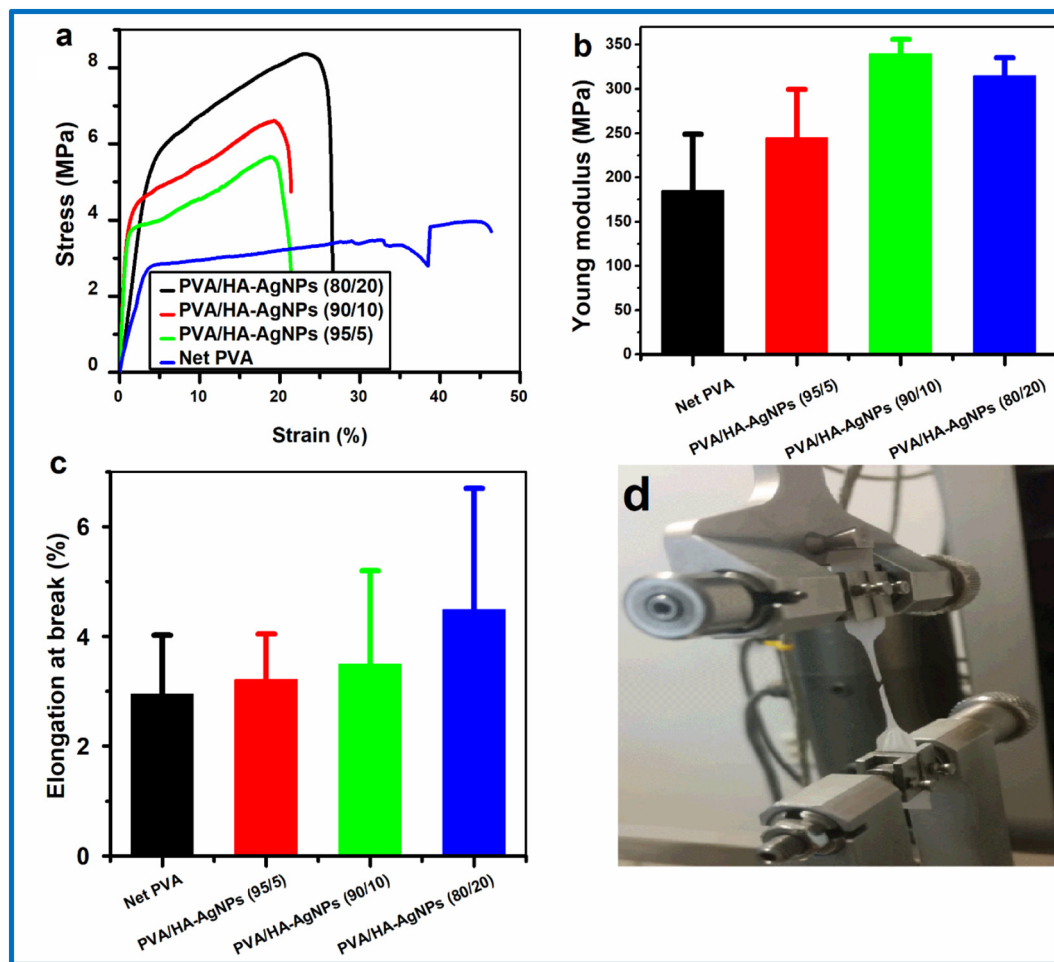
Fig. 6. Mechanical properties of PVA/HA-AgNPs nanofibrous mats. Experimental conditions: (a) Stress-strain curves of nanofibrous mats fabricated using different ratio between PVA and HA-AgNPs; (b) Young modulus of nanofibrous mats; (c) Elongation at break (%); (d) Visualized sample of nanofiber mat after failure. 1% HA, 0.1 M Ag⁺, 1 ml NaOH, 20 min, and different ratio between nanofibrous mats compositions (Neat PVA, PVA/HA-NPs (95/5); PVA/HA-NPs (90/10); PVA/HA-NPs (80/20)).

the tensile strength, Young's modulus and elongation to failure compared with the neat PVA nanofibers was observed. The Young's modulus of the nanofibrous mats was significantly enhanced compared with the neat PVA mat and was increased from 175 MPa to 325 MPa (Fig. 6b, c) by increasing the content of filler in the electrospun nanofibers. The elongation at break also slightly increased. When a higher amount of nanocomposite (reinforcing agent) was added, it could be reasonably attributed to a large aspect ratio and the interaction between HA-AgNPs and the matrix (with a small particle size of AgNPs; Fig. 3), without restrictions to the movement of PVA polymer chains [78,79]. Fig. 6d visualizes the deformation part (from the center) of the nanofibrous mats after failure. We assume that the electrostatic force during the electrospinning process may improve the interaction between PVA and nanofiller, and the size-effect in nanofibers might contribute to the improved mechanical properties. These results confirmed that the nanocomposites consisting of PVA and HA-AgNPs nanofiller might be used for the preparation of high strength nanofibers. One of our hypotheses was proved by enhancing the mechanical properties of the dressing fibers using HA/AgNPs nanocomposite compared to the net PVA sheet which could be used in tissue engineering applications, especially for burnt skin regeneration and drug carrier purposes.

5. Conclusion

A novel wound dressing nanofibrous mats were fabricated from nanocomposite polyvinyl alcohol/hyaluronan silver nanoparticles (PVA/HA-AgNPs) with controlled size and shape of AgNPs by safe and green processing. The following results were obtained as a must to attain the specific hypotheses of our study.

- Hyaluronan was used as a dually functional (reducing and stabilizing) agent for fabrication of silver nanoparticles. Hyaluronan with low molecular weight (150–170 KDa) and polyvinyl alcohol (70 KDa) could prevent the aggregation of AgNPs at low concentration of Ag^+ (up to 0.1 M) and led to the size of the Ag^0 obtained after 20 min of the reaction of about (2–6 nm) with spherical shape morphology. PVA/HA-AgNPs dressing nanofibers were fabricated by electrospinning technique and water was used as a green solvent. It was found that the fiber diameter decreased with increasing the HA/AgNPs content up to 20 wt% with a significant enhancement of the nanofiber mechanical properties. Crystallinity and thermal stability of nanofibrous mats were enhanced using higher ratios of PVA to HA-AgNPs nanocomposite.
- Based on our results, all hypotheses of our work were proved, clearly discussed and the novel nanofibrous mats (PVA/HA-AgNPs) could be further modified and used as nanocarriers for *in-vivo* and *in-vitro* applications with a reduced risk of coagulation and rejection from the immune system. The new nanocomposite nanofibrous mats might be useful in a wide variety of medical and biological purposes that take advantage of the biological activates of HA and antimicrobial properties of AgNPs.

Acknowledgments

Appendix A. Supplementary data

Supplementary data to this article can be found online at https://doi.org/10.1016/j.ijbiomac.2019.07.205.

References

[1] A.M. Abdel-Mohsen, R. Hrdina, L. Burgert, G. Krylova, R.M. Abdel-Rahman, A. Krejcova, M. Steinhart, L. Benes, Green synthesis of hyaluronan fibers with silver nanoparticles, Carbohyd Polym 89 (2) (2012) 411–422.

[2] J. Radhakrishnan, A. Subramanian, U.M. Krishnan, S. Sethuraman, Injectable and 3D bioprinted polysaccharide hydrogels: from cartilage to osteochondral tissue engineering, Biomacromolecules 18 (1) (2017) 1–26.

[3] N. Broguiere, E. Cavalli, G.M. Salzmann, M. Zenobi-Wong, Factor XIII cross-linked hyaluronan hydrogels for cartilage tissue engineering, ACS Biomaterials Science & Engineering 2 (12) (2016) 2176–2184.

[4] F.P. Rojas, M.A. Batista, C.A. Lindburg, D. Dean, A.J. Grodzinsky, C. Ortiz, L. Han, Molecular adhesion between cartilage extracellular matrix macromolecules, Biomacromolecules 15 (3) (2014) 772–780.

[5] J. Seror, Y. Merkher, N. Kampf, L. Collinson, A.J. Day, A. Maroudas, J. Klein, Articular cartilage proteoglycans as boundary lubricants: structure and frictional interaction of surface-attached hyaluronan and hyaluronan–aggrecan complexes, Biomacromolecules 12 (10) (2011) 3432–3443.

[6] K. Valachová, D. Topoľská, R. Mendichi, M.N. Collins, V. Sasinková, L. Šoltés, Hydrogen peroxide generation by the Weissberger biogenic oxidative system during hyaluronan degradation, Carbohydr. Polym. 148 (2016) 189–193.

[7] K. Valachová, M. Baňasová, D. Topoľská, V. Sasinková, I. Juránek, M.N. Collins, L. Šoltés, Influence of tiopronin, captopril and levamisole therapeutics on the oxidative degradation of hyaluronan, Carbohydr. Polym. 134 (2015) 516–523.

[8] Y. Ji, K. Ghosh, X.Z. Shu, B. Li, J.C. Sokolov, G.D. Prestwich, R.A.F. Clark, M.H. Rafailovich, Electrospun three-dimensional hyaluronic acid nanofibrous scaffolds, Biomaterials 27 (20) (2006) 3782–3792.

[9] X. Zhu, T. Chen, B. Feng, J. Weng, K. Duan, J. Wang, X. Lu, Biomimetic bacterial cellulose-enhanced double-network hydrogel with excellent mechanical properties applied for the osteochondral defect repair, ACS Biomaterials Science & Engineering 4 (10) (2018) 3534–3544.

[10] T.M. Tamer, M.N. Collins, K. Valachová, M.A. Hassan, A.M. Omer, M.S. Mohy-Eldin, K. Švík, R. Jurčík, Ľ. Ondruška, C. Bíró, A.B. Albadarin, L. Šoltés, MitoQ loaded chitosan-Hyaluronan composite membranes for wound healing, Materials 11 (4) (2018) 569.

[11] H.S. Han, K.Y. Choi, H. Lee, M. Lee, J.Y. An, S. Shin, S. Kwon, D.S. Lee, J.H. Park, Gold-nanoclustered hyaluronan nano-assemblies for photothermally maneuvered photodynamic tumor ablation, ACS Nano 10 (12) (2016) 10858–10868.

[12] F. Bano, M. Carril, P. Di Gianvincenzo, R.P. Richter, Interaction of Hyaluronan with cationic nanoparticles, Langmuir 31 (30) (2015) 8411–8420.

[13] E.C. Dreaden, S.W. Morton, K.E. Shopsowitz, J.-H. Choi, Z.J. Deng, N.-J. Cho, P.T. Hammond, Bimodal tumor-targeting from microenvironment responsive Hyaluronan layer-by-layer (LbL) nanoparticles, ACS Nano 8 (8) (2014) 8374–8382.

[14] S. Boddohi, N. Moore, P.A. Johnson, M.J. Kipper, Polysaccharide-based polyelectrolyte complex nanoparticles from chitosan, heparin, and hyaluronan, Biomacromolecules 10 (6) (2009) 1402–1409.

[15] Z. Cai, H. Zhang, Y. Wei, F. Cong, Hyaluronan-inorganic nanohybrid materials for biomedical applications, Biomacromolecules 18 (6) (2017) 1677–1696.

[16] A.M. Abdel-Mohsen, J. Jancar, R.M. Abdel-Rahman, L. Vojtek, P. Hyršl, M. Dušková, H. Nejezchlebová, A novel in situ silver/hyaluronan bio-nanocomposite fabrics for wound and chronic ulcer dressing: in vitro and in vivo evaluations, Int. J. Pharm. 520 (1) (2017) 241–253.

[17] C.-H. Chen, S.-H. Chen, K.T. Shalumon, J.-P. Chen, Dual functional core–sheath electrospun hyaluronic acid/polycaprolactone nanofibrous membranes embedded with silver nanoparticles for prevention of peritendinous adhesion, Acta Biomater. 26 (2015) 225–235 Supplement C.

[18] A. Schneider, C. Picart, B. Senger, P. Schaaf, J.-C. Voegel, B. Frisch, Layer-by-layer films from hyaluronan and amine-modified hyaluronan, Langmuir 23 (5) (2007) 2655–2662.

[19] T. Dvir, B.P. Timko, D.S. Kohane, R. Langer, Nanotechnological strategies for engineering complex tissues, Nat. Nanotechnol. 6 (2010) 13.

[20] Q. Liu, B. Duan, X. Xu, L. Zhang, Progress in rigid polysaccharide-based nanocomposites with therapeutic functions, J. Mater. Chem. B 5 (29) (2017) 5690–5713.

[21] M. Gholipourmalekabadi, A.M. Seifalian, A.M. Urbanska, M.D. Omrani, J.G. Hardy, Z. Madjd, S.M. Hashemi, H. Ghanbarian, P. Brouki Milan, M. Mozafari, R.L. Reis, S.C. Kundu, A. Samadikuchaksaraei, 3D protein-based bilayer artificial skin for the guided scarless healing of third-degree burn wounds in vivo, Biomacromolecules 19 (7) (2018) 2409–2422.

[22] X. Yan, F. Li, K.-D. Hu, J. Xue, X.-F. Pan, T. He, L. Dong, X.-Y. Wang, Y.-D. Wu, Y.-H. Song, W.-P. Xu, Y. Lu, Nacre-mimic reinforced Ag@reduced graphene oxide-sodium alginate composite film for wound healing, Sci. Rep. 7 (1) (2017) 13851.

[23] J. Xiong, P. Cui, X. Chen, J. Wang, K. Parida, M.-F. Lin, P.S. Lee, Skin-touch-actuated textile-based triboelectric nanogenerator with black phosphorus for durable biomechanical energy harvesting, Nat. Commun. 9 (1) (2018) 4280.

[24] T.-T. Tsai, T.-H. Huang, C.-J. Chang, N. Yi-Ju Ho, Y.-T. Tseng, C.-F. Chen, Antibacterial cellulose paper made with silver-coated gold nanoparticles, Sci. Rep. 7 (1) (2017) 3155.

[25] S.V. Kumar, A.P. Bafana, P. Pawar, A. Rahman, S.A. Dahoumane, C.S. Jeffryes, High conversion synthesis of <10 nm starch-stabilized silver nanoparticles using microwave technology, Sci. Rep. 8 (1) (2018) 5106.

[26] L. Zhang, H. Fang, K. Zhang, J. Yin, Homologous sodium alginate/chitosan-based scaffolds, but contrasting effect on stem cell shape and osteogenesis, ACS Appl. Mater. Interfaces 10 (8) (2018) 6930–6941.

[27] D. Liang, Z. Lu, H. Yang, J. Gao, R. Chen, Novel asymmetric wettable AgNPs/chitosan wound dressing: in vitro and in vivo evaluation, ACS Appl. Mater. Interfaces 8 (6) (2016) 3958–3968.

[28] D. Annur, Z.-K. Wang, J.-D. Liao, C. Kuo, Plasma-synthesized silver nanoparticles on electrospun chitosan nanofiber surfaces for antibacterial applications, Biomacromolecules 16 (10) (2015) 3248–3255.

[29] M.J. Laudenslager, J.D. Schiffman, C.L. Schauer, Carboxymethyl chitosan as a matrix material for platinum, gold, and silver nanoparticles, Biomacromolecules 9 (10) (2008) 2682–2685.

[30] P. Sahariah, M. Másson, Antimicrobial chitosan and chitosan derivatives: a review of the structure–activity relationship, Biomacromolecules 18 (11) (2017) 3846–3868.

[31] A.-K. Picke, J. Salbach-Hirsch, V. Hintze, S. Rother, M. Rauner, C. Kascholke, S. Möller, R. Bernhardt, S. Rammelt, M.T. Pisabarro, G. Ruiz-Gómez, M. Schnabelrauch, M. Schulz-Siegmund, M.C. Hacker, D. Scharnweber, C. Hofbauer, L.C. Hofbauer, Sulfated hyaluronan improves bone regeneration of diabetic rats by binding sclerostin and enhancing osteoblast function, Biomaterials 96 (2016) 11–23 Supplement C.

[32] M. Swierczewska, H.S. Han, K. Kim, J.H. Park, S. Lee, Polysaccharide-based nanoparticles for theranostic nanomedicine, Adv. Drug Deliv. Rev. 99 (Part A) (2016) 70–84.

[33] A.G. Arranja, V. Pathak, T. Lammers, Y. Shi, Tumor-targeted nanomedicines for cancer theranostics, Pharmacol. Res. 115 (Supplement C) (2017) 87–95.

[34] X. Zhang, M. Yao, M. Chen, L. Li, C. Dong, Y. Hou, H. Zhao, B. Jia, F. Wang, Hyaluronic acid-coated silver nanoparticles as a nanoplatform for in vivo imaging applications, ACS Appl. Mater. Interfaces 8 (39) (2016) 25650–25653.

[35] S. Jiang, Y. Chen, G. Duan, C. Mei, A. Greiner, S. Agarwal, Electrospun nanofiber reinforced composites: a review, Polym. Chem. 9 (20) (2018) 2685–2720.

[36] F. Ding, H. Deng, Y. Du, X. Shi, Q. Wang, Emerging chitin and chitosan nanofibrous materials for biomedical applications, Nanoscale 6 (16) (2014) 9477–9493.

[37] J. Li, Y. Zhou, W. Chen, Z. Yuan, B. You, Y. Liu, S. Yang, F. Li, C. Qu, X. Zhang, A novel 3D in vitro tumor model based on silk fibroin/chitosan scaffolds to mimic the tumor microenvironment, ACS Appl. Mater. Interfaces 10 (43) (2018) 36641–36651.

[38] R. Sridhar, R. Lakshminarayanan, K. Madhaiyan, V. Amutha Barathi, K.H.C. Lim, S. Ramakrishna, Electrosprayed nanoparticles and electrospun nanofibers based on natural materials: applications in tissue regeneration, drug delivery and pharmaceuticals, Chem. Soc. Rev. 44 (3) (2015) 790–814.

[39] T.D. Stocco, N.J. Bassous, S. Zhao, A.E.C. Granato, T.J. Webster, A.O. Lobo, Nanofibrous scaffolds for biomedical applications, Nanoscale 10 (26) (2018) 12228–12255.

[40] S. Ling, W. Chen, Y. Fan, K. Zheng, K. Jin, H. Yu, M.J. Buehler, D.L. Kaplan, Biopolymer nanofibrils: structure, modeling, preparation, and applications, Prog. Polym. Sci. 85 (2018) 1–56.

[41] N. Dalton, R.P. Lynch, M.N. Collins, M. Culebras, Thermoelectric properties of electrospun carbon nanofibres derived from lignin, Int. J. Biol. Macromol. 121 (2019) 472–479.

[42] M. Bernard, E. Jubeli, M.D. Pungente, N. Yagoubi, Biocompatibility of polymer-based biomaterials and medical devices – regulations, in vitro screening and risk-management, Biomaterials Science 6 (8) (2018) 2025–2053.

[43] H. Yoshimoto, Y.M. Shin, H. Terai, J.P. Vacanti, A biodegradable nanofiber scaffold by electrospinning and its potential for bone tissue engineering, Biomaterials 24 (12) (2003) 2077–2082.

[44] S. Zarkoob, R.K. Eby, D.H. Reneker, S.D. Hudson, D. Ertley, W.W. Adams, Structure and morphology of electrospun silk nanofibers, Polymer 45 (11) (2004) 3973–3977.

[45] J.J. Ahire, D.D. Robertson, A.J. van Reenen, L.M.T. Dicks, Polyethylene oxide (PEO)-hyaluronic acid (HA) nanofibers with kanamycin inhibits the growth of listeria monocytogenes, Biomed. Pharmacother. 86 (2017) 143–148.

[46] Y. Deng, X. Zhang, Y. Zhao, S. Liang, A. Xu, X. Gao, F. Deng, J. Fang, S. Wei, Peptide-decorated polyvinyl alcohol/hyaluronan nanofibers for human induced pluripotent stem cell culture, Carbohydr. Polym. 101 (2014) 36–39.

[47] L. Adhikari, N.E. Larm, N. Bhawawet, G.A. Baker, Rapid microwave-assisted synthesis of silver nanoparticles in a halide-free deep eutectic solvent, ACS Sustain. Chem. Eng. 6 (5) (2018) 5725–5731.

[48] Y. Xue, X. Qiu, Z. Liu, Y. Li, Facile and efficient synthesis of silver nanoparticles based on biorefinery wood lignin and its application as the optical sensor, ACS Sustain. Chem. Eng. 6 (6) (2018) 7695–7703.

[49] C. Levard, S. Mitra, T. Yang, A.D. Jew, A.R. Badireddy, G.V. Lowry, G.E. Brown, Effect of chloride on the dissolution rate of silver nanoparticles and toxicity to E. coli, Environmental Science & Technology 47 (11) (2013) 5738–5745.

[50] E. Fantino, A. Chiappone, I. Roppolo, D. Manfredi, R. Bongiovanni, C.F. Pirri, F. Calignano, 3D printing of conductive complex structures with in situ generation of silver nanoparticles, Adv. Mater. 28 (19) (2016) 3712–3717.

[51] M. Lv, S. Su, Y. He, Q. Huang, W. Hu, D. Li, C. Fan, S.-T. Lee, Long-term antimicrobial effect of silicon nanowires decorated with silver nanoparticles, Adv. Mater. 22 (48) (2010) 5463–5467.

[52] Z. Fan, B. Liu, J. Wang, S. Zhang, Q. Lin, P. Gong, L. Ma, S. Yang, A novel wound dressing based on Ag/graphene polymer hydrogel: effectively kill bacteria and accelerate wound healing, Adv. Funct. Mater. 24 (25) (2014) 3933–3943.

[53] G. Khachatryan, K. Khachatryan, J. Grzyb, M. Fiedorowicz, Formation and properties of hyaluronan/nano Ag and hyaluronan-lecithin/nano Ag films, Carbohydr. Polym. 151 (2016) 452–457.

[54] N. Xia, Y. Cai, T. Jiang, J. Yao, Green synthesis of silver nanoparticles by chemical reduction with hyaluronan, Carbohydr. Polym. 86 (2) (2011) 956–961.

[55] N.Q. Hien, D. Van Phu, N.N. Duy, L.A. Quoc, Radiation synthesis and characterization of hyaluronan capped gold nanoparticles, Carbohydr. Polym. 89 (2) (2012) 537–541.

[56] B. Lu, F. Lu, Y. Zou, J. Liu, B. Rong, Z. Li, F. Dai, D. Wu, G. Lan, In situ reduction of silver nanoparticles by chitosan-l-glutamic acid/hyaluronic acid: enhancing antimicrobial and wound-healing activity, Carbohydr. Polym. 173 (2017) 556–565.

[57] X. Cui, C.M. Li, H. Bao, X. Zheng, J. Zang, C.P. Ooi, J. Guo, Hyaluronan-assisted photo-reduction synthesis of silver nanostructures: from nanoparticle to nanoplate, J. Phys. Chem. C 112 (29) (2008) 10730–10734.

[58] M.M. Kemp, A. Kumar, S. Mousa, T.-J. Park, P. Ajayan, N. Kubotera, S.A. Mousa, R.J. Linhardt, Synthesis of gold and silver nanoparticles stabilized with glycosaminoglycans having distinctive biological activities, Biomacromolecules 10 (3) (2009) 589–595.

[59] Z. Yingshan, Y. Dongzhi, N. Jun, Electrospinning of chitosan/poly(vinyl alcohol)/acrylic acid aqueous solutions, J. Appl. Polym. Sci. 102 (6) (2006) 5692–5697.

[60] A.M. Abdelgawad, S.M. Hudson, O.J. Rojas, Antimicrobial wound dressing nanofiber mats from multicomponent (chitosan/silver-NPs/polyvinyl alcohol) systems, Carbohydr. Polym. 100 (2014) 166–178.

[61] H.-J. Li, A.-Q. Zhang, L. Sui, D.-J. Qian, M. Chen, Hyaluronan/tween 80-assisted synthesis of silver nanoparticles for biological application, J. Nanopart. Res. 17 (2) (2015) 111.

[62] H.-M. Liou, L.-R. Rau, C.-C. Huang, M.-R. Lu, F.-Y. Hsu, Electrospun hyaluronan-gelatin nanofibrous matrix for nerve tissue engineering, J. Nanomater. 2013 (2013) 9.

[63] L. Junxing, H. Aihua, H.C. C., F. Dufei, H.B. S., C. Benjamin, Electrospinning of hyaluronic acid (HA) and HA/gelatin blends, Macromol. Rapid Commun. 27 (2) (2006) 114–120.

[64] J.A. Matthews, G.E. Wnek, D.G. Simpson, G.L. Bowlin, Electrospinning of collagen nanofibers, Biomacromolecules 3 (2) (2002) 232–238.

[65] M. Pakravan, M.-C. Heuzey, A. Ajji, Core–shell structured PEO-chitosan nanofibers by coaxial electrospinning, Biomacromolecules 13 (2) (2012) 412–421.

[66] S.S. Ojha, D.R. Stevens, T.J. Hoffman, K. Stano, R. Klossner, M.C. Scott, W. Krause, L.I. Clarke, R.E. Gorga, Fabrication and characterization of electrospun chitosan nanofibers formed via templating with polyethylene oxide, Biomacromolecules 9 (9) (2008) 2523–2529.

[67] S.Y.H. Abdalkarim, H.-Y. Yu, C. Wang, L. Yang, Y. Guan, L. Huang, J. Yao, Sheet-like cellulose nanocrystal-ZnO nanohybrids as multifunctional reinforcing agents in biopolyester composite nanofibers with ultrahigh UV-shielding and antibacterial performances, ACS Applied Bio Materials 1 (3) (2018) 714–727.

[68] A. Mickova, M. Buzgo, O. Benada, M. Rampichova, Z. Fisar, E. Filova, M. Tesarova, D. Lukas, E. Amler, Core/shell nanofibers with embedded liposomes as a drug delivery system, Biomacromolecules 13 (4) (2012) 952–962.

[69] I.C. Um, D. Fang, B.S. Hsiao, A. Okamoto, B. Chu, Electro-spinning and electro-blowing of hyaluronic acid, Biomacromolecules 5 (4) (2004) 1428–1436.

[70] N.T.B. Linh, B.-T. Lee, Electrospinning of polyvinyl alcohol/gelatin nanofiber composites and cross-linking for bone tissue engineering application, J. Biomater. Appl. 27 (3) (2012) 255–266.

[71] Y. Zhao, Z. Fan, M. Shen, X. Shi, Hyaluronic acid-functionalized electrospun polyvinyl alcohol/polyethyleneimine nanofibers for cancer cell capture applications, Adv. Mater. Interfaces 2 (15) (2015), 1500256.

[72] E.K. Brenner, J.D. Schiffman, E.A. Thompson, L.J. Toth, C.L. Schauer, Electrospinning of hyaluronic acid nanofibers from aqueous ammonium solutions, Carbohydr. Polym. 87 (1) (2012) 926–929.

[73] E.R. Morris, D.A. Rees, E.J. Welsh, Conformation and dynamic interactions in hyaluronate solutions, J. Mol. Biol. 138 (2) (1980) 383–400.

[74] P. Gribbon, B.C. Heng, T.E. Hardingham, The molecular basis of the solution properties of hyaluronan investigated by confocal fluorescence recovery after photobleaching, Biophys. J. 77 (4) (1999) 2210–2216.

[75] G. Chen, J. Guo, J. Nie, G. Ma, Preparation, characterization, and application of PEO/HA core shell nanofibers based on electric field induced phase separation during electrospinning, Polymer 83 (2016) 12–19.

[76] C. Tang, C.D. Saquing, J.R. Harding, S.A. Khan, In situ cross-linking of electrospun poly(vinyl alcohol) nanofibers, Macromolecules 43 (2) (2010) 630–637.

[77] Z. Cheng, F. Zhang, W. Liu, L. Cui, L. Kang, A novel preparation for a PVA/l-histidine/AgNPs membrane and its antibacterial property, RSC Adv. 5 (67) (2015) 54182–54187.

[78] B. Wang, Z. Chen, J. Zhang, J. Cao, S. Wang, Q. Tian, M. Gao, Q. Xu, Fabrication of PVA/graphene oxide/TiO2 composite nanofibers through electrospinning and interface sol–gel reaction: effect of graphene oxide on PVA nanofibers and growth of TiO2, Colloids Surf. A Physicochem. Eng. Asp. 457 (2014) 318–325.

[79] W. Chen, L. Yadong, D. Guqiao, X. Xiaoming, J. Mianheng, Preparation and characterization of graphene oxide/poly(vinyl alcohol) composite nanofibers via electrospinning, J. Appl. Polym. Sci. 127 (4) (2013) 3026–3032.

Supporting informations

Electrospinning of hyaluronan/polyvinyl alcohol in presence of *in-situ* silver nanoparticles: preparation and characterization

A.M. Abdel-Mohsen[a,b*], D. Pavliňák[c], M. Čileková[d], P. Lepcio[1], R.M.Abdel-Rahman[1], J. Jančář[a,d]

[a] CEITEC-Central European Institute of Technology, Brno University of Technology, Purkynova 123, Brno, 612 00, Brno, Czechia

[b] Pretreatment and Finishing of Cellulosic Fibers, Textile Research Division, National Research Centre, Dokki, Cairo, Egypt

[c] Department of Physical Electronics, Masaryk University, Brno, Czechia

[d] Institute of Materials Chemistry, Faculty of Chemistry, Brno University of Technology, Purkynova 118, Brno, 612 00, Brno, Czechia
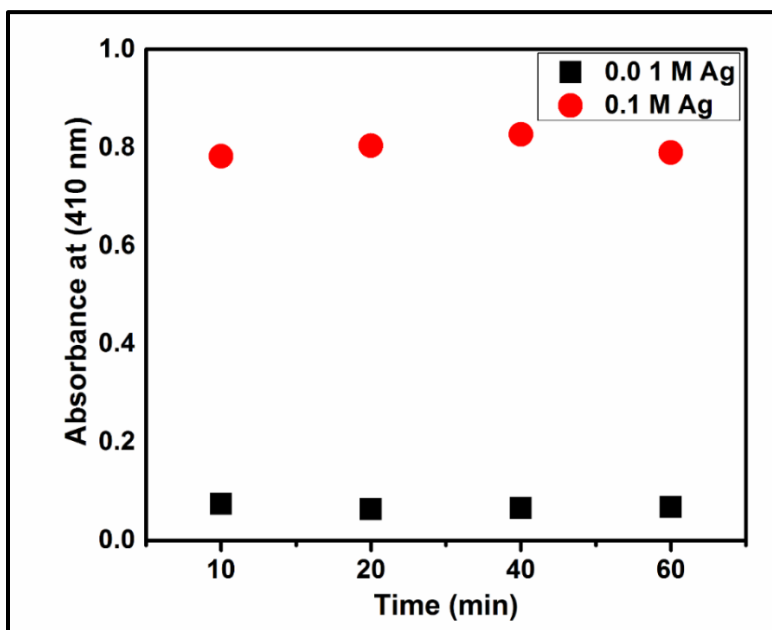
Fig. S1：Time dependence of UV/Vis absorbance at 410 nm

Experimental conditions: 1% HA, 0.1 M and 0. 01 M AgNO₃, 1 ml NaOH, 90 ⁰C and 10 times diluted at different duration time (10, 20, 40, 60 nm)
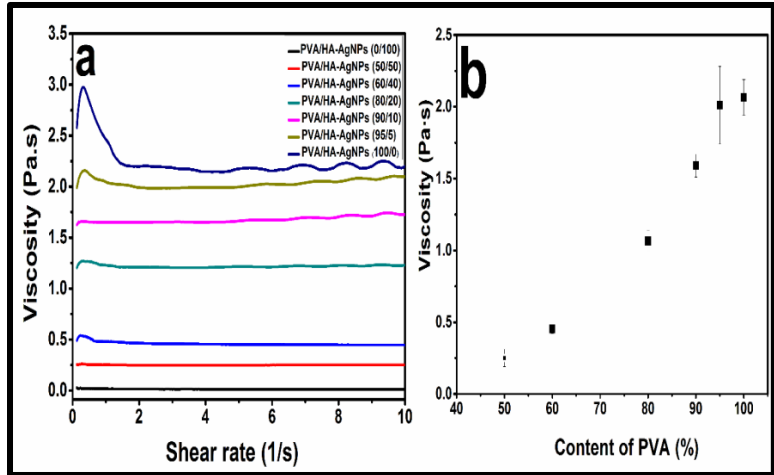
Fig. S2. Rheological properties of PVA/HA-NPs nanocomposites

Experimental conditions :(a) 1 % HA, 0.1 M Ag⁺, 1 ml NaOH, 10 min; different ration between PVA and HA-AgNPs (100/0; 95/5; 90/10; 80/20; 60/40; 50/50; 0/100)
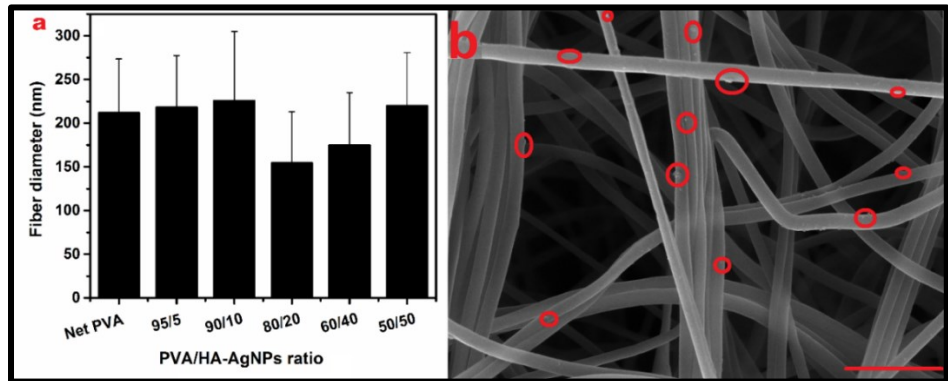
Fig. S3. Effect of different ratios between PVA and HA-AgNPs and distribution of AgNPs into nanofibers

Experimental conditions: (a) Effect of weight ratio between PVA and Ag-NPs (100/0, 95/5, 90/10, 80/20, 60/40 and 50/50). (b) SEM of distribution of AgNPs into PVA/HA nanofibrous mats (20/50).

Table S1. Composition of nanofibrous mats fabricated using different ratios between PVA and HA-AgNPs.

Net PVA	Weight (%)	PVA/HA-AgNPs (80/20)	PVA/HA-AgNPs (60/40)	PVA/HA-AgNPs (50/50)
C	58.1	42.67	46.31	29.22
O	41.9	47.79	46.33	49.41
N	-------	6.63	5.40	5. 92
Na	-----	2.83	1.67	13.92
Ag	-------	0.08	0.29	1.54

Publication 11

US 20150119783A1

(54) **METHOD OF PREPARATION OF POLYSACCHARIDE FIBRES, WOUND COVERS THAT CONTAIN THEM, METHOD OF MANUFACTURING OF WOUND COVERS, AND APPARATUS FOR PREPARATION OF POLYSACCHARIDE FIBRES**

(71) Applicant: **Continpro Biotech s.r.o.**, Dolni Dobrouc (CZ)

(72) Inventors: **Ladislav Burgert**, Pardubice (CZ);
Radim Hrdina, Pardubice (CZ);
Vladimir Velebny, Zamberk (CZ);
Abdel Mohsen Abdel-Lattif, Fayoum City (EG); **Romana Sulakova**, Usti Nad Orlici (CZ); **Lubos Sobotka**, Hradec Kralove (CZ); **Jiri Betak**, Modrany (CZ); **Dzianis Smirnou**, Usti Nad Orlici (CZ)

(57) **ABSTRACT**

The invention relates to the method of the preparation of polysaccharide fibers based on hyaluronic acid, a compound comprising hyaluronic acid and metal ions, schizophylan, chitin/chitosan-glucan complex, a compound comprising chitin/chitosan-glucan complex and metal ions, internal mixture of chitin and chitosan, a compound comprising internal mixture of chitin and metal ions, sodium alginate, potassium alginate, ammonium alginate, xanthane, xanthane sodium salt, xanthane potassium salt, oxycellulose, oxycellulose sodium salt, oxycellulose potassium salt, carboxymethyl cellulose, carboxymethyl cellulose sodium salt, and carboxymethyl cellulose potassium salt, or a mixture of polysaccharides, in a non-stationary coagulation bath. Further the invention relates to covers of internal and external wounds and skin defects based on these fibers, and a method of production thereof, and the apparatus for the preparation of polysaccharide fibers.
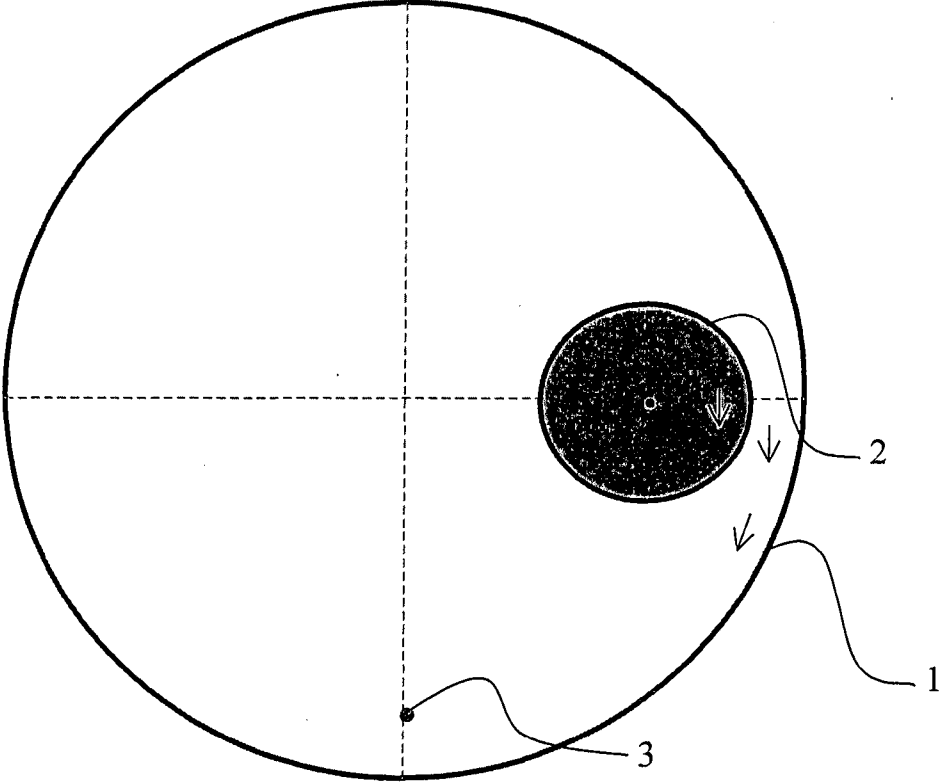
FIG.1A
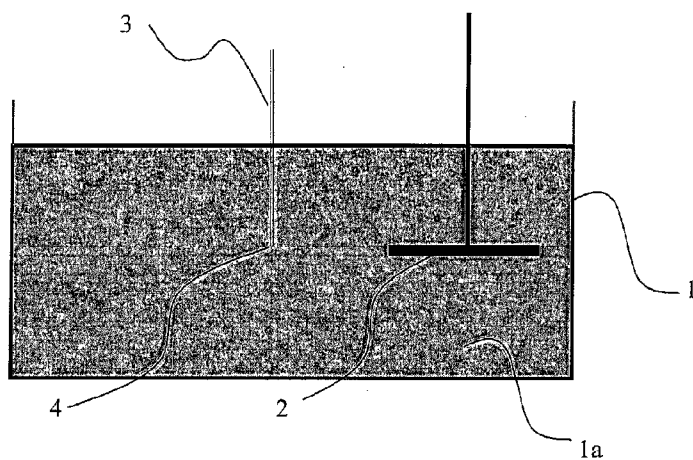
FIG.1B
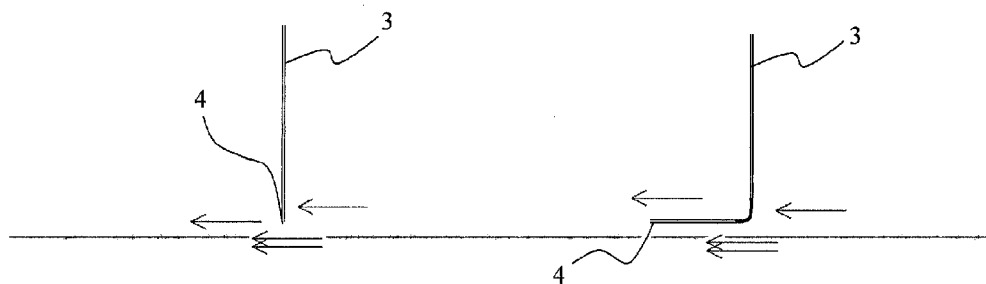
FIG.1C   **FIG.1D**
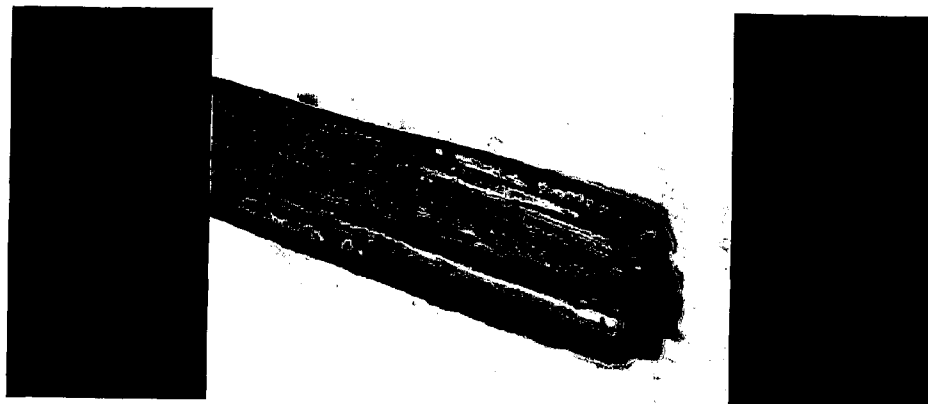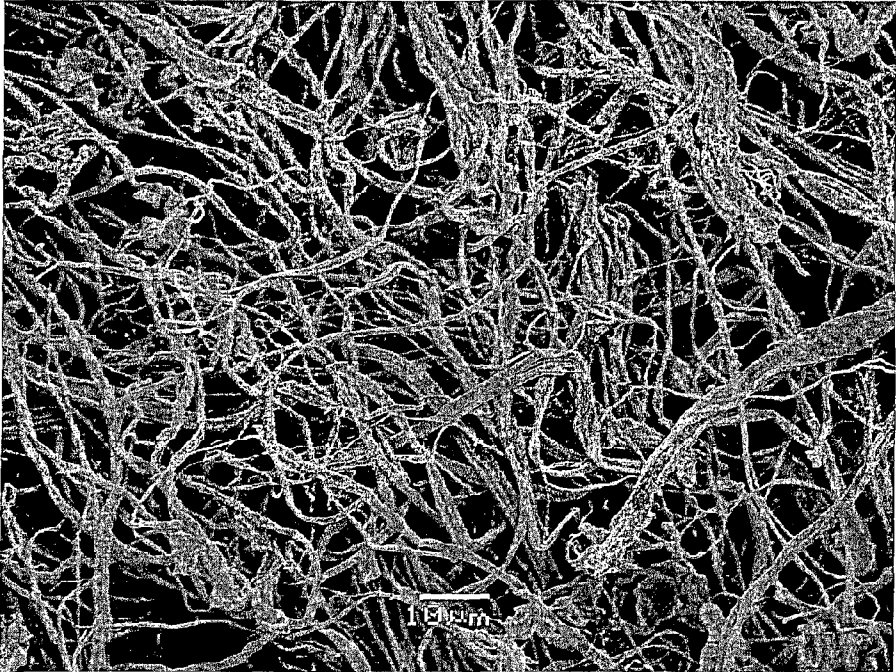
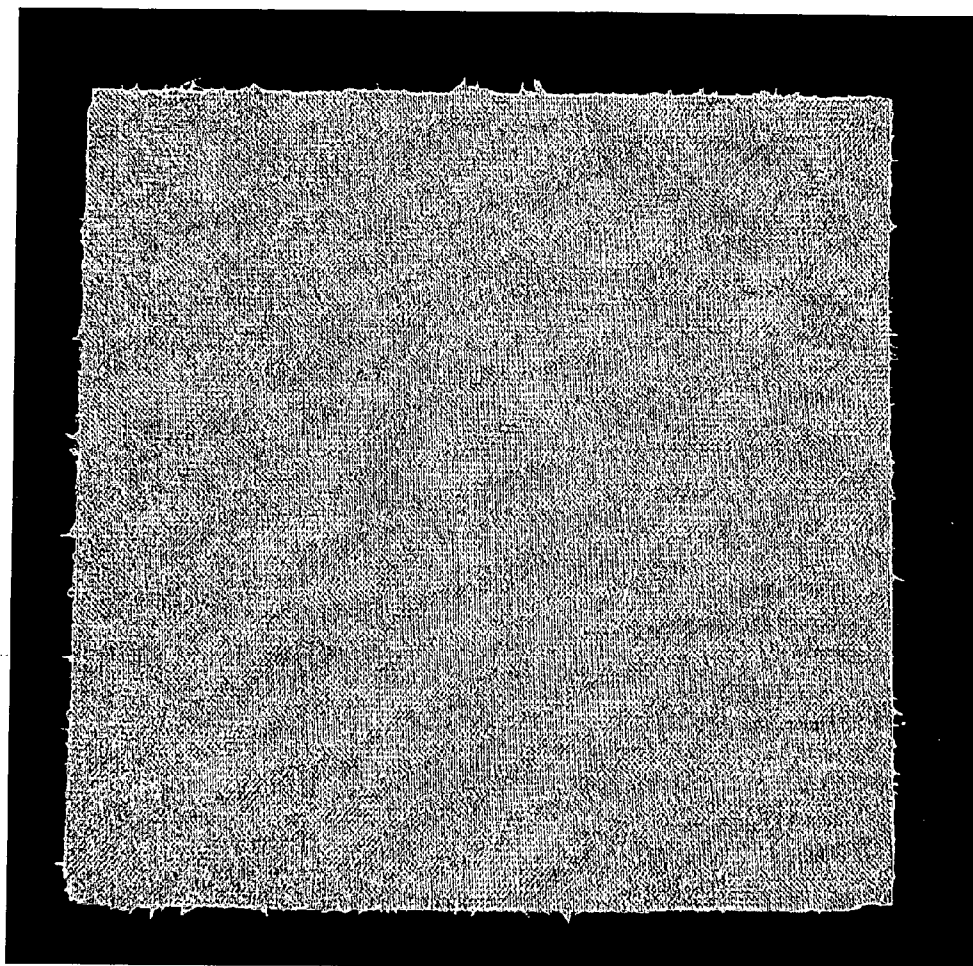**FIG.2**
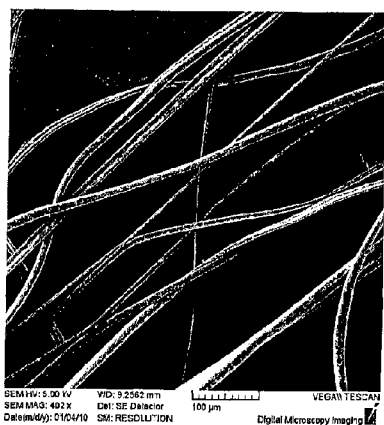
FIG.3A

FIG.3B

FIG.4

FIG.5
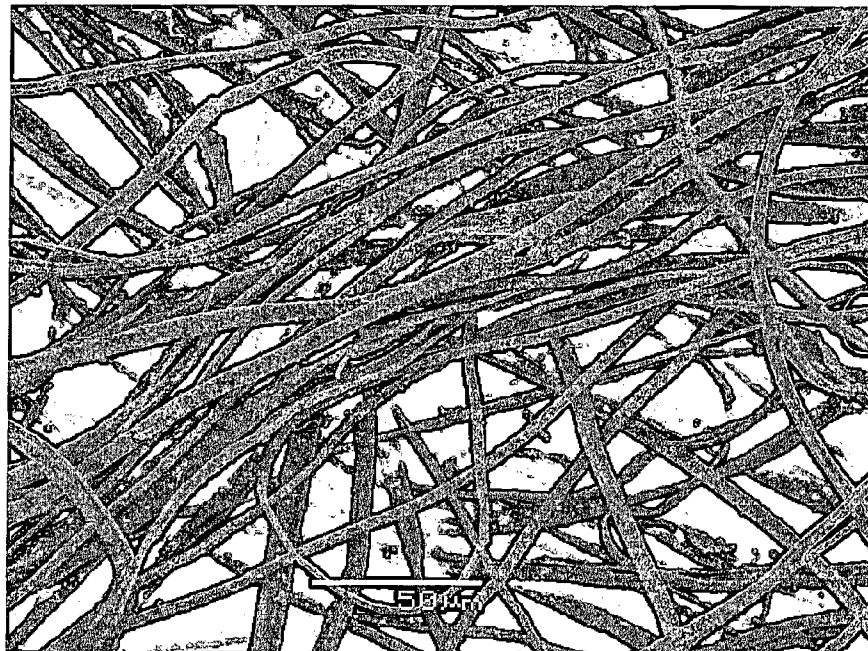
FIG.6
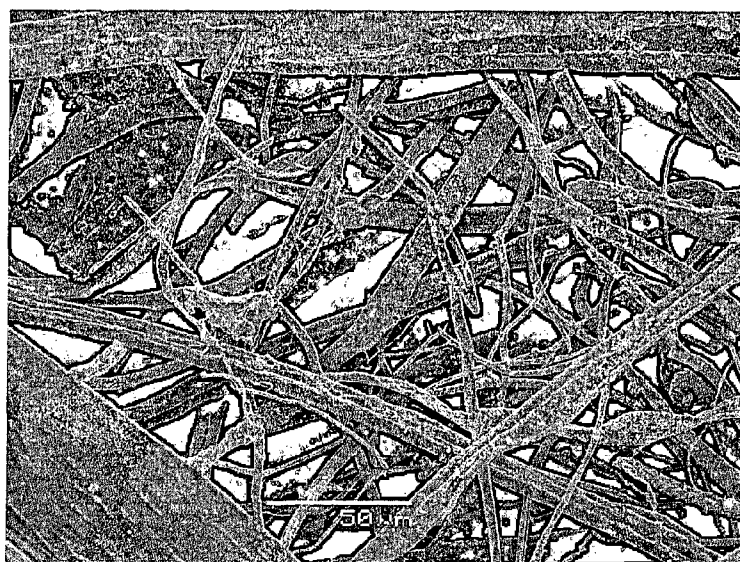
FIG.7
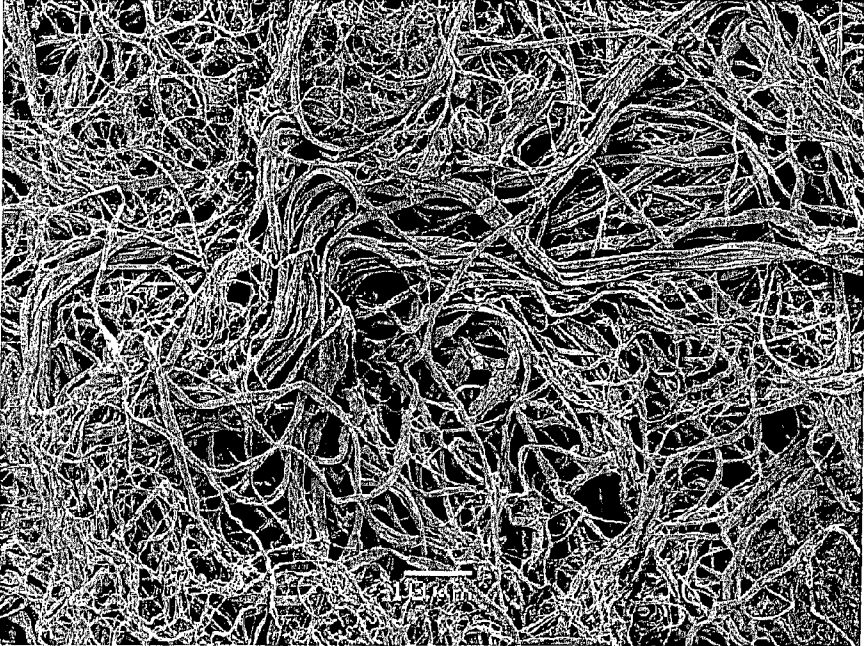
FIG.8

FIG.9
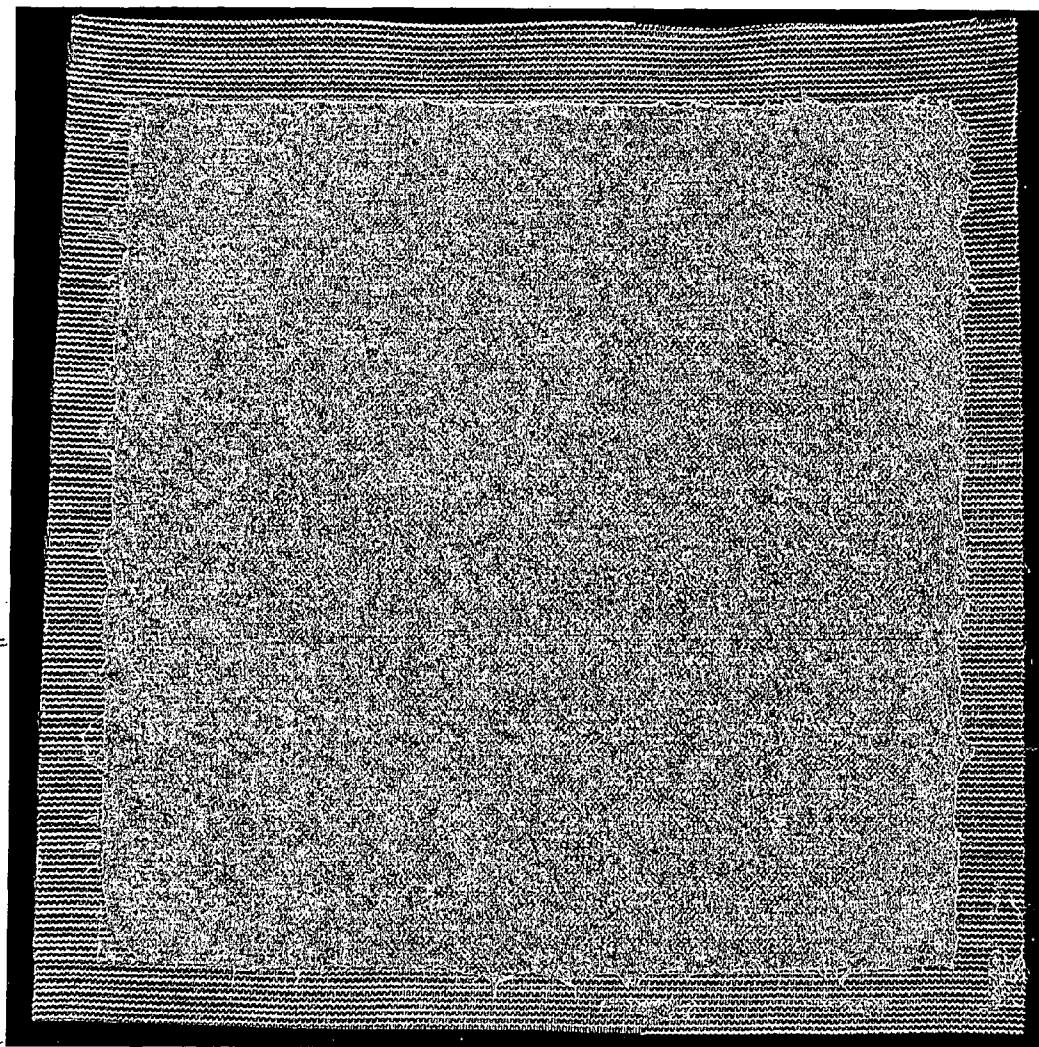
FIG.10a
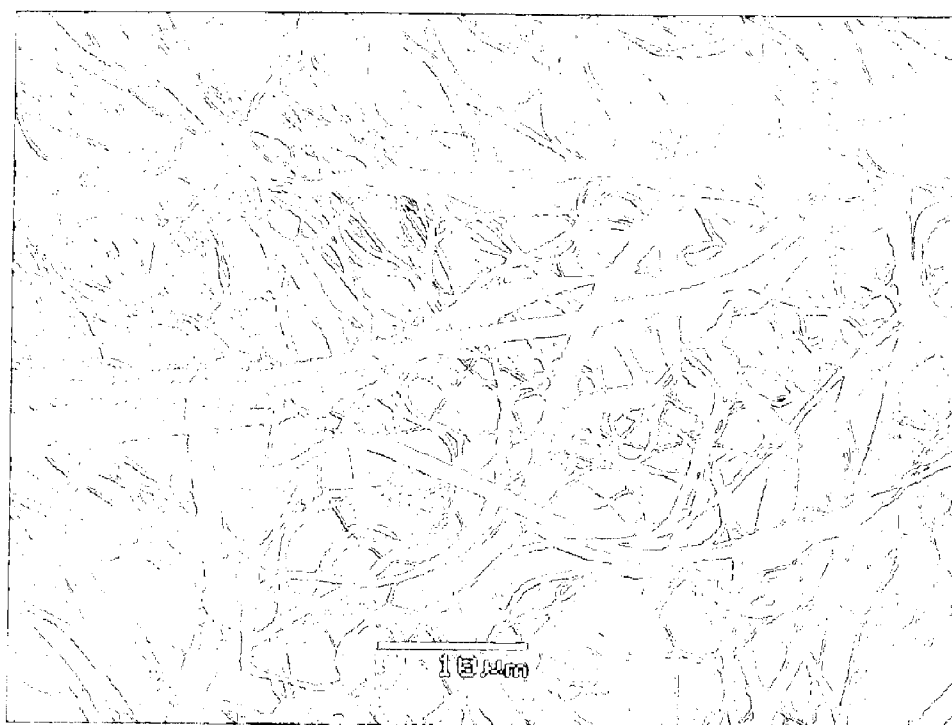
FIG.10b

FIG.11

FIG.12a

FIG.12b

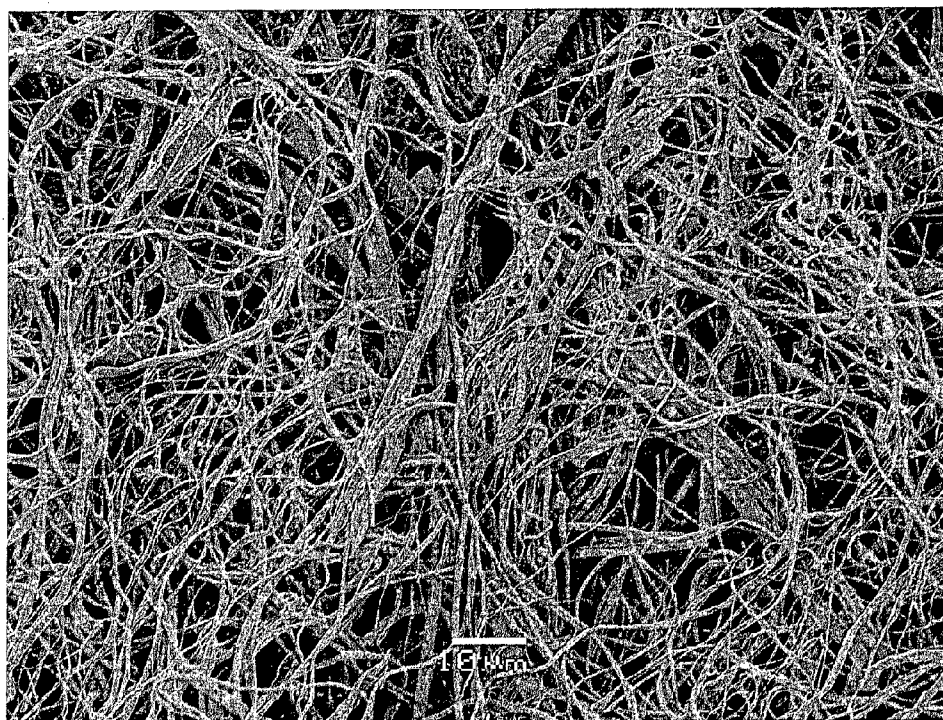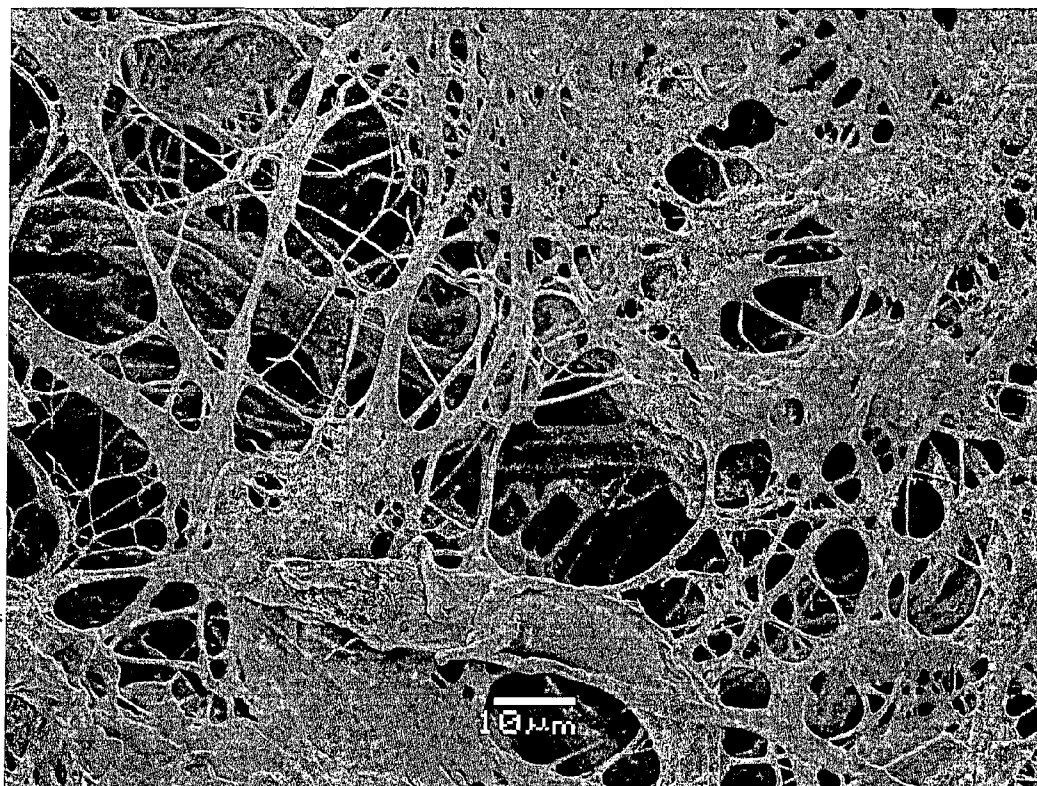**FIG.13**

METHOD OF PREPARATION OF POLYSACCHARIDE FIBRES, WOUND COVERS THAT CONTAIN THEM, METHOD OF MANUFACTURING OF WOUND COVERS, AND APPARATUS FOR PREPARATION OF POLYSACCHARIDE FIBRES

FIELD OF THE INVENTION

[0001]   This invention relates to a method and an apparatus for preparing polysaccharide staple microfibers, wound covers based on the microfibers, and the method of their preparation.

BACKGROUND OF THE INVENTION

[0002]   Treatment of skin defects, and acute, or chronic wounds is a very important part of the modern medicine. This also relates to the increasing age of population being treated with the use of more and more modern procedures. Wound healing is a very complicated process which is nowadays studied intensively. Even though the partial steps of the healing process are known, the whole complex is still undiscovered. Nowadays the wet healing is preferred, based on supplying the humidity from the dressing, and using the regulated drainage of the tissue fluid. Use of a vacuum pump with the low pressure is also modern. During the last 10 years, the system based on the utilization of biological and physical properties of the hyaluronic acid has been prepared. Especially in combination with an appropriate antimicrobial agent, its action in the location of the healing wound is ensured. So far, experience with this therapy has been positive, and the advantageousness of the antiadhesive, hydrophilic, and healing properties of the hyaluronan-iodine complex has been proved in many papers.

[0003]   The wound covers can be further improved by utilization of biopolymers spinning. With the use of this method, a large surface acting on the contact wound surface, better contacting of the cells taking part in the healing with the active substances bound to the fibers, the dressing structure improving the properties of the extracellular matrix of the tissue being healed, and the right circulation of the tissue fluid will be ensured.

[0004]   The staple fibers can be processed into the so-called staple yarns or they can be successfully processed into nonwoven textiles. The nonwoven textiles usually present a continuous layer of staple fibers where the primary fibers are arranged randomly. In contrast to the conventional textiles (prepared by weaving, knitting, crocheting), the unwoven textile is based on a web of these randomly arranged fibers which can be both short and long. This layer-forming nonwoven textile can be compact and paper-like, or it can represent a porous and "fluffy" structure. The layer thickness (nonwoven textile) is usually from 25 μm to several centimeters. The layer weight is therefore from about 5 g/m^2 to 1 kg/m^2. The mechanical properties (nonwoven textile), such as the tear strength, bending strength, and the like, are given by the primary fibers strength, and also by adhesive and physical and chemical forces between the individual fibers, which are crossed randomly (Encyclopedia of Textiles, Fibers, and Nonwoven Fabrics, Encyclopedia Reprint Series, Ed. Martin Grayson, John Wiley & Sons, Inc., 1984).

[0005]   As regards the fibers themselves, they can be classified as conventional fibers, microfibers and nanofibers. The microfibers are defined as the fibers with the sheerness bellow 1 dtex, i.e. the weight of a fiber of 1 000 m long is below 0.1 g. The nanofibers are characterized with their diameter of units to hundreds nanometers, due to their character their sheerness in decitexes is not determined. Unwoven textiles can be prepared from all types of these fibers. As regards the chemical nature of the primary fibers, they can be both natural and synthetic fibers. It is obvious that an unwoven textile can be prepared by mechanical mixing of various fibers of different sheerness or chemical nature. It is also possible to combine a conventional textile (woven textile, knitted textile, and the like) with a nonwoven textile, i.e. a layer of the nonwoven textile is "applied" on the conventional textile. These combinations are used in the cases where e.g. enhancement of the mechanical properties of the final product is demanded, or a "multi-layer" material is desired, or a combination of polymers, where a final product has a particular function, for example it stimulates wound healing and the like, is concerned. The reason for "mixing" various polymers (fibers) can be also economical (a combination of expensive and cheap fibers), especially in case of the so-called functional textiles.

[0006]   Interestingly, in the past the term microfibers was related to the synthetic fibers, especially polyester, and polyamide. The techniques of producing staple fibers from synthetic polymer melt can be found e.g. in the publication Nakajima T, Kajiwara K, McIntyre J E, 1994. *Advanced fiber Spinning Technology*. Woodhead Publishing.

[0007]   Microfibers or nanofibers can be, in general, prepared from a polymer solution by various techniques. Probably the most sophisticated one is the so-called electrospinning, or spinning in a strong electrical field (5 to 50 kV), where a polymer solution (or a melt, in case of synthetic polymers) is injected via a thin nozzle (needle) into electrostatic field, where the nozzle and the collector are connected to a voltage source. A polymer droplet flowing out of the nozzle is stretched by this field, and that leads to the production of a nano- or microfiber, with a solvent evaporating at the same time. We can say that the number of publications discussing the electrospinning increases exponentially during the time (D. Li, Y. Xia. *Electro spinning of Nanofibers: Reinventing the Wheel?*. Advanced Materials. 2004, 16, 1151-1170).

[0008]   The microfibers from, in general, biopolymers, can be obtained also by a strong mechanical action on a "raw" starting natural material. For example, the microfibrillated cellulose (MFC) can be prepared by microfluidization technique from a wood substance (the preparation of MFC is described for example in J. Y. Zhu et al, Green Chem., 2011, 13, 1339).

[0009]   Another method to obtain the microfibers from biopolymers (sodium alginate, starch, keratin) is described in the publications from Polish authors (Dariusz Wawro a kol., Microfibrids from Natural Polymers', Fibres & Textiles in Eastern Europe, v. 10, No. 3/2002 (38), pp. 23-26, 2002), where the principle lies in the use of non-stationary coagulation bath. There is a principle of a stream of a polymer solution coming out of a nozzle being driven by a stream, preferably perpendicular, of the coagulation bath. This leads to the fibrillation and microfibers formation. However, there is a disadvantage of the fibers prepared by this process being very short, according to the said document their length is maximum 800 μm, so they form a hardly processable pulp. The same author described the preparation of chitosan

microfibers by the same method (Dariusz Wawro a kol., Fibres & Textiles in Eastern Europe (2006), 14(3), 97-101.).

[0010] The use of nonstationary coagulation bath is described in the U.S. Pat. No. 5,868,973 (1999) 'Process and apparatus for producing fibers from cellulose derivatives'. The prepared microfibers are also very short.

[0011] Hyaluronic acid (A) has a chemical structure of a linear polyelectrolyte composed of repeatedly altering units of β-(1,3)-D-glucuronic acid and β-(1,4)-N-acetyl-D-gluko-samine repeating continually and creating (-4GlcUAβ1-3GlcNAcβ1-)$_n$ long chains. Every repeating unit has one car-boxyl group, four hydroxyl groups, and an acetamide group.

A
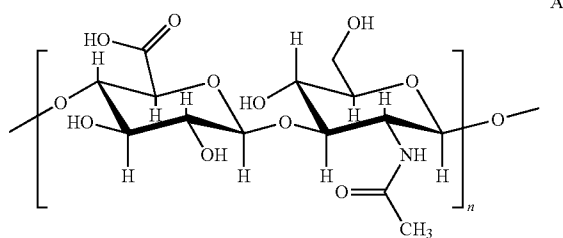
[0012] Primary and secondary hydroxyl groups are moder-ately acidic, and they can be ionized by alkali ionization, for example by sodium hydroxide, where, however, pK_a is above the value of 14. The carboxyl group belongs to a group of medium acids neutralized by alkali into salts, hylauronates, e.g. sodium hyaluronate. The mixture of a salt and a free acid is referred to as hyaluronan. For example, pK_a of the free form of hyaluronic acid in water varies around 3.45, in 0.2M NaCl it is 2.95 (L. Lapčik et al.: Chemické listy 85, 281-298, 1991). Hyaluronic acid is characterized by a high molecular weight of 5.10^4 to 5.10^6 g·mol^{-1}, depending on the source from which it has been obtained. This polysaccharide is water soluble within the whole pH range, in the form of a salt. The hyaluronic acid is a unique biopolymer intended for thera-peutic applications acknowledged as a versatile surface mate-rial improving the biocompatibility of remedies. A review can be found for example in the publication (S. Dumitriu, *Polysaccharides: Structural diversity and functional versa-tility*, Marcel Dekker Inc. 1998, ISBN 0824701275).

[0013] Hyaluronic acid, more specifically hylauronan, has a beneficial effect on wound healing. This is due to its physi-cal, chemical, and biological properties. The polymer is a strong hydrophile, ensuring therefore a good transportation of a tissue fluid, and favourable rheological properties in the location of the healing wound, it prevents its drying, and simultaneously prevents serious adhesion of the bandage to the wound. The biological properties of hyaluronan are asso-ciated with its influence on inflammation processes, new vas-cular tubes formation, bonding on lymphatic vessels, and cell receptors (CD 44 receptors) stimulation. All these effects improve healing of wounds and skin defects (Sobotka L, Smahelova A, Pastorova J, Kusalova M.: *A case report of the treatment of diabetic foot ulcers using a sodium hyaluronate and iodine complex.*

[0014] Int J Low Extrem Wounds. 2007 September; 6(3): 143-7. And Cutting K F: *Wound healing through synergy of hyaluronan and an iodine complex*. J Wound Care. 2011 September; 20(9):424, 426, 428-30).

[0015] Chitin (B1) is the second most common polysaccha-ride found in the nature. It consists of repeating β-(1,4)-N-acetyl glucosamine units. It is water insoluble, soluble in organic solvents such as hexafluoro isopropanole, hexafluro acetone, chlorinated alcohols conjugated with aqueous solu-tions of mineral acids, and N,N-dimethylacetamide contain-ing 5% of lithium salts (M. N. V. Ravi Kumar, *Reactive and Functional Polymers* 46 (2000) 1-27).

[0016] Chitosan (B2) is a form of chitin, where at least 50% of β-(1,4)-N-acetyl glucosamine units are deacetylated. Its properties are influenced by the degree of deacetylation (ratio of acetylated to deacetylated units). This cationic polysaccha-ride is water soluble at acidic pH levels lower than pKa of chitosan (pK_a 6.5). Chitin and chitosan are commercially obtained from seashells (crabs, lobsters, crayfish), or by extraction of the cell walls of certain fungi.

[0017] Both these polysaccharides are of wide industrial use, for example in water treatment, in cosmetics as an addi-tive to soaps and shampoos, or in medicine for preparation of bandages intended to ensure wound hydration in the so-called wet healing (Dai T, Tanaka M, Huang Y Y, Hamblin M R: *Chitosan preparations for wounds and burns: antimicrobial and wound-healing effects*. Expert Rev Anti Infect Ther. 2011, July; 9(7):857-79). Chitin and chitosan are also used for production of skin substitutes (Tseng H J, Tsou T L, Wang H J, Hsu S H.: *Characterization of chitosan-gelatin scaffolds for dermal tissue engineering*. J Tissue Eng Regen Med. 2011 Oct. 28. doi: 10.1002).

[0018] The said polysaccharides have substantial seques-tration effects (they are capable to bond metal ions). Chitosan is renewable and biodegradable, and at the same time it has also an antibacterial effect (N. Liu et al., *Carbohydrate Poly-mers* 2004; 64; 60-65). Its salts with organic (lactate, acetate, glycolate, succinate) and mineral acids (hydrochloride) are water soluble, and at the same time they have haemostatic effect, which can be also related to the ability of bonding haemocoagulative molecules.

B1

B2
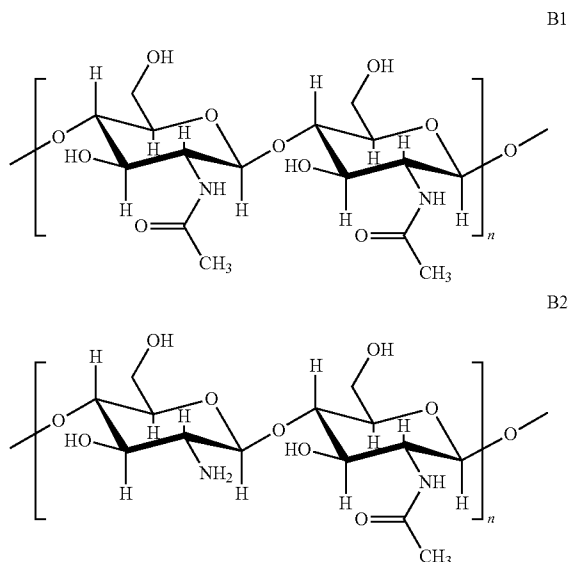
[0019] Chitin/chitosan-glucan complex is obtained from the mycelium of certain fungi species (*Aspergillus* sp., *Peni-*

cillium sp., *Schizophyllum commune*). It is a mixture of chitin/chitosan and β-(1,3)-D-glucan which are joined with a glycosidic bond. The weight ratio of chitin/chitosan and glucan is from 0.001:99.99 to 99.99:0.01. This polysaccharide can be in the form of a pharmacologically acceptable salt—lactate, glycolate, acetate, succinate, hydrochloride.

[0020] Chitin/chitosan-glucan complex can have a beneficial effect on healing due to an immunomodulative effect of glucan. In addition, it can entrap humidity in the defect area, and therefore ensure the so-called wet healing.

[0021] Schizophylan (D) is an extracellular polysaccharide produced by the fungi *Schizophyllan commune* ATCC 38548.

This neutral polysaccharide consists of the chain of β-(1,3)-D-glucopyranose units, where β-(1,6)-D-glucopyranose is bonded on every third β-(1,3)-D-glucopyranose unit, and the molecule forms a triple helix. Its molecular weight varies within the range of $6\text{-}12 \times 10^6$ g·mol^{-1}. In dimethylsulfoxide, at the temperatures above 120° C. or pH above 12, untwisting of triple helix occurs and the molecule is then formed by single chains, which leads to a decrease of the molecular weight by ⅓ (U. Rau, Methods in Biotechnology, 1999, Volume 10, 43-55, DOI: 10.1007/978-1-59259-261-6_4). This polysaccharide is degraded in a mammal body, and it has many remedial and immunomodulative effects (Wakshull, *Immunopharmacology* 41 (1999) 89-107).
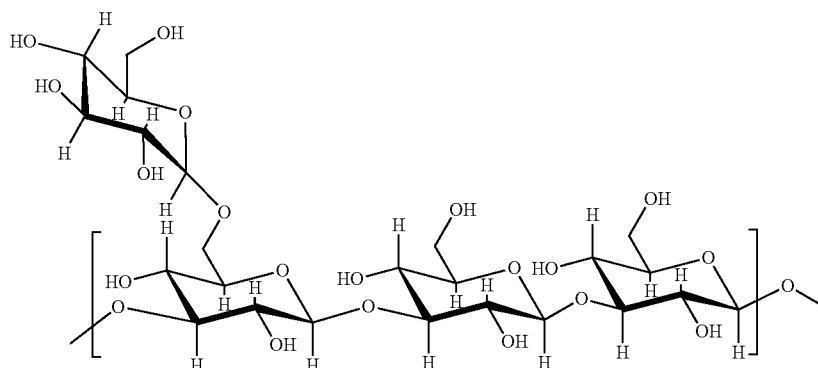
D

[0022] Xanthan (E) is a water-soluble polysaccharide produced by *Xanthomonas campestris* bacteria, and the most frequently it is used as a food additive (Davidson, Robert L. (1980). *Handbook of Water-soluble Gums and Resins*. McGraw Hill. ISBN 0070154716).
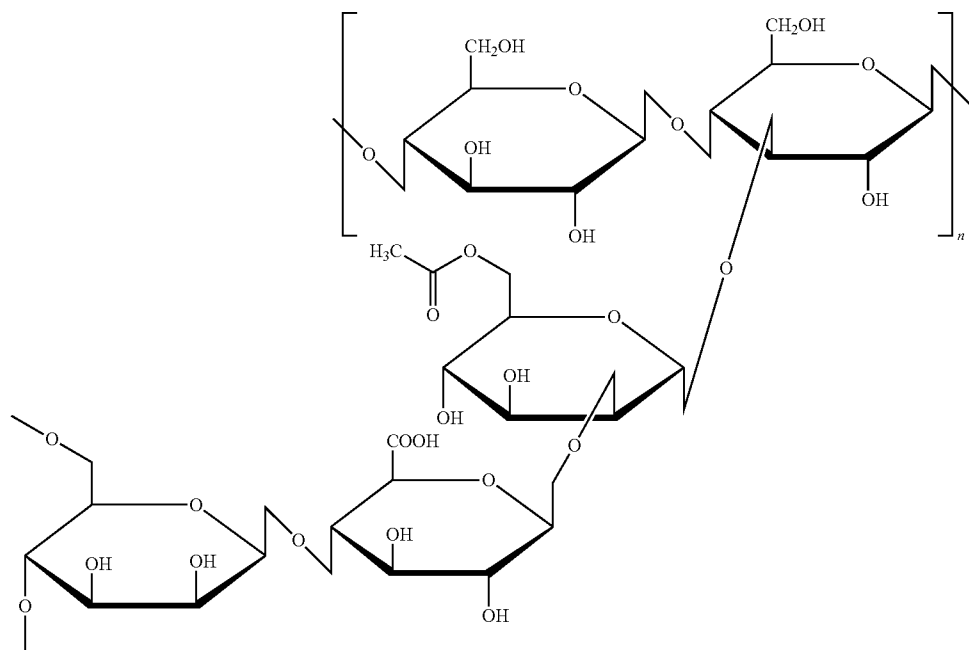
E

[0023] Alginate (F), or the alginic acid, is also a water-soluble anionic polysaccharide which strongly absorbs moisture. The production thereof can be found in (Remminghorst and Rehm (2009). "Microbial Production of Alginate: Biosynthesis and Applications". *Microbial Production of Biopolymers and Polymer Precursors*. Caister Academic Press. ISBN 978-1-904455-36-3). Because of its capability of water entrapping in the location of a wound, alginate is widely used in the cases of the need of wound moisturizing and ensuring the decomposition and gradual dissolving of necrotic tissues. It is often combined with antimicrobial agents.

F
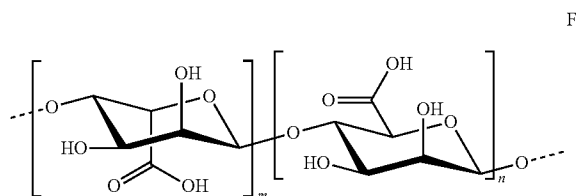
[0024] Oxycellulose is a cellulose derivative where a part of —CH$_2$—OH groups is oxidized into —COOH groups. Oxycellulose water-solubility depends on the content of carboxyl groups. The solubility of almost 100% is achieved when the —COOH groups content is above 20%. Desired haemostatic effects are achieved within the range of 16 to 19% of COOH.

[0025] Carboxymethyl cellulose (G) is a synthetic cellulose derivative, and it is an anionic polysaccharide, often used in the form of a sodium salt which is water soluble. It is also a food additive (Sodium carboxymethyl cellulose (Cellulose gum). *Codex Alimentarius*. 2009).

G
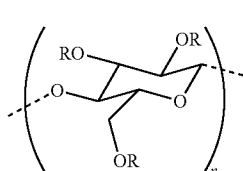
R = H, CH$_2$COOH

[0026] Many biopolymers have the disadvantage of non-fusibility (their melting point is above their decomposition temperature). For spinning, especially for the purpose of non-woven textiles production, it is not possible to use progressive technologies of fiber production, such as "spunbond" (i.e. direct application of a fiber formed form a melt by a nozzle onto an endless belt where a web layer—the base of the nonwoven textile—is formed), or "meltblown" (i.e. the polymer melt leaving the nozzle is entrained with a hot air flow, which helps to form a characteristic type of the fiber as a base of a nonwoven textile).

[0027] As the polysaccharides do not flux, the method called wet spinning is used for preparing the fibers. A polysaccharide dissolved in an appropriate solvent is extruded through various types of nozzles (circular or slot nozzle, or a nozzle with various profiles—radial, spherical triangle, and the like) directly into a non-solvent (precipitation bath), where a fiber or a film is formed. The description of the wet spinning method can be found for example in T. P.

Nevell, S. H. Zeronian: *Cellulose Chemistry and its Applications*. John Wiley & Sons 1985, p. 455-479. Or: J. E. McIntyre: *The Chemistry of Fibres*. Edward Arnold, London 1971, p. 15.

[0028] The wet spinning method can be modified into the so-called dry-wet spinning. It is used, for example, for spinning of certain types of aromatic polyamides or fibers from regenerated cellulose of the Tencell, Lyocell types, and the like. The principle of dry-wet spinning consists in that a stream of a polymer solution leaving the nozzle passes through an air gap before its entering into the precipitation bath, this gap has a length from a few millimeters to a few centimeters (this technique is described e.g. in documents WO 2000/063470, DE 10331342, JP 2008208480). The dry-wet spinning technique has been originally used for spinning of hyaluronan in the document (Burgert L., et al., *Hyaluronová vlákna, způsob jejich přípravy použití*, PV 2010-1001).

[0029] There are known methods of spinning of hyaluronic acid into a fiber, for example A. Rupprecht (Acta Chem. Scand., B33, No. 10, 1979) spun the potassium salt of hyaluronic acid in 75-80% ethanol comprising 0.1M KCl, he coiled the fibers into a disc, so the fibers aglutinated by drying into a film comprising a "spatially orientated" hyaluronic acid. This way of spinning naturally did not lead to fibers processable in the textile industry.

[0030] Further, E. D. T. Atkins et al. (*Biochem. J.* 128, 1255-1263, 1972) prepared model fibers from hyaluronic acid and sodium hyaluronate in such a way that first they prepared a film which they cut into thin strips. For these "model fibers" cut from films (and drawn) they determined a crystal modification with the use of X-ray structural analysis, including the dimensions of an elementary crystal cell. They found out that the elementary cell of a non-drawn sodium hyaluronate fiber was of a hexagonal crystal system and the macromolecules were arranged antiparallely supposing the hydrogen bonds between amide groups of acetylated glucosamine. Base dimension: a=1.17 nm (or 2.02 nm). Macromolecule profile diameter approx. 0.673 nm. Dimension c of the elementary cell (along the fiber axis) was 2.85 nm.

[0031] They have also found that conditioning of sodium hyaluronate based fibers at 60° C. and relative humidity of 75% lead to the formation of a new hexagonal crystal lattice, a=1.87 nm, maintaining c=2.85 nm. The change of the lattice type (with maintaining the crystal modification) is also known in cases of other fibers—polymers—e.g. cellulose in the cotton fiber.

[0032] The same author determined the monoclinic crystal system with the elementary cell dimension of a=1.96 nm (but it is not fully defined) at the fibers prepared from hyaluronic acid (acid form).

[0033] The document WO 2009/050389 describes the preparation of a yarn with the use of wet spinning method, where this yarn comprises hyaluronic acid in the acid form, acetic acid, and it is partially water soluble. The preparation of a fiber consists of the following steps: a) preparation of an aqueous solution of hyaluronic acid, or a salt thereof, preferably sodium salt, where the hyaluronic acid concentration is higher than 0.8%, preferably within the range of 1 to 2% by weight; b) extrusion of the solution through the nozzle into a spinning bath; c) forming the fiber in the bath, which consists of acetic acid and water, where the acetic acid concentration is higher than 80%, preferably higher than 90%, the most preferably 99%. The obtained yarn has a diameter higher than

100 µm. The authors of this document declare that the fibers prepared by their procedure can be used for both the woven and nonwoven textiles. In fact, due to their small strength (according to the comparative example 10, the tearing occurs at the stress of 67 MPa), the fibers are not applicable for the preparation of woven fabric or knitted fabric, so they are applicable for preparation of nonwoven textiles only. The strengths of textile fibers produced in a conventional manner vary within the following intervals: cellulose fibers 1.8 to 2.7 cN·dtext^{-1}; synthetic fibers above 4 cN·dtext^{-1}; coefficient of variation up to 10%. Loop (knot) strength of the fiber should be approximately 80% of the fiber strength without deformation. It applies especially to weaving, knitting, and bobbin lace work. For non-woven textiles, the loop strength of the fiber is not essential.

[0034] The above mentioned document PV 2010-1001 describes the preparation of fibers comprising the hyaluronic acid characterized in that the fiber consists of hyaluronic acid and/or at least one compound comprising hyaluronic acid and metal ions, wherein the fiber can optionally comprise metal salts originating from the production process, having the molecular weight of macromolecules within the range of 100 kDa to 3 MDa. The prepared fibers are characterized by that the fiber (monophile, primary fiber) diameter is 4 µm to 1 mm, length weight 0.1 to 30 g/1000 m (0.1 to 30 tex), tensile strength 0.5 to 3 cN·dtex-1, and loop strength 20 to 80% of tensile strength. The solution is characterized also by the preparation of silk tow comprising 2 to 50 primary fibers. Therefore it concerns the fibers with properties useful for the production of both woven and nonwoven textiles.

[0035] The preparation of chitin fibers via the wet spinning method from chitin solution is described for example in the U.S. Pat. No. 1,029,727 (1977), where chitosan is dissolved in trichloroacetic acid, and the fibers of high strength are prepared by the wet spinning method.

[0036] The Japanese document (OPI) No. 127500/1978 describes a similar method differing only in that chitin is dissolved in dichloroacetic acid. The prepared fiber has a lower strength than when using the method employing trichloroacetic acid.

[0037] The U.S. Pat. No. 3,988,411 (1976) uses hexafluoro isopropyl alcohol or hexafluoro acetone sesquihydrate to dissolve chitin. Acetone is used as the coagulation bath.

[0038] The U.S. Pat. No. 4,029,727 (1977) uses mixtures of trichloroacetic acid or dichloroacetic acid, chloral hydrate, and halogenated hydrocarbon (e.g. CCl_4) to dissolve chitin. Acetone is used as the coagulation bath, then the fibers are neutralized with alkalis, washed with 2-propanol, and dried.

[0039] The U.S. Pat. No. 4,431,601 (1984) uses mixtures of trichloroacetic acid and halogenated hydrocarbon (e.g. CCl_4) to dissolve chitin. Acetone is used as the first coagulation bath, and methanol is used as the second coagulation bath. The produced fibers are useful as surgical sutures. The U.S. Pat. No. 4,932,404 (1990) describes a very similar method.

[0040] The U.S. Pat. No. 4,857,403 describes the preparation of tough fibers of "chitin acetate/formate" and "chitosan acetate/formate". In fact, it concerns a method where the derivatives of chitin and chitosan are prepared first (by O-acylation and N-acylation), and then they are spun by a conventional method. The problem of this patent is that the procedure with chitosan comprises dissolving chitosan (40 g) in formic acid, then adding the ice cold acetic acid, and anhydride (500 ml). The mixture is agitated for 12 hours at 0° C. At these given conditions, the rate of acetylation of chitosan amide

groups, and therefore the conversion of chitosan to chitin, is questionable. N-acetyl and O-acetyl chitin and chitosin derivatives are herein called acetates. Another problem, naturally, is that the amine group protonizes by acid treatment to give the respective salts ($—NH_2+CH_3COOH→—NH_3^{+-}$ $OOCCH_3$). In the end, the resulting fibers are O-acyled and N-acyled chitine and chitosane derivatives. The following U.S. Pat. No. 4,861,527 (1989) tries to solve this problem relating to chitosan in that the fibers prepared by the methods of the previous patent are immersed into the concentrated aqueous solution of NaOH (50-70% by weight of NaOH). This induces O- and N-deacetylation, and also dissapearing of the amide groups and re-creation of $—NH_2$ groups. However, the problem is that chitosan in its neutral form (amine groups are not protonized) does not have haemostatic and antimicrobial effects. Of course, it has a strong chelating effect.

[0041] The preparation of chitosan fibers by the wet spinning method from chitosan solution is described for example in the document (OPI) No. 112937/1981, where chitosan is dissolved in water at acidic conditions, the solution is filtrated and spun into the coagulation bath comprising anion surfactants.

[0042] The document (OPI) No. 116418/1984 describes dissolving of chitosan in water acidified with dichloroacetic acid. Further, this document describes chelation of metal ions by prepared fibers.

[0043] The U.S. Pat. No. 4,464,321 (1984) describes a method of preparation of chitosan hollow fibers designed for ultrafiltrations, where an acidic chitosan solution is spun into an alkaline coagulation bath comprising a plastificator (glycerin). The interesting fact in this method is that the stream leaving the nozzle (designed for forming hollow fibers) passes through an ammonium atmosphere before its entrance into the coagulation bath. Therefore, it concerns a wet-dry spinning method.

[0044] The document (OPI) No. 106901/1988 describes a method, where chitosan is dissolved at 40° C. in water acidified by acetic acid, and thus the solution comprising 3% of chitosan and 0.5% of acetic acid is prepared. The solution is spun at 30° C. in the coagulation bath comprising aqueous 1% NaOH. The formed fibers are washed and dried. The fiber tensile strength is 2.44 g/denier, elongation at break 10.8%, and knot strength 1.77 SG/denier.

[0045] In the publication (Shigehiro Hirano a kol., Carbohydrate Polymers 38 (1999) 293-298) the preparation of staple chitosan fibers, which are in addition plastified by ethylene glycol is described.

[0046] The essential problem of pure chitosan consists in that, according to our experiences, these fibers have a small strength and are fragile. Another problem is that chitosan acidic aqueous solutions are logically spun into an alkaline solution thereby the chitosan has no protonized amino groups and therefore it loses its haemostatic and antibacterial effect (Fouda, M. M. G. et al., *Use of chitosan/polyamine biopolymers based cotton as a model system to prepare antimicrobial wound dressing.* International Journal of Diabetes Mellitus. 2009, 1, 61-64).

[0047] We can conclude that wound covers based on staple microfibers from hyaluronic acid and/or hyaluronan, with the fibers long enough (more than 800 µm) to prepare tough nonwoven textile with a very low surface weight (below 5 g/m^2), cotton wool, tampons, or material usable for spinning, have not been known so far. If a spinning nozzle and a draw-

off (and curling) apparatus is arranged properly, it would be possible to process the forming staple microfibers into staple yarns.

[0048] We can also conclude that neither wound covers based on staple microfibers longer than 800 µm made from pure schizophylan, chitin, chitin/chitosan-glucane complex, internal mixture of chitin and chitosan, or water soluble chitosan salt, are known, even if we take into account the fact that chitin and also chitosan fibers exist and it is not possible to distinguish exactly between chitin and chitosan. Herein, the internal mixture is understood as the individual chitin and chitosan molecules are "entwined" mutually.

[0049] Said drawback is eliminated by the present invention.

SUMMARY OF THE INVENTION

[0050] The invention relates to the method of preparation of polysaccharide fibers, where the spinning solution of a polysaccharide of the concentration of 0.01 to 0.8% by weight is prepared, the polysaccharide having the molecular weight of 60 kDa to 3 MDa and being selected from the group comprising hyaluronic acid, a compound comprising hyaluronic acid and metal ions, schizophylan, chitin/chitosan-glucan complex, a compound comprising chitin/chitosan-glucan complex and metal ions, internal mixture of chitin and chitosan, a compound comprising internal mixture of chitin and metal ions, sodium alginate, potassium alginate, ammonium alginate, xanthan, xanthan sodium salt, xanthan potassium salt, oxycellulose, oxycellulose sodium salt, oxycellulose potassium salt, carboxymethyl cellulose, carboxymethyl cellulose sodium salt, and carboxymethyl cellulose potassium salt, or mixtures of polysaccharides, in an aqueous medium, which is spun in a non-stationary coagulation bath comprising pure C_1-C_3 alcohol. pH of the aqueous medium is preferably from 1 to 13. During the spinning, the content of water in the coagulation bath is within the range of 0.1 to 40% by weight, preferably 10% by weight. The spinning solution can pass through the air passage of the length of 1 to 200 mm before its entry into the coagulation bath. The spinning solution can also be stored for 5 to 24 hours in the refrigerator at the temperature of –40° C. to –10° C. before spinning. In a preferred embodiment, the spinning solution can comprise calcium or zinc salt in the concentration from 0.1 to 50% by weight selected for example from the group comprising acetates, formates, chlorides, sulphates, fluorides, nitrates, and hydrates of these salts.

[0051] The temperature of the coagulation bath is preferably within the range of 18 to 30° C.

[0052] In a preferred embodiment, the fibers are transferred from the coagulation bath to a stationary maturation bath for 20 minutes to 96 hours, wherein the stationary maturation bath comprises C_1-C_3 alcohol, and can comprise also up to 10% by weight of an organic acid.

[0053] In another preferred embodiment of the invention, the fibers are metalized for 20 minutes to 25 days in a metallization bath comprising C_1-C_3 alcohol or a mixture of C_1-C_3 alcohol and an organic acid, and a salt of a polyvalent metal selected from the group comprising calcium, magnesium, copper, manganese, zinc, chromium, iron, and cobalt. The fibers can also be shortened, in a shortening bath comprising C_1-C_3 alcohol or a mixture of C_1-C_3 alcohol and an organic acid, from the starting length of 0.8 to 3 cm to a length suitable for a method of preparation of a nonwoven textile.

[0054] A fiber suspension can preferably be homogenized in a homogenization bath comprising C_1-C_3 alcohol or a mixture of C_1-C_3 alcohol and an organic acid.

[0055] The metallization of fibers can be run directly in the coagulation bath, the maturation bath, the shortening bath, or the homogenization bath by adding a salt of a polyvalent metal, or the fibers are transferred to a new metallization bath. The shortening of fibers can be run directly in the maturation bath or the fibers are transferred to a new shortening bath. The homogenization of fibers can be run directly in the shortening bath or the fibers are transferred to a new homogenization bath.

[0056] Then the fibers can be collected from the last bath and dried, wherein they can first be washed with alcohol before drying.

[0057] Further, the invention relates to the method of production of a cover based on polysaccharide fibers, where the fibers are prepared by the method disclosed above, or the mixture of fibers is prepared by the method disclosed above, or the mixture is prepared of fibers prepared by the method disclosed above and the fibers selected from the group comprising the fibers based on natural mycelium processed by a method maintaining the fiber character of natural mycelium, then the fibers are removed from the solution by filtration and the filtration cake is dried. The filtration cake can be compressed and/or washed with alcohol before drying. For example, in case of hyaluronan, only the "abundant water" is removed by alcohol, whereas the water bound in hyaluronan ensuring the bonds between the —COOH and —NHCOCH$_3$ groups is kept, so the hyaluronan is not denatured in an undesirable way. The fibers can be also filtered off onto a suitable pad, the filtration cake and the pad are compressed and then dried, and the pad can be optionally removed from the dried filtration cake.

[0058] H-bonds are established between the individual fibers by the "wet" compression of the filtration cake, so the nonwoven textile (a cover) is compact, tough and elastic. The same interactions are established also with the fibers from the more hydrophilic pad, for example polyamide.

[0059] After compression, the wet cover of the wound comprises above all the used alcohol, but due to a high hydrophility of, for example, hyaluronic acid, it comprises also a certain amount of water bound in this polymer. Due to this reason it is necessary to define also the relative humidity of the air as the drying medium. The drying can be run at the temperatures of 20° C. to 80° C., and at the relative humidity of air of 15% to 80%, preferably by hot air.

[0060] In a preferred embodiment the dried filtration cake is then inserted into a metallization bath, then the fibers are collected from the metallization bath, washed, and dried.

[0061] Further the invention relates to a wound cover comprising the above mentioned biopolymer staple fibers, the fibers being prepared by the method described above, or the mixture of fibers prepared by the method described above and the fibers selected from the group comprising the fibers based on the natural mycelium processed by a method maintaining the fiber character of natural mycelium, i.e. the material from the natural mycelium has the character of a fiber with the diameter of 1 to 100 µm and the length at least of 0.1 mm. Biopolymer staple microfibers of internal and/or external wounds cover have a diameter of 1 to 100 µm and the length at least of 0.8 cm, preferably the length within the range of 0.8 to 3 cm. The fibers from which the cover is prepared can be non-shortened, i.e. of the length of 0.8 to 3 cm, or shortened

in a shortening bath comprising C_1-C_3 alcohol or a mixture of C_1-C_3 alcohol and an organic acid, to the length suitable for the method of preparation of a nonwoven textile, i.e. the length for example of 1 to 5 mm.

[0062] The wound cover is preferably in the form of nonwoven textile, nonwoven textile fastened on a pad, cotton wool, tampon, or paper stuff.

[0063] Further, the invention also relates to an apparatus for preparation of polysaccharide fibers, the apparatus comprising a cylindrical container for the coagulation bath, and a rotary disc with the vertical axis of rotation passing through the bottom of the cylindrical container in a distance from the vertical axis of the cylindrical container. The apparatus further comprises a spinning nozzle the outlet of which is arranged in the cylindrical container in a distance from its wall, the distance being 70 to 130% of the shortest distance of the rotary disc from the wall of the cylindrical container. The rotary disc diameter is preferably 10 to 30% of the diameter of the cylindrical container. In a preferred embodiment of the invention the angle spacing of the vertical axis of the rotary disc and the outlet of the spinning nozzle is above 80°, with respect to the vertical axis of the container. In another preferred embodiment of the invention the spinning nozzle can be bent on its end comprising the outlet.

[0064] The invention will be described in more detail in the following description.

[0065] Biopolymer, as disclosed herein, is preferably a polysaccharide with the size of macromolecules of 60 kDa to 3 MDa (determined by the conventional SEC-MALLS, Size-Exclusion Chromatography coupled to Multi-Angle Laser Light Scattering method, this method is disclosed in detail for example in the publication: Bezákovã, Z. et al., *Effect of microwave irradiation on the molecular and structural properties of hyaluronan*. Carbohydrate Polymers 2008, 73, (4), 640-646).

[0066] The term polysaccharide in this disclosure is preferably understood as:

[0067] 1. Hyaluronic acid and/or at least one compound comprising hyaluronic acid and metal ions.

[0068] The term "a compound comprising hyaluronic acid and metal ions" comprises any compound comprising hyaluronic acid and metal or metals ions, including salts and metal complex compounds. The character of the bond between hyaluronic acid and a metal depends on the metal, usually it is an ionic bond, a covalent bond (ion-covalent) or a coordinate covalent bond. The said term also comprises the compounds comprising ions of more than one metal. The metals are preferably selected from the group comprising lithium, sodium, potassium, calcium, magnesium, copper, manganese, zinc, chromium, iron, and cobalt.

[0069] 2. Schizophylan

[0070] 3. Chitin/chitosan-glucane complex and/or at least one compound comprising chitin/chitosan-glucane complex and metal ions. The term "a compound comprising chitin/chitosan-glucane complex and metal ions" comprises any compound comprising chitin/chitosan-glucane complex and metal or metals ions, including salts and metal complex compounds. The character of the bond between chitin/chitosan-glucane complex and metal depends on the metal, usually it is an ionic bond, a covalent bond (ion-covalent) or a coordinate covalent bond. The said term also comprises the compounds comprising ions of more than one metal. The metals are preferably selected from the group comprising lithium,

sodium, potassium, calcium, magnesium, copper, manganese, zinc, chromium, iron, and cobalt.

[0071] 4. Internal mixture of chitin and chitosan and/or at least one compound comprising the internal mixture of chitin and chitosan and metal ions. The term "a compound comprising the internal mixture of chitin and chitosan and metal ions" comprises any compound comprising the internal mixture of chitin and chitosan and metal or metals ions, including salts and metal complex compounds. The character of the bond between the internal mixture of chitin and chitosan depends on the metal, usually it is an ionic bond, a covalent bond (ion-covalent) or a coordinate covalent bond. The said term also comprises the compounds comprising ions of more than one metal. The metals are preferably selected from the group comprising lithium, sodium, potassium, calcium, magnesium, copper, manganese, zinc, chromium, iron, and cobalt.

[0072] 5. Sodium, potassium, or ammonium alginate.

[0073] 6. Xanthan and/or its sodium or potassium salt.

[0074] 7. Oxycellulose and/or its sodium or potassium salt.

[0075] 8. Carboxymethyl cellulose and/or its sodium or potassium salt.

[0076] The term "pure C_1-C_3 alcohol" refers to C_1-C_3 alcohol of the concentration of 97.5 to 100%, which is the starting concentration at the beginning of the spinning.

[0077] The method of preparation of staple microfibers according to the present invention is based on the use of a non-stationary coagulation bath, and its principle consists in the preparation of a spinning solution (preferably water solution) comprising a biopolymer or a mixture of biopolymers, and said solution is then spun in a non-stationary coagulation (precipitation) bath comprising alcohol, preferably propane-2-ol. During the spinning the concentration of alcohol decreases due to adding of the spinning solution. Optimum conditions are achieved if the water content varies from 0 to 40% by weight, preferably 10% by weight.

[0078] Preferably the water content in the coagulation bath during the spinning is maximum 10% by weight.

[0079] The coagulation bath does not comprise an acid. We have found by our own study that when the coagulation bath does not comprise an acid, the fiber formation at the nozzle outlet slows down, so the microfibers of the length up to 3 cm are formed and, in addition, the fibers do not stick together.

[0080] The term "coagulation bath" refers to a bath where the microfibers are formed from a spinning solution. This bath can be also denoted as the "spinning bath" or "precipitation bath".

[0081] In the case of water soluble biopolymers the following method is used: first a water solution of biopolymer with pH in the range of 1 to 13, or any mixture of biopolymers, where the concentration of biopolymer (or the sum of biopolymers) in this solution is 0.01 to 8% by weight, is prepared, and this solution is then spun by the nozzle into a non-stationary coagulation bath.

[0082] The water solubility of the biopolymers without —COOH group can be enhanced by adding urea in such a way that its concentration in the spinning solution is 2 to 15% by weight.

[0083] In another embodiment the spinning solution can be agitated for 10 minutes to 1 hour, until the formation of a homogenous solution suitable for spinning. Thereafter, this solution can be preferably stored for 5 to 24 hours in a refrigerator at the temperature of –40° C. to –10° C. Then the solution is taken out, let heat to the room temperature, and this solution is then spun through the nozzle into a non-stationary

coagulation bath. The low temperature causes disruption of the net of inner and outer hydrogen bonds of biopolymer, so the individual molecules separate apart and "linearize", so they spin better from the solution (this technique is described for example for cellulose in the articles: Ying Wang, Yulin Deng. *The Kinetics of Cellulose Dissolution in Sodium Hydroxide Solution at Low Temperatures*. Biotechnology and Bioengineering, 102, 5, 2009; Magali Egal, Tatiana Budtova, Patrick Navard. *The dissolution of microcrystalline cellulose in sodium hydroxide-urea aqueous solutions*. Cellulose, 15, 361, 2008).

[0084] A special issue is the preparation of a spinning solution of chitin-chitosan complex with its content of 0.01 to 8% by weight, where chitin is dissolved in the mixture of dichloroacetic acid and formic acid or acetic acid (1:1 by weight), chitosan is dissolved in formic acid or acetic acid, and both the solutions are combined at agitation. The formed homogenous solution is then spun through the nozzle into a non-stationary coagulation bath.

[0085] In this spinning method the forming microfiber is formed and drawn by the force of a stream of the coagulation bath. Fibre drawing is a process where the fiber is deformed (elongated) along the longitudinal axis of the fiber. The length of the fiber increases, its diameter decreases, and its sheerness increases until forming a microfiber. Due to the orientation of macromolecules and supramolecular forms, and due to the increasing of the crystalline fraction, the mechanical parameters of the fiber enhance: its strength increases and its elongation decreases. During the process of elongation, less stable crystalline modifications can also change into more stable modifications.

[0086] The spinning can be carried out also by the dry-wet method, where an air passage before the entry of the stream of the solution being spun into the coagulation (spinning) bath is 1 to 200 mm.

[0087] The inner diameter of the nozzle is, of course, larger than in the order of μm because it would not be possible to press the solutions, which are relatively viscous, through the nozzle (needle) so narrow. We have found by our own study that in the stream leaving the nozzle, a microfiber bundle is formed in the coagulation bath, these microfibers separate apart in the moving coagulation bath (of course, provided that the twisting thereof does not occur). FIG. 2 shows, by way of example, a bundle of primary microfibers of schizophyllan, displayed under the optical microscope. Other fiber-forming polysaccharides behave in a similar way.

[0088] Afterwards, the microfibers can be removed (filtrated) from the coagulation bath and their strength can be enhanced in a maturation bath. The maturation bath can comprise, in addition to the alcohol, also an acid, which causes, for example in the case of hyaluronan, a change of COONa group into —COOH group and thus forms a system of hydrogen bonds and therefore causes the formation of a tight supramolecular structure. Especially if the fibrils are not tight enough, which can happen due to the absence of an acid in the coagulation bath, the formed microfibers are optionally immersed to the maturation bath for 20 minutes to 96 hours.

[0089] In this embodiment of the invention the maturation bath preferably has the composition selected from the group comprising a mixture consisting of 90 to 100% by weight of an alcohol, and up to 10% by weight of an organic acid, for example formic acid or acetic acid. The bath therefore comprises either an alcohol alone or it can also contain an acid, which helps to stabilize the fiber structure, and therefore the fiber is tighter.

[0090] It is advisable to collect the forming microfiber form the bath immediately to prevent its uncontrollable twisting. The collected fiber can be inserted to a maturation bath. In the maturation bath, the system of hydrogen bonds, having been broken by dissolving of a biopolymer, is reconstituted, or, in other words, a secondary and tertiary structure (supramolecular in general) of a biopolymer, bearing the necessary biological and mechanical characteristics, is restored. It can be concluded that in the coagulation bath the microfiber of suitable dimensions is prepared, and then in the maturation bath the right mechanical characteristics are "prepared".

[0091] As the microfibers formed in the non-stationary coagulation bath are too long for many applications, they can be preferably "shortened" to the length of approximately 1 to 5 mm in an appropriate knife mixer with the use of the maturation bath as the medium. A new bath, the so-called shortening bath, can also be used. The composition of the shortening bath is the same as the coagulation bath or the maturation bath. The shortening is necessary for the following preparation of planar textiles, not for the preparation of cotton wool.

[0092] Then it is optionally possible to further homogenize the fibers formed in this way with the aid of a suitable high speed dispergator in the so-called homogenization bath, where the previous shortening bath is preferably used. A new bath, the so-called homogenization bath, can be also used. The composition of the homogenization bath is the same as the coagulation bath and/or maturation bath.

[0093] The prepared staple microfibers are then collected/filtrated either alone in a suitable filtration apparatus or they are filtrated (fastened) onto a pad, generally a textile, optionally washed with alcohol and dried, again alone or together with the pad. The microfibers layer can be optionally removed from the pad. If it is presumed to remove the pad, it is advisable to use a more hydrophobic pad, for example low molecular polyethylene, which does not form H-bonds with the given fibers.

[0094] In another embodiment the microfibers are filtrated onto a pad, optionally washed, and fastened to this pad by wet compression with the use of a suitable apparatus, and dried (together with the pad).

[0095] The drying temperature of prepared staple microfibers is 20 to 80° C.

[0096] In another embodiment the microfibers of various chemical composition obtained by the previous procedures are mixed together in any ratio in the shortening bath or preferably in the homogenization bath, and they are homogenized in the homogenization bath. The following procedure is then the same as for the previous processes.

[0097] In this invention, the alcohol is methanol, ethanol, propane-1-ol, propane-2-ol, or any mixture thereof. The acid is formic acid, acetic acid, propionic acid, or any mixture thereof.

[0098] In another embodiment the microfibers obtained by the previous processes can be placed into the so-called metallization bath for 20 minutes to 25 days, where various metals are inserted into the microfibers; in this invention it concerns metal ions of calcium, magnesium, copper, manganese, zinc, chromium, iron, and cobalt. From the technological point of view the metallization can be carried out in every bath (coagulation, maturation, shortening, homogenization;

in the case of zinc also in the spinning solution) by adding a salt of polyvalent metal into a proper bath, or a separate metallization bath can be prepared, where this technological step (metallization) can be added to any step, right from the metallization immediately after the coagulation. The metallization is most commonly carried out in the maturation bath. If the metallization step is present, it is necessary to wash the final fibers with alcohol, for example with methanol or isopropanol.

[0099] In the case of biopolymers having the sequestration properties (hyaluronic acid/hyaluronan, internal mixture of chitin and chitosan, chitin/chitosan-glucane complex), the invention is characterized in that the metallization bath is

a) a solution of the salt of polyvalent metal of the concentration of $5 \cdot 10^{-5}$ to $1 \cdot 10^{-2}$ M in the mixture of 1 to 99% by weight of acid, 1 to 99% by weight of alcohol and up to 10% by weight of water, or

b) a solution of the salt of polyvalent metal of the concentration of $5 \cdot 10^{-5}$ to $1 \cdot 10^{-2}$ M in the alcohol comprising up to 10% by weight of water, optionally in the presence of a base selected from the group comprising LiOH, NaOH, KOH, Li_2CO_3, Na_2CO_3, K_2CO_3, $LiHCO_3$, $NaHCO_3$ a $KHCO_3$, with the concentration of the base of $5 \cdot 10^{-5}$ to 1 N.

[0100] As the salts of the polyvalent metal (Mn^{2+}, Ca^{2+}, Cr^{3+}, Fe^{2+}, Co^{3+}, Cu^{2+}, Zn^{2+}), their acetates, formates, chlorides, sulphates, fluorides, nitrates, and hydrates are meant.

[0101] The prepared microfibers are usable as a free cotton wool, further for the production of nonwoven textiles of various types and by various techniques, and, after carding, they can be also used for the production of staple yarn. Nonwoven textiles, cotton wool, tampons, paper stuff, etc. can be made from the fibers.

[0102] The produced nonwoven textile can be "self-supporting" or in the form of a layer of microfibers on a suitable carrier/pad (e.g. textile, preferably fabric or knitted fabric) for the use for suitable wound covers.

[0103] The fastening of microfibers on a suitable textile is a substitution of lyophilization, which is technologically very complicated and expensive.

[0104] The method of spinning according to the present invention in the non-stationary coagulation bath and the following treatments in the consecutive baths exhibits certain advantages. The first advantage is that due to the staple microfiber, which is long enough, it is possible to prepare a nonwoven textile with a very low areal weight (~5 g/m^2) and at the same time tight enough for the common manipulation with the nonwoven textile of this areal weight. The nonwoven textile of the areal weight from 10 g/m^2 can be advantageously used as self-supporting, i.e. without any pad, for example as a cover of internal wounds.

[0105] A further benefit is that during the spinning, at a low concentration of a polymer, e.g. 0.5 to 1% by weight of the aqueous polymer solution, it is possible to prepare the spinning solution only in water and spin it e.g. into propane-2-ol. Due to the fact that NaOH is not added into the spinning solution, the medium is not alkaline, thus the polymer does not degrade. In addition, the complicated removal of organic acids (formic, acetic) and alcohol (methanol, ethanol) from the fiber prepared by the conventional method (PV 2010-1001) is avoided.

[0106] During the spinning of e.g. internal mixture of chitin and chitosan we avoid using the coagulation bath comprising substantial amounts of inorganic salts (10% of NaOH and 30% of sodium acetate). Furthermore, a substantial advan-

tage of this method is that during the spinning in the coagulation bath comprising generally an alcohol (for example propane-2-ol), the ammonium groups (chitosan-$NH_3^+X^-$, $X^- = Cl^-$, CH_3COO^-, etc.) are not converted to amine groups and therefore the microfibers keep their haemostatic and antibacterial effect.

[0107] A certain amount of solvent used during the production process remains in the final microfibers/fibers. This amount can be defined with the aid of NMR spectroscopy within the range of 0.2 to 5% by weight.

[0108] The subject of the invention further comprises covers of internal and external wounds based on the microfibers prepared by the method of the invention. The covers of internal and external wounds can be in the form of woven or nonwoven textiles or cotton wool. The covers of internal and external wounds are for example dressings, bandages, patches, tampons.

[0109] The subject of the invention therefore comprises the covers of internal and external wounds based on staple microfibers consisting of hyaluronic acid and/or at least one compound comprising hyaluronic acid and metal ions, where the fiber can optionally comprise metal salts originating from the production process, which can be prepared by the method according to the present invention, which has the properties of a textile fiber, i.e. nonwoven textiles, cotton wool, tampons, paper stuff, and the like can be made from this fiber. The fiber is composed of hyaluronic acid and/or at least one compound comprising hyaluronic acid and metal ions, where the molecular weight of macromolecules is within the range of 100 kDa to 3 MDa. Preferably the diameter of microfiber (primary fiber) is 1-100 μm and the length 0.8-3 cm.

[0110] The term "a compound comprising hyaluronic acid and metal ions" includes any compound comprising hyaluronic acid and metal or metals ions including salts and metal complex compound. The character of the bond between hyaluronic acid depends on the metal, usually it is an ionic bond, covalent (ionic covalent) or coordinate covalent bond. The said term also comprises the compounds comprising the ions of more than one metal. The metals are preferably selected from the group comprising lithium, sodium, potassium, calcium, magnesium, copper, manganese, zinc, chromium, iron, and cobalt.

[0111] Preferably, the maximum content of these cations in a fiber is as follows:

Metal ion	Maximum content in a fibre (% hm.)
Li+	1.80
Na+	5.72
K+	9.36
Mg2+	3.11
Ca2+	5.03
Mn2+	6.77
Zn2+	7.95
Fe2+	6.87
Cu2+	7.75
Co2+	7.22
Cr3+	4.38
Fe3+	4.69
Co3+	4.93

[0112] The fiber can optionally comprise a metal salt originating from the production process and it refers to acetates, formates, sulphates, chlorides, fluorides, nitrates, phosphates, hydroxides, or oxides of the metals selected from the

group comprising lithium, sodium, potassium, calcium, magnesium, copper, manganese, zinc, chromium, iron, and cobalt. These salts can form a weak or strong interaction with hyaluronic acid. In the case of zinc, the fiber can also comprise the zinc salts Zn^{2+} as the metal salts. The wound covers based on staple microfibers of hyaluronic acid/hyaluronan serve for the construction of bandages absorbing the liquid from the wound and at the same time they stimulate the process of granulation. In the combination with a suitable antiseptic agent they can be utilized for both the acute and chronic non-healing wounds.

[0113] Further, the subject of the invention comprises the covers of internal and external wounds based on staple microfibers consisting of chitin/chitosan-glucan complex, wherein the fiber can optionally comprise metal salts originating from the production process, which can be prepared by the procedure according to the present invention, and has the properties of a textile fiber, i.e. both the woven and nonwoven textiles, cotton wool, tampons, paper stuff, and the like can me made from this fiber. The microfiber/fiber is composed of chitin/chitosan-glucane complex, where the molecular weight of macromolecules is within the range of 70 kDa to 1 MDa. Wound covers based on the staple microfibers of chitin/chitosan-glucane complex serve to cover acute seriously contused and bleeding wounds before their final treatment. They can be of use also in the case of wounds which tend to form necrotic crusts.

[0114] Further, the subject of the invention comprises the covers of internal and external wounds based on staple microfibers consisting of schizophylane, wherein the fiber can optionally comprise metal salts originating from the production process, which can be prepared by the procedure according to the present invention, and has the properties of a textile fiber, i.e. both the woven and nonwoven textiles, cotton wool, tampons, paper stuff, and the like can be made from this fiber. The microfiber/fiber is composed of schizophylane, where the molecular weight of macromolecules is within the range of 200 kDa to 2 MDa. These wound covers can be utilized in combined bandages (wound covers) at the patients who need improvement of local immune processes (e.g. the patients treated with corticosteroids or other immuno suppressants).

[0115] We have found by our own study that amino groups play the key role in spinning of chitin or chitosan. In our opinion, the type of supramolecular structure (helix, double or triple helix, fibers, gels, etc.) depends on the presence of amino groups in the macromolecule. The amino group, due to its sp^3 hybridization, forms 3D structures via the hydrogen bonds. Therefore, it has 3D cross-linking character and thus, these molecules preferentially form gels in water, which are, however, not easy to spin properly. On the contrary, the acylated amino groups, due their H-bonds, form 2D structures, so they support the formation of linear chains (for example double-helixes) suitable for spinning. As it was stated above, the chitin amino groups are mainly acetylated whereas the chitosan amino groups are deacetylated (in other words, there are predominantly the amino groups). The problem consists in that chitin can be spun, but it has not the required biological properties. On the contrary, chitosan has proper biological properties, but it is not possible to prepare fibers from it, or they are of low quality (fragile). The solution is provided by the present invention, where chitin with suitable spinning properties is used on purpose. Further the chitosan with suitable biological properties is used. The principle consists in

dissolving both the polymers, mixing the solutions (in other words, two types of macromolecules are mixed to form chitin-chitosan complex) so that the weight ratio of chitin/chitosan is within the range of 3/4-7/1, and the obtained homogenous solution is spun in the coagulation bath.

[0116] The subject of the invention further comprises covers of internal and external wounds from staple fibers consisting of an internal mixture of chitin and chitosan (i.e. chitin-chitosan complex) that can be prepared by the method according to the present invention, the fibers having the properties of a textile fiber, which means that nonwoven textiles, cotton wool, tampons, paper stuff, and the like can be made from this staple microfiber. The staple microfiber is composed of chitin, where the molecular weight of the macromolecules is within the range of 100 kDa to 1 MDa, and chitosan, where the molecular weight of the macromolecules is within the range of 60 kDa to 1 MDa. These wound covers will be used for the construction of haemostatic and antibacterial bandages.

BRIEF DESCRIPTION OF THE DRAWINGS

[0117] FIG. 1A is a schematic section plan of the apparatus for the preparation of staple microfibers.

[0118] FIG. 1B is a vertical section of the apparatus from the FIG. 1A.

[0119] FIG. 1C shows a straight nozzle (needle).

[0120] FIG. 1D shows a bent nozzle (needle).

[0121] FIG. 2 shows a bundle of schizophylane microfibers.

[0122] FIG. 3 shows the character of the fibers prepared according to the Example 1 (FIG. 3A—magnification of 400×; FIG. 3B—magnification of 5000×).

[0123] FIG. 4 shows a nonwoven textile prepared in the Example 2.

[0124] FIG. 5 shows a cotton wool prepared in the Example 3.

[0125] FIG. 6 shows the character of the fibers prepared according to the Example 4 (magnification of 500×).

[0126] FIG. 7 shows the character of the fiber layer prepared according to the Example 5 (magnification of 500×).

[0127] FIG. 8 shows a microphotography of the layer prepared according to the Example 12 (magnification of 1000×).

[0128] FIG. 9 shows a microphotography of the layer prepared according to the Example 13 (magnification of 1000×).

[0129] FIG. 10a shows the wound cover prepared according to the Example 14—self-supporting, possible to be applied without any supporting knitted fabric.

[0130] FIG. 10b shows the character of a fiber structure (wound cover) prepared from the staple microfibers of hyaluronic acid and native microfibers of chitin/chitosan-glucan complex in the ratio of 1:1 according to the Example 14.

[0131] FIG. 11 shows the wound cover prepared according to the Example 16 (on a supporting textile).

[0132] FIG. 12a shows the wound cover prepared according to the Example 16 (self-supporting layer).

[0133] FIG. 12b shows the wound cover according to the Example 16. The layer character under the electron microscope. Magnification of 1000×.

[0134] FIG. 13 shows the wound cover prepared according to the Example 22. The layer character under the electron microscope. Magnification of 1000×.

PREFERRED EMBODIMENTS OF THE INVENTION

[0135] The pictures of the fibers were made with the microscope Tescan VEGA II LSU (Tescan, Brno). This microscope utilizes wolfram cathode and the maximum resolution is 3 nm. The parameters of measurement were as follows: accelerating voltage of the primary electron beam: 5 kV, working distance—WD: 4-5 mm, pressure in the chamber: high vacuum, display mode: secondary electrons.

[0136] The fibers were stuck on a carbon sticking target and then powdered with gold. The gold layer on the sample: approx. 15 nm, powdering machine: SC7620 Mini Sputter Coater (Quorum Technologies, UK).

[0137] The molecular weight of hyaluronic acid, or hyaluronans, was measured with the aid of HPLC from Shimadzu, equipped with the light scattering detector miniDAWN from Watt Technologies (the so-called SEC-MALLS method).

[0138] The apparent viscosity was measured with ARG2 rheometer from TA Instruments. The cone (40 mm/1°)-plate system of measurement was used. Cone data: first—diameter, second—bevel angle. The metals were determined with the aid of sequential optical emission spectrometer with the ionization in the inductively coupled plasma (Integra XL2, GBC Australia) with the use of ceramic V-groove nebulizer and cyclonic cloud chamber (both from Glass Expansion, Australia).

Example 1

[0139] In the air atmosphere, at intense stirring, 6 grams of sodium hyaluronan with molecular weight of 1.7 MDa (determined by the SEC-MALLS method) was dissolved in 94 g of water with adding of 0.51 g NaOH to obtain a homogenous, well flowing, viscous solution suitable for spinning. This solution was spun by the wet method with a nozzle having the diameter of 0.4 mm into the spinning bath comprising propane-2-ol, stirred with an agitator, more specifically with the Heidolph DIAX 900 dispergator at 2500 rpm. The forming microfiber was collected from the "moving (non-stationary) bath" and transferred to the "maturation bath" consisting of propane-2-ol, where the coagulation of the fiber was completed. After 60 minutes, the microfiber was removed from the maturation bath and dried at the temperature of 60° C. The fiber character is shown in FIG. 3. The length of the microfibers obtained by this method is approximately 5-30 mm. This type of fibers is suitable for the construction of bandages which absorb the liquid from the wound and at the same time they stimulate the process of granulation. In the combination with a suitable antiseptic agent they can be utilized for both the acute and the chronic non-healing wounds. Separately, they can be used for the application into caverns or defects after the teeth extraction. They can also be useful in the field of plastic and correction surgery.

Example 2

[0140] In the air atmosphere, at intense stirring, 6 grams of sodium hyaluronan with the molecular weight of 1.7 MDa (determined by the SEC-MALLS method) was dissolved in 94 g of water with adding of 0.51 g NaOH to obtain a homogenous, well flowing, viscous solution suitable for spinning. This solution was spun by the wet method with a nozzle having the diameter of 0.4 mm into the spinning bath comprising propane-2-ol, stirred with the Heidolph DIAX 900 dispergator at 2500 rpm. The forming microfiber was col-

lected from the "moving bath" and transferred to the "maturation bath" consisting of propane-2-ol, where the coagulation of the fiber was completed. After 60 minutes the maturation bath containing the microfibers was poured into the Eta-Ergo knife mixer, where the fibers were shortened. Then the shortened fiber was filtrated off and the obtained filtration cake was compressed to the form of a "paper" sheet, and the produced product was dried at the room temperature (approx. 25° C.). The paper sheet, or nonwoven textile, is shown in FIG. 4. The length of the microfibers obtained by this method is approximately 5-30 mm.

[0141] This textile is suitable for flat absorption bandages which stimulate the granulation and wound healing. In the combination with an antiseptic agent they can be used for the construction of functional bandages and patches. They can also be useful in the field of plastic and correction surgery.

Example 3

[0142] In the air atmosphere, at intense stirring, 6 grams of sodium hyaluronan with the molecular weight of 1.7 MDa (determined by the SEC-MALLS method) was dissolved in 94 g of water with adding of 0.51 g NaOH to obtain a homogenous, well flowing, viscous solution suitable for spinning. This solution was spun by the wet method with a nozzle having the diameter of 0.4 mm into the spinning bath comprising propane-2-ol, stirred with the Heidolph DIAX 900 dispergator at 2500 rpm. The forming microfiber was collected from the "moving bath" and transferred to the "maturation bath" consisting of propane-2-ol, where the coagulation of the fiber was completed. After 60 minutes the maturation bath containing the microfibers was poured into the Eta-Ergo knife mixer, where the fibers were shortened. Then the shortened fiber was filtrated off and the filtration cake was dried without compression at 20° C. A voluminous layer of microfibers—a cotton wool showed in FIG. 5—was thereby obtained as a base of a nonwoven textile suitable for various uses. The cotton wool is suitable for the direct application into deep wounds and caverns or defects after the teeth extraction. It will also be of use in surgery for improving the healing of various connections and anastomoses. For this purpose, the combination of fibers and an appropriate antiseptic agent is possible.

Example 4

[0143] In the air atmosphere, at intense stirring, 6 grams of sodium hyaluronan with the molecular weight of 19.37 MDa (determined by the SEC-MALLS method) was dissolved in 94 g of water to obtain a homogenous, well flowing, viscous solution suitable for spinning. This solution was spun by the wet method with a nozzle having the diameter of 0.4 mm into the spinning bath comprising propane-2-ol, stirred with the Heidolph DIAX 900 dispergator at 2500 rpm. The forming microfiber was collected from the bath and transferred to methanol where the coagulation of the fiber was completed. After 60 minutes the fiber was dried at the temperature of 60° C. and its character is shown in FIG. 6.

[0144] The use of this fiber is the same as in the Example 1.

Example 5

[0145] In the air atmosphere, at intense stirring, 6 grams of sodium hyaluronan with the molecular weight of 19.37 MDa (determined by the SEC-MALLS method) was dissolved in 94 g of water to obtain a homogenous, well flowing, viscous

solution suitable for spinning. This solution was spun by the wet method with a nozzle having the diameter of 0.4 mm into the spinning bath comprising propane-2-ol, stirred with the Heidolph DIAX 900 dispergator at 2500 rpm. The forming microfiber was collected from the bath and transferred to methanol where the coagulation of the fiber was completed. After 60 minutes the maturation bath containing the microfibers was poured into the Eta-Ergo knife mixer, where the fibers were shortened. Then the shortened fiber was filtrated off, compressed on a calendar (with medium pressure) and dried at the room temperature (approx. 25° C.). The character of the layer is shown in FIG. 7.

[0146] A voluminous layer of microfibers, suitable for the production of nonwoven textile, is thereby obtained.

[0147] This textile is suitable for flat absorption bandages which stimulate the granulation and wound healing. In the combination with an antiseptic agent it can be used for the construction of functional bandages and patches. They will be of use especially for healing of extensive defects. It concerns especially the broken surgical wounds and polytraumas.

Example 6

[0148] In the air atmosphere at intense stirring, 3 g of chitosan from Aldrich company (catalog no. 448869—declared as: Chitosan, low molecular weight, 75-85% deacetylated) were dissolved in 72 g of 2% acetic acid (water solution) to obtain a 4% homogenous, well flowing viscous solution suitable for spinning. In this solution, 3 g of sodium hyaluronan (Contipro Biotech s.r.o.) with the molecular weight of 19.37 kDa (determined by the SEC-MALLS method) was dissolved. The obtained solution was spun by the wet method with a nozzle having the diameter of 0.6 mm into the spinning bath comprising propane-2-ol and stirred with the Heidolph DIAX 900 dispergator at 2200 rpm. The forming microfiber was collected from the bath and transferred to methanol where the coagulation of the fiber was completed. After 60 minutes the maturation bath containing the microfibers was poured into the Eta-Ergo knife mixer, where the fibers were shortened. Then the shortened fiber was filtrated off and the obtained filtration cake was dried at 20° C. without compression.

[0149] This bandage is suitable for acute bleeding wounds. It will be of use especially in traumatology.

Example 7

[0150] In the air atmosphere at intense stirring, 1 g of xanthane (Xanthan Gum—Donau Chem-Typ: 890.235, 402 80 MESH, Ceroga Pharm) was dissolved in 99 g of water to obtain a 1% homogenous, well flowing viscous solution suitable for spinning. This solution was spun by the wet method with a nozzle having the diameter of 0.4 mm into the spinning bath comprising propane-2-ol and stirred with the Heidolph DIAX 900 dispergator at 2500 rpm. The forming microfiber was collected from the bath and transferred to propane-2-ol, where the coagulation of the fiber was completed. After 60 minutes the maturation bath containing the microfibers was poured into the Eta-Ergo knife mixer, where the fibers were shortened. Then the shortened fiber was filtrated off and the obtained filtration cake of xanthane fibers was dried at 20° C. without compression. The xanthane fibers can adjust the adhesiveness and hydration character of combined bandages.

Example 8

[0151] In the air atmosphere at intense stirring, 0.5 g of xanthane (Xanthan Gum—Donau Chem-Typ: 890.235, 402 80 MESH, Ceroga Pharm) and 0.5 g of hyaluronic acid (Contipro Biotech s.r.o. Dolní Dobrouč; 1.7 MDa, determined by the SEC-MALLS method) were dissolved in 99 g of water to obtain a 1% homogenous, well flowing viscous solution suitable for spinning. This solution was spun by the wet method with a nozzle having the diameter of 0.4 mm into the spinning bath comprising propane-2-ol and stirred with the Heidolph DIAX 900 dispergator at 2500 rpm. The forming microfiber was collected from the bath and transferred to propane-2-ol, where the coagulation of the fiber was completed. After 60 minutes the maturation bath containing the microfibers was poured into the Eta-Ergo knife mixer, where the fibers were shortened. The shortened fiber was filtrated off and the obtained filtration cake of mixed fibers (xanthane-hyaluronic acid) was dried at 20° C. without compression.

[0152] The xanthane fibers in the combination with hyaluronan can modify the flow of interstitial fluid and thereby regulate the adhesiveness and hydration character of combined bandages.

Example 9

[0153] In the air atmosphere at intense stirring, 3 g of ammonium alginate (Protamin S—fy. FMC BioPolymer, N-3002 Drammen, Norway) was dissolved in 97 g of water to obtain a 3% homogenous, well flowing viscous solution suitable for spinning. This solution was spun by the wet method with a nozzle having the diameter of 0.4 mm into the spinning bath comprising propane-2-ol and stirred with the Heidolph DIAX 900 dispergator at 2500 rpm. The forming microfiber was collected from the bath and transferred to propane-2-ol, where the coagulation of the fiber was completed. After 60 minutes the maturation bath containing the microfibers was poured into the Eta-Ergo knife mixer, where the fibers were shortened. The shortened fiber was filtrated off and the obtained filtration cake of the fiber of ammonium alginate was dried at 20° C. without compression.

[0154] The alginate staple fibers can be used for example for entrapping the fluid in the area of a dry wound.

Example 10

[0155] In the air atmosphere at intense stirring, 1 g of ammonium alginate and 1 g of sodium hyaluronan (Contipro Biotech s.r.o. Dolní Dobrouč; 1.7 MDa, determined by the SEC-MALLS method) were dissolved in 98 g of water to obtain a 2% homogenous, well flowing viscous solution suitable for spinning. This solution was spun by the wet method with a nozzle having the diameter of 0.4 mm into the spinning bath comprising propane-2-01 and stirred with the Heidolph DIAX 900 dispergator at 2500 rpm. The forming microfiber was collected from the bath and transferred to propane-2-ol, where the coagulation of the fiber was completed. After 60 minutes the maturation bath containing the microfibers was poured into the Eta-Ergo knife mixer, where the fibers were shortened. The shortened fiber was filtrated off and the obtained filtration cake of the mixed fiber of alginate—hyaluronic acid was dried at 20° C. without compression.

[0156] These mixed fibers ensure various hydration and granulation characteristics of the wounds with impaired vascularity.

Example 11

[0157] In the air atmosphere at intense stirring, 0.25 g of schizophylane (Contipro Biotech s.r.o. Dolní Dobrouč; 1.7 MDa, determined by the SEC-MALLS method) was being dissolved in 25 g of water for 24 hours to obtain a homogenous, well flowing viscous solution suitable for spinning. This solution was spun by the wet method with a nozzle having the diameter of 0.4 mm into the spinning bath comprising propane-2-ol and stirred with the Heidolph DIAX 900 dispergator at 2500 rpm. The forming microfiber was collected from the bath and transferred to propane-2-ol, where the coagulation of the fiber was completed. After 60 minutes the maturation bath containing the microfibers was poured into the Eta-Ergo knife mixer, where the fibers were shortened, and further they were shortened and homogenized with the aid of Heidolph DIAX 900 mixer. A layer of this fiber was prepared by the filtration on a suitable pad (knitted fabric from polyamide 6 (silk) with areal weight of approx. 40 $g \cdot m^{-2}$). The obtained filtration cake was compressed (together with the pad) in a two-roll calendar and dried at 20° C. As the layer obtained in this way has no affinity to the pad, it gets unstuck spontaneously during the drying. The areal weight of the obtained fibers (nonwoven textile) from schizophylane was approx. 15 g/m^2. The formed microfiber layer can be applied including the pad or it can be removed—separated—from the pad and the layer of microfibers can be used separately.

[0158] The fibers obtained thereby are of use in combined bandages for the patients who are in need of improvement of local immune processes (e.g. the patients treated with corticosteroids or other immunosuppressants).

Example 12

[0159] In the air atmosphere at intense stirring, 0.25 g of schizophylane (Contipro Biotech s.r.o. Dolní Dobrouč) and 0.25 g of sodium hyaluronan (Contipro Biotech s.r.o. Dolní Dobrouč) with the molecular weight of 1.7 MDa (determined by the SEC-MALLS method) were being dissolved in 50 g of water for 24 hours to obtain a homogenous, well flowing viscous solution suitable for spinning. This solution was spun by the wet method with a nozzle having the diameter of 0.4 mm into the spinning bath comprising propane-2-ol and stirred with the Heidolph DIAX 900 dispergator at 2500 rpm. The forming microfiber was collected from the bath and transferred to propane-2-ol, where the coagulation of the fiber was completed. After 60 minutes the maturation bath containing the microfibers was poured into the Eta-Ergo knife mixer, where the fibers were shortened, and further they were shortened and homogenized with the aid of Heidolph DIAX 900 mixer. The suspension of the mixed fiber was filtrated on a suitable pad (knitted fabric from polyamide 6 (silk) with areal weight of approx. 40 $g \cdot m^{-2}$) and thereby a layer of this mixed fiber was prepared. The obtained filtration cake was wet compressed (including the pad) in a two-roll calendar and dried at 20° C. As the obtained mixed fibers have an affinity to the pad, the layer was not removed from the pad, and the layer of the mixed fibers from schizophylane and hyaluronic acid had the areal weight of approx. 10 g/m^2 (weight of the pad was subtracted). The formed layer of microfibers (FIG. **8**) can be applied including the pad or it can be removed—separated—from the pad and the layer of microfibers can be used separately.

[0160] The combination of schizophylane+HA in mixed fibers is of use for the construction of combined immunomodulating bandages.

Example 13

[0161] In the air atmosphere at intense stirring, 0.5 g of sodium hyaluronan (Contipro Biotech s.r.o. Dolní Dobrouč) with the molecular weight of 1.7 MDa (determined by the SEC-MALLS method) was dissolved in 50 g of water to obtain homogenous, well flowing viscous solution suitable for spinning. This solution was spun by the wet method with a nozzle with the diameter of 0.4 mm into the spinning bath comprising propane-2-ol and stirred with the Heidolph DIAX 900 dispergator at 2500 rpm. The forming microfiber was collected from the bath and transferred to propane-2-ol, where the coagulation of the fiber was completed. After 60 minutes the maturation bath containing the microfibers was poured into the Eta-Ergo knife mixer, where the fibers were shortened, and further they were shortened and homogenized with the aid of Heidolph DIAX 900 mixer. 0.5 g of homogenized fibrous sample of chitin/chitosan-glucane complex (Contipro Biotech s.r.o. Dolní Dobrouč, species: *Aspergillus niger*. dry mass: 93.64%, ash: 0.82%, GLA content: 13.26%) was added to the shortened fiber. The suspension of the mixture of fibers was further homogenized and in the end filtrated on a suitable pad (knitted fabric from polyamide 6 (silk) with areal weight of approx. 40 $g \cdot m^{-2}$) and thereby a layer of this mixture of fibers was prepared. The obtained filtration cake was wet compressed in a two-roll calendar and dried at 20° C. The obtained layer of the mixture of fibers from chitosan-glucane complex and hyaluronic acid had the areal weight of approx. 15 g/m^2 (the weight of the pad was subtracted). The formed layer of microfibers (FIG. **9**) can be applied including the pad or it can be removed—separated—from the pad and the layer of microfibers can be used separately.

[0162] These fibers are suitable for covering acute seriously contused and bleeding wounds before their final treatment. They can also be of use in the case of wounds which tend to form necrotic crusts.

Example 14

[0163] In the air atmosphere at intense stirring, 0.5 g of sodium hyaluronan (Contipro Biotech s.r.o. Dolní Dobrouč) with the molecular weight of 1.7 MDa (determined by the SEC-MALLS method) was dissolved in 50 g of water to obtain a homogenous, well flowing viscous solution suitable for spinning. This solution was spun by the wet method with a nozzle having the diameter of 0.4 mm into the spinning bath comprising propane-2-ol and stirred with the Heidolph DIAX 900 dispergator at 2500 rpm. The forming microfiber was collected from the bath and transferred to propane-2-ol, where the coagulation of the fiber was completed. After 60 minutes the maturation bath containing the microfibers was poured into the Eta-Ergo knife mixer, where the fibers were shortened, and further they were shortened and homogenized with the aid of Heidolph DIAX 900 mixer. 0.5 g of homogenized fibrous sample of chitin/chitosan-glucane complex (Contipro Biotech s.r.o. Dolní Dobrouč, obtained from Schizophyllan commune) was added to the shortened fiber. The suspension of the mixture of fibers was further homogenized and then filtrated on a suitable pad (knitted fabric from polyamide 6 (silk) with areal weight of approx. 40 $g \cdot m^{-2}$) and thereby a layer of this mixture of fibers was prepared. The

obtained filtration cake was wet compressed in the two-roll calendar and dried at 20° C. and relative air humidity of 15%. The obtained layer of the mixture of fibers from chitosan-glucane complex and hyaluronic acid had areal weight of approx. 15 g/m² (weight of the pad was subtracted). The formed layer of microfibers can be applied including the pad or it can be removed—separated—from the pad and the layer of microfibers can be used separately (FIG. 10a, 10b).

[0164] These fibers are suitable for covering acute seriously contused and bleeding wounds before their final treatment. They can also be of use in the case of wounds which tend to form necrotic crusts.

Example 15

[0165] In the air atmosphere at intense stirring, 0.5 g of sodium hyaluronan (Contipro Biotech s.r.o. Dolní Dobrouč) with the molecular weight of 1.7 MDa (determined by the SEC-MALLS method) was dissolved in 50 g of water to obtain a homogenous, well flowing viscous solution suitable for spinning. This solution was spun by the wet method with a nozzle having the diameter of 0.4 mm into the spinning bath comprising propane-2-ol and stirred with the Heidolph DIAX 900 dispergator at 2500 rpm. The forming microfiber was collected from the bath and transferred to propane-2-ol, where the coagulation of the fiber was completed. After 60 minutes the maturation bath containing the microfibers was poured into the Eta-Ergo knife mixer, where the fibers were shortened, and further they were shortened and homogenized with the aid of Heidolph DIAX 900 mixer. 0.5 g of microfibers from chitin/chitosan-glucane complex (the preparation is described in Example 18) was added to the shortened fiber. The suspension of the mixture of fibers was further homogenized and in the end filtrated on a suitable pad (knitted fabric from polyamide 6 (silk) with areal weight of approx. 40 g·m⁻²) and thereby a layer of this mixture of fibers was prepared. The obtained filtration cake was wet compressed in the two-roll calendar and dried at 20° C. The obtained layer of the mixture of fibers from chitosan and hyaluronic acid had areal weight of approx. 15 g/m² (weight of the pad was subtracted). The formed layer of microfibers can be applied including the pad or it can be removed—separated—from the pad and the layer of microfibers can be used separately. These fibers are suitable for covering acute seriously contused and bleeding wounds before their final treatment. They can also be of use in the case of wounds which tend to form necrotic crusts.

Example 16

[0166] In the air atmosphere at intense stirring, 0.5 g of sodium hyaluronan (Contipro Biotech s.r.o. Dolní Dobrouč) with the molecular weight of 1.7 MDa (determined by the SEC-MALLS method) was dissolved in 50 g of water to obtain a homogenous, well flowing viscous solution suitable for spinning. This solution was spun by the wet method with a nozzle having the diameter of 0.4 mm into the spinning bath comprising propane-2-ol and stirred with the Heidolph DIAX 900 dispergator at 2500 rpm. The forming microfiber was collected from the bath and transferred to propane-2-ol, where the coagulation of the fiber was completed. After 60 minutes the maturation bath containing the microfibers was poured into the Eta-Ergo knife mixer, where the fibers were shortened, and further they were shortened and homogenized with the aid of Heidolph DIAX 900 mixer. The suspension of

the fibers was further homogenized and in the end filtrated on a suitable pad (knitted fabric from polyamide 6 (silk) with areal weight of approx. 40 g·m⁻²) and thereby a layer of this mixture of fibers was prepared. The obtained filtration cake was wet compressed in a two-roll calendar and dried at 52° C. and relative air humidity of 18%. The obtained layer of fibers from hyaluronic acid had areal weight of approx. 15 g/m² (the weight of the pad was subtracted). The formed layer of microfibers can be applied including the pad (FIG. 11) or it can be removed—separated—from the pad and the layer of microfibers can be used separately (FIG. 12a).

[0167] The character of the layer of microfibers under the electron microscope is shown in FIG. 12b.

[0168] These fibers are suitable for flat absorption bandages which stimulate the granulation and wound healing. In the combination with an antiseptic agent they can be used for the construction of functional bandages and patches. They can be useful also in the field of plastic and correction surgery.

Example 17

[0169] In the air atmosphere at intense stirring, 1 g of chitosan from Aldrich company (catalog no. 448869—declared as: Chitosan, low molecular weight, 75-85% deacetylated) was dissolved in 100 g of 2% acetic acid (2 g of ice-cold acetic acid and 98 g of water) to obtain a 1% homogenous, well flowing viscous solution suitable for spinning. This solution was spun by the wet method with a nozzle having the diameter of 0.4 mm into the spinning bath comprising propane-2-ol and stirred with the Heidolph DIAX 900 dispergator at 2500 rpm. The forming microfiber was collected from the bath and transferred to propane-2-ol, where the coagulation of the fiber was completed. After 60 minutes the maturation bath containing the microfibers was poured into the Eta-Ergo knife mixer, where the fibers were shortened, and further they were shortened and homogenized with the aid of Heidolph DIAX 900 mixer. To this suspension of fibers, the suspension of fibers from hyaluronic acid prepared according to the Example 22 was further added. The suspension of both types of fibers was further homogenized and in the end filtrated on a suitable pad (knitted fabric from polyamide 6 (silk) with areal weight of approx. 40 g·m⁻²) and thereby a layer of this mixture of fibers was prepared. The obtained filtration cake was wet compressed in a two-roll calendar and dried at 20° C. The obtained layer of fibers from hyaluronic acid and chitosan fibers had areal weight of 15 g/m². The formed layer of microfibers can be applied including the pad or it can be removed—separated—from the pad and the layer of microfibers can be used separately. The formed layer of microfibers is water-insoluble.

[0170] This textile is suitable for the construction of patches for treating smaller wounds and bruises.

Example 18

[0171] In a mixture of acetic acid and formic acid (97 g, mixture 1:1 by weight), 3 g of chitin (University of Pardubice, approx. 1 MDa—determined by viscosimetry), acetylation degree of amine groups approx. 95%, extracted from crab shells provided by VCI Brasil company) were dissolved at stirring, and the solution was stirred for 2 hours at 22° C. (room temperature).

[0172] In another reaction container, 4 g of chitosan (University of Pardubice, approx. 100 kDa—determined by viscosimetry), acetylation degree of amine groups approx. 84%)

were dissolved, at stirring, in 96 g of formic acid, and the solution was stirred for 2 hours at 22° C. (room temperature). Then both solutions were combined and the resulting solution was spun by the wet method with a nozzle having the diameter of 0.4 mm into the spinning bath comprising propane-2-ol and stirred with the Heidolph DIAX 900 dispergator at 2500 rpm. The forming microfiber was collected from the bath and transferred to the maturation bath comprising propane-2-ol, where the coagulation of the fiber was completed. After 120 minutes the maturation bath containing the microfibers was poured into the Eta-Ergo knife mixer, where the fibers were shortened, and further they were shortened and homogenized with the aid of Heidolph DIAX 900 mixer. In the end, the suspension of fibers was filtrated off and thereby the layer of this mixture of fibers was prepared. The obtained filtration cake was washed with methanol and dried at 20° C.

[0173] The bandages based on these fibers are of use for covering smaller acute bleeding wound which tend to dry prematurely.

Example 19

[0174] The procedure was the same as in Example 16. Only the obtained suspension of fibers was diluted 3 times with 2-propanol and the suspension was filtered.

[0175] The obtained layer of fibers form hyaluronic acid had the areal weight of 5 g/m² (the weight of the pad was subtracted). The obtained layer of microfibers can be applied including the pad or it can be removed—separated—from the pad and the layer of microfibers can be used separately.

[0176] This textile is suitable for flat absorption bandages which stimulate the granulation and wound healing. Combined with an antiseptic agent they can be used for the construction of functional bandages and patches. They can be of use mainly in the treatment of extensive defects. It concerns especially broken surgery wounds and polytraumas.

Example 20

[0177] In the air atmosphere at intense stirring, 1.5 g of sodium hyaluronan (Contipro Biotech s.r.o. Dolní Dobrouč) with the molecular weight of 1.7 MDa (determined by the SEC-MALLS method) were dissolved in 200 g of water to obtain a homogenous, well flowing viscous solution suitable for spinning. 0.257 g of $CaCl_2.6H_2O$ in 10 ml of water (sample no. 1) or 0.43 g of $CaCl_2.6H_2O$ in 10 ml of water (sample no. 2) were added to the solution. After thorough mixing, this homogenous solution was spun by the wet method with a nozzle having the diameter of 0.6 mm into the spinning bath comprising propane-2-ol and stirred with the Heidolph DIAX 900 dispergator at 2500 rpm. The forming microfiber was collected from the bath and transferred to propane-2-ol, where the coagulation of the fiber was completed. After 60 minutes the maturation bath containing the microfibers was poured into the Eta-Ergo knife mixer, where the fibers were shortened, and further they were shortened and homogenized with the aid of Heidolph DIAX 900 mixer. The suspension of the fibers was further homogenized and in the end filtrated on a suitable pad (knitted fabric from polyamide 6 (silk) with areal weight of approx. 40 g·m⁻²) and thereby a layer of fibers of calcium salt of hyaluronic acid was prepared. The obtained filtration cake was wet compressed in a two-roll calendar and dried at 20° C. The obtained layer of fibers from calcium salt of hyaluronic acid had areal weight of 15 g/m² (the weight of the pad was subtracted). The formed

layer of micro fibers can be applied including the pad or it can be removed—separated—from the pad and the layer of microfibers can be used separately.

[0178] The content of the calcium ion in microfibers was determined by the method of optical emission spectrometry with inductively coupled plasma. The results are shown in the following table:

Sample	Content of Ca^{2+} (% by weight)
1	2.305
2	3.301

[0179] This textile is suitable as the contact (with the wound) layer for the construction of haemostatic bandages.

Example 21

[0180] In the air atmosphere at intense stirring, 0.5 g of sodium hyaluronan (Contipro Biotech s.r.o. Dolní Dobrouč) with the molecular weight of 1.7 MDa (determined by the SEC-MALLS method) was dissolved in 50 g of water to obtain a homogenous, well flowing viscous solution suitable for spinning. This solution was spun by the wet method with a nozzle having the diameter of 0.4 mm into the spinning bath comprising propane-2-ol and stirred with the Heidolph DIAX 900 dispergator at 2500 rpm. The forming microfiber was collected from the bath and transferred to propane-2-ol, where the coagulation of the fiber was completed. After 60 minutes the maturation bath containing the microfibers was poured into the Eta-Ergo knife mixer, where the fibers were shortened, and then they were shortened and homogenized with the aid of Heidolph DIAX 900 mixer. The suspension of the fibers was further homogenized and in the end filtrated on a suitable pad (knitted fabric from polyamide 6 (silk) with areal weight of approx. 40 g·m⁻²) and thereby a layer of this mixture of fibers was prepared. The obtained filtration cake was wet compressed in a two-roll calendar and dried at 20° C. The obtained layer of fibers from hyaluronic acid had areal weight of 15 g/m² (the weight of the pad was subtracted). The obtained layer of microfibers was inserted without the pad into 100 ml of metallization bath comprising: 65 ml of methanol p.a., 35 ml of formic acid 98% pure, and 1 ml of water, and 2 g of CrF_2 (sample no. 1); or 2 g of $KCr(SO_4)_2.12H_2O$ (sample no. 2); or 2 g of $CuSO_4.5H_2O$ (sample no. 3); or 2 g of $ZnSO_4.7H_2O$ (sample no. 4); or 2 g of $CaCl_2.2 H_2O$ (sample no. 5). The layer of microfibers was left in the metallization bath for 25 days, then it was removed, washed with methanol, and dried at room temperature.

[0181] The content of the respective cations was determined by the method of optical emission spectrometry with inductively coupled plasma.

[0182] The content of the respective metals is shown in the following table.

sample	Cr % by weight	Cu % by weight	Zn % by weight	Ca % by weight
1	3.846	—	—	—
2	2.972	—	—	—
3	—	2.300	—	—
4	—	—	2.806	—
5	—	—	—	0.759

[0183] The samples nos. 1 and 2 (metallization with chromium ions) were water-insoluble.

[0184] The microfibers comprising the metal ions in a farmacologically acceptable concentration are of use in many topical applications. For example the microfibers, or the textile products made of them, comprising calcium ions, can be suitable for the construction of haemostatic bandages. The microfibers, or the textile products made of them, comprising zinc ions or a combination of zinc ions with copper ions, can be utilized as a part of the bandages intended to application on the wounds difficult to heal, as are for example decubitus or venous ulcers. The textile products from the microfibers comprising zinc, copper or chromium ions, or their combination, can be used as a part of covers applied on various forms of pemphigus. The textile products comprising the microfibers bearing zinc ions, or a combination of zinc and copper ions, can be utilized in the combination with various dermatics in preparations suppressing the symptoms of dermatitides. The microfibers comprising zinc or copper ions or their mixtures can be a component of cosmetic masks.

Example 22

[0185] The preparation of the layer from spun HA with the aerial weight of 15 $g \cdot m^{-2}$ on a suitable carrier In the air atmosphere at intense stirring, 0.5 g of sodium hyaluronan (CPN s.r.o. Dolní Dobrouč) with the molecular weight of 1.7 MDa (determined by the SEC-MALLS method) was dissolved in 50 g of water to obtain a homogenous, well flowing viscous solution suitable for spinning. This solution was spun by the wet method with a nozzle having the diameter of 0.4 mm into the spinning bath comprising propane-2-ol and stirred with the Heidolph DIAX 900 dispergator at 2500 rpm. The forming microfiber was collected from the bath and transferred to propane-2-ol, where the coagulation of the fiber was completed. After 60 minutes the maturation bath containing the microfibers was poured into the Eta-Ergo knife mixer, where the fibers were shortened, and further they were shortened and homogenized with the aid of Heidolph DIAX 900 mixer. The suspension of the fibers was further homogenized and in the end filtrated on a suitable pad (knitted fabric from polyamide 6 (silk) with areal weight of approx. 40 $g \cdot m^{-2}$) and thereby a layer of this mixture of fibers was prepared. The obtained filtration cake was wet compressed in a two-roll calendar and dried at 25° C. and relative air humidity of 65%. The obtained layer of fibers from hyaluronic acid had the areal weight of 15 $g \cdot m^{-2}$ (the weight of the pad was subtracted). The obtained layer of microfibers can be applied including the pad or it can be removed—separated—from the pad and the layer of microfibers can be used separately. The character of the layer is shown in FIG. 13.

[0186] The fibers are suitable for flat absorption bandages which stimulate the granulation and wound healing. Combined with an antiseptic agent they can be used for the construction of functional bandages and patches. They can also be useful in the field of plastic and correction surgery.

[0187] The disclosed examples can be preferably carried out on the apparatus according to the invention, which is shown in FIGS. 1A and 1B and which comprises a cylindrical container 1 for the coagulation bath 1a, and a rotary disc 2 with a vertical axis of rotation passing through the bottom of the cylindrical container 1 and in a distance from the vertical axis of the cylindrical container 1. It means that the rotary disc 2 (rotor) which causes the movement of the coagulation bath, is placed asymmetrically in the cylindrical container 1. The diameter of the rotary disc 2 is approximately 10 to 30% of the diameter of the container 1. The distance of the edge of rotary disc 2 from the wall of the container 1 is in the case of laboratory apparatus approximately 5 to 20 mm, for example 15 mm. The advantages of this arrangement are that the formed fibers are not wound up on the rotary disc 2, they do not break, and they are not twisted mutually. The rotary disc 2 is preferably made of steal, glass or ceramics of the thickness of 1 to 3 mm, and the diameter can be for example 60 mm, and it is placed in the coagulation bath. The coagulation bath can be of the volume for example 2000 cm^3, and is placed in the container 1 of a cylindrical character with the diameter of 230 mm. The rotations of the rotary disc 2 are preferably 2000 to 2500 rpm. The arrows in FIGS. 1A and 1C and 1D show the direction of the disc rotation, or the direction of the stream of the coagulation bath. The apparatus further comprises the spinning nozzle 3, the outlet 4 of which is arranged in the cylindrical container 1 in a distance from its wall of 70 to 130% of the shortest distance of the rotary disc 2 form the wall of the cylindrical container 1. The opening of the nozzle 3 (needle) bringing the polymer solution has preferably the diameter of 0.05 to 1.6 mm and is placed in the direction of the stream of the coagulation bath in the distance of 80 to 190° from the axis passing through the centre of the container 1 and the centre of the rotary disc 2 (FIG. 1A). It means that the angle spacing of the vertical axis of the rotary disc 2 and the outlet 4 of the spinning nozzle 3 is preferably above 80°, related to the vertical axis of the container 1. In another preferred embodiment of the invention the spinning nozzle 3 can be bent on its end comprising the outlet 4. The advantage of the bending of the nozzle 3 is that the axis of the stream leaving the nozzle 3 is concurrent with the stream of the coagulation bath and that the bending of the nozzle 3, due to the deformation and narrowing of the diameter in the point of bending, causes a stronger "stress" to the macromolecules of the polymer, and therefore, for example due to the thixiotropic character exhibited by hyaluronan, the kinetic viscosity of the polymer solution is decreased and also a "linear arrangement of the chain of macromolecules" occurs which is a good condition for the formation of tight fibers. According to the method of spinning, the outlet 4 of the nozzle 3 can be placed above or under the level of the coagulation bath 1a.

1. A method of preparation of polysaccharide fibers characterized in that a 0.01 to 8% wt spinning solution of a polysaccharide having the molecular weight of 60 kDa to 3 MDa and being selected from the group comprising hyaluronic acid, a compound comprising hyaluronic acid and metal ions, schizophylan, chitin/chitosan-glucan complex, a compound comprising chitin/chitosan-glucan complex and metal ions, internal mixture of chitin and chitosan, a compound comprising internal mixture of chitin and metal ions, sodium alginate, potassium alginate, ammonium alginate, xanthane, xanthane sodium salt, xanthane potassium salt, oxycellulose, oxycellulose sodium salt, oxycellulose potassium salt, carboxymethyl cellulose, carboxymethyl cellulose sodium salt, and carboxymethyl cellulose potassium salt, or mixtures of polysaccharides, is prepared in an aqueous medium, which is spun in a non-stationary coagulation bath comprising pure C_1-C_3 alcohol.

2. The method according to claim 1 characterized in that during the spinning the water content in the coagulation bath is within the range of 0.1 to 40% by weight.

3. The method according to claim 2 characterized in that the water content is 10% by weight.

4. The method of preparation according to claim **1** characterized in that the spinning solution passes through an air passage of the length of 1 to 200 mm before its entering the coagulation bath.

5. The method of preparation according to claim **1** characterized in that the spinning solution, before entering the coagulation bath, is stored in a refrigerator for 5 to 24 hours at the temperature of $-40°$ C. to $-10°$ C. and then it is left to heat to room temperature.

6. The method of preparation according to claim **1** characterized in that the temperature of the coagulation bath is within the range of 18 to 30° C.

7. The method of preparation according to claim **1** characterized in that the fibers are further transferred for 20 minutes to 96 hours from the coagulation bath to the stationary maturation bath comprising C_1-C_3 alcohol.

8. The method of preparation according to claim **7** characterized in that the maturation bath further comprises up to 10% by weight of organic acid.

9. The method of preparation according to claim **1** characterized in that the spinning solution further comprises a calcium or zinc salt in the concentration of 0.1 to 50% by weight.

10. The method of preparation according to claim **1** characterized in that the fibers are further metallized for 20 minutes to 25 days directly in bath selected form the coagulation bath, maturation bath, shortening bath or homogenization bath, by adding a salt of polyvalent metal, or they are transferred to a new bath, wherein each of the baths comprises C_1-C_3 alcohol, or a mixture of C_1-C_3 alcohol and organic acid, and a salt of polyvalent metal selected from the group comprising calcium, magnesium, copper, manganese, zinc, chromium, iron, and cobalt.

11. The method of preparation according to claim **1** characterized in that the fibers are shortened in the shortening bath comprising C_1-C_3 alcohol, or the mixture of C_1-C_3 alcohol and organic acid, from the starting length of 0.8 to 3 cm to the length of 1 to 5 mm, or the fibers are shortened directly in the maturation bath, or they are transferred to a new shortening bath.

12. The method of preparation according to claim **1** characterized in that the fibers are homogenized in the homogenization bath comprising C_1-C_3 alcohol, or the mixture of C_1-C_3 alcohol and organic acid, or they are homogenized directly in the shortening bath, or they are transferred to a new homogenization bath.

13. The method of the preparation according to claim **1** characterized in that the fibers are removed from the last bath and dried.

14. The method of the preparation according to claim **13** characterized in that the fibers are washed with alcohol before drying.

15. A method of production of a cover based on polysaccharide fibers characterized in that the 30 fibers are prepared by the method defined in claim **1**, or a mixture of fibers prepared by the method defined in claim **1** is prepared, or a mixture of fibers prepared by the method defined in claim **1** and fibers based on the natural mycelium is prepared, and then the fibers are filtrated off the solution and the filtration cake is dried.

16. The method of production of the cover according to claim **15** characterized in that the filtration cake is compressed before drying.

17. The method of production of the cover according to claim **15** characterized in that the fibers are filtrated onto a suitable pad, the filtration cake is compressed with the pad, and then they are dried.

18. The method of production of the cover according to claim **17** characterized in that the pad is removed from the dried filtration cake.

19. The method of production of the cover according to claim **15** characterized in that the filtration cake is washed with alcohol before drying.

20. The method of production of the cover according to claim **15** characterized in that the dried filtration cake is inserted into the metallization bath, then the fibers are removed from the metallization bath, washed with alcohol and dried.

21. The method of production of the cover according to claim **15** characterized in that the drying is carried out at the temperature of 20 to 80° C. and relative air humidity of 15 to 80%.

22. The method of production of the cover according to claim **15** characterized in that the drying is carried out by hot air.

23. A wound cover based on the polysaccharide fibers prepared by the method defined in claim **1** characterized in that it comprises staple microfibers of biopolymer, or a mixture of staple microfibers of biopolymer, or a mixture of staple microfibers of biopolymer and fibers based on the natural mycelium, where its areal weight is at least 5 g/m^2.

24. The wound cover according to claim **23** characterized in that the length of the initial microfibers is within the range of 0.8 to 3 cm.

25. The wound cover according to claim **23** characterized in that it is in the form of nonwoven textile, nonwoven textile fixed on a pad, cotton wool, tampon or paper stuff.

26. (canceled)

27. (canceled)

28. (canceled)

29. (canceled)

30. (canceled)

* * * * *

Publication 12

A novel *in situ* silver/hyaluronan bio-nanocomposite fabrics for wound and chronic ulcer dressing: *In vitro* and *in vivo* evaluations

A.M. Abdel-Mohsen[a,b,c,*], J. Jancar[a,b,d], R.M. Abdel-Rahman[a], L. Vojtek[e], P. Hyršl[e], M. Dušková[e], H. Nejezchlebová[e]

[a] CEITEC—Central European Institute of Technology, Brno University of Technology, Brno, Czechia
[b] SCITEG, a.s., Brno, Czechia
[c] Pretreatment and Finishing of Cellulosic Fibers, Textile Research Division, National Research Centre, Dokki, Cairo, Egypt
[d] Faculty of Chemistry, Institute of Materials Chemistry, Brno University of Technology, Brno, Czechia
[e] Masaryk University, Faculty of Science, Department of Experimental Biology, Brno, Czechia

ABSTRACT

In-situ formed hyaluronan/silver (HA/Ag) nanoparticles (NPs) were used to prepare composite fibers/fabrics for the first time. Different concentrations of silver nitrate (1, 2 mg/100 ml) were added at ambient temperature to sodium hyaluronate solution (40 mg/ml), then the pH was increased to 8 by adding sodium hydroxide. The in-situ formed HA/Ag-NPs were used to prepare fibers/nonwoven fabrics by wet-dry-spinning technique (WDST). UV/vis spectroscopy, SEM, TEM, DLS, XPS, XRD and TGA were employed to characterize the structure and composition of the nanocomposite, surface morphology of fiber/fabrics, particle size of Ag-NPs, chemical interactions of Ag^0 and HA functional groups, crystallinity and thermal stability of the wound dressing, respectively. The resultant HA/Ag-NPs1 and HA/Ag-NPs2 composite showed uniformly dispersed throughout HA fiber/fabrics (SEM), an excellent distribution of Ag-NPs with 25 ± 2, nm size (TEM, DLS) and acceptable mechanical properties. The XRD analysis showed that the *in-situ* preparation of Ag-NPs increased the crystallinity of the resultant fabrics as well as the thermal stability. The antibacterial performance of medical HA/Ag-NPs fabrics was evaluated against gram negative bacteria E. coli K12, exhibiting significant bactericidal activity. The fibers did not show any cytotoxicity against human keratinocyte cell line (*HaCaT*). *In-vivo* animal tests indicated that the prepared wound dressing has strong healing efficacy (non-diabetics/diabetics rat model) compared to the plain HA fabrics and greatly accelerated the healing process. Based on our results, the new HA/Ag-NPs-2 mg nonwoven wound dressing fabrics can be used in treating wounds and chronic ulcers as well as cell carrier in different biological research and tissue engineering.

© 2017 Elsevier B.V. All rights reserved.

1. Introduction

Wound healing is a complex, multi-step process including the activation of a variety of cell types. Re-epithelization during the early phase of wound healing, occurs only after migration and proliferation of keratinocyte cells in the epidermal layer from the wound edge as well as by differentiation of stem cells residing in the bulge of hair follicles (Tjong, 2012; Zanette et al., 2011). Bio-nanocomposites represent a fascinating interdisciplinary area that brings together biology, materials science and nanotechnology. Generally, polymer nanocomposite results from the combination of a suitable biopolymer and filler particles at the nanometer scale. The extraordinary versatility of these new materials stems from the large selection of biopolymers and fillers available (Paul and Robeson, 2008; Potts et al., 2011; Regiel et al., 2013; Tjong, 2012).

The interaction between filler and polymer enables the NPs to act as molecular bridges greatly affecting properties of the polymer matrix (Kalathi et al., 2014; Potts et al., 2011; Tjong, 2012; Zeng et al., 2005). Bio-nanocomposites add a new biological dimension to these enhanced properties introducing bioactivity, biocompatibility and/or resorb-ability.

Sodium hyaluronate (HA) is natural polysaccharide with composed units of D-glucuronic acid and *N*-acetyl glucosamine, present in different connective tissues such as cartilage, bone, and it's the central component for structuring the connective tissue (Abdel-Mohsen et al., 2012c; Harris et al., 1972; Lapčík et al., 1998; Reineck et al., 2003). Moreover, they are environmentally friendly green chemicals. It is also used as a diagnostic marker for different diseases such as cancer, tumor diseases (Alkrad et al., 2003). Recently Raman spectroscopy is used to examine the chemical structure of bulk hyaluronan films (Kvitek et al., 2005; Tao et al., 2003). In order to avoid wound or chronic ulcer infection by bacteria, antibacterial agents must be introduced into neat hyaluronan (Abdel-Mohsen et al., 2013, 2012c). Among various

antimicrobial agents, silver (Ag^0) is the most common and well-studied type of the antibacterial agent due to its wide antibacterial spectrum (Abdel-Mohsen et al., 2014, 2012a, 2013, 2012c). Silver nanoparticles are reported to be effectively against a wide range of gram positive/negative bacteria, fungi and viruses (Barbinta-Patrascu et al., 2014; Cong et al., 2014; Loza et al., 2014; Marsich et al., 2013; Nocchetti et al., 2013; Schneid et al., 2014; Shi et al., 2015; Taheri et al., 2014). Silver nitrate is used as antimicrobial agent for wounds as far back as World War I; the current use of silver agents has been reduced to topical silver derivatives like silver sulfadiazine (cream/gel) in the treatment of burn wounds due to the unique properties of excellent and effective antibiotics (Sun et al., 2013; Szegedi et al., 2014).

Silver nanoparticles (Ag-NPs) are clusters of silver atoms that area in diameter from 1 to 100 nm and attracted interest as antibacterial and antifungal agents for applications in cosmetics (Kokura et al., 2010), textile (Abdel-Mohsen et al., 2012a; Bober et al., 2014) and medicine (Abdel-Mohsen et al., 2012a; Stevens et al., 2011). They are used for coatings on various materials like
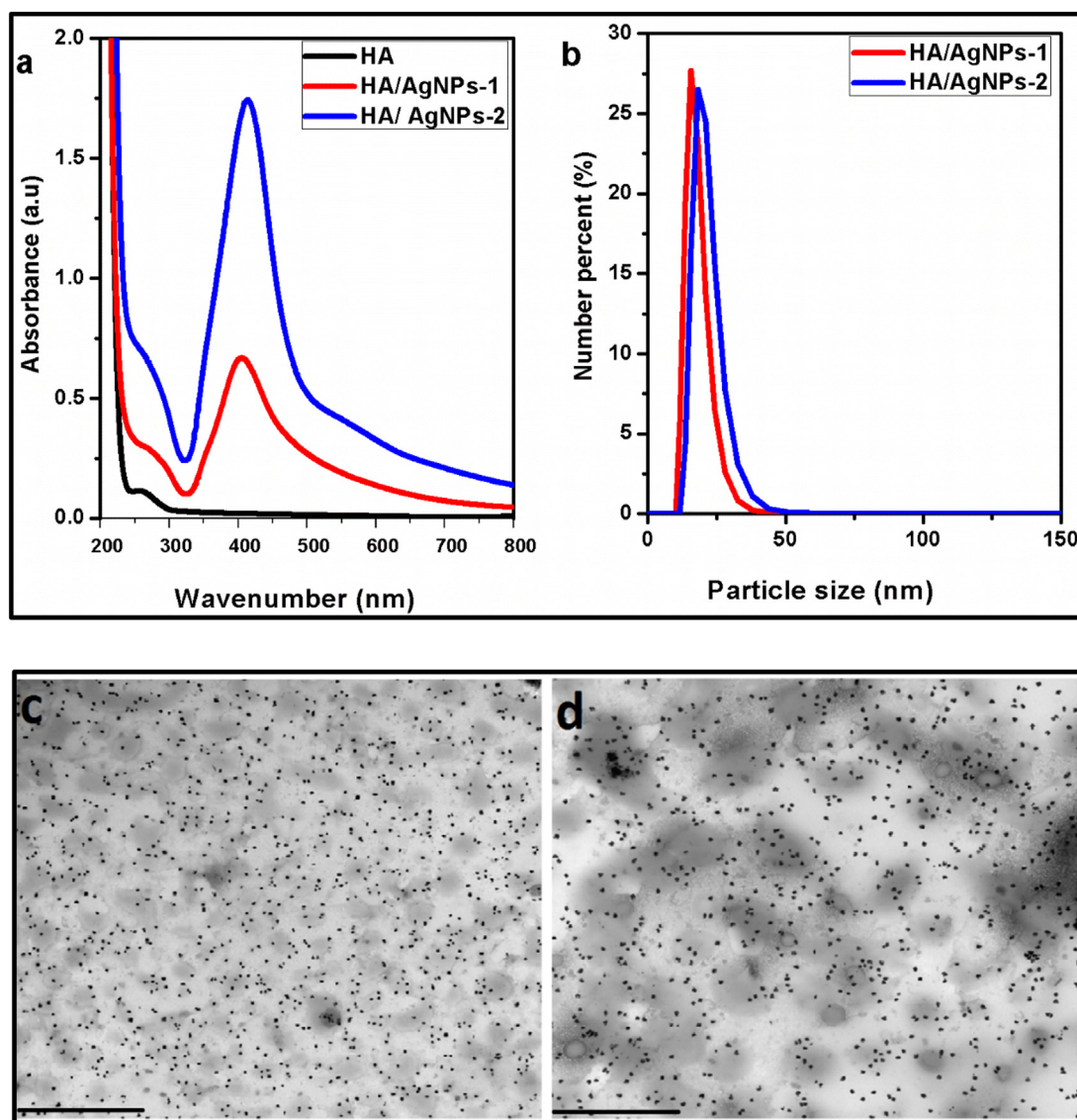

Fig. 1. UV/Vis spectra of plain HA and HA/Ag-NPs-1 mg and HA/Ag-NPs-2 mg (a); DLS of HA/Ag-NPs-1 mg and HA/Ag-NPs-2 mg (b), TEM of HA/Ag-NPs-1 mg (c); TEM of HA/Ag-NPs-2 mg (d); scale bars = 1 μm.

textiles and certain instill for the treatment of burns wounds, as a water disinfectant, and in air-freshener sprays (Sun et al., 2013; Zanette et al., 2011). Recent evidence suggests that Ag-NPs have potentially anti-inflammatory effects and contributes to accelerate wound healing (Banti and Hadjikakou, 2013; Lin et al., 2013; Roy and Banerjee, 2011; Thunus et al., 1995). Skin wound healing proceeds through a cascade of events including different processing steps like coagulation, inflammation, proliferation, matrix and tissue remodeling. The ultimate goal for wound healing is a speedy recovery with minimal scarring and maximum function recovery (Ferreira et al., 2013; Lu et al., 2012; Pal et al., 2014). Hyaluronan fibers with silver nanoparticles were prepared by post treatment technique (Abdel-Mohsen et al., 2012c). The Ag-NPs are completely not interact with hyaluronan functional groups and may be on the surface of the fibers (Abdel-Mohsen et al., 2013, 2012c). In the present work, silver nanoparticles are prepared by *in situ* way for the first time using sodium hyaluronate then the bio-

nanocomposite are used for preparation of fibers/fabrics from the newly composite material. In this study we use the *in situ* way to synthesis Ag-NPs with a view to enhance the physical, thermal, mechanical and biological properties of the newly wound dressing mats for tissue engineering applications. Different wound dressing materials (Abdel-Mohsen et al., 2016; Aly et al., 2011; Barnea et al., 2010; Huang et al., 2014; Li et al., 2015; Pei et al., 2015; Pyun et al., 2015; Singaravelu et al., 2016; Trivedi et al., 2014) that used for wound/chronic ulcer dressing applications are prepared using different biomaterials such as chitosan (Levi-Polyachenko et al., 2016), alginate (Bowler and Parsons, 2016; Li et al., 2016), cellulose (Gustaite et al., 2015), hyaluronan (Abdel-Rahman et al., 2016; Mogoşanu and Grumezescu, 2014), Pullulan (Priya et al., 2016), collagen (Silcock, 2010) and gelatin (Yoon et al., 2016).

In this paper, a new wound dressing material are fabricated from hyaluronan/silver bio-nanocomposite fabrics, in which the Ag-NPs are synthesized by an *in-situ* method. The novel mats are
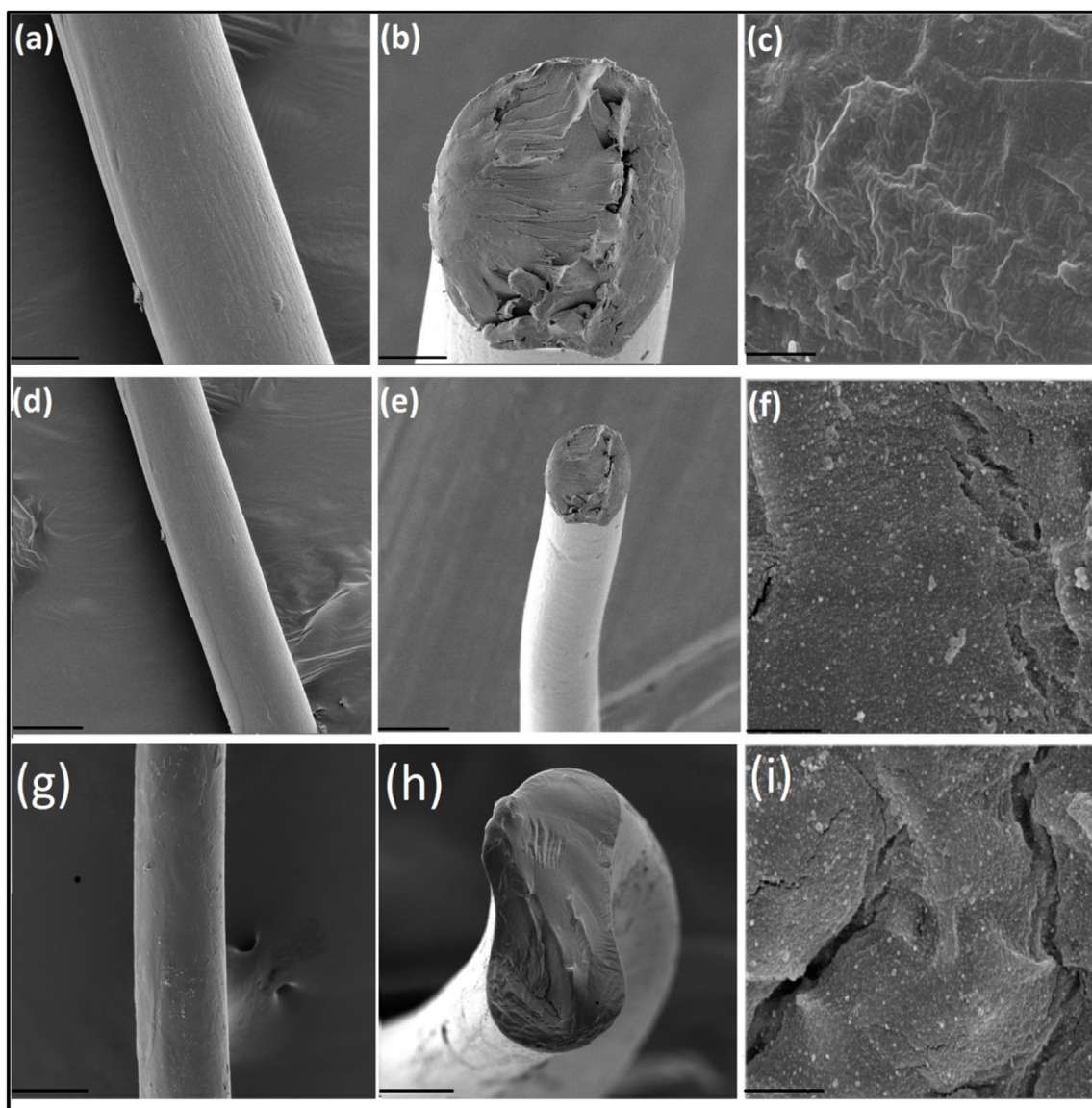

Fig. 2. Scanning electron micrographs of plain HA fibers (a); cross-section of HA fibers (b); HA fibers at high magnification (c); HA/Ag-NPs-1 mg fiber; (d); cross-section of HA/Ag-NPs-1 mg fiber (e); HA/Ag-NPs-1 mg fiber at high magnification (f); HA/Ag-NPs-2 mg fiber; (d); cross-section of HA/Ag-NPs-2 mg fiber (e); HA/Ag-NPs-2 mg fiber at high magnification. Scale bars for a, d, g (100 μm); b, e, h (50 μm), and c, f, i (2 μm).
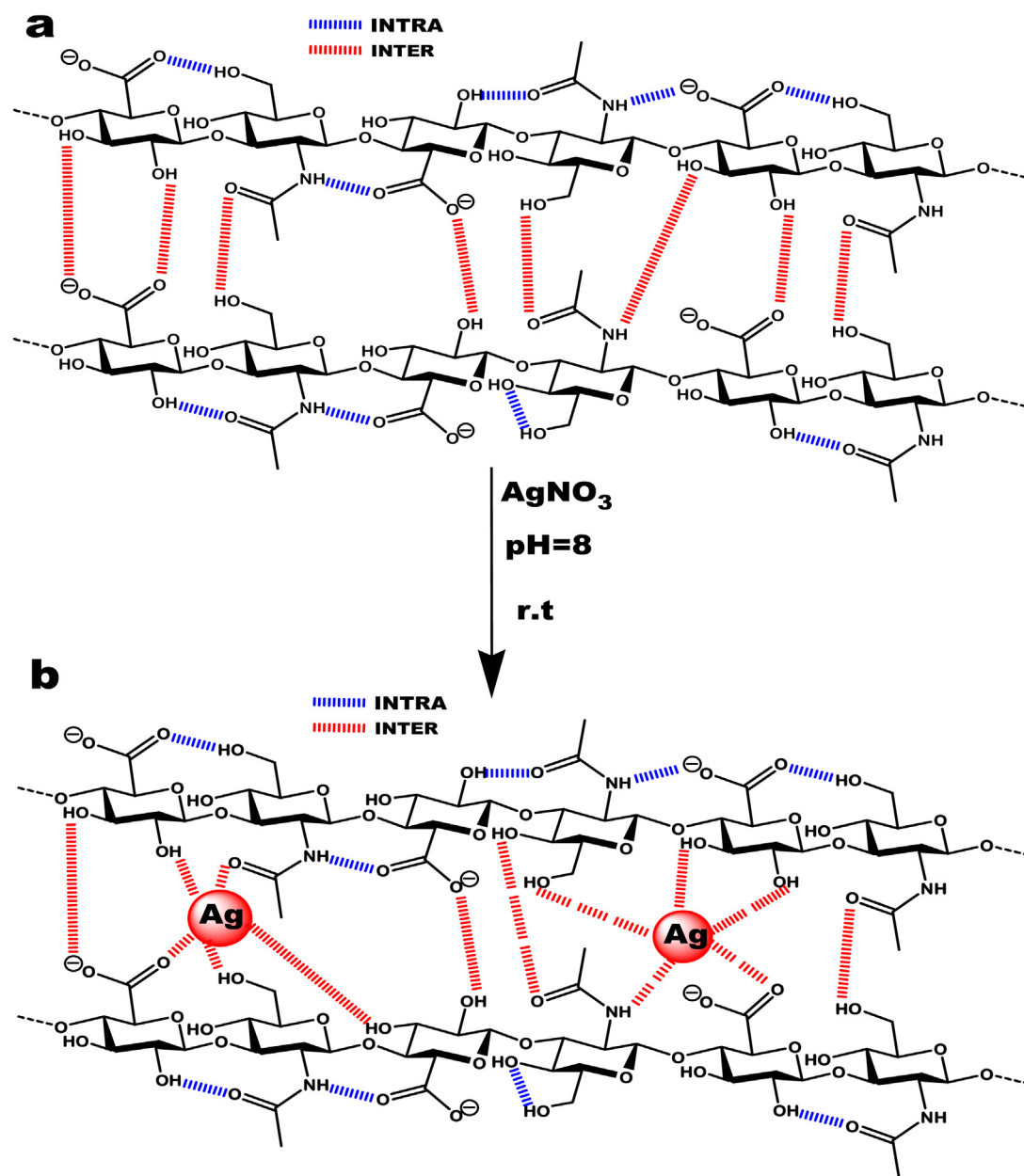
Fig. 3. Intra/intermolecular hydrogen bonds between hyaluronan chains (a); proposed interaction mechanism between hyaluronan functional groups and silver nanoparticles (b).

fabricated by wet-dry-spinning technique. Chemical structure, mechanical properties and biological activity of the new materials are characterized and analyzed.

2. Experimental

2.1. Materials

Sodium hyaluronate with molecular weight of 700–900 kDa was purchased from CPN Ltd., (Czech Republic), sodium hydroxide, acetic acid, isopropyl alcohol were purchased from Lach-Ner (Czech Republic) and silver nitrate was obtained from Sigma-Aldrich (Germany). Demineralized water was used for all the experiments.

2.2. Methods

2.2.1. In-situ *preparation of silver/hyaluronan nanoparticles composite fiber*

Hyaluronan/silver nanocomposite (HA/Ag-NPs) with different Ag nanoparticles contents were synthesized with no external reducing or stabilizing agents. Sodium hyaluronate was used as the reducing and capping agents at the same time. 40 mg of sodium hyaluronate (HA) molecular weight 700–900 kDa was dissolved under stirring in 1 ml of demineralized water into homogenous, viscous solution of suitable for wet-spinning. Silver nitrate solutions (1 and 2 mg) were added independently drop-wise into hyaluronan solution (1 ml) under stirring at room temperature for 1 h. Then, the pH was increased close to pH = 8 by adding few drops
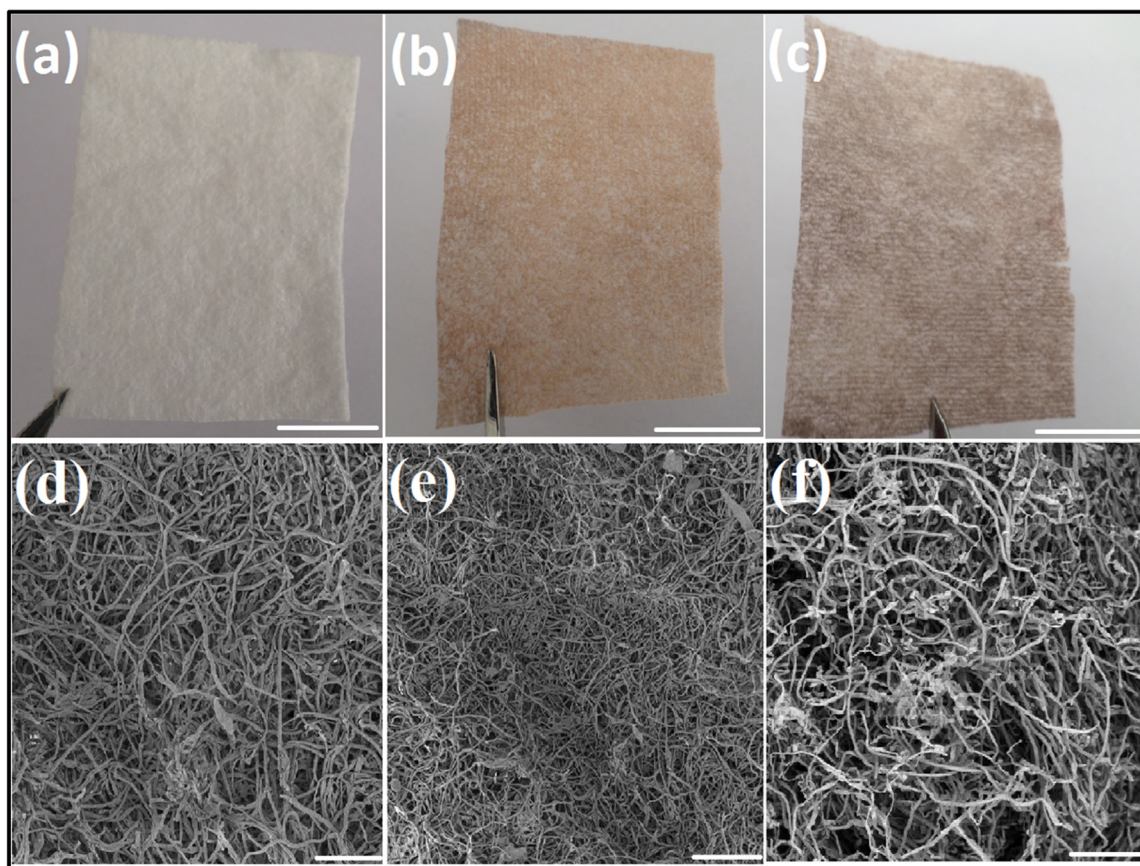
Fig. 4. Visualized photograph of hyaluronan fabrics sheet (a); nonwoven HA/Ag-NPs-1 mg fabrics (b); HA/Ag-NPs-2 mg fabrics (c); SEM of nonwoven HA fabrics sheet (d); nonwoven HA/Ag-NPs-1 mg fabrics (e); nonwoven HA/Ag-NPs-1 mg fabrics (f). Scale bars (a, b, c) were 1 cm and for (d–f) were 50 μm.

of sodium hydroxide (1 M), keep the total volume 100 ml (4 wt.% HA, 0.001% 0.002% Ag⁺). The HA/Ag-NPs solution acquired a clear yellow color indicating formation of silver nanoparticles (Chen et al., 2015; Pauksch et al., 2014; Raza et al., 2015). This solution was extruded through a nozzle with the needle diameter of 0.2 mm to the coagulation bath composed of acetic acid (99.9%)/absolute isopropyl alcohol solvent mixture (30/70; v/v) obtained HA fibers with 30 cm length. The prepared fibers were kept in the coagulation bath to solidify for approximately 0.3 to 15 h. Then, fibers were washed with isopropyl alcohol and air dried. Unmodified neat hyaluronan fibers were prepared employing the same process as described above.

2.2.2. Preparation of wound dressing sheet

After preparation of neat hyaluronan and hyaluronan/Ag⁰ nanoparticle composite (HA/Ag-NPs) fibers, the fibers were removed from the coagulation bath and kept for 1 h in isopropyl alcohol for solidification under fast stirring under mechanical stirrer (2000 rpm/min), then, cut into short fibers using vortex mixer for 5 min. The short fibers were collected and filtered with Buchner funnel, dried at 40 °C for 20 min. To remove the residual isopropyl alcohol, the HA and HA/Ag-NPs nonwoven sheets (200 μm length) were placed in a fume hood for 24 h.

2.3. Physical characterization

Ultraviolet/visible (UV/Vis) spectroscopy measurement was carried out using the UV-160A, (Shimadzu, Japan) equipped with quartz cuvettes with an optical path of 1 cm. The concentration of the measured solutions was kept constant at 1 mg ml⁻¹. The UV/vis

spectra were collected at room temperature (25 ± 2 °C). Transmission electron microscope (TEM) investigations were performed employing the JEOL JEM-2010 (HT) electron microscope (JEOL, Japan), with the accelerating voltage of 150 kV. The samples were dissolved in demineralized water with concentration of 0.5 mg/ml, and a drop was placed on Cu grids pre-coated with carbon films and air dried. Dynamic light scattering measurement was performed utilizing Malvern Zetasizer Nano ZS (Malvern, USA). The samples were filtered using a 0.45 μm nylon syringe filter directly into a poly acrylic cell.

X-ray diffraction was measured at 3 kW diffractometer Smart lab from Rigaku using Cu Kα radiation (λ = 1.54 Å) and detector Dtex Ultra with Bragg-Brentano geometry. Diffraction angle 2-Theta was measured in range from 10° to 90° with step size 0.02° at speed 4°/min. Generator was operated at current 30 mA and voltage 40 kV. Instron 3343 universal tensile testing machine (Instron, USA), pre-tensioned to 0.05 N was used to determine mechanical properties. Cross head speed of 30 mm/min was used. Fabrics were kept at 24 °C and relative humidity of 30% for 1 h. Fabrics were cut into a 5 cm long pieces and axially mounted in the testing jaws of Inston 3343. The fabrics were pre-loaded to 0.05 N (Abdel-Mohsen et al., 2012c; Baker et al., 2016; Zivanovic et al., 2007) followed by constant cross head speed of 30 mm/min tensile deformation until their break. Each measurement was repeated five times and average value and standard deviation was determined.

2.3.1. In vitro and in vivo measurements

Human keratinocyte cell line (HaCaT) was isolated from skin removed during a cosmetic plastic surgery. The samples were
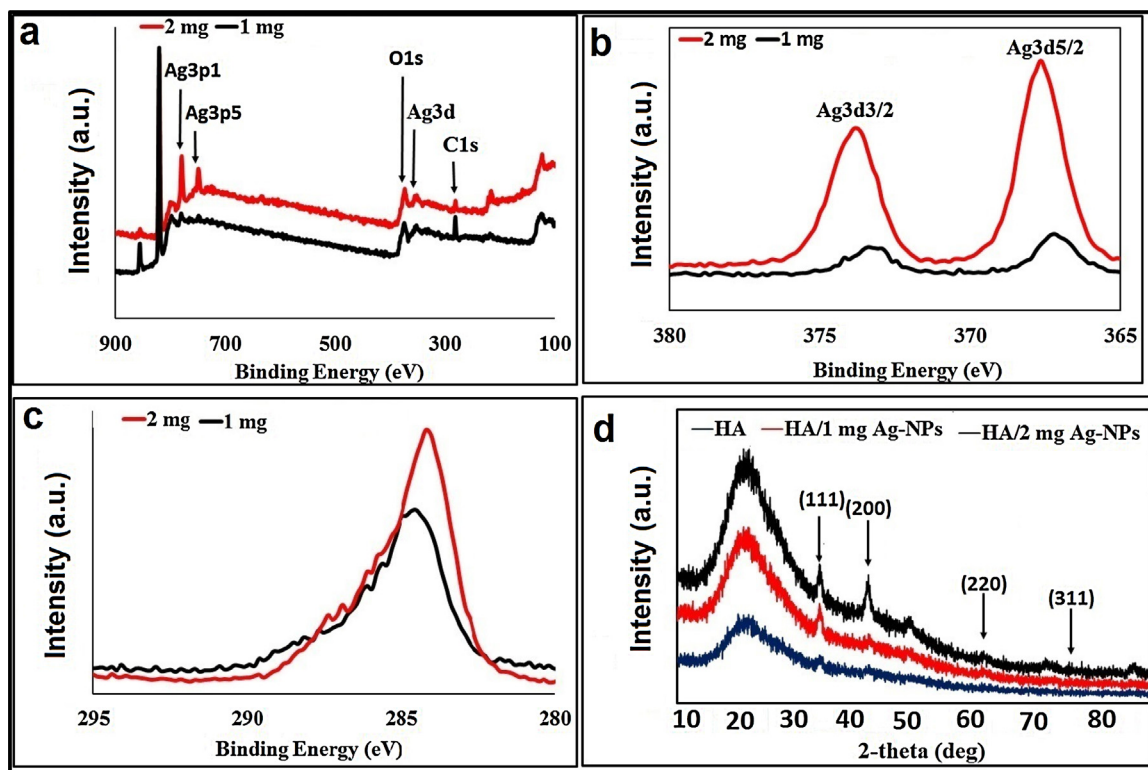
Fig. 5. XPS spectra of HA/Ag-NPs-1 mg and HA/Ag-NPs-2 mg (a); high-resolution Ag3d spectra of HA/Ag-NPs-1 mg and HA/Ag-NPs-2 mg (b); high-resolution C1s spectra of HA/Ag-NPs-1 mg and HA/Ag-NPs-2 mg (c); XRD diffraction patterns of plain HA and HA/Ag-NPs-1 mg and HA/Ag-NPs-2 mg (d).

obtained with informed consent and institutional approval. Keratinocyte cultures were prepared according to the method described previously (Rheinwatd and Green, 1975). Approximately 4000 *HaCaT* cells were seeded to 96-well test plates. The cells were cultured for 24 h before treatment with the cell prepared solution. The tested solution was added to each well so that the final concentration of the tested solution in the well was 1000 μg/mL by diluent medium. Cytotoxicity was measured after 0, 24, 48, 72 h after the treatment with 3-(4.5-dimethylthiazol-2-yl)-2.5-diphenyl tetrazolium bromide assay. MTT assay was described in the previously work (Abdel-Mohsen et al., 2014; Vistejnova et al., 2009). MTT stock solutions were added to the cell culture medium/ plates were incubated at 37 °C for 2.5 h. The supernatant was discarded and cells were lysed in lysis solution for 30 min on a shaker. The optical density was measured in 96-well plate by the Versamax micro-plate reader (Molecular devices, USA) at the wavelength of 570 nm. The *HaCaT* was grown in the 3-(4.5-dimethylthiazol-2-yl)-2.5-diphenyl tetrazolium supplemented with 10% phosphate buffer solution, glutamine, and gentamycin in 5% carbon dioxide at 37 °C. Plain hyaluronan fabrics and hyaluronan/silver nanocomposite fabrics (HA/Ag-NPs-1 mg, HA/Ag-NPs-2 mg) were prepared to obtain concentrations 1000 μg ml^{-1}. The experiments were carried out at least in six independent repeats.

Genetically modified *E. coli* K-12 capable of bioluminescence were exposed to cellulose derivatives which led to the reduction of bacterial viability visualized by real time bioluminescence measurement. Concentrated stock suspension of bacteria was prepared and stored at −80 °C (Atosuo et al., 2013). Final concentration of bacterial cells in the applied suspension was set to approximately 380 000 cells per 100 μl. 200 μl of this suspension was mixed with 5, 10 or 15 mg of plain HA and/or HA/

Ag-NPs-1 mg nonwoven fabrics were suspended in 100 μl of the phosphate buffer. Light (490 nm) was generated by enzymatic reaction in bioluminescent bacteria and measured continuously during 90 min by luminometer LM-01T (Immunotech, Czech Republic) at laboratory temperature. Results are expressed in relative light units (RLU). An average integral, area under the kinetic curve was compared to control and the percentage of bacterial extinction was calculated. Experiments were repeated independently three times. The reduction percent (%; Table S1) of bacteria was calculated from the following Eq. (1).

$$\text{Reduction percent } (\%) = \frac{A - B}{A} \times 100 \tag{1}$$

Where, A was the number of viable number of microorganisms without treatment; B was the viable number of microorganisms after treatment.

Heparinized (50 IU/ml) blood samples were obtained from healthy volunteers with a given informed consent. The number of leukocytes in the blood and their relative differentiation counts were determined using Coulter counter STKS (Coulter, England) and stained blood smears, respectively. Luminol-enhanced CL of the blood phagocytes was measured using a microplate luminometer LM-01T (Immunotech, Czech Republic) as described previously (Atosuo et al., 2013). The assays were run in duplicates. Samples contained 10 ml of the whole blood, luminol and zymosane as the activator of phagocytosis in case of activated chemiluminescence or buffer in case of spontaneous chemiluminescence. The CL emission expressed as relative light units (RLU) was recorded continuously for 90 min at 37 °C.

The wound healing efficacy of various as-prepared nonwoven fabrics sheets as well as the control (non-diabetics, diabetics) samples were evaluated using a rat model. Male Wister rats were
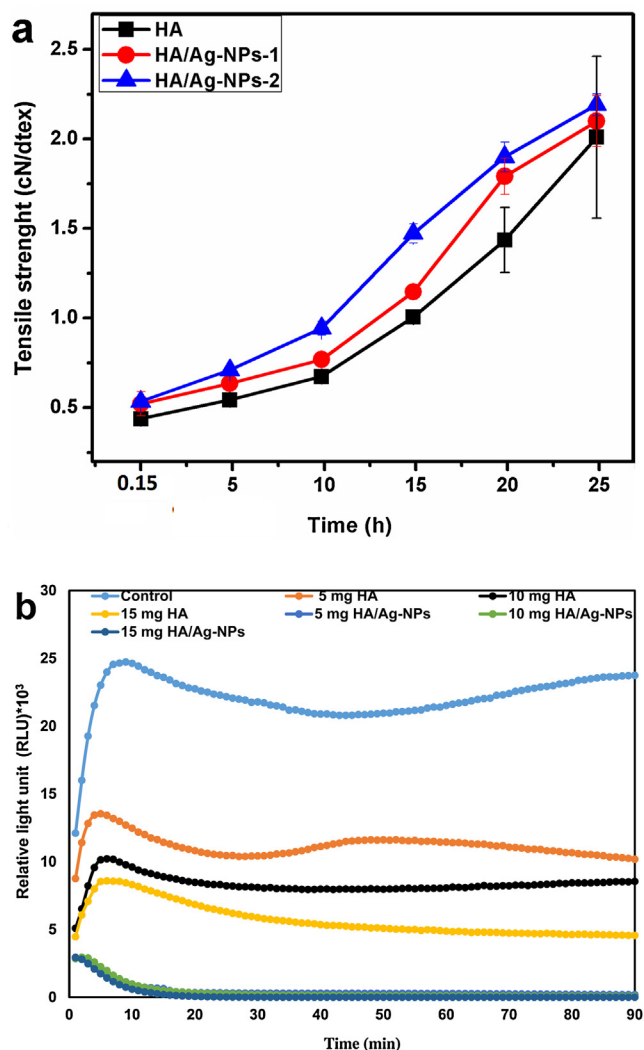
Where, A_{0-} wound area at day 0, Ax wound area at specified time of surgery, respectively.

Excised wound sites fixed in 10 % neutral buffer formalin were processed routinely (dehydration in ascending alcohol series, clearing in xylol, embedded in paraffin wax, and cutting into 4 μm thickness). Sections were dewaxed, rehydrated, and stained with hematoxylin and eosin. The stained samples were examined using Olympus light microscope and photographed at 20×

Fig. 6. (a) Tensile strength and (b) antibacterial activity of wound dressing. Effect of coagulation time on tensile strength of plain HA, HA/Ag-NPs–1 mg, and HA/Ag-NPs–2 mg fibers; SD ± 5 (a). Different concentrations (5, 10 and 15 mg; n = 3) of plain HA nonwoven fabrics and HA/Ag-NPs–1 mg nonwoven mats compared to control sample against gram negative bacteria (E.coli K12) (b).

used divided into six groups (n = 5): first group (untreated non-diabetic healthy control); group two (untreated diabetic health control); group three (treated non-diabetic with plain HA dressing fabrics); group four (treated non-diabetic sample with plain HA/Ag-NPs-2 mg dressing); group five (treated diabetic sample with plain HA dressing fabrics); group six (treated diabetic sample with plain HA/Ag-NPs-2 mg dressing fabrics). A wound was made on the back of each animal. Five animals from each group were sacrificed on the 0st, 5th, 10th and 15th days. In each rat, the healing wound area was measured. The results obtained from the samples taken on the third, tenth, and fifteen days after wounding evaluated and presented decrease of the wound area when compared with untreated rats. After the experiment, rats were kept in separate cages. On 5th, and 15th postoperative days and the wound was photographed. The wound area was measured by outlining the wound area. New dressings were applied to the wound sites after they were cleaned with normal saline solution. The rate of wound closure was determined by the following Eq. (2).

Degree of wound contraction $(\%) = \dfrac{A_0 - Ax}{A_0} \times 100$ (2)
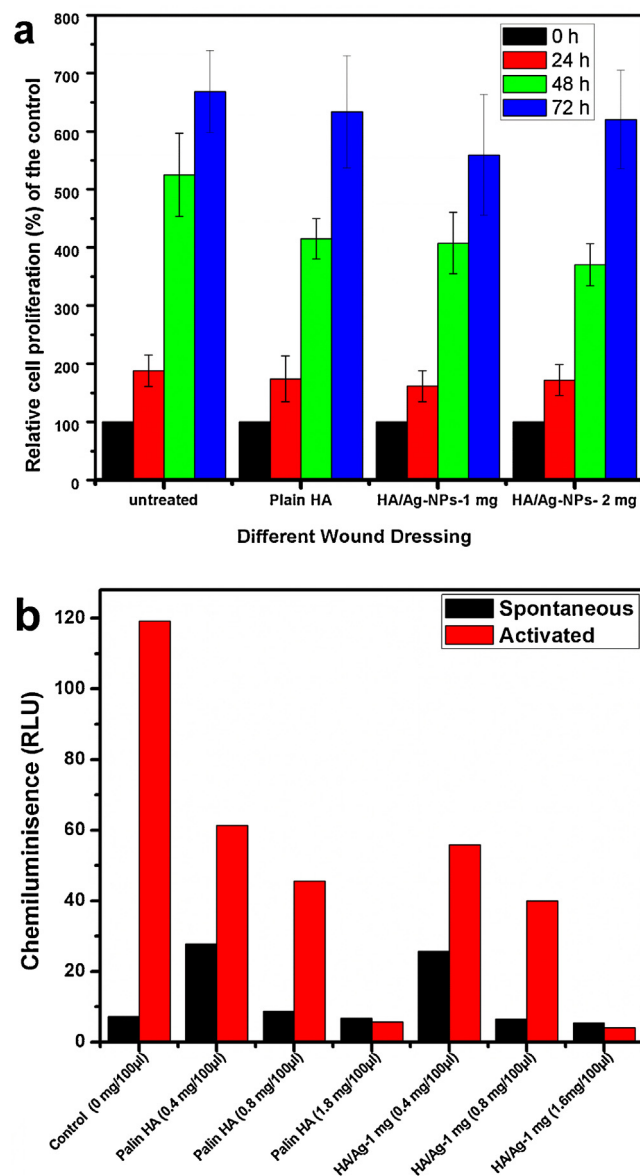
Fig. 7. (a) Cytotoxicity and (b) phagocytes of wound dressing. Cytotoxicity of wound dressing nonwoven mats against keratinocytes cell line. Plain hyaluronan fabrics (HA), hyaluronan/silver nanoparticles (HA-Ag-NPs-1 mg) nonwoven fabrics and hyaluronan/silver nanoparticles (HA-Ag-NPs-2 mg) nonwoven fabrics on the keratinocytes cell line (*HaCaT*), cell viability was measured at 0-72 h. Plain HA dressing (1000 μg/ml), *HaCaT* viability, MTT assay; HA/Ag-NPs-1 mg (1000 μg/ml); *HaCaT* viability, MTT assay; HA/Ag-NPs-2 mg wound dressing (1000 μg/ml); *HaCaT* viability, MTT assay, (n=6). The data were expressed as mean ± SEM (n= 6) **(a)**. Influence of plain hyaluronan and hyaluronan/silver nanoparticles nonwoven mats (HA-Ag-NPs-2 mg) on the spontaneous and zymosan-activated oxidative burst of blood phagocytes. Oxidative burst of phagocytes was analyzed chemiluminome-trically. Light emission expressed as relative light units (RLU) was recorded continuously for 90 min at 37°C and corrected to the number of polymorphonuclear cells **(b)**.
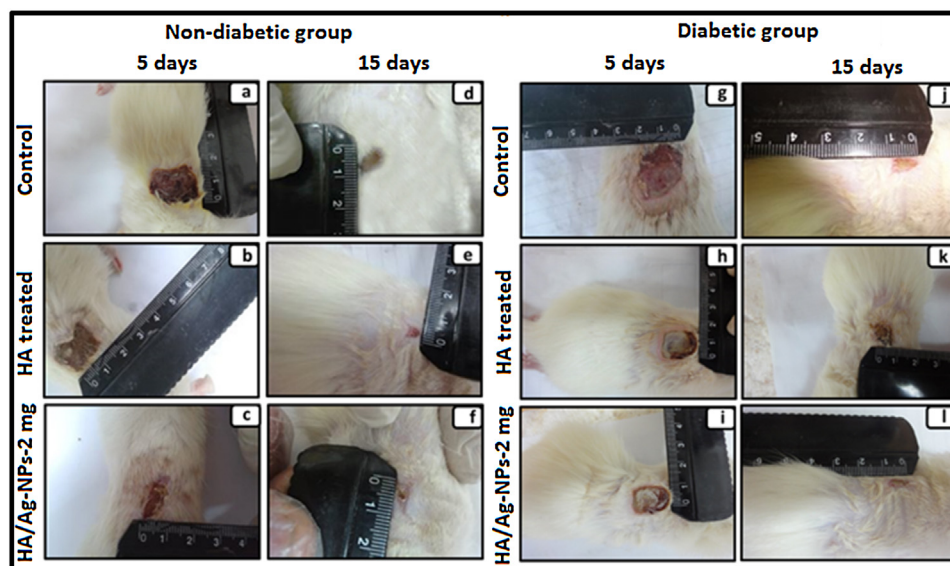
Fig. 8. Photograph of skin rat's observation of the healing treated with HA and HA/Ag-NPs wound dressing mats. Representative photographs of the macroscopic appearance of a 20 mm × 20 mm cutaneous wound created on non-diabetic (left), control (a–d), plain HA wound dressing mats treated (b–e), and HA/Ag-NPs-1 mg wound dressing mats treated (c–f) groups; diabetic (right) control (g–j), HA nonwoven mats treated (h–k), and HA/Ag-NPs-2 mg treated (i–l) groups; on days 5 and 15 post surgery. Note; the complete healing of the HA/Ag-NPs-2 mg treated groups compared with HA wound dressing mats treated and untreated groups. Each group of figures were representative of five rats at each time point.

magnification. All experiments were carried out at least in three to four independent repeats. All animals procedures were carried out in accordance with the Ethics Committee of the National Research Centre (Egypt) confirmed to the "Guide for the care and use of Laboratory Animals" published by the US National Institutes of Health.

3. Results and discussion

3.1. In-situ preparation of Ag-NPs

In-situ silver nanoparticles were prepared for the first time employing a chemically-friendly process. Medium molecular weight sodium hyaluronate was used as capping and stabilizing agent for *in-situ* Ag-NPs preparation. No toxic external reducing agents such as sodium borohydride, hydrazine hydrate, *N,N*-dimethyl formamide *etc.*, (Du et al., 2015; Murphy et al., 1991; Pastoriza-Santos and Liz-Marzán, 2002; Tatarchuk et al., 2013; Van Hyning and Zukoski, 1998) were used in our study, that could be the source of potential biological hazard which used for the preparation of the Ag-NPs. The pH of the reaction mixture was raised to 8 by using sodium hydroxide solution (1 M). 1 and 2 mg of silver nitrate solutions were added to 40 mg of well-dissolved hyaluronan in water, at room temperature ($25 \pm 2\,^{\circ}$C) under mechanical stirring for 1 h. The color of the reaction mixture was changed from colorless to yellowish color that confirmed the formation of *in-situ* Ag-NPs. Fig. 1a showed the UV/vis absorption spectra of plain hyaluronan (HA) and various HA/Ag-NPs blends with different Ag^0 concentrations (1, 2 mg). The plain hyaluronan solution had one UV/vis absorption peak it was observed at 250 nm corresponded to the C=O of carboxylic and acetamide groups of hyaluronan chains. *In-situ* silver nanoparticles lead to absorption peak appeared at 420 nm and the intensity increased with increasing the concentration of Ag^0. The absorption peak of Ag^0 was attributed to surface plasmon resonance of the colloidal silver (Abdel-Mohsen et al., 2014; Chen et al., 2015; Mohiti-Asli et al., 2014; Pauksch et al., 2014), which indicated that the silver in HA/Ag

nanocomposite exists in the form of nanoparticles. The average size of Ag-NPs increased from 20 ± 2 to 25 ± 2 nm when the silver concentration increased from 1 to 2 mg, respectively (Fig. 1b). Transmission electron microscope (TEM) observation of the HA/Ag-NPs (Fig. 1c, d) revealed that the Ag-NPs were homogenously and uniformly distributed without agglomerations. This could be associated with the fact that hyaluronan fibers act as carrier for silver nanoparticles and, in so doing, prevent the nanoparticles from aggregations and agglomerations thereby retaining uniform and homogenous size.

The functional fibers/fabrics were synthesized by wet-dry-spinning technique (WDST) in the biologically benign hyaluronan/water/silver nitrate/sodium hydroxide system. The coagulation bath byproduct was mainly sodium acetate and sodium chloride. Therefore, this bath procedure was a green bio-friendly technology. The HA/Ag-NPs nanoparticles composite were injected into the syringe pump machine connected with the 0.2 μm diameter needle and the edge of needle was kept 1 cm above the coagulation solvent bath. The coagulation bath contained acetic acid/isopropyl as solidifying agents with solvent ratio (30/70 v/v). The obtained fibers were removed from the coagulation bath after 0.3 to15 h and washed three times with isopropyl alcohol (each 1 h) until neutralization, then air dried at room temperature ($25 \pm 2\,^{\circ}$C).

Fig. 2 presents the scanning electron micrographs (SEM) of plain hyaluronan fibers and hyaluronan/silver fiber with different content of Ag^0. Surface morphology of the plain HA fiber (Fig. 2a–c) exhibits a uniform cross section shape without any surface defects. Fig. 2(d) depicts the SEM micrograph of *in-situ* hyaluronan/silver nanoparticles composite fiber (1 mg). Homogenous surfaces and uniform shape were maintained even for the HA/Ag-NPs fiber (Fig. 2e). At higher magnification (Fig. 2f) the particles of silver appeared at the fracture surface of the fibers without exhibiting any agglomeration of the Ag particles. Fig. 2(g–i) explores the surface morphology of hyaluronan/silver nanoparticles with higher content of silver (HA/Ag-NPs–2 mg), showing no significant difference between the HA/Ag-NPs–1 mg and HA/Ag-NPS–2 mg fiber morphology. Observations documented by Figs. 2 and 3 (a, b)
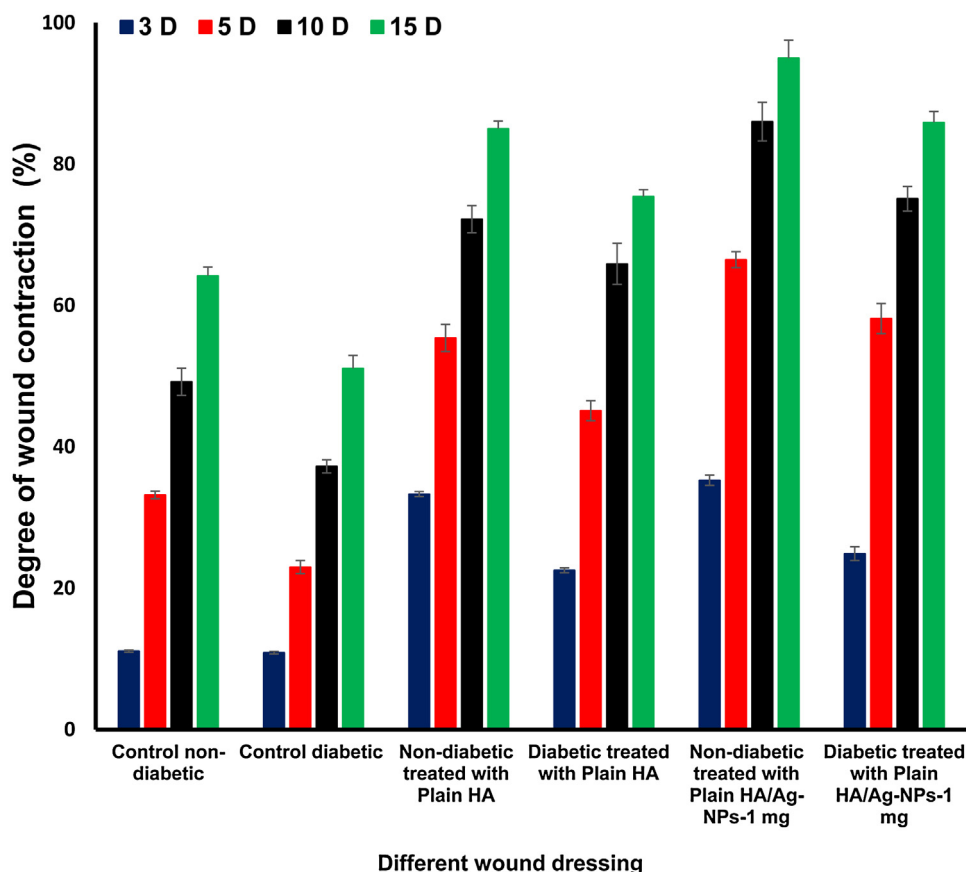
Fig. 9. Wound area closure percentage as a function of postoperative time.

provide solid proof that the hyaluronan acted as stabilizing and capping agent effectively preventing the agglomeration of silver nanoparticles.

Fig. 3(a) shows schematically the inter/intra hydrogen bonds between hyaluronan chains, due to raised/decreased/raised pH of the reaction mixture, the inter/intra hydrogen bonds between the HA chains were destroyed/generated spontaneously (Morris et al., 1980). Silver nanoparticles were interconnected with functional groups of hyaluronan (hydroxyl, carboxyl, acetamide, and partially amino groups) chemically or physically bonded (Fig. 3b). The silver nanoparticles were electrostatically shielded by the hyaluronan groups (Gribbon et al., 1999). Silver nanoparticles acted as cross-linking agents between the hyaluronan chains keeping the helical structure of hyaluronic acid molecule (Almond et al., 1997; Blundell et al., 2006; Sheehan et al., 1977; Winter et al., 1975; Wu et al., 2013).

Fig. 4 shows visualized photographs of nonwoven sheet and SEM of hyaluronan fabrics with/without silver nanoparticles. Comparing between the SEM of monofilament (Fig. 2a–c) and visualized/SEM of short nonwoven HA fiber (Fig. 4a, d), the latter was shorter and thinner diameter than HA fibers. This was due to the highest and fast stirring, the HA/Ag-NPs fibers were well dispersed in the coagulation bath and, they preventing the fibers sticking to each other meanwhile, results in solidification. Fig. 4(b, e) shows that the HA/Ag-NPs-1 mg fabrics, the silver nanoparticles were well dispersed and well homogenized in hyaluronan fabrics with yellowish/brown color sheet. Comparing the diameters of HA/Ag-NPs-1 *mg* (Fig. 4b,e) sheet and HA/Ag-NPs-1 mg monofilaments (Fig. 2d–f), the fiber sheet was more thin and shorter than the

monofilament, due to fast stirring during the preparation step which prevented the adhesive of fibers together. Fig. 4(c, f) explores the visualized photograph of HA/Ag-NPs-2 mg and SEM of HA/Ag-NPs-2 mg, respectively. It was clear that, the Ag^0 was well dispersed into hyaluronan matrix without aggregation (Fig. 1b) with yellowish/brown color. From Fig. 4, the plain HA and HA/Ag-NPs with different forms (colloids, monofilaments, and nonwoven fabrics mats) could prepared by green and environmental safe technology.

The XPS spectra of Ag-NPs interconnected with HA fabrics provided further information about the structure of the chemical interactions between functional groups of HA and Ag-NPs. Fig. 5(a) shows the overall XPS spectra of various silver/hyaluronan nanocomposite fabrics and Fig. 5(b) shows the high-resolution of Ag3d peak apparently composed of two different peaks at 368.64 and 374.55 eV, corresponding to Ag3d5/2 and Ag3d3/2, respectively, indicated the formation of silver nanoparticles (Fan et al., 2014; Suh et al., 2006; Thiel et al., 2007; Woehl et al., 2014). The high-resolution of C1s (Fig. 5c) peaks of carbon-oxygen bonds increases dramatically with increasing the silver content, which indicated that hyaluronan interacting with silver. This data provided solid evidence for the proposed mechanism of HA/Ag-NPs interaction (Fig. 3a, b). XRD of plain HA and HA/Ag-NPs nonwoven sheet were shown in Fig. 5(d). Hyaluronan fabrics were shown only broad peak around 2-theta = 15–30° (Fig. 5d). HA/Ag-NPs–1 mg and HA/Ag-NPs–2 mg nonwoven sheets clearly showed four different peaks appeared at 39.2, 44.5, 65.2, and 77.8° and corresponded to (111), (200), (220) and (311) diffractions of metallic silver nanoparticles (Abdel-Mohsen et al., 2014, 2012b;

Maillard et al., 2003; Nocchetti et al., 2013; Wiley et al., 2005). The intensity of Ag-NPs peaks were increased with the content of Ag^0 (Fig. 5d).

Fig. 6(a) shows the effect of the coagulation time on then relative tensile strength of plain HA and HA/Ag-NPs fabrics with different concentration of Ag-NPs solidified in the acetic acid/isopropyl alcohol solvent. The tensile strength was proportional to the coagulation time, increased with time from 0.15 to 25 h as shown in Fig. 6(a) after 25 h of immersed the plain and fabrics with silver nanoparticles different contents, the tensile strength was increased to 1.92, 2.1 and 2.25 cN/dtex for HA and HA/Ag-NPs-1 mg and HA/Ag-NPs-2 mg, respectively. This improvement in mechanical properties of the fabrics due to the silver nanoparticles (Ag-NPs) act as cross-linker agent between hyaluronan chains chemically/physically interactions.

Bacteria colonize essentially all chronic ulcers, and result in an infection effectively hindering the healing process. Topical antimicrobial agents are used clinically on a variety of infected wounds and ulcers and the object of their use is the control of microbial proliferation (Liakos et al., 2015; Lipsky and Hoey, 2009). Here, the antibacterial activity of silver nanoparticles was investigated using *Escherichia coli* K12 strain (Fig. 6b). Plain HA nonwoven fabrics exhibit moderate antibacterial activity against *E. coli* K12 bacteria, (Supporting Table 1S). This moderate activity of HA fabrics may be caused by the partial deacetylation of hyaluronan during fiber preparation generating free amino groups which can interact with negative charges on the surface of bacteria (Abdel-Mohsen et al., 2012a, 2012b). Fig. 6(b) shows the antibacterial activity of HA/Ag-NPs- 1 mg with average NP diameter of (20 ± 2) nm (Fig. 1c; Supporting Table 1S). The presence of silver nanoparticles (Ag-NPs) increased the bactericidal activity compared to HA substantially (Supporting Table 1). The mechanism of antibacterial activity of silver in HA/Ag-NPs composite fibers particles against bacteria is not well understood.

The antibacterial activity is probably caused by the electrostatic attraction between negatively charged cell membrane of microorganism and positively charged nanoparticles (Liakos et al., 2015; Liu et al., 2012). The bactericidal effect of silver inhibits the protein synthesis inside the cell, inhibits the metabolic pathway and interferes with nucleic acid synthesis (Abdel-Mohsen et al., 2014, 2012a; Fan et al., 2014; Govindan et al., 2012; Lin et al., 2013; Loza et al., 2014; Schneid et al., 2014; Zanette et al., 2011). HA/Ag-NPs-1 mg nanocomposite fabrics exhibit enhanced antibacterial activity also due to large contact area with bacteria (Fig. 6b). All these combined beneficial qualities, make the prepared hyaluronan/silver nanoparticle composites suitable candidates for use as wound and chronic ulcer dressing.

3.2. Cytotoxicity of nonwoven fabrics mats

Because of their antibacterial activity, biocompatibility of the HA/Ag-NP fibers was another important issue in testing the feasibility of their wound and ulcer dressing applications. Fig. 7(a) presents the cytotoxicity of plain HA fabrics and HA/Ag-NPs with different concentrations (1 mg, 2 mg) nonwoven fabrics. Plain HA fabrics were non-toxic and the viability of keratinocytes cell line with concentration 1000 µg after 27 h of seeding with keratinocytes cell line (*HaCaT*). *In-situ* synthesized silver nanoparticles/hyaluronan nonwoven fabrics with different concentrations of Ag^0 (1 mg, 2 mg) was seeded with *HaCaT* cell for 3 days (Fig. 7a). Interestingly, both HA/Ag-NPs-1 mg and HA/Ag-NPs–2 mg were non-cytotoxic against *HaCaT* and compared with control sample. The results conclude that both plain HA and HA/Ag-NPs (1 mg, 2 mg) nonwoven fabrics didn't show any cytotoxicity (Fig. 7a).

Effective wound healing requires a highly organized series of events that include inflammation, re-epithelialization, keratinocyte proliferation, matrix deposition, angiogenesis, and wound contraction (Chen and Abatangelo, 1999). At low concentration
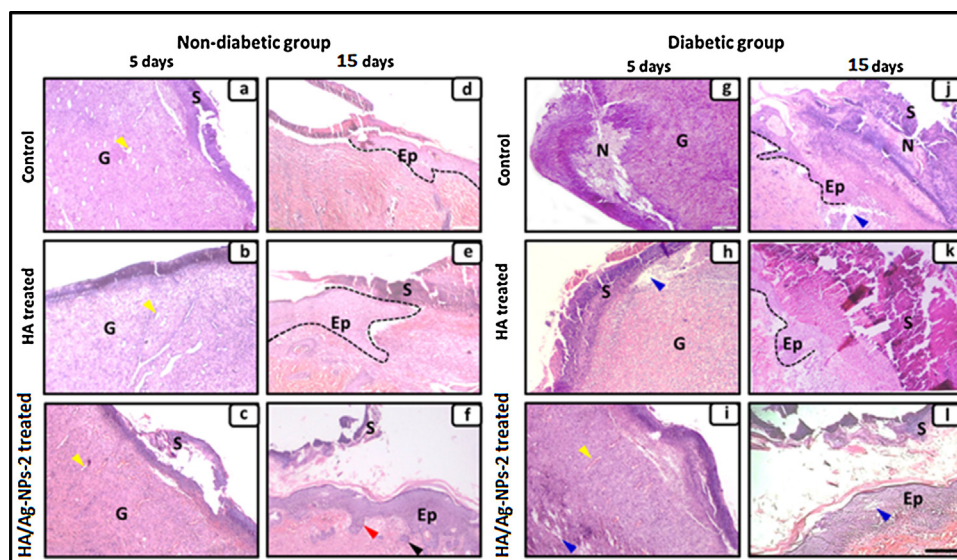

Fig. 10. Histological observations of wound healing after surgery. The healed wound sections stained with hematoxylin and eosin of the fifth and fifteen day post-surgery, 20×. The photomicrographs show sections excised from non-diabetic groups (left) of control (a–d), HA treated (b–e), HA/Ag-NPs-2 mg treated (c–f); diabetic groups (right) of control (g–j), HA nonwoven fabrics treated (h-k), HA/Ag-NPs-2 mg treated (i–l). In the fifth day, Note that a loose crust (S) cover the wounded area was seen clearly in both diabetic and non-diabetic groups, complete inflammatory reaction with prominent cell proliferation beneath the wound crust to form the granulation tissue (G) or neodermis, neovascularization (yellow arrowheads). However, necrotic tissue (N) and some bubbles (Blue arrowheads) were detected especially in diabetic groups indicating a lagging phase of healing rate. In the day fifteen, the demarcation dashed lines show the leading edge of the epithelial tissue (Ep) crawl slowly and started to invade the underlying dermis pushing out the fully formed wound crust to the outside. Notice that in figure (f) the HA/Ag-NPs-2 mg treated non-diabetic group, intact epithelial covering was evident with fully formed hair follicle (red arrowhead) and cross sections of sebaceous gland (black arrowhead) reflecting a higher rate of healing properties than other groups.

(0.4 μg), plain HA fabrics and HA/Ag-NPs fabrics were increased in spontaneous production of ROS by intact phagocytes (Fig. 7b). On the other hand, zymosan-induced ROS production was significantly decreased by both plain HA nonwoven fabrics and HA/Ag-NPs-2 mg mats with increased the concentration of plain HA and HA/Ag-NPs-2 mg nonwoven mats, respectively. From the results shown in Fig. 7b, we can conclude that the presence of silver nanoparticles in hyaluronan fabrics could be responsible for the inhibition of zymosan-activated oxidative burst of phagocytes. This could be important for efficacy of HA/Ag-NP fabrics ulcer treatments since phagocyte derived ROS could damage cells and tissue in healing the wound.

3.3. Healing properties of dressing mats

Aside from antibacterial and biocompatibility examination, in-vivo test was used for evaluating the real wound-healing effect of the fibers under investigation. Fig. 8 shows the optical microscope images of small cuts (2.5 × 2.5 cm) treated with plain HA fabrics; HA/Ag-NPs-2 mg nonwoven fabrics and untreated control sample after 5 and 15 days. In our non-diabetic and diabetics rats model, a full thickness skin wound of was made on the back of the rats. The wound closure rate was evaluated by measured of the wound contraction percentage as a function of time as shown in Fig. 8 at the date of surgery, no visible difference in the wound appearance was observed between the control and both HA and HA/A-g-NPs-1 mg treated groups in non-diabetic and diabetics rats model (data not shown). After 5 days of surgery, the control group (non-diabetic, diabetic) exhibited closure percentage of 33 and 22%, respectively (Fig. 9). The plain HA wound dressing fabrics treated non-diabetic rat group exhibited the wound closure of 55%, for HA nonwoven fabrics treated diabetic exhibited the closure percentage was 45%. For HA/Ag-NPs-1 mg nonwoven fabrics group treated non-diabetic/diabetic rats, the wound closure percentage was 66 and 57%, respectively (Fig. 9). In 15 days of surgery, the treated groups (non-diabetics/diabetics) by HA/Ag-NPs-2 mg nonwoven fabrics has highly closure percentage 95 and 85%. Such an excellent wound healing effect of HA/Ag-NPs-2 mg nonwoven fabrics could be attributed to synergetic effects between antibacterial performance of silver nanoparticles and the functional groups of hyaluronan. During the wound healing process, silver nanoparticles were released from the wound cover and killed and inhibited the bacteria which was infected the wound. Hyaluronan was depolymerized to release N-acetyl-glucosamine, and glucuronic acid by Hyaluronidase enzyme, which initiates fibroblast proliferation and helps in ordered collagen deposition. It was known that new epidermal generated from the edge to the center of the wounds, decreasing the deepness and area of the wounds with time. The rapid wound closure may be attributed to the rapid epidermis migration due to the moist wound healing environment. The epithelization can be further accelerated if the wound was kept moist (Burd et al., 1991; Frenkel, 2014). Furthermore, hyaluronan molecule have been announced to induce migration of inflammatory cells and fibroblasts, being activated to produce various cytokines (Ishihara et al., 2001; Obmińska-Mrukowicz et al., 2006; Ueno et al., 1999; Usami et al., 1998) and accelerating the wound healing process (Ishihara et al., 2001).

Histology of healed skin was investigated to confirm degree of skin regeneration (Fu et al., 2015; Kwan et al., 2014; Munger et al., 2014; Qin et al., 2014). The healing patterns of both diabetic and non-diabetic groups were studied by histological examination of control (diabetic and non-diabetic), plain HA nonwoven fabrics, and HA/Ag-NPs-2 mg treated tissue samples at days 5 and 15 post-operation by hematoxylin and eosin staining. Microscopic observations on day 5 showed small difference between non-diabetic and diabetics groups; the wound consisted of a large (scab) covering the opened area. At the bottom of wounds, newly generated granulation tissue (G) was visualized in Fig. 10. The G consisted of inflammatory cells, newly synthesized blood vessels, fibroblasts and endothelial cells. After 15 day, the leading edge of the epithelial tissue crawl slowly and started to invade the underlying dermis pushing out the fully formed wound crust to the outside. However, necrotic tissue and some bubbles were detected especially in diabetic groups indicated a lagging phase of healing rate. In HA/Ag-NPs-2 mg treated groups, complete wound regeneration of the epithelial covering were prominent and new hair follicles with some sections of sebaceous glands had started to develop reflecting a higher rate of healing properties than other groups.

4. Conclusions

In-situ silver nanoparticles (Ag-NPs) were synthesized by using sodium hyaluronate as stabilizing and capping agents in absence any external reducing agents. Uniform dispersion of almost monodisperse in-situ formed Ag nanoparticles (20–25 ± 2 nm) were obtained by the green process. From the XRD and TGA analysis showed that the in-situ preparation of Ag-NPs increased the crystallinity of the resultant fabrics and thermal stability, respectively. The mechanical properties of the HA/Ag-NPs (1, 2) was enhanced compared with neat HA. The HA/Ag-NPs nano-composite fabrics wound cover exhibited the desired antibacterial activity against gram negative bacterial (E.coli), has no effect on the keratinocyte's cell line growth (HaCaT) and was highly biocompatible. The wound dressing HA/Ag-NPs fabrics wound cover had higher wound healing efficacy compared to the plain HA fabrics covers and control sample, and histological measurements, demonstrated its applicability in wound and chronic ulcer treatment.

Appendix A. Supplementary data

Supplementary data associated with this article can be found, in the online version, at http://dx.doi.org/10.1016/j.ijpharm.2017.02.003.

References

Abdel-Mohsen, A.M., Abdel-Rahman, R.M., Hrdina, R., Imramovský, A., Burgert, L., Aly, A.S., 2012a. Antibacterial cotton fabrics treated with core–shell nanoparticles. Int. J. Biol. Macromol. 50, 1245–1253.

Abdel-Mohsen, A.M., Aly, A.S., Hrdina, R., El-Aref, A., 2012b. A novel method for the preparation of silver/chitosan-O-methoxy polyethylene glycol core shell nanoparticles. J. Polym. Environ. 20, 459–468.

Abdel-Mohsen, A.M., Hrdina, R., Burgert, L., Krylová, G., Abdel-Rahman, R.M., Krejčová, A., Steinhart, M., Beneš, L., 2012c. Green synthesis of hyaluronan fibers with silver nanoparticles. Carbohydr. Polym. 89, 411–422.

Abdel-Mohsen, A.M., Hrdina, R., Burgert, L., Abdel-Rahman, R.M., Hašová, M., Šmejkalová, D., Kolář, M., Pekar, M., Aly, A.S., 2013. Antibacterial activity and cell viability of hyaluronan fiber with silver nanoparticles. Carbohydr. Polym. 92, 1177–1187.

Abdel-Mohsen, A.M., Abdel-Rahman, R.M., Fouda, M.M.G., Vojtova, L., Uhrova, L., Hassan, A.F., Al-Deyab, S.S., El-Shamy, I.E., Jancar, J., 2014. Preparation, characterization and cytotoxicity of schizophyllan/silver nanoparticle composite. Carbohydr. Polym. 102, 238–245.

Abdel-Mohsen, A.M., Jancar, J., Massoud, D., Fohlerova, Z., Elhadidy, H., Spotz, Z., Hebeish, A., 2016. Novel chitin/chitosan-glucan wound dressing: isolation,

characterization, antibacterial activity and wound healing properties. Int. J. Pharm. 510, 86–99.

Abdel-Rahman, R.M., Abdel-Mohsen, A.M., Hrdina, R., Burgert, L., Fohlerova, Z., Pavliňák, D., Sayed, O.N., Jancar, J., 2016. Wound dressing based on chitosan/hyaluronan/nonwoven fabrics: preparation, characterization and medical applications. Int. J. Biol. Macromol. 89, 725–736.

Alkrad, J.A., Mrestani, Y., Stroehl, D., Wartewig, S., Neubert, R., 2003. Characterization of enzymatically digested hyaluronic acid using NMR, Raman, IR, and UV–vis spectroscopies. J. Pharm. Biomed. Anal. 31, 545–550.

Almond, A., Sheehan, J.K., Brass, A., 1997. Molecular dynamics simulations of the two disaccharides of hyaluronan in aqueous solution. Glycobiology 7, 597–604.

Aly, A.S., Abdel-Mohsen, A.M., Hrdina, R., Abou-Okeil, A., 2011. Preparation and characterization of polyethylene glycol/dimethyl siloxane adduct and its utilization as finishing agent for cotton fabric. J. Nat. Fibers 8, 176–188.

Atosuo, J., Lehtinen, J., Vojtek, L., Lilius, E.-M., 2013. Escherichia coli K-12 (pEGFPluxABCDEamp): a tool for analysis of bacterial killing by antibacterial agents and human complement activities on a real-time basis. Luminescence 28, 771–779.

Baker, S.R., Banerjee, S., Bonin, K., Guthold, M., 2016. Determining the mechanical properties of electrospun poly-ε-caprolactone (PCL) nanofibers using AFM and a novel fiber anchoring technique. Mater. Sci. Eng. C 59, 203–212.

Banti, C.N., Hadjikakou, S.K., 2013. Anti-proliferative and anti-tumor activity of silver(i) compounds. Metallomics 5, 569–596.

Barbinta-Patrascu, M.E., Ungureanu, C., Iordache, S.M., Bunghez, I.R., Badea, N., Rau, I., 2014. Green silver nanobioarchitectures with amplified antioxidant and antimicrobial properties. J. Mater. Chem. B 2, 3221–3231.

Barnea, Y., Weiss, J., Gur, E., 2010. A review of the applications of the hydrofiber dressing with silver (Aquacel Ag(®)) in wound care. Ther. Clin. Risk Manag. 6, 21–27.

Blundell, Charles D., Deangelis, Paul L., Almond, A., 2006. Hyaluronan: the absence of amide–carboxylate hydrogen bonds and the chain conformation in aqueous solution are incompatible with stable secondary and tertiary structure models. Biochem. J 396, 487–498.

Bober, P., Liu, J., Mikkonen, K.S., Ihalainen, P., Pesonen, M., Plumed-Ferrer, C., von Wright, A., Lindfors, T., Xu, C., Latonen, R.-M., 2014. Biocomposites of nanofibrillated cellulose, polypyrrole, and silver nanoparticles with electroconductive and antimicrobial properties. Biomacromolecules 15, 3655–3663.

Bowler, P.G., Parsons, D., 2016. Combatting wound biofilm and recalcitrance with a novel anti-biofilm Hydrofiber® wound dressing. Wound Med. 14, 6–11.

Burd, D.A.R., Ritz, M., Regauer, S., Longaker, M.T., Siebert, J.W., Garg, H., 1991. Hyaluronan and wound healing: a new perspective. Br. J. Plast. Surg. 44, 579–584.

Chen, W.Y.J., Abatangelo, G., 1999. Functions of hyaluronan in wound repair. Wound Repair Regen. 7, 79–89.

Chen, C.-H., Chen, S.-H., Shalumon, K.T., Chen, J.-P., 2015. Dual functional core–sheath electrospun hyaluronic acid/polycaprolactone nanofibrous membranes embedded with silver nanoparticles for prevention of peritendinous adhesion. Acta Biomater. 26, 225–235.

Cong, Y., Xia, T., Zou, M., Li, Z., Peng, B., Guo, D., Deng, Z., 2014. Mussel-inspired polydopamine coating as a versatile platform for synthesizing polystyrene/Ag nanocomposite particles with enhanced antibacterial activities. J. Mater. Chem. B 2, 3450–3461.

Du, Y., Su, J., Luo, W., Cheng, G., 2015. Graphene-supported nickel–platinum nanoparticles as efficient catalyst for hydrogen generation from hydrous hydrazine at room temperature. ACS Appl. Mater. Interfaces 7, 1031–1034.

Fan, Z., Liu, B., Wang, J., Zhang, S., Lin, Q., Gong, P., Ma, L., Yang, S., 2014. A novel wound dressing based on Ag/graphene polymer hydrogel: effectively kill bacteria and accelerate wound healing. Adv. Funct. Mater. 24, 3933–3943.

Ferreira, D.S., Marques, A.P., Reis, R.L., Azevedo, H.S., 2013. Hyaluronan and self-assembling peptides as building blocks to reconstruct the extracellular environment in skin tissue. Biomater. Sci. 1, 952–964.

Frenkel, J.S., 2014. The role of hyaluronan in wound healing. Int. Wound J. 11, 159–163.

Fu, C., Liu, T., Li, L., Liu, H., Liang, Q., Meng, X., 2015. Effects of graphene oxide on the development of offspring mice in lactation period. Biomaterials 40, 23–31.

Govindan, S., Nivethaa, E.A.K., Saravanan, R., Narayanan, V., Stephen, A., 2012. Synthesis and characterization of chitosan–silver nanocomposite. Appl. Nanosci. 2, 299–303.

Gribbon, P., Heng, B.C., Hardingham, T.E., 1999. The molecular basis of the solution properties of hyaluronan investigated by confocal fluorescence recovery after photobleaching. Biophys. J. 77, 2210–2216.

Gustaite, S., Kazlauske, J., Bobokalonov, J., Perni, S., Dutschk, V., Liesiene, J., Prokopovich, P., 2015. Characterization of cellulose based sponges for wound dressings. Colloids Surf. A Physicochem. Eng. Asp. 480, 336–342.

Harris, M.J., Herp, A., Pigma, W., 1972. Metal catalysis in the depolymerization of hyaluronic acid by autoxidants. J. Am. Chem. Soc. 94, 7570–7572.

Huang, Y., Zhong, Z., Duan, B., Zhang, L., Yang, Z., Wang, Y., Ye, Q., 2014. Novel fibers fabricated directly from chitin solution and their application as wound dressing. J. Mater. Chem. B 2, 3427–3432.

Ishihara, M., Ono, K., Sato, M., Nakanishi, K., Saito, Y., Yura, H., Matsui, T., Hattori, H., Fujita, M., Kikuchi, M., Kurita, A., 2001. Acceleration of wound contraction and healing with a photocrosslinkable chitosan hydrogel. Wound Repair Regen. 9, 513–521.

Kalathi, J.T., Yamamoto, U., Schweizer, K.S., Grest, G.S., Kumar, S.K., 2014. Nanoparticle diffusion in polymer nanocomposites. Phys. Rev. Lett. 112, 108301.

Kokura, S., Handa, O., Takagi, T., Ishikawa, T., Naito, Y., Yoshikawa, T., 2010. Silver nanoparticles as a safe preservative for use in cosmetics. Nanomed. Nanotechnol. Biol. Med. 6, 570–574.

Kvitek, L., Prucek, R., Panacek, A., Novotny, R., Hrbac, J., Zboril, R., 2005. The influence of complexing agent concentration on particle size in the process of SERS active silver colloid synthesis. J. Mater. Chem. 15, 1099–1105.

Kwan, K.H.L., Yeung, K.W.K., Liu, X., Wong, K.K.Y., Shum, H.C., Lam, Y.W., Cheng, S.H., Cheung, K.M.C., To, M.K.T., 2014. Silver nanoparticles alter proteoglycan expression in the promotion of tendon repair. Nanomed. Nanotechnol. Biol. Med. 10, 1375–1383.

Lapčík, L., Lapčík, L., De Smedt, S., Demeester, J., Chabreček, P., 1998. Hyaluronan: preparation, structure, properties, and applications. Chem. Rev. 98, 2663–2684.

Levi-Polyachenko, N., Jacob, R., Day, C., Kuthirummal, N., 2016. Chitosan wound dressing with hexagonal silver nanoparticles for hyperthermia and enhanced delivery of small molecules. Colloids Surf. B Biointerfaces 142, 315–324.

Li, Y., Jiang, H., Zheng, W., Gong, N., Chen, L., Jiang, X., Yang, G., 2015. Bacterial cellulose-hyaluronan nanocomposite biomaterials as wound dressings for severe skin injury repair. J. Mater. Chem. B 3, 3498–3507.

Li, D., Ye, Y., Li, D., Li, X., Mu, C., 2016. Biological properties of dialdehyde carboxymethyl cellulose crosslinked gelatin–PEG composite hydrogel fibers for wound dressings. Carbohydr. Polym. 137, 508–514.

Liakos, I., Rizzello, L., Hajiali, H., Brunetti, V., Carzino, R., Pompa, P.P., Athanassiou, A., Mele, E., 2015. Fibrous wound dressings encapsulating essential oils as natural antimicrobial agents. J. Mater. Chem. B 3, 1583–1589.

Lin, I.W.-S., Lok, C.-N., Yan, K., Che, C.-M., 2013. A silver complex of N,N[prime or minute]-disubstituted cyclic thiourea as an anti-inflammatory inhibitor of I[small kappa]B kinase. Chem. Commun. 49, 3297–3299.

Lipsky, B.A., Hoey, C., 2009. Topical antimicrobial therapy for treating chronic wounds. Clin. Infect. Dis. 49, 1541–1549.

Liu, Y., Guan, W., Ren, G., Yang, Z., 2012. The possible mechanism of silver nanoparticle impact on hippocampal synaptic plasticity and spatial cognition in rats. Toxicol. Lett. 209, 227–231.

Loza, K., Diendorf, J., Sengstock, C., Ruiz-Gonzalez, L., Gonzalez-Calbet, J.M., Vallet-Regi, M., Koller, M., Epple, M., 2014. The dissolution and biological effects of silver nanoparticles in biological media. J. Mater. Chem. B 2, 1634–1643.

Lu, B., Li, T., Zhao, H., Li, X., Gao, C., Zhang, S., Xie, E., 2012. Graphene-based composite materials beneficial to wound healing. Nanoscale 4, 2978–2982.

Maillard, M., Huang, P., Brus, L., 2003. Silver nanodisk growth by surface plasmon enhanced photoreduction of adsorbed [Ag+]. Nano Lett. 3, 1611–1615.

Marsich, E., Bellomo, F., Turco, G., Travan, A., Donati, I., Paoletti, S., 2013. Nano-composite scaffolds for bone tissue engineering containing silver nanoparticles: preparation, characterization and biological properties. J. Mater. Sci. Mater. Med. 24, 1799–1807.

Mogoşanu, G.D., Grumezescu, A.M., 2014. Natural and synthetic polymers for wounds and burns dressing. Int. J. Pharm. 463, 127–136.

Mohiti-Asli, M., Pourdeyhimi, B., Loboa, E.G., 2014. Novel, silver-ion-releasing nanofibrous scaffolds exhibit excellent antibacterial efficacy without the use of silver nanoparticles. Acta Biomater. 10, 2096–2104.

Morris, E.R., Rees, D.A., Welsh, E.J., 1980. Conformation and dynamic interactions in hyaluronate solutions. J. Mol. Biol. 138, 383–400.

Munger, M.A., Radwanski, P., Hadlock, G.C., Stoddard, G., Shaaban, A., Falconer, J., Grainger, D.W., Deering-Rice, C.E., 2014. In vivo human time-exposure study of orally dosed commercial silver nanoparticles. Nanomed. Nanotechnol. Biol. Med. 10, 1–9.

Murphy, J.A., Ackerman, A.H., Heeren, J.K., 1991. Recovery of silver from and some uses for waste silver chloride. J. Chem. Educ. 68, 602.

Nocchetti, M., Donnadio, A., Ambrogi, V., Andreani, P., Bastianini, M., Pietrella, D., Latterini, L., 2013. Ag/AgCl nanoparticle decorated layered double hydroxides: synthesis, characterization and antimicrobial properties. J. Mater. Chem. B 1, 2383–2393.

Obmińska-Mrukowicz, B., Szczypka, M., Gawęda, B., 2006. Modulatory effects of chitosan adipate on the T and B lymphocyte subsets in mice. J. Vet. Sci. 7, 157–160.

Pal, S., Tak, Y.K., Han, E., Rangasamy, S., Song, J.M., 2014. A multifunctional composite of an antibacterial higher-valent silver metallopharmaceutical and a potent wound healing polypeptide: a combined killing and healing approach to wound care. New J. Chem. 38, 3889–3898.

Pastoriza-Santos, I., Liz-Marzán, L.M., 2002. Synthesis of silver nanoprisms in DMF. Nano Lett. 2, 903–905.

Pauksch, L., Hartmann, S., Rohnke, M., Szalay, G., Alt, V., Schnettler, R., Lips, K.S., 2014. Biocompatibility of silver nanoparticles and silver ions in primary human mesenchymal stem cells and osteoblasts. Acta Biomater. 10, 439–449.

Paul, D.R., Robeson, L.M., 2008. Polymer nanotechnology: nanocomposites. Polymer 49, 3187–3204.

Pei, Y., Ye, D., Zhao, Q., Wang, X., Zhang, C., Huang, W., Zhang, N., Liu, S., Zhang, L., 2015. Effectively promoting wound healing with cellulose/gelatin sponges constructed directly from a cellulose solution. J. Mater. Chem. B 3, 7518–7528.

Potts, J.R., Dreyer, D.R., Bielawski, C.W., Ruoff, R.S., 2011. Graphene-based polymer nanocomposites. Polymer 52, 5–25.

Priya, V.S., Iyappan, K., Gayathri, V.S., William, S., Suguna, L., 2016. Influence of pullulan hydrogel on sutureless wound healing in rats. Wound Med. 14, 1–5.

Pyun, D.G., Yoon, H.S., Chung, H.Y., Choi, H.J., Thambi, T., Kim, B.S., Lee, D.S., 2015. Evaluation of AgHAP-containing polyurethane foam dressing for wound healing: synthesis, characterization, in vitro and in vivo studies. J. Mater. Chem. B 3, 7752–7763.

Qin, H., Cao, H., Zhao, Y., Zhu, C., Cheng, T., Wang, Q., Peng, X., Cheng, M., Wang, J., Jin, G., Jiang, Y., Zhang, X., Liu, X., Chu, P.K., 2014. In vitro and in vivo anti-biofilm

effects of silver nanoparticles immobilized on titanium. Biomaterials 35, 9114–9125.

Raza, Z.A., Rehman, A., Mohsin, M., Bajwa, S.Z., Anwar, F., Naeem, A., Ahmad, N., 2015. Development of antibacterial cellulosic fabric via clean impregnation of silver nanoparticles. J. Clean. Prod. 101, 377–386.

Regiel, A., Irusta, S., Kyzioł, A., Arruebo, M., Santamaria, J., 2013. Preparation and characterization of chitosan–silver nanocomposite films and their antibacterial activity against Staphylococcus aureus. Nanotechnology 24, 015101.

Reineck, I., DeAnna, J., Suleski, T.J., Lee, S.A., Rupprecht, A., 2003. A raman study of the hydration of wet-spun films of Li-hyaluronate. J. Biomol. Struct. Dyn. 21, 153–157.

Rheinwatd, J.G., Green, H., 1975. Seria cultivation of strains of human epidemal keratinocytes: the formation keratinizin colonies from single cell is. Cell 6, 331–343.

Roy, S., Banerjee, A., 2011. Amino acid based smart hydrogel: formation, characterization and fluorescence properties of silver nanoclusters within the hydrogel matrix. Soft Matter 7, 5300–5308.

Schneid, A.C., Roesch, E.W., Sperb, F., Matte, U., da Silveira, N.P., Costa, T.M.H., Benvenutti, E.V., de Menezes, E.W., 2014. Silver nanoparticle-ionic silsesquioxane: a new system proposed as an antibacterial agent. J. Mater. Chem. B 2, 1079–1086.

Sheehan, J.K., Gardner, K.H., Atkins, E.D., 1977. Hyaluronic acid: a double-helical structure in the presence of potassium at low pH and found also with the cations ammonium, rubidium and caesium. J. Mol. Biol. 117, 113–135.

Shi, Z., Tang, J., Chen, L., Yan, C., Tanvir, S., Anderson, W.A., Berry, R.M., Tam, K.C., 2015. Enhanced colloidal stability and antibacterial performance of silver nanoparticles/cellulose nanocrystal hybrids. J. Mater. Chem. B 3, 603–611.

Silcock, D., 2010. 12 – Collagen-Based Dressings as Therapeutic Agents for Wound Healing A2 – Lewis, Andrew, Drug-Device Combination Products. Woodhead Publishing, pp. 280–310.

Singaravelu, S., Ramanathan, G., Muthukumar, T., Raja, M.D., Nagiah, N., Thyagarajan, S., Aravinthan, A., Gunasekaran, P., Natarajan, T.S., Selva, V.N. Geetha, Kim, G., Sivagnanam, J.-H., 2016. Durable keratin-based bilayered electrospun mats for wound closure. J. Mater. Chem. B 4, 3982–3997.

Stevens, K.N.J., Croes, S., Boersma, R.S., Stobberingh, E.E., van der Marel, C., van der Veen, F.H., Knetsch, M.L.W., Koole, L.H., 2011. Hydrophilic surface coatings with embedded biocidal silver nanoparticles and sodium heparin for central venous catheters. Biomaterials 32, 1264–1269.

Suh, M.P., Moon, H.R., Lee, E.Y., Jang, S.Y., 2006. A redox-active two-dimensional coordination polymer: preparation of silver and gold nanoparticles and crystal dynamics on guest removal. J. Am. Chem. Soc. 128, 4710–4718.

Sun, J., Li, J., Fan, H., Ai, S., 2013. Ag nanoparticles and vancomycin comodified layered double hydroxides for simultaneous capture and disinfection of bacteria. J. Mater. Chem. B 1, 5436–5442.

Szegedi, A., Popova, M., Yoncheva, K., Makk, J., Mihaly, J., Shestakova, P., 2014. Silver- and sulfadiazine-loaded nanostructured silica materials as potential replacement of silver sulfadiazine. J. Mater. Chem. B 2, 6283–6292.

Taheri, S., Baier, G., Majewski, P., Barton, M., Forch, R., Landfester, K., Vasilev, K., 2014. Synthesis and antibacterial properties of a hybrid of silver-potato starch nanocapsules by miniemulsion/polyaddition polymerization. J. Mater. Chem. B 2, 1838–1845.

Tao, A., Kim, F., Hess, C., Goldberger, J., He, R., Sun, Y., Xia, Y., Yang, P., 2003. Langmuir-blodgett silver nanowire monolayers for molecular sensing using surface-enhanced raman spectroscopy. Nano Lett. 3, 1229–1233.

Tatarchuk, V.V., Sergievskaya, A.P., Korda, T.M., Druzhinina, I.A., Zaikovsky, V.I., 2013. Kinetic factors in the synthesis of silver nanoparticles by reduction of Ag+ with hydrazine in reverse micelles of triton N-42. Chem. Mater. 25, 3570–3579.

Thiel, J., Pakstis, L., Buzby, S., Raffi, M., Ni, C., Pochan, D.J., Shah, S.I., 2007. Antibacterial properties of silver-doped titania. Small 3, 799–803.

Thunus, L., Dauphin, J.F., Moiny, G., Deby, C., Deby-Dupont, G., 1995. Anti-inflammatory properties of copper, gold and silver, individually and as mixtures. Analyst 120, 967–973.

Tjong, S.C., 2012. Polymer Nanocomposites for Biomedical Applications, Polymer Composites with Carbonaceous Nanofillers. Wiley-VCH Verlag GmbH & Co. KGaA, pp. 285–329.

Trivedi, T.J., Rao, K.S., Kumar, A., 2014. Facile preparation of agarose-chitosan hybrid materials and nanocomposite ionogels using an ionic liquid via dissolution, regeneration and sol-gel transition. Green Chem. 16, 320–330.

Ueno, H., Yamada, H., Tanaka, I., Kaba, N., Matsuura, M., Okumura, M., Kadosawa, T., Fujinaga, T., 1999. Accelerating effects of chitosan for healing at early phase of experimental open wound in dogs. Biomaterials 20, 1407–1414.

Usami, Y., Okamoto, Y., Takayama, T., Shigemasa, Y., Minami, S., 1998. Chitin and chitosan stimulate canine polymorphonuclear cells to release leukotriene B4 and prostaglandin E2. J. Biomed. Mater. Res. 42, 517–522.

Van Hyning, D.L., Zukoski, C.F., 1998. Formation mechanisms and aggregation behavior of borohydride reduced silver particles. Langmuir 14, 7034–7046.

Vistejnova, L., Dvorakova, J., Hasova, M., Muthny, T., Velebny, V., Soucek, K., Kubala, L., 2009. The comparison of impedance-based method of cell proliferation monitoring with commonly used metabolic-based techniques. Neuro Endocrinol. Lett. 30 (Suppl. 1), 121–127.

Wiley, B., Sun, Y., Mayers, B., Xia, Y., 2005. Shape-controlled synthesis of metal nanostructures: the case of silver. Chem. Eur. J. 11, 454–463.

Winter, W.T., Smith, P.J.C., Arnott, S., 1975. Hyaluronic acid: structure of a fully extended 3-fold helical sodium salt and comparison with the less extended 4-fold helical forms. J. Mol. Biol. 99, 219–235.

Woehl, M.A., Ono, L., Riegel Vidotti, I.C., Wypych, F., Schreiner, W.H., Sierakowski, M. R., 2014. Bioactive nanocomposites of bacterial cellulose and natural hydrocolloids. J. Mater. Chem. B 2, 7034–7044.

Wu, S., Ai, L., Chen, J., Kang, J., Cui, S.W., 2013. Study of the mechanism of formation of hyaluronan putty at pH 2.5: part I. Experimental measurements. Carbohydr. Polym. 98, 1677–1682.

Yoon, D.S., Lee, Y., Ryu, H.A., Jang, Y., Lee, K.-M., Choi, Y., Choi, W.J., Lee, M., Park, K.M., Park, K.D., Lee, J.W., 2016. Cell recruiting chemokine-loaded sprayable gelatin hydrogel dressings for diabetic wound healing. Acta Biomater. 38, 59–68.

Zanette, C., Pelin, M., Crosera, M., Adami, G., Bovenzi, M., Larese, F.F., Florio, C., 2011. Silver nanoparticles exert a long-lasting antiproliferative effect on human keratinocyte HaCaT cell line. Toxicol. In Vitro 25, 1053–1060.

Zeng, Q.H., Yu, A.B., Lu, G.Q., Paul, D.R., 2005. Clay-based polymer nanocomposites: research and commercial development. J. Nanosci. Nanotechnol. 5, 1574–1592.

Zivanovic, S., Li, J., Davidson, P.M., Kit, K., 2007. Physical, mechanical, and antibacterial properties of chitosan/PEO blend films. Biomacromolecules 8, 1505–1510.

Supporting information

A novel *in situ* Silver/Hyaluronan Bio-nanocomposite Fabrics for Wound and Chronic Ulcer Dressing: *In vitro* and *In vivo* Evaluations

A.M. Abdel-Mohsen[*], J. Jancar, R. M.Abdel-Rahman, L.Vojtek, P. Hyršl, M. Dušková, H. Nejezchlebová

Reduction percent (%)				
Time (Min)	**Control**	**Plain HA**	**HA/Ag-NPs-1 mg**	**HA/Ag-NPs-2 mg**
30	10 ± 2	20 ± 0.5	87 ± 2	95 ± 0.2
60	15 ± 1	25 ± 0.75	91 ± 1.5	97 ± 0.1
90	17 ± 4	27 ± 0.62	96 ± 1.3	99 ± 0.1

Table S1. Reduction rate of plain HA nonwoven fabrics, HA-Ag-1 mg, HA-Ag-2mg nonwoven fabrics mats.

Publication 13

Wound healing of different molecular weight of hyaluronan; *in-vivo* study

Moustafa M.G. Fouda [a,d,*,1], A.M. Abdel-Mohsen [b,c,d,**,1], Hossam Ebaid [e,f,***,1], Iftekhar Hassan [e], Jameel Al-Tamimi [e], Rasha M. Abdel-Rahman [g], Ali Metwalli [f], Ibrahim Alhazza [e], Ahmed Rady [e], Ayman El-Faham [a,h], J. Jancar [b,c,i]

[a] Chemistry Department, College of Science, King Saud University, P.O. Box 2455, Riyadh 11451, Saudi Arabia
[b] CEITEC-Central European Institute of Technology, Brno University of Technology, Technicka 3058/10, 616 00 Brno, Czech Republic
[c] SCITEG, a.s., Brno, Czech Republic
[d] National Research Centre, Textile Research Division, Pre-treatment and Finishing of Cellulosic Fibers, Dokki, P.O. 12311, Cairo, Egypt
[e] Department of Zoology, College of Science, King Saud University, P.O. Box 2455, Riyadh 11451, Saudi Arabia
[f] Department of Zoology, Faculty of Science, El-Minia University, Egypt
[g] Institute of Organic Chemistry and Technology, Faculty of Chemical Technology, University of Pardubice, Studentská 573, Pardubice CZ-532 10, Czech Republic
[h] Department of Chemistry, Faculty of Science, Alexandria University, P.O. Box 426, Ibrahimia, Alexandria 21321, Egypt
[i] Faculty of Chemistry, Institute of Materials Chemistry, Brno University of Technology, Technicka 3058/10, 616 00 Brno, Czech Republic

ARTICLE INFO

ABSTRACT

Recruitment of cells and mediators is altered during impaired wound healing, thereby delaying this process. To overcome this problem, the correlation of wound healing in older rats, and the impact of different molecular weight of hyaluronan without silver nanoparticles; (low-HA1), (High-HA2), (Medium- HA3) and with silver nanoparticles (High-HA4) is investigated. The superior HA were selected to be further investigated onto diabetic wounds. Our results pointed to a marked deficiency in wounds granulation in older rats, which was accompanied with impairment of healing process. In older rats group treated with HA2 or HA4, granulation and dermal construction were improved. Furthermore, the number of pathogenic bacteria on wounds was declined throughout the first 24 h by HA2 and HA4. The wound size in HA4-treated older rats was significantly smaller than that in other HA1, HA2 or HA3-treated older ones. Also, diabetes impaired the level of inflammatory cytokine, in diabetic model. On contrary, HA4 was found to normalize the level of inflammatory cytokine, in the diabetic model. Furthermore, HA4 was found to recover all oxidative and toxicity markers in diabetic models. This data confirms the critical role of HA4 to improve granulation and inflammatory mediators in impaired older and diabetic rat wound healing.

© 2016 Elsevier B.V. All rights reserved.

1. Introduction

Despite the great clinical efforts, impaired wound healing is still a medical challenge with daily increasing of its health complications. Thus, studies of how aging [1,2] and diabetes effects wound healing have become a research priority. The cell migration, fibroblastic differentiation, collagen remodeling, and proliferation are decreased in impaired healing. This may be attributed not only to cellular defects but also to changes in mediators associated with the senescence [3] and diabetic process.

A combination of various factors comprising hormonal parameter, free oxygen radicals and impaired angiogenesis seems to be the reason of postponed cutaneous healing in elderly [4]. Anti-age agents seemed to assist wound healing by decreasing inflammation
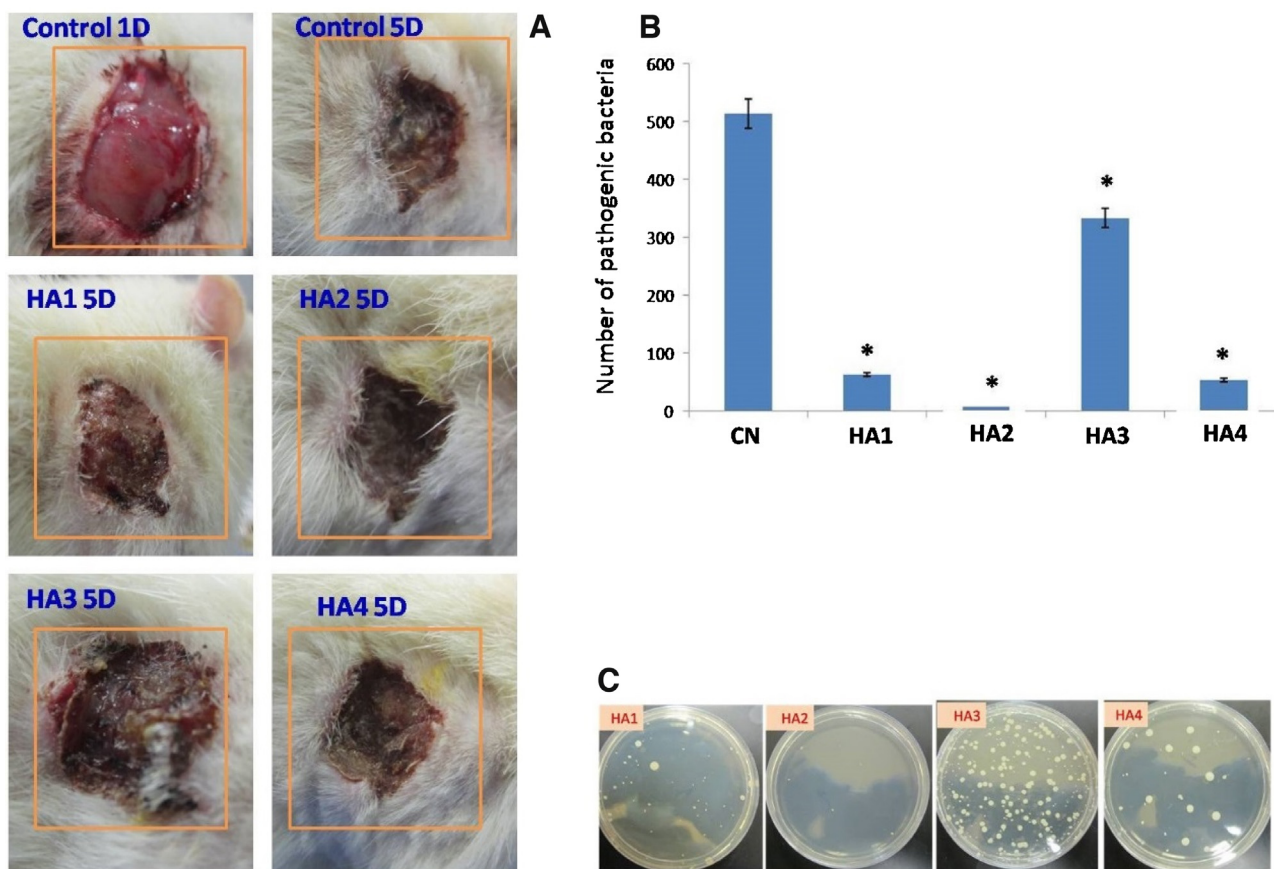
Fig. 1. A: Representative external photographs of full thickness skin wounds in control untreated and different treated groups. Photographs were taken from different rat groups two weeks post-wounding (Wound was rectangle, 10 × 20 mm). This figure shows that the wound size becomes smaller in groups II–IV in comparison to the control wound size or the group I wound size. B: The total count of the pathogenic bacteria grown on the full thickness wounded skin from older untreated (Control) and treated rats. Full thickness skin samples were taken from different rat groups one day post-wounding (Wound was rectangle, 10 × 20 mm). Values shown are means ± SD. *Shows the significance in comparison with the control group. C: Agar bacterial culture from different groups.

and stimulating the recovery process [5]. TGF-β is potentially used for the treatment of wound injuries, including ulcers in the elderly [6].

The wound healing process in diabetic patients can be adversely affected by several elements, comprising unrelieved pressure, infection, and concurrent underlying conditions. Sodium aescinate [7], whey proteins [8,9], chromogenic acid [10] and many other natural products may effectively control and improve wound healing in diabetic rats via its anti-inflammatory and antioxidant activities.

Recently, silver nanoparticles (AgNPs) have gained a great deal of interest among researchers in different area of applications such as textiles [11–16], biomedicine[17], medicine and pharmaceutics. Several green methods of AgNPs preparation such as chemical reduction methods have been reported [17–21].

The treatment of impaired wounds involves the use of biomaterials that can deliver mechanical and biological lines to the surrounding environment [22]. Haluronan (HA) is a straight forward chain glycosaminoglycan polymer consisting of repeating entities of disaccharide and is found in vertebrates [23] and human body, comprising skin and soft tissue [24]. Due to the impact on signaling pathways, HA plays a significant role in wound-healing process [25]. According to Antonella et al. [26], the molecular weight of hyaluronan plays a significant rule in the wound repair process *in vitro*, however, there is no any *in vivo* study in the literature till now focusing on the effect of molecular weights of hyaluronan with and without silver nanoparticles. Also, in this previous study [26], the author(s) claims that, higher molecular weight of HA can accumulate and binds fibrinogen that is essen-

tial for clot formation. Therefore, in our study, the investigation of the effect of different molecular weights of HA with and without silver nanoparticles could be effective factor to study *in-vivo*. The use of hyaluronan leads to better proliferation of granulation tissue as well as epithelialization with respect to wound healing diabetic conditions in rats [27]. Many recent studies investigated the impact of HA either single or in combination with different compounds on wound healing process [28–31]. To the best of our knowledge, there is no such comparative study, *In-vivo,* of molecular weights of nanocomposite (hyaluronan/silver nanoparticles) on the healing of diabetic ulceration. Therefore, for the 1st time, the impact of four different preparations from HA and its combination with silver nanoparticles on impaired wound healing in old and diabetic models are tested and evaluated.

2. Materials and methods

Different molecular weights of hyaluronan (low, medium, high molecular weight) was used, kindly provided by Sigea S.r.L., Trieste (Italy). Milli-Q water was used for all experiments. All chemicals were used before further purification.

2.1. Preparation of hyaluronic acid solution with and without silver nanoparticles

1% of different molecular weight of hyaluronan was dissolved in Milli-Q water under stirring at room temperature and marked as low molecular weight hyaluronan(LHA1), High molecular
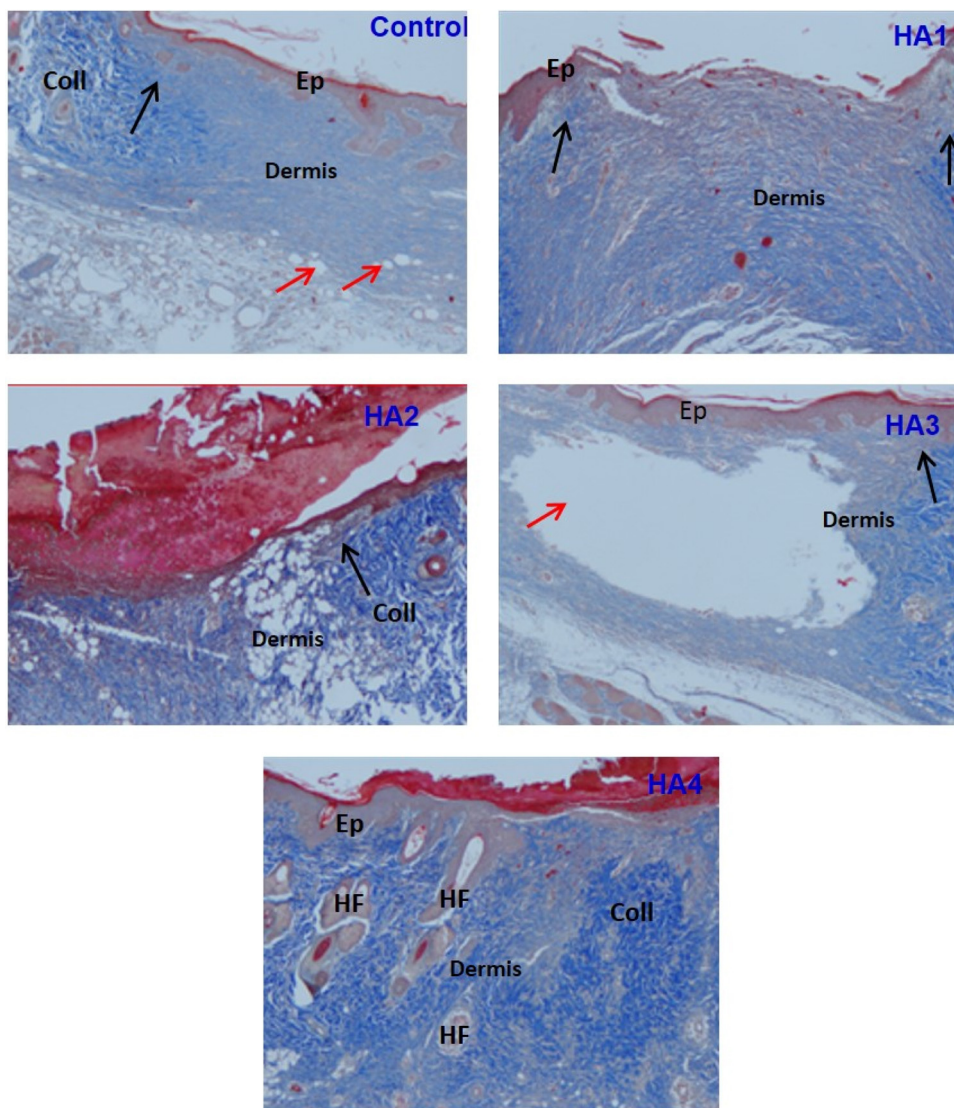
Fig. 2. Representative Masson Trichrome staining of full thickness wounded skin from older untreated (Control) and treated rats (group HA1-HA4) (X 100). Full thickness skin samples were taken from different rat groups two weeks post-wounding (Wound was rectangle, 10 × 20 mm). Epidermal cells (Ep); Collagen fibers (Coll); Epidermal tongues (black arrows); Bubbles (red arrows); Hair follicles (HF).

weight hyaluronan (HHA2), medium molecular weight hyaluronan (MHA3) and high hyaluronan/silver nanoparticles composite (HHA4/AgNPs).

2.2. Preparation of silver/hyaluronan nanoparticles composite

Silver nanoparticles were synthesized according to previous work with small modification [32,33]. High molecular weight hyaluronan was dissolved in Milli-Q water at room temperature with 1% concentration, then 1 ml of 10 mM of silver nitrate was added drop-wise into hyaluronic solution, the pH of the solution was raised until 7-8 with sodium hydroxide (1 M) and the reaction mixture was kept under stirring for 1 h at room temperature until the solution color converted from colorless to yellowish color indicated silver nanoparticles were obtained. The formation of silver nanoparticles was characterized by using UV–vis spectrophotometer, where a sharp significant peak appeared at 420 nm which is corresponding to the silver nanoparticles. Also, TEM was used to measure the size and size distribution of silver nanoparticles formed (the size of AgNPs was 100 nm), (data not shown).

2.3. Experimental design

Two experiments were performed to test the current lab prepared compounds. In the first experiment, about 40 older male rats were divided into 5 equal groups (n = 8). Wounds were performed in all rats in equal sizes to facilitate effect comparison of the four prepared compounds. The first group was remained as a control group. The remained four groups, each of them locally received one of four compounds on the cutaneous wound daily for 7 days. Because their superior effects on wound healing of older rats, compounds 2 and 4 were selected to be tested in the second experiments on the diabetic rat model. In the second experiment, about 40 male rats were divided into 5 equal groups (n = 8). The first group was remained as control un-wounded, while the second group was wounded control. The three other groups were diabetic rats; one of them was wounded and the two groups were wounded and locally received compound 2 and compound 4, respectively.
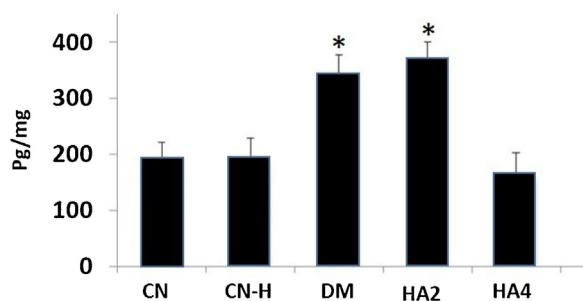
Fig. 3. The level of interferon gamma in the different treated groups. Values shown are means ± SD. *Shows the significance in comparison with the control group.
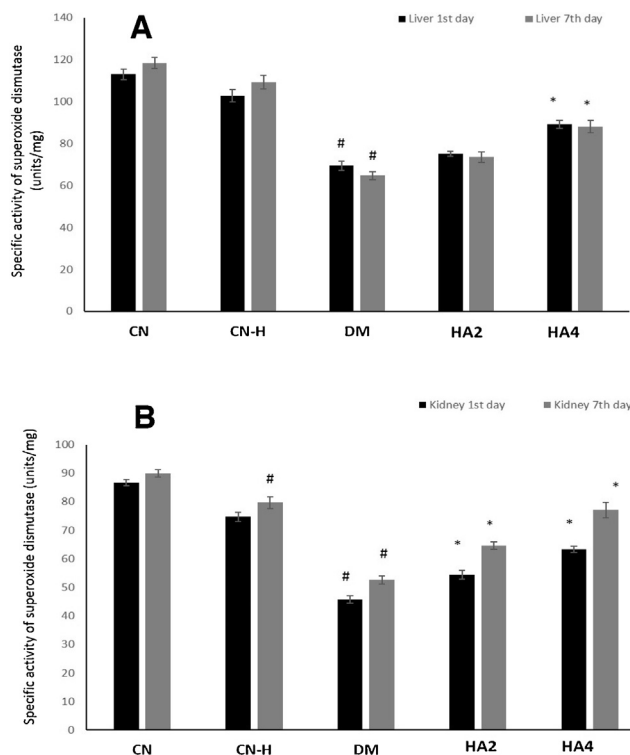

Fig. 4. The level of Superoxide dismutase in liver (A) and kidney (B) tissues from different groups. Values shown are means ± SD. #Shows the significance in comparison with the control group. *Shows the significance in comparison with the diabetic group.

2.4. Ethical approval

"This work did not comprise endangered or protected species". "With respect to the experimental animals, all processes were accompanied in accordance with the standards regular forth explored in guidelines for the care and use of experimental animals by the Committee for the Purpose of Control and Supervision of Experiments on Animals and the National Institutes of Health". "The working protocol (care and handling of experimental animals) was permitted by the Animal Ethics Committee of the Zoology Department at King Saud University, College of Science".

2.5. Excisional wound preparation

"All Rats were subjected to anesthetize, and the rate back was smooth-shaven and disinfected by ethyl alcohol". "The wound cell removal exemplary model which is used in this test was executed as previously designated by Schwentker [34] with minor variation". The clean-shaven skin was subjected to pinched followed by

tucked, and the wound was punched throughout the full thickness of the tucked skin to give 5 mm diameter circle under the shoulder blades of each rat.

2.6. Total bacterial count

The total bacterial count of the injured surface in rats were measured by using the viable cell counting method [35] by passing the sterilized cotton swap on the injured surface and putting the swap in 10 ml physiological rangers solution. The solution was vortexed with the swap. Appropriate dilutions were prepared and plated using the pour plate method with nutrient agar. The plates were incubated aerobically at 37 °C for 48 h.

2.7. Diabetic models

Diabetes was prompted by a single dose of newly dissolved STZ (50 mg/kg of body weight; Sigma, USA) in a 0.1 mol/l citrate buffer (pH 4.5) into the peritoneum. Control group rats were injected with citrate buffer. After seven days of STZ dose, rats were carefully chosen for serum glucose levels. Rats with a serum glucose level ≥ 200 mg/dl after 2 h of glucose absorption were deemed as diabetic and designated for further studies.

2.8. ELISA estimation of INF-γ

The INF-γ level in serum of investigational groups was calculated using specific ELISA kits bought from Abcam, USA. The concentration of INF-γ was determined using a spectrophotometer at 450 nm according to the manufacturers' instructions.

2.9. Histological studies

All rats were subjected to euthanizing overdose of isoflurane. Tissue sections were collected from the wound locations in order to evaluate the wound zone. In order to identify the collagen deposition in the dermal tissues, Mallory Trichrome stain was carefully applied. The tissue damage degree was inspected blindly via a Leica DMRB/E light microscope (Heerbrug, Switzerland). Sections images were taken, followed by digitalization using Adobe Photoshop (Adobe Systems, Mountain View, CA). Wounds were detached from four rats of each handling group, just two days after being wounding by cutting a square area that comprised the whole wound site. The gathered tissues were instantly kept in a solution of formaldehyde; 10%, in phosphate-buttered saline, then washed using PBS, dehydrated in series of alcohol dilutions and inserted in paraffin. Microtome segments were cut vertically thru the wound site and adhered to slides prior to staining.

2.10. Statistics

The statistical study was accomplished by means of MINITAB software (MINITAB, State College, PA, Version 13.1, 2002). All obtained numbers were normally disseminated with uniform alterations. Consequently, one-way ANOVA statistical was utilized to define the whole influence of each treatment. This test was complemented by individual comparison between the different treatments using Tukey's method for pairwise comparisons. The results were expressed as mean (M) ± standard deviation (SD). Only statistically significant changes with P < 0.05 were found between the treatment and the control group, and between the treatment and the older or diabetic group considered.
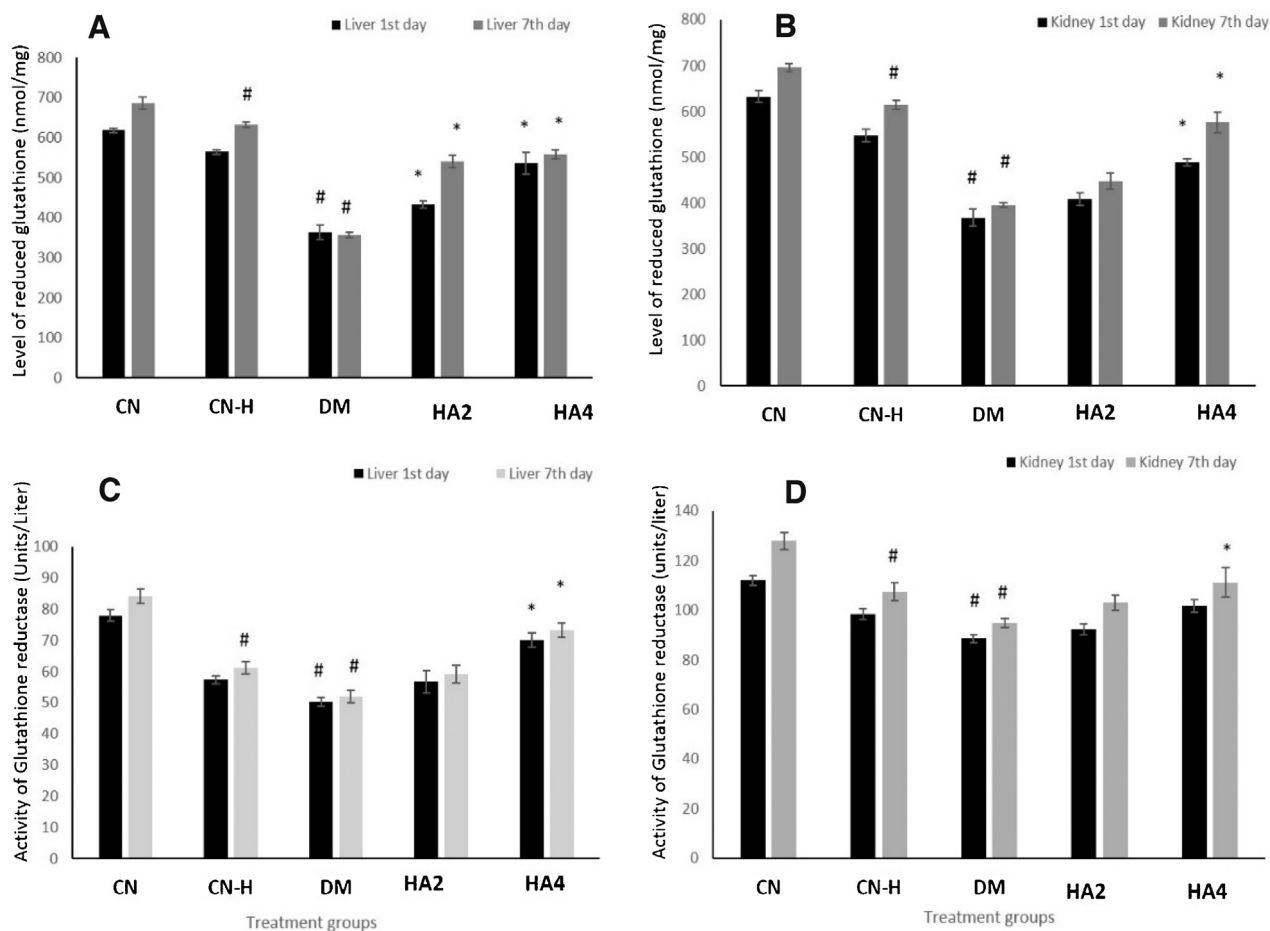
Fig. 5. The level of reduced glutathione (A,B) and glutathione reductase (C,D) in both liver and kidney tissues from different groups. Values shown are means ± SD. #Shows the significance in comparison with the control group. *Shows the significance in comparison with the diabetic group.

3. Results

3.1. Effects of the four HA compounds on old models

3.1.1. External variations in the wound morphology

External variations in the morphology of wound were observed daily during the investigational period. The percentage of older rats displaying wound closure was significantly lesser than that of the control rats. HA4 was found to retrieve the wound closure rate in the older rats to a comparable level to that of the young rats (Fig. 1A).

To observe the improvement of wound healing, morphometric signals were assessed at two day intervals. The size of the wound opening was significantly greater in sections from older rats in contrast to those from the young rats. The wound opening of older rats complemented with HA4 was gradually minimized, nevertheless, to become totally closed by the eighth day after wounding. Moreover, the number of new blood vessels and the depth of the dermal tissue in the wounded area were significantly decreased in older rats in comparison to the younger ones, but HA4 was found to significantly stimulate angiogenesis and the assembly of dermal constituents (Fig. 1A).

3.1.2. Inhibition of Pathogenic bacteria

We detected the quantitative changes of the bacterial load in wounded tissues over time. As shown in Fig. 1(b,c), HA2 and HA4 were found to significantly inhibit the pathogenic bacteria-growing in the wound sites throughout the experimental time in compari-

son to the control non-treated rats. Although, HA1 and HA3 were found to significantly inhibit the pathogenic bacteria growing in the wound sites, they failed to completely suppress this bacterial growing comparing to HA2 and HA4 (Fig. 1b,c).

3.1.3. Histological changes in the wound region

The epidermal cells covered the wounded region and the collagen fibers started to invade the dermal tissue of the control rats. However, some bubbles were noticed in numerous slides from the control rats signifying a slow healing. In HA1 rats, the two epidermal tongues were obviously appeared. In HA2 rats, the epidermal migration under the immature scar was normally extended with some few bubbles. The dermis was very disturbed in the sections from HA3 group. Interestingly, the collagen fibers were fully distinguished and well symmetrically distributed under the new epidermal tissue with mature scar in HA4 group. Noteworthy, is the formation and proliferation of the hair follicles which designate a well dermal contraction and normal repair in comparison to the control group (Fig. 2).

3.2. Effects of the two selected HA (HA2 and HA4) compounds on diabetic models

This part of the study was dedicated to discourse the effect HA2 and HA4 in the diabetes-induced rats. As inflammatory cytokines and oxidative stress are of the major contributive factors in pathogenesis and progression of the disease, so assessment of INF-γ and
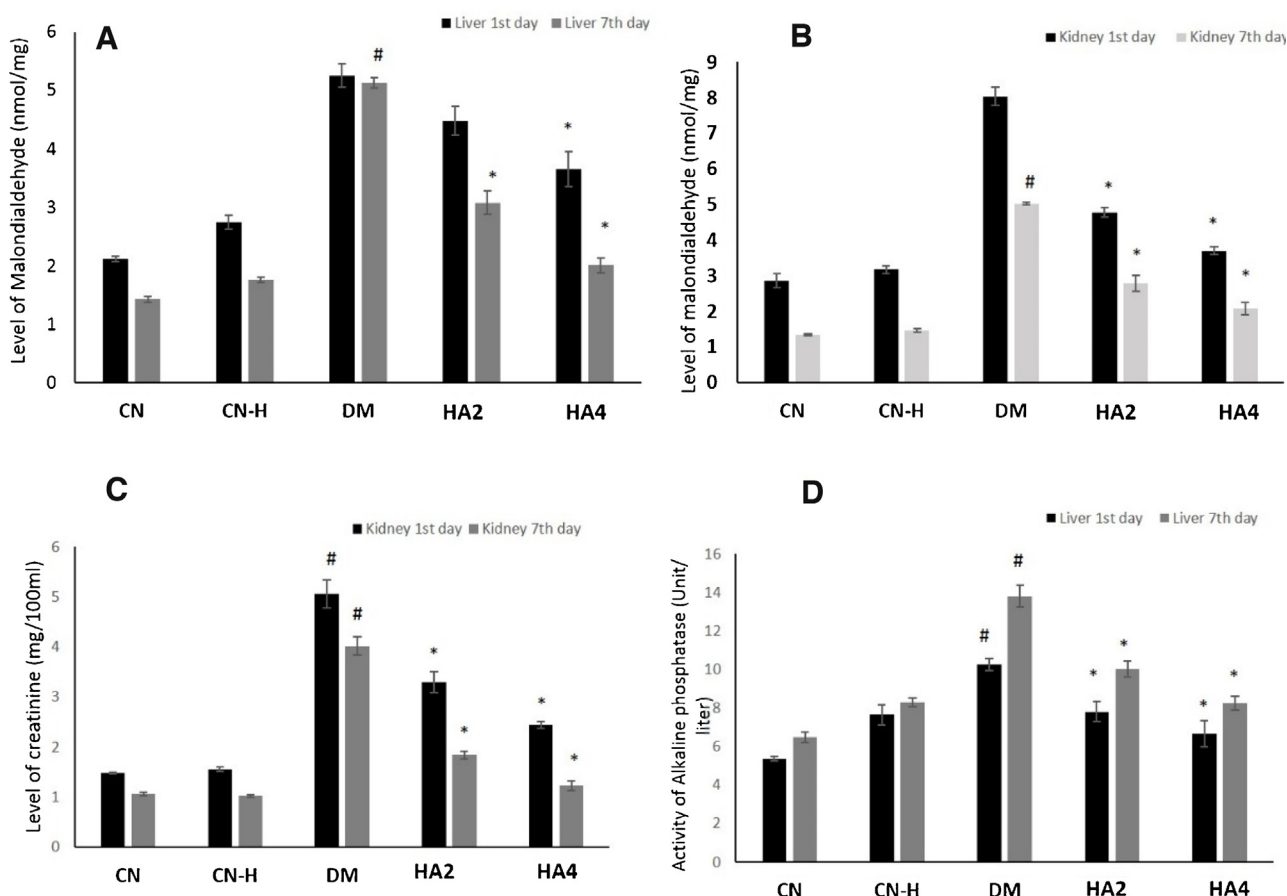
Fig. 6. The level of MDA (A,B), creatinine (C) and alkaline phosphatase (D) in both liver and kidney tissues from different groups. Values shown are means ± SD. #Shows the significance in comparison with the control group. *Shows the significance in comparison with the diabetic group.

oxidative stress markers was the main motto of this section of the study.

3.2.1. Effect of HA2 and HA4 on the level of interferon gamma

Interferon gamma as an inflammatory cytokine was estimated after 24 h of wounding. Diabetes was found to significantly elevate the concentration of interferon gamma in comparison to the control healthy rats. On the other hand, the compound HA4 was found to obviously normalize its level in the diabetic rats. This means that HA4 stopped the elevation of inflammatory cytokines to permit the subsequent normal healing phases (Fig. 3).

3.2.2. Effect of HA2 and HA4 on antioxidant enzymes and proteins of diabetic rats

3.2.2.1. Superoxide dismutase (SOD). **Liver:** After 1st day of the treatment, group DM showed a decline in the specific activity of SOD by 38.55% while the CN-H demonstrated merely 8.96% of decrease as compared to the control. Among the combination groups, HA2 and HA4 exhibited an increase in its activity by 8.35% and 28.44% with respect to the group DM. After 7th day of the treatment, the animals showed similar but stronger pattern. DM group demonstrated a decrease in its activity by 45.35% while HA2 and HA4 showed an increase by 13.67% and 35.94% respectively as compared to group DM (Fig. 4A).

Kidney: After 1st day of the treatment, DM group showed a dip in its activity by 47.19% whereas HA2 and HA4 demonstrated a rise in its activity by 18.75% and 38.28% in the same sequence. After 7th day of the treatment, the decline in DM group was found to

be 41.39% while the group- HA2 and HA4 showed an increase by 22.78% and 46.35% with respect to the DM group (Fig. 4B).

3.2.2.2. Reduced glutathione (GSH). **Liver:** After 1st day of the treatment, DM group showed decrease in GSH level by 41.29% while HA2 and HA4 demonstrated replenishment in its level by 19.34% and 47.50% as compared to the DM group. After 7th day of the treatment, the dip in its level in DM group rose to 47.97% while HA2 and HA4 showed recovery in its level by 26.25% and 56.41% with respect to the DM group (Fig. 5A).

Kidney: After 1st day of the treatment, GSH level was found to be compromised by 41.83% in DM group as compared to the control whereas HA2 and HA4 demonstrated replenishment in its activity by 10.99% and 32.69%. After 7th day of the treatment, its level was decreased by 43.23% in the group DM whereas its level was found to be increased by 13.45% and 45.85% in HA2 and HA4 groups with respect to the DM group (Fig. 5B).

3.2.2.3. Glutathione reductase activity (GR). **Liver:** After 1st day of the treatment, GR activity was decreased by 35.41% and 26.40% in the DM and CN-H groups. The combination groups, HA2 and HA4 showed the increase by 12.84% and 39.35% as compared to the DM group. After 7th day of the treatment, the activity of GR was decreased by 38.41% and 27.35% in DM and CN-H groups respectively while its activity was observed to be improved by 14.04% and 40.86% in HA2 and HA4 groups respectively (Fig. 5C).

Kidney: After 1st day of the treatment, DM group showed a decrease in its activity by 20.90% followed by 12.15% in CN-H group. HA2 and HA4 groups demonstrated an increase in its activity by 4.19% and 14.79% respectively as compared to the DM. After 7th
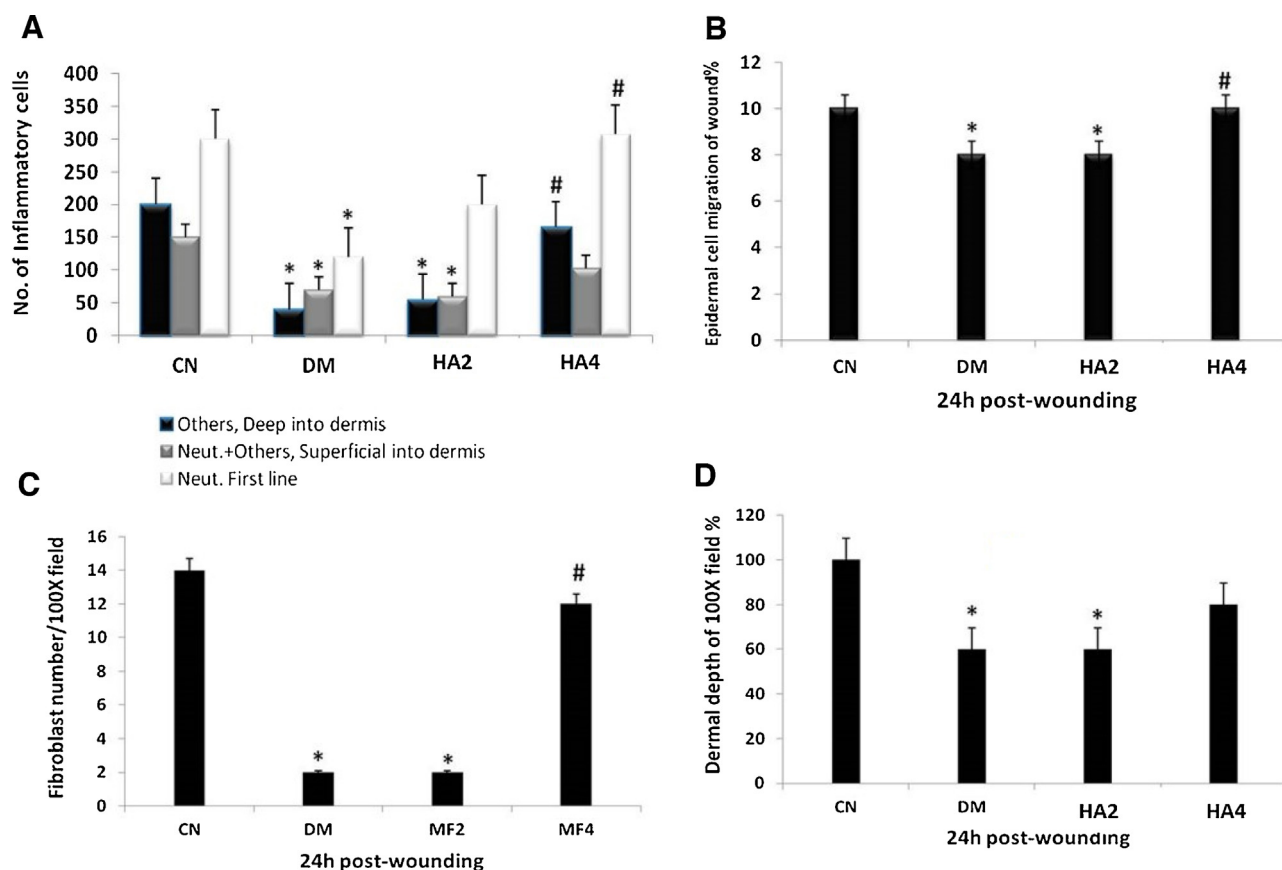
Fig. 7. Histological events one day post-wounding in different groups. A: The number if inflammatory cells (neutrophils in the first wound line, neutrophils and other cells in the superficial line of the damaged dermis and inflammatory cells deep in the damaged dermis) in the wound region. B: The epidermal migration distance (epidermal tongue) from the old epidermal periphery in relation to the wound size. C: The mean of fibroblast number read in the 100× field for each group. D: The dermal depth in relation to the diameter of 100× field. Values shown are means ± SD. *Shows the significance in comparison with the control group. # shows the significance in comparison with the diabetic group.

day of the treatment, DM group exhibited 25.94% of decline followed by 16.04% in the group CN-H while HA2 and HA4 showed the increase in its activity by 8.63% and 17.30% in the same sequence with respect to the DM group (Fig. 5D).

3.2.3. Effect of HA2 and HA4 on toxicity markers of diabetic rats
3.2.3.1. Malondialdehyde (MDA) level. **Liver:** After 1st day of the treatment, DM showed enhancement in the level of MDA by 147.64% followed by 29.24% in CN-H group by as compared to the control. Among the combination groups, HA2 and HA4 demonstrated a decrease in its level by 14.66% and 30.47% respectively. After 7th day of the treatment, DM demonstrated an increase in its level by 258.74% followed by 23.07% in CN-H group. However, HA2 and HA4 groups showed decrease in its level by 39.96% and 60.81% respectively (Fig. 6A).

Kidney: After 1st day of the treatment, DM group showed enhanced the level of MDA by 181.11% followed by 11.18% in CN-H group. HA2 and HA4 groups demonstrated the decrease in its level by 40.54% and 53.98% respectively. After 7th day of the treatment, DM group showed an increase in MDA level by 275% followed by 9.7% in case of CN-H group. However, HA2 and HA4 groups displayed a decrease in its level by 44% and 60% respectively as compared to the DM group (Fig. 6B).

3.2.3.2. Creatinine level. Creatinine is considered as one of the most reliable renal function marker. Its level, after 1st day of the treatment, was found to be raised by 241.89% in DM group while CN-H showed only 4.72% of increment in the kidney samples as compared

to the control. However, HA2 and HA4 showed decrease in its level by 34.78% and 51.77% in respective kidney samples. After 7th day of the treatment, its level rose to 294.11% and 3.77% in DM and CN-H groups respectively. Hitherto, HA2 and HA4 groups showed a marked decrease in its level by 38.04% and 58.58% with respect to the DM group (Fig. 6C).

3.2.3.3. Alkaline phosphatase (ALP) activity. ALP is one of most important liver function markers to assess toxic burden on the liver. In the present study, after 1st day of the treatment, its activity was raised by 42.64% and 90.87% in CN-H and DM groups respectively as compared to the control. However, groups HA2 and HA4 showed decrease in its activity by 23.80% and 34.82% with respect to the DM group. After 7th day of the treatment, DM group showed 112.80% of enhanced activity of ALP followed by 28.08% in CN-H group. However, the combination groups, HA2 and HA4 showed decrease in its activity by 27.19% and 40.17% respectively as compared to the DM group (Fig. 6D).

3.2.4. Effect of HA2 and HA4 on the histological morphometric indices

Our histological outcomes pointed to a marked deficiency in the number of neutrophils in the wounds of diabetic rats, which was complemented with impairment of the healing process. In the group of diabetic rats, inflammatory cell number in the dermal region, declined throughout the first 24 h after wounding. Both the neutrophil number and the inflammatory cell number in the dermal region recovered in diabetic rats, which received
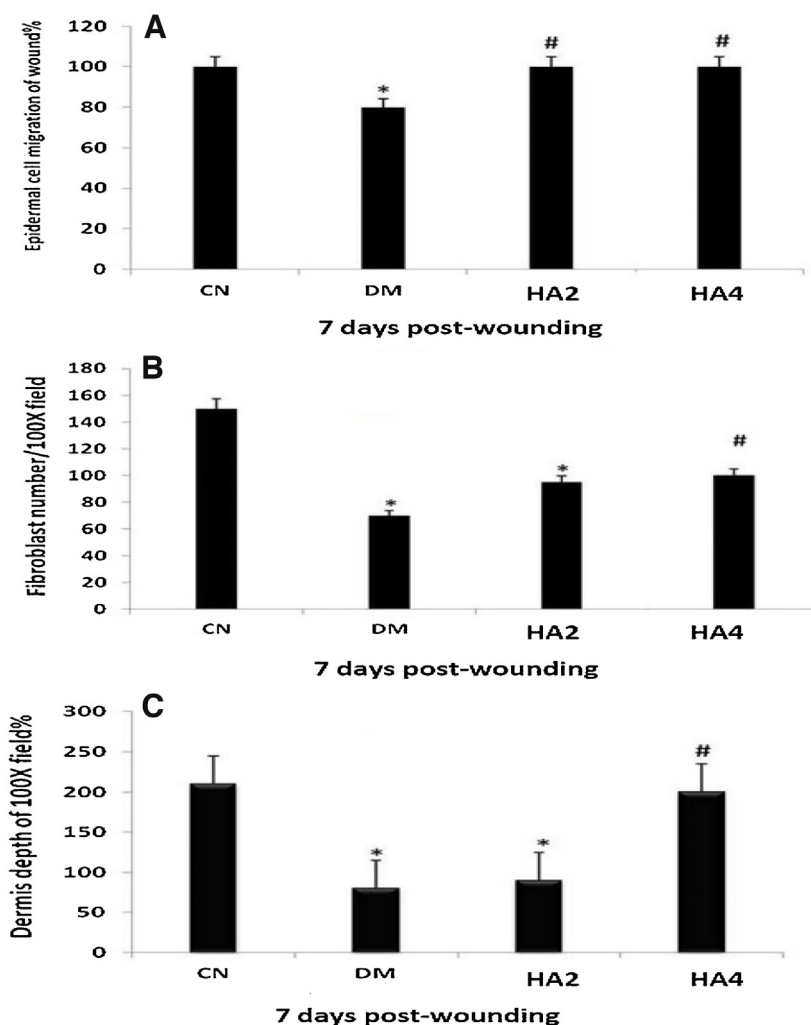
Fig. 8. Histological events seven days post-wounding in different groups. A: The epidermal migration distance (epidermal tongue) from the old epidermal periphery in relation to the wound size. B: The mean of fibroblast number in the $100\times$ field for each group. D: The dermal depth in relation to the diameter of $100\times$ field. Values shown are means $\pm$ SD. *Shows the significance in comparison with the control group. #Shows the significance in comparison with the diabetic group.

HA4 supplementation (Fig. 7A). Interestingly, HA4 was found to significantly recover the epidermal cell migration to the normal one (Fig. 7B). It was observed that fibroblast number was recovered in the HA4 rats (Fig. 7C). Furthermore the dermal depth was normalized by HA4 (Fig. 7D).

After seven days of wounding, the epidermal migration (Fig. 8A), the fibroblast number (Fig. 8B) and the dermal depth (Fig. 8C) were recovered in the HA4 rats. Thus, the wound size in diabetic rats treated with HA4 was significantly lower than that in diabetic ones.

4. Discussion

While it is known that recruitment of cells and mediators is altered during impaired wound healing, thereby delaying this process [1,36], little is performed to find a potential compound to outcome this problem. Recently HA was intensively applied in order to solve the impaired wound healing. Bioactivity of HA-based nanofibrous scaffolds was able to release growth factors that can activate wound healing [37] and HA was beneficial in treating diabetic foot [5] and markedly improved skin mechanical properties [38]. HA derivatives increase the healing progression in burns, epithelial surgical wounds, and chronic wounds [24]. The combination of HA, Col and EGF stimulated cell activity comprising cell migration and proliferation on the adipose tissue in a dia-

betic wound [39]. Here we investigated the impact of four newly prepared compounds from hyaluronic acid on the wound healing events in an older rat model. The high molecular weight of HA (HA2) and its combination with silver nanoparticles (HA4) were found to accelerate the wound healing process in older rat model. Silver nanoparticles also can accelerate the healing process in diabetic/non diabetic rates [32,33,40]. Combination of HA with silver nanoparticles (HA4) was superior on HA2 in the diabetic model.

This part of the study is dedicated to investigate the ameliorative potential of hyaluronic acid (HA2) and its combination with silver nanoparticles (HA4) in the Diabetes Miletus (DM) induced rats. The DM group clearly showed how most of the oxidative stress marker enzymes (SOD and GR) and the proteins (GSH) were significantly compromised concomitant with elevated level of MDA and organ function markers (ALP and creatinine) in the present study. This pattern of redox status clearly suggests that oxidative stress plays a central role in the pathogenesis of Diabetes Miletus. Interestingly, the pattern was found consistent in the DM group animals on the 1st day as well as on the 7th day after the diabetes induction. Moreover, the extent of oxidative stress mediated perturbation was found exacerbated in diabetes induced rats after one week of the induction. All these observations prove that oxidative stress is one of the major causative factors in progression and advancement of the disease that might be attributive involved in

severing of the sufferings of the diabetic patients [41,42]. Furthermore, the behavior of major organ toxicity markers (creatinine and alkaline phosphatase) indicate that the kidney is the target organ in DM group whereas the liver was found target organ in control hurt (CN-H) group. Intriguingly, hyaluronic acid was found as a very efficient antioxidant which further improved with silver nanoparticles in the diabetic induced rats. Both the treatment groups- HA2 and HA4 demonstrated significant restoration of the normal redox status after their single dose on day 1 and this further improved in most of the oxidative parameters on the 7th day of consecutive dosing. The present investigation clearly entails that hyaluronic acid has a significant dose dependent antioxidant and antidiabetic activity that further improves with silver nanoparticles.

It is well established that diabetes mellitus is a metabolic disorder whose pathogenesis and progression are based on altered redox status *in vivo* [43–46]. This notion is well presented by this section of work showing significantly elevated redox and toxicity markers in the diabetic rats that were found to be normalized by hyaluronic acid and its combination silver nanoparticles in dose and time dependent manner.

The liver is considered as a central immunological organ of the whole organism [47,48]. In the CN-H group that was hurt without any treatment, was showing more alteration most of the redox and toxicity markers in the liver sample as compared to their kidney samples. However, in diabetic rats, the kidney becomes the central target with respect to the liver. The constant high glucose concentration in diabetic induced rats put exert extra burden on the glomerular filtration in the kidneys. Besides, the glycation of key biomolecules and cellular components compromise the activity of many enzymes and key protein including the antioxidant enzymes and reduced glutathione and sulfhydryl groups [36,44]. This might be the reason for kidneys being more targeted in DM as compared to the liver. It is well known that hyaluronic acid is an effective antioxidant natural compound that occurs in various types of tissues including epithelial and epidermal cells in living organisms [49,50]. It acts as an important constituting agent as well as an immune-modulator that are important requisites in wound-healing and tissue repair mechanism [51]. Furthermore, silver nanoparticles have been documented for their antioxidant, anti-inflammatory and immune stimulant properties that make them an excellent promising drug delivery system [52,53]. These contemporary studies clearly support our findings that the antioxidant and anti-diabetic properties of hyaluronic acid increases many folds if co-administered with silver nanoparticles. These nanoparticles have the ability to enter into the cytoplasmic vicinities that enhance bioavailability of the drugs in the target organs that consequently improve the overall pharmacodynamics, efficacy and safety profile of the proposed drug.

Conclusions

This data confirms the critical role of HA4 to improve granulation and inflammatory mediators in impaired older and diabetic rat wound healing.

Competing interests

The author declares that there to be no competing interests.

Acknowledgements

References

[1] H. Ebaid, Neutrophil depletion in the early inflammatory phase delayed cutaneous wound healing in older rats: improvements due to the use of un-denatured camel whey protein, Diagn. Pathol. 9 (46) (2014), 1746–1596.

[2] D.J. Kim, T. Mustoe, R.A. Clark, Cutaneous wound healing in aging small mammals: a systematic review, Wound Repair Regen. 23 (3) (2015) 318–339.

[3] C.S. de Melo Rambo, J.A. Silva Jr., A.J. Serra, A.P. Ligeiro, R.P. Vieira, R. Albertini, E.C. Leal-Junior, P. de, Tarso Camillo de Carvalho, Comparative analysis of low-level laser therapy (660 nm) on inflammatory biomarker expression during the skin wound-repair process in young and aged rats, Lasers Med. Sci. 29 (5) (2014) 1723–1733.

[4] O.C. Soybir, S.O. Gurdal, E.S. Oran, F. Tulubas, M. Yuksel, A.I. Akyildiz, A. Bilir, G.R. Soybir, Delayed cutaneous wound healing in aged rats compared to younger ones, Int. Wound J. 9 (5) (2012) 478–487.

[5] P.C. Chang, S.C. Tsai, Y.H. Jheng, Y.F. Lin, C.C. Chen, Soft-tissue wound healing by anti-advanced glycation end-products agents, J. Dent. Res. 93 (4) (2014) 388–393.

[6] D.A. Cox, S. Kunz, N. Cerletti, G.K. McMaster, R.R. Burk, Wound healing in aged animals–effects of locally applied transforming growth factor beta 2 in different model systems, EXS 61 (1992) 287–295.

[7] Z. Zhang, G. Cao, L. Sha, D. Wang, M. Liu, The efficacy of sodium aescinate on cutaneous wound healing in diabetic rats, Inflammation 38 (5) (2015) 1942–1948.

[8] H. Ebaid, K. Hassanein, M. El-Feki, The undenatured whey protein enhanced wound healing in mice, J. Egyptian German Soc. Zool. 47 (2005) 267–287.

[9] H. Ebaid, S.A. Bashandy, I.M. Alhazza, A. Rady, S. El-Shehry, Folic acid and melatonin ameliorate carbon tetrachloride-induced hepatic injury, oxidative stress and inflammation in rats, Nutr. Metab. 10 (1) (2013) 1743–7075.

[10] D. Bagdas, B.C. Etoz, Z. Gul, M.O. Ozyigit, N. Cinkilic, S. Inan, N.I. Buyukcoskun, K. Ozluk, M.S. Gurun, Chlorogenic acid enhances abdominal skin flap survival based on epigastric artery in nondiabetic and diabetic rats, Ann. Plast. Surg. (2014).

[11] A.S. Aly, A.M. Abdel-Mohsen, A. Hebeish, Innovative multifinishing using chitosan-O-PEG graft copolymer/citric acid aqueous system for preparation of medical textiles, J. Text. Inst. 101 (1) (2010) 76–90.

[12] A. Hebeish, M.E. El-Naggar, M.M.G. Fouda, M.A. Ramadan, S.S. Al-Deyab, M.H. El-Rafie, Highly effective antibacterial textiles containing green synthesized silver nanoparticles, Carbohydr. Polym. 86 (2) (2011) 936–940.

[13] M.M.G. Fouda, H.M. Fahmy, Multifunctional finish and cotton cellulose fabric, Carbohydr. Polym. 86 (2) (2011) 625–629.

[14] M.H. El-Rafie, M.E. El-Naggar, M.A. Ramadan, M.M.G. Fouda, S.S. Al-Deyab, A. Hebeish, Environmental synthesis of silver nanoparticles using hydroxypropyl starch and their characterization, Carbohydr. Polym. 86 (2) (2011) 630–635.

[15] A.M. Abdel-Mohsen, A.S. Aly, R. Hrdina, A.S. Montaser, A. Hebeish, Biomedical textiles through multifunctioalization of cotton fabrics using innovative methoxypolyethylene glycol-*N*-chitosan graft copolymer, J. Polymer. Environ. 20 (1) (2011) 104–116.

[16] R.M. Abdel-Rahman, A.M. Abdel-Mohsen, M.M.G. Fouda, S.S. Al Deyab, A.S. Mohamed, Finishing of cellulosic fabrics with chitosan/polyethylene glycol-siloxane to improve their performance and antibacterial properties, Life Sci. J. 10 (4) (2013) 834–839.

[17] M.M.G. Fouda, M.R. El-Aassar, G.F. El Fawal, E.E. Hafez, S.H.D. Masry, A. Abdel-Megeed, K-Carrageenan/poly vinyl pyrollidone/polyethylene glycol/silver nanoparticles film for biomedical application, Int. J. Biol. Macromol. 74 (2015) 179–184.

[18] T. Textor, M.M.G. Fouda, B. Mahltig, Deposition of durable thin silver layers onto polyamides employing a heterogeneous Tollens' reaction, Appl. Surf. Sci. 256 (8) (2010) 2337–2342.

[19] A.M. Abdel-Mohsen, A.S. Aly, R. Hrdina, A.T. El-Aref, A novel method for the preparation of silver/chitosan-*O*-methoxy polyethylene glycol core shell nanoparticles, J. Polym. Environ. 20 (2) (2011) 459–468.

[20] A.M. Abdel-Mohsen, R.M. Abdel-Rahman, R. Hrdina, A. Imramovský, L. Burgert, A.S. Aly, Antibacterial cotton fabrics treated with core–shell nanoparticles, Int. J. Biol. Macromol. 50 (5) (2012) 1245–1253.

[21] M.E. El-Naggar, T.I. Shaheen, M.M.G. Fouda, A.A. Hebeish, Eco-friendly microwave-assisted green and rapid synthesis of well-stabilized gold and core-shell silver-gold nanoparticles, Carbohydr. Polym. 136 (2016) 1128–1136.

[22] T. Tokatlian, C. Cam, T. Segura, Porous hyaluronic acid hydrogels for localized nonviral DNA delivery in a diabetic wound healing model, Adv. Healthc. Mater. 4 (7) (2015) 1084–1091.

[23] N. Ievdokimova, [Hyaluronic acid, receptor CD44, and their role in diabetic complications], Ukrains'kyi biokhimichnyi zhurnal 80 (5) (2008) 5–44.

[24] J. Voigt, V.R. Driver, Hyaluronic acid derivatives and their healing effect on burns, epithelial surgical wounds, and chronic wounds: a systematic review and meta-analysis of randomized controlled trials, Wound Repair Regen. 20 (3) (2012) 317–331.

[25] G. Weindl, M. Schaller, M. Schafer-Korting, H.C. Korting, Hyaluronic acid in the treatment and prevention of skin diseases: molecular biological, pharmaceutical and clinical aspects, Skin Pharmacol. Physiol. 17 (5) (2004) 207–213.

[26] A. D'Agostino, A. Stellavato, T. Busico, A. Papa, V. Tirino, G. Papaccio, A. La Gatta, M. De Rosa, C. Schiraldi, In vitro analysis of the effects on wound healing of high- and low-molecular weight chains of hyaluronan and their hybrid H-HA/L-HA complexes, BMC Cell Biol. 16 (1) (2015) 1–15.

[27] I. Siebenschuh, F. Rosken, M. Koschnick, H. Rakers, K.E. Arfors, W. Mutschler, M.D. Menger, [Local administration of hyaluronic acid for improving wound healing in diabetes], Langenbecks Arch. Chir. Suppl. Kongressbd. 115 (Suppl. I) (1998) 467–468.

[28] B.S. Anisha, R. Biswas, K.P. Chennazhi, R. Jayakumar, Chitosan-hyaluronic acid/nano silver composite sponges for drug resistant bacteria infected diabetic wounds, Int. J. Biol. Macromol. 62 (2013) 310–320.

[29] J.F. Kirk, G. Ritter, I. Finger, D. Sankar, J.D. Reddy, J.D. Talton, C. Nataraj, S. Narisawa, J.L. Millan, R.R. Cobb, Mechanical and biocompatible characterization of a cross-linked collagen-hyaluronic acid wound dressing, Biomatter 3 (4) (2013) 29.

[30] H.J. You, S.K. Han, J.W. Rhie, Randomised controlled clinical trial for autologous fibroblast-hyaluronic acid complex in treating diabetic foot ulcers, J. Wound Care 23 (11) (2014) 521–522.

[31] I. Eroglu, E.H. Gokce, N. Tsapis, S.T. Tanriverdi, G. Gokce, E. Fattal, O. Ozer, Evaluation of characteristics and in vitro antioxidant properties of RSV loaded hyaluronic acid-DPPC microparticles as a wound healing system, Colloids Surf. B Biointerfaces 126 (2015) 50–57.

[32] A.M. Abdel-Mohsen, R. Hrdina, L. Burgert, G. Krylová, R.M. Abdel-Rahman, A. Krejčová, M. Steinhart, L. Beneš, Green synthesis of hyaluronan fibers with silver nanoparticles, Carbohydr. Polym. 89 (2) (2012) 411–422.

[33] A.M. Abdel-Mohsen, R. Hrdina, L. Burgert, R.M. Abdel-Rahman, M. Hašová, D. Šmejkalová, M. Kolář, M. Pekar, A.S. Aly, Antibacterial activity and cell viability of hyaluronan fiber with silver nanoparticles, Carbohydr. Polym. 2 (2013) 1177–1187.

[34] A. Schwentker, Y. Vodovotz, R. Weller, T.R. Billiar, Nitric oxide and wound repair: role of cytokines? Nitric Oxide 7 (1) (2002) 1–10.

[35] A.M. Abdelgawad, S.M. Hudson, O.J. Rojas, Antimicrobial wound dressing nanofiber mats from multicomponent (chitosan/silver-NPs/polyvinyl alcohol) systems, Carbohydr. Polym. 100 (2014) 166–178.

[36] H. Ebaid, Promotion of immune and glycaemic functions in streptozotocin-induced diabetic rats treated with un-denatured camel milk whey proteins, Nutr. Metab. 11 (31) (2014) 1743–7075.

[37] Z. Wang, Y. Qian, L. Li, L. Pan, L.W. Njunge, L. Dong, L. Yang, Evaluation of emulsion electrospun polycaprolactone/hyaluronan/epidermal growth factor nanofibrous scaffolds for wound healing, J. Biomater. Appl. 26 (2015), 0885328215586907.

[38] M. Galeano, F. Polito, A. Bitto, N. Irrera, G.M. Campo, A. Avenoso, M. Calo, P. Lo Cascio, L. Minutoli, M. Barone, F. Squadrito, D. Altavilla, Systemic administration of high-molecular weight hyaluronan stimulates wound healing in genetically diabetic mice, Biochim. Biophys. Acta 7 (2011) 752–759.

[39] S. Kondo, H. Niiyama, A. Yu, Y. Kuroyanagi, Evaluation of a wound dressing composed of hyaluronic acid and collagen sponge containing epidermal growth factor in diabetic mice, J. Biomater. Sci. Polym. Ed. 23 (13) (2012) 1729–1740.

[40] A.M. Abdel-Mohsen, R.M. Abdel-Rahman, M.M.G. Fouda, L. Vojtova, L. Uhrova, A.F. Hassan, S.S. Al-Deyab, I.E. El-Shamy, J. Jancar, Preparation, characterization and cytotoxicity of schizophyllan/silver nanoparticle composite, Carbohydr. Polym. 102 (1) (2014) 238–245.

[41] A.C. Maritim, R.A. Sanders, J.B. Watkins 3rd., Diabetes, oxidative stress, and antioxidants: a review, J. Biochem. Mol. Toxicol. 17 (1) (2003) 24–38.

[42] T.V. Fiorentino, A. Prioletta, P. Zuo, F. Folli, Hyperglycemia-induced oxidative stress and its role in diabetes mellitus related cardiovascular diseases, Curr. Pharm. Des. 19 (32) (2013) 5695–5703.

[43] M.M. Alam, D. Meerza, I. Naseem, Protective effect of quercetin on hyperglycemia, oxidative stress and DNA damage in alloxan induced type 2 diabetic mice, Life Sci. 109 (1) (2014) 8–14.

[44] D. Meerza, I. Naseem, J. Ahmed, Effect of 1, 25(OH)(2) vitamin D(3) on glucose homeostasis and DNA damage in type 2 diabetic mice, J. Diabet. Complications 26 (5) (2012) 363–368.

[45] I. Hassan, S. Chibber, I. Naseem, Ameliorative effect of riboflavin on the cisplatin induced nephrotoxicity and hepatotoxicity under photoillumination, Food Chem. Toxicol. 48 (8–9) (2010) 2052–2058.

[46] I. Hassan, S. Chibber, I. Naseem, Vitamin B(2): a promising adjuvant in cisplatin based chemoradiotherapy by cellular redox management, Food Chem. Toxicol. 59 (2013) 715–723.

[47] C.N. Jenne, P. Kubes, Immune surveillance by the liver, Nat. Immunol. 14 (10) (2013) 996–1006.

[48] V. Racanelli, B. Rehermann, The liver as an immunological organ, Hepatology 43 (2 Suppl. 1) (2006) S54–62.

[49] C. Ke, L. Sun, D. Qiao, D. Wang, X. Zeng, Antioxidant acitivity of low molecular weight hyaluronic acid, Food Chem. Toxicol. 49 (10) (2011) 2670–2675.

[50] G.M. Campo, A. Avenoso, S. Campo, A.M. Ferlazzo, A. Calatroni, Administration of hyaluronic acid and chondroitin-4-sulfate limits endogenous antioxidant depletion and reduces cell damage in experimental acute pancreatitis, Pancreas 28 (2) (2004) E45–53.

[51] M. Prosdocimi, C. Bevilacqua, Impaired wound healing in diabetes: the rationale for clinical use of hyaluronic acid plus silver sulfadiazine, Minerva Med. 103 (6) (2012) 533–539.

[52] R. Cortivo, V. Vindigni, L. Iacobellis, G. Abatangelo, P. Pinton, B. Zavan, Nanoscale particle therapies for wounds and ulcers, Nanomedicine 5 (4) (2010) 641–656.

[53] L. Ge, Q. Li, M. Wang, J. Ouyang, X. Li, M.M.Q. Xing, Nanosilver particles in medical applications: synthesis, performance, and toxicity, Int. J. Nanomed. 9 (2014) 2399–2407.